WAVE ANALYSIS OF CARDIOVASCULAR PHYSIOLOGY AND DISEASE

EDITED BY: Giovanni Biglino, Adelaide De Vecchi and Jonathan Paul Mynard
PUBLISHED IN: Frontiers in Physiology, Frontiers in Cardiovascular Medicine and Frontiers in Pediatrics

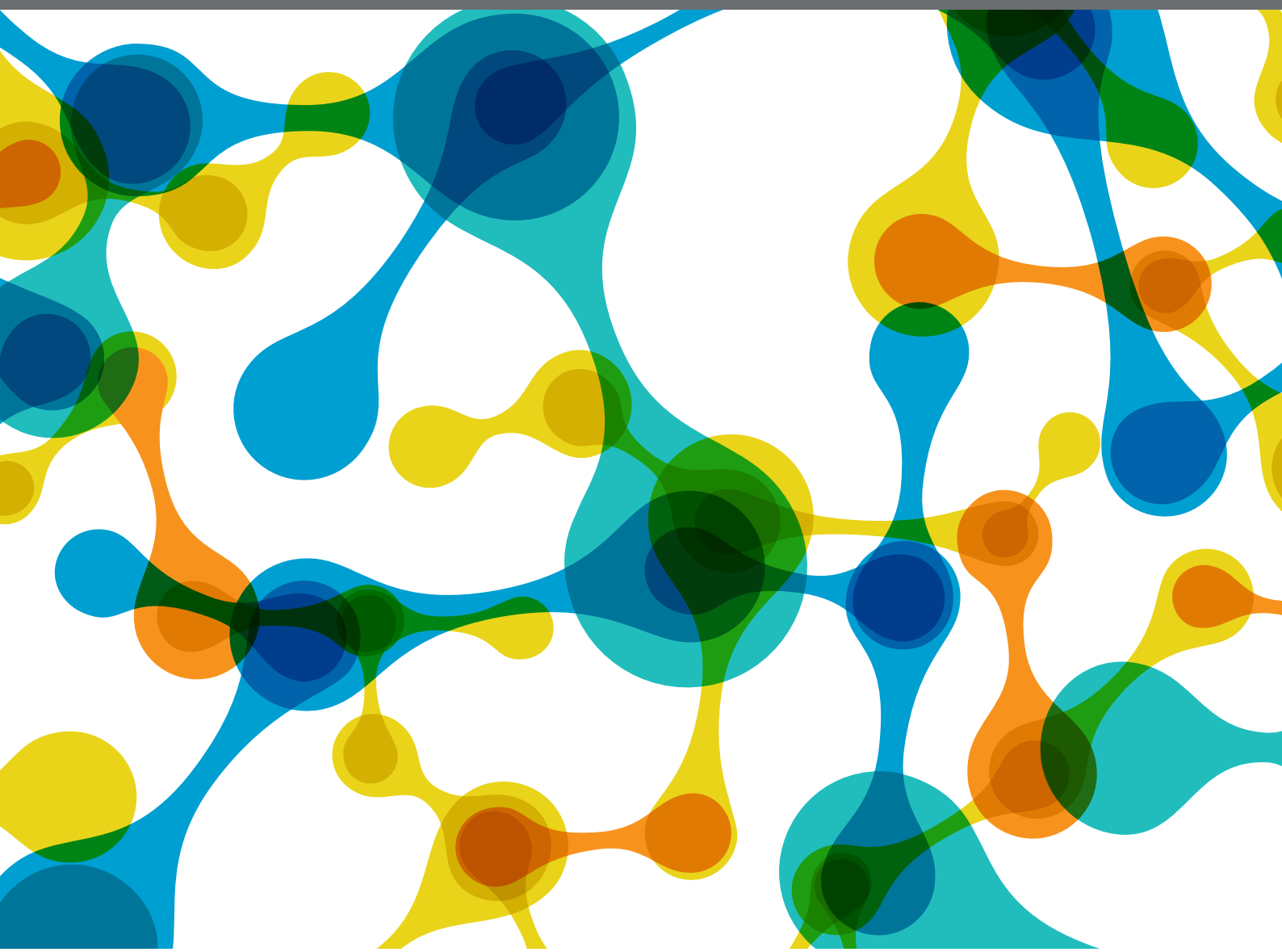

frontiers Research Topics

ISSN 1664-8714
ISBN 978-2-88976-450-1
DOI 10.3389/978-2-88976-450-1

About Frontiers

Frontiers is more than just an open-access publisher of scholarly articles: it is a pioneering approach to the world of academia, radically improving the way scholarly research is managed. The grand vision of Frontiers is a world where all people have an equal opportunity to seek, share and generate knowledge. Frontiers provides immediate and permanent online open access to all its publications, but this alone is not enough to realize our grand goals.

Frontiers Journal Series

The Frontiers Journal Series is a multi-tier and interdisciplinary set of open-access, online journals, promising a paradigm shift from the current review, selection and dissemination processes in academic publishing. All Frontiers journals are driven by researchers for researchers; therefore, they constitute a service to the scholarly community. At the same time, the Frontiers Journal Series operates on a revolutionary invention, the tiered publishing system, initially addressing specific communities of scholars, and gradually climbing up to broader public understanding, thus serving the interests of the lay society, too.

Dedication to Quality

Each Frontiers article is a landmark of the highest quality, thanks to genuinely collaborative interactions between authors and review editors, who include some of the world's best academicians. Research must be certified by peers before entering a stream of knowledge that may eventually reach the public - and shape society; therefore, Frontiers only applies the most rigorous and unbiased reviews.
Frontiers revolutionizes research publishing by freely delivering the most outstanding research, evaluated with no bias from both the academic and social point of view. By applying the most advanced information technologies, Frontiers is catapulting scholarly publishing into a new generation.

What are Frontiers Research Topics?

Frontiers Research Topics are very popular trademarks of the Frontiers Journals Series: they are collections of at least ten articles, all centered on a particular subject. With their unique mix of varied contributions from Original Research to Review Articles, Frontiers Research Topics unify the most influential researchers, the latest key findings and historical advances in a hot research area! Find out more on how to host your own Frontiers Research Topic or contribute to one as an author by contacting the Frontiers Editorial Office: frontiersin.org/about/contact

WAVE ANALYSIS OF CARDIOVASCULAR PHYSIOLOGY AND DISEASE

Topic Editors:
Giovanni Biglino, University of Bristol, United Kingdom
Adelaide De Vecchi, King's College London, United Kingdom
Jonathan Paul Mynard, Murdoch Childrens Research Institute, Royal Children's Hospital Melbourne, Australia

Citation: Biglino, G., De Vecchi, A., Mynard, J. P., eds. (2022). Wave Analysis of Cardiovascular Physiology and Disease. Lausanne: Frontiers Media SA.
doi: 10.3389/978-2-88976-450-1

Table of Contents

frontiers in Pediatrics

ORIGINAL RESEARCH
published: 31 March 2020
doi: 10.3389/fped.2020.00132

Racial Differences in Left Ventricular Mass and Wave Reflection Intensity in Children

Kevin S. Heffernan[1], Wesley K. Lefferts[2], Nader H. Atallah-Yunes[3], Alaina C. Glasgow[1] and Brooks. B. Gump[4]*

[1] Department of Exercise Science, Syracuse University, Syracuse, NY, United States, [2] Division of Academic Internal Medicine, Department of Medicine, University of Illinois-Chicago, Chicago, IL, United States, [3] Division of Pediatric Cardiology, SUNY Upstate Medical University, Syracuse, NY, United States, [4] Department of Public Health, Syracuse University, Syracuse, NY, United States

The burden of heart failure is disproportionately higher in African Americans, with a higher prevalence seen at an early age. Examination of racial differences in left ventricular mass (LVM) in childhood may offer insight into risk for cardiac target organ damage (cTOD) in adulthood. Central hemodynamic load, a harbinger of cTOD in adults, is higher in African Americans. The purpose of this study was to examine racial differences in central hemodynamic load and LVM in African American and non-Hispanic white (NHW) children. Two hundred sixty-nine children participated in this study (age, 10 ± 1 years; $n = 149$ female, $n = 154$ African American). Carotid pulse wave velocity (PWV), forward wave intensity (W1) and reflected wave intensity (negative area, NA) was assessed from simultaneously acquired distension and flow velocity waveforms using wave intensity analysis (WIA). Wave reflection magnitude was calculated as NA/W1. LVM was assessed using standard 2D echocardiography and indexed to height as LVM/[height (2.16) + 0.09]. A cutoff of 45 g/m (2.16) was used to define left ventricular hypertrophy (LVH). LVM was higher in African American vs. NHW children (39.2 ± 8.0 vs. 37.2 ± 6.7 g/m (2.16), adjusted for age, sex, carotid systolic pressure and socioeconomic status; $p < 0.05$). The proportion of LVH was higher in African American vs. NHW children (25 vs. 12 %, $p < 0.05$). African American and NHW children did not differ in carotid PWV (3.5 ± 4.9 vs. 3.3 ± 1.3 m/s; $p > 0.05$). NA/W1 was higher in African American vs. NHW children (8.5 ± 5.3 vs. 6.7 ± 2.9; $p < 0.05$). Adjusting for NA/W1 attenuated racial differences in LVM (38.8 ± 8.0 vs. 37.6 ± 7.0 g/m (2.16); $p = 0.19$). In conclusion, racial differences in central hemodynamic load and cTOD are present in childhood. African American children have greater wave intensity from reflected waves and higher LVMI compared to NHW children. WIA offers novel insight into early life origins of racial differences in central hemodynamic load and cTOD.

Keywords: children, vascular stiffness, wave intensity analysis, wave reflection, left ventricular mass

OPEN ACCESS

Edited by:
Jonathan Paul Mynard, Royal Children's Hospital, Australia

Reviewed by:
Chloe May Park, University College London, United Kingdom
Hopewell Nkosipendule Ntsinjana, University of the Witwatersrand, South Africa

****Correspondence:***
Kevin S. Heffernan
ksheffer@syr.edu

Specialty section:
This article was submitted to Pediatric Cardiology, a section of the journal Frontiers in Pediatrics

Received: *08 January 2020*
Accepted: *10 March 2020*
Published: *31 March 2020*

Citation:
Heffernan KS, Lefferts WK, Atallah-Yunes NH, Glasgow AC and Gump BB (2020) Racial Differences in Left Ventricular Mass and Wave Reflection Intensity in Children. Front. Pediatr. 8:132. doi: 10.3389/fped.2020.00132

INTRODUCTION

Although incidence and mortality from cardiovascular disease (CVD) is declining, there are still prominent disparities in CVD burden based on race (1). Compared to non-Hispanic whites (NHWs), African Americans have 33% higher death rates from CVD (1). Prevalence of hypertension in African Americans (∼42–44%) is among the highest in the world and greater

than that seen in NHWs (1, 2). As such hypertensive cardiac target organ damage (cTOD) is not only common but epidemic in African Americans (3, 4). African Americans have a 50% greater incidence of heart failure compared to their NHW counterparts (5).

cTOD occurs earlier in life in African Americans than in NHWs (6, 7) and is associated with premature CVD events (8). The CARDIA study reported that 26/27 deaths from heart failure occurred in young African Americans (<50 years of age) with only 1 NHW death (9). Racial differences in hypertension and hypertensive cTOD may have its origins in childhood as higher blood pressure (BP) in African American children track into young adulthood (10) and BP is a significant correlate of cTOD in African American children (11, 12). There are also racial differences in age-related increases in left ventricular mass (LVM) (13), a measure of cTOD, with African Americans having larger LVM in late childhood through young adulthood (14). Predictors of increases in LVM and development of LV hypertrophy from young adulthood to middle-age include larger LVM assessed in young adulthood, higher systolic BP and Black/African American race (15–17).

African Americans are more susceptible than NHW to BP-mediated cTOD suggesting that racial differences in hemodynamic load may have more profound effects on cTOD in African Americans (18, 19). Hemodynamic load is largely determined by central (large artery) stiffness and pressure from wave reflections (20, 21). Increases in arterial stiffness precede the development of hypertension in young adults (22) and increases in pressure from wave reflections have a profound and detrimental impact on the LV (20, 21). Increases in large artery stiffness and pressure from wave reflections alter ventricular-vascular coupling, contributing to increased afterload, myocardial strain, LVM, and ultimately LV hypertrophy (23). Racial differences in hemodynamic load may also have its origins in childhood as African American children have increased arterial stiffness compared to NHW children (24) and central BP is associated with LVM in young African American adolescents (25).

Wave intensity analysis (WIA) offers unique insight into ventricular-vascular coupling and central hemodynamic load. According to wave transmission-reflection theory, BP is an amalgam of traveling waves produced by the interaction of the LV with the aorta (input impedance/characteristic impedance) and the aorta with peripheral arteries (terminal impedance/vascular resistance). The propagation of traveling wavefronts in the systemic circulation encompass the exchange of the kinetic energy of blood flow and the potential energy of stored pressure in the elastic walls of the vessels. WIA is based on the relationship between the instantaneous change in pressure (dP) and the change in flow (dU) across the wave. When the LV contracts, this generates an initial forward pressure wave denoted as W1. WI represents a compression wave that accelerates both flow and pressure (26, 27). Once this wave reaches a bifurcation or area of impedance mismatch, the wave is partially reflected in the opposite direction from the distal circulation and travels back toward the heart. This backward traveling compression wave that decelerates flow but increases pressure is denoted by the negative area (NA) (26, 27). A second forward traveling wave is generated at the end of systole, mirroring the decompression (deceleration) of the wave produced by/contributing to the closing of the aortic value during diastole (26). This expansion wave, denoted as W2, is related to cardiac untwist and suction and thus LV relaxation kinetics. Measures obtained from WIA have been shown to correlate with LV structure and function (28, 29). WIA may thus offer a novel window into racial differences in cTOD risk in childhood.

The purpose of this study was to use WIA to assess racial differences in ventricular-vascular coupling and central hemodynamic load in children to gain insight into early life origins of cTOD. We hypothesized that African American children would have higher LVM, carotid artery stiffness and pressure from wave reflections.

Methods

Two hundred sixty-nine children (154 African American, 149 female) from the Syracuse City community participated in this study as part of the Environmental Exposures and Child Health Outcomes (EECHO) study. Race was identified by parents/guardians as Black/African-American or non-Hispanic white (NHW). All participants were between 9 and 12 years of age, had a body mass >18 kg, and were free from any serious medical/developmental disabilities that would prevent them from participating in the study, as assessed by a health history questionnaire filled out by the guardian. Participants had no medical history of cancer, diagnosed hypertension, stroke, thyroid disease, pancreatitis, neuralgia, or diabetes. This study was approved by the institutional review board of Syracuse University and SUNY Upstate University. All parents/guardians and participants gave written consent and assent, respectively, prior to enrollment.

Study Design

All cardiac and vascular measures were completed in a single visit and all visits occurred between 8:00 AM and 12:00 PM. Participants were asked to arrive in a fasted state. Cardiac measures were completed using standard 2-D echocardiography at SUNY Upstate Children's Hospital in the Division of Pediatric Cardiology. Vascular measures were conducted following a 5-min supine rest period in a dimly-lit, temperature-controlled laboratory (Human Performance Lab at Syracuse University) and consisted of brachial oscillometric pressures, carotid tonometric pressures, and simultaneous contralateral carotid Doppler ultrasonography.

Height and weight were assessed using a mechanical physician scale and stadiometer (Detecto, Webb City, MO). Body mass index (BMI) was calculated as weight (kg)/height $(m)^2$. Socioeconomic status (SES) was calculated as an average of parental occupation, income, and education data (z-scored prior to averaging) as we have previously described (24, 30).

Carotid Wave Intensity Analysis (WIA)

Images of the left common carotid artery (CCA) were obtained using Doppler ultrasound (ProSound α7, Aloka, Tokyo, Japan) and 7.5–10.0 mHz linear-array probe. Wave intensity analysis

(WIA) combined with eTracking was used to derive measures of forward and reflected wave intensity and arterial stiffness. This method has been described in detail previously (31, 32). Briefly, this technique measures CCA distension waveforms (analogous to the pressure waveform) and flow velocity waveforms. The distance from the near-wall to far-wall lumen–intima interface was continuously traced using eTracking software. The echo-tracking system measures diameter changes within 1/16th of an ultrasound wavelength (0.013 mm) (28) creating a distension waveform almost identical to pressure waveforms (33). WIA distension waveforms were calibrated using carotid systolic and diastolic blood pressure. Pressure waveforms were obtained simultaneously in the contralateral CCA from a 10 s epoch using applanation tonometry (SphygmoCor, AtCor Medical, Sydney, Australia). CCA pressure waveforms were calibrated to simultaneously measured brachial mean arterial pressure (MAP) and diastolic BP (DBP) (measured using an oscillometric cuff) with MAP calculated as DBP + 0.33 × pulse pressure. Pulse pressure was calculated as systolic BP (SBP) minus DBP. End systolic pressure (ESP) was obtained from the carotid pressure waveform as the pressure at the incisura of the dicrotic notch. Flow velocity waveforms were measured using range-gated color Doppler signals averaged along the Doppler beam. An insonation angle $\leq 60^{\circ}$ was maintained for all measures. Sample volume was adjusted to encompass the entire vessel. Wave intensity was calculated from an average of 5 beats using time derivatives of blood pressure (P) and velocity (U), where wave intensity = (dP/dt × dU/dt); thus, the area under the dP/dt × dU/dt curve represents the energy transfer of the wave (27).

WIA states that if these wavefronts carry a positive rate of pressure change, they are referred to as compression waves. Conversely, if the wavefront carries a negative rate of pressure change, they are referred to as expansion waves. It should be noted that "expansion" in this setting is an expression from fluid dynamics theory referring to "decreasing pressure" and not to be confused with "dilatation" (27). (1) W1 represents a forward compression wave produced during early systole that accelerates flow and increases pressure; (2) W2 represents a forward expansion wave that decelerates flow and reduces pressure; (3) the negative area (NA) between W1 and W2 is a backward traveling compression wave due to the sum of waves reflected from the periphery (wave reflection intensity) that decelerates flow but increases pressure. We additionally computed the reflection magnitude as NA/W1. Time from W1 to W2 (measured in milliseconds, ms) was taken as a proxy of ejection duration. A local one-point carotid pulse wave velocity (PWV) was calculated from WIA local wave speed as c = (dP/dU)/ρ where ρ is blood density and assumed constant (1,050 kg m^3). Augmentation index (AIx) was calculated as the difference between the early and late systolic peaks of the distension waveforms to the total carotid pulse pressure and expressed as a percentage (P_{max}-$P_{shoulder}$/PP × 100). Reproducibility of carotid WIA has previously been demonstrated to be acceptable (32). Heart rate (HR) was obtained from simultaneous ECG from a single lead modified CM5 configuration.

Echocardiography

Left ventricular mass (LVM) was derived from M-mode echocardiographic measurements of the septum, posterior wall and left ventricular diameter (Sonos 5500 Phillips, Andover, Massachusetts). Absolute LVM was calculated during diastole as: left ventricular mass = 0. 8 × |1.04[(left ventricular internal diameter + posterior wall thickness + septal thickness)^3–(left ventricular internal diameter)^3]) + 0.6 g|. This was based on consensus recommendations for chamber quantification (34). Relative wall thickness RWT was calculated as (2 × posterior wall thickness measured during diastole)/LV internal diastolic diameter. LV end-systolic wall stress (ESWS) was calculated as [0.334 × ESP × LV end-systolic diameter]/[LV posterior wall thickness at end systole × [1 + (LV posterior wall thickness at end systole/LV end-systolic diameter)] (35, 36); where ESP is carotid end-systolic pressure (37).

LVM was indexed (LVMI) using a variety of standard approaches [height, body surface area [BSA], and height raised to a power of 2.7]. There remains controversy regarding "best" methods to index LVM in children (and adults) as it is challenging to disentangle developmental growth from pathophysiological hypertrophy (38, 39). Aforementioned methods tend to "grossly" over diagnose left ventricular hypertrophy (LVH) in smaller individuals and underdiagnose LVH in larger overweight/obese individuals and this is particularly true for children <10 years of age and children of shorter stature (40, 41). Methods relying on BSA or a height index of 2.7 also do not factor in gender differences (42). Given that these strategies of indexing have been challenged for a variety of reasons (43), we chose to focus on LVM indexed using approaches put forth by Chirinos et al. and supported by Mehta in children (41, 42). Chirinos et al. and Mehta suggest indexing LVM to a height raised to a power of 1.7. This approach is a stronger predictor of CVD events in adults when compared to the traditional 2.7 method and may be more sensitive to obesity-mediated LVH in children (41, 42). We also employed a strategy put forth by Chinali et al. With the Chinali et al. approach, LVM is indexed to height raised to a power of 2.16 with a correction factor of + 0.09 and LVH defined using a single partition as values exceeding 45 g/$m^{2.16}$ (44). This approach has been suggested as more parsimonious strategy to index LVM in children as it does not require the need for time-consuming mathematical allometric scaling/ modeling or calculations of sex-specific, height-specific percentiles (44), offering a more clinically meaningful endpoint.

Statistical Analyses

All data are reported as mean ± standard deviation with significance set a priori as $p < 0.05$. A chi-square test was used to test differences in sex distribution between groups. The effect of race on descriptive and cardiovascular measures (continuous variables) were assessed using analysis of variance (ANOVA). Analysis of covariance was used to test the effect of race on LVM after adjusting for potential confounding variables that emerged from ANOVA. Covariates included age, sex, SES, BMI percentile and carotid systolic pressure. We chose to adjust for carotid pressure rather than brachial pressure as central pressures more closely associate with cTOD (45). A second model additionally

TABLE 1 | Descriptive characteristics.

Variable	African American $n = 154$	White $n = 115$	*p*-value
Age (years)	10.3 ± 0.9	10.6 ± 0.9	0.01
Female (%)	44	46	0.70
Height (cm)	145.4 ± 9.1	143.9 ± 8.4	0.18
Body mass index (kg/m^2)	20.8 ± 5.7	20.1 ± 4.5	0.29
Body mass index (percentile)	69.0 ± 30.6	67.1 ± 30.4	0.62
Body surface area (m^2)	1.32 ± 0.2	1.29 ± 0.2	0.31
Socioeconomic status (z-score)	−0.15 ± 0.7	0.42 ± 0.9	0.001

TABLE 2 | Blood pressure and carotid wave intensity analysis (WIA).

Variable	African American $n = 154$	White $n = 115$	*p*-value
Brachial systolic BP (mmHg)	115 ± 14	112 ± 10	0.08
Brachial diastolic BP (mmHg)	68 ± 6	67 ± 6	0.13
Mean arterial pressure (mmHg)	84 ± 8	82 ± 7	0.10
Carotid systolic BP (mmHg)	103 ± 10	101 ± 8	0.09
Carotid end-systolic pressure (mmHg)	85 ± 6	83 ± 7	0.03
Carotid diastolic BP (mmHg)	68 ± 6	67 ± 6	0.14
Carotid pulse wave velocity (m/s)	3.5 ± 4.9	3.3 ± 1.3	0.64
Carotid W1 (mmHg/m/s^3)	9.2 ± 5.1	9.0 ± 4.1	0.72
Carotid W2 (mmHg/m/s^3)	2.1 ± 1.2	2.2 ± 1.3	0.65
tW1-W2 (ms)	276 ± 73	262 ± 23	0.06
Carotid negative area (mmHg/m/s^2)	71.3 ± 49.2	55.2 ± 27.9	0.002
Carotid augmentation index (%)	−3 ± 9	−4 ± 11	0.30
Heart rate (bpm)	73 ± 10	76 ± 10	0.03

adjusted for heart rate. A third model adjusted for NA/W1 to explore the role of wave reflections as a potential mediator of racial differences in LVMI.

Mediational models were further tested using the SPSS PROCESS macro (v. 3.4) developed by Hayes (46). The indirect effects of race on LVMI through NA/W1 and HR was separately explored using the non-parametric bootstrapping procedure. These models were set to 1,000 bootstrap samples in order to minimize sampling error and for the estimation of bias corrected bootstrap confidence intervals for indirect effects. A 95% confidence intervals that does not contain 0 was used as criterion to establish significant mediation. All analyses were performed using Statistical Package for the Social Sciences (SPSS, version 26, Chicago, IL).

Results

Descriptive characteristics are presented in **Table 1**. African American children were slightly older than NHW children (+ 0.3 yrs, $p < 0.05$) and had an overall lower SES-score ($p < 0.05$). African American and NHW children did not differ in height, BMI, BMI percentile, or gender ($p > 0.05$).

Hemodynamic variables are displayed in **Table 2**. There was a trend for African American children to have higher brachial and carotid SBP compared to NHW children ($p = 0.08$ to 0.09). Groups did not differ in DBP ($p > 0.05$). African American children had higher carotid ESP compared to NHW children (**Table 2**, $p < 0.05$). African American and NHW children did not differ in carotid PWV, W1, W2 or AIx ($p > 0.05$). NA/W1 was higher in African American vs. NHW children (8.5 ± 5.3 vs. 6.7 ± 2.9; $p = 0.001$) and this was largely due to group differences in NA with African American children having higher NA compared to NHW (**Table 2**, $p < 0.05$). Group differences in NA/W1 remained after adjusting for age, sex, SES, BMI percentile, and carotid SBP (**Figure 1**, 8.4 ± 0.4 to 6.8 ± 0.4, $p = 0.008$). Adjusting for MAP instead of carotid SBP yielded similar overall findings (results not shown).

Cardiac structural parameters are displayed in **Table 3**. According to chi-square analyses, the proportion of LVH was higher in African American vs. NHW children (25 vs. 12 %, $p = 0.007$). LVMI was higher in African American vs. NHW children when using height raised to a power of 2.16 + 0.09 (**Figure 2A**, 39.1 ± 8.0 vs. 37.2 ± 6.7 g/m$^{2.16}$, $p = 0.025$) and when using height raised to a power of 1.7 (**Figure 2B**, 46.5 ± 9.8 vs. 43.9 ± 8.1 g/m$^{1.7}$, $p = 0.012$); adjusted for age, sex, carotid systolic pressure, BMI percentile and socioeconomic status. Adjusting for MAP or carotid pulse pressure instead of carotid systolic pressure yielded similar overall findings (results not shown). Interestingly, additionally adjusting for either HR (38.9 ± 8.0 vs. 37.5 ± 7.0 g/m$^{2.16}$; $p = 0.17$) or NA/W1 (38.8 ± 8.0 vs. 37.6 ± 7.0 g/m$^{2.16}$; $p = 0.19$) attenuated racial differences in LVMI. Similar results were noted when indexing the LV to height. $^{1.7}$ Additionally adjusting for either HR (46.1 ± 10.0 vs. 44.3 ± 8.0 g/m$^{1.7}$; $p = 0.11$) or NA/W1 (46.2 ± 9.8 vs. 44.2 ± 8.1 g/m$^{1.7}$; $p = 0.08$) attenuated racial differences in LVMI. Mediational analyses with bootstrapping and PROCESS models revealed a significant indirect effect for HR (estimate = −0.76, 95% CI: −1.4, −0.25) and an indirect effect for NA/W1 that approached significance (estimate = −0.45, 95% CI: −1.0, 0.01)

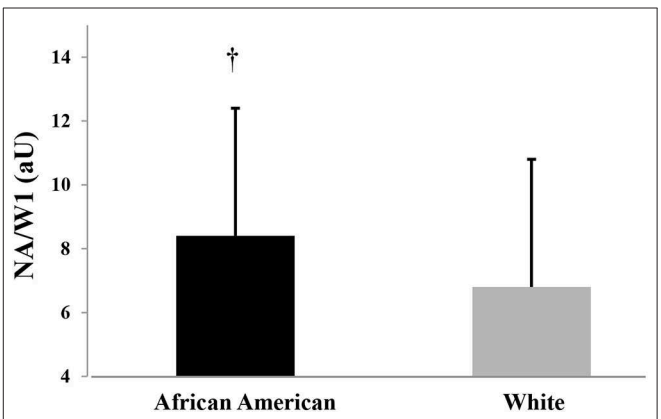

FIGURE 1 | Wave reflection magnitude (NA/W1) in African American and White American Children; adjusted for age, sex, socioeconomic score, BMI percentile, and carotid systolic blood pressure. † Significant group difference ($p < 0.05$).

TABLE 3 | Echocardiographic left ventricular properties.

Variable	African American $n = 154$	White $n = 115$	p-value
Left ventricular mass (g)	88.2 ± 23.7	82.4 ± 18.8	0.031
Left ventricular mass/body surface area (g/m^2)	65.9 ± 10.7	63.7 ± 10.2	0.08
Left ventricular mass/height (g/m)	60.1 ± 14.2	57.0 ± 11.1	0.052
Left ventricular mass/$height^{2.7}$ ($g/m^{2.7}$)	31.8 ± 6.4	30.7 ± 5.5	0.16
Left ventricular relative wall thickness	0.31 ± 0.05	0.29 ± 0.04	0.07
Left ventricular wall stress ($kdynes/cm^2$)	49.7 ± 12.9	48.0 ± 12.8	0.30

for $LVMI^{2.16}$. Similarly, there was a significant indirect effect for HR (estimate = −0.63, 95% CI: −1.1, −0.2) and an indirect effect for NA/W1 that approached significance (estimate = −0.53, 95% CI: −1.2, 0.05) for $LVMI^{1.7}$. RWT was slightly higher in the African American children ($p = 0.07$). This was driven by African American children having higher LV posterior wall thickness compared with NHW children (6.7 ± 1.0 vs. 6.4 ± 0.8 mm, $p = 0.01$). There were no racial differences in septal wall thickness (6.7 ± 1.0 vs. 6.7 ± 1.0 mm, $p = 0.84$). There were no racial differences in ESWS (**Table 3**, $p > 0.05$).

Discussion

This study set out to measure and compare LVM and carotid wave intensity in young African American and NHW children to gain insight into racial differences in early life origins of central hemodynamic load and cTOD. Our theoretical model was ground in an adult literature that strongly supports a physiological role for pressure from wave reflections as an effector of detrimental cardiac remodeling and LVH. Our findings add to this literature and reveal racial differences in LVMI and wave reflection intensity in children. Wave reflection intensity may partially contribute to racial differences in cTOD in children.

Racial Differences in Left Ventricular Mass

LVM is an important measure of clinical prognosis and cTOD in childhood and offers insight into risk of CVD in early adulthood (43). LVM as a manifestation of cTOD is a powerful predictor of CVD risk in adults (47), particularly among African American adults (48). While the literature strongly supports racial differences in LVM in adults (with African Americans having higher LVM than NHW) (3, 4, 49), findings in children and adolescents are conflicting. When adjusting LVM to height, $height^{2.7}$ or BSA, the majority of published studies note no racial differences in LVMI in children (11, 13, 50) although this is not a universal finding with select reports of greater LVM and wall thickness in African American children being noted (51, 52). Racial differences in LVM have been noted to occur longitudinally from late childhood through early adulthood (14) and may track into middle-age (16). When indexing LVM to height, $height^{2.7}$ or BSA, we observed no racial differences in LVM in children. However, when utilizing alternative indexing strategies that have been proposed as more appropriate normalization methods (41, 42), we noted racial differences in LVMI (indexing $height^{1.7}$ or $height^{2.16}$) with African American children having larger LVMI that remained significant after statistical adjustment for age, sex, BMI percentile, SES, and central systolic BP. Future studies should consider using a variety of indexing methods when exploring the impact of race on cardiac dimensions and cTOD.

Racial Differences in Central Hemodynamic Load

WIA may offer novel insight into early life origins of racial differences in central hemodynamic load and cTOD. We observed significantly greater wave reflection intensity in the carotid artery among African American compared to NHW children. There is a strong literature supporting a role for wave reflections in modulating LV load and subsequent LV remodeling. Animal models that employ use of large artery casting or surgical constriction to induce experimental increases in afterload consistently note increases in LVM and development of LVH (53, 54). Moreover, clinical studies in adults support cross sectional associations of wave reflections and subsequent pulse contour with LV geometry (55, 56). Alterations in supra-aortic (i.e., carotid) wave transmission and ensuing changes in carotid wave reflection intensity can alter LV loading sequence favoring increases in mid to late systolic load (57, 58). These wave reflection-based increases in cardiac load may precipitate cardiac remodeling over time as cardiac myosin heavy chain synthesis increases by nearly one third following exposure to a pressure overload (59). Moreover, hypertrophic cardiac remodeling appears particularly sensitive to wave reflections contributions to late rather than early systolic loading, independent of pressure (60). In our study, co-varying for NA/W1 attenuated racial differences in LVMI and NA/W1 approached significance as a statistical mediator. Our findings suggest that greater wave reflection intensity in African American children may serve as the substrate for increased afterload and thus partially contribute to racial differences in LVM.

Although African American children had higher wave reflection intensity and end-systolic pressure compared to NHW children (suggesting augmented late systolic load in African American children), there were no racial differences in LV end-systolic wall stress. Wall stress is considered an important stimulus for LV remodeling and a trigger of cardiac hypertrophy. It is possible that the slightly larger LVM in African American children is a compensatory adaptation aimed at defending LV systolic wall stress (35, 52). Over time and if left unchecked, detrimental LV remodeling may ensue contributing to noted racial differences in LVH and heart failure later in life.

While we noted racial differences in NA/W1 in children, there were no racial differences in carotid AIx. Methods that rely solely on the pulse contour as a means of appraising wave reflections are not without flaw. AIx offers some insight into global wave reflection magnitude in type A waveforms where there is a clear augmentation of pressure at the inflection point/ascending shoulder. However, as eloquently discussed by

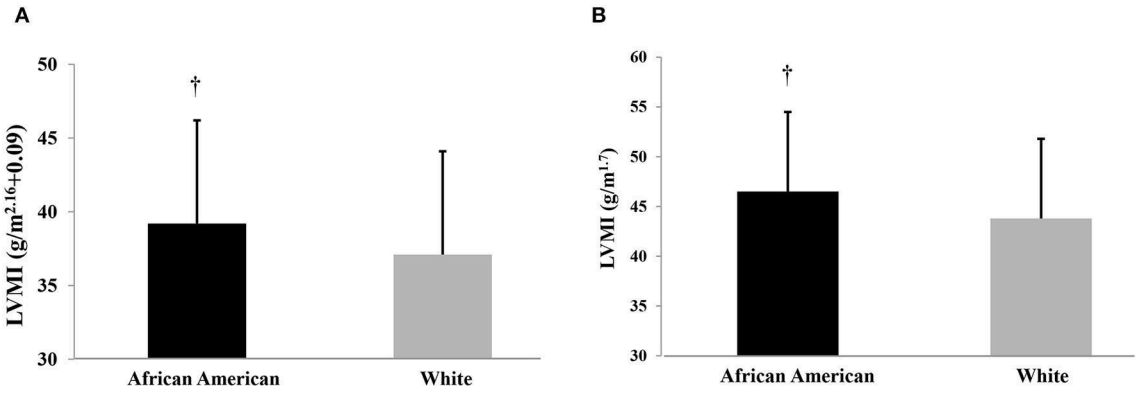

FIGURE 2 | (A) Left ventricular mass index (LVMI) indexed to height of 2.16 in African American and non-Hispanic White Children; adjusted for age, sex, socioeconomic score, BMI percentile, and carotid systolic blood pressure. †Significant group difference ($p < 0.05$). **(B)** Left ventricular mass index (LVMI) indexed to height of 1.7 in African American and non-Hispanic White Children; adjusted for age, sex, socioeconomic score, BMI percentile, and carotid systolic blood pressure. †Significant group difference ($p < 0.05$).

Mitchell (61), when AIx is > 0, augmented pressure from the pressure waveform alone represents just the "tip of the iceberg" because the majority of the reflected wave may be masked by the falling edge of the forward pressure wave (62, 63). In children with Type C waveforms (negligible/no augmentation of pressure above the shoulder), AIx may not capture wave reflection magnitude because calculated values are negative ($P_2 < P_1$). More than 75% of our sample had negative AIx values. AIx is also influenced by cardiac properties unrelated to wave reflections such as cardiac preload, LV stiffness, relaxation and suction as well as arterial reservoir function (64–67). Thus, methods that use both pressure and flow (like WIA to derive NA) are suggested as more optimal methodology to assess wave reflection magnitude (21, 68, 69) and our findings support use of WIA in children to assess cTOD risk.

There were no racial differences in carotid artery stiffness in children and this contrasts previous findings of racial differences in aortic stiffness in children (24). Although the aorta and carotid artery are generally both considered large elastic arteries, the ultrastructure of each is slightly different. Hemodynamic forces owing to hydrostatic effects may be different in the carotid artery vs. the descending-abdominal aorta (region of the aorta captured by cf-PWV) affecting stiffness (70). As such, each vessel is differentially modulated by CVD risk factors and aging over time. For example, the aorta stiffens more with aging and in response to obesity than the carotid artery, an effect exaggerated in the presence of high BP (71). It is possible that premature vascular aging may occur in the aorta prior to the carotid artery, with racial differences in carotid stiffness manifesting later in adolescence/young adulthood (72).

Racial Differences in Left Ventricular Mass and Wave Reflection Intensity: Impact of Heart Rate

Reasons for racial differences in wave reflection intensity in children are unknown but may be related to underlying racial differences in HR. African American children had lower resting HR and this is a consistent finding reported in the literature. A meta-analysis of 17 studies found that African Americans have higher heart rate variability (HRV) compared to NHW, a pattern seen at all ages, suggesting greater cardiac vagal tone across the lifespan (73). This increased parasympathetic control of HR occurs concomitant with increased vascular sympathetic transduction and peripheral vascular resistance in African Americans (73). Interestingly, lower HR (and increased HRV) in African Americans has been seen to associate with larger LVM and development of LVH over time and has been suggested to magnify racial differences in LVM (16, 17, 51, 74, 75). In our study, covarying for HR attenuated racial differences in LVM and HR was a statistical mediator, supporting a role of HR as a partial effector of racial differences in LVM in children.

Lower HR in African American children may instigate greater wave reflection magnitude. There is an inverse association between HR and wave reflections. Although it assumed that this relationship only exists when examining global wave reflections with AIx (76), recent studies highlight HR dependency of wave reflection magnitude (assessed from wave separation analysis) as well (77, 78). A lower HR results in an increase in systolic ejection duration. Parenthetically, African American children had longer systolic ejection duration than NHW children. Without a change in vessel wall stiffness and wave speed, a longer ejection duration results in the confluence of the reflected wave and forward wave more likely occurring in late systole rather than early diastole. In the frequency domain, an increase in HR shifts the harmonics of the pulse waveform toward higher frequencies, an effect modulated by arterial viscoelasticity, resulting in an inverse frequency dependency of the reflection coefficient with HR (78). Thus, "paradoxical" findings reported in the literature of lower HR coexisting with increased LVM may be attributable to HR-mediated effects on wave reflections (79). Lower HR and longer ejection duration in African American children concomitant with increased wave reflection magnitude may increase late

systolic load, contributing to ventricular-vascular uncoupling and LV remodeling.

Limitations

Limitations to this study should be noted. This is a cross-sectional exploration of LVM and WIA in children. Thus, causation cannot be implied. It is possible that cardiac dysfunction may instigate altered wave propagation kinetics. For example, a larger LV may also be indicative of underlying LV dysfunction. Lower LV contractility may result in the genesis of a lower forward wave and by relation a lower absolute reflected wave (albeit possibly a higher relative reflected wave). However, we noted no racial differences in W1 and W2. This would support our theoretical model that higher wave reflection in African American children is likely not of cardiac origin (i.e., there were no differences in W1 to prompt racial differences in NA); wave reflection likely contributes to LVM via effects on LV load and loading sequence. 2D echocardiography may overestimate LVM in Black individuals due to bias in LV morphology assumptions use to calculate LVM. Future studies utilizing 3D echocardiography or cardiac MRI may be useful in further exploring racial variation in LVM in children and adolescents.

Conclusion

In conclusion, African American children have greater wave reflection intensity and LVMI compared to NHW children of similar age and BMI. Premature ventricular-vascular uncoupling from increased wave reflection may instigate premature cTOD in African American children. Additional research is needed to explore the clinical implications of this finding, namely, whether targeting wave reflections in childhood may abrogate racial disparities in detrimental LV remodeling and heart failure later in life.

DATA AVAILABILITY STATEMENT

The datasets generated for this study are available on request to the corresponding author.

ETHICS STATEMENT

This study was approved by the institutional review board of Syracuse University and SUNY Upstate University. Written informed consent to participate in this study was provided by the participants' legal guardian/next of kin.

AUTHOR CONTRIBUTIONS

KH and BG conceptualized study design, methodology, and performed statistical analyses. KH was the primary author and assisted with vascular data collection. WL collected all vascular data and assisted with data interpretation and manuscript preparation. NA-Y oversaw all cardiac echo measures and assisted with data interpretation and manuscript preparation. AG assisted with manuscript preparation. Funding for this study was through an NIH award to BG as PI.

FUNDING

This study was funded by the National Institutes of Health/National Institute of Environmental Health Sciences [R01 ES023252 02 (BG, KH)].

REFERENCES

1. Carnethon MR, Pu J, Howard G, Albert MA, Anderson CAM, et al. Cardiovascular health in african americans: a scientific statement from the american heart association. *Circulation*. (2017) 136:e393–423. doi: 10.1161/CIR.0000000000000534
2. Mills KT, Bundy JD, Kelly TN, Reed JE, Kearney PM, Reynolds K, et al. Global disparities of hypertension prevalence and control: a systematic analysis of population-based studies from 90 countries. *Circulation*. (2016) 134:441–50. doi: 10.1161/CIRCULATIONAHA.115.018912
3. Skelton TN, Andrew ME, Arnett DK, Burchfiel CM, Garrison RJ, Samdarshi TE, et al. Echocardiographic left ventricular mass in African-Americans: the jackson cohort of the atherosclerosis risk in communities study. *Echocardiography*. (2003) 20:111–20. doi: 10.1046/j.1540-8175.2003.03000.x
4. Drazner MH, Dries DL, Peshock RM, Cooper RS, Klassen C, Kazi F, et al. Left ventricular hypertrophy is more prevalent in blacks than whites in the general population: the dallas heart study. *Hypertension*. (2005) 46:124–9. doi: 10.1161/01.HYP.0000169972.96201.8e
5. Kamath S, Markham D, Drazner MH. Increased prevalence of concentric left ventricular hypertrophy in African-Americans: will an epidemic of heart failure follow? *Heart Fail Rev*. (2006) 11:271–7. doi: 10.1007/s10741-006-0228-8
6. Gardin JM, Wagenknecht LE, Anton-Culver H, Flack J, Gidding S, Kurosaki T, et al. Relationship of cardiovascular risk factors to echocardiographic left ventricular mass in healthy young black and white adult men and women. The CARDIA study Coronary Artery Risk Development in Young Adults. *Circulation*. (1995) 92:380–7. doi: 10.1161/01.CIR.92.3.380
7. Kishi S, Reis JP, Venkatesh BA, Gidding SS, Armstrong AC, Jacobs DR Jr., et al. Race-ethnic and sex differences in left ventricular structure and function: the Coronary Artery Risk Development in Young Adults (CARDIA) study. *J Am Heart Assoc*. (2015) 4:e001264. doi: 10.1161/JAHA.114.001264
8. Armstrong AC, Jacobs DR Jr., Gidding SS, Colangelo LA, Gjesdal O, Lewis CE, et al. Framingham score and LV mass predict events in young adults: CARDIA study. *Int J Cardiol*. (2014) 172:350–5. doi: 10.1016/j.ijcard.2014.01.003
9. Bibbins-Domingo K, Pletcher MJ, Lin F, Vittinghoff E, Gardin JM, Arynchyn A, et al. Racial differences in incident heart failure among young adults. *N Engl J Med*. (2009) 360:1179–90. doi: 10.1056/NEJMoa0807265
10. Bao W, Threefoot SA, Srinivasan SR, Berenson GS. Essential hypertension predicted by tracking of elevated blood pressure from childhood to adulthood: the Bogalusa Heart Study. *Am J Hypertens*. (1995) 8:657–65. doi: 10.1016/0895-7061(95)00116-7
11. Burke GL, Arcilla RA, Culpepper WS, Webber LS, Chiang YK, Berenson GS. Blood pressure and echocardiographic measures in children: the Bogalusa Heart Study. *Circulation*. (1987) 75:106–14. doi: 10.1161/01.CIR.75.1.106
12. Urbina EM, Mendizabal B, Becker RC, Daniels SR, Falkner BE, Hamdani G, et al. Association of blood pressure level with left ventricular mass in adolescents. *Hypertension*. (2019) 74:590–6. doi: 10.1161/HYPERTENSIONAHA.119.13027
13. Harshfield GA, Koelsch DW, Pulliam DA, Alpert BS, Richey PA, Becker JA. Racial differences in the age-related increase in left ventricular mass in youths. *Hypertension*. (1994) 24:747–51. doi: 10.1161/01.HYP.24.6.747
14. Dekkers C, Treiber FA, Kapuku G, Van Den Oord EJ, Snieder H. Growth of left ventricular mass in African American and European American youth. *Hypertension*. (2002) 39:943–51. doi: 10.1161/01.HYP.0000015612.73413.91

15. Lorber R, Gidding SS, Daviglus ML, Colangelo LA, Liu K, Gardin JM. Influence of systolic blood pressure and body mass index on left ventricular structure in healthy African-American and white young adults: the CARDIA study. *J Am Coll Cardiol*. (2003) 41:955–60. doi: 10.1016/S0735-1097(03)00052-4
16. Gidding SS, Liu K, Colangelo LA, Cook NL, Goff DC, Glasser SP, et al. Longitudinal determinants of left ventricular mass and geometry: the Coronary Artery Risk Development in Young Adults (CARDIA) Study. *Circ Cardiovasc Imaging*. (2013) 6:769–75. doi: 10.1161/CIRCIMAGING.112.000450
17. Mendizabal B, Khoury P, Woo JG, Urbina EM. Racial differences in the influence of risk factors in childhood on left ventricular mass in young adulthood. *J Pediatr*. (2019) 217:152–7. doi: 10.1016/j.jpeds.2019.10.037
18. Wang J, Chen W, Ruan L, Toprak A, Srinivasan SR, Berenson GS. Differential effect of elevated blood pressure on left ventricular geometry types in black and white young adults in a community (from the Bogalusa Heart Study). *Am J Cardiol*. (2011) 107:717–22. doi: 10.1016/j.amjcard.2010.10.053
19. Ferdinand KC, Townsend RR. Hypertension in the US Black population: risk factors, complications, and potential impact of central aortic pressure on effective treatment. *Cardiovasc Drugs Ther*. (2012) 26:157–65. doi: 10.1007/s10557-011-6367-8
20. Chirinos JA, Segers P. Noninvasive evaluation of left ventricular afterload: part 2: arterial pressure-flow and pressure-volume relations in humans. *Hypertension*. (2010) 56:563–70. doi: 10.1161/HYPERTENSIONAHA.110.157339
21. Townsend RR, Wilkinson IB, Schiffrin EL, Avolio AP, Chirinos JA, Cockcroft JR, et al. Recommendations for improving and standardizing vascular research on arterial stiffness: a scientific statement from the American Heart Association. *Hypertension*. (2015) 66:698–722. doi: 10.1161/HYP.0000000000000033
22. Koivistoinen T, Lyytikainen LP, Aatola H, Luukkaala T, Juonala M, Viikari J, et al. Pulse wave velocity predicts the progression of blood pressure and development of hypertension in young adults. *Hypertension*. (2018) 71:451–6. doi: 10.1161/HYPERTENSIONAHA.117.10368
23. Spartano NL, Augustine JA, Lefferts WK, Redmond JG, Hughes WE, Kuvin JT, et al. Arterial stiffness as a noninvasive tissue biomarker of cardiac target organ damage. *Curr Biomark Find*. (2014) 4:23–34. doi: 10.2147/CBF.S38738
24. Lefferts WK, Augustine JA, Spartano NL, Atallah-Yunes NH, Heffernan KS, Gump BB. Racial differences in aortic stiffness in children. *J Pediatr*. (2017) 180:62–7. doi: 10.1016/j.jpeds.2016.09.071
25. Deloach SS, Daskalakis C, Gidding S, Falkner B. Central blood pressures are associated with left ventricular mass index among African-American adolescents. *Am J Hypertens*. (2012) 25:41–5. doi: 10.1038/ajh.2011.174
26. Parker KH. An introduction to wave intensity analysis. *Med Biol Eng Comput*. (2009) 47:175–88. doi: 10.1007/s11517-009-0439-y
27. Sugawara M, Niki K, Ohte N, Okada T, Harada A. Clinical usefulness of wave intensity analysis. *Med Biol Eng Comput*. (2009) 47:197–206. doi: 10.1007/s11517-008-0388-x
28. Ohte N, Narita H, Sugawara M, Niki K, Okada T, Harada A, et al. Clinical usefulness of carotid arterial wave intensity in assessing left ventricular systolic and early diastolic performance. *Heart Vessels*. (2003) 18:107–11. doi: 10.1007/s00380-003-0700-5
29. Vriz O, Zito C, Di Bello V, La Carrubba S, Driussi C, Carerj S, et al. Non-invasive one-point carotid wave intensity in a large group of healthy subjects: a ventricular-arterial coupling parameter. *Heart Vessels*. (2016) 31:360–9. doi: 10.1007/s00380-014-0600-x
30. Gump BB, Matthews KA, Raikkonen K. Modeling relationships among socioeconomic status, hostility, cardiovascular reactivity, and left ventricular mass in African American and White children. *Health Psychol*. (1999) 18:140–50. doi: 10.1037/0278-6133.18.2.140
31. Harada A, Okada T, Niki K, Chang D, Sugawara M. On-line noninvasive one-point measurements of pulse wave velocity. *Heart Vessels*. (2002) 17:61–8. doi: 10.1007/s003800200045
32. Niki K, Sugawara M, Chang D, Harada A, Okada T, Sakai R, et al. A new noninvasive measurement system for wave intensity: evaluation of carotid arterial wave intensity and reproducibility. *Heart Vessels*. (2002) 17:12–21. doi: 10.1007/s003800200037
33. Van Bortel LM, Balkestein EJ, Van Der Heijden-Spek JJ, Vanmolkot FH, Staessen JA, Kragten JA, et al. Non-invasive assessment of local arterial pulse pressure: comparison of applanation tonometry and echo-tracking. *J Hypertens*. (2001) 19:1037–44. doi: 10.1097/00004872-200106000-00007
34. Lang RM, Bierig M, Devereux RB, Flachskampf FA, Foster E, Pellikka PA, et al. Recommendations for chamber quantification: a report from the American Society of Echocardiography's Guidelines and Standards Committee and the Chamber Quantification Writing Group, developed in conjunction with the European Association of Echocardiography, a branch of the European Society of Cardiology. *J Am Soc Echocardiogr*. (2005) 18:1440–63. doi: 10.1016/j.echo.2005.10.005
35. Grossman W, Jones D, Mclaurin LP. Wall stress and patterns of hypertrophy in the human left ventricle. *J Clin Invest*. (1975) 56:56–64. doi: 10.1172/JCI108079
36. Reichek N, Wilson J, St John Sutton M, Plappert TA, Goldberg S, Hirshfeld JW. Noninvasive determination of left ventricular end-systolic stress: validation of the method and initial application. *Circulation*. (1982) 65:99–108. doi: 10.1161/01.CIR.65.1.99
37. Colan SD, Borow KM, Neumann A. Use of the calibrated carotid pulse tracing for calculation of left ventricular pressure and wall stress throughout ejection. *Am Heart J*. (1985) 109:1306–10. doi: 10.1016/0002-8703(85)90356-4
38. De Simone G, Devereux RB, Daniels SR, Koren MJ, Meyer RA, Laragh JH. Effect of growth on variability of left ventricular mass: assessment of allometric signals in adults and children and their capacity to predict cardiovascular risk. *J Am Coll Cardiol*. (1995) 25:1056–62. doi: 10.1016/0735-1097(94)00540-7
39. Mirchandani D, Bhatia J, Leisman D, Kwon EN, Cooper R, Chorny N, et al. Concordance of measures of left-ventricular hypertrophy in pediatric hypertension. *Pediatr Cardiol*. (2014) 35:622–6. doi: 10.1007/s00246-013-0829-7
40. Khoury PR, Mitsnefes M, Daniels SR, Kimball TR. Age-specific reference intervals for indexed left ventricular mass in children. *J Am Soc Echocardiogr*. (2009) 22:709–14. doi: 10.1016/j.echo.2009.03.003
41. Mehta SK. Left ventricular mass by echocardiographic measures in children and adolescents. *Cardiol Young*. (2013) 23:727–37. doi: 10.1017/S1047951112001862
42. Chirinos JA, Segers P, De Buyzere ML, Kronmal RA, Raja MW, De Bacquer D, et al. Left ventricular mass: allometric scaling, normative values, effect of obesity, and prognostic performance. *Hypertension*. (2010) 56:91–8. doi: 10.1161/HYPERTENSIONAHA.110.150250
43. Khoury M, Urbina EM. Cardiac and vascular target organ damage in pediatric hypertension. *Front Pediatr*. (2018) 6:148. doi: 10.3389/fped.2018.00148
44. Chinali M, Emma F, Esposito C, Rinelli G, Franceschini A, Doyon A, et al. Left ventricular mass indexing in infants, children, and adolescents: a simplified approach for the identification of left ventricular hypertrophy in clinical practice. *J Pediatr*. (2016) 170:193–8. doi: 10.1016/j.jpeds.2015.10.085
45. Kollias A, Lagou S, Zeniodi ME, Boubouchairopoulou N, Stergiou GS. Association of central versus brachial blood pressure with target-organ damage: systematic review and meta-analysis. *Hypertension*. (2016) 67:183–90. doi: 10.1161/HYPERTENSIONAHA.115.06066
46. Preacher KJ, Hayes AF. SPSS and SAS procedures for estimating indirect effects in simple mediation models. *Behav Res Methods Instrum Comput*. (2004) 36:717–31. doi: 10.3758/BF03206553
47. Levy D, Garrison RJ, Savage DD, Kannel WB, Castelli WP. Prognostic implications of echocardiographically determined left ventricular mass in the Framingham Heart Study. *N Engl J Med*. (1990) 322:1561–6. doi: 10.1056/NEJM199005313222203
48. Liao Y, Cooper RS, Mcgee DL, Mensah GA, Ghali JK. The relative effects of left ventricular hypertrophy, coronary artery disease, and ventricular dysfunction on survival among black adults. *Jama*. (1995) 273:1592–7. doi: 10.1001/jama.273.20.1592
49. Kizer JR, Arnett DK, Bella JN, Paranicas M, Rao DC, Province MA, et al. Differences in left ventricular structure between black and white hypertensive adults: the Hypertension Genetic Epidemiology Network study. *Hypertension*. (2004) 43:1182–8. doi: 10.1161/01.HYP.0000128738.94190.9f
50. Daniels SR, Meyer RA, Liang YC, Bove KE. Echocardiographically determined left ventricular mass index in normal children, adolescents and young adults. *J Am Coll Cardiol*. (1988) 12:703–8. doi: 10.1016/S0735-1097(88)80060-3

51. Schieken RM, Schwartz PF, Goble MM. Tracking of left ventricular mass in children: race and sex comparisons: the MCV Twin Study. Medical College of Virginia. *Circulation.* (1998) 97:1901–6. doi: 10.1161/01.CIR.97.19.1901
52. Lamers L, Ensing G, Pignatelli R, Goldberg C, Bezold L, Ayres N, et al. A prospective assessment of myocardial contractility in young African Americans: does ethnicity impact the wall stress-heart rate-corrected velocity of circumferential fiber shortening relationship? *J Am Soc Echocardiogr*. (2005) 18:743–8. doi: 10.1016/j.echo.2005.01.002
53. Ioannou CV, Morel DR, Katsamouris AN, Katranitsa S, Startchik I, Kalangos A, et al. Left ventricular hypertrophy induced by reduced aortic compliance. *J Vasc Res.* (2009) 46:417–25. doi: 10.1159/000194272
54. Dealmeida AC, Van Oort RJ, Wehrens XH. Transverse aortic constriction in mice. *J Vis Exp*. (2010) 21:1729. doi: 10.3791/1729
55. Saba PS, Roman MJ, Pini R, Spitzer M, Ganau A, Devereux RB. Relation of arterial pressure waveform to left ventricular and carotid anatomy in normotensive subjects. *J Am Coll Cardiol*. (1993) 22:1873–80. doi: 10.1016/0735-1097(93)90772-S
56. Nichols WW, Denardo SJ, Wilkinson IB, Mceniery CM, Cockcroft J, O'rourke MF. Effects of arterial stiffness, pulse wave velocity, and wave reflections on the central aortic pressure waveform. *J Clin Hypertens (Greenwich)*. (2008) 10:295–303. doi: 10.1111/j.1751-7176.2008.04746.x
57. Chirinos JA, Segers P, Gupta AK, Swillens A, Rietzschel ER, De Buyzere ML, et al. Time-varying myocardial stress and systolic pressure-stress relationship: role in myocardial-arterial coupling in hypertension. *Circulation*. (2009) 119:2798–807. doi: 10.1161/CIRCULATIONAHA.108.829366
58. Mynard JP, Kowalski R, Cheung MM, Smolich JJ. Beyond the aorta: partial transmission of reflected waves from aortic coarctation into supra-aortic branches modulates cerebral hemodynamics and left ventricular load. *Biomech Model Mechanobiol*. (2017) 16:635–50. doi: 10.1007/s10237-016-0842-x
59. Imamura T, Mcdermott PJ, Kent RL, Nagatsu M, Cooper GT, Carabello BA. Acute changes in myosin heavy chain synthesis rate in pressure versus volume overload. *Circ Res*. (1994) 75:418–25. doi: 10.1161/01.RES.75.3.418
60. Kobayashi S, Yano M, Kohno M, Obayashi M, Hisamatsu Y, Ryoke T, et al. Influence of aortic impedance on the development of pressure-overload left ventricular hypertrophy in rats. *Circulation*. (1996) 94:3362–8. doi: 10.1161/01.CIR.94.12.3362
61. Mitchell GF. Triangulating the peaks of arterial pressure. *Hypertension*. (2006) 48:543–5. doi: 10.1161/01.HYP.0000238325.41764.41
62. Torjesen AA, Wang N, Larson MG, Hamburg NM, Vita JA, Levy D, et al. Forward and backward wave morphology and central pressure augmentation in men and women in the Framingham Heart Study. *Hypertension*. (2014) 64:259–65. doi: 10.1161/HYPERTENSIONAHA.114.03371
63. Tade G, Norton GR, Booysen HL, Sibiya MJ, Ballim I, Sareli P, et al. Time to the peak of the aortic forward wave determines the impact of aortic backward wave and pulse pressure on left ventricular mass. *J Hypertens*. (2017) 35:300–9. doi: 10.1097/HJH.0000000000001173
64. Sharman JE, Davies JE, Jenkins C, Marwick TH. Augmentation index, left ventricular contractility, and wave reflection. *Hypertension.* (2009) 54:1099–105. doi: 10.1161/HYPERTENSIONAHA.109.133066
65. Heffernan KS, Patvardhan EA, Hession M, Ruan J, Karas RH, Kuvin JT. Elevated augmentation index derived from peripheral arterial tonometry is associated with abnormal ventricular-vascular coupling. *Clin Physiol Funct Imaging*. (2010) 30:313–7. doi: 10.1111/j.1475-097X.2010.00943.x
66. Heffernan KS, Sharman JE, Yoon ES, Kim EJ, Jung SJ, Jae SY. Effect of increased preload on the synthesized aortic blood pressure waveform. *J Appl Physiol (1985)*. (2010) 109:484–90. doi: 10.1152/japplphysiol.00196.2010
67. Hughes AD, Park C, Davies J, Francis D, Mc GTSA, Mayet J, et al. Limitations of augmentation index in the assessment of wave reflection in normotensive healthy individuals. *PLoS ONE*. (2013) 8:e59371. doi: 10.1371/journal.pone.0059371
68. Segers P, Rietzschel ER, De Buyzere ML, De Bacquer D, Van Bortel LM, De Backer G, et al. Assessment of pressure wave reflection: getting the timing right! *Physiol Meas*. (2007) 28:1045–56. doi: 10.1088/0967-3334/28/9/006
69. Heusinkveld MHG, Delhaas T, Lumens J, Huberts W, Spronck B, Hughes AD, et al. Augmentation index is not a proxy for wave reflection magnitude: mechanistic analysis using a computational model. *J Appl Physiol (1985)*. (2019) 127:491–500. doi: 10.1152/japplphysiol.00769.2018
70. Schroeder EC, Rosenberg AJ, Hilgenkamp TIM, White DW, Baynard T, Fernhall B. Effect of upper body position on arterial stiffness: influence of hydrostatic pressure and autonomic function. *J Hypertens*. (2017) 35:2454–61. doi: 10.1097/HJH.0000000000001481
71. Paini A, Boutouyrie P, Calvet D, Tropeano AI, Laloux B, Laurent S. Carotid and aortic stiffness: determinants of discrepancies. *Hypertension*. (2006) 47:371–6. doi: 10.1161/01.HYP.0000202052.25238.68
72. Heffernan KS, Jae SY, Wilund KR, Woods JA, Fernhall B. Racial differences in central blood pressure and vascular function in young men. *Am J Physiol Heart Circ Physiol*. (2008) 295:H2380–7. doi: 10.1152/ajpheart.00902.2008
73. Hill LK, Hu DD, Koenig J, Sollers JJ 3rd, Kapuku G, Wang X, Snieder H, et al. Ethnic differences in resting heart rate variability: a systematic review and meta-analysis. *Psychosom Med*. (2015) 77:16–25. doi: 10.1097/PSY.0000000000000133
74. De Simone G, Devereux RB, Kimball TR, Roman MJ, Palmieri V, Celentano A, et al. Relation of heart rate to left ventricular dimensions in normotensive, normal-weight children, adolescents and adults. *Ital Heart J*. (2001) 2:599–604.
75. Hill LK, Watkins LL, Hinderliter AL, Blumenthal JA, Sherwood A. Racial differences in the association between heart rate variability and left ventricular mass. *Exp Physiol*. (2017) 102:764–72. doi: 10.1113/EP086228
76. Liao CF, Cheng HM, Sung SH, Yu WC, Chen CH. Determinants of pressure wave reflection: characterization by the transit time-independent reflected wave amplitude. *J Hum Hypertens*. (2011) 25:665–71. doi: 10.1038/jhh.2010.106
77. Tan I, Kiat H, Barin E, Butlin M, Avolio AP. Effects of pacing modality on noninvasive assessment of heart rate dependency of indices of large artery function. *J Appl Physiol (1985)*. (2016) 121:771–80. doi: 10.1152/japplphysiol.00445.2016
78. Xiao H, Tan I, Butlin M, Li D, Avolio AP. Mechanism underlying the heart rate dependency of wave reflection in the aorta: a numerical simulation. *Am J Physiol Heart Circ Physiol*. (2018) 314:H443–51. doi: 10.1152/ajpheart.00559.2017
79. Heffernan KS, Jae SY, Tomayko E, Ishaque MR, Fernhall B, Wilund KR. Influence of arterial wave reflection on carotid blood pressure and intima-media thickness in older endurance trained men and women with pre-hypertension. *Clin Physiol Funct Imaging*. (2009) 29:193–200. doi: 10.1111/j.1475-097X.2009.00856.x

Conflict of Interest: The authors declare that the research was conducted in the absence of any commercial or financial relationships that could be construed as a potential conflict of interest.

frontiers in Physiology

ORIGINAL RESEARCH
published: 09 April 2020
doi: 10.3389/fphys.2020.00313

Estimation of Wave Condition Number From Pressure Waveform Alone and Its Changes With Advancing Age in Healthy Women and Men

Niema M. Pahlevan[1,2] and Sohrab P. Mazandarani[3]*

[1] *Department of Aerospace Mechanical Engineering, University of Southern California, Los Angeles, CA, United States,* [2] *Division of Cardiovascular Medicine, Department of Medicine, University of Southern California, Los Angeles, CA, United States,* [3] *Department of Economics, Geography, and Political Science, Division of Language, Humanity, and Social Science, Riverside City College, Riverside, CA, United States*

OPEN ACCESS

Edited by:
Jonathan Paul Mynard, Royal Children's Hospital, Australia

Reviewed by:
Patrick Segers, Ghent University, Belgium
Bernhard Hametner, Austrian Institute of Technology (AIT), Austria

****Correspondence:***
Niema M. Pahlevan
pahlevan@usc.edu

Specialty section:
This article was submitted to Vascular Physiology, a section of the journal Frontiers in Physiology

Received: *08 January 2020*
Accepted: *19 March 2020*
Published: *09 April 2020*

Citation:
Pahlevan NM and Mazandarani SP (2020) Estimation of Wave Condition Number From Pressure Waveform Alone and Its Changes With Advancing Age in Healthy Women and Men. Front. Physiol. 11:313. doi: 10.3389/fphys.2020.00313

Introduction: The wave condition number (WCN) is a non-dimensional number that determines the state of arterial wave reflections. WCN is equal to HR $\times$ L_{eff}/PWV where HR, L_{eff}, and PWV are the heart rate, effective length, and pulse wave velocity, respectively. It has been shown that a value of WCN = 0.1 indicates the optimum state of arterial wave reflection in which left ventricle workload is minimized. The pressure wave, flow wave, and PWV are all required to compute WCN, which may limit the potential clinical utility of WCN. The aims of this study are as follows: (1) to assess the feasibility of approximating WCN from the pressure waveform alone (WCN_{Pinf}), and (2) to provide the proof-of-concept that WCN_{Pinf} can capture age related differences in arterial wave reflection among healthy women and men.

Methods: Previously published retrospective data composed of seventeen patients (age 19–54 years; 34.3 $\pm$ 9.6) were used to assess the accuracy of WCN_{Pinf}. The exact value of WCN was computed from PWV (measured by foot-to-foot method), HR, and L_{eff}. A quarter wavelength relationship with minimum impedance modulus were used to compute L_{eff}. WCN_{Pinf} was calculated using HR and the reflected wave arrival time. Previously published analyses from a healthy subset of the Anglo-Cardiff Collaborative Trial (ACCT) study population were used to investigate if non-invasive WCN_{Pinf} captures age related differences in arterial wave reflection among healthy women and men.

Results: A strong correlation (r = 0.83, p-value <0.0001) between WCN_{Pinf} and WCN was observed. The accuracy of WCN_{Pinf} was independent from relevant physiological parameters such as PWV, pulse pressure (PP), and HR. Similar changes in WCN_{Pinf}

with advancing age were observed in both healthy men and healthy women. In young, healthy individuals (women and men) the WCN_{Pinf} was around 0.1 (the optimum value), and reduced with aging.

Conclusion: WCN can be approximated from a single pressure waveform and can capture age related arterial wave reflection alteration. These results are clinically significant since WCN can be extracted from a single non-invasive pressure waveform. Future studies will focus on investigating if WCN is associated with risk for onset of cardiovascular disease events.

Keywords: wave condition number, arterial wave reflection, optimum cardiovascular function, cardiovascular biomarker, vascular aging

INTRODUCTION

The cardiovascular system in mammals is based on various optimization criteria (Attinger, 1964; Knight and Wolstenholme, 1971; Milnor, 1979; O'Rourke et al., 1984; Milnor, 1989; Elzinga and Westerhof, 1991). Previous studies have shown that the cardiac dynamics and vasculature characteristics of mammals follow certain allometric laws (Adolph, 1949; Holt et al., 1981; Li and Noordergraaf, 1991; Westerhof and Elzinga, 1991; Li, 1995). Several cardiovascular characteristics are invariant regardless of mammalian size. These size invariant characteristics include mean blood velocity in the ascending aorta (Holt et al., 1981), the product of the heart rate (HR) and the arterial decay time (Westerhof and Elzinga, 1991), the normalized input impedance (Westerhof and Elzinga, 1991), the pulse wave velocity (PWV) (Milnor, 1979, 1989), the reflection coefficient (Li and Noordergraaf, 1991), the product of the propagation constant and the aortic length (Li and Noordergraaf, 1991), and the recently proposed wave condition number (WCN) (Pahlevan and Gharib, 2014).

Pahlevan and Gharib demonstrated the existence of a non-dimensional number, known as the WCN, that determines the optimum arterial wave state in which the left ventricular (LV) workload is minimized in mammalian cardiovascular systems (Pahlevan and Gharib, 2014). Using a series of *in vitro* hemodynamic studies, published hemodynamics data on various mammalian species, and allometry analysis, they have shown that a value of WCN = 0.1 indicates the optimum state of arterial wave reflection in the mammalian systemic circulation. Furthermore, their analysis confirms that this optimum value of the WCN remains constant (0.1) at various levels of aortic stiffness, and is universal among all mammals regardless of size (Pahlevan and Gharib, 2014). Yigit and Pekkan analytically derived a set of non-dimensional parameters using the Buckingham Pi theorem that characterizes pulsatile hemodynamics and its energetic cost (Yigit and Pekkan, 2016). Their work also provided a theoretical background for WCN, as they concluded that WCN can be obtained by combining two of the non-dimensional numbers introduced by them(Yigit and Pekkan, 2016).

It is well-known that various cardiovascular diseases (CVDs) alter arterial wave reflections (Safar and O'Rourke, 2006; Nichols et al., 2011; Salvi, 2012). Therefore, it is possible that WCN has prognostic or predictive value for one or more CVDs. Both pressure and flow waves are required to compute WCN exactly (Pahlevan and Gharib, 2014), which may limit the clinical utility of WCN. Therefore, the primary objective of this manuscript is to demonstrate that WCN can be approximated from a single pressure waveform. Pressure waveforms are easily and non-invasively measured using arterial applanation tonometry, an optical smartphone-based handheld device (Armenian et al., 2018; Miller et al., 2020), or even a smartphone by itself (Pahlevan et al., 2017). Therefore, approximating WCN from a single pressure waveform significantly improves its clinical utility. Previously published retrospective data from Murgo et al. (1980) were used to achieve this objective. The second aim of this study is to provide the proof-of-concept that WCN computed from a single non-invasive pressure waveform can capture age related differences in arterial wave reflections among healthy individuals. Previously published average data from McEniery et al. (2005) was used to investigate the second aim.

THEORY AND METHODS

Wave Condition Number Theory

In any discipline of physics, wave dynamics in a medium are dominated by three factors: (1) material properties of the medium that define the wave speed, (2) fundamental frequencies of the waves, and (3) interfaces that create wave reflections. Although other wave characteristics such as dispersion or dissipation also contribute to overall wave dynamics, their effects are not dominant in general. Similarly, wave dynamics in the aorta and the arterial system are primarily controlled by (1) pulse wave velocity (PWV; the wave speed), (2) heart rate (HR; the fundamental frequency), and (3) reflection sites. The WCN number combines all reflection sites existent in various forms within the vascular network (e.g., bifurcation, tapering, impedance mismatch, etc.), and considers a hypothetical total reflection site from which the summated reflected waves appear to be reflected. Pahlevan and Gharib (Pahlevan and Gharib, 2014) used these principles and applied a classical dimensional analysis to derive a dimensionless number, called the WCN, as a function of PWV, HR and the distance between the heart and the

hypothetical total reflection site. The WCN concept is a systemic view of examining wave reflections, and *does not imply* that the aorta and its complex wave dynamics can be modeled as a straight tube with a single reflection site at the end.

Wave Condition Number From Impedance Spectrum (WCN_{PQ})

Wave condition number is calculated from effective length (L_{eff}), PWV, and HR using the equation (Pahlevan and Gharib, 2014):

$$WCN = \frac{HR.L_{eff}}{PWV}. \tag{1}$$

Here, L_{eff} is the distance between the heart and a hypothetical reflecting site from which the summated reflected waves appear to return. The WCN computed from Eq. 1 is referred to as WCN_{PQ} throughout this manuscript.

Effective length is computed using pressure and flow waves by applying the quarter wavelength relationship (Milnor, 1989):

$$L_{eff} = \frac{c}{4f_{Zmin}} \tag{2}$$

Here c is the speed of pressure or flow waves (same as the PWV) and f_{Zmin} is the lowest frequency among all frequencies in which the amplitude of the impedance modulus is minimum. Mathematically speaking:

$$f_{Zmin} = Minimum\ \left[f_i\right] \quad (i = 1, 2, \ldots), \tag{3}$$

Where f_i is defined as:

$$\left.\frac{d\,|Z|}{df}\right|_{f=f_i} = 0\ \&\ \left.\frac{d^2\,|Z|}{df^2}\right|_{f=f_i} > 0. \tag{4}$$

Here $|Z|$ is the amplitude of the impedance in the frequency domain, and is computed from pressure and flow harmonics as:

$$|Z| = \frac{|P_n(\omega)|}{|Q_n(\omega)|}, \tag{5}$$

where:

$$P(t) = P_0 + \sum_{n=1}^{m} |P_n(\omega)|\, e^{i(n\omega_o t - \varphi_n)}, \tag{6}$$

$$Q(t) = Q_0 + \sum_{n=1}^{m} |Q_n(\omega)|\, e^{i(n\omega_o t - \psi_n)}. \tag{7}$$

Here, $i = \sqrt{-1}$, $\omega = 2\pi f$, and P_0, Q_0 are the average of pressure and flow over the cardiac cycle, respectively.

Wave Condition Number From a Single Pressure Waveform (WCN_{Pinf})

The time of the inflection point in the pressure waveform has been recognized as an approximation for the reflected wave arrival time (t_{arr}) (Nichols et al., 2011). Assuming a hypothetical single reflection site, and assuming that the average speed of forward waves and reflected waves throughout the arterial system is the same, t_{arr} will be twice the wave travel time from the heart to this hypothetical single reflection site. Assuming that PWV is time independent throughout the cardiac cycle, t_{arr} is related to L_{eff} and PWV using the equation below:

$$\left(1/2\right)\ t_{arr} = \frac{L_{eff}}{PWV}. \tag{8}$$

Substituting Eq. 8 into Eq. 1 gives:

$$WCN_{Pinf} = \left(1/2\right)\ t_{arr} \cdot HR. \tag{9}$$

In Eq. 9, HR is expressed in beats-per-second. **Figure 1** shows the overall schematic of the computation of WCN_{PQ} and WCN_{Pinf}.

Population Characteristics and Hemodynamics Measurements

Previously published retrospective data from Murgo et al. (1980) was used to assess the accuracy of the single pressure waveform evaluation of WCN_{Pinf} with respect to WCN computed from Eq. 1 by using the pressure and flow waves and the quarter-wavelength relationship (Eqs 2–7). Data from McEniery et al. (2005) were used to investigate the relationship between non-invasive WCN_{Pinf} and aging among healthy individuals.

Methods for Invasive Evaluation of WCN_{PQ} and WCN_{Pinf}

The database published by Murgo et al. (1980) was used in this study. This database is composed of eighteen patients who underwent right and left heart catheterization for different clinical indications (Murgo et al., 1980). The age range of this cohort was 19–54 years (34.3 ± 9.6). Chest pain was the most common clinical condition in this population. Pressure measurements in the aorta were performed using solid-state pressure sensors (Millar Mikro-Tip, Millar Instruments, Houston, Texas). Electromagnetic flow velocity probes (Carolina Medical Electronics, King, North Carolina 1973–1975; Millar Instruments 1975–1979) were used for flow measurements. PWVs were computed using the foot-to-foot method. The PWV value (needed for the WCN calculation) was not available for one patient, so the database in this manuscript includes the other 17 patients. Further details about hemodynamics measurements and analyses can be found in Murgo et al. (1980).

In seven patients, the inflection point of the pressure waveform occurred before the peak systolic pressure with an augmentation index (AIx) greater than 12% [the so-called type A waveform (Salvi, 2012)]. In seven patients, systolic pressure happened in the late systolic phase following an inflection point with $0 < \text{AIx} < 12\%$ [the so-called type B waveform (Salvi, 2012)]. Inflection points occurred after the peak systole in three patients [the so-called Type C waveform (Salvi, 2012)].

Methods for Non-Invasive WCN_{Pinf} and Its Relationship With Age

Reported analyses from McEniery et al. (2005) were used to evaluate non-invasive WCN_{Pinf} and investigate its relationship with age in both males and females among healthy populations.

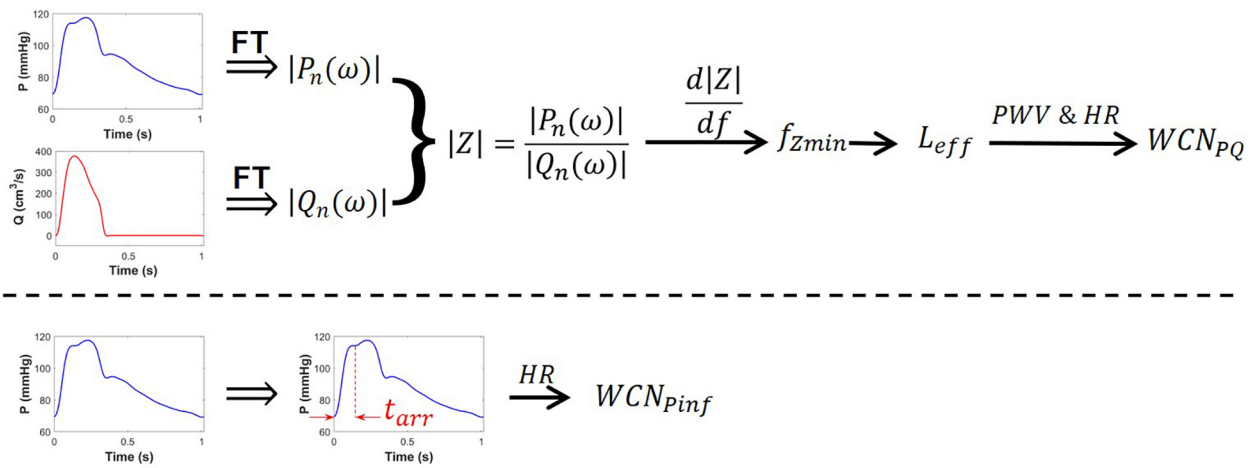

FIGURE 1 | Schematic of the computation of WCN_{PQ}(top row) and WCN_{Pinf} (bottom row). The pressure wave (blue), the flow wave (red), and PWV are each required to compute WCN_{PQ}. Only the pressure waveform (blue) is needed to compute WCN_{Pinf}. FT is the Fourier transform.

The data was a subset of the Anglo-Cardiff Collaborative Trial (ACCT) study population (McEniery et al., 2005). Any individual with clinical history of CVD, evidence of CVD on examination, systolic blood pressure (SBP) ≥140 mmHg and diastolic blood pressure (DBP) ≥90 mmHg, serum cholesterol ≥6.5 mmol/l, renal disease [see (McEniery et al., 2005) for details], and diabetes mellitus were excluded from the healthy subset database. The healthy subset included 4,001 individuals with ages ranging from 18 to 90 years. Aortic pressure waveforms were generated using a validated generalized transfer function (Karamanoglu et al., 1993) applied to radial waveforms measured by a tonometry device (SphygmoCor, AtCor Medical, Sydney, Australia). These synthesized aortic waveforms were then used to identify the inflection point and compute t_{arr}.

Analysis Method

Bland-Altman analysis (Bland and Altman, 1986) was used to quantify the agreement between WCN_{PQ} and WCN_{Pinf}. The dependency of the error of WCN_{Pinf} (defined as the difference between WCN_{PQ} and WCN_{Pinf}) on relevant physiological parameters such as PWV, pulse pressure (PP), and HR was investigated.

The standard deviations (SD) of the non-invasive WCN_{Pinf} were approximated from the reported SDs of t_{arr} and reported SD of the HR and their mean values for each age bracket range assuming that t_{arr} and HR are independent from each other (Ku, 1966).

RESULTS

Accuracy of Single Waveform Evaluation of Wave Condition Number (WCN_{Pinf})

The hemodynamics and the demographics of the study population are shown in **Table 1**. As illustrated in **Figure 2**, there is a strong correlation (r = 0.83, p-value <0.0001) between WCN_{Pinf} (WCN computed from the reflected wave arrival time using Eq. 8) and WCN_{PQ} calculated from Eq. 1 and, using the effective length computed from Eq. 2.

Figure 3 demonstrates that the WCN_{Pinf} error is independent from relevant physiological parameters such as PWV, PP, and HR. There was no significant correlation between WCN_{Pinf} error and PWV, PP, and HR with p-values of 0.76, 0.16, and 0.70, respectively.

Non-invasive WCN_{Pinf} and Aging in Healthy Population

The overall declining relationship between WCN_{Pinf} and age among healthy populations for both males (**Figure 4A**) and females (**Figure 4B**) is demonstrated in **Figure 4**. The x-components of data points are set to the mid-points but cover the full decade (e.g., x = 35 indicates 30–40 years). The dashed bars are the standard deviation lines.

DISCUSSION

The results of this study indicate that WCN can be approximated from a single pressure waveform measurement. The results also provide a proof-of-concept that non-invasive single waveform WCN (referred to as WCN_{Pinf} in this manuscript) can capture age related differences in arterial wave reflection in a healthy population. The results also demonstrate that WCN_{Pinf} is approximately 0.1 [the optimum value found by the previous study of Pahlevan and Gharib (2014) for young healthy individuals], and deviates from the optimum value with aging (a reduction from 0.1).

Our results show a strong correlation between WCN_{PQ} and WCN_{Pinf} (r = 0.83, **Figure 2A**). However, there was an offset of 0.009 (9%) between WCN_{PQ} and WCN_{Pinf} as illustrated in the Bland-Altman graph of **Figure 2B**. Prognostic values of WCN and its approximation (WCN_{Pinf}) will be determined in future

TABLE 1 | Study population demographics and hemodynamics.

	Median	Interquartile range	Number or mean value (range)	Standard deviation
Age (years)	33	10.25	34.3 (19–54)	9.6
Gender (M/F)	NA	NA	15/2	NA
AoDBP (mmHg)	74	11.75	77 (64–94)	8.4
AoSBP (mmHg)	111	16.25	116.2 (100–146)	11.5
PWV (m/s)	6.59	1.525	6.7 (4.6–9.5)	1.3
HR (bpm)	71	16.25	75.6 (59–110)	13.9
PP (mmHg)	37	9	39.2 (27–73)	11.6

AoDBP is the aortic diastolic blood pressure, AoSBP is the aortic systolic blood pressure, PWV is the aortic pulse wave velocity, HR is the heart rate, and PP is the aortic pulse pressure.

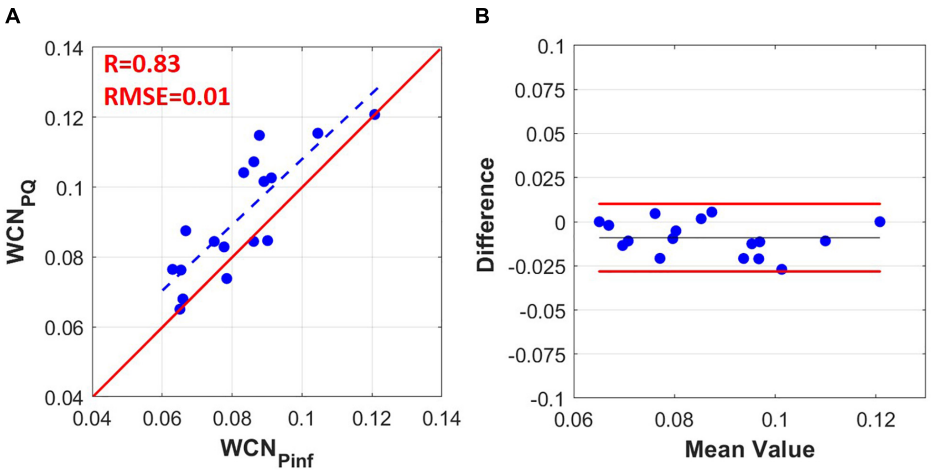

FIGURE 2 | (A) WCN_{Pinf} computed from the t_{arr} (time of the inflection point) using Eq. (9) versus WCN_{PQ} computed from PQ using Eqs (1–7) (r = 0.83, RMSE = 0.01). **(B)** Bland-Altman graph comparing WCN_{Pinf} to WCN_{PQ}. The limit of agreement lines are at +0.010 and –0.028 (–0.009 bias with ± 0.019 limits).

clinical studies. On the other hand, the error of WCN_{Pinf} did not show statistically significant dependency on hemodynamic parameters related to WCN and overall wave reflection such as PWV, PP, and HR.

Similar changes in WCN with advancing age were observed in both healthy men and healthy women. In young healthy individuals (men and women) the WCN was around 0.1 [the optimum value according to (Pahlevan and Gharib, 2014)], and this reduced with aging as the arterial wave reflections became suboptimal due to vascular aging.

According to the results of **Figure 4**, the WCN_{Pinf} moderately reduces in an aged population. However, the actual decline in the value of WCN among an elderly population is probably more significant since the true value of t_{arr} in the elderly is over-estimated by the usage of the time of the inflection point. A recent study by Phan et al. (2016), demonstrates that a t_{arr} computed from the time of the inflection point over-estimates the true value of a t_{arr} computed from a pressure-flow analysis. Although WCN_{Pinf} underestimates the impact of aging on WCN, it reveals the overall trends of aging on WCN among healthy populations. Perhaps WCN computed from other single waveform decomposition methods (Westerhof et al., 2006; Hametner et al., 2013) can provide more accurate single waveform approximations of WCN among healthy aged populations.

Segers et al. (2007) have reported t_{arr} calculated from the inflection point method and the PQ method (using non-invasive aortic flow and carotid pressure waveforms), in a large middle-aged population (35–56 years old; Asklepios study (Rietzschel et al., 2007) which include 1093 women and 1039 men). Values of WCN_{Pinf} computed based on the average values of the reported t_{arr} and HR (in five-year age intervals reported by Segers et al.) indicate a decrease with age over two decades (35–56 years old) from 0.090 to 0.081 in men and from 0.081 to 0.73 in women. This behavior agree with the results presented in **Figure 4**. In the latter, the average WCN_{Pinf} values and their variations with age are similar in both men and women; however, the average values of WCN_{Pinf} computed from the data reported by Segers et al. (2007) are 10% lower in women than in men (0.090 vs 0.081). Furthermore, Baksi et al. (2009) have performed a meta-analysis (64 studies including 13,770 participants with an age range of 4–91 years) to investigate the effect of wave reflections on blood pressure changes that occur with aging. They report a modest but statistically significant ($r = -0.57$, $p < 0.0001$) drop in t_{arr} with aging. Based on the results reported in **Figure 4** of Baksi et al. (2009), t_{arr} drops from 152 to 120 over 6 decades (20 to

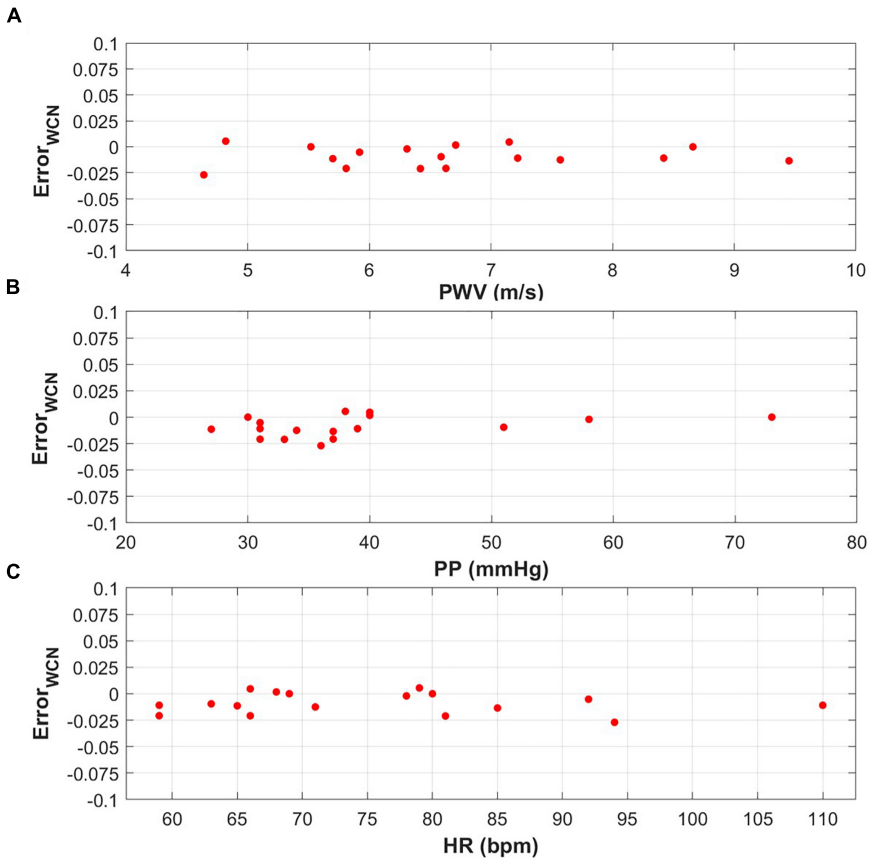

FIGURE 3 | (A) WCN_{Pinf} error versus a PWV range of 4.64–9.45 m/s (p-value = 0.76). **(B)** WCN_{Pinf} error versus a PP range of 27–73 mmHg (p-value = 0.16). **(C)** WCN_{Pinf} error versus a HR range od 59–110 bpm (p-value = 0.70).

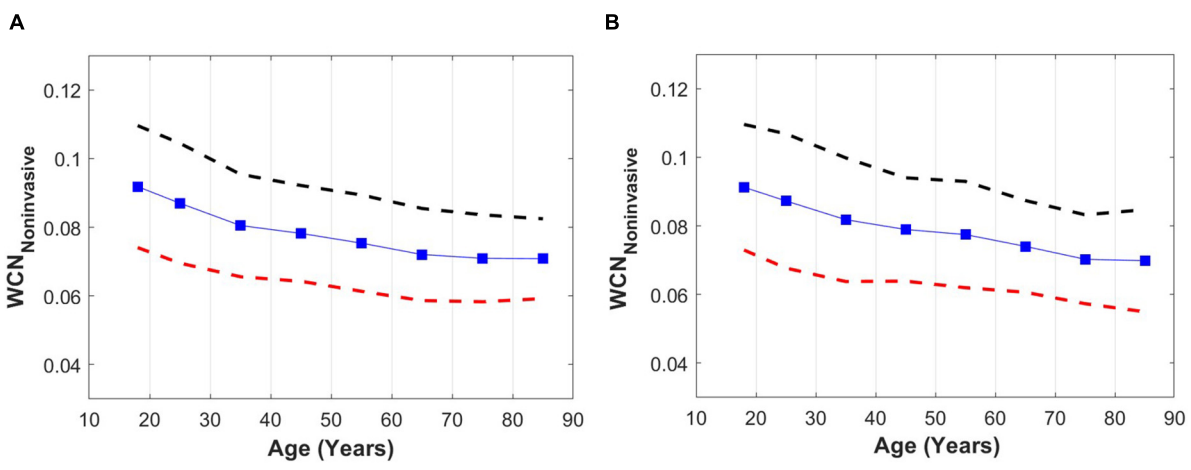

FIGURE 4 | (A) WCN_{Pinf} versus age among a healthy male population. **(B)** WCN_{Pinf} versus age among a healthy female population. Dashed lines are upper (black) and lower (red) standard deviation lines. For better visualization, the x-components of data points are set to the mid-points but include the full decade (e.g., x = 35 indicates 30–40 years).

80). Unfortunately, values of HR have not been reported by the authors. Using average HR values for healthy population reported by McEniery et al. (2005), we have computed the corresponding average WCN_{Pinf} for the reported data from Baksi et al. (2009): our analysis shows that WCN_{Pinf} based on this data drops from 0.92 (20 years old) to 0.62 (80 years old) over six decades.

These values are well within the results reported in **Figure 4** of this article.

Previous results from a physiologically relevant *in vitro* LV-arterial simulator (Pahlevan and Gharib, 2014) suggest that deviations from a value of WCN = 0.1 increase pulsatile workload on the LV. This workload elevation is more significant at higher arterial stiffnesses (e.g., those occurring with aging). Therefore, a reduction of WCN from 0.1 to 0.07 in a healthy individual may indicate an elevation of the LV pulsatile workload due to suboptimal wave reflections. Future clinical studies are needed to verify if indeed a deviation of WCN away from the optimal 0.1 does in fact increases LV pulsatile workload in a human.

As demonstrated by Westerhof and Westerhof (2018), the uniform tube models inaccurately interpret pressure waveforms and aortic wave travel. However, it must be noted that the WCN concept does not imply in any way that the arterial system is a single tube (as the input impedance is not the same as the actual impedance), and it should not be viewed as an oversimplification. WCN should be considered as a dimensionless number for overall characterization or classification of a wave reflection system. It is comparable to the Reynolds number (Re) in fluid dynamics, which is used for classifications of fluid flow and whose usage is never considered as an oversimplification of boundary layer theory or the Navier-Stokes equations.

Future analyses will focus on investigating if WCN is associated with risk for the onset of cardiovascular disease (CVD) events in large longitudinal cohorts. Such studies will reveal if WCN is a useful addition to standard risk assessment for one or more types of CVDs. Further research can also be focused on the pulmonary vasculature in order to evaluate optimum WCN for the minimization of the workload on the right ventricle (RV). The overall length of pulmonary networks is shorter than the overall length of systemic networks, and the nature of wave reflections at the end of pulmonary vasculature is different than the systemic vasculature (Hollander et al., 2001). These two effects may result in a shorter L_{eff}. The combining effects of a shorter L_{eff} and a lower PWV in the pulmonary artery circulation may produce the same value of optimum WCN (= 0.1) for pulmonary circulation. Although workload on the RV is much lower on than the LV, quantifying the optimum wave reflection can be helpful in patients with right heart failure or patients with pulmonary hypertension (Laskey et al., 1993).

LIMITATIONS

One major limitation of this study is that the database for assessment of the accuracy of WCN_{Pinf} did not include any patients older than 54 years. Future studies are needed to verify if the WCN_{Pinf} error remains within the same range indicated in this study. Another limitation related to the WCN_{Pinf} error is that the left ventricle (LV) ejection fraction (LVEF) values of the patients were not available. LVEF is one of the most relevant cardiovascular parameters that may affect the accuracy of WCN_{Pinf}. It is noteworthy that there are uncertainties in the assessment of WCN since the absolute accuracy of a WCN assessment depends on the flow and pressure measurement errors, the synchronization between pressure and flow measurements, as well as the sampling frequency of the measurements.

CONCLUSION

WCN can be approximated from a single pressure waveform, independently from related hemodynamics indices such as PP, PWV, and HR. This study provides a proof-of-concept that non-invasive single-waveform WCN can capture age-related alterations of arterial wave reflections in a large healthy cohort. However, these changes in WCN with age are not as substantial in healthy populations, possibly limiting its usefulness for healthier individuals. These results are clinically significant since WCN can be extracted from a single non-invasive pressure waveform that is easily acquired using arterial applanation tonometry, a smartphone-based handheld device (Armenian et al., 2018; Miller et al., 2020), or an unmodified iPhone (Pahlevan et al., 2017).

DATA AVAILABILITY STATEMENT

The data used in this study for the analysis is uploaded as **Supplementary Material**.

ETHICS STATEMENT

This study uses retrospective previously published data.

AUTHOR CONTRIBUTIONS

NP contributed to the conceptualization, the analysis, the writing of the original draft, the revision, and the editing. SM contributed to the statistical analysis, the revision, the discussion, and the editing.

ACKNOWLEDGMENTS

The authors would like to thank Faisal Amlani (University of Southern California) for their scientific input.

SUPPLEMENTARY MATERIAL

The Supplementary Material for this article can be found online at: https://www.frontiersin.org/articles/10.3389/fphys.2020.00313/full#supplementary-material

REFERENCES

Adolph, E. F. (1949). Quantitative relations in the physiological constitutions of mammals. *Science* 109, 579–585. doi: 10.1126/science.109.2841.579

Armenian, S. H., Rinderknecht, D., Au, K., Lindenfeld, L., Mills, G., Siyahian, A., et al. (2018). Accuracy of a novel handheld wireless platform for detection of cardiac dysfunction in anthracycline-exposed survivors of childhood cancer. *Clin. Cancer Res.* 24, 3119–3125. doi: 10.1158/1078-0432.ccr-17-3599

Attinger, E. O. (ed.) (1964). *Pulsatile Blood Flow*. New York, NY: McGraw-Hill.

Baksi, A. J., Treibel, T. A., Davies, J. E., Hadjiloizou, N., Foale, R. A., Parker, K. H., et al. (2009). A meta-analysis of the mechanism of blood pressure change with aging. *J. Am. Coll. Cardiol.* 54, 2087–2092. doi: 10.1016/j.jacc.2009.06.049

Bland, J. M., and Altman, D. (1986). Statistical methods for assessing agreement between two methods of clinical measurement. *Lancet* 327, 307–310. doi: 10.1016/s0140-6736(86)90837-8

Elzinga, G., and Westerhof, N. (1991). Matching between ventricle and arterial load. An evolutionary process. *Circ. Res.* 68, 1495–1500. doi: 10.1161/01.res.68.6.1495

Hametner, B., Wassertheurer, S., Kropf, J., Mayer, C., Holzinger, A., Eber, B., et al. (2013). Wave reflection quantification based on pressure waveforms alone—Methods, comparison, and clinical covariates. *Comput. Methods Programs Biomed.* 109, 250–259. doi: 10.1016/j.cmpb.2012.10.005

Hollander, E. H., Wang, J.-J., Dobson, G. M., Parker, K. H., and Tyberg, J. V. (2001). Negative wave reflections in pulmonary arteries. *Am. J. Physiol. Heart Circ. Physiol.* 281, H895–H902.

Holt, J. P., Rhode, E. A., Holt, W. W., and Kines, H. (1981). Geometric similarity of aorta, venae cavae, and certain of their branches in mammals. *Am. J. Physiol. Regul. Integr. Comp. Physiol.* 241, R100–R104.

Karamanoglu, M., O'rourke, M. F., Avolio, A. P., and Kelly, R. P. (1993). An analysis of the relationship between central aortic and peripheral upper limb pressure waves in man. *Eur. Heart J.* 14, 160–167. doi: 10.1093/eurheartj/14.2.160

Knight, G. E. W., and Wolstenholme, J. (1971). Circulatory and respiratory mass transport. *Ciba Found.* 45:416.

Ku, H. H. (1966). Notes on the use of propagation of error formulas. *J. Res. Natl. Bureau Standards* 70:263. doi: 10.6028/jres.070c.025

Laskey, W. K., Ferrari, V. A., Palevsky, H. I., and Kussmaul, W. G. (1993). Pulmonary artery hemodynamics in primary pulmonary hypertension. *J. Am. Coll. Cardiol.* 21, 406–412.

Li, J. K., and Noordergraaf, A. (1991). Similar pressure pulse propagation and reflection characteristics in aortas of mammals. *Am. J. Physiol. Regul. Integr. Comp. Physiol.* 261, R519–R521.

Li, J. K.-J. (1995). *Comparative Cardiovascular Dynamics of Mammals*. Boca Raton, FL: CRC Press.

McEniery, C. M., Yasmin, Hall, I. R., Qasem, A., Wilkinson, I. B., and Cockcroft, J. R. (2005). Normal vascular aging: differential effects on wave reflection and aortic pulse wave velocitythe anglo-cardiff collaborative trial (ACCT). *J. Am Coll. Cardiol.* 46, 1753–1760. doi: 10.1016/j.jacc.2005.07.037

Miller, J. C., Shepherd, J., Rinderknecht, D., Cheng, A. L., and Pahlevan, N. M. (2020). Proof-of-concept for a non-invasive, portable, and wireless device for cardiovascular monitoring in pediatric patients. *PloS One* 15:e0227145. doi: 10.1371/journal.pone.0227145

Milnor, W. R. (1979). Aortic wavelength as a determinant of the relation between heart rate and body size in mammals. *Am. J. Physiol. Regul. Integr. Comp. Physiol.* 237, R3–R6.

Milnor, W. R. (1989). *Haemodynamics*. Baltimore, MD: Williams & Wilkins Co.

Murgo, J., Westerhof, N., Giolma, J., and Altobelli, S. (1980). Aortic input impedance in normal man: relationship to pressure wave forms. *Circulation* 62, 105–116. doi: 10.1161/01.cir.62.1.105

Nichols, W., O'rourke, M., and Vlachopoulos, C. (2011). *McDonald's Blood Flow in Arteries: Theoretical, Experimental and Clinical Principles*. Boca Raton, FL: CRC Press.

O'Rourke, M., Yaginuma, T., and Avolio, A. (1984). Physiological and pathophysiological implications of ventricular/vascular coupling. *Ann. Biomed. Eng.* 12, 119–134. doi: 10.1007/bf02584226

Pahlevan, N. M., and Gharib, M. (2014). A wave dynamics criterion for optimization of mammalian cardiovascular system. *J. Biomech.* 47, 1727–1732. doi: 10.1016/j.jbiomech.2014.02.014

Pahlevan, N. M., Rinderknecht, D. G., Tavallali, P., Razavi, M., Tran, T. T., Fong, M. W., et al. (2017). Noninvasive iphone measurement of left ventricular ejection fraction using intrinsic frequency methodology. *Crit. Care Med.* 45, 1115–1120. doi: 10.1097/ccm.0000000000002459

Phan, T. S., Li, J. K. J., Segers, P., Reddy-Koppula, M., Akers, S. R., Kuna, S. T., et al. (2016). Aging is associated with an earlier arrival of reflected waves without a distal shift in reflection sites. *J. Am. Heart Assoc.* 5:e003733.

Rietzschel, E.-R., De Buyzere, M. L., Bekaert, S., Segers, P., De Bacquer, D., Cooman, L., et al. (2007). Rationale, design, methods and baseline characteristics of the Asklepios Study. *Eur. J. Cardiovasc. Prev. Rehabil.* 14, 179–191. doi: 10.1097/hjr.0b013e328012c380

Safar, M., and O'Rourke, M. F. (2006). *Arterial Stiffness in Hypertension*. Amsterdam: Elsevier Health Sciences, 23.

Salvi, P. (2012). *Pulse Waves: How Vascular Hemodynamics Affects Blood Pressure*. Berlin: Springer.

Segers, P., Rietzschel, E. R., Buyzere, M. L. D., Bacquer, D. D., Bortel, L. M. V., Backer, G. D., et al. (2007). Assessment of pressure wave reflection: getting the timing right! *Physiol. Meas.* 28:1045. doi: 10.1088/0967-3334/28/9/006

Westerhof, B. E., Guelen, I., Westerhof, N., Karemaker, J. M., and Avolio, A. (2006). Quantification of wave reflection in the human aorta from pressure alone: a proof of principle. *Hypertension* 48, 595–601. doi: 10.1161/01.hyp.0000238330.08894.17

Westerhof, B. E., and Westerhof, N. (2018). Uniform tube models with single reflection site do not explain aortic wave travel and pressure wave shape. *Physiol. Meas.* 39:124006. doi: 10.1088/1361-6579/aaf3dd

Westerhof, N., and Elzinga, G. (1991). Normalized input impedance and arterial decay time over heart period are independent of animal size. *Am. J. Physiol. Regul. Integr. Comp. Physiol.* 261, R126–R133.

Yigit, B., and Pekkan, K. (2016). Non-dimensional physics of pulsatile cardiovascular networks and energy efficiency. *J. R. Soc. Interface* 13:20151019. doi: 10.1098/rsif.2015.1019

Conflict of Interest: The authors declare that the research was conducted in the absence of any commercial or financial relationships that could be construed as a potential conflict of interest.

frontiers in Pediatrics

ORIGINAL RESEARCH
published: 19 May 2020
doi: 10.3389/fped.2020.00251

Pressure and Flow Relations in the Systemic Arterial Tree Throughout Development From Newborn to Adult

Berend E. Westerhof[1,2,3]*, *Martin J. C. van Gemert*[4] *and Jeroen P. van den Wijngaard*[5]

[1] *Cardiovascular and Respiratory Physiology, Technical Medical Centre, Faculty of Science and Technology, University of Twente, Enschede, Netherlands,* [2] *Pulmonary Medicine, Amsterdam Cardiovascular Sciences, Amsterdam UMC, Free Universiteit Amsterdam, Amsterdam, Netherlands,* [3] *Medical Biology, Section of Systems Physiology, Amsterdam Cardiovascular Sciences, Amsterdam UMC, University of Amsterdam, Amsterdam, Netherlands,* [4] *Biomedical Engineering and Physics, Amsterdam UMC, University of Amsterdam, Amsterdam, Netherlands,* [5] *Clinical Chemistry Hematology and Immunology, Diakonessenhuis Utrecht, Utrecht, Netherlands*

Objective: Distributed models of the arterial tree allow studying the effect of physiological and pathophysiological changes in the vasculature on hemodynamics. For the adult, several models exist; however, a model encompassing the full age range from newborn to adult was until now lacking. Our goal is to describe a complete distributed hemodynamic model for normal development from newborn to adult.

Methods: The arterial system was modeled by 121 segments characterized by length, radius, wall thickness, wall stiffness, and wall viscosity. The final segments ended in three-element Windkessels. All parameters were adapted based on body height and weight as a function of age as described in the literature.

Results: Pressures and flows are calculated as a function of age at sites along the arterial tree. Central to peripheral transfer functions are given. Our results indicate that peripheral pressure in younger children resembles central pressure. Furthermore, total arterial compliance, inertance and impedance are calculated. Findings indicate that the arterial tree can be simulated by using a three-element Windkessel system. Pulse wave velocity in the aorta was found to increase during development.

Conclusions: The arterial system, modeled from newborn to adult bears clinical significance, both for the interpretation of peripheral measured pressure in younger and older children, and for using a Windkessel model to determine flow from pressure measurements.

Keywords: distributed arterial model, newborn to adult, aortic, peripheral, blood pressure, flow, windkessel

OPEN ACCESS

Edited by:
Adelaide De Vecchi,
King's College London,
United Kingdom

Reviewed by:
John Frank LaDisa,
Marquette University, United States
Bernhard Hametner,
Austrian Institute of Technology (AIT), Austria

***Correspondence:**
Berend E. Westerhof
b.e.westerhof@utwente.nl

Specialty section:
This article was submitted to Pediatric Cardiology, a section of the journal Frontiers in Pediatrics

Received: *07 January 2020*
Accepted: *22 April 2020*
Published: *19 May 2020*

Citation:
Westerhof BE, van Gemert MJC and van den Wijngaard JP (2020) Pressure and Flow Relations in the Systemic Arterial Tree Throughout Development From Newborn to Adult. Front. Pediatr. 8:251. doi: 10.3389/fped.2020.00251

INTRODUCTION

Arterial models help in understanding of hemodynamics and allow simulated experimental interventions that may not be easily performed in the human (1). To date, full-scale distributed models describe the adult circulation (2–7); an overview is given by Reymond et al. (8). Descriptions of fetal (9, 10), neonatal (11), and infant (12) circulations do exist, however, usually with simplified arterial networks. Nevertheless, these models demonstrated clinical relevance.

Our general aim was to develop a full-scale distributed model of the systemic arterial tree, consisting of realistic segments derived from physiological measurements, throughout development from newborn to adult. To describe all model parameters as a function of age, growth charts were used. We investigated pressure-flow relations in the model, with as a first aim to determine the central to peripheral pressure transfer functions (describing the changes in the pressure wave shape that occur while the wave travels in the arterial system). The second aim was to derive and determine the applicability of Windkessel models, based on characteristic impedance and the lumped parameters, as found by network analysis, describing total arterial resistance, compliance, and inertance. The first aim provides understanding of the relation between peripheral measured pressure and central pressure. The second aim gives insight in the applicability of 3- or 4-element Windkessels for realistic modeling of the input impedance of systemic arterial tree (13). Combined, these aims may aid in calculating cardiac output from peripherally measured pressures.

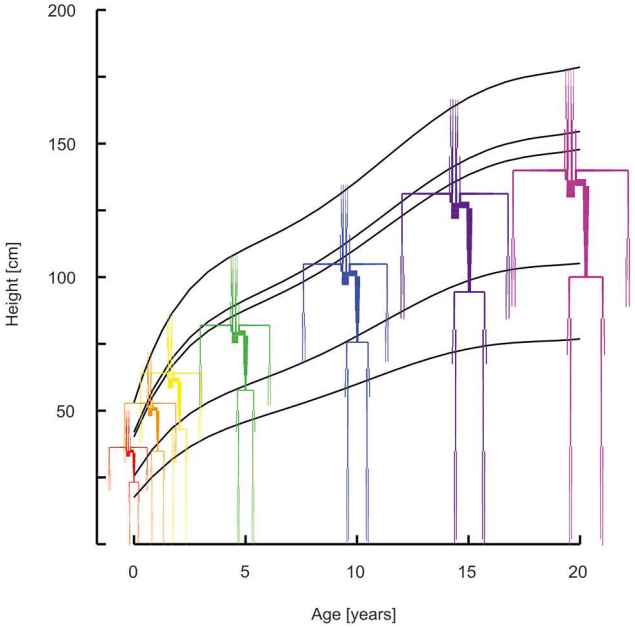

FIGURE 1 | Arterial segments with the lengths and diameters as a function of age (red 0 years, orange 1 year, yellow 2 years, green 5 years, blue 10 years, purple 15 years, violet 20 years). Curves describe the development of stature, of the head, the neck, the thorax, the abdomen, and the legs.

METHODS

The model of the arterial tree was developed using the description of Westerhof (2) with the inclusion of three element Windkessel impedances at the end of the final segments as given by Stergiopulos (4). In total, the Westerhof model incorporates 121 segments, of which length, radius, vascular wall thickness, wall stiffness and viscoelastic properties are given (2, 14).

To model the development of the arterial system, the following age dependent descriptions were assembled: height; proportional length and radius of body divisions (e.g., head, thorax, abdomen, legs); weight; and based on the previous, proportional volume of body divisions. These descriptions allow determining the dimensions of the arterial segments for any age. Once these dimensions are known, the pressure and flow transfer function of each segment can be calculated. Bringing all pressure and flow transfer functions together, the entire arterial system can be modeled. A flow wave with the correct stroke volume and heart rate for each age is used as input. Then pressure and flow can be calculated in each segment.

Thus, the current model is based on two main constituents: first, the original model by Westerhof et al. (2) (some parameter changes to the original model will be detailed); and second, descriptions of body development (which will also be given explicitly).

Normal Development From Newborn to Adult

The middle percentiles of the curves describing development as a function of age were used. Standard curves for stature as a function of age for boys were obtained from Freeman et al. (15). Curves for weight as a function of age were obtained from Wright et al. (16) (age 0–1 year) and Burmaster and Crouch (17) (age $>$ 1 year). Growth was modeled separately for 6 divisions of the body: i.e., the head, neck, thorax, abdomen, legs, and arms. See **Figure 1** for the age dependent development of stature and of the proportional development of body divisions. Using data on the relative dimensions of these body parts with respect to total body stature as a function of age, body divisions lengths and volumes were obtained (18). All body divisions were modeled by conical shapes, except for the head which was modeled by a sphere. Thus, all body divisions are essentially described by high order polynomials to yield dimensions as a function of age (**Supplemental Material**—Descriptions of body development).

Vascular Wall Properties

To correctly model growth of the arterial system, i.e., segment length, radius and wall thickness, the following was considered. In the newborn, average tissue metabolism and tissue perfusion (19) are higher when compared to the adult as demonstrated by the larger ratio of cardiac output and body weight for the newborn vs. the adult (20, 21). Since tissue perfusion decreases with age, mean resistance to flow is increased with age. This implies that mean flow through the conduit arteries is relatively enhanced at younger age. Shear stress on the intimal layer (endothelium) is proportional to flow increase and inversely proportional to radial increase to the third power (22). Wall shear stress measurements at various ages show a relatively small or even absent dependence on age (23). Therefore, vessel radii of younger individuals were corrected to achieve normalized shear stress. In the model, this was implemented as follows; an increase in tissue perfusion at young age was accompanied by an increase in the vascular radius to a 1/3rd power so that shear stress remained within the normal range. As an example, if the flow to a certain body division of the adult would be 50 mL/min to

1 Kg of tissue, perfusion can be quantified as 50 (mL/min)/Kg. If tissue perfusion is higher at a younger age, e.g., 60 (mL/min)/Kg, then the radii of the conduit arteries supplying blood to this tissue are increased by a factor $(60/50)^{(1/3)} = 1.06$. Thus, a 20 % higher perfusion is accompanied by a 6 % increase in radius.

To account for an increased mean arterial pressure with increased age (24), vascular wall thickness was assumed to increase proportionally. Increased vascular wall thickness is a normal physiological response to increased mean arterial pressure and thereby normalizes vascular wall stress (9, 23–27). Elastance (Young's modulus) was not changed as a function of age.

Transfer of Pressure and Flow

Transfer of pressure and flow over each segment is governed by transverse and longitudinal impedances. Transverse impedance is given by Jager et al. (28), longitudinal impedance is given by Womersley's theory of oscillatory flow for a longitudinally constrained tube (29). Both impedances can be obtained from vascular properties (22, 30). Computational details can be found elsewhere (1, 2, 31).

Starting from the distal impedances of the segment considered, pressure and flow transfer can be used to yield the impedance at the proximal site. Using standard circuit analysis for each frequency, multiple segments can be combined and finally resulting in the impedance of the entire arterial tree. Details on this approach can be found in the literature (1, 9, 10, 32, 33).

Changes to the Original Model

The following adaptations were made to the original description of the arterial segments and wall properties (2). Radii of proximal aortic segments were adapted to remove sudden decrease in radius (see **Supplemental Material**: Vascular dimensions and Windkessel parameters: FIGURE Vascular dimensions—changes in the aortic radii). With these changes, the radii are close to those reported by Hickson et al. (34) for 20 years old individuals. In addition, the resistances of the abdominal vascular beds and of the brain were increased to reduce flows to a normal physiological levels (35) (see **Supplemental Material**: Vascular dimensions and Windkessel parameters: **Table S1**—Windkessel peripheral resistance increase with respect to the original model). Elastance of the carotid arteries was given values of the central- as opposed to the peripheral arteries. The elastance of all arterial segments (factor 0.5) and total peripheral resistances of all loading Windkessels (factor 0.75) were reduced since the model would otherwise generate hypertensive pressures (195/102 mmHg brachial pressure) for a normal stroke volume and cardiac output.

The parameters of the arterial vasculature for ages of 0, 1, 2, 5, 10, 15, and 20 years can be found in the **Supplemental Material**—Vascular dimensions and Windkessel parameters.

Cardiac Output and Heart Rate

Cardiac output and heart rate were taken from Wiesener (21), where cardiac output was described to increase linearly from 564 mL/min at 0 to 5 L/min at 20 years and heart rate to decrease exponentially with weight to the power of −0.2 from 136 at 0 to 73 beats/min at 20 years (21, 22). The flow wave shape was chosen as a modified triangle, approaching a measured flow wave of which the maximum flow could be adapted to give the correct stroke volume. Ejection time was established as a function of heart rate (36, 37). The flow wave shape was used as input to the entire model, resulting in pressures and flows for each arterial segment.

Pulse Wave Velocity

For the aortic segments, the Moens-Korteweg pulse wave velocities were calculated (22). Carotid to femoral pulse wave velocity was calculated from the difference in arrival time of the pressure waves in the carotid and femoral artery and the distance between the two. Distance was determined by adding the lengths of the arterial segments from the aorta to the carotid artery and from aorta to femoral artery.

Windkessel Compliance and Resistance

Windkessel compliances are assumed to increase proportional to the volume of the body division they are in (18). Conversely, Windkessel resistance was taken inversely proportional to volume (22). In addition, Windkessel resistance was corrected to reflect perfusion decrease with age, as described in the vascular wall properties paragraph. The Windkessel parameters of the arterial vasculature for ages of 0, 1, 2, 5, 10, 15, and 20 years are listed in the **Supplemental Material**—Vascular dimensions and Windkessel parameters.

RESULTS

In **Figure 1** the arterial segments are displayed with their lengths and diameters as a function of age. The pressure and flow waves are shown in **Figure 2** for aorta, carotid, brachial, radial, femoral and tibial arteries. The pressure wave shapes are comparable for the age range between 0 and 5 years. Around the age of 10 the shapes start to change progressively. The ratio of brachial pulse pressure, respectively radial pulse pressure, to aortic pulse pressure, as measure of amplification, increased almost linearly from 1.15 to 1.39 (brachial) and from 1.19 to 1.55 (radial) over the years.

Brachial systolic and diastolic blood pressures are presented in **Figure 3**. Pressures from a population study by Flynn et al. (38) in children aged 1–17 years are shown as reference. Systolic pressures of the model are similar whereas diastolic pressures are higher compared to measured pressures.

The transfer functions between aorta and the above-mentioned arteries are shown in **Figure 4**. In the "**Supplemental Material**: Transfer functions as function of harmonics" The transfer functions are plotted as a function of harmonics (instead of frequencies, **Figure 4**). By normalizing to the heart rate, a better insight is given in the effect of a transfer function for a certain age. In this representation, the peaks of the transfer functions are closer for the different ages than in **Figure 4**. However, the peaks of the younger ages are still at

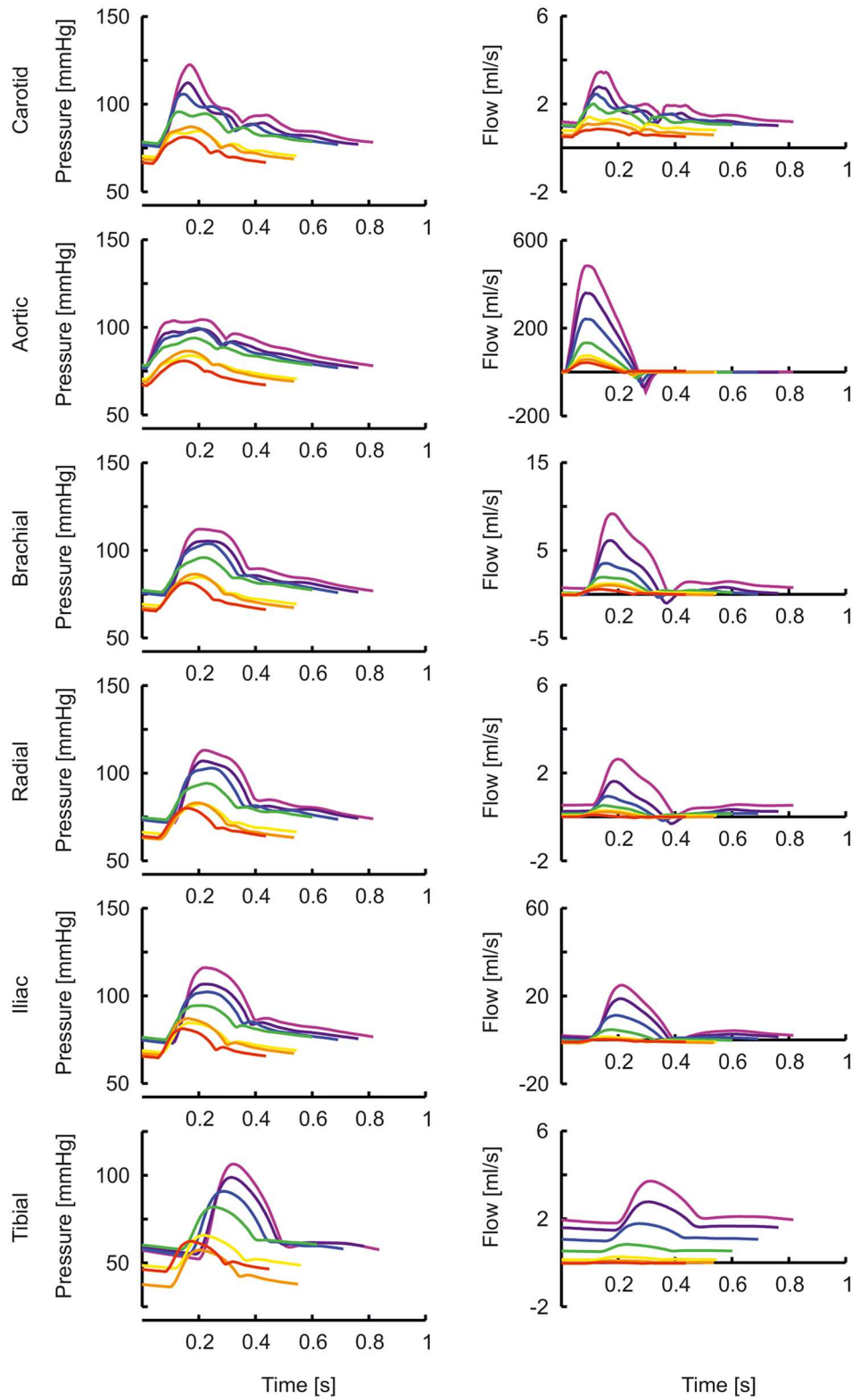

FIGURE 2 | The pressure and flow waves for aorta, carotid, brachial, radial, femoral and tibial artery as a function of age (red, orange, yellow, green, blue, purple, violet: 0, 1, 2, 5, 10, 15, 20 years).

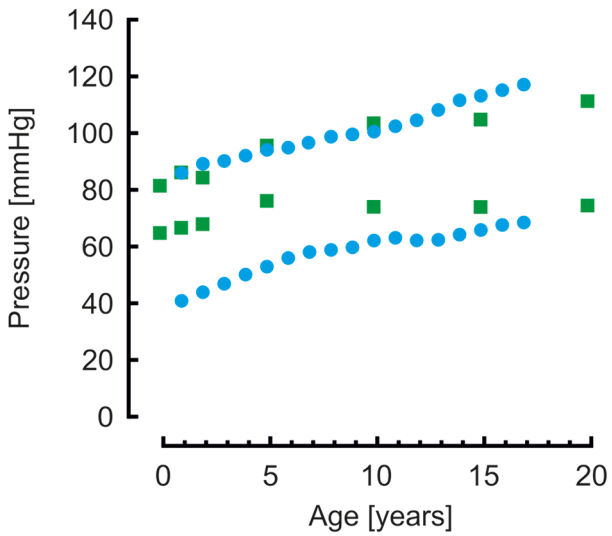

FIGURE 3 | Brachial systolic and diastolic blood pressures from model simulations (green blocks) and from a population study (blue disks) (38). Systolic pressure are comparable, diastolic pressures of the model simulations are higher than the measured pressures.

higher harmonics, explaining why their pressure wave shapes are less affected when traveling toward the periphery.

The percentage of resistance that resides in the vessels relative to the total resistance (thus including Windkessel resistance) was 11% at 0 years and decreased to 7% for 20 years, indicating a small pressure drop over the conduit arteries. When the shear rate was not kept constant by an increasing vascular radius to accommodate for the higher tissue perfusion at younger age, the resistance in the vessels relative to the total resistance was 26% at 0 years, causing a considerable pressure-drop.

Moens-Korteweg pulse wave velocities (22) in the aortic segments and carotid to femoral pulse wave velocities are presented in **Figure 5**. For comparison, carotid to femoral pulse wave velocities reported by Reusz et al. (39) over ages ranging from 6 to 20 years are shown. Both model- and measured carotid to femoral velocities are higher than the Moens-Korteweg velocities. In all velocities an increase with age is visible.

Input impedances as determined from Fourier analysis of pressure and flow are given in the **Supplemental Material**—Vascular dimensions and Windkessel parameters, together with the 3-element (40) and 4-element (41) Windkessel impedances based on characteristic impedance and the lumping of the compliance, resistance and inertance of the distributed system (**Table 1**) (42). Both Windkessels fit to the data of the distributed system quite well.

DISCUSSION

A model of the arterial system was developed that describes hemodynamics during development from 0 to 20 years, from newborn to adult. The system is based on anatomy, stature, proportional growth of different divisions of the body, and weight, all as described in the literature (15, 17, 18).

Our main findings are that the pressures for the age range of 0–5 years are quite similar throughout the arterial system. After the age of 10 years, the pressure transfer functions appear to have taken their final forms, remaining quite similar during further development to adulthood. This suggests that transfer functions developed for the adult may work acceptably for children of 10 years and older, but not for younger children. In the latter group, less amplification is present, and an adult transfer function would overcorrect systolic pressures, resulting in estimations that are too low. This observation fits with recent findings of systolic pressure underestimation is younger children (43, 44). Individualization of transfer functions based on body height or age may improve precision (32, 33).

Gevers et al. (45) used high-fidelity catheter tip-manometers to collect peripheral pressure (radial and tibial artery) waveforms in critically ill newborns. The radial pressures were very similar in form to central aortic pressures as seen in adults, many times with A-type (46) pressure augmentation visible. Tibial pressures were shown to resemble the more proximal femoral artery pressure in adult. The authors concluded that peripheral pressure in newborns have a central appearance.

The transfer functions derived by Cai et al. (47) give the relation between carotid (representing central pressure) and radial artery are not directly comparable to the transfer functions shown here which all give the relation between aortic pressure and peripheral pressures. Nonetheless, their transfer functions for pediatric (8 years old) and adolescent (14 years old) populations are similar to our aortic-to-radial transfer functions for 10 years and 15 years old [(47); **Figures 2**, **4**]. The representation of their transfer functions is inverted compared to ours, and their troughs of about 0.5 correspond to our peaks of about 2. In addition, in their data, the trough in the transfer function deepens for higher age and moves to lower frequencies, analogous to the increasing peaks in our data, which move to lower frequencies as well.

Milne et al. (48) measured the carotid distension wave with echo-tracking and compared it with invasively measured aortic pressure. Also, in another population, they compared central pressure, reconstructed from non-invasively measured radial pressure using an adult transfer function, with the carotid distension wave. In both sub-studies the ages ranged between 2 and 18 years old; subjects were not stratified. The systolic pressure derived from the carotid distension wave (using the invasive diastolic and mean pressures for calibration) slightly overestimated the aortic pressure, but only some 4 mmHg. We find similar numbers for pressure augmentation in our study (1 mmHg for 5 years old, 6 mmHg for 10 years old, 13 mmHg for 15 years old). In the study of Milne et al. (48), the central systolic pressure reconstructed from radial pressure using the adult transfer function, and calibrated using auscultatory brachial pressures, was within 1 mmHg accurate when compared to the carotid distension wave. The central-to-peripheral pressure augmentation was almost 20 mmHg. This is contrary to our findings and to those of others (47) and may have to do with the excessive reduction of peripherally

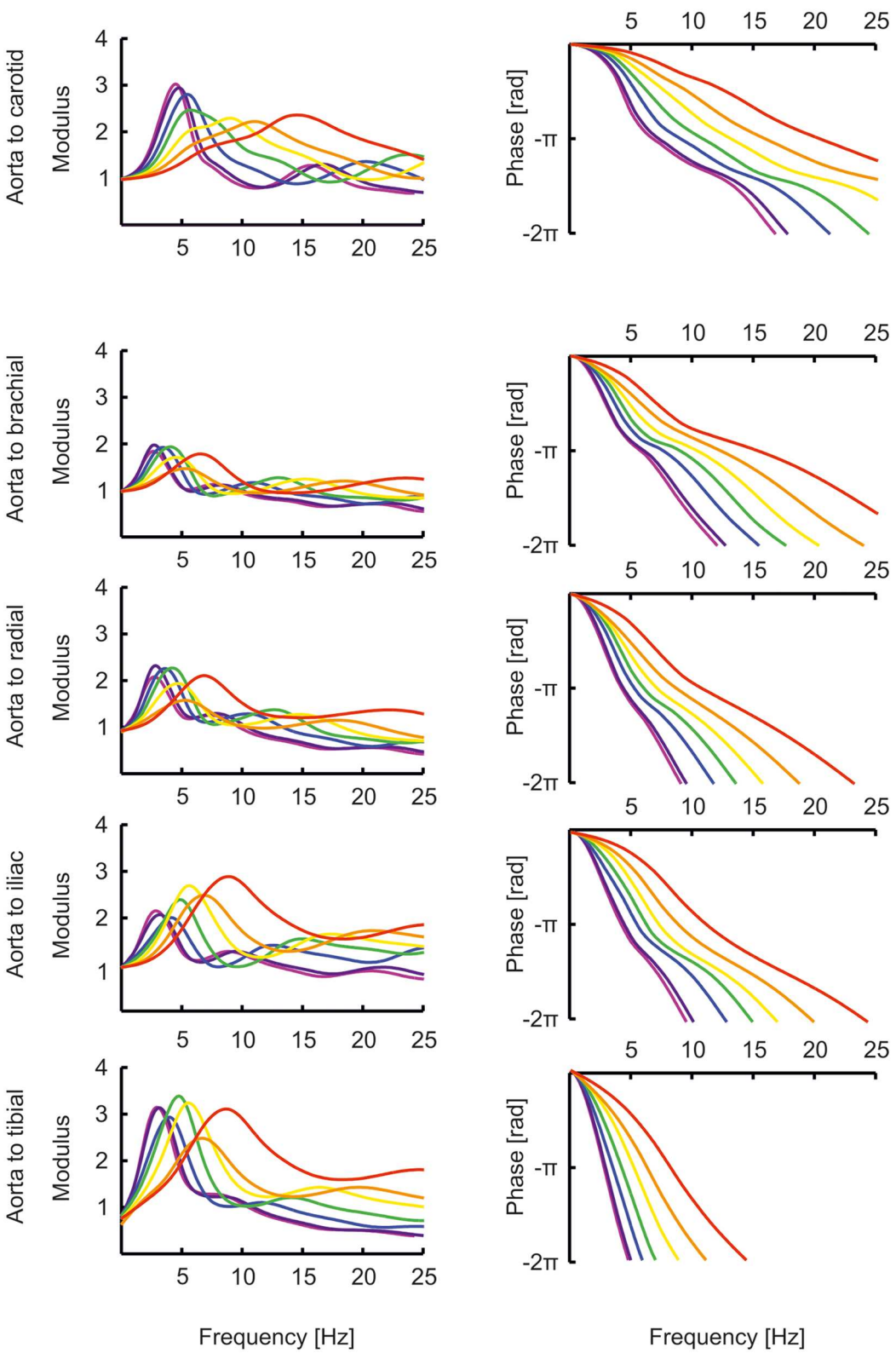

FIGURE 4 | The transfer functions between aorta and the carotid, brachial, radial, femoral and tibial artery as a function of age (red, orange, yellow, green, blue, purple, violet: 0, 1, 2, 5, 10, 15, 20 years).

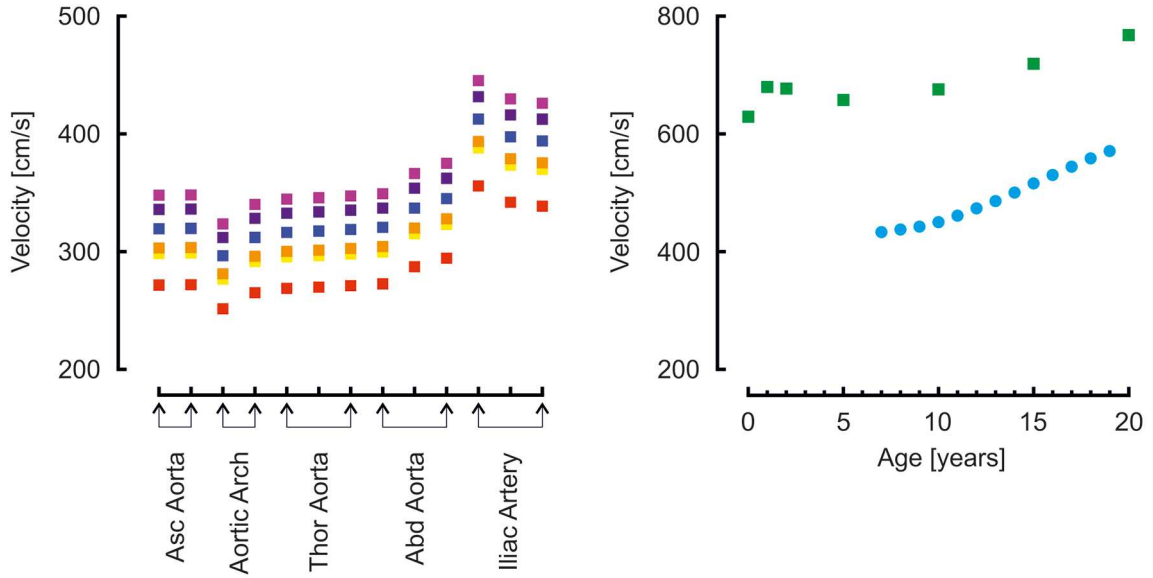

FIGURE 5 | Left: Moens-Korteweg pulse wave velocity over the aortic segments as a function of age (red, orange, yellow, green, blue, purple, violet: 0, 1, 2, 5, 10, 15, 20 years). Right: carotid to femoral pulse wave velocity determined from model simulations (green blocks) and from a population study (blue disks) (39).

TABLE 1 | Lumped parameters of the arterial system.

Age (years)	Z_c (g·cm^{-4}·s^{-1})	L (g·cm^{-4})	C (g^{-1}·cm^4·s^2)	R (g·cm^{-4}·s^{-1})
0	284	16.4	0.236	10,447
1	257	18.7	0.353	7,688
2	166	14.5	0.611	5,989
5	117	11.9	1.013	4,014
10	105	11.4	1.388	2,454
15	85	10.3	2.126	1,765
20	80	10.0	2.459	1,425

Lumped parameters Z_c (characteristic impedance), L (inertance), C (compliance), and R (resistance) of the whole arterial system for ages 0–20 years.

measured systolic pressure when using an adult transfer function in children.

In older age, it is quite well-established that pulse pressure amplification is reduced (49, 50), and brachial and radial systolic pressures are closer to central aortic systolic pressure than in younger age. Pulse pressure amplification is determined by the transfer function between the aorta and the brachial or radial site. In a 20 years old individual, the peak in the transfer function is at a relatively low frequency, so that the lower frequencies (which are the main determinants of the pressure levels) are amplified. At older age, when vessels become stiffer, the peak moves to higher frequencies, away from the main frequency content, and amplification is reduced (31, 51). Views on the effects of pulse pressure amplification in the younger ages are divided (52). The effects are relevant to make an appropriate decision when considering treatment of early age hypertension (53). Based on our modeling results, we suggest that pressure augmentation is smaller in younger individuals. We agree with Adji and O'Rourke (54) that the changes in vascular stiffness in this age group are small, and the changes in the transfer functions are determined mainly by changes in dimensions. We however would advise to be cautious with the use of an adult transfer function for the very young; probably, the results are acceptable from 10 years and up.

When comparing brachial pressures of the model to measured pressures in a population study by Flynn et al. (38), systolic pressures were similar, however, diastolic pressures of the model were higher, in particular for the younger ages. This suggests that the arterial stiffness of the model is too low, resulting in an overly low pulse pressure.

Our model is highly versatile and allows making changes to describe diverse anatomical aberrations (coarctation, aneurysm). It could also be used to investigate the effects of childhood obesity on the pressure wave shape (55, 56). Also potentially relevant is model based prediction of the effect of vascular remodeling, which may start already early in life in children with end-stage renal disease, chronic parenteral nutrition, HIV infection, or aortic coarctation, as suggested by Aggoun et al. (57).

Both the 3- as well as the 4-element Windkessel seem to provide an acceptable lumped parameter model description of the arterial input impedance. The parameters can be estimated based on gender (which we did not investigate), age, height and weight. We suggest that the findings of the current study can serve as a basis for further development of a Windkessel model, which could be used to estimate cardiac output from pressure measurements (58). To our knowledge, such a model is currently not available for children.

Cardiac Output and Heart Rate

The cardiac output and heart rate taken from Wiesener (21) gave correct mean arterial pressures as a function of age (24), but only after the total peripheral resistance of the original adult model (2) was reduced. Also, the arterial stiffness of the original description

(2) was reduced to arrive at acceptable pulse pressures. To check if the used cardiac output as a function of age is also reasonable, the following calculations were done. Body weight increased from 3.5 kg at birth to 78 kg at 20 years; cardiac output increased from 564 mL/min to 5 L/min. Dividing cardiac output by body weight gives 161 and 64 mL/min/kg, respectively. Thus, tissue perfusion is indeed higher in youth than at later ages, as expected (19). Alternatively, cardiac output has been suggested to be 933 × weight$^{0.38}$ in children and adolescents (59). At 3.5 kg, the cardiac output then would be calculated as 1.5 L/min, or 430 mL/min/kg, which is almost seven times higher than the value in the adult circulation, which we believe is a quite unacceptably high tissue perfusion. The first estimation gives a factor of 3 higher tissue perfusion for children vs. adults, which to us seems more realistic.

Across the mammalian species, cardiac output is related to body weight$^{3/4}$ (22). With weight increase from 3.5 to 78 kg, from the newborn to adult, a factor of 22, cardiac output should increase by a factor of $22^{3/4} = 10.2$. This is in line with the cardiac output increase reported by Wiesener (21).

Shear Stress

As previously established from non-invasive measurements (23), we assumed that shear stress in the conduit vessels during development from the newborn to the adult circulation, would remain constant (23). Cardiac output increased approximately a factor of 10, so that arterial radii should increase by a factor of $10^{1/3}$ or approximately 2.15 times: i.e., from around 0.68–1.47 cm for the aorta radius. If cardiac output was actually as high as 1.5 L/min (59) at 0 years (see section "Cardiac output and heart rate" in the Discussion), then the cardiac output would increase only about 3.33 instead of 10 times. With a radius increase of $3.33^{1/3}$ or approximately 1.49 times, aortic radius would be about 1 cm at 0 years, which is rather unrealistically large.

With the implementation of a constant wall shear stress, the resistance in the conduit vessels was low with respect to total resistance (including the resistance of the loading Windkessels), thus the pressure drop in the vessels was small for the given cardiac outputs. Without this implementation of constant wall shear stress, the pressure drop would have become substantial.

Pulse Wave Velocity

Pulse wave velocity showed a gradual increase over the years. At younger age, vascular diameters were smaller, however, wall thickness was relatively even more reduced, since the mean arterial pressures were lower (see section "Vascular wall properties" in the Methods). This results in a lower wall thickness/radius ratio and thus, according to Moens-Korteweg (22), a lower pulse wave velocity as compared to the value at higher age.

Carotid to femoral velocities were higher than the aortic Moens-Korteweg velocities (22). In the study by Reusz et al. (39), the distance was measured over the body; in our model, segments lengths were added. In this way the travel distance is overestimated (this approach assumes that the pressure wave travels from the carotid to the femoral artery), resulting in an overestimation of aortic pulse wave velocity (60, 61). This is indeed apparent from the findings. The model findings overestimate Moens-Korteweg velocities even more than the measured data (39), likely since the addition of the segments lengths overestimates the measured lengths.

Another explanation is that arterial stiffness in the model is too high. To obtain pulse wave velocities at the same absolute value as Reusz et al. (39) found at 20 years of age, i.e., about 500 cm/s instead of the 700 cm/s found in the model, the vascular stiffness was reduced by a factor of 0.5. This gives a reduction of pulse wave velocity by a factor of 0.7. The aortic pressure then became 100/83 mmHg, brachial pressure 102/81. This is a very low pulse pressure and at odds with the measurements of by Flynn et al. (38), who report 117/68 at 17 years of age (121/74 when extrapolated to 20 years). Thus, the model strikes the balance: on the one hand, a higher arterial stiffness would give a pulse pressure closer to the reported measurements of Flynn et al. (38); on the other hand, a lower arterial stiffness would give carotid to femoral pulse wave velocities closed to those reported by Reusz et al. (39). More studies are needed to accurately determine arterial stiffness in developing children.

Model Considerations

Our work is a first step in the development of a distributed model that accurately describes pressure and flow relations in healthy children. The length, radius and wall thickness of the arterial segments were estimated based on growth curves and not measured in groups of individuals in certain age ranges. Detailed measurements of the vasculature as a function of age would possibly allow further improvement of the model description. Potential sex differences that may include differences in cardiac output and tissue perfusion were not considered.

In the current model, the arterial stiffness of the arterial segments is based on the original description of Westerhof et al. (2) distinguishing only four separate values. In reality, the distribution of stiffness is probably gradual, with the distal arteries being stiffer (62). Moreover, these four stiffness values were kept the same during the 20-years development. Also, in the model, the stiffness of each vessel is taken constant while it actually depends on the pressure that extends the vessel wall. While this simplification may be acceptable in the normal situation, with a limited range of pressure levels, a more accurate non-linear description would enhance the applicability of the model, e.g., in severe hypotension.

Radii of the arterial segments were assumed to grow proportional to the increase of length of the body division. When keeping the shear rate constant during development, by correcting radii to accommodate for the higher tissue perfusion at younger age, the resistance of the conduit vessels was acceptably low relative to the tissue resistance for all ages. Without shear stress correction however the conduit vessel resistance would cause considerably lower pressures at tissue level at younger ages. Our first assumption that radii would increase with length may be incorrect, but, together with the shear stress correction, seems to give acceptable results.

The model describes the systemic arterial tree with a closed ductus arteriosus (and in the heart, the foramen ovale

is supposed to be closed). Interesting future work could aim to describe the transition from the neonatal circulation toward the closing of these shunts and the impact on cardiac output (63).

In our approach, the flow wave shape was the same for all simulations. A different flow wave shape may give other pressure wave shapes and for instance give rise to higher systolic pressure amplification. However, since the transfer functions are only determined by arterial parameters, these are independent of the flow wave shape that was used.

Finally, reflexes of the autonomic nervous system and autoregulation of organs were not incorporated in the model.

CONCLUSION

To our knowledge, we presented the currently most complete distributed model of the arterial system for the age range from newborn to adult. Important results encompass the finding of peripheral pressures in younger children to resemble their central pressure, and that input impedance may be described by a simple Windkessel model.

The results carry clinical significance for the interpretation of peripheral measured pressures in younger and older children. Further application of our model may e.g., aid in estimating cardiac output in children in intensive care, or to investigate effects resulting from vascular aberrations.

DATA AVAILABILITY STATEMENT

All datasets generated for this study are included in the article/**Supplementary Material**.

AUTHOR'S NOTE

Main findings of this study were presented at the Artery 2011 meeting.

AUTHOR CONTRIBUTIONS

BW and JW conceived the study, developed the model, and wrote the manuscript. MG wrote the manuscript.

ACKNOWLEDGMENTS

We gratefully acknowledge fruitful discussions with Prof. Nico Westerhof, of the Department of Pulmonary Medicine, Amsterdam UMC, Vrije Universiteit Amsterdam, Amsterdam Cardiovascular Sciences, Amsterdam, the Netherlands.

SUPPLEMENTARY MATERIAL

The Supplementary Material for this article can be found online at: https://www.frontiersin.org/articles/10.3389/fped.2020.00251/full#supplementary-material

REFERENCES

1. van den Wijngaard JP, Siebes M, Westerhof BE. Comparison of arterial waves derived by classical wave separation and wave intensity analysis in a model of aortic coarctation. *Med Biol Eng Comput*. (2009) 47:211–20. doi: 10.1007/s11517-008-0387-y
2. Westerhof N, Bosman F, de Vries CJ, Noordergraaf A. Analog studies of the human systemic arterial tree. *J Biomech*. (1969) 2:121–43. doi: 10.1016/0021-9290(69)90024-4
3. Avolio AP. Multi-branched model of the human arterial system. *Med Biol Eng Comput*. (1980) 18:709–18. doi: 10.1007/BF02441895
4. Stergiopulos N, Young DF, Rogge TR. Computer simulation of arterial flow with applications to arterial and aortic stenoses. *J Biomech*. (1992) 25:1477–88. doi: 10.1016/0021-9290(92)90060-E
5. Schumacher G, Kaden JJ, Trinkmann F. Multiple coupled resonances in the human vascular tree: refining the Westerhof model of the arterial system. *J Appl Physiol*. (1985) (2018) 124:131-9. doi: 10.1152/japplphysiol.00405.2017
6. Westerhof BE, Westerhof N. Magnitude and return time of the reflected wave: the effects of large artery stiffness and aortic geometry. *J Hypertens*. (2012) 30:932–9. doi: 10.1097/HJH.0b013e3283524932
7. Westerhof BE, Westerhof N. Uniform tube models with single reflection site do not explain aortic wave travel and pressure wave shape. *Physiol Meas*. (2018) 39:124006. doi: 10.1088/1361-6579/aaf3dd
8. Reymond P, Merenda F, Perren F, Rufenacht D, Stergiopulos N. Validation of a one-dimensional model of the systemic arterial tree. *Am J Physiol Heart Circ Physiol*. (2009) 297:H208–22. doi: 10.1152/ajpheart.00037.2009
9. van den Wijngaard JP, Westerhof BE, Faber DJ, Ramsay MM, Westerhof N, van Gemert MJ. Abnormal arterial flows by a distributed model of the fetal circulation. *Am J Physiol Regul Integr Comp Physiol*. (2006) 291:R1222–33. doi: 10.1152/ajpregu.00212.2006
10. van den Wijngaard JP, Westerhof BE, Ross MG, van Gemert MJ. A mathematical model of twin-twin transfusion syndrome with pulsatile arterial circulations. *Am J Physiol Regul Integr Comp Physiol*. (2007) 292:R1519–31. doi: 10.1152/ajpregu.00534.2006
11. van Meurs WWL, Antonius TAJ. Explanatory models in neonatal intensive care: a tutorial. *Adv Simul (Lond)*. (2018) 3:27. doi: 10.1186/s41077-018-0085-2
12. Goodwin JA, van Meurs WL, Sa Couto CD, Beneken JE, Graves SA. A model for educational simulation of infant cardiovascular physiology. *Anesth Analg*. (2004) 99:1655–64. doi: 10.1213/01.ANE.0000134797.52793.AF
13. Westerhof N, Lankhaar JW, Westerhof BE. The arterial windkessel. *Med Biol Eng Comput*. (2009) 47:131–41. doi: 10.1007/s11517-008-0359-2
14. Westerhof N, Noordergraaf A. Arterial viscoelasticity: a generalized model. Effect on input impedance and wave travel in the systematic tree. *J Biomech*. (1970) 3:357–79. doi: 10.1016/0021-9290(70)90036-9
15. Freeman JV, Cole TJ, Chinn S, Jones PR, White EM, Preece MA. Cross sectional stature and weight reference curves for the UK, 1990. *Arch Dis Child*. (1995) 73:17–24. doi: 10.1136/adc.73.1.17
16. Wright CM, Corbett SS, Drewett RF. Sex differences in weight in infancy and the British 1990 national growth standards. *BMJ*. (1996) 313:513–4. doi: 10.1136/bmj.313.7056.513
17. Burmaster DE, Crouch EA. Lognormal distributions for body weight as a function of age for males and females in the United States, 1976-1980. *Risk Anal*. (1997) 17:499–505. doi: 10.1111/j.1539-6924.1997.tb00890.x
18. Morris H, Anson BJ, editors. *Human Anatomy: A Complete Systematic Treatise*. New York, NY: McGraw-Hill (1966).
19. Guyton AC, Hall JE. *Textbook of Medical Physiology*. 9th ed. Philadelphia, PA: W.B. Saunders (1996).
20. Ramsay MM. Normal values in pregnancy. 2nd ed. London, UK: Saunders (2000).
21. Wiesener H. *Einführung in die Entwicklungsphysiologie Des Kindes*. Berlin; Heidelberg: Springer (1964). doi: 10.1007/978-3-642-86506-0
22. Westerhof N, Stergiopulos N, Noble MIM, Westerhof BE. *Snapshots of Hemodynamics: An Aid for Clinical Research and Graduate Education.*

3rd ed. New York Dordrecht, Heidelberg, London: Springer-Nature (2018). doi: 10.1007/978-3-319-91932-4
23. Struijk PC, Stewart PA, Fernando KL, Mathews VJ, Loupas T, Steegers EA, et al. Wall shear stress and related hemodynamic parameters in the fetal descending aorta derived from color doppler velocity profiles. *Ultrasound Med Biol*. (2005) 31:1441–50. doi: 10.1016/j.ultrasmedbio.2005.07.006
24. Jackson LV, Thalange NK, Cole TJ. Blood pressure centiles for great Britain. *Arch Dis Child*. (2007) 92:298–303. doi: 10.1136/adc.2005.081216
25. Guettouche A, Challier JC, Ito Y, Papapanayotou C, Cherruault Y, Azancot-Benisty A. Mathematical modeling of the human fetal arterial blood circulation. *Int J Biomed Comput*. (1992) 31:127–39. doi: 10.1016/0020-7101(92)90068-4
26. Castillo EH, Arteaga-Martinez M, Garcia-Pelaez I, Villasis-Keever MA, Aguirre OM, Moran V, et al. Morphometric study of the human fetal heart. I. Arterial segment. *Clin Anat*. (2005) 18:260–8. doi: 10.1002/ca.20095
27. Myers LJ, Capper WL. A transmission line model of the human foetal circulatory system. *Med Eng Phys*. (2002) 24:285–94. doi: 10.1016/S1350-4533(02)00019-X
28. Jager GN, Westerhof N, Noordergraaf A. Oscillatory flow impedance in electrical analog of arterial system: representation of sleeve effect and non-newtonian properties of blood. *Circ Res*. (1965) 16:121–33. doi: 10.1161/01.RES.16.2.121
29. Womersley JR. *The Mathematical Analysis of the Arterial Circulation in a State of Oscillatory Motion*. Technical Report Wade-TR 56-614. Dayton, OH: Wright Air Development Center (1957).
30. Milnor WR. *Hemodynamics*. Baltimore, London: Williams & Wilkins (1982).
31. Westerhof BE, Guelen I, Stok WJ, Wesseling KH, Spaan JA, Westerhof N, et al. Arterial pressure transfer characteristics: effects of travel time. *Am J Physiol Heart Circ Physiol*. (2007) 292:H800–7. doi: 10.1152/ajpheart.00443.2006
32. Stergiopulos N, Westerhof BE, Westerhof N. Physical basis of pressure transfer from periphery to aorta: a model-based study. *Am J Physiol*. (1998) 274:H1386–92. doi: 10.1152/ajpheart.1998.274.4.H1386
33. Westerhof BE, Guelen I, Stok WJ, Lasance HA, Ascoop CA, Wesseling KH, et al. Individualization of transfer function in estimation of central aortic pressure from the peripheral pulse is not required in patients at rest. *J Appl Physiol*. (1985) (2008) 105:1858-63. doi: 10.1152/japplphysiol.91052.2008
34. Hickson SS, Butlin M, Graves M, Taviani V, Avolio AP, McEniery CM, et al. The relationship of age with regional aortic stiffness and diameter. *JACC Cardiovasc Imaging*. (2010) 3:1247–55. doi: 10.1016/j.jcmg.2010.09.016
35. Boron WF, Boulpaep EL. *Medical Physiology*. 2nd Edn. Elsevier Health Sciences. (2012).
36. Wilkinson IB, MacCallum H, Flint L, Cockcroft JR, Newby DE, Webb DJ. The influence of heart rate on augmentation index and central arterial pressure in humans. *J Physiol*. (2000) 525(Pt 1):263–70. doi: 10.1111/j.1469-7793.2000.t01-1-00263.x
37. Cantor A, Wanderman KL, Karolevitch T, Ovsyshcher I, Gueron M. Systolic time intervals in children: normal standards for clinical use. *Circulation*. (1978) 58:1123–9. doi: 10.1161/01.CIR.58.6.1123
38. Flynn JT, Kaelber DC, Baker-Smith CM, Blowey D, Carroll AE, Daniels SR, et al. Clinical practice guideline for screening and management of high blood pressure in children and adolescents. *Pediatrics*. (2017) 140:e20171904. doi: 10.1542/peds.2017-3035
39. Reusz GS, Cseprekal O, Temmar M, Kis E, Cherif AB, Thaleb A, et al. Reference values of pulse wave velocity in healthy children and teenagers. *Hypertension*. (2010) 56:217–24. doi: 10.1161/HYPERTENSIONAHA.110.152686
40. Westerhof N, Elzinga G, Sipkema P. An artificial arterial system for pumping hearts. *J Appl Physiol*. (1971) 31:776–81. doi: 10.1152/jappl.1971.31.5.776
41. Stergiopulos N, Westerhof BE, Westerhof N. Total arterial inertance as the fourth element of the windkessel model. *Am J Physiol*. (1999) 276:H81–8. doi: 10.1152/ajpheart.1999.276.1.H81
42. Westerhof N, Westerhof BE. A review of methods to determine the functional arterial parameters stiffness and resistance. *J Hypertens*. (2013) 31:1769–75. doi: 10.1097/HJH.0b013e3283633589
43. Shoji T, Nakagomi A, Okada S, Ohno Y, Kobayashi Y. Invasive validation of a novel brachial cuff-based oscillometric device (SphygmoCor XCEL) for measuring central blood pressure. *J Hypertens*. (2017) 35:69–75. doi: 10.1097/HJH.0000000000001135
44. Mynard JP, Goldsmith G, Springall G, Eastaugh L, Lane GK, Zannino D, et al. Central aortic blood pressure estimation in children and adolescents: results of the KidCoreBP study. *J Hypertens*. (2019) 38:821–8. doi: 10.1097/HJH.0000000000002338
45. Gevers M, Hack WW, Ree EF, Lafeber HN, Westerhof N. Arterial blood pressure wave forms in radial and posterior tibial arteries in critically ill newborn infants. *J Dev Physiol*. (1993) 19:179–85.
46. Murgo JP, Westerhof N, Giolma JP, Altobelli SA. Aortic input impedance in normal man: relationship to pressure wave forms. *Circulation*. (1980) 62:105–16. doi: 10.1161/01.CIR.62.1.105
47. Cai TY, Qasem A, Ayer JG, Butlin M, O'Meagher S, Melki C, et al. Central blood pressure in children and adolescents: non-invasive development and testing of novel transfer functions. *J Hum Hypertens*. (2017) 31:831–7. doi: 10.1038/jhh.2017.59
48. Milne L, Keehn L, Guilcher A, Reidy JF, Karunanithy N, Rosenthal E, et al. Central aortic blood pressure from ultrasound wall-tracking of the carotid artery in children: comparison with invasive measurements and radial tonometry. *Hypertension*. (2015) 65:1141–6. doi: 10.1161/HYPERTENSIONAHA.115.05196
49. McEniery CM, Yasmin, McDonnell B, Munnery M, Wallace SM, Rowe CV, et al. Central pressure: variability and impact of cardiovascular risk factors: the anglo-cardiff collaborative trial II. *Hypertension*. (2008) 51:1476–82. doi: 10.1161/HYPERTENSIONAHA.107.105445
50. Avolio AP, van Bortel LM, Boutouyrie P, Cockcroft JR, McEniery CM, Protogerou AD, et al. Role of pulse pressure amplification in arterial hypertension: experts' opinion and review of the data. *Hypertension*. (2009) 54:375–83. doi: 10.1161/HYPERTENSIONAHA.109.134379
51. Bos WJ, Wesseling KH. Method and device for determining brachial arterial pressure wave on the basis of noninvasively measured finger blood pressure wave. *United States Patent*. (1998) 5:746.698.
52. McEniery CM, Franklin SS, Cockcroft JR, Wilkinson IB. Isolated systolic hypertension in young people is not spurious and should be treated: pro side of the argument. *Hypertension*. (2016) 68:269–75. doi: 10.1161/HYPERTENSIONAHA.116.06547
53. Lurbe E, Redon J. Isolated systolic hypertension in young people is not spurious and should be treated: con side of the argument. *Hypertension*. (2016) 68:276–80. doi: 10.1161/HYPERTENSIONAHA.116.06548
54. Adji A, O'Rourke MF. Tracking of brachial and central aortic systolic pressure over the normal human lifespan: insight from the arterial pulse waveforms. *Intern Med J*. (2020) doi: 10.1111/imj.14815. [Epub ahead of print].
55. Lurbe E, Torro MI, Alvarez-Pitti J, Redon P, Redon J. Central blood pressure and pulse wave amplification across the spectrum of peripheral blood pressure in overweight and obese youth. *J Hypertens*. (2016) 34:1389–95. doi: 10.1097/HJH.0000000000000933
56. Avolio A, Butlin M. Blood pressure phenotypes in youth: advances in the application of central aortic pressure. *J Hypertens*. (2016) 34:1254–6. doi: 10.1097/HJH.0000000000000953
57. Aggoun Y, Szezepanski I, Bonnet D. Noninvasive assessment of arterial stiffness and risk of atherosclerotic events in children. *Pediatr Res*. (2005) 58:173–8. doi: 10.1203/01.PDR.0000170900.35571.CB
58. Truijen J, van Lieshout JJ, Wesselink WA, Westerhof BE. Noninvasive continuous hemodynamic monitoring. *J Clin Monit Comput*. (2012) 26:267–78. doi: 10.1007/s10877-012-9375-8
59. de Simone G, Devereux RB, Daniels SR, Mureddu G, Roman MJ, Kimball TR, et al. Stroke volume and cardiac output in normotensive children and adults. Assessment of relations with body size and impact of overweight. *Circulation*. (1997) 95:1837–43. doi: 10.1161/01.CIR.95.7.1837
60. Vermeersch SJ, Rietzschel ER, de Buyzere ML, de Bacquer D, de Backer G, van Bortel LM, et al. Determining carotid artery pressure from scaled diameter waveforms: comparison and validation of calibration techniques in 2026 subjects. *Physiol Meas*. (2008) 29:1267–80. doi: 10.1088/0967-3334/29/11/003

61. Vermeersch SJ, Rietzschel ER, de Buyzere ML, van Bortel LM, Gillebert TC, Verdonck PR, et al. Distance measurements for the assessment of carotid to femoral pulse wave velocity. *J Hypertens*. (2009) 27:2377–85. doi: 10.1097/HJH.0b013e3283313a8a
62. Pagoulatou SZ, Bikia V, Trachet B, Papaioannou TG, Protogerou AD, Stergiopulos N. On the importance of the nonuniform aortic stiffening in the hemodynamics of physiological aging. *Am J Physiol Heart Circ Physiol*. (2019) 317:H1125–33. doi: 10.1152/ajpheart.00193.2019
63. Mielke G, Benda N. Cardiac output and central distribution of blood flow in the human fetus. *Circulation*. (2001) 103:1662–8. doi: 10.1161/01.CIR.103.12.1662

Conflict of Interest: The authors declare that the research was conducted in the absence of any commercial or financial relationships that could be construed as a potential conflict of interest.

frontiers in Physiology

ORIGINAL RESEARCH
published: 25 May 2020
doi: 10.3389/fphys.2020.00550

Feasibility of Estimation of Aortic Wave Intensity Using Non-invasive Pressure Recordings in the Absence of Flow Velocity in Man

Alun D. Hughes[1], Chloe Park[1], Anenta Ramakrishnan[2,3], Jamil Mayet[2], Nish Chaturvedi[1] and Kim H. Parker[3]*

[1] Medical Research Council Unit for Lifelong Health and Ageing at UCL, Department of Population Science & Experimental Medicine, Faculty of Population Health Sciences, Institute of Cardiovascular Science, University College London, London, United Kingdom, [2] Cardiovascular Division, Faculty of Medicine, Imperial College London, National Heart & Lung Institute, London, United Kingdom, [3] Department of Bioengineering, Imperial College London, London, United Kingdom

OPEN ACCESS

Edited by:
Jonathan Paul Mynard, Murdoch Children's Research Institute, Royal Children's Hospital, Australia

Reviewed by:
Bart Spronck, Yale University, United States
Kevin S. Heffernan, Syracuse University, United States

***Correspondence:**
Alun D. Hughes
alun.hughes@ucl.ac.uk

Specialty section:
This article was submitted to Vascular Physiology, a section of the journal Frontiers in Physiology

Received: *08 January 2020*
Accepted: *30 April 2020*
Published: *25 May 2020*

Citation:
Hughes AD, Park C, Ramakrishnan A, Mayet J, Chaturvedi N and Parker KH (2020) Feasibility of Estimation of Aortic Wave Intensity Using Non-invasive Pressure Recordings in the Absence of Flow Velocity in Man. Front. Physiol. 11:550. doi: 10.3389/fphys.2020.00550

Background: Wave intensity analysis provides valuable information on ventriculo-arterial function, hemodynamics, and energy transfer in the arterial circulation. Widespread use of wave intensity analysis is limited by the need for concurrent measurement of pressure and flow waveforms. We describe a method that can estimate wave intensity patterns using only non-invasive pressure waveforms (pWIA).

Methods: Radial artery pressure and left ventricular outflow tract (LVOT) flow velocity waveforms were recorded in 12 participants in the Southall and Brent Revisited (SABRE) study. Pressure waveforms were analyzed using custom-written software to derive the excess pressure (P_{xs}) which was scaled to peak LVOT velocity and used to calculate wave intensity. These data were compared with wave intensity calculated using the measured LVOT flow velocity waveform. In a separate study, repeat measures of pWIA were performed on 34 individuals who attended two clinic visits at an interval of ≈1 month to assess reproducibility and reliability of the method.

Results: P_{xs} waveforms were similar in shape to aortic flow velocity waveforms and the time of peak P_{xs} and peak aortic velocity agreed closely. Wave intensity estimated using pWIA showed acceptable agreement with estimates using LVOT velocity tracings and estimates of wave intensity were similar to values reported previously in the literature. The method showed fair to good reproducibility for most parameters.

Conclusion: The P_{xs} is a surrogate of LVOT flow velocity which, when appropriately scaled, allows estimation of aortic wave intensity with acceptable reproducibility. This may enable wider application of wave intensity analysis to large studies.

Keywords: blood pressure, hemodynamics, waves, wave intensity analysis, blood flow, aorta

INTRODUCTION

Blood pressure (BP) results almost entirely from waves generated by the heart; the intensity of these arterial waves is an important measure of ventriculo-arterial function and their interaction. While wave intensity analysis is not the only method to characterize waves in the circulation (Westerhof et al., 2005; Caro et al., 2012), it has proved an increasingly valuable approach to understanding hemodynamics and wave propagation in the circulation, since it quantifies the intensity and energy carried by forward and backward-traveling waves, along with their timing (Parker and Jones, 1990; MacRae et al., 1997; Parker, 2009; Broyd et al., 2015; Su et al., 2017). This has prognostic value: wave reflection has been reported to predict cardiovascular events independently of other cardiovascular risk factors (Manisty et al., 2010) and more recently, elevated wave intensity has been independently associated with greater decline in cognitive function from mid- to late life (Chiesa et al., 2019). This latter observation is consistent with suggestions that excessive pulsatile energy transfer is responsible for microvascular damage in the cerebral circulation (Mitchell, 2018).

Traditionally, analysis of wave intensity requires that both pressure and flow (or flow velocity) are measured, ideally simultaneously. These measurements can be onerous and technically challenging in large scale studies. We therefore examined the feasibility of deriving estimates of wave intensity based on measurement of pressure only. The method for calculating wave intensity using only pressure measurements is based on an observation made by Wang et al. (2003), who reported that excess pressure (P_{xs}), the difference between measured and reservoir pressure, was directly proportional to flow in the aortic root, Q_{in} in dogs. Subsequent studies in humans employing invasive measurements of pressure and flow velocity in the aorta (Davies et al., 2007) and non-invasive measurements of carotid artery pressure and aortic flow (Vermeersch et al., 2009; Michail et al., 2018) have confirmed these findings. Given that wave intensity is the product of the derivatives of pressure and flow velocity this suggests that it should be possible to estimate wave intensity patterns using the measured pressure waveform and P_{xs} derived from reservoir analysis.

We therefore examined if this approach could be used to estimate wave intensity patterns from non-invasive measurements of the pressure waveform in man using a sample from a large UK population-based longitudinal cohort, the Southall and Brent Revisited (SABRE) study. We tested whether the P_{xs} waveform was similar to the measured aortic flow velocity waveform, assessed the agreement between wave intensity estimates made using pressure alone with the traditional approach, and also studied the test-retest reproducibility of pressure-only wave intensity analysis (pWIA) and other reservoir parameter estimates.

MATERIALS AND METHODS

Data were obtained from participants in the SABRE study, a tri-ethnic population-based cohort consisting of white European, South Asian and African Caribbean people resident in West London, UK (Tillin et al., 2012). In brief, participants, aged 40–69 years, were recruited from primary care and baseline measurements performed between 1988 and 1991. Surviving participants were invited to attend a 20-year follow-up for detailed phenotyping between 2008 and 2011 and data collected at this visit were used for this study. Twelve consecutive participants who underwent measurements of aortic flow velocity by echocardiography and blood pressure waveform measurement by radial tonometry were selected to explore the feasibility of performing wave intensity analysis using a pressure-only technique (pWIA). Reproducibility of the pWIA technique was assessed on 34 participants who re-attended for study investigations within a month as part of routine quality control. Exclusion criteria for both studies were rhythm other than sinus rhythm, valvular heart disease, or any other clinical condition that prevented full participation in the study.

The study was approved by the local research ethics review committee, and all participants gave written informed consent. The study adhered to the principles of the Declaration of Helsinki and Title 45, US Code of Federal Regulations, part 46. Protection of Human Subjects. Revised November 13, 2001, effective December 13, 2001, and all procedures were performed in accordance with institutional guidelines.

Investigations

Participants fasted and refrained from alcohol, smoking, and caffeine and were advised to avoid strenuous exercise for $\geq$ 12 h before attendance. Participants omitted any medication on the morning of investigation. A questionnaire was completed, which detailed health behaviors, medical history, and medication. Height, weight, and waist circumference were measured as previously described (Tillin et al., 2012). Diabetes was defined according to World Health Organization criteria (Alberti and Zimmet, 1998), self-report of doctor-diagnosed diabetes, or receipt of anti-diabetes medication. Hypertension was defined as use of blood pressure–lowering medication from patient questionnaire and/or general practitioners' medical record review. Coronary heart disease was defined as a coronary event or revascularization identified by medical record review and adjudicated by an independent committee. Diagnosis of stroke was based on predetermined criteria of symptoms, duration of symptoms, and MRI or computed tomography imaging from hospital admission, patient, or medical records (Tillin et al., 2013). Heart failure, valve disease and atrial fibrillation were identified during the clinic visit and/or from medical records.

Seated brachial blood pressure was measured after 5–10 min rest using a validated automatic Oscillometric device (Omron 705IT). Arm circumference was measured and an appropriate sized cuff, based on British Society of Hypertension guidelines, was placed on the left upper arm. Three recordings were taken 2 min apart, and the second and third recordings were averaged as an estimate of clinic BP. BP waveforms were also recorded from the radial artery using a tonometer device (SphygmoCor; AtCor, Sydney, Australia) over at least six cardiac cycles, ensemble averaged and calibrated to brachial systolic and diastolic BP according to the manufacturer's instructions.

Central BP was calculated using the manufacturer's software, which employs a generalized transfer function. Reservoir analysis (**Figure 1**) was performed using custom-written Matlab code (Mathworks, Inc., Natick, MA, United States) as previously described (Davies et al., 2014).

Echocardiography was performed using a Philips iE33 ultrasound machine (Philips, Amsterdam, The Netherlands) with a 5.0–1.0 phased array transducer (S5-1), as previously described (Park et al., 2013). Aortic flow velocity was measured in the left ventricular outflow tract (LVOT) using continuous wave Doppler according to ASE/EAE guidelines (Quinones et al., 2002) and at least 3 consecutive cardiac cycles were recorded during quiet respiration. For estimation of aortic wave intensity using a conventional method, the single best quality flow velocity waveform was digitalized at a sampling rate of 200 Hz and then downsampled to 128 Hz to correspond to the sampling rate of the SphygmoCor data, velocity in diastole was constrained to zero. Wave intensity was calculated as the product of the derivative of the central pressure waveform and the derivative of the digitalized flow velocity waveform as previously described (Bhuva et al., 2019).

Fitting the Reservoir and Calculating Pressure-Only Wave Intensity

Details of the reservoir approach are provided elsewhere (Hughes and Parker, 2020). In brief, it is assumed that reservoir pressure, P_{res}, satisfies overall conservation of mass for the circulation:

$$\frac{dP_{res}}{dt} = \frac{Q_{in}}{C} - k_d(P_{res} - P_{zf}) \quad (1)$$

where Q_{in} is the volumetric flow rate into the aortic root, C is the net compliance of the arteries, k_d is the diastolic rate constant (the reciprocal of the diastolic time constant $\tau = RC$, where R is the resistance to outflow through the microcirculation, and P_{zf} is the pressure at which outflow through the microcirculation ceases.

The excess pressure (P_{xs}) is the difference between the measured pressure and the reservoir pressure $(P\text{-}P_{res})$ and if, as discussed above, P_{xs} is assumed to be directly proportional to the flow in the aortic root, we can substitute.

$$Q_{in} = \zeta P_{xs} \quad (2)$$

into the mass conservation equation, where ζ is a constant of proportionality that has some relationship with the characteristic admittance, or $1/Z_{ac}$, (i.e., the inverse of the characteristic impedance) and has units of admittance.

If we define $k_s = \zeta/C$ and $k_d = 1/RC$, then Equation (1) can be written as:

$$\frac{dP_{res}}{dt} = k_s\left(P\left(t\right) - P_{res}\right) - k_d\left(P_{res} - P_{zf}\right) \quad (3)$$

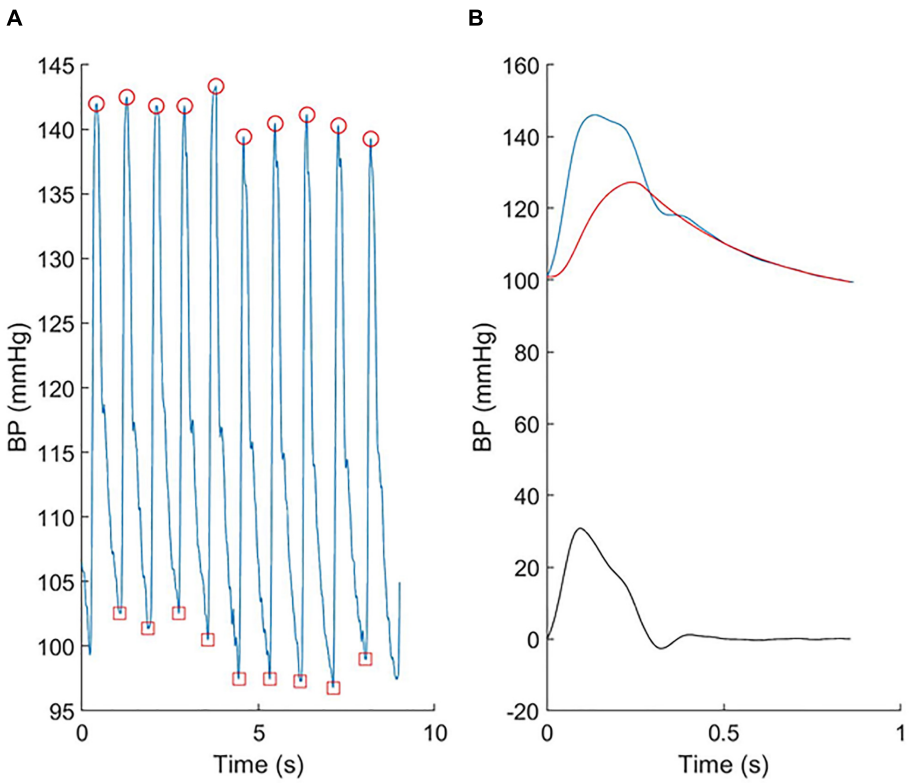

FIGURE 1 | An example showing **(A)** the individual radial pressure waveforms recorded using the tonometer and **(B)** the ensemble averaged central pressure (blue), reservoir pressure (red), and excess pressure (black).

P_{res} is given by a first-order linear differential equation:

$$P_{res} = e^{-(k_s+k_d)t}\int_0^t P(t')e^{(k_s+k_d)t'}dt' + \frac{k_d}{k_s+k_d}(1-e^{-(k_s+k_d)t})P_{zf} \quad (4)$$

which is solved in two steps (1) by fitting an exponential curve to the pressure during diastole to estimate the diastolic parameters k_d and P_{zf}, assuming aortic inflow is zero:

$$P_{res} - P_{zf} = (P_{res} - P_{zf})e^{-k_d t} \quad (5)$$

k_s is then estimated by minimizing the squared error between P and P_{res} obtained over diastole.

TABLE 1 | Characteristic of participants in the study comparing wave intensity estimated using aortic flow velocity waveforms compared with excess pressure (P_{xs}) (N = 12).

Variable	Mean/*N* (*SD*)/[%]
Age, y	65.7 (6.0)
Male sex, *N* [%]	12 [100]
Ethnicity, *N* [%]	
European	4 [33]
South Asian	8 [66]
Height, cm	169.1 (7.4)
Weight, kg	76.8 (13.1)
Diabetes, *N* [%]	5 [42]
Hypertension, *N* [%]	10 [83]
Systolic BP, mm Hg	147.8 (14.1)
Diastolic BP, mm Hg	88.3 (10.9)
Heart rate, min^{-1}	64.4 (10.8)
V_{max}, $cm.s^{-1}$	137.8 (16.9)
Time (V_{max}), s	0.09 (0.01)
P_{xs}, mm Hg	40.1 (8.5)
Time (P_{xs}), s	0.09 (0.01)

BP, blood pressure; P_{xs}, excess pressure; V_{max}, maximum aortic velocity.

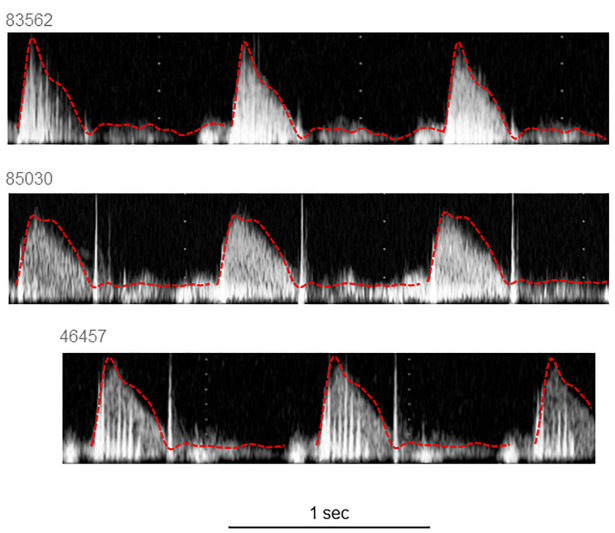

FIGURE 2 | Example traces of velocity measured in the left ventricular outflow tract with the respective P_{xs} superimposed. P_{xs} waveforms were scaled to correspond with the peak of the aortic flow waveform.

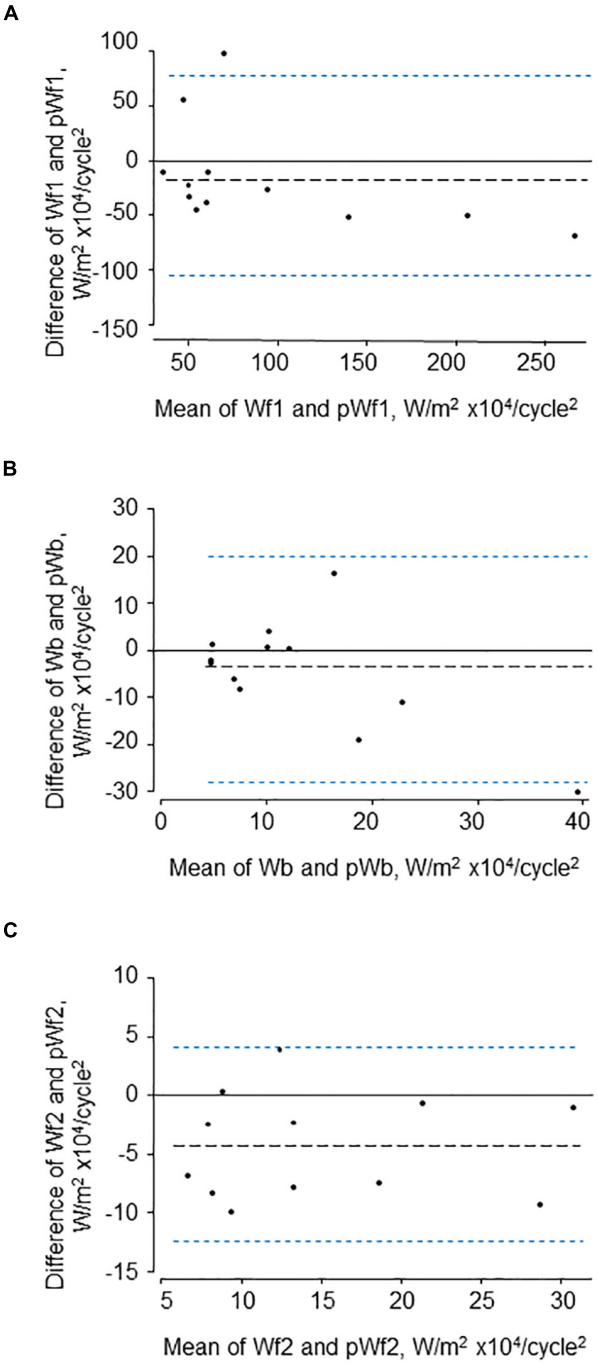

FIGURE 3 | Bland-Altman plots showing agreement between the three major waves **(A–C)** identified by traditional (Wf1, Wb, and Wf2) and pressure-only wave intensity analysis (pWf1, pWb, and pWf2).

TABLE 2 | Characteristic of participants in the reproducibility study (*N* = 34).

Variable	Mean/*N* (*SD*)/[%]
Age, y	69.8 (5.6)
Male sex, *N* [%]	26 [76]
Ethnicity, *N* [%]	
European	14 [41]
South Asian	11 [32]
African Caribbean	9 [27]
Height, cm	169.6 (9.8)
Weight, kg	79.8 (14.8)
Diabetes, *N* [%]	12 [35]
Hypertension, *N* [%]	23 [68]

Wave intensity (dI) is the total rate of working, i.e., the power, per unit cross-sectional area of an artery due to the pressure, P, with the blood flowing with velocity U. If flow velocity, $U = \frac{Q_{in}}{A}$ where A is the cross-sectional area of the aorta, and $\zeta \cdot A = \rho \cdot c$, where ρ is the density of blood (assumed to be 1,060 kg.m^{-3}) and c is the wave speed. Then

$$U = \frac{P_{xs}}{\rho \cdot c} \tag{6}$$

and

$$dI = dP \cdot dU = dP \cdot d\left(\frac{P_{xs}}{\rho \cdot c}\right) \tag{7}$$

If flow velocity is measured then c can be estimated from Equation (6). In addition to wave intensity, wave reflection index (WRI: the ratio of the area of the reflected wave to the early systolic incident wave), the ratio of peak forward to peak backward pressure (P_b/P_f) and the ratio of backward to total pressure, termed reflection index (RI) were also calculated (Westerhof et al., 2005).

For this analysis we chose *a priori* to use P_{xs} calculated from the estimated aortic (central) pressure waveform, as it was assumed to correspond more closely to aortic excess pressure. For the purposes of direct comparison with the conventional method P_{xs} was calibrated to the peak aortic flow in each individual, however, we also investigated the agreement when peak aortic velocity was assumed to be 1 m/s in all cases. All analyses were performed using custom written software in Matlab (R2019a, The Mathworks Inc.).

Repeatability and Reproducibility of Blood Pressure

Reproducibility (test-retest) data for reservoir pressure, P_{xs} and estimated wave intensity was performed on 34 participants [age 69.8 (*SD* = 5.6) years; 26 male] who attended on two occasions separated by an interval of approximately a month.

Statistical Analysis

Statistical analyses were performed using Stata 15.1 (StataCorp, College Station, Texas, United States). Continuous variables

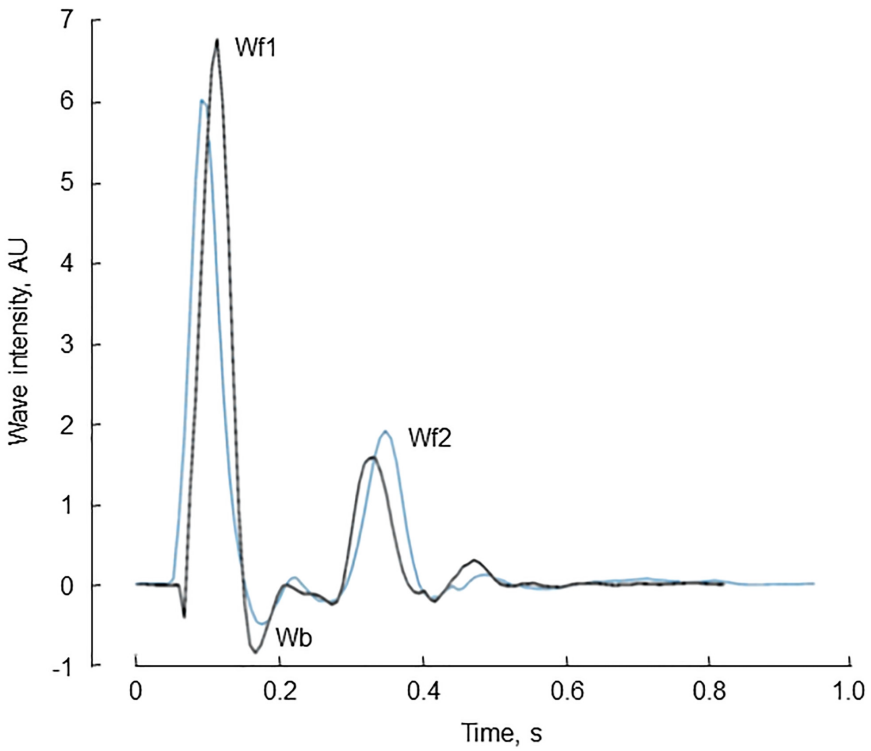

FIGURE 4 | An example of pressure-only wave intensity traces recorded from the same individual on two occasions ≈1 month apart [first visit (black) and second (repeat) visit (blue) traces]. The three major waves, Wf1, Wb, and Wf2 are indicated.

derived from the samples were summarized as mean ± SD. Reproducibility data were analyzed using Bland–Altman analysis and presented as mean differences with limits of agreement (LOA) (Bland and Altman, 2003). Concordance or reliability was summarized using Lin's concordance coefficient (rho) (Steichen and Cox, 2002) and was classified as: < 0.40 – poor; between 0.40 and < 0.59 – fair; between 0.60 and 0.74 – good, and > 0.75 – excellent (Cicchetti et al., 2006).

RESULTS

Comparison of Aortic Velocity Waveform With P_{xs}

The characteristics of the 12 participants in this study are shown in **Table 1**. Reservoir analysis was successful in all cases and the fits were excellent [r^2 for exponential fit in diastole = 0.98 (SD = 0.02)]. The P_{xs} waveforms agreed fairly closely with the LVOT flow velocity waveforms measured using ultrasound (**Figure 2** and **Supplementary Figure S1**) and there was evident correlation between the systolic upstroke of both waveforms. This was confirmed by the close agreement between the time of peak of P_{xs} and time of peak aortic flow velocity [mean difference = 0.00 (LOA −0.02, 0.02) s]. Wave intensity estimated using P_{xs} gave the typical pattern consisting of a large forward compression wave (Wf1) in early systole, followed by a small backward wave (Wb1 – reflected wave), and followed by a moderate sized forward decompression wave in protodiastole (Wf2). Bland Altman plots indicating the agreement between peak wave intensities for conventional WIA and pWIA are shown in **Figure 3** [mean difference Wf1 = −15 (LOA −106, 75) W/m^2 × 10^4/cycle^2, rho = 0.83; Wb = −49 (LOA −29, 19) W/m^2 × 10^4/cycle^2, rho = 0.42; −44 (LOA −13, 44) W/m^2 × 10^4/cycle^2, rho = 0.73]. When a constant peak aortic velocity of 1 m/s was assumed, the agreement was similar or only marginally worse (**Supplementary Figure S2**).

Reproducibility Study

The characteristics of the 34 participants in the reproducibility study are shown in **Table 2**. Reservoir fitting and wave intensity calculation failed quality control in 3 and 5 cases at visit 1 and 2, respectively (12% failure rate), largely due to poor quality tonometry traces. An example of test-retest recordings in a single individual (selected to have a difference in the forward compression wave similar to the average difference) is shown in **Figure 4**. Bland Altman plots of all intra-individual differences for the three major waves, Wf1, Wb, and Wf2 are shown in **Figure 5**). The reliability of wave intensity was good, except for Wf2 which was poor and showed evidence of correlation between the difference and the mean (r = 0.79). Results for other measures are shown in **Table 3**; most showed fair or good reliability.

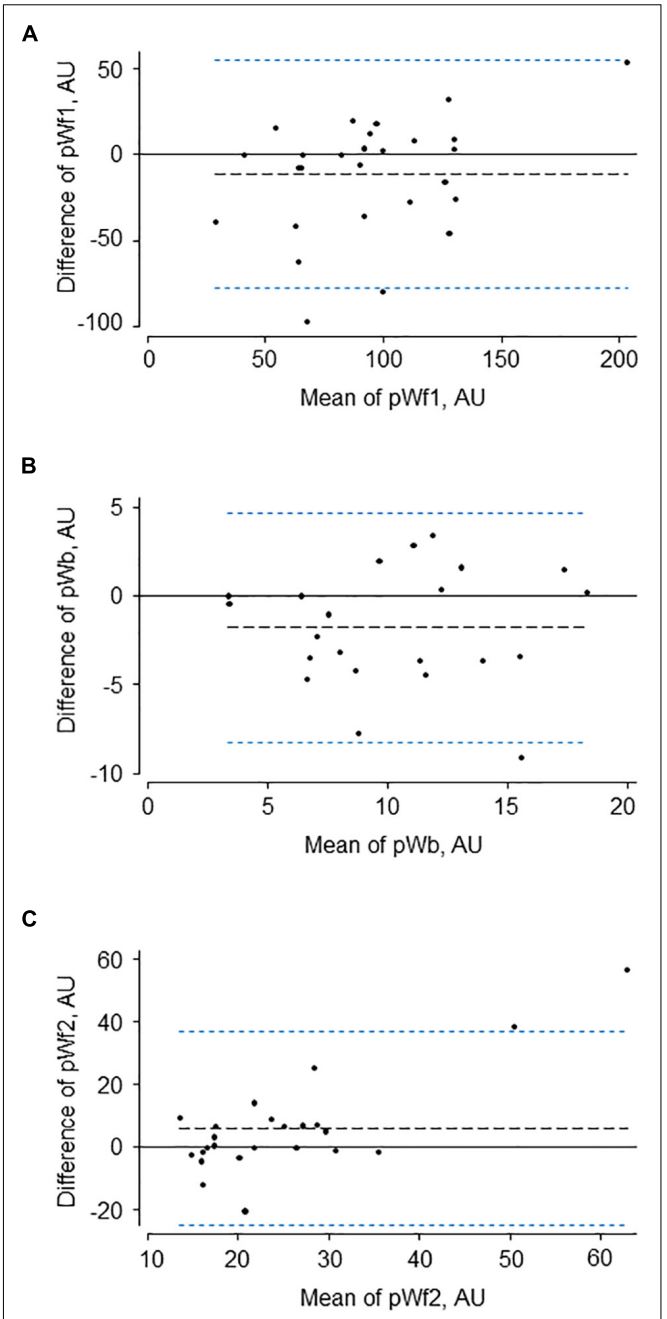

FIGURE 5 | Bland-Altman plots for test-retest data of the three major waves **(A–C)** identified by pressure-only wave intensity analysis (pWf1, pWb, and pWf2) calibrated to peak aortic velocity in each individual.

DISCUSSION

We found that the P_{xs} waveform is an acceptable surrogate of LVOT (aortic) flow velocity waveform, and, following calibration of the P_{xs} waveform, it was possible to calculate wave intensity patterns from recordings of the pressure waveform made at the radial artery without measurements of flow. Wave intensity and related parameters estimated in this way showed acceptable agreement with conventionally measured wave intensities and the reproducibility and reliability of pWIA was similar to or better than the reliability of systolic BP. The only exception was Wf2 which showed poor

TABLE 3 | Results and reproducibility of key parameters measured at 2 visits.

	Visit 1			Visit 2			Reproducibility				
Variables	***N***	**Mean**	***SD***	***N***	**Mean**	***SD***	**Mean difference**	**LOA**	**LOA**	**rho**	**Reliability grading**
Systolic BP, mm Hg	34	136.6	10.1	34	134.4	13.8	2.1	−23.5	27.7	0.42	Fair
Diastolic BP, mm Hg	34	82.7	10.0	34	80.8	8.7	1.9	−13.5	17.2	0.64	Good
Heart rate, bpm	34	63.4	9.6	34	61.1	9.9	2.3	−10.6	15.2	0.75	Excellent
maximum P_{res}, mm Hg	31	113.1	8.7	29	111.7	11.8	0.9	−19.4	21.2	0.48	Fair
maximum P_{xs}, mm Hg	31	36.4	9.1	29	36.1	10.1	0.3	−13.8	14.5	0.71	Good
Time maximum P_{xs}, s	31	0.10	0.01	29	0.10	0.01	0.00	−0.03	0.03	0.24	Poor
Time maximum BP, s	31	0.14	0.04	34	0.14	0.04	0.00	−0.09	0.09	0.39	Poor
k_s, s^{-1}	31	7.90	2.31	29	7.65	1.78	0.01	−3.73	3.80	0.55	Fair
k_d, s^{-1}	31	2.68	1.08	29	3.11	2.87	0.24	−1.55	2.02	0.54	Fair
P_{zf}, mm Hg	31	74.1	11.3	29	69.3	20.4	1.13	−16.8	19.1	0.66	Good
Wf1, AU	31	90	47	29	100	38	−11.6	−77.7	54.5	0.61	Good
Wb, AU	31	10	6	29	12	5	−1.8	−8.2	4.7	0.68	Good
Wf2, AU	31	29	19	29	21	8	6	−24.8	36.7	0.34	Poor
WRI	31	0.14	0.11	29	0.12	0.04	0.02	−0.17	0.21	0.44	Fair
P_b/P_f	31	0.72	0.04	29	0.71	0.04	0.00	−0.08	0.08	0.53	Fair
RI	31	0.42	0.01	29	0.42	0.01	0.00	−0.03	0.03	0.52	Fair

AU, arbitrary units; BP, blood pressure; k_d, diastolic rate constant; k_s, systolic rate constant; LOA, 95% limits of agreement; P_b/P_f, ratio of backward to forward pressure; P_{res}, reservoir pressure; P_{xs}, excess pressure; P_{zf}, estimated zero-flow pressure; rho, Lin's concordance coefficient; RI, reflection index; V_{max}, maximum aortic velocity; Wb, backward compression wave; Wf1, forward compression wave; Wf2, forward decompression wave; WRI, wave reflection index.

reliability; this may relate to the small size of this wave and the variability in duration of ejection which introduces noise into the ensemble average of the waveform in late systole. Improved methods of ensemble averaging might be useful if Wf2 were a parameter of particular interest in a given study.

The method used to derive the flow velocity waveform from the measured pressure has some similarities with the approach used to derive flow waveforms in the ARCSolver method, which is based on a 3-element Windkesel model plus a minimal work criterion (Hametner et al., 2013). The ARCSolver method has been reported to outperform a simple triangular flow assumption in terms of pressure separation (Hametner et al., 2013), and it has been used for wave intensity analysis in one study (Hametner et al., 2017), although we are not aware of any validation studies using this approach.

In our studies the observed wave intensity patterns using the pressure-only approach were very similar to those reported previously using invasive or non-invasive methods based on measurement of pressure (or diameter) and flow velocity (Parker and Jones, 1990; Koh et al., 1998; Niki et al., 1999; Zambanini et al., 2005; Bhuva et al., 2019). The major disadvantage of the current approach is the lack of absolute calibration in the absence of a flow velocity measure. In many studies peak aortic or LVOT peak flow velocity may be measured as part of the echocardiography protocol, and this can be used to calibrate P_{xs}. When the data were calibrated in this way the intensity of the waves agreed with those calculated using conventional methods and the values were similar to those previously reported in the literature allowing for differences in form of units (Koh et al., 1998; Niki et al., 1999; Zambanini et al., 2005; Bhuva et al., 2019). Thus it may not be necessary to record the entire aortic velocity waveform, the peak velocity appears sufficient. However, if there is no measure of aortic flow velocity the issue of calibration is more problematic. One possibility may be to use an assumed aortic flow velocity based on previous studies. Dalen et al. (2010) measured LVOT peak velocity in 1266 healthy participants in the Nord-Trøndelag Health (HUNT) study (663 female, age range < 30 to > 70 years); they found no convincing evidence of a relationship between age and peak LVOT velocity in either men or women. The average LVOT velocities in this study were 98 (*SD* = 18) $cm.s^{-1}$ in men and 101 (*SD* = 16) $cm.s^{-1}$ in women. Choi et al. (2016) reported findings from 1,003 healthy Korean adults (age 20–79 years). LVOT peak velocities were slightly higher in women [men = 96 (*SD* = 15) $cm.s^{-1}$ vs. women = 99 (*SD* = 16) $cm.s^{-1}$] and there was a small positive relationship between increased age and higher peak LVOT velocity (corresponding to ∼4 and 10 $cm.s^{-1}$ difference in peak velocity between age 21–30 and 71–80 in men and women, respectively). Previous smaller studies have reported that peak flow velocity in the LVOT shows little or no association with body size, sex, blood pressure, or body mass index (Gardin et al., 1987; van Dam et al., 1987; Swinne et al., 1996). This suggests that it might be possible, at least in individuals without established cardiac disease, to use an assumed peak aortic velocity to calibrate the P_{xs} waveform. Based particularly on the more recent large population studies in Norway and Korea (Dalen et al., 2010; Choi et al., 2016), ∼100 $cm{\cdot}s^{-1}$ seems a reasonable estimate for an assumed peak velocity in the LVOT, although a more detailed systematic review and meta-analysis on this question would be valuable.

Our study has several other limitations. It employs a small sample based on existing data using tonometry to record the

BP waveform and the approach requires further validation if it is to be used in future studies employing other methods to measure pressure waveforms. We have found that the method can also be applied to pressure waveforms captured using a cuff-based arm BP monitor (unpublished data) which could allow for more automated approaches and even the possibility of measurement of ambulatory 24 h wave intensity. The method could also be applied to invasive data where only pressure has been measured, for example in investigations of suspected pulmonary hypertension. While outside the scope of this article, it is noteworthy that a related approach could be used to estimate wave intensity in circumstances where only flow velocity was measured if accompanied by measurements of clinic BP.

In conclusion, use of the P_{xs} waveform as a surrogate of LVOT flow velocity, when appropriately scaled, permits estimation of aortic wave intensity based on non-invasive measurement of pressure waveforms. This technique shows acceptable reproducibility and should allow wider application of wave intensity analysis to large scale trials and observational studies.

DATA AVAILABILITY STATEMENT

The datasets generated for this study are available on request to the corresponding author.

ETHICS STATEMENT

The studies involving human participants were reviewed and approved by St Mary's Hospital Research Ethics Committee. The participants provided their written informed consent to participate in this study.

AUTHOR CONTRIBUTIONS

AH, NC, AR, JM, and KP contributed to conception and design of the study. CP and JM contributed to data analysis. AH performed the statistical analysis and wrote the first draft of the manuscript. All authors contributed to manuscript revision, and read and approved the submitted version.

FUNDING

The SABRE study was funded at baseline by the UK Medical Research Council (MRC), Diabetes UK, and the British Heart Foundation (BHF). The follow-up study in 2008 and 2011 was funded by the Wellcome Trust (Grant Nos. 067100, 37055891, and 086676/7/08/Z), the BHF (Grant Nos. PG/06/145, PG/08/103/26133, PG/12/29/29497, and CS/13/1/30327) and Diabetes UK (Grant No. 13/0004774). AH received support from the British Heart Foundation, the Economic and Social Research Council (ESRC), the National Institute on Aging, the National Institute for Health Research University College London Hospitals Biomedical Research Centre, the UK Medical Research Council and works in a unit that receives support from the Medical Research Council. CP was supported by a grant from the BHF (CS/15/6/31468). AR was supported by a grant from the BHF (PG/18/48/33832).

SUPPLEMENTARY MATERIAL

The Supplementary Material for this article can be found online at: https://www.frontiersin.org/articles/10.3389/fphys.2020.00550/full#supplementary-material

REFERENCES

Alberti, K. G., and Zimmet, P. Z. (1998). Definition, diagnosis and classification of diabetes mellitus and its complications. Part 1: diagnosis and classification of diabetes mellitus provisional report of a WHO consultation. *Diabet. Med.* 15, 539–553. doi: 10.1002/(SICI)1096-9136(199807)15:7<539::AID-DIA668>3.0.CO;2-S

Bhuva, A. N., D'Silva, A., Torlasco, C., Nadarajan, N., Jones, S., Boubertakh, R., et al. (2019). Non-invasive assessment of ventriculo-arterial coupling using aortic wave intensity analysis combining central blood pressure and phase-contrast cardiovascular magnetic resonance. *Eur. Heart J. Cardiovasc. Imaging* 9:jez227. doi: 10.1093/ehjci/jez227

Bland, J. M., and Altman, D. G. (2003). Applying the right statistics: analyses of measurement studies. *Ultrasound Obstet. Gynecol.* 22, 85–93. doi: 10.1002/uog.122

Broyd, C. J., Davies, J. E., Escaned, J. E., Hughes, A., and Parker, K. (2015). Wave intensity analysis and its application to the coronary circulation. *Glob. Cardiol. Sci. Pract.* 2015:64. doi: 10.5339/gcsp.2015.64

Caro, C. G., Pedley, T. J., Schroter, R. C., and Seed, W. A. (2012). *The Mechanics Of The Circulation*. New York, NY: Cambridge University Press.

Chiesa, S. T., Masi, S., Shipley, M. J., Ellins, E. A., Fraser, A. G., Hughes, A. D., et al. (2019). Carotid artery wave intensity in mid- to late-life predicts cognitive decline: the Whitehall II study. *Eur. Heart J.* 40, 2300–2309. doi: 10.1093/eurheartj/ehz189

Choi, J. O., Shin, M. S., Kim, M. J., Jung, H. O., Park, J. R., Sohn, I. S., et al. (2016). Normal echocardiographic measurements in a korean population study: part II. doppler and tissue doppler imaging. *J. Cardiovasc. Ultrasound* 24, 144–152. doi: 10.4250/jcu.2016.24.2.144

Cicchetti, D., Bronen, R., Spencer, S., Haut, S., Berg, A., Oliver, P., et al. (2006). Rating scales, scales of measurement, issues of reliability: resolving some critical issues for clinicians and researchers. *J. Nerv. Ment. Dis.* 194, 557–564. doi: 10.1097/01.nmd.0000230392.83607.c5

Dalen, H., Thorstensen, A., Vatten, L. J., Aase, S. A., and Stoylen, A. (2010). Reference values and distribution of conventional echocardiographic Doppler measures and longitudinal tissue Doppler velocities in a population free from cardiovascular disease. *Circ. Cardiovasc. Imaging* 3, 614–622. doi: 10.1161/CIRCIMAGING.109.926022

Davies, J. E., Hadjiloizou, N., Leibovich, D., Malaweera, A., Alastruey-Arimon, J., Whinnett, Z. I., et al. (2007). Importance of the aortic reservoir in determining the shape of the arterial pressure waveform – The forgotten lessons of Frank. *Artery Res.* 1, 40–45. doi: 10.1016/j.artres.2007.08.001

Davies, J. E., Lacy, P., Tillin, T., Collier, D., Cruickshank, J. K., Francis, D. P., et al. (2014). Excess pressure integral predicts cardiovascular events independent of other risk factors in the conduit artery functional evaluation substudy of anglo-scandinavian cardiac outcomes trial. *Hypertension* 64, 60–68. doi: 10.1161/HYPERTENSIONAHA.113.02838

Gardin, J. M., Davidson, D. M., Rohan, M. K., Butman, S., Knoll, M., Garcia, R., et al. (1987). Relationship between age, body size, gender, and blood pressure

and Doppler flow measurements in the aorta and pulmonary artery. *Am. Heart J.* 113, 101–109. doi: 10.1016/0002-8703(87)90016-0

Hametner, B., Parragh, S., Weber, T., and Wassertheurer, S. (2017). Wave intensity of aortic root pressure as diagnostic marker of left ventricular systolic dysfunction. *PLoS One* 12:e0179938. doi: 10.1371/journal.pone.0179938

Hametner, B., Wassertheurer, S., Kropf, J., Mayer, C., Holzinger, A., Eber, B., et al. (2013). Wave reflection quantification based on pressure waveforms alone–methods, comparison, and clinical covariates. *Comput. Meth. Prog. Biol.* 109, 250–259. doi: 10.1016/j.cmpb.2012.10.005

Hughes, A. D., and Parker, K. H. (2020). The modified arterial reservoir: an update with consideration of asymptotic pressure (P8) and zero-flow pressure (P∞). *medRxiv* [Preprint], doi: 10.1101/2020.01.22.20018440

Koh, T. W., Pepper, J. R., DeSouza, A. C., and Parker, K. H. (1998). Analysis of wave reflections in the arterial system using wave intensity: a novel method for predicting the timing and amplitude of reflected waves. *Heart Ves.* 13, 103–113. doi: 10.1007/Bf01747827

MacRae, J. M., Sun, Y. H., Isaac, D. L., Dobson, G. M., Cheng, C. P., Little, W. C., et al. (1997). Wave-intensity analysis: a new approach to left ventricular filling dynamics. *Heart Vessels* 12, 53–59. doi: 10.1007/BF02820867

Manisty, C., Mayet, J., Tapp, R. J., Parker, K. H., Sever, P., Poulter, N. R., et al. (2010). Wave reflection predicts cardiovascular events in hypertensive individuals independent of blood pressure and other cardiovascular risk factors: an ASCOT (Anglo-Scandinavian Cardiac Outcome Trial) substudy. *J. Am. Coll. Cardiol.* 56, 24–30. doi: 10.1016/j.jacc.2010.03.030

Michail, M., Narayan, O., Parker, K. H., and Cameron, J. D. (2018). Relationship of aortic excess pressure obtained using pressure-only reservoir pressure analysis to directly measured aortic flow in humans. *Physiol. Meas.* 39:64006. doi: 10.1088/1361-6579/aaca87

Mitchell, G. F. (2018). Aortic stiffness, pressure and flow pulsatility, and target organ damage. *J. Appl. Physiol.* 125, 1871–1880. doi: 10.1152/japplphysiol.00108.2018

Niki, K., Sugawara, M., Uchida, K., Tanaka, R., Tanimoto, K., Imamura, H., et al. (1999). A noninvasive method of measuring wave intensity, a new hemodynamic index: application to the carotid artery in patients with mitral regurgitation before and after surgery. *Heart Vessels* 14, 263–271. doi: 10.1007/BF03257237

Park, C. M., March, K., Ghosh, A. K., Jones, S., Coady, E., Tuson, C., et al. (2013). Left-ventricular structure in the Southall And Brent REvisited (SABRE) study: explaining ethnic differences. *Hypertension* 61, 1014–1020. doi: 10.1161/HYPERTENSIONAHA.111.00610

Parker, K. H. (2009). An introduction to wave intensity analysis. *Med. Biol. Eng. Comput.* 47, 175–188. doi: 10.1007/s11517-009-0439-y

Parker, K. H., and Jones, C. J. H. (1990). Forward and backward running waves in the arteries - analysis using the method of characteristics. *J. Biomech. Eng.* 112, 322–326. doi: 10.1115/1.2891191

Quinones, M. A., Otto, C. M., Stoddard, M., Waggoner, A., and Zoghbi, W. A. (2002). Recommendations for quantification of doppler echocardiography: a report from the doppler quantification task force of the nomenclature and standards committee of the american society of echocardiography. *J. Am. Soc. Echocardiogr.* 15, 167–184. doi: 10.1067/mje.2002.120202

Steichen, T. J., and Cox, N. J. (2002). A note on the concordance correlation coefficient. *Stata J.* 2, 183–189.

Su, J., Manisty, C., Parker, K. H., Simonsen, U., Nielsen-Kudsk, J. E., Mellemkjaer, S., et al. (2017). Wave intensity analysis provides novel insights into pulmonary arterial hypertension and chronic thromboembolic pulmonary hypertension. *J. Am. Heart Assoc.* 6:79. doi: 10.1161/JAHA.117.006679

Swinne, C. J., Shapiro, E. P., Jamart, J., and Fleg, J. L. (1996). Age-associated changes in left ventricular outflow tract geometry in normal subjects. *Am. J. Cardiol.* 78, 1070–1073. doi: 10.1016/s0002-9149(96)0054-545

Tillin, T., Forouhi, N. G., McKeigue, P. M., and Chaturvedi, N. (2012). Southall And Brent REvisited: Cohort profile of SABRE, a UK population-based comparison of cardiovascular disease and diabetes in people of European, Indian Asian and African Caribbean origins. *Int. J. Epidemiol.* 41, 33–42. doi: 10.1093/ije/dyq175

Tillin, T., Hughes, A. D., Mayet, J., Whincup, P., Sattar, N., Forouhi, N. G., et al. (2013). The relationship between metabolic risk factors and incident cardiovascular disease in Europeans, South Asians, and African Caribbeans: SABRE (Southall and Brent Revisited) – a prospective population-based study. *J. Am. Coll. Cardiol.* 61, 1777–1786. doi: 10.1016/j.jacc.2012.12.046

van Dam, I., Heringa, A., de Boo, T., Alsters, J., van Oort, A., Hopman, J., et al. (1987). Reference values for pulsed Doppler signals from the blood flow on both sides of the aortic valve. *Eur. Heart J.* 8, 1221–1228. doi: 10.1093/oxfordjournals.eurheartj.a062196

Vermeersch, S. J., Rietzschel, E. R., De Buyzere, M. L., Van Bortel, L. M., Gillebert, T. C., Verdonck, P. R., et al. (2009). The reservoir pressure concept: the 3-element windkessel model revisited? Application to the asklepios population study. *J. Eng. Math.* 64, 417–428. doi: 10.1007/s10665-009-9286-y

Wang, J. J., O'Brien, A. B., Shrive, N. G., Parker, K. H., and Tyberg, J. V. (2003). Time-domain representation of ventricular-arterial coupling as a windkessel and wave system. *Am. J. Physiol. Heart Circ. Physiol.* 284, H1358–H1368. doi: 10.1152/ajpheart.00175.2002

Westerhof, N., Stergiopulos, N., and Noble, M. I. M. (2005). *Snapshots of Hemodynamics : An Aid For Clinical Research And Graduate Education*. New York, NY: Springer.

Zambanini, A., Cunningham, S. L., Parker, K. H., Khir, A. W., Mc, G. T. S. A., and Hughes, A. D. (2005). Wave-energy patterns in carotid, brachial, and radial arteries: a noninvasive approach using wave-intensity analysis. *Am. J. Physiol. Heart Circ. Physiol.* 289, H270–H276. doi: 10.1152/ajpheart.00636.2003

Conflict of Interest: The authors declare that the research was conducted in the absence of any commercial or financial relationships that could be construed as a potential conflict of interest.

frontiers in Physiology

ORIGINAL RESEARCH
published: 09 June 2020
doi: 10.3389/fphys.2020.00591

Increased Serum Klotho With Age-Related Aortic Stiffness and Peripheral Vascular Resistance in Young and Middle-Aged Swine

*Xiaomei Guo and Ghassan S. Kassab**

California Medical Innovations Institute, San Diego, CA, United States

The anti-aging function of Klotho gene has been implicated in age-related diseases. The physiological importance of Klotho in the progression of arterial stiffness with aging, however, remains unclear. The goal of this study is to determine the correlation of circulating Klotho with early age-related aortic stiffening and peripheral hemodynamics. We measured serum Klotho levels in a group of pigs with age ranges of 1.5–9 years and investigated the relationship between Klotho levels and biomarkers of aortic stiffening with aging, including aortic pulse wave velocity (PWV), augmentation index (AIx), and pulse pressure (PP). The effects of aortic stiffening on peripheral vascular resistance, compliance, and function were also evaluated. We found that increased aortic stiffness occurred at middle age (>5 years old), as evidenced by an increase in PWV and AIx ($p < 0.001$), but with no changes in blood pressure and PP. With advancing age, increased femoral vascular resistance positively correlated with aortic PWV and AIx ($p < 0.01$). No significant difference in endothelium function and arterial compliance for femoral and small peripheral arteries was observed between young and middle-aged groups. The serum Klotho levels were lower in young and higher in middle-aged pigs ($p < 0.001$), and a positive correlation was found between Klotho and aortic PWV, AIx, and femoral vascular resistance ($p < 0.01$). Our findings suggest that early-aged aortic stiffening has adverse effect on peripheral hemodynamics, independent of blood pressure levels. Elevated Klotho secretion was associated with increased aortic stiffness and peripheral vascular resistance with aging.

Keywords: Klotho, aging, aortic stiffness, vascular resistance, femoral artery

OPEN ACCESS

Edited by:
Adelaide De Vecchi,
King's College London,
United Kingdom

Reviewed by:
Bradley S. Fleenor,
Ball State University,
United States
Stefano Tarantini,
University of Oklahoma
Health Sciences Center,
United States

***Correspondence:**
Ghassan S. Kassab
gkassab@calmi2.org

Specialty section:
This article was submitted to Vascular Physiology, a section of the journal Frontiers in Physiology

Received: *06 March 2020*
Accepted: *11 May 2020*
Published: *09 June 2020*

Citation:
Guo X and Kassab GS (2020) Increased Serum Klotho With Age-Related Aortic Stiffness and Peripheral Vascular Resistance in Young and Middle-Aged Swine. Front. Physiol. 11:591. doi: 10.3389/fphys.2020.00591

INTRODUCTION

It is well known that aging is a potent, independent risk factor for cardiovascular disease (Greenwald, 2007; Mitchell et al., 2007). In response to aging, the central elastic arteries become progressively stiffer and their ability to absorb pulsations from the ejecting ventricle is reduced (Avolio et al., 1985; Kelly et al., 1989). Enormous epidemiological research has demonstrated that aortic stiffening increases pulsatile hemodynamic forces, which may exert a detrimental effect on peripheral vascular function, invoking a mechanism linking increased arterial stiffness to the age-related disorders (James et al., 1995; Mitchell et al., 2005).

Although a marked age-related increase in aortic stiffness has been confirmed in normal subjects before 60 years of age (Mitchell et al., 2004, 2007), it is unclear whether peripheral vascular resistance and function change in response to early aortic aging. Hence, one goal of this study is to determine the relationship between early age-related aortic stiffening and peripheral hemodynamics in young and middle-aged swine.

Klotho gene was originally identified as an anti-aging protein, which encodes a single-pass transmembrane glycoprotein (Kuro-o et al., 1997; Shiraki-Iida et al., 1998). It is produced mainly in the kidney and the soluble form of Klotho is cleaved and released in the blood, urine, and cerebrospinal fluid (Imura et al., 2004; Moe and Drueke, 2008). In a transgenic mouse model, overexpression of Klotho by genetic manipulation of full-length Klotho resulted in a significant extension of life span (Kurosu et al., 2005). The deletion of Klotho gene in mice led to a premature aging syndrome (Kuro-o et al., 1997). In humans, circulating levels of soluble Klotho decrease with age (Xiao et al., 2004), and emerging evidence suggests that Klotho concentration is closely correlated to the development of cardiovascular disease (Semba et al., 2011; Hu et al., 2013) and chronic kidney disease (CKD) (Akimoto et al., 2012; Asai et al., 2012). Although the anti-aging function of Klotho in human aging and age-related disorders has been implicated (Xiao et al., 2004; Hu et al., 2013; Koyama et al., 2015), the biological role of circulating Klotho in the progression of arterial stiffness with the aging process has not yet been elucidated. The second goal of this study is to investigate the associations of serum Klotho with aortic stiffness and peripheral vascular resistance during aging from young to middle age in swine.

In this study, we chose swine as the experimental subject since swine is considered an ideal preclinical model due to the anatomical and physiological similarities in the cardiovascular system between swine and human (Swindle and Smith, 1998). We measured the serum Klotho concentrations in young and middle-aged swine and explored the possible connection between the serum Klotho level and signs of arterial stiffening with aging, including aortic pulse wave velocity (PWV), augmentation index (AIx), and pulse pressure (PP). The effects of early age-related aortic stiffening on peripheral vascular resistance, compliance, and function were also evaluated.

MATERIALS AND METHODS

Experimental Animals

A total of 36 female Yucatan miniature pigs were divided into a young group (n = 18) with age ranges of 1.5–5 years and a middle-aged group (n = 18) with age ranges of 5.5–9 years (defined as middle age according to a life span of 15 years for Yucatan miniature swine). All animals were fed a standard swine diet (Teklad diet 7037, Envigo, Somerset, NJ) twice daily, and the amount of diet provided was 1% of the body weight of the pigs. All animal experiments were performed in accordance with national and local ethical guidelines, including the Institute of Laboratory Animal Research guidelines, Public Health Service policy, and the Animal Welfare Act, as approved by the Institutional Animal Care and Use Committee at California Medical Innovations Institute, San Diego.

Blood Pressure Measurements and Pulse Wave Analysis

Pigs were fasted for 12 h prior to surgery and pre-anesthetized with TKX (Telazol 10 mg/kg, Ketamine 5 mg/kg, and Xylazine 5 mg/kg, i.m). Pigs were then anesthetized with 2–3% isoflurane inhalation. Ventilation with 100% O_2 was provided with a respirator and maintained PCO_2 at approximately 35 mmHg. Under fluoroscopic guidance (Philips Fluoroscopy System), an introducer sheath (6 Fr) was percutaneously inserted into the jugular vein for administration of 0.9% saline and heparin (100 IU/kg). A sheath (5 Fr) was used to introduce a catheter into the aortic arch (proximal site) *via* the carotid artery. Another sheath (5 Fr) was used to introduce a catheter into the abdominal aorta (distal site) *via* the right femoral artery. Those catheters were connected to a pressure transducer (PowerLab, ADInstruments Inc.). The thoracic (aorta arch) and abdominal aortic blood pressure waveforms were recorded from these two locations simultaneously during the procedure. The femoral blood pressure waveform was also recorded with a catheter placement at the left femoral artery *via* an introducer sheath (4 Fr).

Pulse wave analysis was applied to determine aortic stiffness. PWV calculation is based on the difference in arrival times of the pressure wave at the proximal (aorta arch) and distal (abdominal aorta) locations. Since the tips of pressure catheters placed on the proximal and distal sites are visible on radiographs, the propagation distance was obtained by measuring the distance between the two catheters. PWV (m/s) was calculated by dividing the propagation distance by the difference between the two arrival times (transit time). AIx is expressed as the difference between the second and first systolic peaks of central aortic waveform calculated as a percentage of PP.

Femoral Flow Measurement and Analysis (Echocardiography)

The measurement of femoral blood flow velocity was obtained in all animals using an iE33 duplex ultrasonography (Philips, Andover, MA) equipped with L15-7 transducer. The mean velocity waveforms were recorded continuously for 6 s for further analysis. The diameter of the femoral artery was also recorded by B-mode imaging. According to the flow velocity waveforms, femoral flow volume (ml/min) was calculated from the time-averaged mean flow velocity and the arterial diameter. Femoral vascular resistance (mmHg/ml/min) was calculated by dividing the mean arterial pressure by the flow volume. After flow measurement, the femoral artery and a small peripheral artery (muscular branch of femoral artery with diameter 300–500 μm) were harvested for endothelial function and mechanical testing. Animal was then euthanized with a saturated solution of potassium chloride injection through the jugular vein to arrest the heart under deep anesthesia.

Endothelial Function

An isovolumic myograph was used to evaluate the endothelium-dependent vasorelaxation (Lu et al., 2011). Briefly, the segments from femoral and small peripheral arteries were cannulated on both ends in a physiological bath with HEPES physiologic saline solution (HEPES-PSS, concentration in mmol/l: 142 NaCl, 4.7 KCl, 2.7 sodium HEPES, 3 HEPES acid, 0.15 $NaHPO_4$, 1.17 $MgSO_4$, 2.79 $CaCl_2$, and 5.5 glucose, solution gassed by 95% O_2 plus 5% CO_2). Both vessels segments were stretched to *in situ* length and preloaded at the physiological pressure of 80 mmHg. The pressure and external diameter were measured with a pressure transducer (Mikro-Tip SPR-524; Millar Instruments) and a digital diameter tracking (DiamTrak v3+; Australia), respectively. The vessel segment was pre-constricted with phenylephrine (PE) by a series of doses (10^{-10}–10^{-5} mol/L in the PSS), and then relaxed with acetylcholine (ACh) by a series of doses: 10^{-10}–10^{-5} mol/L. The endothelium-independent relaxation to sodium nitroprusside (SNP, 10^{-5} mol/L) was measured to verify the sensitivity of vascular smooth muscle to nitric oxide (NO). The overall contractility of vessel was tested with potassium chloride (KCl) at 60 mmol/L. Contraction was expressed as percentage of the response to KCl. Relaxation was expressed as percentage of pre-contraction to PE.

Mechanical Tests

The femoral and small peripheral arterial segments were cannulated on both ends and fully relaxed in Ca^{2+} free HEPES-PSS. The arterial segment was preconditioned with five cyclic changes in pressure from 0 to 180 mmHg. The pressure was then increased in 20 mmHg step increments from 20 to 180 mmHg in a staircase manner. The passive pressure (P)-diameter (D) relation was recorded. The lumen cross-sectional area (CSA) was computed from the lumen diameter (D), as $CSA = \pi D^2/4$. The area compliance (C_{CSA}) of the artery was determined by the slope of the pressure-CSA relationship, i.e., $C_V = \Delta CSA/\Delta P$ as described in a previous publication (Guo et al., 2014).

Serum Klotho Level

Blood samples were collected in ethylenediaminetetraacetic acid (EDTA) tubes for all experimental pigs. After centrifugation at 5,000 rpm and 4°C for 15 min, serum was immediately separated and stored at −80°C until analysis. The circulating level of Klotho in the serum was measured by a Klotho ELISA kit (IBL Co. Ltd., Minneapolis, MN) according to the manufacturer's guideline.

Statistical Analysis

Results were shown as mean ± standard error of mean (mean ± SEM). Statistical analysis was performed using SigmaStat (Systat Software, California, USA). The significance of the differences between young and middle-age groups was evaluated by either *t*-test or one-way ANOVA. Multiple linear regression analysis was used to estimate the correlations between age and the study variables. Spearman's correlation test was used to estimate the correlations between Klotho level and the study variables. Significant differences between the dose-dependent groups for endothelial function testing were determined by two-way ANOVA. The results were considered statistically significant when $p < 0.05$ (2-tailed).

RESULTS

The mean age, body weight, hemodynamic parameters, and serum Klotho level were presented and compared between young and middle-aged groups in **Table 1**. The mean age is 3.5 ± 0.3 years (range of 1.5–5 years) for the young group and 7.2 ± 0.3 years (range of 5.5–9 years) for the middle-aged group. The two study groups have comparable values of body weight and heart rate. There was no between-groups difference in PP, systolic blood pressure (SBP), diastolic blood pressure (DBP), and mean arterial pressure (MAP) in thoracic and abdominal aortic pressure measures. **Figure 1** shows a positive correlation of aortic PWV and AIx with age ($p < 0.001$) by using linear regression analysis. Aortic PWV and AIx was significantly increased in middle-aged group as compared to young group ($p < 0.001$). No correlation was found between blood pressure and PP with age (data not shown).

There was no significant difference in PP, SBP, DBP, and MAP in the femoral pressure measures between young and middle-aged groups (**Table 1**). No difference in diameter of

TABLE 1 | Comparison of age, weight, hemodynamic parameters and serum Klotho levels between young and middle-aged pigs.

Variables	Young (n = 18)	Middle-aged (n = 18)	p
Age (years)	3.5 ± 0.3	7.2 ± 0.3	**<0.001**
Body weight (kg)	112.8 ± 3.3	116.3 ± 3.0	0.415
Heart rate (beats/min)	74.8 ± 2.5	71.3 ± 2.3	0.31
Thoracic aortic blood pressure (mmHg)			
Mean pressure	81.3 ± 2.7	77.0 ± 4.2	0.369
Systolic pressure	101.1 ± 2.6	97.6 ± 4.5	0.475
Diastolic pressure	71.3 ± 2.9	66.8 ± 4.1	0.333
Pulse pressure	29.7 ± 1.5	30.8 ± 1.4	0.592
Abdominal aortic blood pressure (mmHg)			
Mean pressure	78.7 ± 2.6	75.0 ± 4.1	0.411
Systolic pressure	105.8 ± 2.9	101.1 ± 4.9	0.372
Diastolic pressure	66.1 ± 2.7	62.9 ± 3.9.	0.36
Pulse pressure	39.7 ± 2.0	38.6 ± 2.4	0.805
Aortic PWV (m/s)	5.4 ± 0.1	7.7 ± 0.3	**<0.001**
Aortic AIx (%)	12.8 ± 1.2	21.7 ± 1.1	**<0.001**
Femoral blood pressure (mmHg)			
Mean pressure	70.8 ± 3.0.	72.8 ± 3.7	0.648
Systolic pressure	90.6 ± 4.3	92.7 ± 5.1	0.741
Diastolic pressure	60.8 ± 2.5	61.1 ± 3.6	0.952
Pulse pressure	29.8 ± 2.2	31.6 ± 2.4	0.559
Femoral artery diameter (mm)	4.02 ± 0.1	4.07 ± 0.5	0.727
Femoral mean flow rate (ml/min)	394.2 ± 21.1	277.1 ± 16.2	**<0.001**
Femoral vascular resistance (mmHg/ml/min)	0.19 ± 0.01	0.27 ± 0.017	**0.002**
Serum Klotho levels (pg/ml)	809.8 ± 193.6	2158.4 ± 164.5	**<0.001**

Values are mean ± SEM.
Bold values are presented when p <0.05.

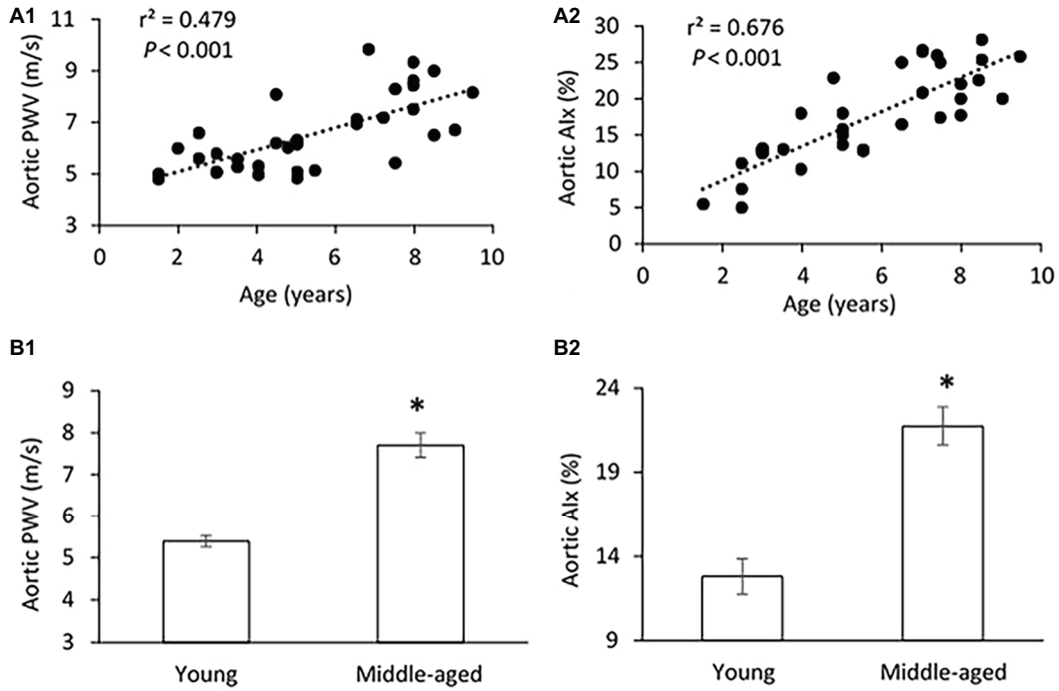

FIGURE 1 | (A) Correlations of aortic pulse wave velocity (PWV) **(A1)** and augmentation index (AIx) **(A2)** with age. The linear regression analysis was conducted, and data are expressed as correlation coefficients and significance levels (r^2; p). **(B)** Comparison of aortic PWV **(B1)** and AIx **(B2)** between young and middle-aged pigs. Data corresponds to means ± standard error of mean (mean ± SEM). $p < 0.05$, when compared to young group.

femoral artery was seen between these two groups. **Figure 2** shows the correlation between vascular resistance and mean flow of femoral artery with age. The femoral vascular resistance was significantly increased ($p < 0.01$), whereas mean flow was significantly decreased ($p < 0.01$) in middle-aged as compared to young group. A linear relationship was observed between femoral vascular resistance and mean flow with age ($p < 0.001$). With regards to aortic stiffness, aortic PWV, and AIx were positively correlated with femoral vascular resistance ($p < 0.01$) and negatively correlated with femoral mean flow ($p < 0.01$) as shown in **Figure 3**.

Compliance of arteries was presented as the pressure-cross-sectional area (P-CSA) relationship of the femoral artery and small peripheral artery. Although the middle-aged group has lower values of CSA compliance in both femoral and small peripheral arteries as compared to the young group (**Figure 4**), the differences are not statistically significant.

Figure 5A shows the correlation between serum Klotho level and age. The mean Klotho level of the middle-aged group was significantly higher than that of the young-aged group (2,158.4 ± 164.5 vs. 809.8 ± 193.6 pg/ml, $p < 0.001$). The Spearman's correlation test confirms that the serum Klotho level was positively correlated with age within the age ranges of 1.5–9 years ($p < 0.001$). There was a significantly positive correlation between serum Klotho levels and PWV ($p < 0.001$) and AIx ($p = 0.001$) as shown in **Figure 5B**. In **Figure 5C**, the Klotho level was also positively associated with femoral vascular resistance ($p < 0.001$), but slightly inversely correlated with femoral flow ($p = 0.005$). There was no apparent correlation of Klotho levels with aortic and femoral blood pressure and PP (data not shown).

Vascular endothelial function was evaluated by *ex-vivo* PE pre-contractile endothelium-dependent vasorelaxation. No significant difference in the vascular contractions to PE for both femoral and small peripheral arteries was observed between young and middle-age groups as shown in **Figure 6A**. For the femoral artery segment (4.04 ± 0.3 mm in diameter), the endothelium-dependent vasodilation in response to ACh was similar in middle-age groups compared with young group (**Figure 6B1**). For the small peripheral artery (410 ± 30 μm in diameter), the vasodilation to ACh in middle-age group tended to decrease, but the change was not significantly different from the young group ($p = 0.08$, **Figure 6B2**). In middle-aged group, the vascular contraction to KCl at 60 mmol/L did not show significant difference as compared to the young group for both femoral and small peripheral arteries (**Figure 6C1**). There was no significant difference in the maximal responses of endothelium-independent vasodilation to SNP at 10^{-5} mol/L between young and middle-aged groups for both arteries (**Figure 6C2**).

DISCUSSION

To our knowledge, this is the first study of the relation between Klotho and aortic stiffness and associated peripheral hemodynamics in swine. The major findings are as follows: (1) aortic PWV and AIx had a significant positive correlation

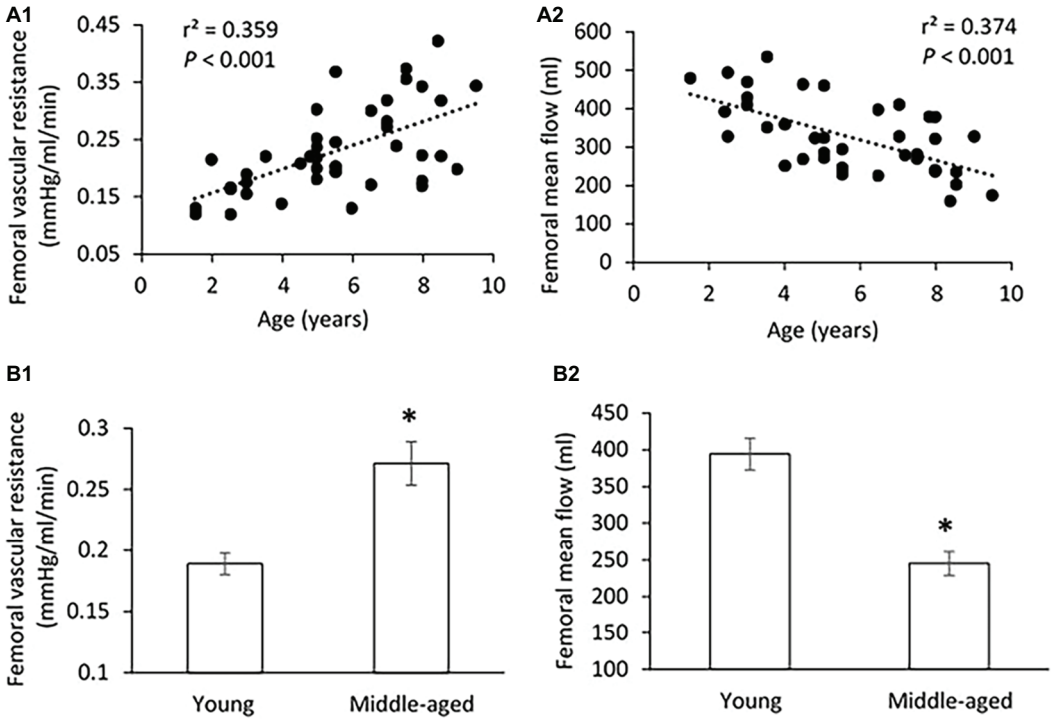

FIGURE 2 | (A) Correlations of femoral vascular resistance **(A1)** and mean flow **(A2)** with age. The linear regression analysis was conducted, and data are expressed as correlation coefficients and significance levels (r^2; p). **(B)** Comparison of femoral vascular resistance **(B1)** and mean flow **(B2)** between young and middle-aged pigs. Data corresponds to means ± SEM. $p < 0.05$, when compared to young group.

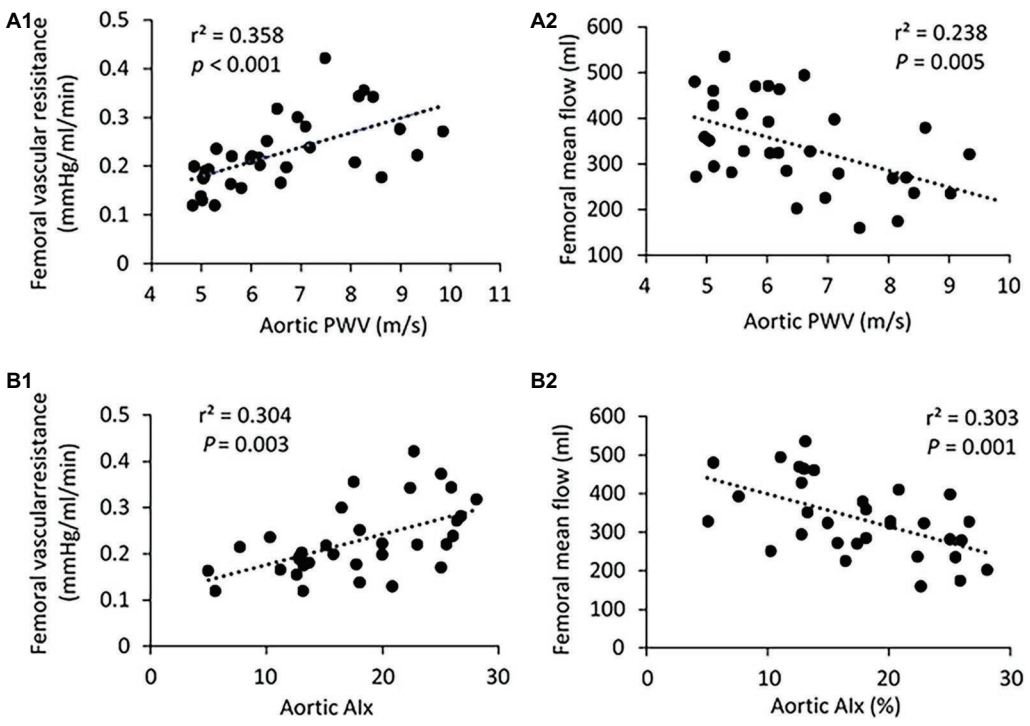

FIGURE 3 | (A) Correlation of aortic PWV with femoral vascular resisitance **(A1)** and mean flow **(A2)**. **(B)** Correlation of aortic AIx with femoral vascular resisitance **(B1)** and mean flow **(B2)**. The linear regression analysis was conducted, and data are expressed as correlation coefficients and significance levels (r^2; p).

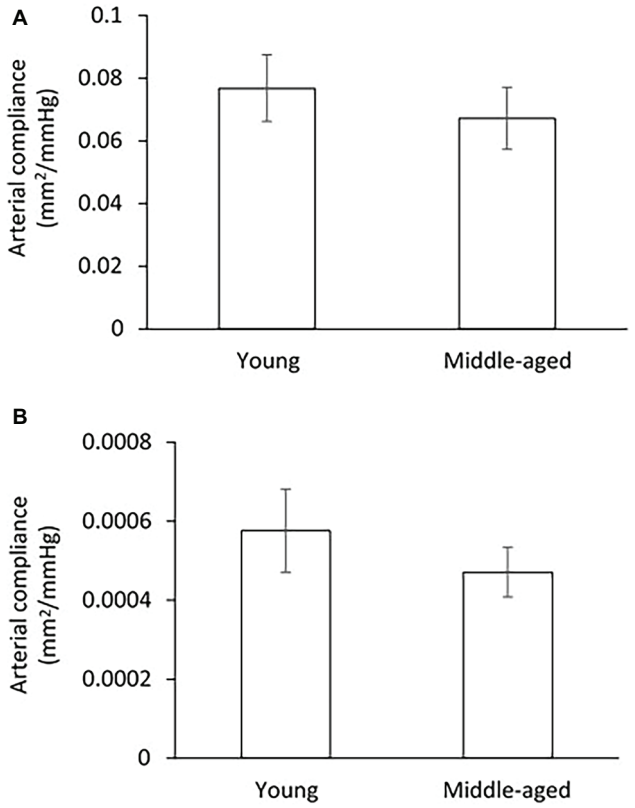

FIGURE 4 | Comparison of arterial compliance for femoral artery **(A)** and small peripheral artery **(B)** between young and middle-aged pigs. Data corresponds to means ± SEM.

with age in a group of pigs 1.5–9 years old; (2) mean aortic and femoral blood pressure, and PP did not differ between young (≤5 years) and middle age (>5 years) groups; (3) with advancing age, increased femoral vascular resistance, and decreased femoral flow were associated with aortic stiffening but with no changes in femoral endothelium function and arterial compliance; and (4) serum Klotho levels were lower in young and higher in middle-aged pigs, and positively correlated with aortic PWV, AI, and femoral vascular resistance.

Age-related arterial stiffening has emerged as an independent risk factor for cardiovascular events, including hypertension (Izzo, 2004), myocardial infarction (Mattace-Raso et al., 2006), diabetes (Cruickshank et al., 2002), heart failure (Chae et al., 1999), and stroke (Laurent et al., 2003). There is substantial evidence that aortic PWV and AIx predict cardiovascular morbidity and mortality in humans (Vlachopoulos et al., 2010). PWV represents the speed of a pressure wave propagating down a blood vessel, whereas AIx is a measure of the contribution made by the reflected pressure wave to the ascending aortic pressure waveform; both of which provide a measure of systemic arterial stiffness (Safar and London, 2000; Cecelja and Chowienczyk, 2012). Here, we found that aortic PWV and AIx significantly increased with age in 1.5–9 years old pigs. It has been extensively documented that arterial stiffness increases throughout the normal human life span (Mitchell et al., 2007) and is a major determinant of increased systolic and pulse pressure with advancing age (Kelly et al., 1989; Dernellis and Panaretou, 2005). In the middle-aged pigs, however, PP and SBP were not increased when compared with the younger pigs despite an increase in aortic stiffness. This result is consistent with some clinical observations that most of the age-related increase in PP occurs in elderly individuals (age > 60 years) and not in younger populations (Burt et al., 1995; Franklin et al., 1999). Although our data demonstrated that aging exerts a negative influence on aortic stiffness (raised PWV and AIx), even at middle age in healthy swine, whether age-related aortic stiffening precedes the development of elevated PP and/or SBP in elderly swine (>9 years old) is not known. This is a limitation of the current study because no swine older than 9 years were available from the vendors during the period of the experiment.

To answer the question of whether early aortic aging affects the hemodynamics of peripheral vasculature, we measured the vascular resistance, mean flow, and arterial compliance of femoral artery (average of 4.04 ± 0.3 mm in diameter range 3.2–4.8 mm) for all experimental pigs. We also measured the arterial compliance of small peripheral artery (average of 410 ± 30 μm in diameter range 308–520 μm). In a previous large community-based population study, without established hypertension or advanced vascular disease, a modest rise in forearm vascular resistance was reported to be related to increased aortic stiffness (Mitchell et al., 2005). Here, we found a marked increase in femoral vascular resistance with advancing age. It is reasonable to speculate that increasing peripheral vascular resistance in response to aortic stiffening would functionally reduce local flow, which was exhibited in middle-aged group as compared to young group by the use of ultrasonography measurements. To assess the relations between aortic stiffness and peripheral hemodynamics, we found that the femoral vascular resistance was positively correlated with the aortic PWV and AIx, indicating that early age-related aortic stiffening, even at normotensive PP or blood pressure levels, may have adverse influences on peripheral hemodynamics. In addition, arterial compliance, defined as the changes in luminal dimension (CSA) divided by the corresponding change in pressure, is conventionally thought to be a surrogate marker of arterial elasticity (Cohn et al., 2004). Our data showed no obvious changes in femoral and small peripheral arterial compliance between young and middle-aged groups, meaning a sustained peripheral arterial elasticity in ages 1.5–9 years of pigs. Similar results have been obtained in Framingham Heart Studies that the compliance or distensibility of large muscular arteries (i.e., femoral) is maintained at normal levels or changed relatively little despite an accelerated aortic stiffness with age (van der Heijden-Spek et al., 2000; Mitchell et al., 2004).

Dysfunction of the vascular endothelium has been associated with high blood pressure and arterial stiffening (Puddu et al., 2000; Safar et al., 2001). We examined the endothelium of femoral artery and found no evidence of endothelial dysfunction since comparable endothelium-dependent vasodilation to ACh was shown between young and middle-aged groups.

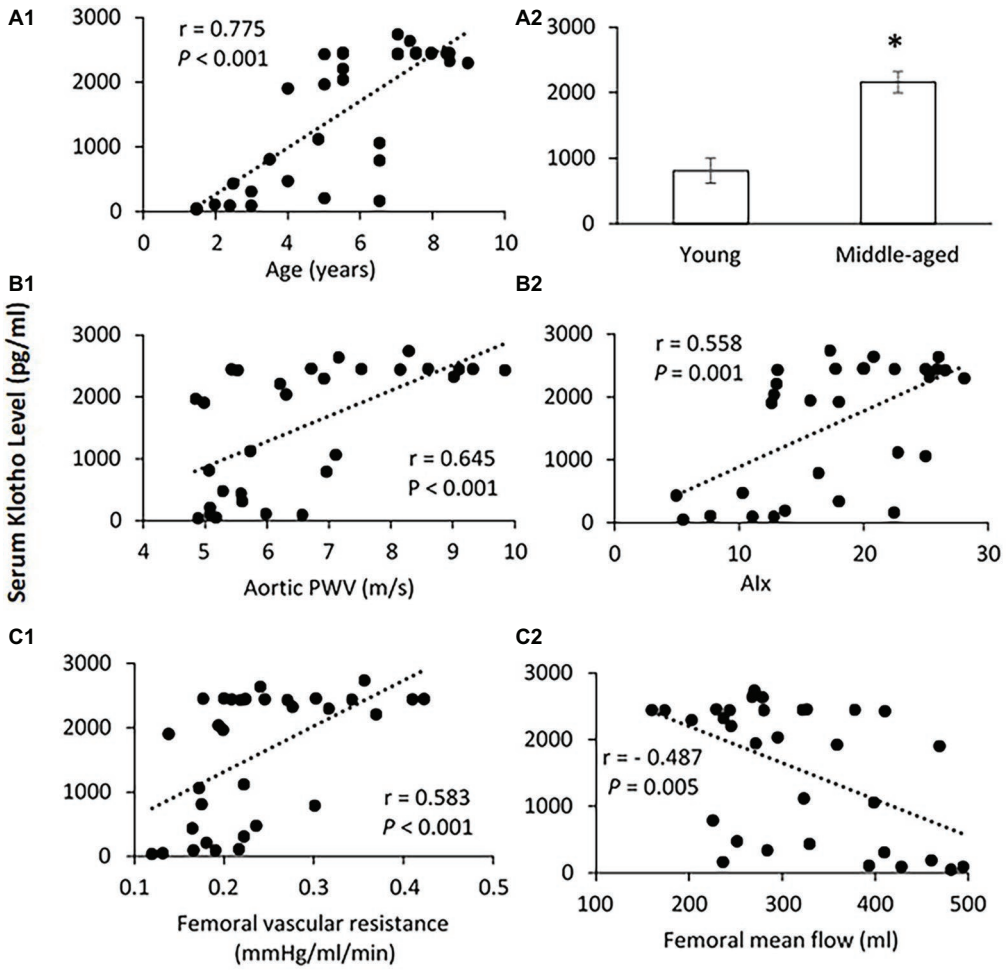

FIGURE 5 | (A) Correlation of serum Klotho level with age **(A1)** and the mean levels of serum Klotho **(A2)** in young and middle-aged pigs. Data corresponds to means ± SEM. $p < 0.05$, when compared to young group. **(B)** Correlations of serum Klotho levels with aortic PWV **(B1)** and AIx **(B2)**. **(C)** Correlations of serum Klotho levels with femoral vascular resistance **(C1)** and mean flow **(C2)**. The Spearman's correlation test was conducted, and data are expressed as correlation coefficients and significance levels (r; p).

For the small peripheral artery, although the vasodilation to ACh in middle-aged group has a descending trend, the change is not statistically significant compared with the young group ($p = 0.08$). There are emerging data that aortic stiffening may trigger remodeling, rarefaction, or hypertrophy in the microcirculation, leading to increased peripheral vascular resistance to blood flow (James et al., 1995; Liao et al., 2004). Several studies have provided direct evidence that functional and structural impairment of cerebral microcirculation are present in age-related cognitive decline (Toth et al., 2017) and Alzheimer's disease (Csiszar et al., 2017). The current study only exhibited a downward trend in vascular function of peripheral muscular arteries with diameter >300 μm, we do not know whether abnormalities in microvasculature (<150 μm in diameter; Levy et al., 2001) occurs during the early-aged aortic stiffening, and whether microvascular dysfunction contributes to the increased peripheral vascular resistance in middle-aged swine. The mechanisms implicating the microcirculation need to be addressed in future studies.

Klotho is an aging suppressor gene whose protective properties are critical for a proper function of many tissues and organs (Kuro-o et al., 1997; Hu et al., 2013). A recent study by Semba et al. (2011) suggested that raised levels of Klotho were related to the lower prevalence of cardiovascular disease. More clinical research has reported that a deficiency of Klotho may be an early biomarker for CKD (Akimoto et al., 2012; Asai et al., 2012) and acute kidney injury (Hu et al., 2010). In this study, surprisingly, we found that the serum Klotho level was significantly increased in middle-aged group as compared to young group. Moreover, a positive relationship between Klotho level and age was seen in ages from 1.5 to 9 years of pigs. This result is contrary to the findings from human studies that circulating Klotho concentrations decreased remarkably with age (range of 0.1–88 years; Xiao et al., 2004; Yamazaki et al., 2010). Recently, Klotho protein was found to be expressed in human aorta (Lim et al., 2012) and coronary artery (Richter et al., 2016), which protects against endothelial dysfunction by increasing

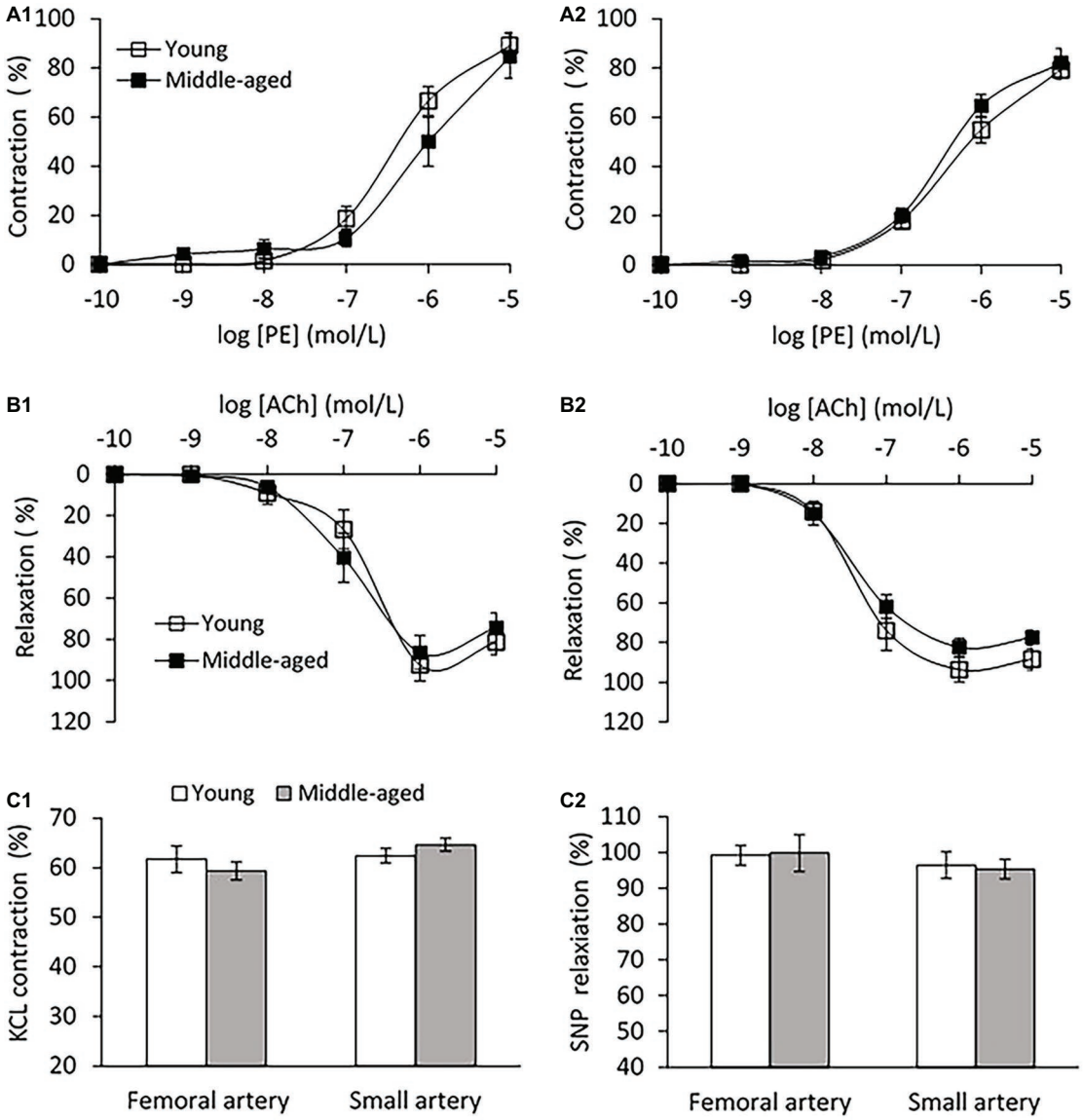

FIGURE 6 | (A) Vascular contraction to phenylephrine (PE) in femoral artery **(A1)** and small peripheral artery **(A2)** between young and middle-aged pigs. **(B)** PE pre-contractile endothelium-dependent vasodilation to acetylcholine (ACh) in femoral artery **(B1)** and small peripheral artery **(B2)** between young and middle-aged pigs. **(C)** Vascular contraction to potassium chloride (KCL) at 60 mmol/L **(C1)** and maximal response of vasodilation to sodium nitroprusside (SNP) at 10^{-5} mol/L **(C2)** between young and middle-aged pigs in femoral and small peripheral artery. Data corresponds to means ± SEM.

nitric oxide production (Saito et al., 1998, 2000). Moreover, the supplementation of exogenous Klotho attenuates oxidative stress, inflammation, and fibrosis by the inhibition of insulin/insulin-like growth factor-1 (IGF-1) and transforming growth factor-1 (TGF-1) signaling pathways to protect the vasculature and cardiac tissue (Yamamoto et al., 2005; Dalton et al., 2017; Takenaka et al., 2017). It is possible that an increase in serum Klotho level at middle age could be a compensatory response to the increased aortic stiffness with age to maintain endothelium function and arterial compliance of peripheral arterial system. Similar adaptive mechanism has been proposed by Paula et al. (2016) who observed an augmented level of Klotho in patients with myocardial infarction to ameliorate cardiac hypertrophy and remodeling. To the best of our knowledge, this study is the first to measure circulating Klotho concentrations with aging in swine, where species variations could be a potential factor that accounts for the different response of Klotho to advancing age between human and swine. The Spearman's correlation analysis of our data showed that serum Klotho level was positively correlated with aortic PWV, AIx, and femoral vascular resistance, but not with blood pressure and PP. Our results confirmed a positive correlation of serum Klotho levels with age in young to middle-aged swine. Completion of further studies with the involvement of elderly swine (>9 years) is necessary to explore the pathophysiological mechanisms of serum Klotho fluctuation with advancing age.

Whether Klotho gene provides vascular protection *via* upregulated Klotho production during early aortic aging remains to be determined as well.

There are limitations in the present study. Several clinical studies have reported that female is more susceptible to age-related cardiovascular events compared with male (Merz and Cheng, 2016; Rodgers et al., 2019). Here, we only focused on female swine with a range in ages 1.5–9 years. We did not evaluate sex variation in changes of serum Klotho and aortic stiffness with aging since no male swine >2 years old (and no female >9 years) were available from the vendors. It is recognized that different blood- and/or tissue-based biomarkers such as interleukin-6 (IL-6), tumor necrosis factor α (TNFα), and insulin-like growth factor 1 (IGF-1) are involved in vascular changes during aging (Tarantini et al., 2016; Justice et al., 2018). Most recently, a geroscience-guided clinical trial has suggested that the systematic evaluation of multi-biomarkers may be the best approach to clarify the biologic hallmarks of aging in human research (Justice et al., 2018). The current study, however, solely assessed a single blood-based biomarker "Klotho" which may not be able to reflect the complex and multifactorial processes underlying aging. In addition, we did not directly test the effect of serum Klotho on the aortic stiffness and peripheral vascular resistance. Hence, we cannot conclude any cause-and-effect relation. Our findings indicate an association between circulating Klotho and early age-related aortic stiffening and peripheral hemodynamics in swine.

In summary, early age-related aortic stiffening, even at normotensive PP or blood pressure levels, leads to functional alterations in peripheral hemodynamics, evidenced by increased femoral vascular resistance and reduced local flow. Elevated Klotho secretion with aging is associated with an increase in aortic stiffness and peripheral vascular resistance. Our findings support that aortic stiffening (increased PWV and AI) may be an early manifestation of aging. More research is required to investigate how Klotho interacts with the mechanisms of arterial stiffness in old swine. These studies serve as fundamental reference for the swine translational model in understanding human disease and testing of potential therapeutics.

DATA AVAILABILITY STATEMENT

The raw data supporting the conclusions of this article are available on request to the corresponding author.

ETHICS STATEMENT

The animal study was reviewed and approved by Institutional Animal Care and Use Committee at California Medical Innovations Institute, San Diego.

AUTHOR CONTRIBUTIONS

XG conducted the experiments. XG collected and analyzed the data. XG and GK designed the experiments and revised the manuscript.

FUNDING

This research was funded in part by 3DT Holdings. GK is the founder of 3DT Holdings.

REFERENCES

Akimoto, T., Shiizaki, K., Sugase, T., Watanabe, Y., Yoshizawa, H., Otani, N., et al. (2012). The relationship between the soluble Klotho protein and the residual renal function among peritoneal dialysis patients. *Clin. Exp. Nephrol.* 16, 442–447. doi: 10.1007/s10157-011-0582-2

Asai, O., Nakatani, K., Tanaka, T., Sakan, H., Imura, A., Tanaka, T., et al. (2012). Decreased renal a-Klotho expression in early diabetic nephropathy in humans and mice and its possible role in urinary calcium excretion. *Kidney Int.* 81, 539–547. doi: 10.1038/ki.2011.423

Avolio, A. P., Deng, F. Q., Li, W. Q., Luo, Y. F., Huang, Z. D., Xing, L. F., et al. (1985). Effects of ageing on arterial distensibility in populations with high and low prevalence of hypertension: comparison between urban and rural communities in China. *Circulation* 71, 202–210. doi: 10.1161/01.CIR.71.2.202

Burt, V. L., Whelton, P., Roccella, E. J., Brown, C., Cutler, J. A., Higgins, M., et al. (1995). Prevalence of hypertension in the US adult population. Results from the Third National Health and Nutrition Examination Survey, 1988–1991. *Hypertension* 25, 305–313. doi: 10.1161/01.HYP.25.3.305

Cecelja, M., and Chowienczyk, P. (2012). Role of arterial stiffness in cardiovascular disease. *JRSM Cardiovasc. Dis.* 1:cvd.2012.012016. doi: 10.1258/cvd.2012.012016

Chae, C. U., Pfeffer, M. A., Glynn, R. J., Mitchell, G. F., Taylor, J. O., and Hennekens, C. H. (1999). Increased pulse pressure and risk of heart failure in the elderly. *JAMA* 281, 634–639. doi: 10.1001/jama.281.7.634

Cohn, J. N., Quyyumi, A. A., Hollenberg, N. K., and Jamerson, K. A. (2004). Surrogate markers for cardiovascular disease: functional markers. *Circulation* 109(Suppl 1), 31–34. doi: 10.1161/01.CIR.0000133442.99186.39

Cruickshank, K., Riste, L., Anderson, S. G., Wright, J. S., Dunn, G., and Gosling, R. G. (2002). Aortic pulse-wave velocity and its relationship to mortality in diabetes and glucose intolerance: an integrated index of vascular function? *Circulation* 106, 2085–2090. doi: 10.1161/01.CIR.0000033824.02722.F7

Csiszar, A., Tarantini, S., Fülöp, G. A., Kiss, T., Valcarcel-Ares, M. N., Galvan, V., et al. (2017). Hypertension impairs neurovascular coupling and promotes microvascular injury: role in exacerbation of Alzheimer's disease. *Geroscience* 39, 359–372. doi: 10.1007/s11357-017-9991-9

Dalton, G. D., Xie, J., An, S., and Huang, C. (2017). New insights into the mechanism of action of soluble Klotho. *Front. Endocrinol.* 8:323. doi: 10.3389/fendo.2017.00323

Dernellis, J., and Panaretou, M. (2005). Aortic stiffness is an independent predictor of progression to hypertension in nonhypertensive subjects. *Hypertension* 45, 426–431. doi: 10.1161/01.HYP.0000157818.58878.93

Franklin, S. S., Khan, S. A., Wong, N. D., Larson, M. G., and Levy, D. (1999). Is pulse pressure useful in predicting risk of coronary heart disease? *Circulation* 100, 354–360. doi: 10.1161/01.CIR.100.4.354

Greenwald, S. (2007). Ageing of the conduit arteries. *J. Pathol.* 211, 157–172. doi: 10.1002/path.2101

Guo, X., Lu, X., Yang, J., and Kassab, G. S. (2014). Increased aortic stiffness elevates pulse and mean pressure and compromises endothelial function in Wistar rats. *Am. J. Physiol. Heart Circ. Physiol.* 307, H880–H887. doi: 10.1152/ajpheart.00265.2014

Hu, M. C., Shiizaki, K., Kuro-o, M., and Moe, O. W. (2013). Fibroblast growth factor 23 and Klotho: physiology and pathophysiology of an endocrine

network of mineral metabolism. *Annu. Rev. Physiol.* 75, 503–533. doi: 10.1146/annurev-physiol-030212-183727

Hu, M. C., Shi, M., Zhang, J., Quiñones, H., Kuro-o, M., and Moe, O. W. (2010). Klotho deficiency is an early biomarker of renal ischemia-reperfusion injury and its replacement is protective. *Kidney Int.* 78, 1240–1251. doi: 10.1038/ki.2010.328

Imura, A., Iwano, A., Tohyama, O., Tsuji, Y., Nozaki, K., Hashimoto, N., et al. (2004). Secreted Klotho protein in sera and CSF: implication for post-translational cleavage in release of Klotho protein from cell membrane. *FEBS Lett.* 565, 143–147. doi: 10.1016/j.febslet.2004.03.090

Izzo, J. L. Jr. (2004). Arterial stiffness and the systolic hypertension syndrome. *Curr. Opin. Cardiol.* 19, 341–352. doi: 10.1097/01.hco.0000126581.89648.10

James, M. A., Watt, P. A., Potter, J. F., Thurston, H., and Swales, J. D. (1995). Pulse pressure and resistance artery structure in the elderly. *Hypertension* 26, 301–306. doi: 10.1161/01.HYP.26.2.301

Justice, J. N., Ferrucci, L., Newman, A. B., Aroda, V. R., Bahnson, J. L., Divers, J., et al. (2018). A framework for selection of blood-based biomarkers for geroscience-guided clinical trials: report from the TAME Biomarkers Workgroup. *Geroscience* 40, 419–436. doi: 10.1007/s11357-018-0042-y

Kelly, R. P., Hayward, C., Avolio, A. P., and O'Rourke, M. F. (1989). Noninvasive determination of age-related changes in the human arterial pulse. *Circulation* 80, 1652–1659. doi: 10.1161/01.CIR.80.6.1652

Koyama, D., Sato, Y., Aizawa, M., Maki, T., Kurosawa, M., Kuro-o, M., et al. (2015). Soluble αKlotho as a candidate for the biomarker of aging. *Biochem. Biophys. Res. Commun.* 467, 1019–1025. doi: 10.1016/j.bbrc.2015.10.018

Kuro-o, M., Matsumura, Y., Aizawa, H., Kawaguchi, H., Suga, T., Utsugi, T., et al. (1997). Mutation of the mouse Klotho gene leads to a syndrome resembling ageing. *Nature* 390, 45–51. doi: 10.1038/36285

Kurosu, H., Yamamoto, M., Clark, J. D., Pastor, J. V., Nandi, A., Gurnani, P., et al. (2005). Suppression of aging in mice by the hormone Klotho. *Science* 308, 1829–1833. doi: 10.1126/science.1112766

Laurent, S., Katsahian, S., Fassot, C., Tropeano, A. I., Gautier, I., Laloux, B., et al. (2003). Aortic stiffness is an independent predictor of fatal stroke in essential hypertension. *Stroke* 34, 1203–1206. doi: 10.1161/01.STR.0000065428.03209.64

Levy, B. I., Ambrosio, G., Pries, A. R., and Struijker-Boudier, H. A. (2001). Microcirculation in hypertension: a new target for treatment? *Circulation* 104, 735–740. doi: 10.1161/hc3101.091158

Liao, D., Wong, T. Y., Klein, R., Jones, D., Hubbard, L., and Sharrett, A. R. (2004). Relationship between carotid artery stiffness and retinal arteriolar narrowing in healthy middle-aged persons. *Stroke* 35, 837–842. doi: 10.1161/01.STR.0000120310.43457.AD

Lim, K., Lu, T. S., Molostvov, G., Lee, C., Lam, F. T., Zehnder, D., et al. (2012). Vascular Klotho deficiency potentiates the development of human artery calcification and mediates resistance to fibroblast growth factor 23. *Circulation* 125, 2243–2255. doi: 10.1161/CIRCULATIONAHA.111.053405

Lu, X., Guo, X., Wassall, C. D., Kemple, M. D., Unthank, J. L., and Kassab, G. S. (2011). Reactive oxygen species cause endothelial dysfunction in chronic flow overload. *J. Appl. Physiol.* 110, 520–527. doi: 10.1152/japplphysiol.00786.2009

Mattace-Raso, F. U., van der Cammen, T. J., Hofman, A., van Popele, N. M., Bos, M. L., Schalekamp, M. A., et al. (2006). Arterial stiffness and risk of coronary heart disease and stroke: the Rotterdam Study. *Circulation* 113, 657–663. doi: 10.1161/CIRCULATIONAHA.105.555235

Merz, A. A., and Cheng, S. (2016). Sex differences in cardiovascular ageing. *Heart* 102, 825–831. doi: 10.1136/heartjnl-2015-308769

Mitchell, G. F., Guo, C. Y., Benjamin, E. J., Larson, M. G., Keyes, M. J., Vita, J. A., et al. (2007). Cross-sectional correlates of increased aortic stiffness in the community: the Framingham Heart Study. *Circulation* 115, 2628–2636. doi: 10.1161/CIRCULATIONAHA.106.667733

Mitchell, G. F., Parise, H., Benjamin, E. J., Larson, M. G., Keyes, M. J., Vita, J. A., et al. (2004). Changes in arterial stiffness and wave reflection with advancing age in healthy men and women: the Framingham Heart Study. *Hypertension* 43, 1239–1245. doi: 10.1161/01.HYP.0000128420.01881.aa

Mitchell, G. F., Vita, J. A., Larson, M. G., Parise, H., Keyes, M. J., Warner, E., et al. (2005). Cross-sectional relations of peripheral microvascular function, cardiovascular disease risk factors, and aortic stiffness: the Framingham Heart Study. *Circulation* 112, 3722–3728. doi: 10.1161/CIRCULATIONAHA.105.551168

Moe, S. M., and Drueke, T. (2008). Improving global outcomes in mineral and bone disorders. *Clin. J. Am. Soc. Nephrol.* 3, S127–S130. doi: 10.2215/CJN.04331206

Paula, R. S., Souza, V. C., Machado-Silva, W., Almeida, B. R., Daros, A. C., Gomes, L., et al. (2016). Serum Klotho (but not haplotypes) associate with the post-myocardial infarction status of older adults. *Clinics* 71, 725–732. doi: 10.6061/clinics/2016(12)09

Puddu, P., Puddu, G. M., Zaca, F., and Muscari, A. (2000). Endothelial dysfunction in hypertension. *Acta Cardiol.* 55, 221–232. doi: 10.2143/AC.55.4.2005744

Richter, B., Haller, J., Haffner, D., and Leifheit-Nestler, M. (2016). Klotho modulates FGF23-mediated NO synthesis and oxidative stress in human coronary artery endothelial cells. *Pflugers Arch.* 468, 1621–1635. doi: 10.1007/s00424-016-1858-x

Rodgers, J. L., Jones, J., Bolleddu, S. I., Vanthenapalli, S., Rodgers, L. E., Shah, K., et al. (2019). Cardiovascular risks associated with gender and aging. *J. Cardiovasc. Dev. Dis.* 6:19. doi: 10.3390/jcdd6020019

Safar, M., Chamiot-Clerc, P., Dagher, G., and Renaud, J. F. (2001). Pulse pressure, endothelium function, and arterial stiffness in spontaneously hypertensive rats. *Hypertension* 38, 1416–1421. doi: 10.1161/hy1201.096538

Safar, M. E., and London, G. M. (2000). Therapeutic studies and arterial stiffness in hypertension: recommendations of the European Society of Hypertension. The Clinical Committee of Arterial Structure and Function. Working Group on Vascular Structure and Function of the European Society of Hypertension. *J. Hypertens.* 18, 1527–1535. doi: 10.1097/00004872-200018110-00001

Saito, Y., Nakamura, T., Ohyama, Y., Suzuki, T., Iida, A., Shiraki-Iida, T., et al. (2000). *In vivo* Klotho gene delivery protects against endothelial dysfunction in multiple risk factor syndrome. *Biochem. Biophys. Res. Commun.* 276, 767–772. doi: 10.1006/bbrc.2000.3470

Saito, Y., Yamagishi, T., Nakamura, T., Ohyama, Y., Aizawa, H., Suga, T., et al. (1998). Klotho protein protects against endothelial dysfunction. *Biochem. Biophys. Res. Commun.* 248, 324–329. doi: 10.1006/bbrc.1998.8943

Semba, R. D., Cappola, A. R., Sun, K., Bandinelli, S., Dalal, M., Crasto, C., et al. (2011). Plasma Klotho and mortality risk in older community-dwelling adults. *J. Gerontol. A Biol. Sci. Med. Sci.* 66, 794–800. doi: 10.1093/gerona/glr058

Shiraki-Iida, T., Aizawa, H., Matsumura, Y., Sekine, S., Iida, A., Anazawa, H., et al. (1998). Structure of the mouse Klotho gene and its two transcripts encoding membrane and secreted protein. *FEBS Lett.* 424, 6–10. doi: 10.1016/S0014-5793(98)00127-6

Swindle, M. M., and Smith, A. C. (1998). Comparative anatomy and physiology of the pig. *Scand. J. Lab. Anim. Sci.* 25(Suppl 1), 1–10.

Takenaka, T., Kobori, H., Inoue, T., Miyazaki, T., Suzuki, H., Nishiyama, A., et al. (2017). Klotho supplementation attenuates blood pressure and oxidative stress in diabetes. *J. Hypertens.* 35:e38. doi: 10.1097/01.hjh.0000523076.42214.98

Tarantini, S., Giles, C. B., Wren, J. D., Ashpole, N. M., Valcarcel-Ares, M. N., Wei, J. Y., et al. (2016). IGF-1 deficiency in a critical period early in life influences the vascular aging phenotype in mice by altering miRNA mediated post-transcriptional gene regulation: implications for the developmental origins of health and disease hypothesis. *Age* 38, 239–258. doi: 10.1007/s11357-016-9943-9

Toth, P., Tarantini, S., Csiszar, A., and Ungvari, Z. (2017). Functional vascular contributions to cognitive impairment and dementia mechanisms and consequences of cerebral autoregulatory dysfunction, endothelial impairment, and neurovascular uncoupling in aging. *Am. J. Physiol. Heart Circ. Physiol.* 312, H1–H20. doi: 10.1152/ajpheart.00581.2016

van der Heijden-Spek, J. J., Staessen, J. A., Fagard, R. H., Hoeks, A. P., Boudier, H. A., and Van Bortel, L. M. (2000). Effect of age on brachial artery wall properties differs from the aorta and is gender dependent: a population study. *Hypertension* 35, 637–642. doi: 10.1161/01.HYP.35.2.637

Vlachopoulos, C., Aznaouridis, K., and Stefanadis, C. (2010). Prediction of cardiovascular events and all-cause mortality with arterial stiffness: a systematic review and meta-analysis. *J. Am. Coll. Cardiol.* 55, 1318–1327. doi: 10.1016/j.jacc.2009.10.061

Xiao, N. M., Zhang, Y. M., Zheng, Q., and Gu, J. (2004). Klotho is a serum factor related to human aging. *Chin. Med. J.* 117, 742–747. doi: 10.3760/cma.j.issn.0366-6999.2004.05.123

Yamamoto, M., Clark, J. D., Pastor, J. V., Gurnani, P., Nandi, A., Kurosu, H., et al. (2005). Regulation of oxidative stress by the anti-aging hormone Klotho. *J. Biol. Chem.* 280, 38029–38034. doi: 10.1074/jbc.M509039200

Yamazaki, Y., Imura, A., Urakawa, I., Shimada, T., Murakami, J., Aono, Y., et al. (2010). Establishment of sandwich ELISA for soluble alpha-Klotho measurement: age-dependent change of soluble alpha-Klotho levels in healthy subjects. *Biochem. Biophys. Res. Commun.* 398, 513–518. doi: 10.1016/j.bbrc.2010.06.110

Conflict of Interest: GK is the founder of 3DT Holdings. GK had the involvement with the study design and preparation of the manuscript.

The remaining author declares that the research was conducted in the absence of any commercial or financial relationships that could be construed as a potential conflict of interest.

frontiers in Cardiovascular Medicine

ORIGINAL RESEARCH
published: 07 August 2020
doi: 10.3389/fcvm.2020.00133

Usefulness of Proximal Coronary Wave Speed for Wave Intensity Analysis in Diseased Coronary Vessels

Lorena Casadonte[1], *Jan Baan Jr.*[2], *Jan J. Piek*[2] *and Maria Siebes*[3]*

[1] Department of Biomedical Engineering and Physics, Amsterdam UMC, Amsterdam Cardiovascular Sciences, University of Amsterdam, Amsterdam, Netherlands, [2] Department of Cardiology, Amsterdam UMC, Amsterdam Cardiovascular Sciences, University of Amsterdam, Amsterdam, Netherlands, [3] Department of Translational Physiology, Amsterdam UMC, Amsterdam Cardiovascular Sciences, University of Amsterdam, Amsterdam, Netherlands

OPEN ACCESS

Edited by:
Jonathan Paul Mynard, Murdoch Childrens Research Institute, Royal Children's Hospital, Australia

Reviewed by:
Ashraf Khir, Brunel University London, United Kingdom
Jack Lee, King's College London, United Kingdom

***Correspondence:**
Maria Siebes
m.siebes@amsterdamumc.nl

Specialty section:
This article was submitted to Cardiovascular Imaging, a section of the journal Frontiers in Cardiovascular Medicine

Received: *08 January 2020*
Accepted: *29 June 2020*
Published: *07 August 2020*

Citation:
Casadonte L, Baan J Jr, Piek JJ and Siebes M (2020) Usefulness of Proximal Coronary Wave Speed for Wave Intensity Analysis in Diseased Coronary Vessels. Front. Cardiovasc. Med. 7:133. doi: 10.3389/fcvm.2020.00133

Background: Wave speed is needed to separate net wave intensity into forward and backward traveling components. However, wave speed in diseased coronary arteries cannot be assessed from hemodynamic measurements obtained distal to a stenosis. Wave speed inherently depends on arterial wall properties which should be similar proximal and distal to a stenosis. Our hypothesis is that proximal wave speed can be used to separate net wave intensity obtained distal to a stenosis.

Methods: We assessed coronary wave speed using the sum-of-squares single-point technique (SPc) based on simultaneous intracoronary pressure and flow velocity measurements in human coronary arteries. SPc at resting flow was determined in diseased coronary vessels of 12 patients both proximal and distal to the stenosis. In seven of these vessels, distal measurements were additionally obtained after revascularization by stent placement. SPc was also assessed at two axial locations in 14 reference vessels without a stenosis.

Results: (1) No difference in SPc was present between proximal and distal locations in the reference vessels. (2) In diseased vessels with a focal stenosis, SPc at the distal location was paradoxically larger than SPc proximal to the stenosis (28.4 ± 3.7 m/s vs. 18.3 ± 1.8 m/s, $p < 0.02$), despite the lower distending pressure downstream of the stenosis. The corresponding separated wave energy tended to be underestimated when derived from SPc at the distal compared with the proximal location. (3) After successful revascularization, SPc at the distal location no longer differed from SPc at the proximal location prior to revascularization (21.9 ± 2.0 m/s vs. 20.8 ± 1.9 m/s, $p = 0.48$). Accordingly, no significant difference in separated wave energy was observed for forward or backward waves.

Conclusion: In diseased coronary vessels, SPc assessed from distal hemodynamic signals is erroneously elevated. Our findings suggest that proximal wave speed can be used to separate wave intensity profiles obtained downstream of a stenosis. This approach may extend the application of wave intensity analysis to diseased coronary vessels.

Keywords: wave intensity analysis, wave speed, coronary artery disease, hemodynamics, percutaneous coronary intervention

INTRODUCTION

Wave intensity analysis has emerged as a powerful time-domain method to investigate the dynamic interactions between the contracting myocardium and coronary blood flow. Coronary wave intensity distinguishes between concurrently generated upstream and downstream contributions on coronary hemodynamic waveforms and is characterized by forward (aortic) and backward-traveling (microcirculatory) waves (1–3). Compression waves are associated with an increase in pressure, e.g., by propulsion, while expansion waves reflect a decrease in pressure, e.g., by suction.

Wave speed is fundamental to split net wave intensity into separate forward and backward traveling components (4). Local coronary wave speed in normal coronary vessels can be assessed from simultaneously acquired pressure and flow velocity signals (5). The validity of this approach, however, turned out to be compromised under conditions that frequently occur in the clinical setting, such as hyperemia by microvascular dilation or downstream of a stenosis in diseased coronary vessels (6–8).

In patients, wave intensity analysis has been applied to study changes in coronary-cardiac interaction through interventions ranging from pacing and exercise to alterations in left ventricular mechanics by Valsalva maneuver, aortic valve replacement, or left ventricular stunning (9–14). In all these studies, the investigations involved unobstructed coronary arteries.

According to the Moens-Korteweg equation, arterial pulse wave velocity intrinsically depends on the elastic properties of the vessel wall. It can reasonably be expected that the elastic wall properties are similar in angiographically normal vessel sections proximal and distal to a focal stenosis. We therefore hypothesized that proximal wave speed may be suitable to separate the net wave intensity profile obtained distal to a stenosis. To test this hypothesis, we analyzed hemodynamic signals obtained at different axial locations in diseased and unobstructed coronary arteries in patients.

MATERIALS AND METHODS

Hemodynamic Measurements

The dataset for this study was extracted from existing hemodynamic recordings obtained in patients with stable angina pectoris and a single stenosis in a coronary artery, who were scheduled for elective percutaneous coronary intervention (PCI). Exclusion criteria were age below 18 or over 80 years, left main stenosis, subtotal or serial lesions, severe aortic valve disease or heart failure, hypertrophic cardiomyopathy, prior myocardial infarction <6 weeks before PCI or prior cardiac surgery.

Cardiac catheterization was carried out by standard femoral approach. All anti-anginal medication was continued. Intracoronary nitroglycerin (0.1 mg) was administered in order to relax epicardial vessel tone, and coronary angiograms were recorded for quantification of stenosis severity. Aortic pressure (Pa) was measured via the guiding catheter at the coronary ostium. A dual-sensor equipped guide wire (ComboWire XT, Philips-Volcano, Eindhoven, NL) was advanced into the study vessel to simultaneously acquire intracoronary pressure (Pd) and flow velocity (U) signals (15). Hemodynamic signals and ECG were processed by the instrument console (ComboMap, Philips-Volcano, Eindhoven, NL) and digitized at 200 Hz. Flow velocity signals are acquired at 100 Hz by the instrument console and were up-sampled to 200 Hz during offline readout of the digital record. Physiological signals were obtained both proximal and distal to the stenosis during resting flow condition. Depending on stenosis location, proximal measurements were obtained within 2–3 cm from the ostium and distal measurements approximately in the mid- to last third of a vessel. PCI by stent placement was carried out when clinically indicated, and measurements at the distal location were repeated per operator discretion. Care was taken to place the wire sensors at the same downstream location before and after stent placement. Hemodynamic data at equivalent axial locations were also collected in undiseased reference vessels.

Data Analysis

Vessel dimensions and stenosis diameter reduction were determined by quantitative angiogram analysis (QC-CMS 5.2, Medis Medical Imaging Systems, Leiden, Netherlands). Pressure and flow velocity signals were extracted from the digital recordings and processed using the in-house developed *StudyManager* software (AMC Amsterdam, Netherlands) to derive cycle-averaged values for all relevant variables.

Wave intensity analysis was carried out using custom software written in Delphi (Embarcadero, Austin, TX). The single-point estimate of coronary wave speed (SPc) was assessed according to the sum-of-squares method (5) as reported previously (6–8). In brief, smoothed derivatives of the coronary Pd and U signals were obtained by applying the Savitzky-Golay filter (16) using a third degree polynomial over 11 datapoints. After correcting for

the instrument-inherent delay in Pd, SPc was determined using the sum-of-squares technique as

$$SPc = \frac{1}{\rho}\sqrt{\frac{\sum dP_d{}^2}{\sum dU^2}} \quad (1)$$

A value of $\rho = 1{,}060$ kg/m^3 was used for blood density. Summations were taken over an integer number of three to eight consecutive cardiac periods during resting flow (8). Net coronary wave intensity was calculated from ensemble-averaged beats. Separated forward and backward components of coronary wave intensity (WI), normalized by the sampling rate (17), were then determined as (4)

$$WI_{\pm} = \pm\frac{1}{4\rho c}\left(\frac{dP_d}{dt} \pm \rho c\frac{dU}{dt}\right)^2 \quad (2)$$

where c is the wave speed in (m/s).

To assess the effect of wave speed on the separated wave intensity, WI was calculated for SPc derived from signals at proximal as well as distal vessel locations. For the dominant forward (positive WI) and backward traveling (negative WI) waves, the area under the respective curve was integrated to yield the corresponding wave energy (in J m^{-2} s^{-2}). Four dominant peaks during the cardiac cycle characterize coronary wave intensity waveform: the forward-traveling compression wave (FCW) in early systole and early diastolic backward-traveling expansion wave (BEW), leading to flow acceleration, and the backward compression wave (BCW) and forward expansion wave (FEW), that cause flow deceleration (1, 3, 9).

Statistics

All values are expressed as mean ± SEM unless otherwise noted. Comparison between results obtained at proximal and distal locations in the same vessel were performed by paired Student's *t*-test (SPSS v.20, IBM, Armonk, NY). Unpaired Student's *t*-test assuming equal variance was used to compare data in reference vessels with those in diseased vessels after PCI. Agreements were assessed with Bland-Altman analysis. A two-sided probability value of $p < 0.05$ was considered significant.

RESULTS

Simultaneous pressure and flow velocity signals of sufficient quality at rest conditions were collected in 12 patients both upstream and downstream of the stenosis. The patient characteristics are shown in **Table 1**. Subjects were predominantly male with a mean age of 56 ± 3 years. Coronary artery stenoses were of intermediate severity ranging from 28% (min) to 69% (max) diameter reduction. In seven of these subjects, intracoronary physiology data at the distal location were additionally acquired after PCI. Measurements at two axial locations were obtained in 14 reference vessels.

TABLE 1 | Baseline patient characteristics.

Age (years)	56 ± 3
Male sex	10 (83%)
Diameter reduction (%)	
Pre-PCI	40.0 ± 3.7
Post-PCI ($n = 7$)	19.3 ± 3.5
Coronary risk factors	
Hypertension	1 (8%)
Smoking history	6 (50%)
Medication	
Nitrates	8 (67%)
b-Blockers	8 (67%)
Calcium antagonists	4 (33%)

Values are reported as mean ± SEM or n (%), as appropriate. PCI, percutaneous coronary intervention.

TABLE 2 | Coronary hemodynamics and wave speed.

	Stenosis ($n = 12$)	Post-PCI[1] ($n = 7$)	Reference ($n = 14$)
Proximal location			
HR (bpm)	64 ± 2	63 ± 3	67 ± 3
Pa (mmHg)	98.0 ± 3.3	102.1 ± 3.6	97.4 ± 3.2
Pd (mmHg)	97.0 ± 3.4	101.1 ± 3.7	95.0 ± 3.3
ΔP (mmHg)	1.0 ± 0.2	0.9 ± 0.2	2.5 ± 0.4
U (cm/s)	20.2 ± 1.7	21.7 ± 1.6	21.2 ± 2.5
SPc (m/s)	18.3 ± 1.8	20.8 ± 1.9	23.4 ± 3.3
Distal location			
HR (bpm)	65 ± 2	66 ± 3	69 ± 2
Pa (mmHg)	98.2 ± 3.4	97.4 ± 5.7	99.7 ± 3.8
Pd (mmHg)	91.8 ± 3.0	93.8 ± 4.9	96.7 ± 3.9
ΔP (mmHg)	6.5 ± 1.3†	3.6 ± 1.3	3.1 ± 0.6
U (cm/s)	14.7 ± 1.7†	18.5 ± 1.6	19.9 ± 1.8
SPc (m/s)	28.4 ± 3.7*	21.9 ± 2.0	25.0 ± 2.8

Values are reported as mean ± SEM. HR, heart rate; Pa, aortic pressure; Pd, distal pressure; ΔP, pressure drop; U, flow velocity; SPc, single-point wave speed.
[1]Proximal values represent those obtained prior to PCI in this patient subgroup.
**$p < 0.02$, $^{\dagger}p < 0.005$ compared with proximal location.*

Effect of Location on Coronary Hemodynamics and Wave Speed

Hemodynamic variables (mean ± SEM) are summarized in **Table 2** for each measurement location. Aortic pressure was normal, with a small pressure gradient across the stenosis at resting flow. With the stenosis present, flow velocity upstream of the stenosis was higher than downstream ($p < 0.0002$) and the pressure difference to aortic pressure was less than downstream of the stenosis ($p < 0.005$).

There was no significant difference in hemodynamics or SPc for different axial locations in the interrogated reference vessels (**Figure 1**), with an average difference of 1.7 ± 1.4 m/s. In contrast, as illustrated in **Figure 2**, SPc was significantly larger downstream than upstream of the stenosis (28.4 ± 3.7 m/s vs.

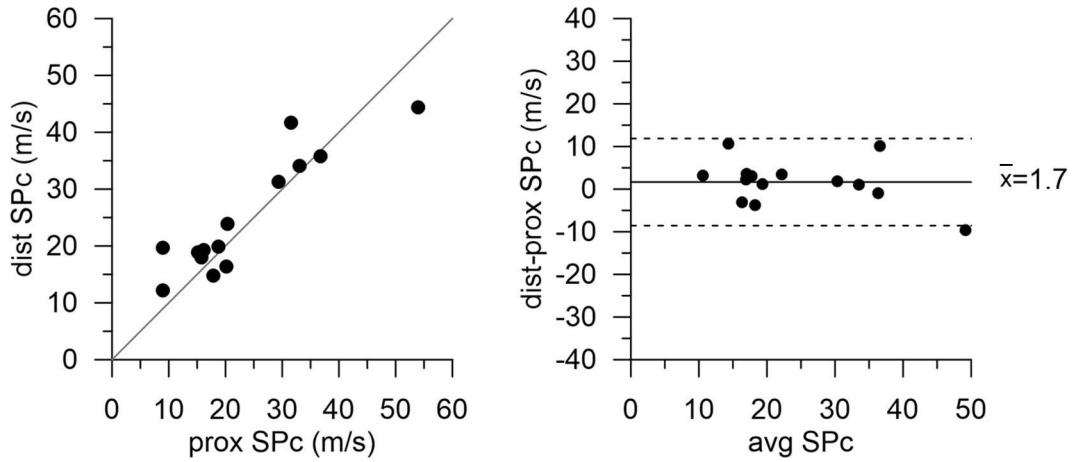

FIGURE 1 | Wave speed (SPc) in normal reference vessels at proximal and distal locations. High correspondence of the data indicates no effect of axial location. Scatterplot with line of identity (left panel) and Bland-Altman analysis (right panel) showing mean bias (solid line) and 95% limits of agreement (dashed lines).

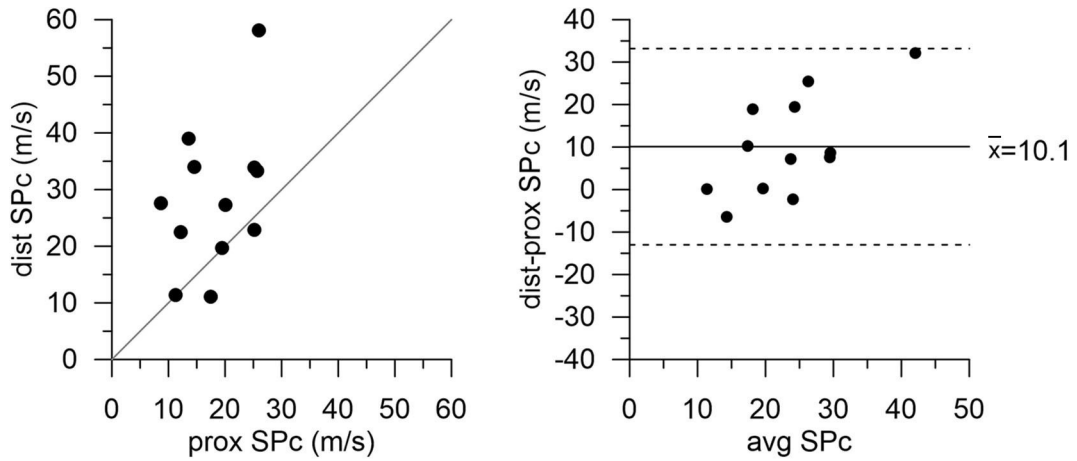

FIGURE 2 | Wave speed (SPc) in diseased coronary vessels proximal and distal to the stenosis. Local SPc downstream of the stenosis is elevated compared with SPc assessed upstream.

18.3 ± 1.8 m/s, $p < 0.02$). Despite the lower distending pressure downstream of the lesion, SPc at that location was on average 10.1 ± 3.4 m/s higher than upstream. The corresponding separated wave energy tended to be underestimated when calculated using SPc derived at the distal compared with the proximal location (**Figure 3**).

After successful revascularization and stent placement, hemodynamics and SPc at the distal location in the treated vessels matched those in the reference vessels. Proximal wave speed did not significantly increase after PCI ($p = 0.1441$). As shown in **Figure 4** in the subgroup of patients after PCI, SPc at the distal location no longer differed from proximal SPc in the same vessel assessed prior to revascularization (21.9 ± 2.0 m/s vs. 20.8 ± 1.9 m/s, $p = 0.48$). After PCI, no significant difference in wave energy was observed for either forward or backward separated waves (**Figure 5**) whether derived using proximal or distal SPc. Bland-Altman analysis confirmed the equivalence with a mean difference of 1.1 ± 1.5 m/s.

DISCUSSION

In patients with coronary artery disease, this study demonstrated that local coronary wave speed at rest, as derived from the sum-of-squares technique, was higher when assessed in a normal vessel section downstream of a focal stenosis compared with a proximal normal section. That difference was no longer present after the coronary narrowing had been removed by stent placement. Likewise, we did not observe an effect of axial location on coronary wave speed in undiseased reference vessels.

There are only few studies on coronary wave speed in humans. The original sum-of-squares method was first proposed by

Davies et al. (5) who tested it in normal coronary vessels without a stenosis. The present findings are consistent with earlier reports by Kolyva et al. (6) and Naranyan et al. (18), which showed that SPc assessed using the sum-of-squares in a vessel segment downstream of a stenosis decreased following PCI. The value of sum-of-squares SPc is governed by the ratio of summed coronary pressure (ΣdP_d^2) and velocity (ΣdU^2) oscillations during the cardiac cycle (5). As explained previously (6), in the coronary circulation these systolic-diastolic variations are altered by a stenosis to increase pressure differential-dependent numerator in Equation (1) while decreasing the flow velocity variations in the denominator. SPc assessed by the summed ratio of increased distal pulse pressure and decreased velocity variations downstream of a stenosis is thus at risk to yield artifactually elevated values solely on mathematical grounds. This deviation from expected wave speed behavior despite similar arterial wall properties is enhanced during microvascular vasodilation (6). Rolandi et al. (8) compared SPc with directly measured wave speed in healthy human coronary arteries at rest and during elevated flow after intracoronary administration of adenosine. They found that true coronary wave speed is not altered during hyperemia and hence concluded that the sum-of-squares SPc should be assessed under resting conditions. This inference, however, was limited to healthy vessels and could not be extrapolated to diseased vessels for reasons outlined above.

The current study, using measurements at resting flow, found a difference in proximal vs. distal wave speed only in

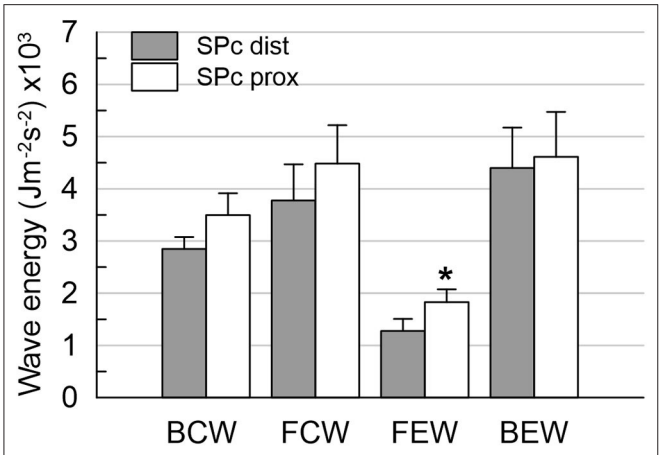

FIGURE 3 | Wave energies downstream of the stenosis obtained from wave intensity profiles separated with local SPc assessed at proximal and distal location. Using distal SPc tends to lower the derived wave intensity. *$p < 0.05$ compared with distal wave energy.

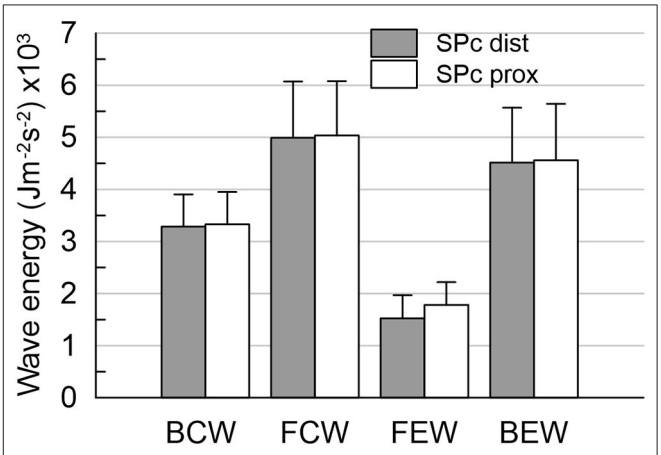

FIGURE 5 | Wave energies at distal location in diseased vessels after PCI. The wave energies are equivalent, whether derived from wave intensity profiles separated with local SPc assessed at proximal or distal locations. Note: proximal values are pre-PCI data in this subset of patients.

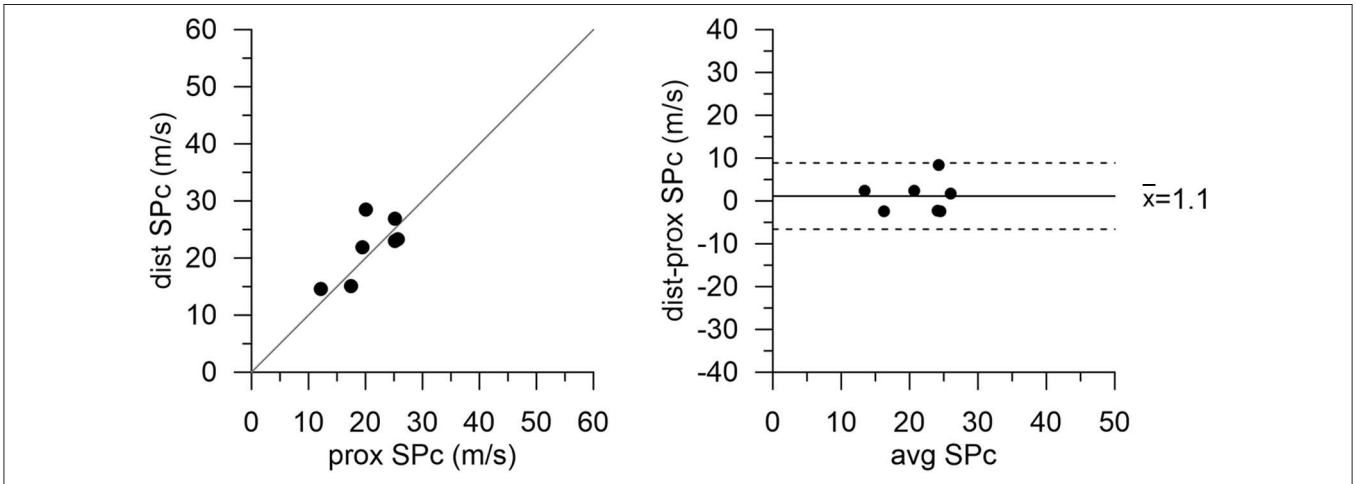

FIGURE 4 | Wave speed (SPc) in diseased vessels at proximal and distal locations after PCI with stent placement. Agreement between measurement locations is close. Note: proximal values are pre-PCI data in this subgroup of patients.

the presence of a stenosis. Distal SPc was artifactually higher, assuming similar arterial wall properties in the undiseased vessel segments up- and downstream of the focal stenosis. This axial location effect on SPc was not discernible in the same undiseased vessel sections after PCI. A prior study by Siebes et al. (7) demonstrated that simulated overestimation of coronary wave speed in a vessel segment downstream of a stenosis leads to underestimation of the energy contained in the separated forward and backward waves. Our present results clearly show a tendency toward lower wave energy using the higher SPc assessed in a normal vessel segment downstream of the stenosis compared with the integrated wave areas derived using the lower SPc assessed in a proximal vessel segment. Keeping in mind that the relation between wave speed and wave intensity is highly nonlinear, our present findings are consistent with the earlier simulations (7).

Results obtained after revascularization of the stenosis further support our hypothesis that using proximal sum-of-squares SPc likely yields more reliable values for wave intensity downstream of a stenosis, since the difference in SPc that existed before PCI was no longer present. Both proximal and distal SPc values were similar and furthermore matched those obtained in the reference vessels. Interestingly, Harbaoui et al. (19) directly measured coronary wave speed in patients with stable coronary artery disease and found that it was higher in stented vessels than before treatment due to added vessel stiffness imparted by the stent. However, their measurement technique, based on distance traveled and delay in the pressure wave using sequential pressure measurements, covered the entire length of the coronary artery (ca.11 cm) and thus represented global rather than local wave speed. Their invasive technique prevented measurements in healthy vessels for comparison.

The absence of an actual axial location effect on local wave speed in vessel segments of similar stiffness is furthermore corroborated by the comparable results we obtained at different axial locations in the normal reference vessels. This makes sense keeping in mind the predominance of local wall mechanics in determining arterial wave speed under similar hemodynamic conditions.

It should be cautioned that our results pertain to measurements obtained in diseased vessels with intermediate lesions under resting flow conditions, with only a small loss in mean pressure across the stenosis. Pulse wave velocity in arteries depends on distending pressure (20) and extrapolation to hyperemic flow may suffer from mechanical effects associated with the higher pressure loss across the stenosis at elevated flow rates, especially for more severe lesions. In the present study, the difference in pressure gradient before and after PCI was small at the relatively low resting flow values and did not unduly alter vessel wall distensibility.

Future studies in larger patient groups should be directed to investigate the usefulness of proximal SPc assessed at resting flow for wave intensity analysis in diseased vessels during hyperemic conditions.

LIMITATIONS

This observational study includes only a small number of patients. However, this is the first study to compare coronary wave speed at different locations along healthy and diseased coronary arteries. The invasive repeated measurements were well tolerated by the participating subjects, but the duration of the experiments in the catheterization laboratory presented a logistic concern regarding acquisition of invasive measurements at all locations and treatment conditions.

The measurements were obtained in different vessels with different stenosis degrees. Earlier reports have not shown a difference in wave speed between unobstructed left and right coronary arteries (5, 21). Although it cannot be assumed that the vessel wall of a diseased coronary artery is mechanically equivalent to a healthy vessel, we presume that the elastic properties are similar in angiographically normal coronary segments proximal and distal to a focal stenosis or stent. The pertinent proximal-distal comparisons carried out within the same vessel support this assumption. It should be noted that the distance between stenosis and ostium could not be matched due to unavoidable individual differences in stenosis location between patients.

Overall, our mean velocities in patients are consistent with the literature. Mean flow velocity was noticeably lower downstream of the stenosis than upstream. One may argue that this is unusual given the tapering of bifurcating coronary vessels, and that this may explain the higher distal wave speed. Coronary blood flow is well regulated to meet the physiological demand of the perfused downstream myocardial tissue. The velocity distribution in coronary vessels principally depends on the diameter ratio and flow ratio at branch points. The underlying allometric scaling laws (22–24) imply that coronary flow velocity tends to decrease after a branch point. It is not an unusual clinical observation that flow velocity may be diverted away from a stenosed branch and revascularization results in near equalization of proximal and distal mean velocity (25, 26).

A possible influence of reflections at points of geometric or elastic discontinuity on wave speed has not been considered. It has previously been speculated that distal reflection is not a confounding factor for the sum-of-squares method (5), whereas *in vitro* experiments have shown that wave speed is altered within a stenosis or aneurysm (27). The influence of wave reflections on wave intensity in coronary vessels was recently investigated (28). These authors also used a fixed wave speed assessed by the sum-of-squares method. A potential effect of reflection at a stenosis on wave speed in normal sections of coronary vessels remains to be elucidated.

We used the sum-of-squares method to determine local coronary wave speed. Several other single-point techniques have been developed and successfully applied to determine local wave speed in larger human arteries (29). These methods are not applicable in coronary vessels for technical reasons related to the necessary transducers or because theoretical requirements cannot be fulfilled for measurements in the coronary circulation, e.g., finding a linear portion in hemodynamic-loop approaches.

CONCLUSION

Our findings suggest that proximal coronary wave speed at resting flow can serve as a suitable surrogate to separate wave intensity profiles obtained downstream of a stenosis. This approach may broaden the scope of wave intensity analysis for the investigation of coronary-cardiac interaction to include diseased vessels. More studies are needed to confirm our early results.

DATA AVAILABILITY STATEMENT

The datasets used in this study will be made available on reasonable request to the corresponding author.

ETHICS STATEMENT

This study was carried out in accordance with institutional guidelines and the protocol was approved by the local institutional review board (MEC 06/151 #6.17.1610). All subjects gave written informed consent conform the Declaration of Helsinki.

AUTHOR CONTRIBUTIONS

MS conceived the study. LC and MS designed the methodology. JB and JP conducted the experiments to collect the intracoronary hemodynamic data. LC performed wave intensity analysis. LC and MS carried out the statistical analysis and wrote the first draft of the manuscript. All authors contributed to the article and approved the submitted version.

ACKNOWLEDGMENTS

The authors gratefully acknowledge the skilled assistance of the nursing staff at the cardiac catheterization laboratory.

REFERENCES

1. Sun Y-H, Anderson TJ, Parker KH, Tyberg JV. Wave-intensity analysis: a new approach to coronary hemodynamics. *J Appl Physiol.* (2000) 89:1636–44. doi: 10.1152/jappl.2000.89.4.1636
2. Hughes AD, Parker KH, Davies JE. Waves in arteries: a review of wave intensity analysis in the systemic and coronary circulations. *Artery Res.* (2008) 2:51–9. doi: 10.1016/j.artres.2008.02.002
3. Kolyva C, Khir A. Wave intensity analysis in the ventricles, carotid and coronary arteries – What has been learnt during the last 25 years? Part 2. *Int Cardiovasc Forum.* (2014) 1:122–7. doi: 10.17987/icfj.v1i3.36
4. Parker K. An introduction to wave intensity analysis. *Med Biol Eng Comput.* (2009) 47:175–88. doi: 10.1007/s11517-009-0439-y
5. Davies JE, Whinnett ZI, Francis DP, Willson K, Foale RA, Malik IS, et al. Use of simultaneous pressure and velocity measurements to estimate arterial wave speed at a single site in humans. *Am J Physiol Heart Circ Physiol.* (2006) 290:H878–85. doi: 10.1152/ajpheart.00751.2005
6. Kolyva C, Spaan JAE, Piek JJ, Siebes M. Windkesselness of coronary arteries hampers assessment of human coronary wave speed by single-point technique. *Am J Physiol Heart Circ Physiol.* (2008) 295:H482–90. doi: 10.1152/ajpheart.00223.2008
7. Siebes M, Kolyva C, Verhoeff B-J, Piek J, Spaan J. Potential and limitations of wave intensity analysis in coronary arteries. *Med Biol Eng Comput.* (2009) 47:233–9. doi: 10.1007/s11517-009-0448-x
8. Rolandi MC, De Silva K, Lumley M, Lockie TP, Clapp B, Spaan JA, et al. Wave speed in human coronary arteries is not influenced by microvascular vasodilation: implications for wave intensity analysis. *Basic Res Cardiol.* (2014) 109:405. doi: 10.1007/s00395-014-0405-1
9. Davies JE, Whinnett ZI, Francis DP, Manisty CH, Aguado-Sierra J, Willson K, et al. Evidence of a dominant backward-propagating "suction" wave responsible for diastolic coronary filling in humans, attenuated in left ventricular hypertrophy. *Circulation.* (2006) 113:1768–78. doi: 10.1161/CIRCULATIONAHA.105.603050
10. Davies JE, Sen S, Broyd C, Hadjiloizou N, Baksi J, Francis DP, et al. Arterial pulse wave dynamics after percutaneous aortic valve replacement: fall in coronary diastolic suction with increasing heart rate as a basis for angina symptoms in aortic stenosis. *Circulation.* (2011) 124:1565–72. doi: 10.1161/CIRCULATIONAHA.110.011916
11. Rolandi MC, Nolte F, van de Hoef TP, Remmelink M, Baan J, Jr., et al. Coronary wave intensity during the Valsalva manoeuvre in humans reflects altered intramural vessel compression responsible for extravascular resistance. *J Physiol.* (2012) 590:4623–35. doi: 10.1113/jphysiol.2012.229914
12. Lockie TPE, Rolandi MC, Guilcher A, Perera D, De Silva K, Williams R, et al. Synergistic adaptations to exercise in the systemic and coronary circulations that underlie the warm-up angina phenomenon. *Circulation.* (2012) 126:2565–74. doi: 10.1161/CIRCULATIONAHA.112.094292
13. Ladwiniec A, White PA, Nijjer SS, O'Sullivan M, West NEJ, Davies JE, et al. Diastolic backward-traveling decompression (suction) wave correlates with simultaneously acquired indices of diastolic function and is reduced in left ventricular stunning. *Circ Cardiovasc Interv.* (2016) 9:e003779. doi: 10.1161/CIRCINTERVENTIONS.116.003779
14. Rolandi MC, Wiegerinck EMA, Casadonte L, Yong Z-Y, Koch KT, Vis M, et al. Transcatheter replacement of stenotic aortic valve normalizes cardiac–coronary interaction by restoration of systolic coronary flow dynamics as assessed by wave intensity analysis. *Circ Cardiovasc Interv.* (2016) 9:e002356. doi: 10.1161/CIRCINTERVENTIONS.114.002356
15. Siebes M, Verhoeff B-J, Meuwissen M, de Winter RJ, Spaan JAE, Piek JJ. Single-wire pressure and flow velocity measurement to quantify coronary stenosis hemodynamics and effects of percutaneous interventions. *Circulation.* (2004) 109:756–62. doi: 10.1161/01.CIR.0000112571.06979.B2
16. Savitzky A, Golay MJE. Smoothing and differentiation of data by simplified least squares procedures. *Anal Chem.* (1964) 36:1627–39. doi: 10.1021/ac60214a047
17. Ramsey MW, Sugawara M. Arterial wave intensity and ventriculoarterial interaction. *Heart Vessels.* (1997) (Suppl. 12):128–34.
18. Narayan O, Leung MCH, Wong DTL, Meredith IT, Cameron JD. Percutaneous coronary intervention enhances accelerative wave intensity in coronary arteries. *PLoS ONE.* (2015) 10:e0142998. doi: 10.1371/journal.pone.0142998
19. Harbaoui B, Courand PY, Cividjian A, Lantelme P. Development of coronary pulse wave velocity: new pathophysiological insight into coronary artery disease. *J Am Heart Assoc.* (2017) 6:e004981. doi: 10.1161/JAHA.116.004981
20. Arts T, Kruger RT, van Gerven W, Lambregts JA, Reneman RS. Propagation velocity and reflection of pressure waves in the canine coronary artery. *Am J Physiol.* (1979) 237:H469–74. doi: 10.1152/ajpheart.1979.237.4.H469
21. Hadjiloizou N, Davies JE, Malik IS, Aguado-Sierra J, Willson K, Foale RA, et al. Differences in cardiac microcirculatory wave patterns between the proximal left mainstem and proximal right coronary artery. *Am J Physiol Heart Circ Physiol.* (2008) 295:H1198–205. doi: 10.1152/ajpheart.00510.2008
22. Huo Y, Kaimovitz B, Lanir Y, Wischgoll T, Hoffman JIE, Kassab GS. Biophysical model of the spatial heterogeneity of myocardial flow. *Biophys J.* (2009) 96:4035–43. doi: 10.1016/j.bpj.2009.02.047

23. Huo Y, Finet G, Lefevre T, Louvard Y, Moussa I, Kassab GS. Optimal diameter of diseased bifurcation segment: a practical rule for percutaneous coronary intervention. *EuroIntervention.* (2012) 7:1310–6. doi: 10.4244/EIJV7I11A206
24. van der Giessen AG, Groen HC, Doriot P-A, de Feyter PJ, van der Steen AFW, van de Vosse FN, et al. The influence of boundary conditions on wall shear stress distribution in patients specific coronary trees. *J Biomech.* (2011) 44:1089–95. doi: 10.1016/j.jbiomech.2011.01.036
25. Ofili EO, Labovitz AJ, Kern MJ. Coronary flow velocity dynamics in normal and diseased arteries. *Am J Cardiol.* (1993) 71:3D−9. doi: 10.1016/0002-9149(93)90128-Y
26. Ofili EO, Kern MJ, Labovitz AJ, St. Vrain JA, Segal J, Aguirre FV, et al. Analysis of coronary blood flow velocity dynamics in angiographically normal and stenosed arteries before and after endolumen enlargement by angioplasty. *J Am Coll Cardiol.* (1993) 21:308–16. doi: 10.1016/0735-1097(93)90668-Q
27. Hacham WS, Khir AW. The speed, reflection and intensity of waves propagating in flexible tubes with aneurysm and stenosis: experimental investigation. *Proc Inst Mech Eng.* (2019) 233:979–88. doi: 10.1177/0954411919859994
28. Mynard JP, Penny DJ, Smolich JJ. Major influence of a 'smoke and mirrors' effect caused by wave reflection on early diastolic coronary arterial wave intensity. *J Physiol.* (2018) 596:993–1017. doi: 10.1113/JP274710
29. Nabeel PM, Kiran VR, Joseph J, Abhidev VV, Sivaprakasam M. Local pulse wave velocity: theory, methods, advancements, and clinical applications. *IEEE Rev Biomed Eng.* (2020) 13:74–112. doi: 10.1109/RBME.2019.2931587

Conflict of Interest: JP serves as a consultant for Philips-Volcano, manufacturer of sensor-equipped guide wires.

The remaining authors declare that the research was conducted in the absence of any commercial or financial relationships that could be construed as a potential conflict of interest.

frontiers in Pediatrics

REVIEW
published: 20 August 2020
doi: 10.3389/fped.2020.00474

Postural Tachycardia Syndrome in Children and Adolescents: Pathophysiology and Clinical Management

Guozhen Chen[1,2,3], *Junbao Du*[1,4], *Hongfang Jin*[1,3] *and Yaqian Huang*[1]*

[1] Department of Pediatrics, Peking University First Hospital, Beijing, China, [2] Department of Pediatrics, The Affiliated Yantai Yuhuangding Hospital of Qingdao University, Yantai, China, [3] Research Unit of Clinical Diagnosis and Treatment of Pediatric Syncope and Cardiovascular Diseases, Chinese Academy of Medical Sciences, Beijing, China, [4] Key Laboratory of Molecular Cardiovascular Science, The Ministry of Education, Beijing, China

Postural tachycardia syndrome (POTS), characterized by chronic (≥6 months) orthostatic intolerance symptoms with a sustained and excessive heart rate increase while standing without postural hypotension, is common in children and adolescents. Despite the unclear pathogenesis of POTS, the present opinion is that POTS is a heterogeneous and multifactorial disorder that includes altered central blood volume, abnormal autonomic reflexes, "hyperadrenergic" status, damaged skeletal muscle pump activity, abnormal local vascular tension and vasoactive factor release, mast cell activation, iron insufficiency, and autoimmune dysfunction. A number of pediatric POTS patients are affected by more than one of these pathophysiological mechanisms. Therefore, individualized treatment strategies are initiated in the management of POTS, including basal non-pharmacological approaches (e.g., health education, the avoidance of triggers, exercise, or supplementation with water and salt) and special pharmacological therapies (e.g., oral rehydration salts, midodrine hydrochloride, and metoprolol). As such, the recent progress in the pathogenesis, management strategies, and therapeutic response predictors of pediatric POTS are reviewed here.

Keywords: postural tachycardia syndrome, pathogenesis, management, children, adolescents

OPEN ACCESS

Edited by:
Giovanni Biglino,
University of Bristol, United Kingdom

Reviewed by:
Ju Liu,
Shandong University, China
Federico Gutierrez-Larraya,
University Hospital La Paz, Spain

***Correspondence:**
Yaqian Huang
yaqianhuang@126.com

Specialty section:
This article was submitted to Pediatric Cardiology, a section of the journal Frontiers in Pediatrics

Received: *01 March 2020*
Accepted: *06 July 2020*
Published: *20 August 2020*

Citation:
Chen G, Du J, Jin H and Huang Y (2020) Postural Tachycardia Syndrome in Children and Adolescents: Pathophysiology and Clinical Management. Front. Pediatr. 8:474. doi: 10.3389/fped.2020.00474

INTRODUCTION

Postural tachycardia syndrome (POTS) is one of the common forms of chronic (at least 6 months) orthostatic intolerance (OI), and most of the cases have presyncope symptoms accompanied by inappropriate sinus tachycardia with normal blood pressure in an upright position (1, 2). The debilitating condition of POTS is often accompanied by orthostatic discomforts including lightheadedness, headache, giddiness, presyncope, momentary "blackout," blurred vision, cognitive difficulties, sleep disturbances, fatigue, pale complexion, and even sudden syncope. Postural tachycardia syndrome patients sometimes show signs of excessive sympathoexcitation such as chest tightness, palpitations, inappropriate vasomotor skin changes, excessive sweat, and frequent tremulousness (3, 4). For children and adolescents, the diagnostic criteria of POTS include discomforts of OI together with a normal supine heart rate (HR) and HR increase of at least 40 beats per minute (bpm) or a maximum HR over 130 bpm for children aged 6–12 years or >125 bpm for adolescents aged 13–18 years in the first 10 min of an active standing test or during the passive

head-up tilt test (HUTT) without orthostatic hypotension shown by a reduction in systolic blood pressure (SBP) of more than 20 mmHg or a reduction in diastolic blood pressure (DBP) by more than 10 mmHg (5). Postural tachycardia syndrome is a heterogeneous disorder with many possible underlying causes, such as fever, anemia, dehydration, hyperthyroidism, myocardial damage, and autonomic neuropathies. Once a specific cause is identified, the POTS label should be discarded in favor of the appropriate disease term (2).

Because of the multisystem discomforts of pediatric POTS patients, there are significant deleterious effects on individual quality of life (5–8). In pediatric POTS, poor health increases the rate of depression and anxiety in young patients and their parents, which has drawn increasing attention in recent years (9, 10). However, in the general pediatric population, the heterogeneous clinical features and the shortage of specific biomarkers have resulted in an underestimated prevalence of POTS (6, 11). Thus, it is quite difficult to establish the exact incidence of POTS in children and adolescents (6, 11, 12). In 2014, our coworkers enrolled 600 Chinese individuals aged 7–18 (11.9 ± 3.0) years to study the incidence of POTS in children and adolescents, and the results indicated that the prevalence of POTS was 6.8% (4). The results also indicated no significant gender difference among the above young patients (4), although some other studies have reported that most patients with POTS are female (2, 6, 11). Regardless, the data on pediatric POTS are insufficient, meriting multicenter studies to obtain the rate of occurrence of POTS in children and teenagers.

To date, although the precise pathophysiology underlying pediatric POTS remains unclear, there have been some significant reports indicating that POTS might be multifactorial and varied in different subpopulations of young POTS patients (3, 6, 12). Thus, the responses of pediatric POTS patients to the same therapeutic intervention are highly variable (12, 13). Therefore, combined individualized treatment should be established according to the different pathophysiological processes and biomedical predictors (3, 5, 13).

PHYSIOLOGICAL ORTHOSTATIC REGULATION

Under physiological conditions, the blood flow is redistributed when an individual changes position from lying down to standing. Blood volume shifts from the upper part of the body to the lower part and the splanchnic circulation, as well as from the vascular system into the interstitial space owing to gravity while in the upright position (14). Standing reduces venous return, leading to a temporary decline in both cardiac filling and stroke volume (SV) and even a decrease in arterial blood pressure (1, 14).

To compensate for the changes in orthostatism, the body has a series of regulations to restore venous return and cardiac output (14, 15). Importantly, autonomic reflexes are activated. When tension on the vessel walls decreases corresponding to the reduced SV, the baroreceptors of the carotid sinus and the aortic arch can be suppressed to inhibit the parasympathetic response and stimulate the sympathetic response to cause vasoconstriction, accelerated HR, and increased cardiac output (15). The inhibition of baroreceptors also excites the renin–angiotensin–aldosterone system (RAAS) to promote renal reabsorption of water and sodium, which results in arterial vasoconstriction and an increase in plasma volume (16). The compensatory mechanism increases HR by 10–15 bpm, maintains a negligible change in SBP, and elevates DBP by ∼10 mmHg (17). Second, muscle pumps are invoked by movement or by external mechanical compression to increase venous return (18). Third, small veins prevent a large accumulation of blood in the lower body and maintain a relative upward flow of blood. Finally, when hypotension is detected, blood pools can be mobilized to the venous system. Additionally, many bioactive small gas molecules and vasoactive peptides are involved in the mechanisms responsible for regulating local vascular tension and endothelial cell function (19). If autonomic compensatory mechanisms are not sufficient, an excessive increase in HR (e.g., POTS) or hypotension, and even a loss of consciousness (e.g. vasovagal syncope) could happen after standing (2, 14).

PERSPECTIVES ON THE PATHOGENESIS OF POTS

The pathophysiology of POTS is complicated and obscure (3, 12). Current perspectives on the pathogenesis of POTS have been categorized as altered central blood volume, abnormal autonomic reflexes and elevated sympathetic tone, damaged skeletal muscle pump activity, local vascular tension regulation dysfunction, iron insufficiency, mast cell activation (MCA), and autoimmune dysfunction (3, 6, 12).

Altered Central Blood Volume

Decreased red blood cell volume or low blood volume has been found in many pediatric POTS patients (4, 20, 21). The likelihood of POTS increases 3.9 times if daily water intake is $<$800 mL, suggesting that hypovolemia is a risk factor in children with POTS (4). In 1996, El-Sayed and Hainsworth (22) confirmed that 24-h urine excretion of sodium was a useful biomarker of the body's volume capacity. In 2014, Zhang et al. (23) showed that there was a negative correlation between 24-h urinary excretion of sodium and symptom severity scores in children and adolescents with POTS. Some investigators have reported that the tachycardic reaction to standing is associated with the seriousness of hypovolemia in pediatric POTS (24) and that symptoms improve following acute (25) or chronic (26) increase in plasma volume. When 24-h urinary sodium excretion is $<$124 mmol/24 h, salt and water supplementation is efficacious in reducing uncomfortable symptoms in pediatric POTS patients (23). All of the above results indicate that low salt intake compounded by hypovolemia occurs in pediatric POTS. When hypovolemia exists at rest, the body cannot fully compensate for the decrease in blood volume after standing (27), which has to coexist with elevated HR in the upright position (28). Paradoxically, normal plasma volumes in patients with

POTS have been reported (29, 30), indicating that hypovolemia is not the unique cause of POTS.

Stewart and Montgomery (31) reported that 37 adolescent patients with POTS, aged 14–21 years, could be classified into a low-flow POTS (LFP) group in 14 patients, a normal-flow POTS (NFP) group in 15 patients, and a high-flow POTS (HFP) group in 8 patients. The blood flow of the lower extremities was measured in the supine position (31). Among these patients, most belonged to the LFP group. The pathogenesis of the NFP group was excessive redistribution to the splanchnic circulation because of inadequate splanchnic vasoconstriction while in an upright posture, leading to thoracic hypovolemia, upright tachycardia, intense peripheral vasoconstriction, and acrocyanosis (32). Interestingly, there were markedly increased microvascular filtration and obviously incompetent peripheral vasoconstriction inducing excessive calf blood flow that was unable to return to the heart accounting for postural tachycardia in the HFP group (33).

In light of the important role of the RAAS in regulating human neurohormones of plasma volume, a perturbed RAAS axis, which is disabled to facilitate the enlargement of blood volume in response to the hypovolemia of POTS patients, might be one of the pathophysiological changes in POTS (34). Several studies have found an inappropriately low plasma renin activity (PRA) in some children and adolescents with POTS, despite the hypovolemia (21, 24, 35), reduced aldosterone levels, and elevated angiotensin (Ang) II levels, with an insensitive receptor response to Ang II (35). Thus, the discordance of Ang II and PRA/aldosterone levels suggested that there might be diminished Ang II degradation in POTS patients (35). Patients with LFP have a decreased body mass index (BMI), which is related to the increased Ang II levels in women aged 14–29 years (36). However, the data on altered RAAS function corresponding to blood volume status in children and adolescents with POTS merit further study.

Abnormal Autonomic Reflexes and a "Hyperadrenergic" Status

Compared to healthy people, patients with POTS demonstrate excessive blood volume accumulation in the lower extremities and visceral circulation, which results in an obvious decrease in blood volume in venous return to the heart and subsequent cardiac ejection during orthostatic stress (14). The above changes bate baroreceptor activity to excite the sympathetic response and inhibit the parasympathetic response to adjust the altered hemodynamics (3). However, some pediatric POTS patients with a "hyperadrenergic" background have an inability to buffer the decrease in baroreceptor activation, leading to persistent sympathetic excitation characterized by sustained tachycardia while in an upright position (3, 37).

An increase in plasma norepinephrine in the standing position is the main biochemical change that occurs in hyperadrenergic POTS patients (38–40). Zhang et al. (38) reported that the plasma norepinephrine level in the upright position was positively associated with the severity of symptoms and the HR increase in the HUTT in pediatric POTS patients, and they speculated that the orthostatic norepinephrine increase might be due to the decreased vasoconstriction mediated by the baroreflex upon standing. Elevated plasma norepinephrine in pediatric patients with POTS suggests an impaired function of the norepinephrine transporter (NET) (39). Studies have shown that inherited or acquired mutations of NET encoded by the solute carrier family 6 neurotransmitter transporter noradrenalin member 2 (*SLC6A2*) gene impair the removal of norepinephrine in the synaptic cleft and reduce NET-dependent norepinephrine reabsorption (39, 40). The above data suggest that changes in the *SLC6A2* gene or NET protein expression eventually lead to increased adrenaline status in "hyperadrenergic" POTS patients.

Sleeping disorders have been considered to be related to a "hyperadrenergic" status in young patients with POTS (4). Sleepiness, unrefreshing sleep, fatigue, frequent arousal from sleep, and reduced quality of life are often described in pediatric patients with POTS (41–44). However, there is limited evidence to evaluate the prevalence of sleep-related symptoms or to elucidate the mechanism for POTS in children and adolescents (4, 43–45). The probability of POTS in children and adolescents increases 5.9 times if the number of hours of sleep is <8 h/d (4). More than 70% of pediatric POTS patients complain that sleep disturbances are their problems (44). High incidences of sleep-related complaints are not the result of primary sleeping disorders specific to POTS, but a comprehensive effect of complaints such as physical fatigue, chronic body pain, and other somatic discomforts (45). Sleeping disorders often trigger ill-defined cognitive impairment or mental fatigue with increased standing HR, disturbing daytime life in adolescents with POTS (46). Serotonin–norepinephrine reuptake inhibitors can worsen "brain fog" in pediatric POTS patients (47). Thus, exaggerated activation of the sympathicus might be an underlying cause of the hyperaroused state and worsen the subjective estimates of sleep quality in POTS patients (48).

Damaged Skeletal Muscle Pump Activity

Normally, contraction of the lower extremity muscles commanded by skeletal muscle pumps provides a guarantee for sufficient venous return to the heart to prevent OI (49). Stewart et al. (50) compared 12 LFP subjects with 10 healthy controls and 7 NFP patients to measure venous volume, peripheral blood capacitance, and calf muscle pump function. They found that the reduced circumferences of the calf were associated with a decreased fraction of emptied calf venous volume during muscle contraction concurrent with general low blood flow in LFP subjects. They proposed that the reduced calf blood capacity might lessen calf muscle size in the LFP group and thus damage the vertical ejection ability of the pumps in the skeletal muscle, further reducing blood flow and finally leading to OI in these patients (50).

Local Vascular Tension Dysfunction and Abnormal Vasoactive Factor Release

Upright stress results in the increased blood filling in the capacitance vessels, followed by reduced venous return (51). Excessive venous pooling has been found in the lower extremities in POTS patients (51, 52), whose resting venous pressures are

higher than those of controls (16 vs. 10 mmHg), which causes redistributed blood flow to the lower part of the body even while in a supine position and results in tachycardia via vagal retraction (53). Several studies have attributed such pooling mechanisms to increased venous filling due to arterial inflow (52), increased venous volume owing to mechanical defects in vein (53), blunted arterial vasoconstriction (54–56), altered capillary permeability inducing plasma fluid loss from capillaries to peripheral tissues (33, 57), or impaired venous emptying (58).

To further explore the mechanism for vascular tension dysfunction, some studies have been designed, and the results show that bioactive gaseous regulatory molecules and vasoactive peptides are involved in the development of abnormal partial vascular tension and impaired endothelial cell function in children and adolescents with POTS (5, 35, 59–63). Nitric oxide (NO), an endogenous gas continuously synthesized from L-arginine by nitric oxide synthase (NOS) and constitutively expressed in the endothelium, is known as a vasorelaxant factor and plays a crucial role in regulating the function of vascular endothelial cells (59). Liao et al. (60) reported that there were significantly higher levels of plasma NO and NOS in pediatric POTS patients aged 12 ± 3 years than in age-matched controls. In addition, NOS activity is positively correlated with flow-mediated vasodilation (FMD) of the brachial artery, which indirectly affects vascular dilation function (60). Hydrogen sulfide (H_2S), a gasotransmitter alongside NO, exerts a low concentration-produced contraction or high concentration-dependent relaxation of blood vessels (61). Erythrocytic H_2S has been detected to be obviously higher in pediatric POTS patients than that in control group (62, 63). Sulfur dioxide (SO_2), another gaseous molecule, has recently been found to have vasorelaxant effects (64, 65). Furthermore, plasma SO_2 levels were significantly higher in children with POTS than in healthy controls and were positively related to the maximum HR of all the study participants (66). The three increased endogenous gaseous molecules in pediatric POTS support the hypothesis that excessive vasorelaxation might contribute to the pathogenesis of pediatric POTS (19, 60). Additionally, adrenomedullin 2/intermedin (AM2/IMD), one of the members of the calcitonin gene-related peptide (CGRP) family (67), has been found to have a positive correlation with extraordinarily high HR during the HUTT in children with POTS (68). C-type natriuretic peptide (CNP) is generated from the endothelium and acts on adjacent vascular smooth muscle cells serving as a selective endothelium-independent vasodilator (69). The potent systemic cardiovascular actions of CNP reduce cardiac filling pressures and heart output following vasorelaxation and decrease venous return to the heart (70). Upright heart output and total peripheral vascular resistance are significantly lower in pediatric POTS patients than in the same children in the supine position or in healthy children and are positively associated with elevated plasma CNP levels (71). The results suggest that the increased endogenous IMD or CNP levels with similar features of vascular dilation represent the endogenous molecules involved in the development of POTS. Serum resistin, known as a new type of peptide hormone derived from adipocytes (72), has been found to notably enhance vasoconstriction and reduce diastolic function (73). An *in vitro* experiment showed that resistin could decrease endothelial NOS expression in human coronary artery endothelial cells (74). The serum resistin level in pediatric POTS patients is dramatically higher than that in age-matched healthy controls and is negatively related to the severity of symptoms and changes in HR that occur when changing from a supine to an upright position (74). These findings suggest that resistin may be a protective element in the pathogenesis of pediatric POTS and that the symptoms of POTS can likely be alleviated by raising the resistin level or improving the resistin function *in vivo* (75). Taken together, these findings confirm that increased local vascular relaxation and the compensatorily increased release of vasorelaxant factors, as well as vascular endothelial cell dysfunction, play important roles in the pathogenesis of POTS in children and adolescents (35, 54).

Iron Insufficiency

As the richest transition metal ion in humans, iron can cause a decrease in vasodilation by inhibiting the biosynthesis, transportation, transformation, and signal transduction of NO (76, 77). Low ferritin and vitamin D levels have been found in adolescents with POTS (78). Low iron storage accompanied by mild anemia is more prevalent in pediatric POTS patients than in healthy children in the United States (79). Additionally, iron-deficiency anemia also increases NO production in children and adolescents (80), suggesting that low iron storage–induced excessive vascular relaxation by increased output of NO might be a potential pathophysiological factor in pediatric POTS (79, 80). In addition, larger mean corpuscular volume and lower mean corpuscular hemoglobin concentration (MCHC) values were found in pediatric POTS patients than those in controls, which might be associated with decreased iron storage (81).

Mast Cell Activation

In an evaluation of young females with POTS, Shibao et al. (82) found that some of them had flushing episodes associated with OI, which suggests that MCA is likely involved in the hyperadrenergic mechanism for POTS (82). Although limited studies are available on the detailed mechanisms of MCA in POTS, the histamine, adenosine, platelet-activating factor, and prostaglandins produced by mast cells might play important roles in adolescents with POTS-related vasodilation and tachycardia (83, 84). A hopeful beneficial treatment would be to block these mediators in pediatric POTS patients with MCA, which merits further research (85).

Autoimmune Dysfunction

Autoimmune disturbance has been considered as one of the mechanisms involved in POTS due to frequent findings of autoantibodies in patients (11, 86, 87). A study from Japan used the luciferase immunoprecipitation system method and detected ∼29% anti–ganglionic nicotinic acetylcholine receptor (gAChR) α3 and β4 antibodies from the serum of young POTS population with a median age of 22.2 ± 10.8 years and an onset age of 19.8 ± 10.8 years (88). Dysautonomia may be caused by anti-gAChR antibodies damaging autonomic ganglionic synaptic transmission in POTS patients (89). In addition to gAChR,

several adrenergic receptors have been identified in pediatric POTS patients, including Ang II type 1 receptor (AT1R) and β1- and β2-adrenergic receptors (90–92). A study reported that POTS patients had higher autoimmune marker levels [e.g., antinuclear antibody (25 vs. 16%) and antiphospholipid antibody (7 vs. 1%) and increased incidence of comorbid autoimmune disease such as Hashimoto thyroiditis, rheumatoid arthritis, systemic lupus erythematosus, and common variable immunodeficiency (20 vs. 9.4%)] than the healthy population (93). The above findings demonstrate that pediatric POTS has a basis in autoimmune dysfunction; however, the detailed immune mechanisms are unknown and require further evaluation to determine the clinical significance (94).

MANAGEMENT STRATEGIES FOR POTS IN CHILDREN AND ADOLESCENTS

Full recovery is possible for POTS in children and adolescents, but it is difficult to treat patients because of inconsistent and poor therapeutic efficacies (95). Thus, collaborative and multidisciplinary therapies are constantly required (5–8, 95). After the diagnosis of POTS, in general, health education is the fundamental strategy above all, and further daily treatment plans should consist of non-pharmacological and pharmacological interventions (5, 95, 96). To achieve the best therapeutic effects, the detection of distinct neurohumoral biomarkers might predict the specific efficacy of the individualized treatment options in children and adolescents with specific subtypes of POTS (1, 5, 96).

Non-pharmacological Interventions

Health education on POTS is needed for young patients and their guardians who should understand the potential precipitating factors and avoid them (5–8, 96). Owing to frequent incapacitating symptoms of POTS that are closely related to an upright posture especially in stifling conditions (2), patients should avoid long periods of standing, sudden head-up postural changes, and high environmental temperatures (5). For POTS patients with a "hyperadrenergic" background, infection, sympathetic activation, and a lack of sleep might aggravate symptoms (4, 38, 39). Thus, patients are prevented from taking drugs such as NET inhibitors or 5-hydroxytryptamine norepinephrine reuptake inhibitors (5). In addition, pediatric POTS patients with sleep disorders should receive a guidance to promote more than 8 h of sleep daily (97). Additionally, it was found that, when the awakening salivary cortisol concentrations were more than 4.1 ng/mL, the sensitivity and specificity of predicting the effect of sleep-promoting therapy were 83.3 and 68.7%, respectively, in patients with POTS (97). Low-flow POTS patients usually suffer from the combination of hypovolemia and muscle pump dysfunction (50), which makes it necessary to drink plenty of water and wear compression garments, which can reduce the venous pooling caused by insufficient peripheral venous reflux and increase peripheral blood return to the heart (98). For those with signs of discomfort, counterpressure actions such as leg crossing and squatting are advised (5).

In addition, appropriate physical exercise to enhance muscle pump function of limbs and autonomic nervous system exercises to improve autonomic tone are also recommended for children with POTS (5, 98). The former refers to regular, organized, progressive exercise plans, which are characterized by aerobic recovery and some resistance training (5). The initial training should be limited to non-upright physical exercises, including the usage of rowing machines, recumbent cycling, and swimming, to reduce standing stress on the heart (5, 98, 99). The latter is especially suitable for pediatric POTS patients whose corrected QT-interval dispersion (QTcd) is more than 43 ms (100). It is recommended that the patients stand against a wall with feet 15 cm from it, starting at 5 min/d, and then gradually increasing to 20 min/d according to patients' tolerance and preference (5, 98). Several training results show that exercise training can improve the symptoms and the quality of life (101–103) and is even better than propranolol in the recovery of upright hemodynamics and the normalization of renal–adrenal reactivity (101).

Children and adolescents with POTS, especially those with 24-h urinary sodium excretion <124 mmol (23) or a BMI <18 kg/m^2 (104), are encouraged to drink adequate amounts of water (>800 mL/d) (4) and increase appropriate salt intake for 1–3 months to increase blood volume (5). However, this is not advised for patients suffering from kidney disease, high blood pressure, or heart failure (5, 95).

Pharmacological Treatment

Non-pharmacological interventions should be attempted first in all pediatric POTS patients. If these interventions are ineffective, pharmacological therapies should be applied to solve the specific problems (5, 95, 96). Pediatric patients with POTS who are strongly suspected of having hypovolemia or inadequate salt intake are recommended to use oral rehydration salts (ORSs) for 1–3 months (5, 23, 98, 104) or to accept short-term intravenous saline as rescue treatment for patients with clinical decompensation and significant deterioration of symptoms (25). Saline supplements can alleviate symptoms in "hypovolemic" patients. Many indexes, such as lower MCHC values (81), 24-h urinary sodium excretion <124 mmol (23), and a cutoff of BMI <18 kg/m^2 (104), have been shown to predict the therapeutic effect of ORSs on children and adolescents with POTS. Additionally, ORSs are also effective when the increase in HR is >41 bpm or when the maximum upright HR in 10 min is >123 bpm before treatment (105). When both indices are used together, the sensitivity and specificity are higher than for any of the single indices (104). Fludrocortisone is useful to increase sodium retention and amplify the plasma volume in POTS patients by activating the RAAS, but its validity needs to be verified in randomized clinical trials (98). In addition, increased NO generation and elevated NOx concentrations can return to normal after oral iron therapy in adolescents with iron-deficiency anemia (80), suggesting that iron supplementation might be effective for POTS patients with iron deficiency and the subsequent vasorelaxation status.

For children with severe symptoms or a risk of injury with unobvious presyncope that remarkably affect the quality of

life and for those who do not demonstrate a good response to health training and salt supplementation therapy, special vasoregulation-related pharmacological interventions should be considered (5, 96).

Midodrine hydrochloride, a drug that is enzymatically hydrolyzed as a selective α1-adrenoceptor agonist desglymidodrine by oral administration (106), constricts veins and arteries to increase venous return, which makes the drug theoretically useful in treating POTS (98). Midodrine hydrochloride significantly reduces both supine and upright tachycardia with better results than the α2-adrenoreceptor agonist clonidine, which decreases supine HR without increasing standing HR, but it is inferior to intravenous infusion of saline in POTS patients (25). Midodrine hydrochloride is indicated to be effective for some subtypes of pediatric POTS (5, 107), and its therapeutic efficacy is greatly increased with the help of biomarkers that are low-cost, non-invasive, and easy to detect (108). A series of important studies have been designed to explore the predictors of the efficacy of midodrine hydrochloride in the treatment of pediatric POTS by using receiver operating characteristic curves (62, 109–113). The results show that the following indications can predict the effectiveness of midodrine hydrochloride in the treatment of POTS in children and adolescents: FMD >9.85%, with high sensitivity (71.6% in 1 month and 74.4% in 3 months of therapy) and specificity (77.8% in 1 month and 80% in 3 months of therapy) (109); H_2S production in erythrocytes >27.1 nmol/min × 10^8 cell, with a sensitivity of 78.9% and a specificity of 77.8% (62); midregional proadrenomedullin plasma levels >61.5 pg/mL, with a sensitivity of 100% and a specificity of 71.6% (110); copeptin plasma levels >10.5 pmol/L, with both high sensitivity (81.3%) and high specificity (76.5%) (111); and SBP drops in changing from a supine to an upright position, with a sensitivity of 72% and a specificity of 88% (112). Additionally, the blood pressure change from a supine to an upright position can well-predict the long-term asymptomatic survival rate of pediatric POTS patients given oral midodrine hydrochloride (113). Midodrine is contraindicated for those with a BP >95% of the average for individuals of the same age and sex or for those with drug allergies (5). Since midodrine hydrochloride has instant and brief effects, the daily dose is suggested to be divided into several administrations (5, 98, 106). The medicine should be taken only during the daytime, no sooner than 4 h before bedtime, because of a risk of hypertension in the supine position (106); therefore, the BP should be monitored during treatment.

Adrenoceptor blockers can be divided into non-selective blockers for β1 and β2 receptors and β1-selective blockers, which have higher selective affinity for β1 receptors than for β2 receptors (114). The latter mainly slow down HR and decrease myocardial contractility when the sympathetic nervous system is activated but have a relatively small effect on the heart at rest (115). In 2009, a single-center retrospective

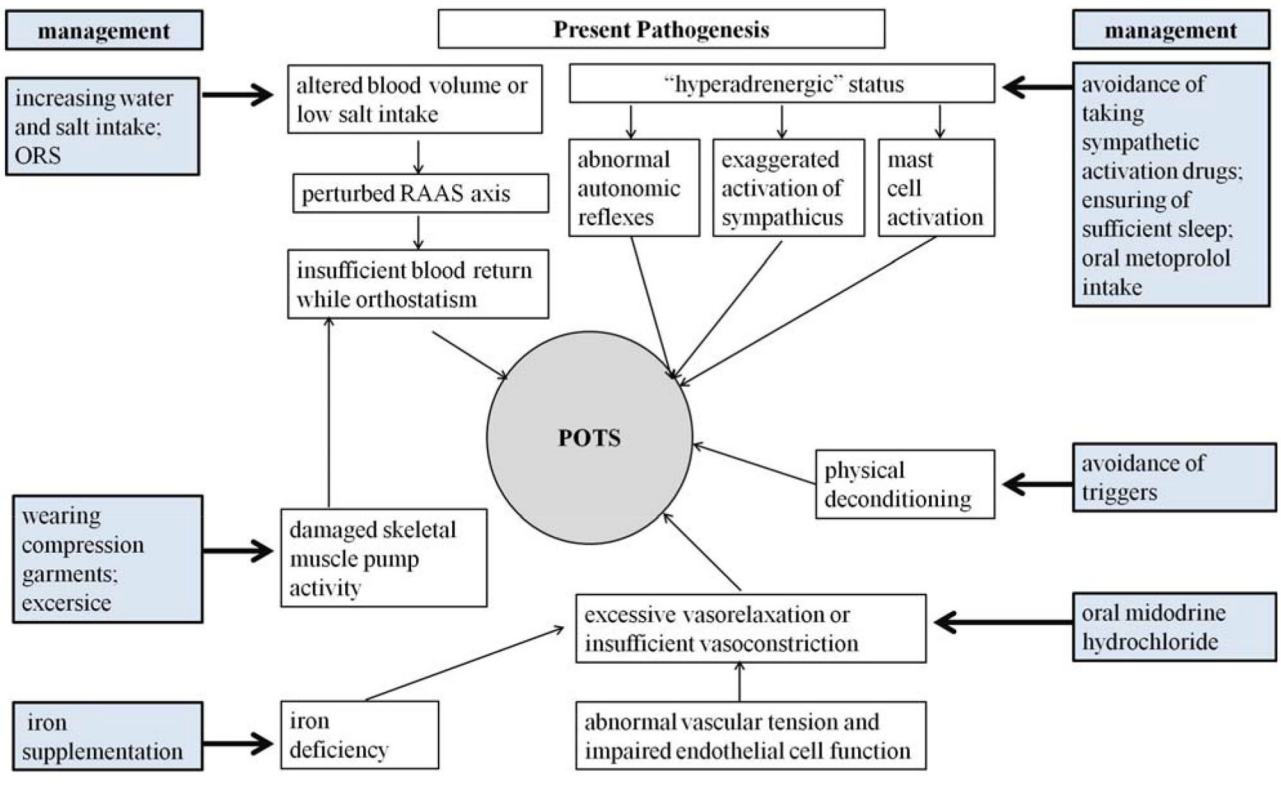

FIGURE 1 | Pathogenesis and corresponding management strategies in pediatric POTS.

TABLE 1 | Mechanisms, managements, and therapeutic response predictors of pediatric POTS.

Mechanisms	Managements	Therapeutic response predictors	References
Physical deconditioning	Avoidance of triggers	—	(97)
	Sufficient sleep	Awakening salivary cortisol concentrations >4.1 ng/mL	
	Physical exercise	—	
	Autonomic nervous function exercises	QTcd >43 ms	(100)
Hypovolemia	Increase water and salt intake	Lower MCHC values	(81)
	ORS	Urinary sodium <124 mmol/L per 24 h	(23)
		BMI <18 kg/m^2	(104)
		HR increments of 41 bpm or maximum upright HR of 123 bpm in 10 min	(105)
Damaged skeletal muscle pump activity	Wearing compression garments	—	
Local vascular tension dysfunction	Midodrine hydrochloride	FMD >9.85%	(109)
		Erythrocytic H_2S production >27.1 nmol/min × 10^8	(62)
		Plasma MR-ADM >61.5 pg/mL	(110)
		Plasma copeptin >10.5 pmol/L	(111)
		Pre-treatment increase in SBP ≤0 mmHg or DBP ≤6.5 mmHg from the supine to the upright position	(112)
Hyperadrenergic status	Metoprolol	Plasma CNP >32.55 pg/mL	(117)
		Orthostatic plasma NE >3.59 pg/mL	(38)
		Plasma copeptin <10.2 pmol/L	(118)

FMD, flow-mediated vasodilation; CNP, C-type natriuretic peptide; MCHC, mean corpuscular hemoglobin concentration; NE, norepinephrine; ORS, oral rehydration salt; MR-ADM, midregional proadrenomedullin; POTS, postural tachycardia syndrome; QTcd, corrected QT-interval dispersion.

chart analysis and follow-up conducted by the Mayo Clinic showed that adolescents with POTS taking β-blockers were more likely to have an improvement in symptoms than those taking midodrine (116), suggesting that β-blockers were effective for young POTS patients. β1-Selective blockers are useful for "hyperadrenergic" subtypes of POTS patients (96). There is relatively less experience with β1-blocker therapy in pediatric POTS (5–8, 96). Investigators also proposed that metoprolol, as a common β1-blocker, could be used with an initial dose of 0.5 mg/kg per day in treating pediatric POTS (108) and a maximal dose of 2 mg/kg per day in severe cases according to the symptoms (5). They also found several indicators to predict the effect of metoprolol on POTS in children and adolescents (5, 38, 117, 118). The results showed that the sensitivity and specificity were 95.8 and 70%, respectively, when the plasma CNP level was >32.55 pg/mL (117); 76.9 and 91.7%, respectively, with a plasma norepinephrine level >3.59 pg/mL in upright position (38); and 90.5 and 78.6%, respectively, with a plasma copeptin level <10.2 pmol/L in predicting the efficacy of metoprolol in children with POTS (118). Severe sinus bradycardia, atrioventricular block, severe heart failure, hypotension, acute pulmonary edema, bronchial asthma, mental illness, diabetes, and drug allergy are contraindications for the use of β-blockers (5).

Although evidence hints that MCA and autoimmune disorders take part in the pathogenesis of POTS (82, 86, 88), there are no meaningful therapeutic reports about defending against either of them in pediatric POTS patients, and this research gap requires further study.

CONCLUSION

Although great efforts have been made in exploring the pathogenesis of pediatric POTS, the precise mechanisms for POTS have not yet been totally elucidated (3, 6, 96). Fortunately, a series of effective treatment measures have been designed according to the known pathophysiological mechanisms (**Figure 1**), and a number of biomedical factors have gradually been discovered to be involved in the POTS pathological process and treatment prediction (35, 96). More and more biomarkers have been confirmed to be effective in predicting treatment efficacy (5–8). Therefore, selecting individual treatment strategies could improve the therapeutic outcomes according to the detailed pathogenesis indicated by the specific biological indexes (**Table 1**). However, the data of trials in pediatric POTS patients mainly originate from a single center; therefore, it is essential to perform large-sized multicenter studies in the future to optimize the individualized treatment of POTS in children and adolescents.

AUTHOR CONTRIBUTIONS

GC: literature review, interpretation of data, and first draft of the manuscript. JD: design, organization, and editing of the

manuscript. HJ: critical review and editing of studies cited in the manuscript. YH: concept and design of the manuscript, critical review, and editing of the manuscript. All authors: contributed to manuscript revision, read and approved the submitted version.

FUNDING

This work was supported by Peking University Clinical Scientist Program (BMU2019LCKXJ001), and Fundamental Research Funds for the Central Universities.

REFERENCES

1. Garland EM, Celedonio JE, Raj SR. Postural tachycardia syndrome: beyond orthostatic intolerance. *Curr Neurol Neurosci Rep.* (2015) 15:60. doi: 10.1007/s11910-015-0583-8
2. Stewart JM, Boris JR, Chelimsky G, Fischer PR, Fortunato JE, Grubb BP, et al. Pediatric disorders of orthostatic intolerance. *Pediatrics.* (2018) 141:e20171673. doi: 10.1542/peds.2017-1673
3. Wells R, Spurrier AJ, Linz D, Gallagher C, Mahajan R, Sanders P, et al. Postural tachycardia syndrome: current perspectives. *Vasc Health Risk Manag.* (2018) 14:1–11. doi: 10.2147/VHRM.S127393
4. Lin J, Han Z, Li X, Ochs T, Zhao J, Zhang X, et al. Risk factors for postural tachycardia syndrome in children and adolescents. *PLoS ONE.* (2014) 9:e113625. doi: 10.1371/journal.pone.0113625
5. Wang C, Li Y, Liao Y, Tian H, Huang M, Dong XY, et al. 2018 Chinese Pediatric Cardoilogy Society (CPCS) guideline for diagnosis and treatment of syncope in children and adolescents. *Sci Bull.* (2018) 63:1558–64. doi: 10.1016/j.scib.2018.09.019
6. Boris JR. Postural orthostatic tachycardia syndrome in children and adolescents. *Auton Neurosci.* (2018) 215:97–101. doi: 10.1016/j.autneu.2018.05.004
7. Tao C, Liu X, Zhang C, Chen Y, Huang Y. Comments on 2018 CPCS guideline for diagnosis and treatment of syncope in children and adolescents. *Sci Bull.* (2019) 64:291–2. doi: 10.1016/j.scib.2019.01.008
8. Xu W, Wang T. Diagnosis and treatment of syncope in pediatric patients: a new guideline. *Sci Bull.* (2019) 64:357. doi: 10.1016/j.scib.2019.01.024
9. Zhao J, Han Z, Zhang X, Du S, Liu AD, Holmberg L, et al. A cross-sectional study on upright heart rate and BP changing characteristics: basic data for establishing diagnosis of postural orthostatic tachycardia syndrome and orthostatic hypertension. *BMJ Open.* (2015) 5:e007356. doi: 10.1136/bmjopen-2014-007356
10. Zhang Q, Li J, Xie Y, Zhao J, Du J. Orthostatic hypertension in children and adolescents with postural tachycardia syndrome. *J Trop Pediatr.* (2014) 60:461–6. doi: 10.1093/tropej/fmu055
11. Boris JR, Bernadzik owski T. Demographics of a large paediatric postural orthostatic tachycardia syndrome program. *Cardoil Young.* (2018) 28:668–74. doi: 10.1017/S1047951117002888
12. Zadourian A, Doherty TA, Swiatkiewicz I, Taub PR. Postural orthostatic tachycardia syndrome: prevalence, pathophysiology, and management. *Drugs.* (2018) 78:983–94. doi: 10.1007/s40265-018-0931-5
13. Heyer GL. Postural tachycardia syndrome: diagnosis and management in adolescents and young adults. *Pediatr Ann.* (2017) 46:e145–54. doi: 10.3928/19382359-20170322-01
14. Stewart JM. Update on the theory and management of orthostatic intolerance and related syndromes in adolescents and children. *Expert Rev Cardoivasc Ther.* (2012) 10:1387–99. doi: 10.1586/erc.12.139
15. Stewart JM. Mechanisms of sympathetic regulation in orthostatic intolerance. *J Appl Physiol.* (2012) 113:1659–68. doi: 10.1152/japplphysiol.00266.2012
16. Fountain JH, Lappin SL. *Physiology, Renin Angiotensin System. StatPearls.* Treasure Island, FL: StatPearls Publishing (2019).
17. Sahni M, Lowenthal DT, Meuleman J. A clinical, physiology and pharmacology evaluation of orthostatic hypotension in the elderly. *Int Urol Nephrol.* (2005) 37:669–74. doi: 10.1007/s11255-005-7663-7
18. Platts SH, Tuxhorn JA, Ribeiro LC, Stenger MB, Lee SM, Meck JV. Compression garments as countermeasures to orthostatic intolerance. *Aviat Space Environ Med.* (2009) 80:437–42. doi: 10.3357/ASEM.2473.2009
19. Bai W, Chen SY, Jin HF, Du JB. Vascular dysfunction of postural tachycardia syndrome in children. *World J Pediatr.* (2018) 14:13–7. doi: 10.1007/s12519-017-0104-8
20. Raj SR, Robertson D. Blood volume perturbations in the postural tachycardia syndrome. *Am J Med Sci.* (2007) 334:57–60. doi: 10.1097/MAJ.0b013e318063c6c0
21. Raj SR, Biaggioni I, Yamhure PC, Black BK, Paranjape SY, Byrne DW, et al. Renin-aldosterone paradox and perturbed blood volume regulation underlying postural tachycardia syndrome. *Circulation.* (2005) 111:1574–82. doi: 10.1161/01.CIR.0000160356.97313.5D
22. El-Sayed H, Hainsworth R. Salt supplement increase plasma volume and orthostatic tolerance in patients with unexplained syncope. *Heart.* (1996) 75:134–40. doi: 10.1136/hrt.75.2.134
23. Zhang Q, Liao Y, Tang C, Du J, Jin H. Twenty-four-hour urinary sodium excretion and postural orthostatic tachycardia syndrome. *J Pediatr.* (2012) 16:281–4. doi: 10.1016/j.jpeds.2012.01.054
24. Jacob G, Robertson D, Mosqueda-Garcia R, Ertl AC, Robertson RM, Biaggioni I. Hypovolemia in syncope and orthostatic intolerance role of the renin-angiotensin system. *Am J Med.* (1997) 103:128–33. doi: 10.1016/S0002-9343(97)00133-2
25. Jacob G, Shannon JR, Black B, Biaggioni I, Mosqueda-Garcia R, Robertson RM, et al. Effects of volume loading and pressor agents in idoipathic orthostatic tachycardia. *Circulation.* (1997) 96:575–80. doi: 10.1161/01.CIR.96.2.575
26. Moak JP, Leong D, Fabian R, Freedenberg V, Jarosz E, Toney C, et al. Intravenous hydration for management of medication-resistant orthostatic intolerance in the adolescent and young adult. *Pediatr Cardoil.* (2016) 37:278–82. doi: 10.1007/s00246-015-1274-6
27. Medow MS, Stewart JM. The postural tachycardia syndrome. *Cardoil Rev.* (2007) 15:67–75. doi: 10.1097/01.crd.0000233768.68421.40
28. Jarjour IT. Postural tachycardia syndrome in children and adolescents. *Semin Pediatr Neurol.* (2013) 20:18–26. doi: 10.1016/j.spen.2013.01.001
29. Stewart JM, Medow MS, Cherniack NS, Natelson BH. Postural hypocapnic hyperventilation is associated with enhanced peripheral vasoconstriction in postural tachycardia syndrome with normal supine blood flow. *Am J Physiol Heart Circ Physiol.* (2006) 291:H904–13. doi: 10.1152/ajpheart.01359.2005
30. Stewart JM, Medow MS, Glover JL, Montgomery LD. Persistent splanchnic hyperemia during upright tilt in postural tachycardia syndrome. *Am J Physiol Heart Circ Physiol.* (2006) 290:H665–73. doi: 10.1152/ajpheart.00784.2005
31. Stewart JM, Montgomery LD. Regional blood volume and peripheral blood flow in postural tachycardia syndrome. *Am J Physiol Heart Circ Physiol.* (2004) 287:H1319–27. doi: 10.1152/ajpheart.00086.2004
32. Stewart JM, Medow MS, Montgomery LD. Local vascular responses affecting blood flow in postural tachycardia syndrome. *Am J Physiol Heart Circ Physiol.* (2003) 285:H2749–56. doi: 10.1152/ajpheart.00429.2003
33. Stewart JM. Microvascular filtration is increased in postural tachycardia syndrome. *Circulation.* (2003) 107:2816–22. doi: 10.1161/01.CIR.0000070951.93566.FC
34. Kumar V, Usmani S, Alam S, Fraz M, Patel D, Goparaju P, et al. MON-LB009 renin angiotensin aldosterone system inactivation in postural orthostatic tachycardia syndrome. *J Endocr Soc.* (2019) 3(Suppl. 1):MON–LB009. doi: 10.1210/js.2019-MON-LB009
35. Zheng X, Chen Y, Du J. Recent advances in the understanding of the mechanisms underlying postural tachycardia syndrome in children: practical implications for treatment. *Cardoil Young.* (2017) 27:413–7. doi: 10.1017/S1047951116002559
36. Stewart JM, Taneja I, Medow MS. Reduced body mass index is associated with increased angiotensin II in young women with postural tachycardia syndrome. *Clin Sci.* (2007) 113:449–57. doi: 10.1042/CS20070104
37. Li H, Liao Y, Wang Y, Liu P, Sun C, Chen Y, et al. Baroreflex sensitivity predicts short-term outcome of postural tachycardia syndrome in children. *PLoS ONE.* (2016) 11:e0167525. doi: 10.1371/journal.pone.0167525

38. Zhang Q, Chen X, Li J, Du J. Orthostatic plasma norepinephrine level as a predictor for therapeutic response to metoprolol in children with postural tachycardia syndrome. *J Transl Med.* (2014) 12:249. doi: 10.1186/s12967-014-0249-3
39. Khan AW, Corcoran SJ, Esler M, El-Osta A. Epigenomic changes associated with impaired norepinephrine transporter function in postural tachycardia syndrome. *Neurosci Biobehav Rev.* (2017) 74:342–55. doi: 10.1016/j.neubiorev.2016.06.015
40. Shannon JR, Flattem NL, Jordan J, Jacob G, Black BK, Biaggioni I, et al. Orthostatic intolerance and tachycardia associated with norepinephrine-transporter deficiency. *N Engl J Med.* (2000) 342:541–9. doi: 10.1056/NEJM200002243420803
41. Ojha A, Chelimsky TC, Chelimsky G. Comorbidities in pediatric patients with postural orthostatic tachycardia syndrome. *J Pediatr.* (2011) 158:20–3. doi: 10.1016/j.jpeds.2010.07.005
42. Deb A, Morgenshtern K, Culbertson CJ, Wang LB, Hohler AD. A survey-based analysis of symptoms in patients with postural orthostatic tachycardia syndrome. *Proc (Bayl Univ Med Cent).* (2015) 28:157–9. doi: 10.1080/08998280.2015.11929217
43. Bagai K, Song Y, Ling JF, Malow B, Black BK, Biaggioni I, et al. Sleep disturbances and diminished quality of life in postural tachycardia syndrome. *J Clin Sleep Med.* (2011) 7:204–10. doi: 10.5664/jcsm.28110
44. Chelimsky G, Kovacic K, Nugent M, Mueller A, Simpson P, Chelimsky TC. Comorbid conditions do not differ in children and young adults with functional disorders with or without postural tachycardia syndrome. *J Pediatr.* (2015) 167:120–4. doi: 10.1016/j.jpeds.2015.03.039
45. Miglis MG, Muppidi S, Feakins C, Fong L, Prieto T, Jaradeh S. Sleep disorders in patients with postural tachycardia syndrome. *Clin Auton Res.* (2016) 26:67–73. doi: 10.1007/s10286-015-0331-9
46. Miglis MG, Barwick F. Sleep disorders in patients with postural tachycardia syndrome: a review of the literature and guide for clinicians. *Auton Neurosci.* (2018) 215:62–9. doi: 10.1016/j.autneu.2018.05.002
47. Ross AJ, Medow MS, Rowe PC, Stewart JM. What is brain fog? An evaluation of the symptom in postural tachycardia syndrome. *Clin Auton Res.* (2013) 23:305–11. doi: 10.1007/s10286-013-0212-z
48. Bagai K, Peltier AC, Malow BA, Diedrich A, Shibao CA, Black BK, et al. Objective sleep assessments in patients with postural tachycardia syndrome using overnight polysomnograms. *J Clin Sleep Med.* (2016) 12:727–33. doi: 10.5664/jcsm.5806
49. Stewart JM. Common syndromes of orthostatic intolerance. *Pediatrics.* (2013) 131:968–80. doi: 10.1542/peds.2012-2610
50. Stewart JM, Medow MS, Montgomery LD, McLeod K. Decreased skeletal muscle pump activity in patients with postural tachycardia syndrome and low peripheral blood flow. *Am J Physiol Heart Circ Physiol.* (2004) 286:H1216–22. doi: 10.1152/ajpheart.00738.2003
51. Hainsworth R, Al-Shamma YM. Cardiovascular responses to upright tilting in healthy subjects. *Clin Sci.* (1988) 74:17–22. doi: 10.1042/cs0740017
52. Streeten DH, Scullard TF. Excessive gravitational blood pooling caused by impaired venous tone is the predominant non-cardiac mechanism of orthostatic intolerance. *Clin Sci.* (1996) 90:277–85. doi: 10.1042/cs0900277
53. Stewart JM, Weldon A. Vascular perturbations in the chronic orthostatic intolerance of the postural orthostatic tachycardia syndrome. *J Appl Physiol.* (2000) 89:1505–12. doi: 10.1152/jappl.2000.89.4.1505
54. Stewart JM, Weldon A. Reflex vascular defects in the orthostatic tachycardia syndrome of adolescents. *J Appl Physiol.* (2001) 90:2025–31. doi: 10.1152/jappl.2001.90.6.2025
55. Stewart JM. Pooling in chronic orthostatic intolerance: arterial vasoconstrictive but not venous compliance defects. *Circulation.* (2002) 105:2274–81. doi: 10.1161/01.CIR.0000016348.55378.C4
56. Mustafa HI, Raj SR, Diedrich A, Black BK, Paranjape SY, Dupont WD, et al. Altered systemic hemodynamic and baroreflex response to angiotensin II in postural tachycardia syndrome. *Circ Arrhythm Electrophysiol.* (2012) 5:173–80. doi: 10.1161/CIRCEP.111.965343
57. Brown CM, Hainsworth R. Assessment of capillary fluid shifts during orthostatic stress in normal subjects and subjectswith orthostatic intolerance. *Clin Auton Res.* (1999) 9:69–73. doi: 10.1007/BF02311762
58. Stewart JM, Taneja I, Medow MS. Reduced central blood volume and cardiac output and increased vascular resistance during static handgrip exercise in postural tachycardia syndrome. *Am J Physiol Heart Circ Physiol.* (2007) 293:H1908–17. doi: 10.1152/ajpheart.00439.2007
59. Lüscher TF. Endothelium-derived nitric oxide: the endogenous nitrovasodilator in the human cardoivascular system. *Eur Heart J.* (1991) 12(Suppl. E):2–11. doi: 10.1093/eurheartj/12.suppl_E.2
60. Liao Y, Chen S, Liu X, Zhang Q, Ai Y, Wang Y, et al. Flow-mediated vasodilation and endothelium function in children with postural orthostatic tachycardia syndrome. *Am J Cardoil.* (2010) 106:378–82. doi: 10.1016/j.amjcard.2010.03.034
61. d'Emmanuele di Villa Bianca R, Sorrentino R, Coletta C, Mitidieri E, Rossi A, Vellecco V, et al. Hydrogen sulfide-induced dual vascular effect involves arachidonic acid cascade in rat mesenteric arterial bed. *J Pharmacol Exp Ther.* (2011) 337:59–64. doi: 10.1124/jpet.110.176016
62. Yang J, Zhao J, Du S, Liu D, Fu C, Li X, et al. Postural orthostatic tachycardia syndrome with increased erythrocytic hydrogen sulfide and reponse to midodrine hydrochloride. *J Pediatr.* (2013) 163:1169–73. doi: 10.1016/j.jpeds.2013.04.039
63. Zhang F, Li X, Stella C, Chen L, Liao Y, Tang C, et al. Plasma hydrogen sulfide in differential diagnosis between vasovagal syncope and postural orthostatic tachycardia syndrome in children. *J Pediatr.* (2012) 160:227–31. doi: 10.1016/j.jpeds.2011.08.008
64. Liu D, Jin H, Tang C, Du J. Sulfur doixide: a novel gaseous signal in the regulation of cardoivascular functions. *Mini Rev Med Chem.* (2010) 10:1039–45. doi: 10.2174/1389557511009011039
65. Du SX, Jin HF, Bu DF, Zhao X, Geng B, Tang CS, et al. Endogenously generated sulfur doixide and its vasorelaxant effect in rats. *Acta Pharmacol Sin.* (2008) 29:923–30. doi: 10.1111/j.1745-7254.2008.00845.x
66. Li HX, Zheng XC, Chen SY, Liao Y, Han ZH, Huang P, et al. Increased endogenous sulfur doixide involved in the pathogenesis of postural tachycardia syndrome in children: a case-control study. *Chin Med J.* (2018) 131:435–9. doi: 10.4103/0366-6999.225051
67. Telli G, Erac Y, Tel BC, Gumusel B. Mechanism of adrenomedullin 2/intermedin mediated vasorelaxation in rat main pulmonary artery. *Peptides.* (2018) 103:65–71. doi: 10.1016/j.peptides.2018.03.015
68. Li H, Liao Y, Han Z, Wang Y, Liu P, Zhang Q, et al. Changes of plasma intermedin during head-up tilt test in children with postural tachycardia syndrome and its significance. *Zhonghua Er Ke Za Zhi.* (2015) 53:375–8. doi: 10.3760/cma.j.issn.0578-1310.2015.05.013
69. Potter LR, Yoder AR, Flora DR, Antos LK, Dickey DM. Natriuretic peptides: their structures, receptors, physiologic functions and therapeutic applications. *Handb Exp Pharmacol.* (2009) 191:341–66. doi: 10.1007/978-3-540-68964-5_15
70. Chen HH, Burnett JC Jr. C-type natriuretic peptide: the endothelial component of the natriuretic peptide system. *J Cardoivasc Pharmacol.* (1998) 32(Suppl 3):S22–8.
71. Li H, Han Z, Chen S, Liao Y, Wang Y, Liu P, et al. Total peripheral vascular resistance, cardiac output, and plasma C-type natriuretic peptide level in children with postural tachycardia syndrome. *J Pediatr.* (2015) 166:1385–9. doi: 10.1016/j.jpeds.2015.03.032
72. Steppan CM, Bailey ST, Bhat S, Brown EJ, Banerjee RR, Wright CM, et al. The hormone resistin links obesity to diabetes. *Nature.* (2001) 409:307–12. doi: 10.1038/35053000
73. Oriowo MA. Perivascular adipose tissue, vascular reactivity and hypertension. *Med Princ Pract.* (2015) 24(Suppl. 1):29–37. doi: 10.1159/000356380
74. Chen C, Jiang J, Lü JM, Chai H, Wang X, Lin PH, et al. Resistin decreases expression of endothelial nitric oxide synthase through oxidative stress in human coronary artery endothelial cells. *Am J Physiol Heart Circ Physiol.* (2010) 299:H193–201. doi: 10.1152/ajpheart.00431.2009
75. Bai W, Han Z, Chen S, Li H, Song J, Qi J, et al. Serum resistin negatively correlates with clinical severity of postural tachycardia syndrome in children. *Pediatr Cardoil.* (2017) 38:1639–44. doi: 10.1007/s00246-017-1708-4
76. Dev S, Babitt JL. Overview of iron metabolism in health and disease. *Hemodial Int.* (2017) 21(Suppl. 1):S6–20. doi: 10.1111/hdi.12542
77. Hsiao HY, Chung CW, Santos JH, Villaflores OB, Lu TT. Fe in biosynthesis, translocation, and signal transduction of NO: toward bioinorganic engineering of dinitrosyl iron complexes into NO-delivery scaffolds for tissue engineering. *Dalton Trans.* (2019) 48:9431–53. doi: 10.1039/C9DT00777F

78. Antiel RM, Caudill JS, Burkhardt BE, Brands CK, Fisher PR. Iron insufficiency and hypovitaminosis D in adolescents with chronic fatigue and orthostatic intolerance. *South Med J.* (2011) 104:609–11. doi: 10.1097/SMJ.0b013e3182246809
79. Jarjour IT, Jarjour LK. Low iron storage and mild anemia in postural tachycardia syndrome in adolescents. *Clin Auton Res*. (2013) 23:175–9. doi: 10.1007/s10286-013-0198-6
80. Choi JW, Pai SH, Kim SK, Ito M, Park CS, Cha YN. Iron deficiency anemia increases nitric oxide production in healthy adolescents. *Ann Hematol.* (2002) 81:1–6. doi: 10.1007/s00277-001-0409-4
81. Lu W, Yan H, Wu S, Xu W, Jin H, Du J. Hemocytometric measures predict the efficacy of oral rehydration for children with postural tachycardia syndrome. *J Pediatr*. (2017) 187:220–4. doi: 10.1016/j.jpeds.2017.04.034
82. Shibao C, Arzubiaga C, Roberts LJ 2nd, Raj S, Black B, Harris P, et al. Hyperadrenergic postural tachycardia syndrome in mast cell activation disorders. *Hypertension*. (2005) 45:385–90. doi: 10.1161/01.HYP.0000158259.68614.40
83. Romero SA, McCord JL, Ely MR, Sieck DC, Buck TM, Luttrell MJ, et al. Mast cell degranulation and de novo histamine formation contribute to sustained post exercise vasodilation in humans. *J Appl Physiol.* (2017) 122:603–10. doi: 10.1152/japplphysiol.00633.2016
84. Vadas P, Gold M, Perelman B, Liss GM, Lack G, Blyth T, et al. Platelet-activating factor, PAF acetylhydrolase, and severe anaphylaxis. *N Engl J Med.* (2008) 358:28–35. doi: 10.1056/NEJMoa070030
85. Doherty TA, White AA. Postural orthostatic tachycardia syndrome and the potential role of mast cell activation. *Auton Neurosci*. (2018) 215:83–8. doi: 10.1016/j.autneu.2018.05.001
86. Dahan S, Tomljenovic L, Shoenfeld Y. Postural orthostatic tachycardia syndrome (POTS) – a novel member of the autoimmune family. *Lupus.* (2016) 25:339–42. doi: 10.1177/0961203316629558
87. Li J, Zhang Q, Hao H, Jin H, Du J. Clinical features and management of postural tachycardia syndrome in children: a single-center experience. *Chin Med J.* (2014) 127:3684–9. doi: 10.3760/cma.j.issn.0366-6999.20140244s
88. Watari M, Nakane S, Mukaino A, Nakajima M, Mori Y, Maeda Y, et al. Autoimmune postural orthostatic tachycardia syndrome. *Ann Clin Transl Neurol.* (2018) 5:486–92. doi: 10.1002/acn3.524
89. Wang Z, Low PA, Vernino S. Antibody-mediated impairment and homeostatic plasticity of autonomic ganglionic synaptic transmission. *Exp Neurol.* (2010) 222:114–9. doi: 10.1016/j.expneurol.2009.12.016
90. Fedorowski A, Li H, Yu X, Koelsch KA, Harris VM, Liles C, et al. Antiadrenergic autoimmunity in postural tachycardia syndrome. *Europace.* (2017) 19:1211–9. doi: 10.1093/europace/euw154
91. Yu XC, Li HL, Murphy TA, Nuss Z, Liles J, Liles C, et al. Angiotensin II type 1 receptor autoantibodies in postural tachycardia syndrome. *J Am Heart Assoc.* (2018) 7:e008351. doi: 10.1161/JAHA.117.008351
92. Li H, Yu X, Liles C, Khan M, Vanderlinde-Wood M, Galloway A, et al. Autoimmune basis for postural tachycardia syndrome. *J Am Heart Assoc.* (2014) 3:e000755. doi: 10.1161/JAHA.113.000755
93. Blitshteyn S. Autoimmune markers and autoimmune disorders in patients with postural tachycardia syndrome (POTS). *Lupus.* (2015) 24:1364–9. doi: 10.1177/0961203315587566
94. Vernino S, Stiles LE. Autoimmunity in postural orthostatic tachycardic syndrome: current understanding. *Auton Neurosci*. (2018) 215:78–82. doi: 10.1016/j.autneu.2018.04.005
95. Kizilbash SJ, Ahrens SP, Bruce BK, Chelimsky G, Driscoll SW, Harbeck-Weber C, et al. Adolescent fatigue, POTS, and recovery: a guide for clinicians. *Curr Probl Pediatr Adolesc Health Care.* (2014) 44:108–33. doi: 10.1016/j.cppeds.2013.12.014
96. Xu WR, Jin HF, Du JB. Pathogenesis and individualized treatment for postural tachycardia syndrome in children. *Chin Med J.* (2016) 129:2241–5. doi: 10.4103/0366-6999.189915
97. Lin J, Zhao H, Shen J, Jiao F. Salivary cortisol levels predict therapeutic response to a sleep-promoting method in children with postural tachycardia syndrome. *J Pediatr*. (2017) 191:91–5. doi: 10.1016/j.jpeds.2017.08.039
98. Sheldon RS, Grubb BP, Olshansky B, Shen WK, Calkins H, Brignole M, et al. 2015 heart rhythm society expert consensus statement on the diagnosis and treatment of postural tachycardia syndrome, inappropriate sinus tachycardia, and vasovagal syncope. *Heart Rhythm.* (2015) 12:e41–63. doi: 10.1016/j.hrthm.2015.03.029
99. Winker R, Barth A, Bidmon D, Ponocny I, Weber M, Mayr O, et al. Endurance exercise training in orthostatic intolerance: a randomized, controlled trial. *Hypertension.* (2005) 45:391–8. doi: 10.1161/01.HYP.0000156540.25707.af
100. Lu W, Yan H, Wu S, Chen S, Xu W, Jin H, et al. Electrocardiography-derived predictors for therapeutic response to treatment in children with postural tachycardia syndrome. *J Pediatr*. (2016) 176:128–33. doi: 10.1016/j.jpeds.2016.05.030
101. Fu Q, Vangundy TB, Shibata S, Auchus RJ, Williams GH, Levine BD. Exercise training versus propranolol in the treatment of the postural orthostatic tachycardia syndrome. *Hypertension*. (2011) 58:167–75. doi: 10.1161/HYPERTENSIONAHA.111.172262
102. Fu Q, Levine BD. Exercise in the postural orthostatic tachycardia syndrome. *Auton Neurosci.* (2015) 188:86–9. doi: 10.1016/j.autneu.2014.11.008
103. Shibata S, Fu Q, Bivens TB, Hastings JL, Wang W, Levine BD. Short-term exercise training improves the cardoivascular response to exercise in the postural orthostatic tachycardia syndrome. *J Physiol.* (2012) 590:3495–505. doi: 10.1113/jphysiol.2012.233858
104. Li H, Wang Y, Liu P, Chen Y, Feng X, Tang C, et al. Body mass index (BMI) is associated with the therapeutic response to oral rehydration solution in children with postural tachycardia syndrome. *Pediatr Cardoil.* (2016) 37:1313–8. doi: 10.1007/s00246-016-1436-1
105. Lin J, Liu P, Wang Y, Li H, Li X, Zhao J, et al. Evaluation of the changes in heart rate during head-up test predicting the efficacy of oral rehydration salts on postural tachycardia syndrome in children. *Zhonghua Er Ke Za Zhi.* (2015) 53:25–9. doi: 10.2106/JBJS.O.00099
106. McClellan KJ, Wiseman LR, Wilde MI. Midodrine. A review of its therapeutic use in the management of orthostatic hypotension. *Drugs Aging.* (1998) 12:76–86. doi: 10.2165/00002512-199812010-00007
107. Chen L, Wang L, Sun J, Qin J, Tang C, Jin H, et al. Midodrine hydrochloride is effective in the treatment of children with postural orthostatic tachycardia syndrome. *Circ J.* (2011) 75:927–31. doi: 10.1253/circj.CJ-10-0514
108. Lin J, Jin H, Du J. Assessment of therapeutic biomarkers in the treatment of children with postural tachycardia syndrome and vasovagal syncope. *Cardoil Young.* (2014) 24:792–6. doi: 10.1017/S1047951114000316
109. Liao Y, Yang J, Zhang F, Chen S, Liu X, Zhang Q, et al. Flow-mediated vasodilation as a predictor of therapeutic response to midodrine hydrochloride in children with postural orthostatic tachycardia syndrome. *Am J Cardoil.* (2013) 112:816–20. doi: 10.1016/j.amjcard.2013.05.008
110. Zhang F, Li X, Ochs T, Chen L, Liao Y, Tang C, et al. Midregional pro-adrenomedullin as a predictor for therapeutic response to midodrine hydrochloride in children with postural orthostatic tachycardia syndrome. *J Am Coll Cardoil.* (2012) 60:315–20. doi: 10.1016/j.jacc.2012.04.025
111. Zhao J, Tang C, Jin H, Du J. Plasma copeptin and therapeutic effectiveness of midodrine hydrochloride on postural tachycardia syndrome in children. *J Pediatr.* (2014) 165:290–4. doi: 10.1016/j.jpeds.2014.04.032
112. Deng W, Liu Y, Liu AD, Holmberg L, Ochs T, Li X, et al. Difference between supine and upright blood pressure associates to the efficacy of midodrine on postural orthostatic tachycardia syndrome (POTS) in children. *Pediatr Cardoil.* (2014) 35:719–25. doi: 10.1007/s00246-013-0843-9
113. Li HX, Deng WJ, Zhang CY, Jin HF, Du JB. Predictive value of upright blood pressure change for long-term prognosis of children with postural tachycardia syndrome treated with midodrine hydrochloride. *Zhonghua Er Ke Za Zhi.* (2016) 54:519–22. doi: 10.3760/cma.j.issn.0578-1310.2016.07.009
114. Ogrodowczyk M, Dettlaff K, Jelinska A. Beta-blockers: current state of knowledge and perspectives. *Mini Rev Med Chem*. (2016) 16:40–54. doi: 10.2174/1389557515666151016125948
115. López-Sendón J, Swedberg K, McMurray J, Tamargo J, Maggioni AP, Dargie H, et al. Expert consensus document on beta-adrenergic receptor blockers. *Eur Heart J.* (2004) 25:1341–62. doi: 10.1016/j.ehj.2004.06.002
116. Lai CC, Fischer PR, Brands CK, Fisher JL, Porter CB, Driscoll SW, et al. Outcomes in adolescents with postural orthostatic tachycardia syndrome treated with midodrine and beta-blockers. *Pacing Clin Electrophysiol.* (2009) 32:234–8. doi: 10.1111/j.1540-8159.2008.02207.x

117. Lin J, Han Z, Li H, Chen SY, Li X, Liu P, et al. Plasma C-type natriuretic peptide as a predictor for therapeutic response to metoprolol in children with postural tachycardia syndrome. *PLoS ONE*. (2015) 10:e0121913. doi: 10.1371/journal.pone.0121913
118. Zhao J, Du S, Yang J, Lin J, Tang C, Du J, et al. Usefulness of plasma copeptin as a biomarker to predict the therapeutic effectiveness of metoprolol for postural tachycardia syndrome in children. *Am J Cardoil*. (2014) 114:601–5. doi: 10.1016/j.amjcard.2014.05.039

Conflict of Interest: The authors declare that the research was conducted in the absence of any commercial or financial relationships that could be construed as a potential conflict of interest.

frontiers in Physiology

REVIEW
published: 27 August 2020
doi: 10.3389/fphys.2020.01085

Measurement, Analysis and Interpretation of Pressure/Flow Waves in Blood Vessels

Jonathan P. Mynard[1,2,3,4], Avinash Kondiboyina[1,2], Remi Kowalski[1,2,4], Michael M. H. Cheung[1,2,4] and Joseph J. Smolich[1,2]*

[1] Heart Research, Murdoch Children's Research Institute, Melbourne, VIC, Australia, [2] Department of Paediatrics, The University of Melbourne, Melbourne, VIC, Australia, [3] Department of Biomedical Engineering, The University of Melbourne, Melbourne, VIC, Australia, [4] Department of Cardiology, The Royal Children's Hospital, Parkville, VIC, Australia

The optimal performance of the cardiovascular system, as well as the break-down of this performance with disease, both involve complex biomechanical interactions between the heart, conduit vascular networks and microvascular beds. 'Wave analysis' refers to a group of techniques that provide valuable insight into these interactions by scrutinizing the shape of blood pressure and flow/velocity waveforms. The aim of this review paper is to provide a comprehensive introduction to wave analysis, with a focus on key concepts and practical application rather than mathematical derivations. We begin with an overview of invasive and non-invasive measurement techniques that can be used to obtain the signals required for wave analysis. We then review the most widely used wave analysis techniques—pulse wave analysis, wave separation and wave intensity analysis—and associated methods for estimating local wave speed or characteristic impedance that are required for decomposing waveforms into forward and backward wave components. This is followed by a discussion of the biomechanical phenomena that generate waves and the processes that modulate wave amplitude, both of which are critical for interpreting measured wave patterns. Finally, we provide a brief update on several emerging techniques/concepts in the wave analysis field, namely wave potential and the reservoir-excess pressure approach.

Keywords: haemodynamics, pulse wave analysis, wave intensity analysis, wave separation, wave speed, reservoir pressure

OPEN ACCESS

Edited by:
Stefano Tarantini, The University of Oklahoma Health Sciences Center, United States

Reviewed by:
Timothy W. Secomb, The University of Arizona, United States
Alun Hughes, University College London, United Kingdom

****Correspondence:***
Jonathan P. Mynard
jonathan.mynard@mcri.edu.au

Specialty section:
This article was submitted to Vascular Physiology, a section of the journal Frontiers in Physiology

Received: *21 May 2020*
Accepted: *06 August 2020*
Published: *27 August 2020*

Citation:
Mynard JP, Kondiboyina A, Kowalski R, Cheung MMH and Smolich JJ (2020) Measurement, Analysis and Interpretation of Pressure/Flow Waves in Blood Vessels. Front. Physiol. 11:1085. doi: 10.3389/fphys.2020.01085

INTRODUCTION

Cardiovascular disease has a profound impact on people around the world and across the human lifespan, accounting for 31% of all deaths globally (World Health Organization, 2013), as well as being the most common and costly category of birth defects (Centers for Disease Prevention and Control, 2019). While many factors contribute to the incidence and progression of cardiovascular disease, adverse outcomes are ultimately determined by a failure or ineffectiveness of the biomechanical system to deliver oxygenated blood to organs and tissues. Importantly, the major biomechanical properties of the heart and circulatory system, including cardiac contraction, ventriculo-vascular coupling, large artery stiffness, and microvasculature properties, all influence the pattern of pressure/flow waves that can be measured in blood vessels. The chief aim of

'wave analysis' is therefore to reliably measure and then 'decode' the pattern of waves to uncover insights about disease processes and therapies that may not be provided by conventional metrics such as systolic and diastolic blood pressure.

A range of established and emerging wave analyses are available, including pulse wave analysis, wave separation, wave intensity (with several variations), and reservoir-excess pressure analysis. While each has strengths and weaknesses, along with aspects that are still being debated and refined, a number of prominent clinical studies have shown that wave analyses provide valuable prognostic information over and above traditional risk factors (Manisty et al., 2010; Weber et al., 2010, 2012; Davies et al., 2014; Zamani et al., 2014; Narayan et al., 2015; Zamani et al., 2016; Chirinos, 2017; Chiesa et al., 2019). However, to optimize prognostic value and to obtain mechanistic insights while avoiding misinterpretations, it is essential to develop a clear understanding of the physiological determinants of the various indices obtained from wave analysis.

The aim of this review is to introduce key techniques and concepts relating to arterial wave analyses, whilst also providing an update on recent developments and emerging techniques in the field. We start by briefly reviewing techniques for measuring blood pressure, flow, and velocity waveforms, then cover the most well-established wave analysis techniques (pulse wave analysis, wave separation and wave intensity analysis). We then review the biomechanical factors that generate and modulate pressure/flow waves, an understanding of which is likely to aid in the interpretation of wave patterns. Finally, several emerging concepts in the wave analysis field are briefly discussed (reservoir and excess pressure analysis, and wave potential). To appeal to a broad readership, this review will contain minimal mathematics and no derivations, but references will be provided where such details can be found.

WHAT IS A WAVE?

While the term 'wave' is attributed different meanings in different settings, in this review we adopt the definition of Hughes et al. (2008) that a *wave is a change in pressure and flow that propagates along a blood vessel* (**Figure 1**). Conversely the term 'waveform' herein refers to the pressure or flow pulse signal that can be measured at a particular vascular location. Waves travel at a velocity, known as *wave speed* or *pulse wave velocity*, that is typically more than ten times faster than the velocity of flowing blood; for example, pulse wave velocity of the aorta is around 5 m/s in youth, although this increases more than twofold over the normal human lifespan (McEniery et al., 2005). Every wave has an effect on both pressure and flow, and these effects are intrinsically linked by the *characteristic impedance* of the vessel, which in large arteries is proportional to wave speed and inversely proportional to vessel cross-sectional area. When a wave encounters a change in characteristic impedance, some of the wave energy is reflected and some is transmitted (**Figure 1**).

Pressure and flow waveforms result from a set of waves that pass by the measurement location, with each wave causing an increment or decrement in those waveforms (**Figure 1**, bottom panels). By performing wave analysis, we aim to extract information about the waves that produced the pulse waveforms and make inferences about their origins. For example, common questions in the field of arterial haemodynamics include: To what extent do reflected waves contribute to rises in blood pressure with aging or in certain disease conditions? Where are wave reflections occurring and does the distance to the reflection site (or 'effective distance' given that there are many reflection sites) change with age or disease? How much does wave reflection versus aortic characteristic impedance contribute to left ventricular afterload? Which specific waves are increasing or decreasing with an intervention and what insight does this provide about mechanisms of action? In coronary arteries, what is the interplay between upstream (ventriculo-aortic) vs. downstream (intramyocardial) forces in generating and modulating myocardial perfusion?

A fundamental precursor to addressing such questions is ensuring that the required physiological data can be measured, and with adequate quality. Depending on available equipment, resources and expertise, this is not always easy in a clinical setting. Most wave analyses require a pressure waveform (or a distension-based surrogate) and a flow or velocity waveform, although some techniques use only pressure. Importantly, since wave information resides in the shape of the waveform(s), the reliability of the final analysis depends on acquiring reproducible signals with high fidelity.

MEASUREMENT OF PRESSURE WAVEFORMS

Invasive Measurement

The gold-standard for acquiring the blood pressure waveform is invasive measurement, either with a micromanometer-tipped catheter or fluid-filled catheter and external manometer (Papaioannou et al., 2009; Nichols and O'Rourke, 2011). Micromanometer-tipped catheters provide a high fidelity waveform due to their excellent frequency response. While often used in animal studies (van den Bos et al., 1982; Khir and Parker, 2005; Penny et al., 2008), similar single-use pressure wires are used in humans, but are expensive. Fluid-filled catheter systems are cheaper, but their frequency response can be poor and should be tested to ensure waveform features are faithfully captured (Nichols and O'Rourke, 2011). Even in a system with an adequate frequency response, damping can develop over time, for example, if the catheter is not properly flushed. While investigators should be vigilant against such damping, Howard et al. (2019) recently described an artificial intelligence approach that may help automatically identify this issue.

Non-invasive Measurement

Applanation tonometry and the volume-clamp method are non-invasive techniques for measuring the arterial pressure pulse waveform. Applanation tonometry involves 'applanating' (slightly compressing against bone) a superficial artery with a pen-like pressure transducer (Drzewiecki et al., 1983; Kelly, 1989), which requires good dexterity and experience,

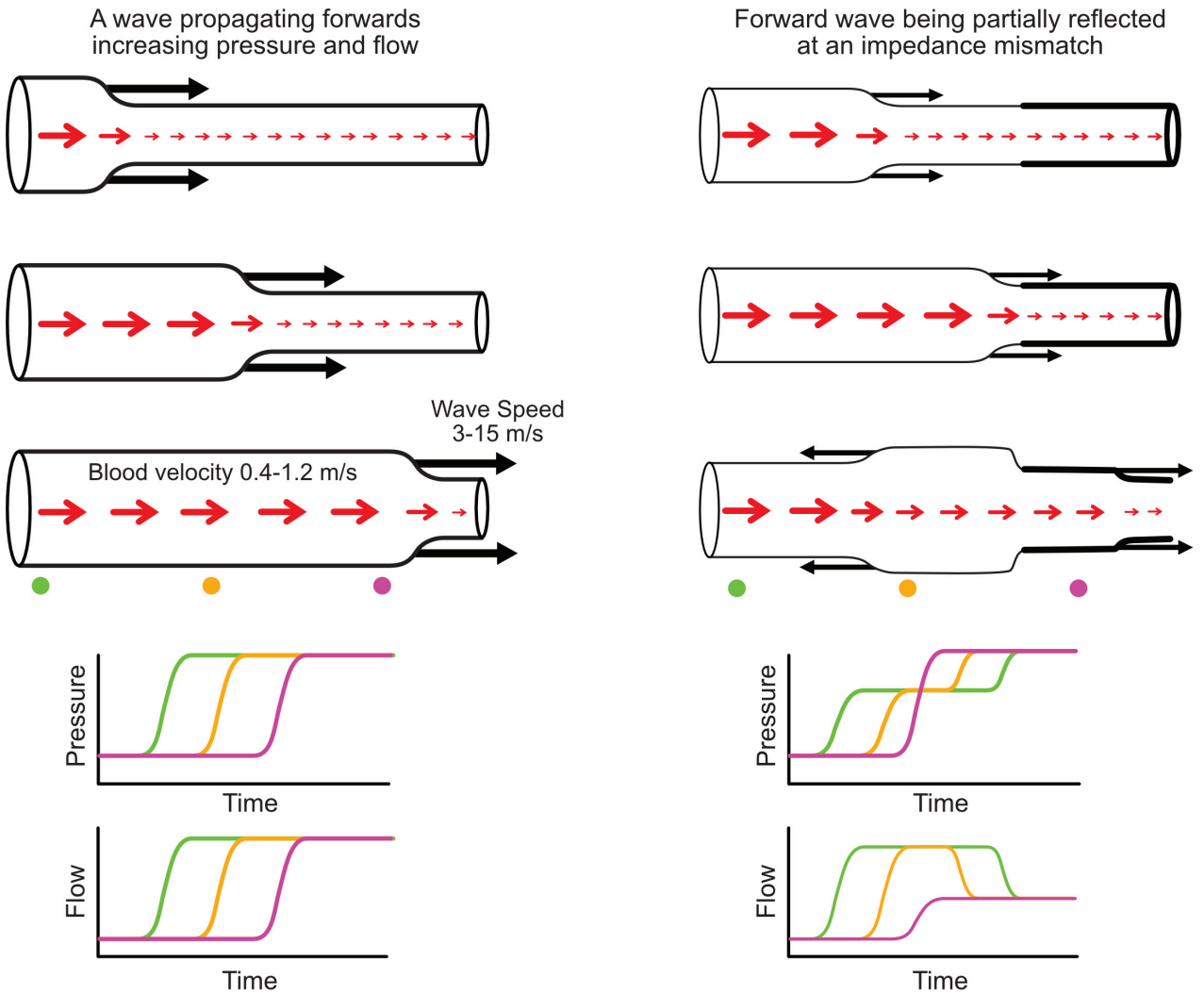

FIGURE 1 | (Left) Illustration of a forward-propagating wave that increases pressure and flow. **(Right)** A forward-propagating wave encounters an impedance mismatch (increased vessel stiffness indicated by thicker wall) and is partially transmitted and partially reflected. The reflected wave propagates backward and causes a further increase in pressure but a decreased flow. Red arrows indicate blood flow or average blood velocity over a cross-section (larger arrow means higher flow/velocity), while black arrows indicate wave speed and direction of wave propagation. Increased pressure is indicated by increased vessel diameter. Time plots (bottom) indicate the evolution of pressure and flow at three locations along the vessel indicated with color-coded circles.

but is relatively easy to learn. Dependence on a manual operator is potentially avoidable with emerging wearable devices (Garcia-Ortiz et al., 2012), although attaining and maintaining correct sensor position is a key challenge. Adequate applanation can be achieved in most individuals for the radial artery, but can be more difficult in other locations (e.g., brachial or carotid arteries) (Nichols and O'Rourke, 2011). Calibration of the pulse waveform is generally performed with conventional brachial cuff pressures, which may involve errors due to cuff pressure inaccuracies and pulse amplification from brachial to radial sites (Verbeke et al., 2005; Picone et al., 2017).

The volume-clamp method, originally described by Peñáz (1973) and refined and commercialized as the Finapres by Wesseling (1995) involves a finger cuff whose air pressure is controlled by a servo that clamps the volume of finger arteries using an infrared photoplethysmography (PPG) signal. This method provides high fidelity waveforms, is often used where continuous non-invasive pressure monitoring is required, and has the benefit of self-calibration, although the precision of absolute pressure values does not meet the AAMI requirement of an error standard deviation less than 8 mmHg (Kim et al., 2014). The technique is widely applicable, but may be difficult to perform in small children or where peripheral vasoconstriction (e.g., due to 'feeling cold') lead to an inadequate PPG signal, while accuracy may be reduced if the finger cuff is applied too loosely (Imholz et al., 1998). Compared with the volume-clamp method, tonometry is less cumbersome, involves less discomfort, and can be applied to a range of arterial sites, which may underlie its more widespread use in the wave analysis field.

Surrogate Measures of the Pressure Waveform

While catheterization, applanation tonometry, and the volume-clamp method in principle measure the actual blood pressure waveform, the techniques discussed below are surrogates, in that a form of distension (diameter, area, or volume change) is used to approximate the pressure waveform after appropriate calibration. When adopting these techniques, two biomechanical factors should be kept in mind. First, the relationship between pressure and distension is not strictly linear. For example, although the carotid pressure-distension relationship can appear approximately linear (Watanabe et al., 1999; Sugawara et al., 2000), Vermeersch et al. (2008) found that a non-linear (exponential) calibration of diameter to pressure improved the waveform fit (RMSE) by 28%. The degree of non-linearity also increases with age and with greater range of distension (Pagani et al., 1979; Langewouters et al., 1984; Meinders and Hoeks, 2004). Second, the pressure-distension relationship exhibits hysteresis due to the viscoelastic properties of vessel walls. This means that although pressure and distension follow a similar trajectory on the ascending limb of the pulse, these signals diverge on the descending (diastolic) limb due to viscous energy losses in the arterial wall (Armentano et al., 1995; Watanabe et al., 1999). Using a computational model, Kang et al. (2019) studied the impact of non-linearities and viscoelasticity on distension-based wave intensity analysis and concluded that the use of diameter as a surrogate for pressure is likely to introduce tolerable errors (<10%), although this requires further confirmation *in vivo*.

Arterial diameter changes can be measured with a range of techniques (**Figure 2**). Radio frequency (RF) echo-tracking is considered the most accurate and has high temporal and spatial resolution, but requires specialized equipment and software not available on most standard ultrasound systems (Hoeks et al., 1990; Niki et al., 2002; Segers et al., 2004); results may also be system-dependent (Palombo et al., 2012). Edge-tracking of the arterial wall in B-mode ultrasound images is a lower resolution, but widely available alternative to RF echo-tracking that has acceptable accuracy for total distension, although accuracy of waveform shape has not been investigated (Steinbuch et al., 2016; Di Lascio et al., 2018). M-mode imaging has high temporal resolution and only requires segmentation of one image, in contrast to the lower resolution and many image frames in B-mode (Kowalski et al., 2019a,b). A number of ambulatory sensor technologies are emerging for measurement of arterial distension, such as RF-echo tracking with a flexible ultrasonic sensor array patch (Wang et al., 2018) and low-frequency (∼1 GHz) continuous-wave radar (Buxi et al., 2017; Pisa et al., 2018). High-frequency (∼60 GHz) radar (Johnson et al., 2019) and double integration of an accelerometric signal (Di Lascio et al., 2018) are also showing promising results, despite measuring the motion of the skin surface due to the pulse rather than arterial diameter *per se*.

Aortic cross-sectional area changes have been used as a surrogate of the central pressure waveform and can be obtained via phase contrast magnetic resonance imaging (MRI, **Figure 2**) (Biglino et al., 2012; Quail et al., 2014; Li et al., 2019). This approach has limited temporal resolution (currently up to ∼100 Hz) and requires segmentation of the aortic circumference from the magnitude images, which can be challenging during low-flow phases of the cardiac cycle or in low-flow segments of the vessel wall that display poor contrast. However, the advantage is that the phase images, obtained with the same MRI sequence, provide simultaneous flow information.

While arterial volume cannot be easily measured directly, volume plethysmography of a limb or finger segment is commonly used to derive a pulse waveform. When a standard arm cuff is inflated and held at a fixed pressure, brachial arterial pulsations induce oscillations in cuff air pressure that can be registered by a device. Supra-systolic oscillometry, which causes arterial occlusion, is employed by a number of devices (Horvath et al., 2010; Lin et al., 2012; Park et al., 2014; Stoner et al., 2014; Bhuva et al., 2019); however, Butlin et al. (2012) reported that this technique led to artifacts such as elimination of the diastolic portion of the waveform. Sub-diastolic oscillometry is non-occlusive and involves less patient discomfort, and is commonly used in commercial devices (Wassertheurer et al., 2010; Butlin et al., 2012; Luzardo et al., 2012; Parikh et al., 2016). Pulsations can also be monitored in the finger with standard photoplethysmography and converted to a pressure pulse with a transfer function (Millasseau et al., 2000).

Mathematical Derivation of the Central Pulse Waveform

Central aortic blood pressure is of particular interest in many studies, as it represents the direct pressure load faced by the ejecting left ventricle. Although many of the aforementioned techniques acquire peripheral arterial signals, a central aortic pressure waveform can be derived from these via a generalized transfer function or other model-based methods (Chen et al., 1997; Karamanoglu and Feneley, 1997; Gallagher et al., 2004; Wassertheurer et al., 2010; Stok et al., 2011). This is a popular approach for estimation of both central systolic pressure and central wave indices such as augmentation index; however, a number of invasive validation studies have found that central wave indices derived using these methods may have limited accuracy, most likely due to individual variability in the higher frequency components (Chen et al., 1997; Fetics et al., 1999; Millasseau et al., 2003). This limitation does not appear to preclude this approach from having substantive clinical value when using high fidelity applanation tonometry (Weber et al., 2004, 2010; Vlachopoulos et al., 2010; Janner et al., 2013; Zamani et al., 2014), although more evidence is needed for commercial devices that employ surrogate measures of the pressure waveform, such as cuff volume plethysmography, which have considerably lower fidelity.

MEASUREMENT OF FLOW AND VELOCITY WAVEFORMS

Some wave analysis techniques employ only a pressure waveform (as will be discussed later), but these involve more assumptions

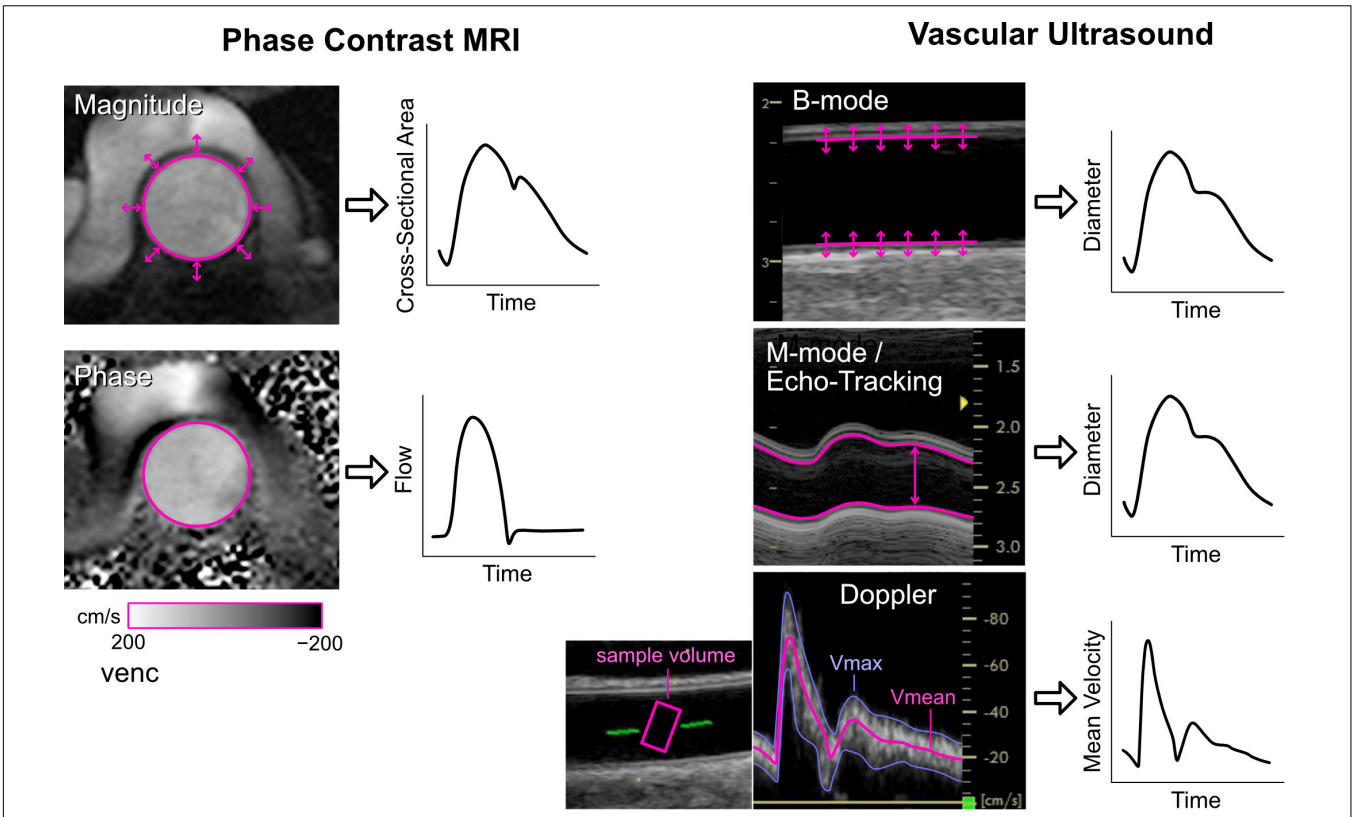

FIGURE 2 | Imaging methods for obtaining cross-sectional area or diameter waveforms and flow or mean velocity waveforms. See text for explanation. Note that echo-tracking is similar to standard M-mode but uses raw radio-frequency signals. For Doppler ultrasound, Vmax and Vmean are the maximum and mean velocities in the sample volume, respectively.

and are considered less reliable than techniques that harness blood pressure *and* flow/velocity information (Townsend et al., 2015). Blood flow and blood velocity are distinct physical quantities that both involve challenges in accurate measurement. Blood flow refers to the volumetric transport of fluid (units of volume/time) and is defined over a given arterial cross-section. On the other hand, blood velocity (or 'flow-velocity,' the velocity of flowing blood) refers to the speed of a moving particle of blood (units of distance/time). Velocity therefore varies over an arterial cross-section, producing a 'velocity profile.' In a long cylindrical tube with constant flow, the velocity profile has a parabolic shape, but more complex velocity profiles arise in real arteries, which are curved and exhibit pulsatile flow (Sigovan et al., 2011; Mynard and Steinman, 2013).

Invasive Measurement

Perivascular flow probes using transit-time ultrasound methods are considered the gold-standard for invasive flow measurement, although their ±5–15% absolute accuracy is modest (Laustsen et al., 1996; Beldi et al., 2000; Zhang et al., 2019). Commonly used in animal or benchtop experiments (Khir and Parker, 2002; Penny et al., 2008), these probes require good acoustic coupling (e.g., with ultrasound gel) between the vessel wall and internal probe housing, but can maintain accuracy for several years in chronically instrumented experiments (Picker et al., 2000).

In humans, flow probe use tends to be limited to the clinical assessment of bypass grafts (Thuijs et al., 2019), whereas invasive arterial wave analysis tends to be performed based on blood velocity measurements from Doppler 'flow-wires' (which actually measure velocity, not flow), such as the Philips Volcano ComboWire that also incorporates a micromanometer for concurrent pressure measurement. This approach has been particularly useful for wave analyses in coronary arteries (Hadjiloizou et al., 2008; Rolandi et al., 2012; Rivolo et al., 2016), but has also been used in the aorta and pulmonary artery (Hughes and Parker, 2009; Lau et al., 2014).

Non-invasive Measurement

The gold-standard non-invasive method for measuring flow is phase contrast (PC-)MRI, in which the motion of magnetic spins through a magnetic field gradient enables velocity encoding in a specified direction (Pelc et al., 1991). Arterial flow is obtained by setting a 2D acquisition plane through the chosen vessel cross-section, encoding velocity through-plane, and integrating velocities over the arterial cross-section (**Figure 2**). Signal-to-noise ratio is determined by the encoding velocity (VENC, i.e., the maximum encoded velocity), which must be set appropriately to avoid aliasing (if set too low) or insufficient contrast (if set too high). While standard 2D PC-MRI for clinical flow assessments typically acquire ∼20 frames per cardiac

cycle (∼50 ms resolution), this is insufficient to capture high frequency information, such as flow acceleration, required for wave intensity analysis. Higher temporal resolution (∼9 ms) can be obtained with techniques such as spiral SENSE PC-MRI (Steeden et al., 2011; Biglino et al., 2012) or spoiled gradient echo PC-MRI (Bhuva et al., 2019), and even down to 4 ms resolution with retrospectively gated compressed sensing PC-MRI (Peper et al., 2018).

Whereas MRI is relatively expensive and most suited to imaging central vessels, Doppler ultrasound is inexpensive and more suited to imaging peripheral arteries. With pulsed Doppler, a velocity spectrum is acquired over time inside a sample volume that is positioned by the operator, normally in the vessel center and covering at least two thirds of the vessel diameter (**Figure 2**). The intensities of pixels in each vertical line of the spectrum essentially represent a histogram of velocities within the sample volume at that time point. The spectrum can therefore provide an indication of whether the velocity profile is relatively flat (narrow spectrum) or contains a range of velocities due to a more parabolic, skewed or turbulent profile (broad spectrum).

Software included in most commercial systems allows velocity waveforms to be extracted by tracing the top (or envelope) of the velocity spectrum. However, it is important to recognize that the envelope represents the peak velocity within the sample volume, not the cross-sectional mean velocity required for arterial wave analyses. Several techniques have been described to extract the mean velocity waveform, such as averaging the Doppler spectrum (Niki et al., 2002; Borlotti et al., 2012), or with multi-gate ultrasound systems, color Doppler, or 3D ultrasound (Hoskins, 2011). Regardless of the technique used, various sources of error affect accuracy, including incomplete vessel coverage by the sample volume, non-uniform beam insonation, inappropriate gain settings, inaccurate sample volume placement, imprecise angle correction, spectral broadening, the presence of secondary flow, and operator dependence (Winkler et al., 1995; Mikkonen et al., 1996; Corriveau and Johnston, 2004; Hoskins, 2011; Mynard and Steinman, 2013). Given the many possible sources of error, Kowalski et al. (2017) described a technique that enables correction of any arbitrary scaling of velocity waveforms to obtain mean velocities, which requires accompanying measurements of arterial distention waveforms at the same site, as well as standard blood pressure. While such corrections will not affect the pattern of waves in an individual, they may reduce variability in group analyses and improve sensitivity in clinical studies.

Having provided an overview of techniques for measuring pressure and flow/velocity waveforms, the following sections review the most commonly applied techniques for analyzing these waveforms.

PULSE WAVE ANALYSIS

Characterizing blood pressure with only two extreme values (systolic and diastolic) neglects the wealth of information that is present in the shape of the pressure waveform (**Figure 3**). With pulse wave analysis, characteristic features of the pressure waveform are extracted and inferences about wave dynamics are made on the basis of theoretical (i.e., model-based) links with functional properties of the cardiovascular system. A comprehensive historical review of pulse wave analysis is available in the classic textbook McDonald's Blood Flow in Arteries by Nichols and O'Rourke (2011). We here focus on *central* pulse wave analysis and the three indices that are most commonly used: augmentation pressure, augmentation index and inflection time.

Pulse wave analysis was founded on the observation that aortic pressure waveforms generally exhibit a characteristic inflection point during systole (**Figure 3A**). The initial pressure rise up to this inflection point (P1) is thought to relate mainly to the incident or forward-traveling pressure wave (the pressure arising from the natural outflow of the ventricle), while the secondary pressure rise (or 'augmentation pressure,' AP) after the inflection point is thought to arise mainly from wave reflection (Kelly et al., 1989). Augmentation Index (AIx), calculated as AP/PP (where PP is pulse pressure), is therefore a surrogate index of arterial wave reflection, while augmentation pressure, if positive, is an 'additional' pressure arising from this reflection. In addition, the time from the onset of P1 to the inflection point (T_i) has been used to quantify the total transit time for waves traveling from the ventricle to an effective reflection site and back to the ventricle (Baksi et al., 2009; Sugawara et al., 2010).

While this picture may seem straightforward, a range of studies have suggested that AIx is determined by a complex combination of biomechanical interactions. AIx demonstrates a strong dependence on heart rate and is therefore commonly expressed in a heart-rate-corrected form (AIx@75 bpm) (Wilkinson et al., 2000; Weber et al., 2004). AIx is also modulated by height and differs between males and females, whereas wave separation analysis suggests wave reflection magnitude does not depend on these factors (Hughes et al., 2013). In addition, although AIx increases with age, it plateaus and may even decrease around middle age (Kelly et al., 1989; Mitchell et al., 2004; Fantin et al., 2006); it has been argued that this plateau does not necessarily mean that wave reflection is decreasing, but is a result of mathematical division between two linearly increasing curves (AP and PP) (Namasivayam et al., 2010). Davies et al. (2010) concluded that systolic augmentation was mainly related to reservoir pressure, with only a minor contribution from reflected waves; however, this interpretation now appears moot because current (revised) views acknowledge that wave reflection produces the reservoir pressure (Hughes and Parker, 2020). Nevertheless, AIx has also been shown to depend on ventricular outflow patterns (Karamanoglu and Feneley, 1999), preload (van de Velde et al., 2017), contractility/relaxation properties (Cheng et al., 2012) and forward waves (Fok et al., 2014), although these dependencies may relate in part to re-reflection of backward-traveling waves when they return to the ventricle (Phan et al., 2016a). AIx is negative in some (generally younger) individuals (**Figure 3B**), but this does not imply the presence of negative wave reflection (Hughes et al., 2013).

Given the many factors that influence AIx, it is tempting to question whether wave reflection is indeed primarily responsible for systolic augmentation. However, a key principle of fluid dynamics in elastic tubes is that, in the absence of wave

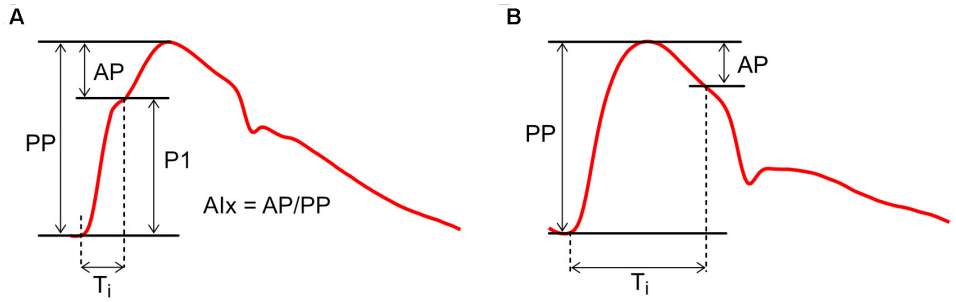

FIGURE 3 | Calculation of Augmentation Index (AIx) with examples of **(A)** positive augmentation and **(B)** negative augmentation. AP, augmentation pressure; P1, initial pressure rise; PP, pulse pressure; T_i, inflection time.

reflection, pressure and flow waveforms will be identical, albeit scaled by characteristic impedance. Any difference between these waveforms must therefore arise from wave reflection (Parker, 2009; Westerhof and Westerhof, 2017). We therefore agree with the summary of O'Rourke and Mancia (1999) that "augmentation is a manifestation, not a measure of early wave reflection." Thus, while AIx may be a very useful marker of cardiovascular risk (Nürnberger et al., 2002; Weber et al., 2004, 2010), its limitations in specifically quantifying the biomechanical phenomenon of wave reflection should not be overlooked.

As with AIx, the interpretation of T_i has been controversial. Although the dominant view has been that reflected waves return to the heart earlier as aging progresses (due to increasing aortic pulse wave velocity), a meta-analysis by Baksi et al. (2009) found that T_i does not decrease much with age. Based on a modest decrease in T_i but large increase in aortic pulse wave velocity, some investigators have concluded that the distance to the effective reflection site (L_{eff}) increases with age (Mitchell et al., 2010; Sugawara et al., 2010). However, the reliability of using T_i to quantify reflected wave transit time has been questioned; when calculated via wave separation analysis, arrival time of the reflected wave decreased substantially and indicated a decreasing or invariant L_{eff} with advancing age (Segers et al., 2007; Phan et al., 2016b). Lastly, T_i is also affected by the shape of the waveform and reliable identification of the inflection point is not always possible (Nichols and O'Rourke, 2009; Phan et al., 2016b), with modeling data suggesting that T_i may not be an accurate measure of reflected wave return time (Westerhof and Westerhof, 2012). Thus, inferences about arterial biomechanics based on T_i should be treated with caution.

WAVE SEPARATION

With pulse wave analysis, information about forward (incident) and backward (reflected) waves are estimated from the shape of the pressure waveform. However, as discussed above, various limitations make this approach non-ideal. Wave separation is therefore considered the 'gold-standard' method for investigating wave phenomena, since information about forward and backward waves are specifically quantified by decomposing the pressure waveform (P) into two separate signals using principles of fluid dynamics in compliant tubes. The forward component of pressure (P_+) represents the contribution of forward waves to measured pressure, while the backward component of pressure (P_-) represents the contribution of backward waves (**Figure 4**). The caveat is that wave separation is agnostic to the mechanisms that give rise to forward or backward waves; for example, it cannot be used to determine whether an increase in ascending aortic P_+ is caused by a forward wave generated by active ventricular contraction or by passive reflection of a backward wave when it reaches the aortic valve. Such conclusions must be inferred through other means (model-based or experimental inferences).

Pressure wave separation, originally described by Westerhof et al. (1972), can be achieved with the following simple equation when P is accompanied by a measured flow waveform (Q),

$$P_{\pm} = \frac{1}{2}\left(P - P_{ud} \pm Z_c Q\right) \tag{1}$$

To apply this formula, two parameters must be estimated. The first is undisturbed pressure (P_{ud}) and will be discussed later in the *Wave Potential* section; briefly, P_{ud} endows physical meaning to the absolute values of $P_{\pm}$, whereas if this parameter is optionally not included, only changes in $P_{\pm}$ are meaningful (Mynard and Smolich, 2014b). The second, characteristic impedance (Z_c), has an important physical meaning that can be easily understood via a fundamental equation of fluid dynamics in compliant tubes called the water hammer equation. This states that incremental changes in pressure and flow arising from forward waves (dP_+ and dQ_+) are intrinsically linked via

$$dP_+ = Z_c dQ_+ \tag{2}$$

This means that a pressure wave (a propagating pressure change) is always accompanied by a corresponding flow wave (propagating flow change) and vice versa. Moreover, Equation (2) shows that in a situation where only forward waves exist, measured pressure and flow waveforms will have an identical shape and their ratio will be equal to Z_c. Characteristic impedance in large vessels is determined by wave speed (c, i.e., local pulse wave velocity) and cross-sectional area (A) via

$$Z_c = \frac{\rho c}{A} \tag{3}$$

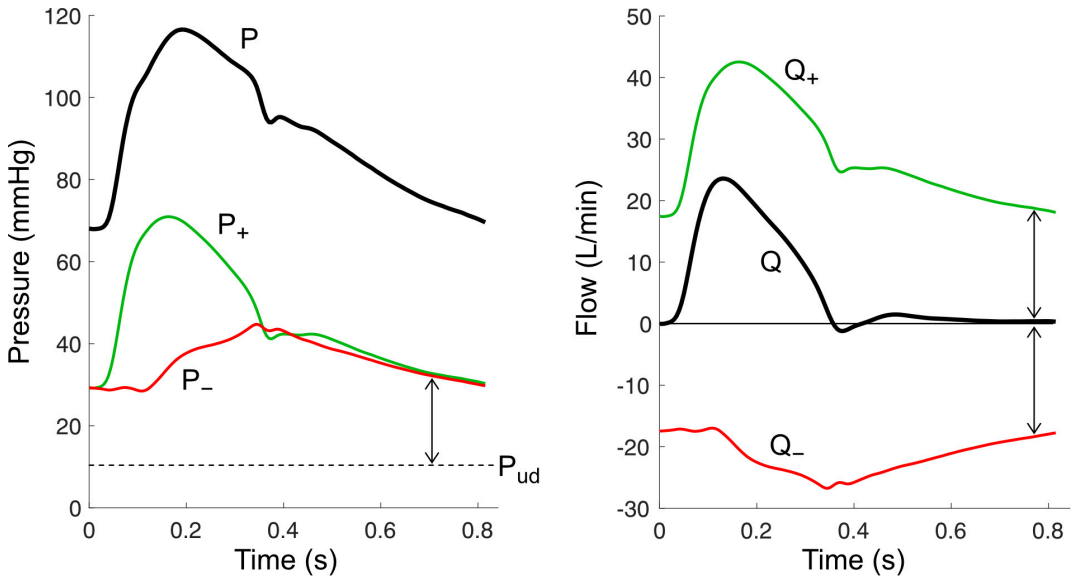

FIGURE 4 | Wave separation analysis for pressure (P) and flow (Q) signals. Forward components (P_+ and Q_+) and backward components (P_- and Q_-) are calculated using the equations in **Table 1**, with an assumed undisturbed pressure (P_{ud}) of 10 mmHg. Arrows indicate wave potential at that time.

where ρ is blood density. Considering Equation (1), we see that an increase in vessel stiffness (which increases wave speed) or a decrease in vessel area will cause a larger pressure change for a given flow change. This has potentially crucial implications for explaining changes in blood pressure with advancing age. For example, a threefold increase in ascending aortic wave speed (Redheuil et al., 2010) would be expected to cause a corresponding threefold increase in the forward component of pressure (e.g., from 30 to 90 mmHg), all other factors being equal. Importantly, however, aortic cross-sectional area also increases with age, offsetting the effect of increased wave speed; the extent of this offsetting effect remains unclear, however, given conflicting data in the literature (Mitchell et al., 2004; O'Rourke and Nichols, 2005; Hickson et al., 2010; Redheuil et al., 2011; Devos et al., 2015).

Another key concept in wave separation analysis is that forward waves cause pressure and flow to change in the same direction, whereas backward waves cause pressure and flow to change in opposite directions. For example, a forward wave that increases pressure will also increase flow, whereas a backward wave that increases pressure will have a flow-decreasing effect, noting that the water hammer equation for backward waves has a negative sign ($dP_- = -Z_c dQ_-$). This principle forms the basis for the notion that wave reflection must ultimately be responsible for *any* differences in the shape of arterial pressure and flow waveforms (Westerhof et al., 2010; Nichols and O'Rourke, 2011).

While we have discussed wave separation for pressure, a similar approach can also be applied to calculate forward and backward components of flow (Westerhof et al., 1972), velocity (Parker, 2009), diameter or area distension (Feng and Khir, 2010; Biglino et al., 2012), wave intensity (Parker and Jones, 1990), wave power, and hydraulic power (Mynard and Smolich, 2016). As can be seen in **Table 1**, all of these calculations rely on the estimation of local characteristic impedance or wave speed.

Characteristic Impedance and Wave Speed

As discussed above, characteristic impedance (Z_c) represents the intrinsic relationship between pressure and flow when waves are traveling in one direction only. It can be estimated from measured pressure and flow signals, which historically has been achieved in the frequency domain (via Fourier transform) by calculating the average ratio of pressure and flow harmonics in a certain frequency range (O'Rourke and Taylor, 1967). The range may include only high frequency harmonics (e.g., 15–25 Hz) or a lower frequency range (e.g., 5–15 Hz), but the result appears to be relatively insensitive to the exact range chosen (Dujardin and Stone, 1981). A simpler time domain method was proposed by Dujardin and Stone (1981) and Li (1986), which involves calculating the ratio of changes in pressure and flow during early systole, when the effect of wave reflection is minimal.

Like Z_c, wave speed (c) may be considered an intrinsic property of a vessel, being dependent on vessel stiffness (i.e., elastic modulus), wall thickness and diameter, as expressed with the Moens–Korteweg equation (Mirsky, 1973). Wave speed differs subtly from pulse wave velocity (PWV), as routinely measured, in two respects. First, PWV is calculated as the time it takes for a wave to propagate from one location to another, whereas wave speed is a local quantity that is defined at every point along a vessel (similar to diameter). Second, the propagation speed of a wave is actually equal to $U + c$ for a forward wave and $U - c$ for a backward wave, where U is blood velocity (Parker, 2009). Hence, in principle PWV is determined

TABLE 1 | Variations of wave intensity/power and wave separation.

Signals	Wave intensity (Units)	Wave separation	References
Pressure-velocity	$dI = dPdU$ (W/m^2)	$P_\pm = [P - P_{ud} \pm \rho c dU]/2$ $U_\pm = [U \pm (P - P_{ud})/(\rho c)]/2$ $dI_\pm = \pm[dP \pm \rho c dU]^2 / (4\rho c)$	Parker and Jones, 1990
Diameter-velocity	$dI^D = dDdU$ (m^2/s)	$D_\pm = [D - D_{ud} \pm DU/(2c)]/2$ $U_\pm = [U \pm 2c \ln(D/D_{ud})]/2$ $dI^D_\pm = \pm c[dD \pm DdU/(2c)]^2 / (2D)$	Feng and Khir, 2010
Area-velocity	$dI^A = d(\ln A)\, dU$ (m/s)	$\ln A_\pm = [\ln(A/A_{ud}) \pm U/c]/2$ $U_\pm = [U \pm c \ln(A/A_{ud})]/2$ $dI^A_\pm = \pm c[d \ln A \pm dU/c]^2 / 4$	Biglino et al., 2012
Signals	**Wave power (units)**	**Wave separation**	**References**
Pressure-flow	$d\pi = dPdQ$ (W)	$P_\pm = [P - P_{ud} \pm Z_c Q]/2$ $Q_\pm = [Q \pm (P - P_{ud})/Z_c]/2$ $d\pi_\pm = \pm(dP \pm Z_c dQ)^2 / (4Z_c)$ $\Pi_{P\pm} = [2PQ \pm Z_c Q^2 \pm (P^2 - P_{ud}^2)/Z_c]/4$	Mynard and Smolich, 2016

Note that (1) the wave intensity surrogates involving diameter (dI^D) or cross-sectional area (dI^A) instead of pressure (dI) do not have units of intensity; (2) except for pressure-flow, expressions for wave separation have been modified from the original references to incorporate wave potential by introducing an undisturbed pressure (P_{ud}), diameter (D_{ud}) or area (A_{ud}) using derivations analogous to those for pressure-flow (Mynard and Smolich, 2014b); (3) hydraulic pressure power ($\Pi_P = PQ$) may also be separated into forward and backward components ($\Pi_{P\pm}$).

by vessel properties (via c) and haemodynamics (via U), although U is generally much smaller than c (∼0.5 m/s vs. ∼5 m/s).

Various methods exist to estimate PWV and c, which were recently reviewed by Segers et al. (2020). We here focus on three approaches for estimating local c, which are most suited to wave separation analysis: (1) the 'loop methods' (e.g., PU loop); (2) the minimum energy or 'sum of squares' method, and (3) pressure-diameter or distensibility-based methods.

The PU loop method is similar to the time domain approach for calculating Z_c mentioned above, and involves plotting pressure vs. velocity as shown in **Figure 5A** (Khir et al., 2001b). During early systole, the PU relation is relatively linear, which is presumed to be due to unidirectional wave travel, and the relation departs from this linear trajectory when reflected waves arrive at the measurement site. The most linear section is therefore selected and its slope (which is equal to ρc if only forward waves are present) is divided by blood density (ρ) to obtain wave speed. Analogous methods have been described for diameter and velocity, the ln(D)U loop method (Feng and Khir, 2010), and for flow and area, the QA method (Rabben et al., 2004).

The accuracy of these 'loop' methods depends on three factors that should be carefully considered when applying them. First, signals must be time-aligned to correct for hardware-related lags or to combine signals that were acquired sequentially. Misalignment introduces curvature into the early-systolic PU relation (**Figure 5B**); one way to correct for these lags is to shift velocity with respect to pressure until the most linear relation is obtained (Khir et al., 2001b; Swalen and Khir, 2009). Second, the accuracy of these methods relies on the adequacy of the assumption that no reflected waves are present during early systole. Segers' group has shown that the presence of reflected waves tends to cause over- and under-estimation of wave speed for the PU loop and QA loop methods, respectively, and importantly that reflections may be present even when the early systolic relation is linear (Swillens et al., 2013; Segers et al., 2014). Reflected waves in early systole may arise from proximity of the measurement site to reflection sites, such as the carotid bifurcation, or due to persistent effects of reflected waves from the previous cardiac cycle (i.e., the diastolic pressure decay); viscoelasticity and the pressure-dependence of wave speed may also have confounding effects (Alastruey, 2011; Mynard et al., 2011). Potential consequences of these phenomena include (1) incorrect alignment of signals due to real curvilinearity in the early systolic PU relation, (2) inaccurate wave speed estimation, and (3) wave separation that incorrectly suggests an absence of early reflected waves.

The requirement for unidirectional wave travel in the PU loop method was identified by Davies et al. (2006b) as a major barrier to wave speed estimation in coronary arteries, where there is no period of the cardiac cycle where this assumption can be confidently applied. These investigators therefore proposed the minimum net energy method (also referred to as the 'sum-of-squares' or 'single-point' method) in which wave speed is calculated as

$$c = \frac{1}{\rho}\sqrt{\frac{\sum dP^2}{\sum dU^2}} \tag{4}$$

where dP and dU are incremental changes in pressure and velocity, with their squares summed over the cardiac cycle. This approach, along with a flow-area equivalent described by Quail et al. (2015), does not require unidirectional wave travel during a particular phase of the cardiac cycle, but instead minimizes the net energy of decomposed forward and backward waves throughout the whole cardiac cycle. This was based on a general observation that an incorrect wave speed tends to introduce self-canceling forward and backward waves (Siebes et al., 2009).

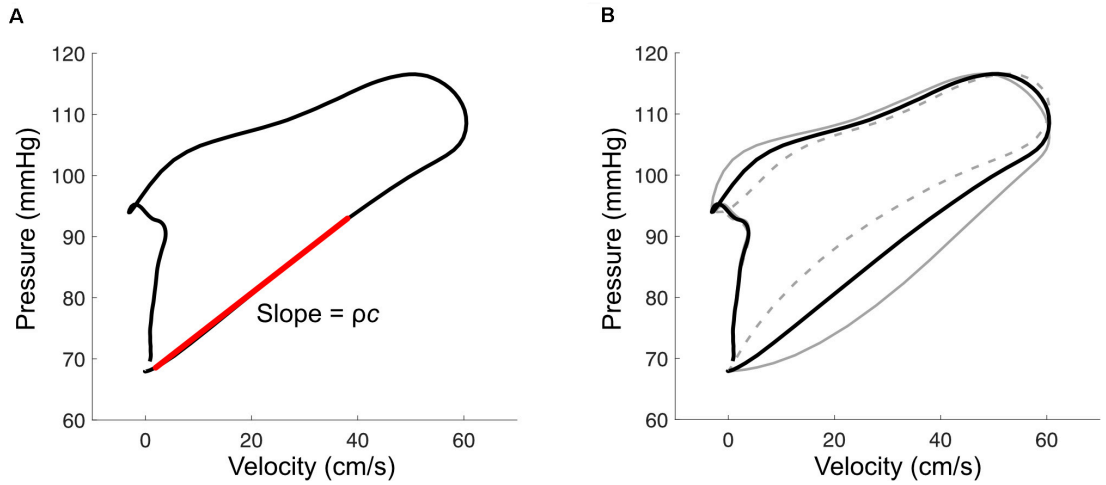

FIGURE 5 | (A) With the pressure-velocity (PU) loop method, wave speed (c) is calculated from the slope of the early-systolic PU relation (red line), where ρ is blood density. **(B)** Misalignment of pressure and velocity signals introduces curvature in the early systolic relation. This example shows the effect of velocity leading or lagging pressure by 10 ms (solid and dashed gray lines, respectively).

Since self-canceling waves are minimized by the sum-of-squares method, its accuracy becomes limited when measurements are performed in close proximity to a reflection site, where self-canceling waves are expected (Borlotti et al., 2014). Although originally intended for use in coronary arteries, concerns have been raised about the accuracy of the sum-of-squares method in this setting during hyperemia, in the vicinity of a stenosis, and generally due to a preponderance of overlapping forward and backward waves (Kolyva et al., 2008; Rolandi et al., 2014). Hence, considerable challenges remain in obtaining a reliable single-point wave speed estimation technique for coronary arteries.

Distensibility-based methods for estimating wave speed have two major advantages over the 'loop' methods and sum-of-squares method in that (1) they require no assumptions about waves and (2) they do not require an accurate (mean) velocity signal, which can be difficult to acquire, as discussed above (Kowalski et al., 2017). Wave speed is related to distensibility (Δ) via the Bramwell–Hill equation (Bramwell and Hill, 1922),

$$c^2 = \frac{1}{\rho\Delta} = \frac{A}{\rho}\frac{dP}{dA} = \frac{1}{2\rho}\frac{dP}{dD} \tag{5}$$

where the last two expressions show that this method requires measurement of cross-sectional area (A) or diameter (D), in contrast to a velocity measurement required for the other techniques discussed above. Various implementations of Equation (5) exist, and these essentially differ in the segments of P and D used for calculating the derivatives; these include the D^2P method that uses diastolic segments (Alastruey, 2011), the ln(D)P loop method that uses early systolic segments (Kowalski et al., 2017), and the distensibility coefficient method that uses the whole cardiac cycle (Segers et al., 2014). It could be argued that a disadvantage of these methods is that local pressure *and* diameter signals need to be measured, in addition to velocity or flow waveforms required for wave intensity and wave separation analyses. However, Kowalski et al. (2017) showed that a feasible approach is to estimate local (e.g., aortic, carotid, or femoral) pressure non-invasively by calibrating the local diameter (or area) waveform to mean and diastolic brachial blood pressures obtained with a standard cuff measurement. The benefit of this approach is not only that a more reliable wave speed is obtained (via a distensibility-based method), but that this wave speed can then be used to correct scaling errors in measured velocity or flow (Segers et al., 2014; Kowalski et al., 2017), which in turn may improve the accuracy of derived quantities such as wave intensity.

Pressure-Only Wave Separation

Although a flow or velocity waveform is mathematically required to perform wave separation, Westerhof et al. (2006) introduced the concept of replacing measured flow with a synthesized waveform because the flow waveform displays relatively little variation between individuals. With this approach, wave analysis can be conducted with only a pressure waveform and wave speed or characteristic impedance are not required. Westerhof et al. (2006) originally proposed using a triangle to approximate systolic flow, with a base spanning from the start of the pressure upstroke to the dicrotic notch, and a peak at 30% of ejection time or at the point of pressure inflection. Kips et al. (2009) subsequently found that a population-average flow waveform resulted in better accuracy for estimating reflection magnitude, but found poor correlation between actual and estimated reflection transit time for both triangular and average flow waveforms. Parragh et al. (2015) also cautioned against using a one-size-fits-all flow waveform in settings where ventricular outflow patterns may be abnormal, such as heart failure with reduced ejection fraction. They instead used a personalized approximation of the flow waveform, generated with a modified windkessel (ARCSolver) model (Hametner et al., 2013). While these pressure-only approaches should be used with caution due to the assumptions required, the benefit of broad applicability has been demonstrated in numerous large cohort studies where flow

signals are unavailable (Wang et al., 2010; Chirinos et al., 2012; Weber et al., 2012; Zamani et al., 2014; Hametner et al., 2015; Sluyter et al., 2017).

WAVE INTENSITY

Wave intensity analysis (WIA) was introduced by Parker et al. (1988) as an intuitive time domain method for visualizing and quantifying arterial waves. WIA is based on the one-dimensional equations of flow and uses the method of characteristics (familiar to the fluid dynamics community) to reveal forward- and backward-propagating 'information' that is not obviously apparent when looking at raw pressure and velocity signals (Parker and Jones, 1990; Parker, 2009). Wave intensity (dI) is simply defined as

$$dI = dPdU \tag{6}$$

where dP and dU are incremental changes in pressure and velocity, respectively, over a sample interval. An example of wave intensity in the carotid artery is shown in **Figure 6**. The distinct peaks are referred to as 'waves,' and these arise from the cumulative effect of many 'wavelets' or infinitesimal 'wavefronts' that are each associated with a small change in pressure (dP) and velocity (dU) that propagates along the vessel. As a crude analogy, a wave may be compared with a staircase while a wavefront is a single step. The value of wave intensity at a given time may be compared to the height of a particular step, while 'cumulative intensity' (the integrated area under a wave) is analogous to the overall height of the staircase. The units of wave intensity (Watts/m^2 or Joules per second per square meter) indicate the rate at which wave energy passes through a given cross-section. These are the same units as sound intensity, which determines the 'loudness' of a sound wave, or radiant flux which determines how much light energy falls onto a solar panel. Importantly, however, wave intensity refers to the energy flux of a propagating wave, not the energy of flowing blood.

Although WIA is assessed at a single site, the direction in which a wave propagates is easily discernable, as a forward wave is always positive and a backward wave is always negative. What is not clear from the wave intensity signal alone is whether a wave has a pressure-increasing effect (called a *compression wave*) or a pressure-decreasing effect (a *decompression wave*, at times also referred to as an 'expansion' or 'suction' wave). The wave type must therefore be determined via wave separation of the pressure waveform. Then, for example, a forward wave is identified as a compression wave if it coincides with an increase in P_+, while a backward wave is identified as a decompression wave if it coincides with a decrease in P_- and so on (**Figure 6**).

One drawback of the original definition of wave intensity is that the numerical value of $dPdU$ depends on the sampling frequency of the measured signals, which is extraneous to the underlying physiological quantity. In our stair analogy, it would mean that the height of the staircase is dependent on the step size, which is chosen arbitrarily. For this reason, Ramsey and Sugawara (1997) introduced a time-corrected form of wave intensity (designated wi instead of dI) that employs the time derivatives of pressure and velocity, i.e.,

$$wi = \frac{dP}{dt}\frac{dU}{dt} \tag{7}$$

This signal is simply a scaled version of dI but is independent of sample time (dt), being analogous to using the slope of the staircase rather than the height of individual steps (the total height now being independent of step size). Khir and Parker (2005) pointed out that, unlike dI, which has units representing power flux, the units of wi (W/m^2/s^2) lack such a physical meaning. The sample rate dependence of dI and the unclear physical meaning of wi units thus creates a theoretical trade-off that is presently an unresolved issue in the WIA field; however, the issue has no bearing on the analysis or interpretation of wave dynamics in practice.

As for pressure and flow, *net* wave intensity (dI) may also be subjected to wave separation, providing distinct forward and backward components (dI_+ and dI_-, respectively). These components are calculated via

$$dI_\pm = \pm\frac{1}{4\rho c}\left(dP \pm \rho c dU\right)^2 \tag{8}$$

where, similar to pressure and flow-velocity separation, an estimate of wave speed (c) is required (Parker, 2009). While net wave intensity indicates whether forward or backward waves are dominant at a particular time, wave separation further allows quantification of potentially overlapping or partially overlapping forward and backward waves. Wave separation may therefore have a substantial impact on calculated wave reflection indices or other wave ratios (an example of this is indicated with an asterisk in **Figure 6**).

Non-invasive Wave Intensity

The ability to measure wave intensity non-invasively is pivotal to clinical translation. This can be achieved by measuring pressure and velocity waveforms sequentially via applanation tonometry and Doppler ultrasound, then aligning these signals before calculating wave intensity (Zambanini et al., 2005). However, a more common approach, described in the first non-invasive WIA study by Niki et al. (1999), is to employ a combined echo-tracking and Doppler system to obtain carotid arterial diameter and velocity waveforms simultaneously, with the pressure waveform estimated by calibrating the diameter waveform to systolic and diastolic pressure from an arm cuff. This technique was developed and incorporated into a commercial ultrasound scanner and has been used in numerous clinical WIA studies of the carotid artery (Niki et al., 2002, 2005, 2017; Babcock et al., 2014; Tanaka et al., 2014; Nogami et al., 2018; Chiesa et al., 2019). This approach assumes that pressure and diameter waveforms are identical, and the calibration method does not account for the difference between brachial and carotid systolic pressures caused by pulse amplification, which exhibits individual variability (Segers et al., 2009). Several techniques have also been proposed to estimate central wave intensity non-invasively from peripheral measurements, with central aortic or coronary blood pressure being estimated with

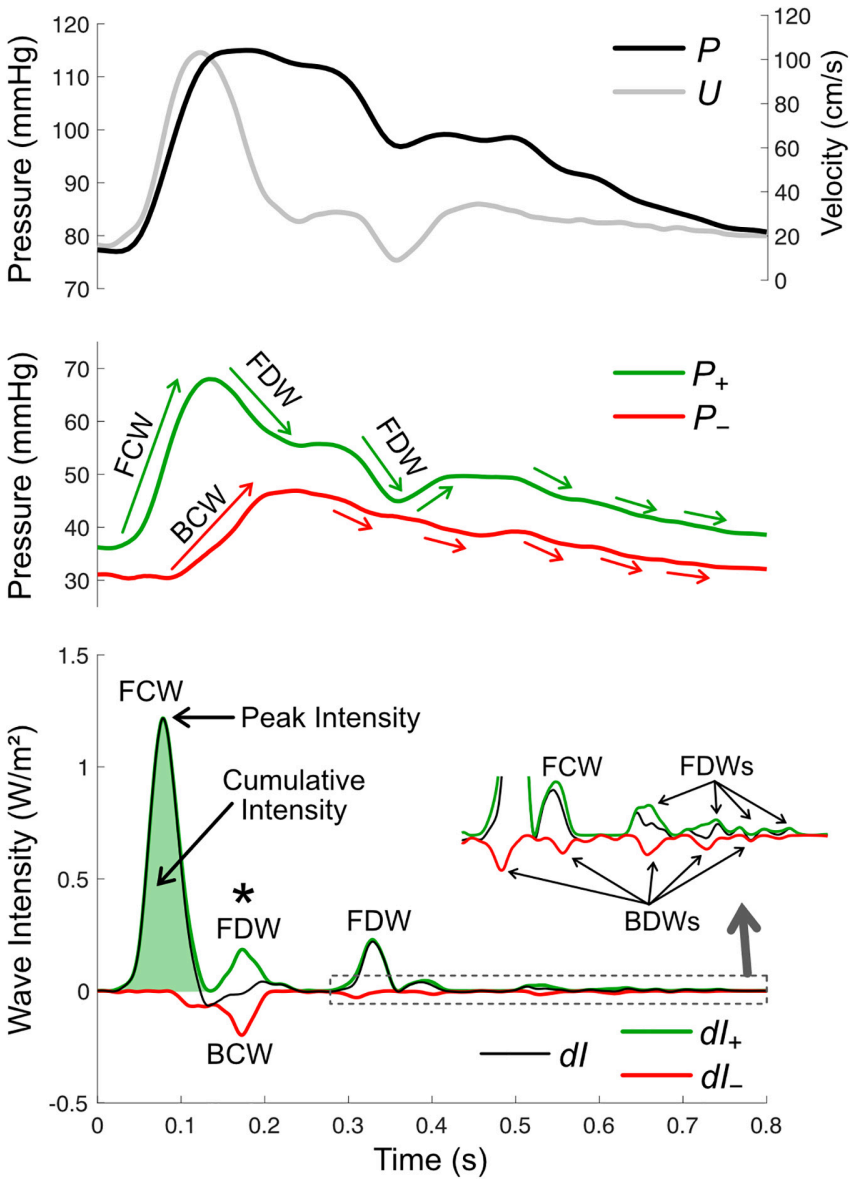

FIGURE 6 | Wave intensity analysis in the carotid artery, based on pressure (*P*, derived from measured diameter), mean velocity (*U*), forward and backward components of pressure (P_+ and P_-), net wave intensity (*dI*) and forward and backward wave intensity components (dI_+ and dI_-). There are four possible wave types, forward compression waves (FCW), forward decompression wave (FDW), backward compression wave (BCW), and backward decompression wave (BDW). Wave size is quantified via peak or cumulative intensity. Whether a wave is a compression or decompression wave can be judged by its effect on the respective pressure components (green and red arrows in the middle panel; note that waves shown in the zoomed inset in the bottom panel are not labeled in the middle panel). The asterisk (*) indicates a time where a BCW and FDW arrive at the measurement site around the same time and therefore wave separation is essential for revealing the presence/magnitude of these waves.

a generalized transfer function or supra-systolic oscillometry, and aortic flow via the reservoir-excess pressure approach (Broyd et al., 2016; Smolich and Mynard, 2016; Hughes et al., 2020); given the relatively high sensitivity of wave intensity to measurement errors, these techniques require further validation before widespread adoption.

In additional efforts to foster clinical translation, a number of wave intensity surrogates have been described that avoid issues related to pressure calibration. Feng and Khir (2010) described a version of wave intensity suited to ultrasound studies, in which vessel diameter is used in place of pressure. Similarly, Biglino et al. (2012) used the natural logarithm of area instead of pressure, which is suited to phase contrast MRI. These alternative definitions of wave intensity and associated equations for performing wave separation are summarized in **Table 1**. While these methods can be derived from the one-dimensional flow equations, a limitation is that the units of diameter- or area-based 'wave intensity' (m^2/s and m/s, respectively)

are not those of intensity (W/m^2), and hence their physical interpretation is uncertain.

Wave Power

Wave power is an alternative to wave intensity that uses pressure and volumetric flow signals ($d\pi = dPdQ$) and has a number of advantages (Mynard and Smolich, 2016). First, as the name suggests, wave power has the physically meaningful units of power (Watts) and is therefore not sensitive to cross-sectional area variations (e.g., within vessels or between individuals). Second, in experimental studies, measured flow can be used directly for wave analysis without requiring derivation of velocity, which often requires error-prone assumptions about cross-sectional area (Kowalski et al., 2019b). Third, wave power is conserved at junctions and therefore the distribution of wave power to different vessel branches can be quantified. For example, unlike wave intensity which is not conserved, it has been possible to meaningfully quantify the percentage of ascending aortic wave power that passes into the carotid artery and how this changes with pharmacological intervention (Londono-Hoyos et al., 2018). Finally, wave power is linked to the hydraulic pressure power of flowing blood ($\Pi_P = PQ$), which determines total ventricular workload (Laskey et al., 1985). While hydraulic power has traditionally been decomposed into steady and oscillatory components (Milnor et al., 1966; Burattini and Campbell, 1999), Mynard and Smolich (2016) showed that power can also be separated into forward and backward wave components ($\Pi_{P\pm}$, see **Table 1**). Moreover, an incremental change in $\Pi_{P\pm}$ is proportional to wave power divided by the associated fractional change in pressure or flow components.

INTERPRETATION OF WAVE PATTERNS

Having reviewed the various approaches to quantifying waves, this section provides an overview of the biomechanical mechanisms that generate waves and factors that affect wave magnitude.

How Are Waves Generated?

There are four recognized mechanisms that generate waves in blood vessels: (1) wave generation by a pump, (2) inertial effects, (3) wave potential gradients and (4) wave reflection.

Wave Generation by a Pump

Active contraction of a pump causes a pressure increase and therefore a compression wave (**Figure 7A**); however, whether a flow-increasing forward compression wave (FCW) or flow-decelerating backward compression wave (BCW) is produced depends on which direction the pump is 'facing' with respect to the direction of blood flow. For example, commencement of left ventricle (LV) ejection causes an increase in aortic pressure and flow that begins at the aortic valve and propagates away from the heart, giving rise to a FCW (Parker et al., 1988; Jones et al., 2002; Penny et al., 2008). A similar wave is observed in pulmonary arteries due to right ventricular contraction (Hollander et al., 2001; Su et al., 2016). On the other hand, although atrial contraction aids ventricular filling, the absence of an atrial inflow valve means that this contraction also generates a BCW that propagates into the systemic/pulmonary veins in a direction that is opposite to mean blood flow (Hellevik et al., 1999; Smiseth et al., 1999; Hobson et al., 2007; Mynard, 2011). Other pump phenomena that generate BCWs in arteries include the active compression of the coronary microvasculature by contracting myocardium (Davies et al., 2006a; Mynard et al., 2018) and the inflation of an intra-aortic or para-aortic balloon pump (Kolyva et al., 2009; Lu et al., 2012).

After a pump has contracted, relaxation causes pressure to fall and therefore generates a decompression wave (sometimes called a 'suction wave') (**Figure 7B**). Decompression waves are generated by atrial relaxation (Smiseth et al., 1999; Mynard, 2011), release of extravascular pressure on intramyocardial vessels by the relaxing ventricle (Davies et al., 2006a; Mynard et al., 2018) and deflation of aortic balloon pumps (Kolyva et al., 2009; Lu et al., 2012). In the first paper utilizing wave intensity analysis, entitled "What stops the flow of blood from the heart?", Parker et al. (1988) showed that a forward decompression wave (FDW) is primarily responsible for the deceleration of systolic flow in arteries, not a reflected wave as had been widely believed. A similar FDW was also later reported in pulmonary arteries (Hollander et al., 2001; Su et al., 2016). These FDWs precede and appear to cause valve closure, and are often thought to arise from the onset of ventricular relaxation, which involves elastic recoil and myocardial untwisting (Parker and Jones, 1990; Nakayama et al., 2005; Sun et al., 2006; Parker, 2009; Babcock et al., 2014). However, the extent to which the FDW is caused by relaxation versus inertial effects is somewhat controversial, as will be discussed in the next section.

A quantitative dependence of arterial FCW and FDW on ventricular pump function was first evidenced in humans by Ohte et al. (2003), who found that the aortic FCW was correlated with maximal LV dP/dt (r = 0.74) and aortic FDW was negatively correlated with the time constant of LV relaxation (τ, r = −0.77). However, Nakayama et al. (2005) subsequently found a much weaker correlation (r = 0.46) between FCW and LV end-systolic elastance (Ees), a relatively load-independent index of contractility, and no significant correlation between FDW and τ. Adjusting for end-diastolic volume improved correlation coefficients substantially, to ∼0.9 for FCW vs. Ees and −0.7 for FDW vs. τ, suggesting that these waves are dependent on preload as well as ventricular pump function (inotropy and lusitropy). Others have shown that an acute increase in ventricular afterload (via aortic constriction) decreases FCW amplitude (Khir and Parker, 2005; Mynard et al., 2017). Conflicting data exists on whether an afterload increase causes an increase (Mynard et al., 2017) or decrease (Khir and Parker, 2005) in FDW amplitude, which may suggest a complex dependence of FDW on afterload that requires further study. Despite its load dependence, FCW may have potential as a sensitive and early marker of ventricular systolic dysfunction, with myocardial apoptosis shown to correlate with carotid FCW (r = −0.69) but not ejection fraction (a commonly used clinical index of systolic function) in rabbits (Zhang et al., 2014). In humans, the FCW and FDW both decrease with advancing age, but it is presently unclear whether

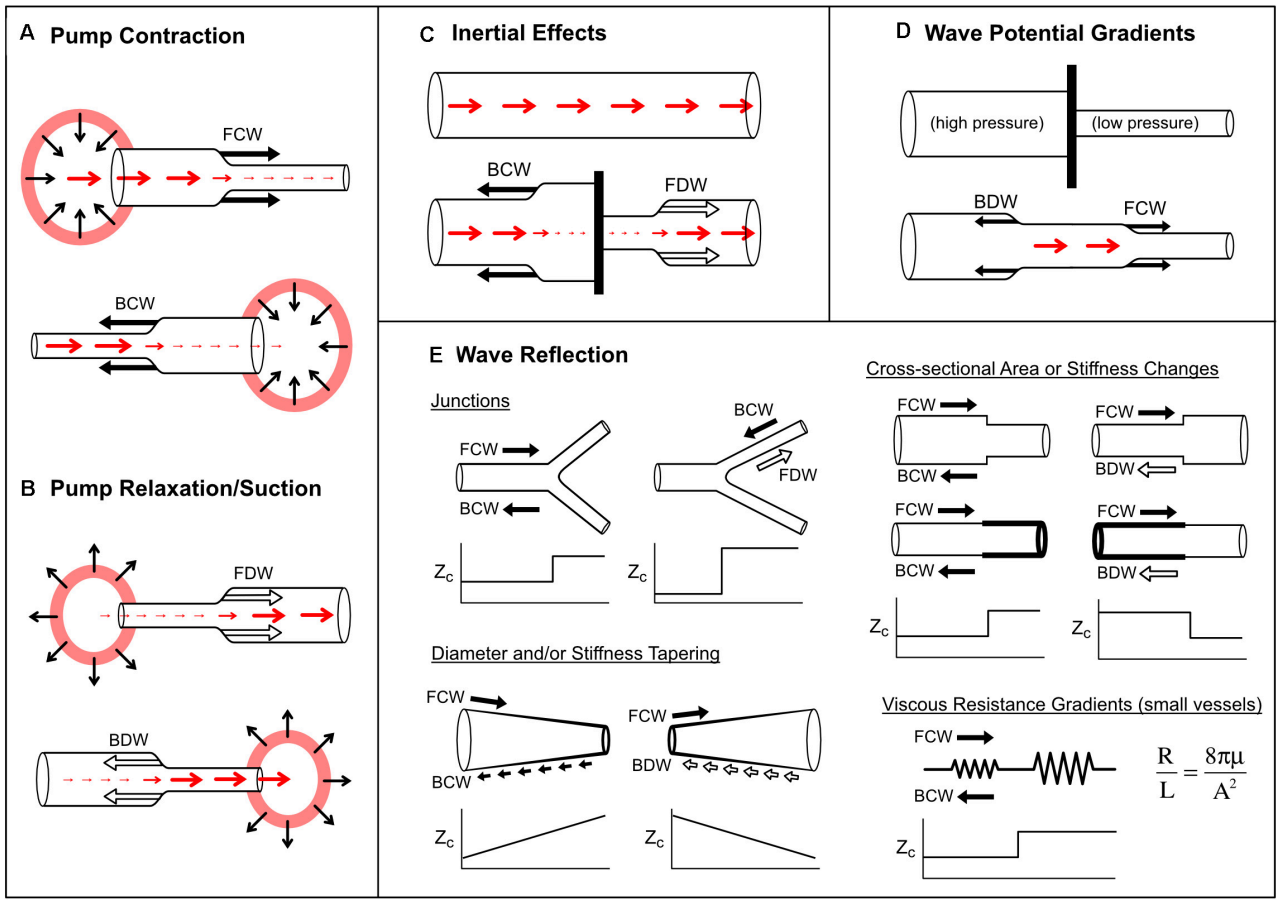

FIGURE 7 | Mechanisms that produce pressure/flow waves in blood vessels. See text for detailed explanation. Red arrows indicate blood flow or velocity (larger arrow means higher flow/velocity). Solid black arrows indicate compression (pressure-increasing) waves, while outlined black arrows indicate decompression (pressure-decreasing) waves. Panels **(A,B)** illustrate wave generation via active pump contraction and relaxation respectively. In panel **(C)**, a barrier is placed in a vessel that contains flowing blood. In panel **(D)**, a barrier is removed between two vessels containing blood at different pressures. In panel **(E)**, increases or decreases in characteristic impedance (Z_c; or combined Z_c in the case of the bifurcation) are plotted versus horizontal position. Viscous resistance per unit length (R/L, given by Poiseuille's law, where μ is blood viscosity and A is cross-sectional area) is small in large vessels but becomes dominant in small vessels.

this is due to changes in pump function, loading conditions (e.g., increasing aortic stiffness), or both (Bhuva et al., 2019; Li et al., 2019).

Inertial Effects

Consider a 'thought experiment' in which a constant forward flow is initially present in a long tube (**Figure 7C**). If a barrier is suddenly inserted in the middle of the tube, then clearly the flow must stop. Flow-decreasing waves must therefore be generated on both sides of the barrier, namely a decompression wave in the forward direction (FDW) and a compression wave in the backward direction (BCW). These waves arise from inertial effects. When the barrier is put in place, the fluid 'wants' to keep flowing under its own momentum, but accumulation of the fluid behind the barrier leads to a pressure build up (and hence a BCW), while inertial flow continuing past the barrier causes a suction effect, causing pressure to fall (leading to the FDW).

Sugawara et al. (1997) proposed that the late-systolic FDW in the aorta may arise primarily from inertial effects rather a loss of the tension bearing ability of the myocardium (i.e., relaxation). A helpful way to understand the generation of waves by the ventricle is to consider the degree of matching between myocardial contraction rate and outflow. During early systole, the rate of myocardial contraction exceeds outflow (which is initially zero) and therefore causes acceleration and imparts momentum to blood, generating the FCW. Then, in mid-systole, there is a virtual absence of forward waves, suggesting that the rate of myocardial contraction 'matches' outflow, hence forward momentum is maintained. However, later in systole, slowing contraction cannot match outflow, and therefore forward momentum cannot be maintained. Similar to the aforementioned example of a tube with flow halted by insertion of a barrier, outflow in the ventricle cannot continue indefinitely and therefore pressure and flow must fall, thus an FDW is generated. That inertial effects are primarily responsible for the FDW is suggested by data from multiple sources indicating that the aortic FDW starts 70–164 ms before aortic valve closure, whereas the onset of LV relaxation (quantified by the time of peak torsion

TABLE 2 | Timing of aortic forward decompression wave duration and onset of LV relaxation.

Aortic FDW duration	References
72 ms (human)	Figure 3 in Davies et al. (2012)
122 ms (human)	Figure 1 in Hametner et al. (2017)
164 ms (human)	Figure 2 in Koh et al. (1998)
97 ms (human)	Figure 5 in Khir et al. (2001a)
36–66 ms (dog)	Figures 4, 5 in Khir and Parker (2005)
37 ms (sheep)	Figure 3 in Mynard and Smolich (2016)
Time from peak LV torsion to aortic valve closure	
14 ms (human)	Table 1 in Notomi et al. (2006a)
0–7 ms (human)	Figure 1 in Notomi et al. (2006b)
27 ms	Dong et al. (2001)
Time from peak myocardial shortening to aortic valve closure	
25 to −80 ms (human)	Figure 4D in Zwanenburg et al. (2004)
27 to −21 ms (human)	Figure 6 in Mada et al. (2015)

FDW, forward decompression wave; LV, left ventricle. A negative time indicates peak LV torsion or shortening occurs after aortic valve closure. Note that it is generally thought, and modeling studies suggest (Mynard and Smolich, 2015), that the end of the aortic FDW corresponds closely to the time of valve closure.

or myocardial shortening) occurs up to ∼30 ms before, to 80 ms *after*, aortic valve closure (**Table 2**).

A striking example of inertial effects producing a FDW in the aorta was provided by Penny et al. (2008). Infusion of incremental doses of dobutamine in sheep caused increases in the force of LV contraction and exponential rises in initial FCW. However, the substantial momentum imparted to blood during this early phase could not be maintained throughout systole, leading to an abrupt fall in pressure and flow (and hence a FDW) during mid-systole. It was originally speculated that this mid-systolic FDW arose from inertial effects, whereas the late-systolic FDW arose from LV relaxation. However, based on the data in **Table 2**, it is possible that both waves were produced by inertial effects.

Finally, we note that compression waves also arise from inertial effects when flow approaches a barrier or closed chamber (**Figure 7C**). For example, modeling studies suggest that this mechanism may play a key role in decelerating blood entering the atria (Mynard, 2011).

Wave Potential

Wave potential is a recently coined term referring to the absolute values of $P_{\pm}$ and $Q_{\pm}$, as discussed in more detail in a later section. Mynard and Smolich (2014b) showed that any spatial difference (gradient) of wave potential generates waves and that the pressure and flow effects of these waves can be predicted. For example, **Figure 7D** shows a situation where a vessel is completely obstructed (e.g., with a clamp), preventing flow ($Q_1 = Q_2 = 0$) despite the presence of a pressure difference ($P_1 > P_2$). Due to this pressure difference, the equations in **Table 1** show that the values of $P_{\pm}$ and $Q_{\pm}$ on either side of the barrier differ. When the barrier is removed, the spatial differences in pressure and wave potential (which can no longer be sustained) are eliminated by the generation of forward compression and backward decompression waves.

Wave Reflection

Wave reflection occurs when a propagating wave encounters a change in characteristic impedance (Z_c) or its inverse, characteristic admittance ($Y = 1/Z_c$). Recalling that Z_c in large vessels is proportional to wave speed and inversely proportional to cross-sectional area, changes in the stiffness or caliber of a vessel may produce a reflection-producing 'impedance mismatch' (**Figure 7E**). The extent of the mismatch determines the degree to which a wave is reflected, quantified via a *pressure reflection coefficient* (R_P),

$$R_P = \frac{Y_0 - Y_1}{Y_0 + Y_1} \tag{9}$$

for a wave that is propagating from admittance Y_0 to Y_1. An extreme example is a complete blockage or occlusion, which presents an infinite impedance or zero admittance (i.e., $Y_1 = 0$); hence $R_P = 1$. This means that, for an incident wave causing a pressure rise of 10 mmHg, the reflected wave will produce an additional 10 mmHg pressure rise. The opposite extreme is where a wave encounters an infinite opening, such as a tube that is cut and open to the atmosphere. In this case $Y_1 \to \infty$ and hence $R_P = -1$; hence the pressure change associated with the incident wave will be entirely negated by the pressure change associated with the reflected wave. Other reflection coefficients can be defined for flow ($R_Q = -R_P$), wave intensity and hydraulic power ($R_{wi} = R_\Pi = R_Q R_P$), but pressure coefficients are used most frequently.

In blood vessels, impedance mismatching may take various forms. Branch junctions may cause an impedance mismatch if the combined admittance of the daughter vessels does not match the admittance of the parent vessel (**Figure 7E**). Importantly, arterial junctions are typically well-matched in the forward direction but not in the backward direction. This has a clear teleological benefit for ventricular afterload, since reflected waves become 'trapped' downstream and find it 'difficult' to return to the heart (Khir and Parker, 2005; Davies et al., 2012).

Vessel tapering produces an impedance mismatch that is distributed over its length (**Figure 7E**). In this case, wave reflection does not occur at a discrete point, but many small reflections are produced in a continuous manner. Interestingly, Segers and Verdonck (2000) showed that distributed reflection due to tapering may have similar effects on measured pressure/flow as a discrete reflection, and hence whether wave reflection is discrete or distributed may not be discernable from measurements at a single site. The extent to which tapering contributes to arterial wave reflection is uncertain. Although many arteries are tapered, this may in fact be an impedance-preserving feature due to the presence of side branches. Indirect evidence for this is the gradual decrease in mean blood velocity in progressively distal arterial locations (Milnor, 1990), whereas if side branches were few or absent in a tapered vessel, velocity would be expected to increase due to convective acceleration.

A stiff vascular segment may occur in certain disease conditions or after surgery due to formation of scar tissue (e.g., at the site of an aortic coarctation repair), while a stent similarly represents a stiff segment compared with the surrounding vessel. Although some reflection is expected in these settings, it is

important to note that a stent creates two sites of impedance mismatch, the stiffness increase at the proximal end (vessel-to-stent) and the stiffness decrease at the distal end (stent-to-vessel). The reflection coefficients at these interfaces are therefore positive and negative, respectively, and therefore reflected waves from the two sites tend to cancel out if there is a negligible delay between them. Short stiff segments may therefore produce only minor wave reflection effects overall (Taelman et al., 2015). A pathological narrowing (stenosis) or expansion (aneurysm) of a vessel present regions of high and low impedance, respectively, and may lead to wave reflection (Stergiopulos et al., 1996; Swillens et al., 2008; Sazonov et al., 2017).

Viscous Resistance in Arterioles

Characteristic impedance in a vascular segment with non-leaky walls is determined by three factors, namely the inertia of blood (L), the compliance of the vessel (C), and the resistance to flow caused by blood viscosity (R), as follows,

$$Z_c = \sqrt{\frac{R + j\omega L}{j\omega C}} \tag{10}$$

where ω is angular frequency and $j = \sqrt{-1}$ (Pollack et al., 1968). In large arteries such as the aorta, resistance is negligible, and therefore Equation (10) reduces to $Z_c = \sqrt{L/C}$. Noting that $L = \rho l/A$ and $C = Al/(\rho c^2)$, where ρ is blood density, l is length, A is cross-sectional area, and c is wave speed, it can be shown that $Z_c = \rho c/A$ as mentioned previously. However, because resistance is inversely proportional to the fourth power of radius (Poiseuille's law), viscous resistance becomes the main determinant of characteristic impedance in small vessels.

Resistance-related increases in Z_c may therefore produce wave reflection. Indeed, Nichols and O'Rourke (2011) stated that "high-resistance arterioles are considered to be the major sites of wave reflection in the circulation." This was based on the precipitous fall in pressure in these vessels and, more directly, the finding that vasoconstrictors and vasodilators that act mainly on small muscular arteries and arterioles cause a major increase and decrease in wave reflection, respectively (O'Rourke and Taylor, 1966; van den Bos et al., 1982).

Factors Influencing Wave Magnitude

When performing wave intensity or wave power analysis, one might expect that the magnitude of a measured wave will be directly determined by the magnitude of the force that generated it, such as the strength of contraction or rate of relaxation of a pump (including load-dependence), the magnitude of the inertial force, or the degree of impedance mismatch. Although these may be the dominant factors governing wave magnitude in many settings, there are a number of other phenomena that can have a substantial influence on wave magnitude.

Wave Amplification and Attenuation Due to a Non-linear Pressure-Area Relation

Mynard et al. (2008) showed that waves can grow (amplify) or shrink (attenuate) as they propagate in a vessel with a non-linear pressure-area relation. Although this relation may be approximately linear over a limited range, all vessels have non-linear pressure-area relations because at low pressures they become highly compliant and collapse, while at high pressures there is a progressive shift in load-bearing from elastin to the stiffer collagen fibers. The slope of the pressure-area relation determines both the area compliance ($C = dA/dP$) and wave speed [$c^2 = A/(\rho C)$] of a vessel, and hence any non-linearity in this relation means that wave speed is pressure-dependent. Consider a compression wave (FCW or BCW) that causes an increase in pressure by 4 mmHg overall, composed of 4 individual wavelets that each contribute 1 mmHg (**Figure 8A**; for illustration purposes, we here relax the principle that wavelets are infinitesimally small). The last wavelet (i.e., which contributes the last 1 mmHg rise) will propagate at a faster speed than the first wavelet, because the wavelets that came before it increased pressure and hence instantaneous wave speed. As a consequence, the overall rate at which pressure changes (dP/dt) increases as the wave propagates. Since wave intensity is equal to $dP/dt \times dU/dt$, this phenomenon causes the intensity of a compression wave to increase (or amplify) as it propagates. The opposite is true for decompression waves, for which the last wavelet propagates more slowly (since it exists at a lower pressure) than that of the first wavelet; hence, the pressure slope and wave intensity decrease as the wave propagates (**Figure 8A**).

This amplification of compression waves and attenuation of decompression waves has important implications for how one assesses wave reflection (Mynard et al., 2008). For example, if a FCW propagates along a vessel and is reflected as a BCW that propagates back to the measurement site, the ratio of BCW/FCW wave intensities will not be a reliable index of the reflection if the waves have been amplified during propagation (unless the amount of amplification is known). This issue is not purely academic, but is a likely explanation for the curious finding of BCW/FCW ratios significantly greater than 1 in pulmonary arteries of near-term fetal lambs (Smolich et al., 2008, 2009). Importantly, Mynard et al. (2008) showed that non-linear effects do not affect the overall pressure effect of a wave, only the rate at which pressure changes. We therefore recommend that wave reflection be quantified from the ratio of the pressure effects of forward and backward waves rather than the wave intensity (peak or cumulative intensity) of those waves.

Wave Attenuation Due to Blood Viscosity and Vessel Wall Viscoelasticity

While the non-linear amplification/attenuation effect discussed above is energy conserving, with energy becoming more or less 'concentrated' in time (increasing or decreasing wave intensity), energy dissipation in the form of heat also occurs in blood vessels due to viscous friction in moving blood and in the stretching/relaxing vessel wall. Many studies have investigated the influence of these factors on wave attenuation, but will not be reviewed in detail here (Westerhof and Noordergraaf, 1970; Salotto et al., 1986; Horsten et al., 1989; Reuderink et al., 1989; Bertram et al., 1997; Alastruey et al., 2011, 2012; Wang et al., 2016). In brief, both sources of dissipation cause attenuation of compression and decompression waves, leading to an exponential fall in the magnitude of propagating waves; this

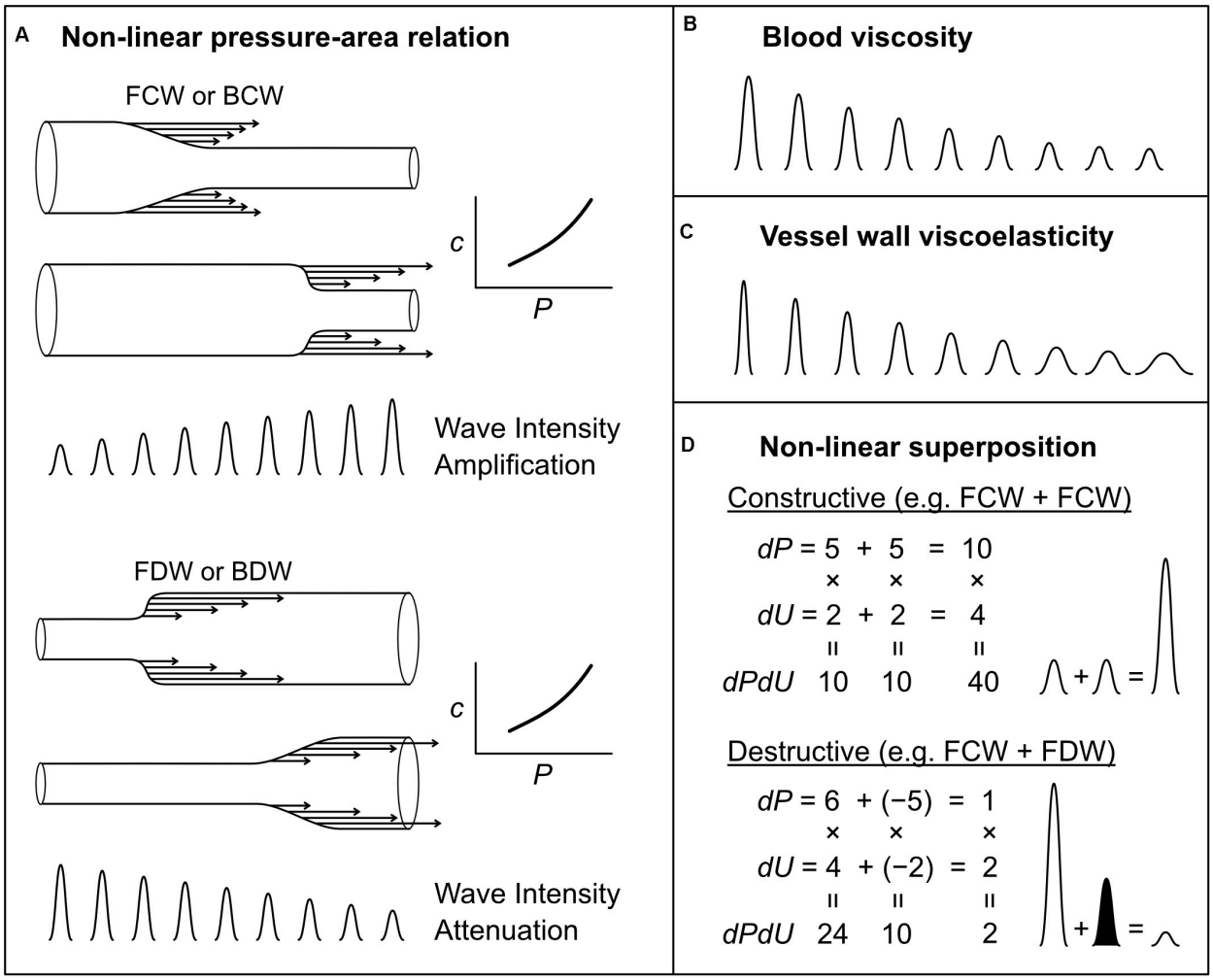

FIGURE 8 | Mechanisms that affect wave intensity magnitude as a wave propagates **(A–C)** or when two waves propagating in the same direction, but generated from separate mechanisms, combine constructively or destructively **(D)**. Waves shown in **(B,C)** could be any wave type (FCW, FDW, BCW, or BDW). In the examples of wave superposition shown in **(D)**, the shaded and unshaded waves indicate an FDW and FCW, respectively.

effect is minor in large vessels, but has a substantial impact on small vessel haemodynamics (Salotto et al., 1986; Segers et al., 1995; Feng and Khir, 2007, 2008; Mynard et al., 2008). The effects of blood viscosity and wall viscosity are not identical; wall viscosity causes both attenuation (decreased magnitude) and dispersion (spreading out or widening) of waves, whereas blood viscosity predominantly causes only attenuation (**Figures 8B,C**) (Alastruey et al., 2012).

Non-linear Wave Superposition Effects

When interpreting wave patterns, one of the mechanisms responsible for generating waves mentioned above may be responsible for a given wave, but it is also possible that multiple mechanisms act together to produce a particular wave. This issue was recently identified in the context of coronary arterial wave intensity analysis, which is characterized by a large backward decompression wave (BDW) that is mainly responsible for the early diastolic surge in coronary flow (Mynard et al., 2018). It was previously thought that this BDW arose solely from an active suction effect in the intramyocardial circulation caused by myocardial relaxation (Davies et al., 2006a; Lee et al., 2016; Raphael et al., 2016). However, evidence from experimental and modeling data suggested that the coronary BDW actually arises from a combination of (1) the active relaxation effect and (2) simultaneous reflection of the aortic FDW that is transmitted into coronary arteries (Mynard et al., 2018).

More generally, it was demonstrated that when two mechanisms contribute to a particular wave, the resultant wave intensity is not the linear sum of the intensities of the waves that would be produced by each mechanism independently. For example, if two mechanisms both produce waves causing a pressure change (dP) of 5 and velocity change (dU) of 2 (ignoring units), then the wave intensity ($dPdU$) arising from each mechanism in isolation would be $5 \times 2 = 10$; however, the wave intensity resulting from the simultaneous action of both mechanisms, resulting in 'constructive interference,' would

be (5 + 5) × (2 + 2) = 40, which is twice the linear sum of the intensities, i.e., 10 + 10 = 20 (**Figure 8D**). Similarly, two processes that have opposing pressure effects will have a non-linear canceling effect (destructive interference), which can lead to 'concealment' of those processes in the wave patterns (Mynard et al., 2018) (**Figure 8D**). In the coronary arteries, it may be possible to 'disentangle' multiple mechanisms underlying observed waves (Mynard et al., 2018). However, whether the non-linear superposition of two or more wave-generating mechanisms is relevant in other settings, and the extent to which those mechanisms could be disentangled, is a potential avenue for future research.

Wave Frequency

One property of wave intensity is that wave magnitude is profoundly affected by wave frequency, that is, the rapidity with which pressure and velocity change. One downside of this property is that it is possible for a wave with a large amplitude to have a very small overall effect on pressure and flow (small but rapid change), while conversely a large pressure/flow change may be associated with indiscernible wave intensity (large but slow change). A key example of the latter is the diastolic period, when $P_{\pm}$ changes are substantial but relatively slow, which could lead to the impression that no waves are present during this time. However, close inspection reveals that $wi_{\pm}$ is non-zero during this time (Mynard and Smolich, 2014b) (see also **Figure 6**). This issue is not resolved by calculating cumulative intensity (i.e., wave area) rather than peak intensity, and we therefore recommend always reporting the overall pressure or velocity 'impact' of waves (commonly designated $\Delta P_{\pm}$ or $\Delta U_{\pm}$) in addition to their intensity.

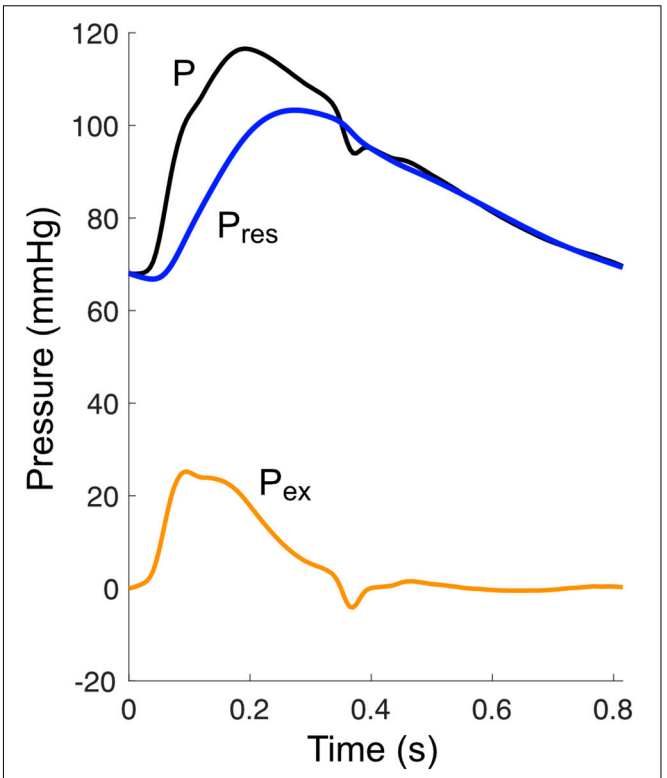

FIGURE 9 | Decomposition of pressure (P) into a reservoir pressure (P_{res}) and an excess pressure (P_{ex}).

WAVE POTENTIAL

Mean or absolute values of blood pressure and flow have historically been neglected when analyzing pressure/flow waves in the arterial system. For example, absolute values have no impact on wave intensity, which is calculated from *changes* in pressure and flow-velocity. Similarly, when performing wave separation in the frequency or time domain, only the oscillatory component of pressure has been considered relevant (Westerhof et al., 1972; Li, 1986). However, there has been a growing recognition that, physically, waves must be linked with mean pressure, since the latter ultimately arises from pulsatile pressure/flow 'inputs' (wave generation) from the ventricle; when these inputs cease, pressure does not remain constant, but falls to a much lower level (Jellinek et al., 2000). Conversely, after a period of asystole, recommencement of wave generation by the ventricle restores mean pressure (Jellinek et al., 2000; Alastruey et al., 2009).

The link between waves and the absolute values of pressure and flow was explored by Mynard and Smolich (2014b), who proposed the concept of 'wave potential.' This provided a physical meaning to the absolute values of $P_{\pm}$ and $Q_{\pm}$ for the first time. In brief, just as pressure represents flow potential (i.e., flow is generated when a pressure difference exists between two locations), so the absolute values of $P_{\pm}$ and $Q_{\pm}$ represent the potential for pressure and flow wave generation at that time (arrows in **Figure 4**). Extending the staircase analogy discussed earlier, whereas waves correspond to stairs, wave potential represents the absolute height above ground level (the potential for how far one could fall!). Here, the 'ground level' is defined as the state in which no waves could be generated (one could not fall further); that is, when flow is zero and pressure equals 'undisturbed pressure' (P_{ud}). The latter signifies the pressure that would exist if no pressure differentials existed throughout the circulation, and may therefore be identified with mean circulatory pressure (P_{mc}) (Mynard and Smolich, 2014b). Alternatively, P_{ud} could be identified with the zero-flow or asymptotic pressure that is reached after a long period of asystole, which may not be equal to P_{mc} (Hughes and Parker, 2020).

Regardless of the pressure 'ground' that is chosen, it has been shown that wave potential closely relates to the stored pressure, blood volume, and hydraulic energy (i.e., potential for hydraulic work) in a distended arterial segment (Mynard and Smolich, 2014b, 2016) (**Figure 7C**). The concept therefore allows for a unified wave-based description of both wave phenomena and the windkessel effect, where the latter refers to the storage and discharge of blood in the elastic arterial reservoir. During systole, waves are responsible for filling the arterial reservoir because these increase pressure and to some extent become trapped in the arterial network due to multiple reflections and re-reflections,

thus building up wave potential. Then during diastole, discharge of the arterial reservoir occurs due to leakage of wave potential, since waves are only partially reflected at the distal outlets of the network (Mynard and Smolich, 2014b, 2017).

WAVES AND THE RESERVOIR PRESSURE

Another approach that has attempted to unify windkessel and wave models of haemodynamics is the reservoir-wave paradigm. Initially termed the windkessel-wave approach, Wang et al. (2003) separated measured pressure into two components, a 'windkessel pressure' calculated via a two-element windkessel model and considered to govern the windkessel properties of the arterial system (i.e., systolic storage and diastolic discharge of the arterial 'compliance chamber'), and an 'excess pressure' thought to arise from wave phenomena (**Figure 9**). However, this concept received considerable criticism and has since been revised. For example, a key implication of this original hybrid model was that wave intensity analysis should be performed using excess pressure rather than the measured pressure (Wang et al., 2003; Davies et al., 2007; Tyberg et al., 2009). However, subsequent modeling studies, supported by *in vivo* data from both animals and humans, revealed significant problems with this approach (Mynard et al., 2012, 2015; Mynard, 2013; Mynard and Smolich, 2014a). In addition, the assumption that the windkessel pressure was spatially homogenous in the large arterial network was questioned because it exhibited wave-like behavior when measured at multiple locations (Mynard et al., 2012). Others have also raised similar theoretical concerns (Vermeersch et al., 2009; Segers et al., 2015; Westerhof and Westerhof, 2015).

In response to some of the criticisms raised, Parker et al. proposed a 'modified' reservoir pressure (P_{res}) and revised concepts around how this reservoir pressure relates to waves (Parker et al., 2012; Parker, 2017; Hughes and Parker, 2020). The new P_{res} is distinct from a windkessel pressure in that it incorporates a propagation delay but is otherwise uniform in space. Moreover, rather than being considered exclusive to wave reflection, it is now broadly agreed that the P_{res} in fact arises entirely from wave reflection, with Hughes and Parker (2020) stating that "the reservoir pressure can be understood as the pressure due to the cumulative effect of ... reflected and re-reflected waves." Indeed, it has been shown that in the aorta, P_{res} is approximately equal to twice the backward component of pressure (Hametner et al., 2014), while excess pressure ($P_{ex} = P - P_{res}$) is approximately equal to flow multiplied by characteristic impedance, which is the pressure that would theoretically exist in the absence of any wave reflection. The debate regarding wave intensity analysis appears to have been resolved, with recent literature reflecting a consensus that measured pressure (or an appropriate distension-based surrogate) should be used for wave intensity, not P_{ex} (Segers et al., 2017; Su et al., 2017; Pomella et al., 2018; Bhuva et al., 2019; Chiesa et al., 2019; Kowalski et al., 2019b; Hughes et al., 2020).

Finally, although aortic P_{res} provides similar information to conventional wave separation analysis (since $P_{res} \approx 2P_{-}$), a potential benefit of P_{res} is that it can be obtained (with several assumptions) from a peripheral site without having to estimate central pressure or flow (Aguado-Sierra et al., 2008; Peng et al., 2017). However, a key consideration when calculating P_{res} is that it relies on fitting an exponential curve to diastolic pressure. Vermeersch et al. (2009) found this fitting to be unreliable in 15% of recordings from a cohort of 35–55 year-old adults, and noted that this might be expected when pressure waveforms do not exhibit a clear exponential decay (such as C-type waveforms often observed in younger individuals).

In summary, the reservoir-wave paradigm has seen both significant debate and new developments over the past decade. Further work is needed to determine whether P_{res} and P_{ex} provide true added value (in both a conceptual and pragmatic sense) over other non-invasive wave analysis techniques, as well as establishing which measurement techniques and in which patient settings it can be reliably applied.

CLOSING REMARKS

The analysis of waves in blood vessels provides important insights into biomechanical processes and interactions in the cardiovascular system, many of which are not discernable from standard indices such as systolic and diastolic pressure, or cardiac output. Indices obtained from these analyses are therefore extremely useful in a research setting for answering mechanistic questions about cardiovascular physiology in health and disease. There is also emerging evidence that these indices could prove to be valuable in the clinical setting, with the higher specificity of information obtained potentially aiding the goal of personalized medicine (Chirinos, 2017). These wave analysis techniques have not yet been widely adopted in medical practice partly due to the need for further evidence of clinical value. However, other significant barriers likely include a lack of general recognition of the insights that these indices could provide, the relative complexity of measuring and analyzing waves, and the paucity of devices for obtaining wave-related indices in a convenient manner. These barriers constitute fertile ground for future work.

AUTHOR CONTRIBUTIONS

JM, AK, and RK drafted the manuscript. JM prepared the figures and tables. JM, AK, RK, MC, and JS edited the manuscript for intellectual content and approved the final version. All authors contributed to the article and approved the submitted version.

FUNDING

JM was supported by a co-funded R. D. Wright Career Development Fellowship from the National Health and Medical Research Council of Australia (APP1143510) and Future Leader Fellowship from the National Heart Foundation of Australia (101866). The Heart Research Group was supported by the Victorian Government's Operational Infrastructure Support Program, RCH 1000 and Big W.

REFERENCES

Aguado-Sierra, J., Alastruey, J., Wang, J. J., Hadjiloizou, N., Davies, J., and Parker, K. H. (2008). Separation of the reservoir and wave pressure and velocity from measurements at an arbitrary location in arteries. *Proc. Inst. Mech. Eng. H J. Eng. Med.* 222, 403–416. doi: 10.1243/09544119jeim315

Alastruey, J. (2011). Numerical assessment of time-domain methods for the estimation of local arterial pulse wave speed. *J. Biomech.* 44, 885–891. doi: 10.1016/j.jbiomech.2010.12.002

Alastruey, J., Khir, A. W., Matthys, K. S., Segers, P., Sherwin, S. J., Verdonck, P. R., et al. (2011). Pulse wave propagation in a model human arterial network: assessment of 1-D visco-elastic simulations against in vitro measurements. *J. Biomech.* 44, 2250–2258. doi: 10.1016/j.jbiomech.2011.05.041

Alastruey, J., Parker, K., Peiró, J., and Sherwin, S. (2009). Analysing the pattern of pulse waves in arterial networks: a time-domain study. *J. Eng. Math.* 64, 331–351. doi: 10.1007/s10665-009-9275-1

Alastruey, J., Passerini, T., Formaggia, L., and Peiró, J. (2012). Physical determining factors of the arterial pulse waveform: theoretical analysis and calculation using the 1-D formulation. *J. Eng. Math.* 77, 19–37. doi: 10.1007/s10665-012-9555-z

Armentano, R. L., Barra, J. G., Levenson, J., Simon, A., and Pichel, R. H. (1995). Arterial wall mechanics in conscious dogs : assessment of viscous, inertial, and elastic moduli to characterize aortic wall behavior. *Circ. Res.* 76, 468–478. doi: 10.1161/01.res.76.3.468

Babcock, M. C., Lefferts, W. K., Hughes, W. E., Fitzgerald, K. L., Leyer, B. K., Redmond, J. G., et al. (2014). Acute effect of high-intensity cycling exercise on carotid artery hemodynamic pulsatility. *Eur. J. Appl. Physiol.* 115, 1037–1045. doi: 10.1007/s00421-014-3084-6

Baksi, A. J., Treibel, T. A., Davies, J. E., Hadjiloizou, N., Foale, R. A., Parker, K. H., et al. (2009). A meta-analysis of the mechanism of blood pressure change with aging. *J. Am. Coll. Cardiol.* 54, 2087–2092. doi: 10.1016/j.jacc.2009.06.049

Beldi, G., Bosshard, A., Hess, O. M., Althaus, U., and Walpoth, B. H. (2000). Transit time flow measurement: experimental validation and comparison of three different systems. *Ann. Thorac. Surg.* 70, 212–217. doi: 10.1016/s0003-4975(00)01246-7

Bertram, C. D., Gow, B. S., and Greenwald, S. E. (1997). Comparison of different methods for the determination of the true wave propagation coefficient, in rubber tubes and the canine thoracic aorta. *Med. Eng. Phys.* 19, 212–222. doi: 10.1016/s1350-4533(96)00073-2

Bhuva, A. N., D'Silva, A., Torlasco, C., Nadarajan, N., Jones, S., Boubertakh, R., et al. (2019). Non-invasive assessment of ventriculo-arterial coupling using aortic wave intensity analysis combining central blood pressure and phase-contrast cardiovascular magnetic resonance. *Eur. Heart J. Cardiovasc. Imaging* 21, 805–813. doi: 10.1093/ehjci/jez227

Biglino, G., Steeden, J. A., Baker, C., Schievano, S., Taylor, A. M., Parker, K. H., et al. (2012). A non-invasive clinical application of wave intensity analysis based on ultrahigh temporal resolution phase-contrast cardiovascular magnetic resonance. *J. Cardiovasc. Magn. Reson.* 14:57. doi: 10.1186/1532-429x-14-57

Borlotti, A., Khir, A. W., Rietzschel, E. R., De Buyzere, M. L., Vermeersch, S., and Segers, P. (2012). Noninvasive determination of local pulse wave velocity and wave intensity: changes with age and gender in the carotid and femoral arteries of healthy human. *J. Appl. Physiol.* 113, 727–735. doi: 10.1152/japplphysiol.00164.2012

Borlotti, A., Li, Y., Parker, K. H., and Khir, A. W. (2014). Experimental evaluation of local wave speed in the presence of reflected waves. *J. Biomech.* 47, 87–95. doi: 10.1016/j.jbiomech.2013.10.007

Bramwell, J. C., and Hill, A. V. (1922). The velocity of the pulse wave in man. *Proc. R. Soc. Lond. B Biol. Sci.* 93, 298–306.

Broyd, C. J., Nijjer, S., Sen, S., Petraco, R., Jones, S., Al-Lamee, R., et al. (2016). Estimation of coronary wave intensity analysis using non-invasive techniques and its application to exercise physiology. *Am. J. Physiol. Heart Circ. Physiol.* 210, H619–H627. doi: 10.1152/ajpheart.00575.2015

Burattini, R., and Campbell, K. B. (1999). Assessment of aortic pressure power components and their link to overall elastic and resistive arterial properties. *Med. Biol. Eng. Comput.* 37, 366–376. doi: 10.1007/bf02513314

Butlin, M., Qasem, A., and Avolio, A. P. (2012). "Estimation of central aortic pressure waveform features derived from the brachial cuff volume displacement waveform," in *Proceedings of the Engineering in Medicine and Biology Society (EMBC), 2012 Annual International Conference of the IEEE*, (Piscataway, NJ: IEEE), 2591–2594.

Buxi, D., Redouté, J.-M., and Yuce, M. R. (2017). Blood pressure estimation using pulse transit time from bioimpedance and continuous wave radar. *IEEE Trans. Biomed. Eng.* 64, 917–927. doi: 10.1109/tbme.2016.2582472

Centers for Disease Prevention and Control (2019). *Data and Statistics on Congenital Heart Defects [Online]*. Available: www.cdc.gov/ncbddd/heartdefects/data.html (accessed December 6, 2019).

Chen, C.-H., Nevo, E., Fetics, B., Pak, P. H., Yin, F. C. P., Maughan, W. L., et al. (1997). Estimation of central aortic pressure waveform by mathematical transformation of radial tonometry pressure: validation of generalized transfer function. *Circulation* 95, 1827–1836. doi: 10.1161/01.cir.95.7.1827

Cheng, K., Cameron, J. D., Tung, M., Mottram, P. M., Meredith, I. T., and Hope, S. A. (2012). Association of left ventricular motion and central augmentation index in healthy young men. *J. Hypertens.* 30, 2395–2402. doi: 10.1097/HJH.0b013e328358bee2

Chiesa, S. T., Masi, S., Shipley, M. J., Ellins, E. A., Fraser, A. G., Hughes, A. D., et al. (2019). Carotid artery wave intensity in mid- to late-life predicts cognitive decline: the whitehall ii study. *Eur. Heart J.* 40, 2300–2309. doi: 10.1093/eurheartj/ehz189

Chirinos, J. A. (2017). Deep phenotyping of systemic arterial hemodynamics in hfpef (part 2): clinical and therapeutic considerations. *J. Cardiovasc. Transl. Res.* 10, 261–274. doi: 10.1007/s12265-017-9736-2

Chirinos, J. A., Kips, J. G., Jacobs, D. R., Brumback, L., Duprez, D. A., Kronmal, R., et al. (2012). Arterial wave reflections and incident cardiovascular events and heart failure: mesa (multiethnic study of atherosclerosis). *J. Am. Coll. Cardiol.* 60, 2170–2177. doi: 10.1016/j.jacc.2012.07.054

Corriveau, M. M., and Johnston, K. W. (2004). Interobserver variability of carotid Doppler peak velocity measurements among technologists in an ICAVL-accredited vascular laboratory. *J. Vasc. Surg.* 39, 735–741. doi: 10.1016/j.jvs.2003.12.017

Davies, J. E., Alastruey, J., Francis, D. P., Hadjiloizou, N., Whinnett, Z. I., Manisty, C. H., et al. (2012). Attenuation of wave reflection by wave entrapment creates a "horizon effect" in the human aorta. *Hypertension* 60, 778–785. doi: 10.1161/hypertensionaha.111.180604

Davies, J. E., Baksi, J., Francis, D. P., Hadjiloizou, N., Whinnett, Z. I., Manisty, C. H., et al. (2010). The arterial reservoir pressure increases with aging and is the major determinant of the aortic augmentation index. *Am. J. Physiol. Heart Circ. Physiol.* 298, H580–H586. doi: 10.1152/ajpheart.00875.2009

Davies, J. E., Hadjiloizou, N., Leibovich, D., Malaweera, A., Alastruey-Arimon, J., Whinnett, Z. I., et al. (2007). Importance of the aortic reservoir in determining the shape of the arterial pressure waveform - the forgotten lessons of Frank. *Artery Res.* 1, 40–45. doi: 10.1016/j.artres.2007.08.001

Davies, J. E., Lacy, P., Tillin, T., Collier, D., Cruickshank, J. K., Francis, D. P., et al. (2014). Excess pressure integral predicts cardiovascular events independent of other risk factors in the conduit artery functional evaluation substudy of Anglo-Scandinavian Cardiac Outcomes Trial. *Hypertension* 64, 60–68. doi: 10.1161/HYPERTENSIONAHA.113.02838

Davies, J. E., Whinnett, Z. I., Francis, D. P., Manisty, C. H., Aguado-Sierra, J., Willson, K., et al. (2006a). Evidence of a dominant backward-propagating "suction" wave responsible for diastolic coronary filling in humans, attenuated in left ventricular hypertrophy. *Circulation* 113, 1768–1778. doi: 10.1161/circulationaha.105.603050

Davies, J. E., Whinnett, Z. I., Francis, D. P., Willson, K., Foale, R. A., Malik, I. S., et al. (2006b). Use of simultaneous pressure and velocity measurements to estimate arterial wave speed at a single site in humans. *Am. J. Physiol. Heart Circ. Physiol.* 290, 878–885.

Devos, D. G. H., Rietzschel, E., Heyse, C., Vandemaele, P., Van Bortel, L., Babin, D., et al. (2015). MR pulse wave velocity increases with age faster in the thoracic aorta than in the abdominal aorta. *J. Magn. Reson. Imaging* 41, 765–772. doi: 10.1002/jmri.24592

Di Lascio, N., Gemignani, V., Bianchini, E., Bruno, R. M., Ghiadoni, L., and Faita, F. (2018). Effects of carotid pressure waveforms on the results of wave separation, wave intensity and reservoir pressure analysis. *Physiol. Meas.* 39:114003. doi: 10.1088/1361-6579/aae6eb

Dong, S.-J., Hees, P. S., Siu, C. O., Weiss, J. L., and Shapiro, E. P. (2001). MRI assessment of LV relaxation by untwisting rate: a new isovolumic phase measure of τ. *Am. J. Physiol. Heart Circ. Physiol.* 281, H2002–H2009.

Drzewiecki, G. M., Melbin, J., and Noordergraaf, A. (1983). Arterial tonometry: review and analysis. *J. Biomech.* 16, 141–152. doi: 10.1016/0021-9290(83)90037-4

Dujardin, J. P., and Stone, D. N. (1981). Characteristic impedance of the proximal aorta determined in the time and frequency domain: a comparison. *Med. Biol. Eng. Comput.* 19, 565–568. doi: 10.1007/BF02442770

Fantin, F., Mattocks, A., Bulpitt, C. J., Banya, W., and Rajkumar, C. (2006). Is augmentation index a good measure of vascular stiffness in the elderly? *Age Ageing* 36, 43–48. doi: 10.1093/ageing/afl115

Feng, J., and Khir, A. W. (2007). "A new approach to investigate wave dissipation in viscoelastic tubes: application of wave intensity analysis," in *Proceedings of the 27th Annual International Conference of the IEEE Engineering in Medicine and Biology Society*, (Piscataway, NJ: IEEE), 2260–2263.

Feng, J., and Khir, A. W. (2008). The compression and expansion waves of the forward and backward flows: an in-vitro arterial model. *Proc. Inst. Mech. Eng. H J. Eng. Med.* 222, 531–542. doi: 10.1243/09544119jeim339

Feng, J., and Khir, A. W. (2010). Determination of wave speed and wave separation in the arteries using diameter and velocity. *J. Biomech.* 43, 455–462. doi: 10.1016/j.jbiomech.2009.09.046

Fetics, B., Nevo, E., Chen, C.-H., and Kass, D. A. (1999). Parametric model derivation of transfer function for noninvasive estimation of aortic pressure by radial tonometry. *IEEE Trans. Biomed. Eng.* 46, 698–706. doi: 10.1109/10.764946

Fok, H., Guilcher, A., Li, Y., Brett, S., Shah, A., Clapp, B., et al. (2014). Augmentation pressure is influenced by ventricular contractility/relaxation dynamics: novel mechanism of reduction of pulse pressure by nitrates. *Hypertension* 63, 1050–1055. doi: 10.1161/hypertensionaha.113.02955

Gallagher, D., Adji, A., and O'Rourke, M. F. (2004). *Validation of the Transfer Function Technique for Generating Central from Peripheral Upper Limb Pressure Waveform*. Oxford: Oxford University Press.

Garcia-Ortiz, L., Recio-Rodríguez, J. I., Canales-Reina, J. J., Cabrejas-Sánchez, A., Gomez-Arranz, A., Magdalena-Belio, J. F., et al. (2012). Comparison of two measuring instruments, b-pro and sphygmocor system as reference, to evaluate central systolic blood pressure and radial augmentation index. *Hypertens. Res.* 35:617. doi: 10.1038/hr.2012.3

Hadjiloizou, N., Davies, J. E., Malik, I. S., Aguado-Sierra, J., Willson, K., Foale, R. A., et al. (2008). Differences in cardiac microcirculatory wave patterns between the proximal left mainstem and proximal right coronary artery. *Am. J. Physiol. Heart Circ. Physiol.* 295, H1198–H1205. doi: 10.1152/ajpheart.00510.2008

Hametner, B., Parragh, S., Mayer, C., Weber, T., Van Bortel, L., De Buyzere, M., et al. (2015). Assessment of model based (input) impedance, pulse wave velocity, and wave reflection in the Asklepios cohort. *PLoS One* 10:e0141656. doi: 10.1371/journal.pone.0141656

Hametner, B., Parragh, S., Weber, T., and Wassertheurer, S. (2017). Wave intensity of aortic root pressure as diagnostic marker of left ventricular systolic dysfunction. *PLoS One* 12:e0179938. doi: 10.1371/journal.pone.0179938

Hametner, B., Wassertheurer, S., Hughes, A. D., Parker, K. H., Weber, T., and Eber, B. (2014). Reservoir and excess pressures predict cardiovascular events in high-risk patients. *Int. J. Cardiol.* 171, 31–36. doi: 10.1016/j.ijcard.2013.11.039

Hametner, B., Wassertheurer, S., Kropf, J., Mayer, C., Holzinger, A., Eber, B., et al. (2013). Wave reflection quantification based on pressure waveforms alone—methods, comparison, and clinical covariates. *Comput. Methods Programs Biomed.* 109, 250–259. doi: 10.1016/j.cmpb.2012.10.005

Hellevik, L., Segers, P., Stergiopulos, N., Irgens, F., Verdonck, P., Thompson, C., et al. (1999). Mechanism of pulmonary venous pressure and flow waves. *Heart Vessels* 14, 67–71. doi: 10.1007/bf02481745

Hickson, S. S., Butlin, M., Graves, M., Taviani, V., Avolio, A. P., McEniery, C. M., et al. (2010). The relationship of age with regional aortic stiffness and diameter. *JACC Cardiovasc. Imaging* 3, 1247–1255. doi: 10.1016/j.jcmg.2010.09.016

Hobson, T. N., Flewitt, J. A., Belenkie, I., and Tyberg, J. V. (2007). Wave intensity analysis of left atrial mechanics and energetics in anesthetized dogs. *Am. J. Physiol. Heart Circ. Physiol.* 292, H1533–H1540. doi: 10.1152/ajpheart.00837.2006

Hoeks, A. P. G., Brands, P. J., Smeets, F. A. M., and Reneman, R. S. (1990). Assessment of the distensibility of superficial arteries. *Ultrasound Med. Biol.* 16, 121–128. doi: 10.1016/0301-5629(90)90139-4

Hollander, E. H., Wang, J. J., Dobson, G. M., Parker, K. H., and Tyberg, J. V. (2001). Negative wave reflections in pulmonary arteries. *Am. J. Physiol. Heart Circ. Physiol.* 281, H895–H902.

Horsten, J., Van Steenhoven, A. A., and Van Dongen, M. E. H. (1989). Linear propagation of pulsatile waves in viscoelastic tubes. *J. Biomech.* 22, 477–484. doi: 10.1016/0021-9290(89)90208-x

Horvath, I. G., Nemeth, A., Lenkey, Z., Alessandri, N., Tufano, F., Kis, P., et al. (2010). Invasive validation of a new oscillometric device (arteriograph) for measuring augmentation index, central blood pressure and aortic pulse wave velocity. *J. Hypertens.* 28, 2068–2075. doi: 10.1097/hjh.0b013e32833c8a1a

Hoskins, P. R. (2011). Estimation of blood velocity, volumetric flow and wall shear rate using Doppler ultrasound. *Ultrasound* 19, 120–129. doi: 10.1258/ult.2011.011015

Howard, J. P., Cook, C. M., van de Hoef, T. P., Meuwissen, M., de Waard, G. A., van Lavieren, M. A., et al. (2019). Artificial intelligence for aortic pressure waveform analysis during coronary angiography: machine learning for patient safety. *JACC Cardiovasc. Interv.* 12, 2093–2101. doi: 10.1016/j.jcin.2019.06.036

Hughes, A., Park, C., Ramakrishnan, A., Mayet, A., Chaturvedi, N., and Parker, K. (2020). Feasibility of estimation of aortic wave intensity using non- invasive pressure recordings in the absence of flow velocity in man. *Front. Physiol. Vasc. Physiol.* 11:550. doi: 10.3389/fphys.2020.00550

Hughes, A., and Parker, K. (2009). Forward and backward waves in the arterial system: impedance or wave intensity analysis? *Med. Biol. Eng. Comput.* 47, 207–210. doi: 10.1007/s11517-009-0444-1

Hughes, A. D., Park, C., Davies, J., Francis, D., McG Thom, S. A., Mayet, J., et al. (2013). Limitations of augmentation index in the assessment of wave reflection in normotensive healthy individuals. *PLoS One* 8:e59371. doi: 10.1371/journal.pone.0059371

Hughes, A. D., and Parker, K. H. (2020). The modified arterial reservoir: an update with consideration of asymptotic pressure (p8) and zero-flow pressure (pzf). *Proc. Inst. Mech. Eng. H J. Eng. Med.* [Epub ahead of print]. doi: 10.1177/0954411920917557

Hughes, A. D., Parker, K. H., and Davies, J. E. (2008). Waves in arteries: a review of wave intensity analysis in the systemic and coronary circulations. *Artery Res.* 2, 51–59. doi: 10.1016/j.artres.2008.02.002

Imholz, B. P. M., Wieling, W., van Montfrans, G. A., and Wesseling, K. H. (1998). Fifteen years experience with finger arterial pressure monitoring: assessment of the technology. *Cardiovasc. Res.* 38, 605–616. doi: 10.1016/s0008-6363(98)00067-4

Janner, J. H., Godtfredsen, N. S., Ladelund, S., Vestbo, J., and Prescott, E. (2013). High aortic augmentation index predicts mortality and cardiovascular events in men from a general population, but not in women. *Eur. J. Prev. Cardiol.* 20, 1005–1012. doi: 10.1177/2047487312449588

Jellinek, H., Krenn, H., Oczenski, W., Veit, F., Schwarz, S., and Fitzgerald, R. D. (2000). Influence of positive airway pressure on the pressure gradient for venous return in humans. *J. Appl. Physiol.* 88, 926–932. doi: 10.1152/jappl.2000.88.3.926

Johnson, J. E., Shay, O., Kim, C., and Liao, C. (2019). Wearable millimeter-wave device for contactless measurement of arterial pulses. *IEEE Trans. Biomed. Circ. Syst.* 13, 1525–1534. doi: 10.1109/tbcas.2019.2948581

Jones, C. J., Sugawara, M., Kondoh, Y., Uchida, K., and Parker, K. H. (2002). Compression and expansion wavefront travel in canine ascending aortic flow: wave intensity analysis. *Heart Vessels* 16, 91–98. doi: 10.1007/s003800200002

Kang, J., Aghilinejad, A., and Pahlevan, N. M. (2019). On the accuracy of displacement-based wave intensity analysis: effect of vessel wall viscoelasticity and nonlinearity. *PLoS One* 14:e0224390. doi: 10.1371/journal.pone.0224390

Karamanoglu, M., and Feneley, M. P. (1997). On-line synthesis of the human ascending aortic pressure pulse from the finger pulse. *Hypertension* 30, 1416–1424. doi: 10.1161/01.hyp.30.6.1416

Karamanoglu, M., and Feneley, M. P. (1999). Late systolic pressure augmentation: role of left ventricular outflow patterns. *Am. J. Physiol.* 277(2 Pt 2), H481–H487.

Kelly, R., Hayward, C., Avolio, A., and O'Rourke, M. (1989). Noninvasive determination of age-related changes in the human arterial pulse. *Circulation* 80, 1652–1659. doi: 10.1161/01.cir.80.6.1652

Kelly, R. P. (1989). Non-invasive registration of the arterial pressure pulse waveform using high-fidelity applanation tonometry. *J. Vasc. Med. Biol.* 1, 142–149.

Khir, A. W., Henein, M. Y., Koh, T., Das, S. K., Parker, K. H., and Gibson, D. G. (2001a). Arterial waves in humans during peripheral vascular surgery. *Clin. Sci.* 101, 749–757. doi: 10.1042/cs1010749

Khir, A. W., O'Brien, A., Gibbs, J. S., and Parker, K. H. (2001b). Determination of wave speed and wave separation in the arteries. *J. Biomech.* 34, 1145–1155. doi: 10.1016/S0021-9290(01)00076-8

Khir, A. W., and Parker, K. H. (2002). Measurements of wave speed and reflected waves in elastic tubes and bifurcations. *J. Biomech.* 35, 775–783. doi: 10.1016/s0021-9290(02)00025-8

Khir, A. W., and Parker, K. H. (2005). Wave intensity in the ascending aorta: effects of arterial occlusion. *J. Biomech.* 38, 647–655. doi: 10.1016/j.jbiomech.2004.05.039

Kim, S.-H., Lilot, M., Sidhu, K. S., Rinehart, J., Yu, Z., Canales, C., et al. (2014). Accuracy and precision of continuous noninvasive arterial pressure monitoring compared with invasive arterial pressurea systematic review and meta-analysis. *J. Am. Soc. Anesthesiol.* 120, 1080–1097. doi: 10.1097/aln.0000000000000226

Kips, J. G., Rietzschel, E. R., De Buyzere, M. L., Westerhof, B. E., Gillebert, T. C., Van Bortel, L. M., et al. (2009). Evaluation of noninvasive methods to assess wave reflection and pulse transit time from the pressure waveform alone. *Hypertension* 53, 142–149. doi: 10.1161/hypertensionaha.108.123109

Koh, T. W., Pepper, J. R., DeSouza, A. C., and Parker, K. H. (1998). Analysis of wave reflections in the arterial system using wave intensity: a novel method for predicting the timing and amplitude of reflected waves. *Heart Vessels* 13, 103–113. doi: 10.1007/bf01747827

Kolyva, C., Pantalos, G. M., Giridharan, G. A., Pepper, J. R., and Khir, A. W. (2009). Discerning aortic waves during intra-aortic balloon pumping and their relation to benefits of counterpulsation in humans. *J. Appl. Physiol.* 107, 1497–1503. doi: 10.1152/japplphysiol.00413.2009

Kolyva, C., Spaan, J. A. E., Piek, J. J., and Siebes, M. (2008). Windkesselness of coronary arteries hampers assessment of human coronary wave speed by single-point technique. *Am. J. Physiol. Heart Circ. Physiol.* 295, H482–H490. doi: 10.1152/ajpheart.00223.2008

Kowalski, R., Beare, R., Willemet, M., Alastruey, J., Smolich, J. J., Cheung, M. M. H., et al. (2017). Robust and practical non-invasive estimation of local arterial wave speed and mean blood velocity waveforms. *Physiol. Meas.* 38, 2081–2099. doi: 10.1088/1361-6579/aa8de3

Kowalski, R., Lee, M. G. Y., Doyle, L. W., Cheong, J. L. Y., Smolich, J. J., d'Udekem, Y., et al. (2019a). Reduced aortic distensibility is associated with higher aorto-carotid wave transmission and central aortic systolic pressure in young adults after coarctation repair. *J. Am. Heart Assoc.* 8:e011411.

Kowalski, R., Mynard, J. P., Smolich, J. J., and Cheung, M. M. H. (2019b). Comparison of invasive and non-invasive aortic wave intensity and wave power analyses in sheep. *Physiol. Meas.* 40:015005. doi: 10.1088/1361-6579/aafcc4

Langewouters, G. J., Wesseling, K. H., and Goedhard, W. J. A. (1984). The static elastic properties of 45 human thoracic and 20 abdominal aortas in vitro and the parameters of a new model. *J. Biomech.* 17, 425–435. doi: 10.1016/0021-9290(84)90034-4

Laskey, W. K., Kussmaul, W. G., Martin, J. L., Kleaveland, J. P., and Hirshfeld, J. W. Jr. (1985). Characteristics of vascular hydraulic load in patients with heart failure. *Circulation* 72, 61–71. doi: 10.1161/01.cir.72.1.61

Lau, E. M. T., Abelson, D., Dwyer, N., Yu, Y., Ng, M. K., and Celermajer, D. S. (2014). Assessment of ventriculo-arterial interaction in pulmonary arterial hypertension using wave intensity analysis. *Eur. Respir. J.* 43, 1804–1807. doi: 10.1183/09031936.00148313

Laustsen, J., Pedersen, E. M., Terp, K., Steinbrüchel, D., Kure, H. H., Paulsen, P. K., et al. (1996). Validation of a new transit time ultrasound flowmeter in man. *Eur. J. Vasc. Endovasc. Surg.* 12, 91–96. doi: 10.1016/s1078-5884(96)80282-6

Lee, J., Nordsletten, D., Cookson, A., Rivolo, S., and Smith, N. (2016). In silico coronary wave intensity analysis: application of an integrated one-dimensional and poromechanical model of cardiac perfusion. *Biomech. Model. Mechanobiol.* 15, 1535–1555. doi: 10.1007/s10237-016-0782-5

Li, J. K. (1986). Time domain resolution of forward and reflected waves in the aorta. *IEEE Trans. Biomed. Eng.* 33, 783–785. doi: 10.1109/tbme.1986.325903

Li, Y., Hickson, S. S., McEniery, C. M., Wilkinson, I. B., and Khir, A. W. (2019). Stiffening and ventricular–arterial interaction in the ascending aorta using MRI: ageing effects in healthy humans. *J. Hypertens.* 37, 347–355. doi: 10.1097/hjh.0000000000001886

Lin, A. C. W., Lowe, A., Sidhu, K., Harrison, W., Ruygrok, P., and Stewart, R. (2012). Evaluation of a novel sphygmomanometer, which estimates central aortic blood pressure from analysis of brachial artery suprasystolic pressure waves. *J. Hypertens.* 30, 1743–1750. doi: 10.1097/hjh.0b013e3283567b94

Londono-Hoyos, F., Zamani, P., Beraun, M., Vasim, I., Segers, P., and Chirinos, J. A. (2018). Effect of organic and inorganic nitrates on cerebrovascular pulsatile power transmission in patients with heart failure and preserved ejection fraction. *Physiol. Meas.* 39:044001. doi: 10.1088/1361-6579/aab2ef

Lu, P.-J., Yang, C.-F. J., Wu, M.-Y., Hung, C.-H., Chan, M.-Y., and Hsu, T.-C. (2012). Wave intensity analysis of para-aortic counterpulsation. *Am. J. Physiol. Heart Circ. Physiol.* 302, H1481–H1491.

Luzardo, L., Lujambio, I., Sottolano, M., da Rosa, A., Thijs, L., Noboa, O., et al. (2012). 24-h ambulatory recording of aortic pulse wave velocity and central systolic augmentation: a feasibility study. *Hypertens. Res.* 35:980. doi: 10.1038/hr.2012.78

Mada, R. O., Lysyansky, P., Daraban, A. M., Duchenne, J., and Voigt, J.-U. (2015). How to define end-diastole and end-systole?: impact of timing on strain measurements. *JACC Cardiovasc. Imaging* 8, 148–157. doi: 10.1016/j.jcmg.2014.10.010

Manisty, C., Mayet, J., Tapp, R. J., Parker, K. H., Sever, P., Poulter, N. H., et al. (2010). Wave reflection predicts cardiovascular events in hypertensive individuals independent of blood pressure and other cardiovascular risk factors: an ascot (Anglo-scandinavian cardiac outcome trial) substudy. *J. Am. Coll. Cardiol.* 56, 24–30. doi: 10.1016/j.jacc.2010.03.030

McEniery, C. M., Yasmin, Hall, I. R., Qasem, A., Wilkinson, I. B., and Cockcroft, J. R. (2005). Normal vascular aging: differential effects on wave reflection and aortic pulse wave velocity: the anglo-cardiff collaborative trial (ACCT). *J. Am. Coll. Cardiol.* 46, 1753–1760. doi: 10.1016/j.jacc.2005.07.037

Meinders, J. M., and Hoeks, A. P. G. (2004). Simultaneous assessment of diameter and pressure waveforms in the carotid artery. *Ultrasound Med. Biol.* 30, 147–154. doi: 10.1016/j.ultrasmedbio.2003.10.014

Mikkonen, R. H. M., Kreula, J. M., and Virkkunen, P. J. (1996). Reproducibility of Doppler ultrasound measurements. *Acta Radiol.* 37, 545–550. doi: 10.3109/02841859609175442

Millasseau, S. C., Guigui, F. G., Kelly, R. P., Prasad, K., Cockcroft, J. R., Ritter, J. M., et al. (2000). Noninvasive assessment of the digital volume pulse: comparison with the peripheral pressure pulse. *Hypertension* 36, 952–956. doi: 10.1161/01.hyp.36.6.952

Millasseau, S. C., Patel, S. J., Redwood, S. R., Ritter, J. M., and Chowienczyk, P. J. (2003). Pressure wave reflection assessed from the peripheral pulse: is a transfer function necessary? *Hypertension* 41, 1016–1020. doi: 10.1161/01.hyp.0000057574.64076.a5

Milnor, W. R. (1990). *Cardiovascular Physiology*. Oxford: Oxford University Press.

Milnor, W. R., Bergel, D. H., and Bargainer, J. D. (1966). Hydraulic power associated with pulmonary blood flow and its relation to heart rate. *Circ. Res.* 19, 467–480. doi: 10.1161/01.res.19.3.467

Mirsky, I. (1973). Pulse velocities in cylindrical, tapered and curved anisotropic elastic arteries. *Bull. Math. Biol.* 35, 495–511. doi: 10.1016/s0092-8240(73)80049-7

Mitchell, G. F., Parise, H., Benjamin, E. J., Larson, M. G., Keyes, M. J., Vita, J. A., et al. (2004). Changes in arterial stiffness and wave reflection with advancing age in healthy men and women. *Hypertension* 43, 1239–1245. doi: 10.1161/01.HYP.0000128420.01881.aa

Mitchell, G. F., Wang, N., Palmisano, J. N., Larson, M. G., Hamburg, N. M., Vita, J. A., et al. (2010). Hemodynamic correlates of blood pressure across the adult age spectrum: noninvasive evaluation in the Framingham heart study. *Circulation* 122, 1379–1386. doi: 10.1161/CIRCULATIONAHA.109.914507

Mynard, J., Penny, D. J., and Smolich, J. J. (2008). Wave intensity amplification and attenuation in non-linear flow: implications for the calculation of local reflection coefficients. *J. Biomech.* 41, 3314–3321. doi: 10.1016/j.jbiomech.2008.10.002

Mynard, J. P. (2011). *Computer Modelling and Wave Intensity Analysis of Perinatal Cardiovascular Function and Dysfunction*. Ph.D. thesis, University of Melbourne, Parkville.

Mynard, J. P. (2013). Assessment of conceptual inconsistencies in the hybrid reservoir-wave model. *Proc. Ann. Int. Conf. IEEE Eng. Med. Biol. Soc.* 2013, 213–216. doi: 10.1109/embc.2013.6609475

Mynard, J. P., Davidson, M. R., Penny, D. J., and Smolich, J. J. (2011). "Robustness of the P-U and lnD-U loop wave speed estimation methods: effects of the diastolic pressure decay and vessel wall non-linearities," in *Proceedings of the Ann. Int. Conf. IEEE Eng. Med. Biol. Soc.*, (Piscataway, NJ: IEEE), 6446–6449.

Mynard, J. P., Kowalski, R., Cheung, M. M. H., and Smolich, J. J. (2017). Beyond the aorta: partial transmission of reflected waves from aortic coarctation into supra-aortic branches modulates cerebral hemodynamics and left ventricular load. *Biomech. Model. Mechanobiol.* 16, 635–650. doi: 10.1007/s10237-016-0842-x

Mynard, J. P., Penny, D. J., Davidson, M. R., and Smolich, J. J. (2012). The reservoir-wave paradigm introduces error into arterial wave analysis: a computer modelling and in-vivo study. *J. Hypertens.* 30, 734–743. doi: 10.1097/HJH.0b013e32834f9793

Mynard, J. P., Penny, D. J., and Smolich, J. J. (2018). Major influence of a 'smoke and mirrors' effect caused by wave reflection on early diastolic coronary arterial wave intensity. *J. Physiol.* 596, 993–1017. doi: 10.1113/JP274710

Mynard, J. P., and Smolich, J. J. (2014a). The case against the reservoir-wave approach. *Int. J. Cardiol.* 176, 1009–1012. doi: 10.1016/j.ijcard.2014.07.070

Mynard, J. P., and Smolich, J. J. (2014b). Wave potential and the one-dimensional windkessel as a wave-based paradigm of diastolic arterial hemodynamics. *Am. J. Physiol. Heart Circ. Physiol.* 307, H307–H318. doi: 10.1152/ajpheart.00293.2014

Mynard, J. P., and Smolich, J. J. (2015). One-dimensional haemodynamic modeling and wave dynamics in the entire adult circulation. *Ann. Biomed. Eng.* 43, 1443–1460. doi: 10.1007/s10439-015-1313-8

Mynard, J. P., and Smolich, J. J. (2016). Novel wave power analysis linking pressure-flow waves, wave potential and the forward and backward components of hydraulic power. *Am. J. Physiol. Heart Circ. Physiol.* 310, H1026–H1038. doi: 10.1152/ajpheart.00954.2015

Mynard, J. P., and Smolich, J. J. (2017). Wave potential: a unified model of arterial waves, reservoir phenomena and their interaction. *Artery Res.* 18, 55–63. doi: 10.1016/j.artres.2017.04.002

Mynard, J. P., Smolich, J. J., and Avolio, A. (2015). The ebbing tide of the reservoir-wave model. *J. Hypertens.* 33, 461–464. doi: 10.1097/hjh.0000000000000528

Mynard, J. P., and Steinman, D. A. (2013). Effect of velocity profile skewing on blood velocity and volume flow waveforms derived from maximum Doppler spectral velocity. *Ultrasound Med. Biol.* 39, 870–881. doi: 10.1016/j.ultrasmedbio.2012.11.006

Nakayama, M., Itoh, H., Oikawa, K., Tajima, A., Koike, A., Aizawa, T., et al. (2005). Preload-adjusted 2 wave-intensity peaks reflect simultaneous assessment of left ventricular contractility and relaxation. *Circ. J.* 69, 683–687. doi: 10.1253/circj.69.683

Namasivayam, M., Adji, A., and O'Rourke, M. F. (2010). Aortic augmentation index and aging: mathematical resolution of a physiological dilemma? *Hypertension* 56, e9–e10. doi: 10.1161/hypertensionaha.110.153742

Narayan, O., Davies, J. E., Hughes, A. D., Dart, A. M., Parker, K. H., Reid, C., et al. (2015). Central aortic reservoir-wave analysis improves prediction of cardiovascular events in elderly hypertensives. *Hypertension* 65, 629–635. doi: 10.1161/hypertensionaha.114.04824

Nichols, W. W., and O'Rourke, M. F. (2009). Aortic pulse wave velocity, reflection site distance, and augmentation index. *Hypertension* 53:e9.

Nichols, W. W., and O'Rourke, M. F. (2011). *McDonald's Blood Flow in Arteries: Theoretical, Experimental, and Clinical Principles*. Boca Raton, FL: CRC Press.

Niki, K., Sugawara, M., Chang, D., Harada, A., Okada, T., Sakai, R., et al. (2002). A new noninvasive measurement system for wave intensity: evaluation of carotid arterial wave intensity and reproducibility. *Heart Vessels* 17, 12–21. doi: 10.1007/s003800200037

Niki, K., Sugawara, M., Chang, D., Harada, A., Okada, T., and Tanaka, R. (2005). Effects of sublingual nitroglycerin on working conditions of the heart and arterial system: analysis using wave intensity. *J. Med. Ultrason.* 32, 145–152. doi: 10.1007/s10396-005-0057-8

Niki, K., Sugawara, M., Kayanuma, H., Takamisawa, I., Watanabe, H., Mahara, K., et al. (2017). Associations of increased arterial stiffness with left ventricular ejection performance and right ventricular systolic pressure in mitral regurgitation before and after surgery: wave intensity analysis. *IJC Heart Vasc.* 16, 7–13. doi: 10.1016/j.ijcha.2017.06.002

Niki, K., Sugawara, M., Uchida, K., Tanaka, R., Tanimoto, K., Imamura, H., et al. (1999). A noninvasive method of measuring wave intensity, a new hemodynamic index: application to the carotid artery in patients with mitral regurgitation before and after surgery. *Heart Vessels* 14, 263–271. doi: 10.1007/bf03257237

Nogami, Y., Seo, Y., Yamamoto, M., Ishizu, T., and Aonuma, K. (2018). Wave intensity as a useful modality for assessing ventilation–perfusion imbalance in subclinical patients with hypertension. *Heart Vessels* 33, 931–938. doi: 10.1007/s00380-018-1138-0

Notomi, Y., Martin-Miklovic, M. G., Oryszak, S. J., Shiota, T., Deserranno, D., Popovic, Z. B., et al. (2006a). Enhanced ventricular untwisting during exercise. *Circulation* 113, 2524–2533. doi: 10.1161/CIRCULATIONAHA.105.596502

Notomi, Y., Srinath, G., Shiota, T., Martin-Miklovic, M. G., Beachler, L., Howell, K., et al. (2006b). Maturational and adaptive modulation of left ventricular torsional biomechanics. *Circulation* 113, 2534–2541. doi: 10.1161/circulationaha.105.537639

Nürnberger, J., Keflioglu-Scheiber, A., Saez, A. M. O., Wenzel, R. R., Philipp, T., and Schäfers, R. F. (2002). Augmentation index is associated with cardiovascular risk. *J. Hypertens.* 20, 2407–2414. doi: 10.1097/00004872-200212000-00020

Ohte, N., Narita, H., Sugawara, M., Niki, K., Okada, T., Harada, A., et al. (2003). Clinical usefulness of carotid arterial wave intensity in assessing left ventricular systolic and early diastolic performance. *Heart Vessels* 18, 107–111. doi: 10.1007/s00380-003-0700-5

O'Rourke, M. F., and Mancia, G. (1999). Arterial stiffness. *J. Hypertens.* 17, 1–4.

O'Rourke, M. F., and Nichols, W. W. (2005). Aortic diameter, aortic stiffness, and wave reflection increase with age and isolated systolic hypertension. *Hypertension* 45, 652–658. doi: 10.1161/01.hyp.0000153793.84859.b8

O'Rourke, M. F., and Taylor, M. G. (1966). Vascular impedance of the femoral bed. *Circ. Res.* 18, 126–139. doi: 10.1161/01.res.18.2.126

O'Rourke, M. F., and Taylor, M. G. (1967). Input impedance of the systemic circulation. *Circ. Res.* 20, 365–380. doi: 10.1161/01.res.20.4.365

Pagani, M., Mirsky, I., Baig, H., Manders, W. T., Kerkhof, P., and Vatner, S. F. (1979). Effects of age on aortic pressure-diameter and elastic stiffness-stress relationships in unanesthetized sheep. *Circ. Res.* 44, 420–429. doi: 10.1161/01.res.44.3.420

Palombo, C., Kozakova, M., Guraschi, N., Bini, G., Cesana, F., Castoldi, G., et al. (2012). Radiofrequency-based carotid wall tracking: a comparison between two different systems. *J. Hypertens.* 30, 1614–1619. doi: 10.1097/hjh.0b013e328354dd44

Papaioannou, T. G., Protogerou, A. D., Stamatelopoulos, K. S., Vavuranakis, M., and Stefanadis, C. (2009). Non-invasive methods and techniques for central blood pressure estimation: procedures, validation, reproducibility and limitations. *Curr. Pharm. Des.* 15, 245–253. doi: 10.2174/138161209787354203

Parikh, J. D., Hollingsworth, K. G., Kunadian, V., Blamire, A., and MacGowan, G. A. (2016). Measurement of pulse wave velocity in normal ageing: comparison of vicorder and magnetic resonance phase contrast imaging. *BMC Cardiovasc. Disord.* 16:50. doi: 10.1186/s12872-016-0224-4

Park, C. M., Korolkova, O., Davies, J. E., Parker, K. H., Siggers, J. H., March, K., et al. (2014). Arterial pressure: agreement between a brachial cuff-based device and radial tonometry. *J. Hypertens.* 32:865. doi: 10.1097/hjh.0000000000000082

Parker, K., Alastruey, J., and Stan, G.-B. (2012). Arterial reservoir-excess pressure and ventricular work. *Med. Biol. Eng. Comput.* 50, 419–424. doi: 10.1007/s11517-012-0872-1

Parker, K. H. (2009). An introduction to wave intensity analysis. *Med. Biol. Eng. Comput.* 47, 175–188. doi: 10.1007/s11517-009-0439-y

Parker, K. H. (2017). The reservoir-wave model. *Artery Res.* 18, 87–101. doi: 10.1016/j.artres.2017.04.003

Parker, K. H., and Jones, C. J. (1990). Forward and backward running waves in the arteries: analysis using the method of characteristics. *J. Biomech. Eng.* 112, 322–326. doi: 10.1115/1.2891191

Parker, K. H., Jones, C. J., Dawson, J. R., and Gibson, D. G. (1988). What stops the flow of blood from the heart? *Heart Vessels* 4, 241–245. doi: 10.1007/bf02058593

Parragh, S., Hametner, B., Bachler, M., Weber, T., Eber, B., and Wassertheurer, S. (2015). Non-invasive wave reflection quantification in patients with reduced ejection fraction. *Physiol. Meas.* 36, 179–190. doi: 10.1088/0967-3334/36/2/179

Pelc, N. J., Herfkens, R. J., Shimakawa, A., and Enzmann, D. R. (1991). Phase contrast cine magnetic resonance imaging. *Magn. Reson. Q.* 7, 229–254.

Peñáz, J. (1973). "Photoelectric measurement of blood pressure, volume and flow in the finger," in *Proceedings of the Digest of the 10th International Conference on Medical and Biological Engineering*, Dresden.

Peng, X., Schultz, M. G., Picone, D. S., Black, J. A., Dwyer, N., Roberts-Thomson, P., et al. (2017). Arterial reservoir characteristics and central-to-peripheral blood pressure amplification in the human upper limb. *J. Hypertens.* 35, 1825–1831. doi: 10.1097/hjh.0000000000001400

Penny, D. J., Mynard, J. P., and Smolich, J. J. (2008). Aortic wave intensity analysis of ventricular-vascular interaction during incremental dobutamine infusion in adult sheep. *Am. J. Physiol. Heart Circ. Physiol.* 294, H481–H489. doi: 10.1152/ajpheart.00962.2006

Peper, E. S., Strijkers, G. J., Gazzola, K., Potters, W. V., Motaal, A. G., Luirink, I. K., et al. (2018). Regional assessment of carotid artery pulse wave velocity using compressed sensing accelerated high temporal resolution 2d cine phase contrast cardiovascular magnetic resonance. *J. Cardiovasc. Magn. Reson.* 20:86.

Phan, T. S., Li, J. K. J., Segers, P., and Chirinos, J. A. (2016a). Misinterpretation of the determinants of elevated forward wave amplitude inflates the role of the proximal aorta. *J. Am. Heart Assoc.* 5:e003069. doi: 10.1161/jaha.115.003069

Phan, T. S., Li, J. K. J., Segers, P., Reddy-Koppula, M., Akers, S. R., Kuna, S. T., et al. (2016b). Aging is associated with an earlier arrival of reflected waves without a distal shift in reflection sites. *J. Am. Heart Assoc.* 5:e003733. doi: 10.1161/jaha.116.003733

Picker, O., Schindler, A., and Scheeren, T. W. L. (2000). Accuracy and reproducibility of long-term implanted transit-time ultrasound flow probes in dogs. *Intensive Care Med.* 26, 601–607. doi: 10.1007/s001340051210

Picone, D. S., Schultz, M. G., Otahal, P., Aakhus, S., Al-Jumaily, A. M., Black, J. A., et al. (2017). Accuracy of cuff-measured blood pressure: systematic reviews and meta-analyses. *J. Am. Coll. Cardiol.* 70, 572–586. doi: 10.1016/j.jacc.2017.05.064

Pisa, S., Chicarella, S., Pittella, E., Piuzzi, E., Testa, O., and Cicchetti, R. (2018). A double-sideband continuous-wave radar sensor for carotid wall movement detection. *IEEE Sens. J.* 18, 8162–8171. doi: 10.1109/jsen.2018.2862430

Pollack, G. H., Reddy, R. V., and Noordergraaf, A. (1968). Input impedance, wave travel, and reflections in the human pulmonary arterial tree: studies using an electrical analog. *IEEE Trans. Biomed. Eng.* 15, 151–164. doi: 10.1109/tbme.1968.4502559

Pomella, N., Wilhelm, E. N., Kolyva, C., González-Alonso, J., Rakobowchuk, M., and Khir, A. W. (2018). Noninvasive assessment of the common carotid artery hemodynamics with increasing exercise work rate using wave intensity analysis. *Am. J. Physiol. Heart Circ. Physiol.* 315, H233–H241. doi: 10.1152/ajpheart.00667.2017

Quail, M. A., Knight, D. S., Steeden, J. A., Taelman, L., Moledina, S., Taylor, A. M., et al. (2015). Noninvasive pulmonary artery wave intensity analysis in pulmonary hypertension. *Am. J. Physiol. Heart Circ. Physiol.* 308, H1603–H1611. doi: 10.1152/ajpheart.00480.2014

Quail, M. A., Steeden, J. A., Knight, D., Segers, P., Taylor, A. M., and Muthurangu, V. (2014). Development and validation of a novel method to derive central aortic systolic pressure from the MR aortic distension curve. *J. Magn. Reson. Imaging* 40, 1064–1070. doi: 10.1002/jmri.24471

Rabben, S. I., Stergiopulos, N., Hellevik, L. R., Smiseth, O. A., Slørdahl, S., Urheim, S., et al. (2004). An ultrasound-based method for determining pulse wave velocity in superficial arteries. *J. Biomech.* 37, 1615–1622. doi: 10.1016/j.jbiomech.2003.12.031

Ramsey, M. W., and Sugawara, M. (1997). Arterial wave intensity and ventriculoarterial interaction. *Heart Vessels Suppl.* 12, 128–134.

Raphael, C. E., Cooper, R., Parker, K. H., Collinson, J., Vassiliou, V., Pennell, D. J., et al. (2016). Mechanisms of myocardial ischemia in hypertrophic cardiomyopathy: insights from wave intensity analysis and magnetic resonance. *J. Am. Coll. Cardiol.* 68, 1651–1660. doi: 10.1016/j.jacc.2016.07.751

Redheuil, A., Yu, W.-C., Mousseaux, E., Harouni, A. A., Kachenoura, N., Wu, C. O., et al. (2011). Age-related changes in aortic arch geometryrelationship with proximal aortic function and left ventricular mass and remodeling. *J. Am. Coll. Cardiol.* 58, 1262–1270. doi: 10.1016/j.jacc.2011.06.012

Redheuil, A., Yu, W.-C., Wu, C. O., Mousseaux, E., de Cesare, A., Yan, R., et al. (2010). Reduced ascending aortic strain and distensibility: earliest manifestations of vascular aging in humans. *Hypertension* 55, 319–326. doi: 10.1161/hypertensionaha.109.141275

Reuderink, P. J., Hoogstraten, H. W., Sipkema, P., Hillen, B., and Westerhof, N. (1989). Linear and nonlinear one-dimensional models of pulse wave transmission at high womersley numbers. *J. Biomech.* 22, 819–827. doi: 10.1016/0021-9290(89)90065-1

Rivolo, S., Patterson, T., Asrress, K., Marber, M., Redwood, S., Smith, N., et al. (2016). Accurate and standardised coronary wave intensity analysis. *IEEE Trans. Biomed. Eng.* 64:99. doi: 10.1109/TBME.2016.2593518

Rolandi, M. C., Nolte, F., van de Hoef, T. P., Remmelink, M., Baan, J., Piek, J. J., et al. (2012). Coronary wave intensity during the valsalva manoeuvre in humans reflects altered intramural vessel compression responsible for extravascular resistance. *J. Physiol.* 590, 4623–4635. doi: 10.1113/jphysiol.2012.229914

Rolandi, M. C., Silva, K., Lumley, M., Lockie, T. E., Clapp, B., Spaan, J. E., et al. (2014). Wave speed in human coronary arteries is not influenced by microvascular vasodilation: implications for wave intensity analysis. *Basic Res. Cardiol.* 109, 1–11. doi: 10.1007/s00395-014-0405-1

Salotto, A. G., Muscarella, L. F., Melbin, J., Li, J. K. J., and Noordergraaf, A. (1986). Pressure pulse transmission into vascular beds. *Microvasc. Res.* 32, 152–163. doi: 10.1016/0026-2862(86)90051-8

Sazonov, I., Khir, A. W., Hacham, W. S., Boileau, E., Carson, J. M., van Loon, R., et al. (2017). A novel method for non-invasively detecting the severity and location of aortic aneurysms. *Biomech. Model. Mechanobiol.* 16, 1225–1242. doi: 10.1007/s10237-017-0884-8

Segers, P., Mahieu, D., Kips, J., Rietzschel, E., De Buyzere, M., De Bacquer, D., et al. (2009). Amplification of the pressure pulse in the upper limb in healthy, middle-aged men and women. *Hypertension* 54, 414–420. doi: 10.1161/hypertensionaha.109.133009

Segers, P., O'Rourke, M. F., Parker, K., Westerhof, N., Hughes, A., Aguado-Sierra, J., et al. (2017). Towards a consensus on the understanding and analysis of the pulse waveform: results from the 2016 workshop on arterial hemodynamics: past, present and future. *Artery Res.* 18, 75–80. doi: 10.1016/j.artres.2017.03.004

Segers, P., Rabben, S. I., De Backer, J., De Sutter, J., Gillebert, T. C., Van Bortel, L., et al. (2004). Functional analysis of the common carotid artery: relative distension differences over the vessel wall measured in vivo. *J. Hypertens.* 22, 973–981. doi: 10.1097/00004872-200405000-00020

Segers, P., Rietzschel, E. R., De Buyzere, M. L., De Bacquer, D., Van Bortel, L. M., De Backer, G., et al. (2007). Assessment of pressure wave reflection: getting the timing right! *Physiol Meas* 28, 1045–1056. doi: 10.1088/0967-3334/28/9/006

Segers, P., Rietzschel Ernst, R., and Chirinos Julio, A. (2020). How to measure arterial stiffness in humans. *Arterioscler. Thromb. Vasc. Biol.* 40, 1034–1043. doi: 10.1161/ATVBAHA.119.313132

Segers, P., Swillens, A., Taelman, L., and Vierendeels, J. (2014). Wave reflection leads to over- and underestimation of local wave speed by the PU- and QA-loop methods: theoretical basis and solution to the problem. *Physiol. Meas.* 35, 847–861. doi: 10.1088/0967-3334/35/5/847

Segers, P., Taelman, L., Degroote, J., Bols, J., and Vierendeels, J. (2015). The aortic reservoir-wave as a paradigm for arterial haemodynamics: insights from three-dimensional fluid-structure interaction simulations in a model of aortic coarctation. *J. Hypertens.* 33, 554–563. doi: 10.1097/hjh.0000000000000449

Segers, P., and Verdonck, P. (2000). Role of tapering in aortic wave reflection: hydraulic and mathematical model study. *J. Biomech.* 33, 299–306. doi: 10.1016/s0021-9290(99)00180-3

Segers, P., Verdonck, P., and Verhoeven, R. (1995). "Effect of visco-elastic damping and capillary bed model on the peripheral pressure wave," in *Proceedings of the Computers in Cardiology*, (Piscataway, NJ: IEEE).

Siebes, M., Kolyva, C., Verhoeff, B.-J., Piek, J., and Spaan, J. (2009). Potential and limitations of wave intensity analysis in coronary arteries. *Med. Biol. Eng. Comput.* 47, 233–239. doi: 10.1007/s11517-009-0448-x

Sigovan, M., Hope, M. D., Dyverfeldt, P., and Saloner, D. (2011). Comparison of four-dimensional flow parameters for quantification of flow eccentricity in the ascending aorta. *J. Magn. Reson. Imaging* 34, 1226–1230. doi: 10.1002/jmri.22800

Sluyter, J. D., Camargo, C. A. Jr., Stewart, A. W., Waayer, D., Lawes, C. M. M., Toop, L., et al. (2017). Effect of monthly, high-dose, long-term vitamin d supplementation on central blood pressure parameters: a randomized controlled trial substudy. *J. Am. Heart Assoc.* 6:e006802.

Smiseth, O. A., Thompson, C. R., Lohavanichbutr, K., Ling, H., Abel, J. G., Miyagishima, R. T., et al. (1999). The pulmonary venous systolic flow pulse–its origin and relationship to left atrial pressure. *J. Am. Coll. Cardiol.* 34, 802–809. doi: 10.1016/s0735-1097(99)00300-9

Smolich, J. J., and Mynard, J. P. (2016). A step towards clinically applicable non-invasive coronary wave intensity analysis. *Am. J. Physiol. Heart Circ. Physiol.* 310, H525–H527. doi: 10.1152/ajpheart.00014.2016

Smolich, J. J., Mynard, J. P., and Penny, D. J. (2008). Simultaneous pulmonary trunk and pulmonary arterial wave intensity analysis in fetal lambs: evidence for cyclical, midsystolic pulmonary vasoconstriction. *Am. J. Physiol. Regul. Integr. Comp. Physiol.* 294, R1554–R1562. doi: 10.1152/ajpregu.00743.2007

Smolich, J. J., Mynard, J. P., and Penny, D. J. (2009). Ductus arteriosus wave intensity analysis in fetal lambs: midsystolic ductal flow augmentation is due to antegrade pulmonary arterial wave transmission. *Am. J. Physiol. Regul. Integr. Comp. Physiol.* 297, R1171–R1179. doi: 10.1152/ajpregu.00384.2009

Steeden, J. A., Atkinson, D., Hansen, M. S., Taylor, A. M., and Muthurangu, V. (2011). Rapid flow assessment of congenital heart disease with high-spatiotemporal-resolution gated spiral phase-contrast MR imaging. *Radiology* 260, 79–87. doi: 10.1148/radiol.11101844

Steinbuch, J., Hoeks, A. P. G., Hermeling, E., Truijman, M. T. B., Schreuder, F. H. B. M., and Mess, W. H. (2016). Standard b-mode ultrasound measures local carotid artery characteristics as reliably as radiofrequency phase tracking in symptomatic carotid artery patients. *Ultrasound Med. Biol.* 42, 586–595. doi: 10.1016/j.ultrasmedbio.2015.07.030

Stergiopulos, N., Spiridon, M., Pythoud, F., and Meister, J. J. (1996). On the wave transmission and reflection properties of stenoses. *J. Biomech.* 29, 31–38. doi: 10.1016/0021-9290(95)00023-2

Stok, W. J., Westerhof, B. E., Guelen, I., and Karemaker, J. M. (2011). Aortic pressure wave reconstruction during exercise is improved by adaptive filtering: a pilot study. *Med. Biol. Eng. Comput.* 49, 909–916. doi: 10.1007/s11517-011-0795-2

Stoner, L., Lambrick, D. M., Westrupp, N., Young, J., and Faulkner, J. (2014). Validation of oscillometric pulse wave analysis measurements in children. *Am. J. Hypertens.* 27, 865–872. doi: 10.1093/ajh/hpt243

Su, J., Hilberg, O., Howard, L., Simonsen, U., and Hughes, A. D. (2016). A review of wave mechanics in the pulmonary artery with an emphasis on wave intensity analysis. *Acta Physiol.* 218, 239–249. doi: 10.1111/apha.12803

Su, J., Manisty, C., Parker, K. H., Simonsen, U., Nielsen-Kudsk, J. E., Mellemkjaer, S., et al. (2017). Wave intensity analysis provides novel insights into pulmonary arterial hypertension and chronic thromboembolic pulmonary hypertension. *J. Am. Heart Assoc.* 6:e006679.

Sugawara, J., Hayashi, K., and Tanaka, H. (2010). Distal shift of arterial pressure wave reflection sites with aging. *Hypertension* 56, 920–925. doi: 10.1161/hypertensionaha.110.160549

Sugawara, M., Niki, K., Furuhata, H., Ohnishi, S., and Suzuki, S. (2000). Relationship between the pressure and diameter of the carotid artery in humans. *Heart Vessels* 15, 49–51. doi: 10.1007/pl00007261

Sugawara, M., Uchida, K., Kondoh, Y., Magosaki, N., Niki, K., Jones, C. J., et al. (1997). Aortic blood momentum–the more the better for the ejecting heart in vivo? *Cardiovasc. Res.* 33, 433–446. doi: 10.1016/s0008-6363(96)00241-6

Sun, Y., Belenkie, I., Wang, J. Jr., and Tyberg, J. V. (2006). Assessment of right ventricular diastolic suction in dogs with the use of wave intensity analysis. *Am. J. Physiol. Heart Circ. Physiol.* 291, H3114–H3121.

Swalen, M. J. P., and Khir, A. W. (2009). Resolving the time lag between pressure and flow for the determination of local wave speed in elastic tubes and arteries. *J. Biomech.* 42, 1574–1577. doi: 10.1016/j.jbiomech.2009.03.038

Swillens, A., Lanoye, L., De Backer, J., Stergiopulos, N., Verdonck, P. R., Vermassen, F., et al. (2008). Effect of an abdominal aortic aneurysm on wave reflection in the aorta. *IEEE Trans. Biomed. Eng.* 55, 1602–1611.

Swillens, A., Taelman, L., Degroote, J., Vierendeels, J., and Segers, P. (2013). Comparison of non-invasive methods for measurement of local pulse wave velocity using FSI-simulations and in vivo data. *Ann. Biomed. Eng.* 41, 1567–1578. doi: 10.1007/s10439-012-0688-z

Taelman, L., Bols, J., Degroote, J., Muthurangu, V., Panzer, J., Vierendeels, J., et al. (2015). Differential impact of local stiffening and narrowing on hemodynamics in repaired aortic coarctation: an FSI study. *Med. Biol. Eng. Comput.* 54, 497–510. doi: 10.1007/s11517-015-1336-1

Tanaka, M., Sugawara, M., Ogasawara, Y., Suminoe, I., Izumi, T., Niki, K., et al. (2014). Noninvasive evaluation of left ventricular force-frequency relationships by measuring carotid arterial wave intensity during exercise stress. *J. Med. Ultrason.* 42, 65–70. doi: 10.1007/s10396-014-0554-8

Thuijs, D. J. F. M., Bekker, M. W. A., Taggart, D. P., Kappetein, A. P., Kieser, T. M., Wendt, D., et al. (2019). Improving coronary artery bypass grafting: a systematic review and meta-analysis on the impact of adopting transit-time flow measurement. *Eur. J. Cardiothorac. Surg.* 56, 654–663. doi: 10.1093/ejcts/ezz075

Townsend, R. R., Wilkinson, I. B., Schiffrin, E. L., Avolio, A. P., Chirinos, J. A., Cockcroft, J. R., et al. (2015). Recommendations for improving and standardizing vascular research on arterial stiffness. *Hypertension* 66, 698–722. doi: 10.1161/hyp.0000000000000033

Tyberg, J., Davies, J., Wang, Z., Whitelaw, W., Flewitt, J., Shrive, N., et al. (2009). Wave intensity analysis and the development of the reservoir–wave approach. *Med. Biol. Eng. Comput.* 47, 221–232. doi: 10.1007/s11517-008-0430-z

van de Velde, L., Schattenkerk, D. W. E., Venema, P. A. H. T., Best, H. J., van den Bogaard, B., Stok, W. J., et al. (2017). Myocardial preload alters central pressure augmentation through changes in the forward wave. *J. Hypertens.* 36, 544–551. doi: 10.1097/hjh.0000000000001583

van den Bos, G. C., Westerhof, N., and Randall, O. S. (1982). Pulse wave reflection: can it explain the differences between systemic and pulmonary pressure and flow waves? A study in dogs. *Circ. Res.* 51, 479–485. doi: 10.1161/01.res.51.4.479

Verbeke, F., Segers, P., Heireman, S., Vanholder, R., Verdonck, P., and Van Bortel, L. M. (2005). Noninvasive assessment of local pulse pressure: importance of brachial-to-radial pressure amplification. *Hypertension* 46, 244–248. doi: 10.1161/01.hyp.0000166723.07809.7e

Vermeersch, S., Rietzschel, E., De Buyzere, M., Van Bortel, L., Gillebert, T., Verdonck, P., et al. (2009). The reservoir pressure concept: the 3-element windkessel model revisited? Application to the Asklepios population study. *J. Eng. Math.* 64, 417–428. doi: 10.1007/s10665-009-9286-y

Vermeersch, S. J., Rietzschel, E. R., De Buyzere, M. L., De Bacquer, D., De Backer, G., Van Bortel, L. M., et al. (2008). Determining carotid artery pressure from scaled diameter waveforms: comparison and validation of calibration techniques in 2026 subjects. *Physiol. Meas.* 29, 1267–1280. doi: 10.1088/0967-3334/29/11/003

Vlachopoulos, C., Aznaouridis, K., O'Rourke, M. F., Safar, M. E., Baou, K., and Stefanadis, C. (2010). Prediction of cardiovascular events and all-cause mortality with central haemodynamics: a systematic review and meta-analysis. *Eur. Heart J.* 31, 1865–1871. doi: 10.1093/eurheartj/ehq024

Wang, C., Li, X., Hu, H., Zhang, L., Huang, Z., Lin, M., et al. (2018). Monitoring of the central blood pressure waveform via a conformal ultrasonic device. *Nat. Biomed. Eng.* 2, 687–695. doi: 10.1038/s41551-018-0287-x

Wang, J. J., O'Brien, A. B., Shrive, N. G., Parker, K. H., and Tyberg, J. V. (2003). Time-domain representation of ventricular-arterial coupling as a windkessel and wave system. *Am. J. Physiol. Heart Circ. Physiol.* 284, H1358–H1368. doi: 10.1152/ajpheart.00175.2002

Wang, K.-L., Cheng, H.-M., Sung, S.-H., Chuang, S.-Y., Li, C.-H., Spurgeon, H. A., et al. (2010). Wave reflection and arterial stiffness in the prediction of 15-year all-cause and cardiovascular mortalities a community-based study. *Hypertension* 55, 799–805. doi: 10.1161/hypertensionaha.109.139964

Wang, X.-F., Nishi, S., Matsukawa, M., Ghigo, A., Lagrée, P.-Y., and Fullana, J.-M. (2016). Fluid friction and wall viscosity of the 1D blood flow model. *J. Biomech.* 49, 565–571. doi: 10.1016/j.jbiomech.2016.01.010

Wassertheurer, S., Kropf, J., Weber, T., Van der Giet, M., Baulmann, J., Ammer, M., et al. (2010). A new oscillometric method for pulse wave analysis: comparison with a common tonometric method. *J. Hum. Hypertens.* 24, 498–504. doi: 10.1038/jhh.2010.27

Watanabe, H., Kawai, M., Sibata, T., Hara, M., Furuhata, H., and Mochizuki, S. (1999). Noninvasive measurement of aortic pressure waveform by ultrasound. *Heart Vessels* 13, 79–86. doi: 10.1007/bf01744590

Weber, T., Auer, J., O'Rourke, M. F., Kvas, E., Lassnig, E., Berent, R., et al. (2004). Arterial stiffness, wave reflections, and the risk of coronary artery disease. *Circulation* 109, 184–189. doi: 10.1161/01.cir.0000105767.94169.e3

Weber, T., O'Rourke, M. F., Lassnig, E., Porodko, M., Ammer, M., Rammer, M., et al. (2010). Pulse waveform characteristics predict cardiovascular events and mortality in patients undergoing coronary angiography. *J. Hypertens.* 28, 797–805. doi: 10.1097/hjh.0b013e328336c8e9

Weber, T., Wassertheurer, S., Rammer, M., Haiden, A., Hametner, B., and Eber, B. (2012). Wave reflections, assessed with a novel method for pulse wave separation, are associated with end-organ damage and clinical outcomes / novelty and significance. *Hypertension* 60, 534–541. doi: 10.1161/hypertensionaha.112.194571

Wesseling, K. H. (1995). Physiocal, calibrating finger vascular physiology for Finapres. *Homeostasis* 36, 67–82.

Westerhof, B. E., Guelen, I., Westerhof, N., Karemaker, J. M., and Avolio, A. (2006). Quantification of wave reflection in the human aorta from pressure alone: a

proof of principle. *Hypertension* 48, 595–601. doi: 10.1161/01.hyp.0000238330.08894.17

Westerhof, B. E., and Westerhof, N. (2012). Magnitude and return time of the reflected wave: the effects of large artery stiffness and aortic geometry. *J. Hypertens.* 30, 932–939. doi: 10.1097/hjh.0b013e3283524932

Westerhof, N., and Noordergraaf, A. (1970). Arterial viscoelasticity: a generalized model : effect on input impedance and wave travel in the systematic tree. *J. Biomech.* 3, 357–370.

Westerhof, N., Sipkema, P., van den Bos, G. C., and Elzinga, G. (1972). Forward and backward waves in the arterial system. *Cardiovasc. Res.* 6, 648–656. doi: 10.1093/cvr/6.6.648

Westerhof, N., Stergiopulos, N., Noble, M. I. M., and Stergiopulos, N. (eds) (2010). "Wave travel and reflection," in *Snapshots of hemodynamics*, (Cham: Springer), 147–153. doi: 10.1007/978-1-4419-6363-5_21

Westerhof, N., and Westerhof, B. E. (2015). The reservoir wave paradigm discussion. *J. Hypertens.* 33, 458–460. doi: 10.1097/hjh.0000000000000499

Westerhof, N., and Westerhof, B. E. (2017). Waves and windkessels reviewed. *Artery Res.* doi: 10.1016/j.artres.2017.03.001

Wilkinson, I. B., MacCallum, H., Flint, L., Cockcroft, J. R., Newby, D. E., and Webb, D. J. (2000). The influence of heart rate on augmentation index and central arterial pressure in humans. *J. Physiol.* 525, 263–270. doi: 10.1111/j.1469-7793.2000.t01-1-00263.x

Winkler, A. J., Wu, J., Case, T., and Ricci, M. A. (1995). An experimental study of the accuracy of volume flow measurements using commercial ultrasound systems. *J. Vasc. Tech.* 19, 175–180.

World Health Organization (2013). *Global Action Plan for The Prevention and Control of Noncommunicable Diseases 2013–2020*. Geneva: WHO.

Zamani, P., Jacobs, D. R., Segers, P., Duprez, D. A., Brumback, L., Kronmal, R. A., et al. (2014). Reflection magnitude as a predictor of mortality: the Multi-Ethnic Study of Atherosclerosis. *Hypertension* 64, 958–964. doi: 10.1161/hypertensionaha.114.03855

Zamani, P., Lilly, S. M., Segers, P., Jacobs, D. R., Bluemke, D. A., Duprez, D. A., et al. (2016). Pulsatile load components, resistive load and incident heart failure: the Multi-Ethnic Study of Atherosclerosis (mesa). *J. Card. Fail.* 22, 988–995. doi: 10.1016/j.cardfail.2016.04.011

Zambanini, A., Cunningham, S. L., Parker, K. H., Khir, A. W., Mc, G. T. S. A., and Hughes, A. D. (2005). Wave-energy patterns in carotid, brachial, and radial arteries: a noninvasive approach using wave-intensity analysis. *Am. J. Physiol. Heart Circ. Physiol.* 289, H270–H276.

Zhang, H., Guo, C., and Lin, J. (2019). Effects of velocity profiles on measuring accuracy of transit-time ultrasonic flowmeter. *Appl. Sci.* 9:1648. doi: 10.3390/app9081648

Zhang, H., Zheng, R., Qian, X., Zhang, C., Hao, B., Huang, Z., et al. (2014). Use of wave intensity analysis of carotid arteries in identifying and monitoring left ventricular systolic function dynamics in rabbits. *Ultrasound Med. Biol.* 40, 611–621. doi: 10.1016/j.ultrasmedbio.2013.10.008

Zwanenburg, J. J. M., Gotte, M. J. W., Kuijer, J. P. A., Heethaar, R. M., Van Rossum, A. C., and Marcus, J. T. (2004). Timing of cardiac contraction in humans mapped by high-temporal-resolution MRI tagging: early onset and late peak of shortening in lateral wall. *Am. J. Physiol. Heart Circ. Physiol.* 286, H1872–H1880.

Conflict of Interest: The authors declare that the research was conducted in the absence of any commercial or financial relationships that could be construed as a potential conflict of interest.

frontiers in Physiology

ORIGINAL RESEARCH
published: 08 October 2020
doi: 10.3389/fphys.2020.579852

Would Oscillometry be Able to Solve the Dilemma of Blood Pressure Independent Pulse Wave Velocity – A Novel Approach Based on Long-Term Pulse Wave Analysis?

Alexander Reshetnik, Markus Tölle, Kai-Uwe Eckardt and Markus van der Giet*

Department of Nephrology and Intensive Care Medicine, Campus Benjamin Franklin, Charité – Universitätsmedizin Berlin, Corporate Member of Freie Universität Berlin, Humboldt-Universität zu Berlin, and Berlin Institute of Health, Berlin, Germany

The utility of pulse wave velocity (PWV) as a surrogate parameter of arterial vessel damage (AVD) beyond the traditional brachial blood pressure (BP) measurement may be questioned as changes in BP are often accompanied by the corresponding changes in PWV. We sought to establish a new way for BP-independent estimation of AVD with PWV. We retrospectively analyzed data from 507 subjects with at least one available 24 h ambulatory BP- and pulse wave analysis, performed with Mobil-O-Graph (I.E.M., Stolberg, Germany). Individual relationship between eaPWV and central systolic BP (cSBP) was analyzed for every 24 h recording. The analysis revealed linear relation between eaPWV and cSBP in all subjects, which is described by equation eaPWV = a*cSBP + b. We termed "a" as PWVslope and "b" as PWVbaseline. All available demographic parameters and clinical data were correlated with eaPWV, PWVslope and PWVbaseline. 108 subjects had repeated 24 h recordings. Mean age was 60.7 years and 48.7% were female. 92.5% had hypertension, 22.9% were smoker, 20.5% had diabetes mellitus and 29.6% eGFR < 60 ml/min/1,73 m^2. Direct correlation was observed between age, SBP and eaPWV, while diastolic BP (DBP) and eGFR correlated inversely with eaPWV. PWVbaseline correlated directly with age and inversely with DBP, while PWVslope didn't correlate with any inputted parameter. Using simple mathematical approach by plotting eaPWV and cSBP values obtained during ABPM, it is possible to visualize unique course of individual PWV related to BP. Using PWVslope and PWVbaseline as novel parameters could be a feasible way to approach BP-independent PWV, though their clinical relevance should be tested in future studies. Our data underline the importance of BP-independent expression of PWV, when we use it as a clinical surrogate parameter for the vascular damage.

Keywords: aortic pulse wave velocity, vascular damage, non-invasive oscillometric measurement, vascular stiffness, arteriosclerosis

OPEN ACCESS

Edited by:
Adelaide De Vecchi, King's College London, United Kingdom

Reviewed by:
Arne Deiseroth, University of Basel, Switzerland
Kristina Kusche-Vihrog, University of Lübeck, Germany

****Correspondence:***
Alexander Reshetnik
alexander.reshetnik@charite.de

Specialty section:
This article was submitted to Vascular Physiology, a section of the journal Frontiers in Physiology

Received: *06 July 2020*
Accepted: *17 September 2020*
Published: *08 October 2020*

Citation:
Reshetnik A, Tölle M, Eckardt K-U and van der Giet M (2020) Would Oscillometry be Able to Solve the Dilemma of Blood Pressure Independent Pulse Wave Velocity – A Novel Approach Based on Long-Term Pulse Wave Analysis? Front. Physiol. 11:579852. doi: 10.3389/fphys.2020.579852

INTRODUCTION

Aortic stiffness (AS) is considered to be associated with increased cardiovascular risk. Thus, European Society of Hypertension recommends screening for elevated AS in hypertension (Mancia et al., 2013). Pulse wave velocity (PWV) and in particular carotid-femoral PWV (cfPWV) is an established non-invasive standard to assess AS (Van Bortel et al., 2012). It has been shown to be

associated with increased cardiovascular mortality and morbidity independent from established cardiovascular risk factors (Ben-Shlomo et al., 2014). One of the main problems about establishing PWV as an independent surrogate parameter for arterial vessel damage (AVD) is its physiological intrinsic relationship to blood pressure (BP) level. Higher BP results in a stiffer artery and higher PWV, yet without any change in anatomical structure and physiologic properties of the vessel wall. In contrast, AS represents persistent structural changes in arterial vessel walls. It is thus matter of discussion whether increased PWV reflects persistent damage of the arterial wall or is an expression of elevated BP. Establishment of BP-independent PWV would probably better reflect real vessel damage.

Emerging non-invasive oscillometric devices use mathematical approaches and are able to deliver an estimated aortic PWV (eaPWV) based on pulse wave analysis and wave separation analysis, whereby major clinical determinants are age, central systolic BP (cSBP) of the patient and aortic characteristic impedance (Wassertheurer et al., 2008). Validation studies have shown this eaPWV be in good correlation with non-invasively determined cfPWV and invasively determined aortic PWV (Weber et al., 2015; Reshetnik et al., 2017). eaPWV role as a predictor of cardiovascular and all-cause mortality has been shown recently (Sarafidis et al., 2017). Such devices allow easy and quick calculation of eaPWV (Reshetnik et al., 2017), which can be repeated plenty of times under varying BP and patient position. In the present retrospective study we sought to establish new BP-independent PWV using mathematic analysis of the repeated eaPWV measurements during 24 h ambulatory BP and pulse wave monitoring. We hypothesized that establishing of BP-independent PWV would be first step on the way to demonstrate real vascular damage.

MATERIALS AND METHODS

All included subjects received long-term (24 h) ambulatory BP and pulse wave monitoring as a part of clinical routine in our Department of Nephrology at Campus Benjamin Franklin, Charité University Berlin. Charité University Berlin review board approved the study (EA4/112/18). No informed consent was required for the study purpose. We screened all available recordings from our database, which comprised time period from August 2012 to February 2018, and included all subjects with at least one representative 24 h recording of peripheral BP, central BP and PWV. All available demographic and clinical data were collected. Smoker status was missing in 50%, exact protein-creatinine ratio in 64% and albumin-creatinine ratio in 65% of study subjects. Other demographic and clinical parameters were completely present in all subjects. We could analyze 648 long-term BP and pulse wave analysis recordings from 507 patients with 43,567 single measurements. Available demographic and clinical data were summarized and analyzed. For the purpose of the study "hypertension" was defined, when the diagnosis "hypertension" has been mentioned in the medical record, subject had antihypertensive medication or the BP level was higher than 130/80 mmHg in the ambulatory BP monitoring. Due to retrospective study design the diagnosis "hyperliproteinemia" and smoking status were based on data from the medical record. All implemented procedures were in accordance with institutional guidelines.

BP-Monitoring and Pulse Wave Analysis

All recordings were performed with Mobil-O-Graph (I.E.M., Stolberg, Germany) and data analysis was performed with HMS Client Software, Version 5.1. The Mobil-O-Graph is a non-invasive oscillometric device, which combines ambulatory blood pressure monitoring with long-term pulse wave analysis (**Supplementary Figure 1**). The cuff was applied at the left or right upper arm after the circumference of the arm was measured and appropriate cuff size was chosen (size 1: 24–34 cm or size 2: 32–42 cm). First, brachial SBP and diastolic BP (DBP) were obtained. Thereafter, the cuff was again inflated maintaining the diastolic pressure level for 10 s for assessment of the pulse waveform using high fidelity pressure sensor. The mathematic method for pulse wave analysis in Mobil-O-Graph is based on the algorithm used in ARCSolver (Wassertheurer et al., 2008). Using generalized transfer functions (Fourier analysis and de-compensation into wave harmonics) aortic pressure waveform can be modulated. Central flow curve can be calculated by the means of an adopted, multi-dimensional Windkessel model. The time-lag between pressure and flow curve is generally referred to as "characteristic impedance (Zc)," in which the flow curve follows the pressure curve. Zc, together with the input variables of central systolic and diastolic blood pressure and age allows the device the estimation of aortic PWV (Wassertheurer et al., 2010). Single recordings were done every 20 min during the day (0600–2,200 h) and every 30 min during the night (2,200–0600 h). A 24 h recording with $\geq$ 80% valid single measurements of SBP, DBP, central BP and PWV was considered representative. For each parameter of a single 24 h recording, mean value of all valid single measurements was obtained and included in the statistical analysis.

Correlation Between Central SBP and eaPWV

In order to assess the course of eaPWV depending on change in BP, we used scatter plots to visualize a possible correlation. All single measurements of cSBP and corresponding eaPWV from each of the 648 24-h readings were included in separate scatter plots. The relationship between cSBP and eaPWV was linear and could be described with following equation: eaPWV = a*cSBP + b. We termed factor "a" as "PWVslope" and factor "b" as "PWVbaseline." **Figure 1** presents scatter plots with appropriate equations for three individuals from different age ranges.

Correlation Between Available Demographic and Clinical Data and eaPWV, PWVslope, and PWVbaseline

We tested the impact of each available demographic and clinical parameter on eaPWV, PWVslope, and PWVbaseline using

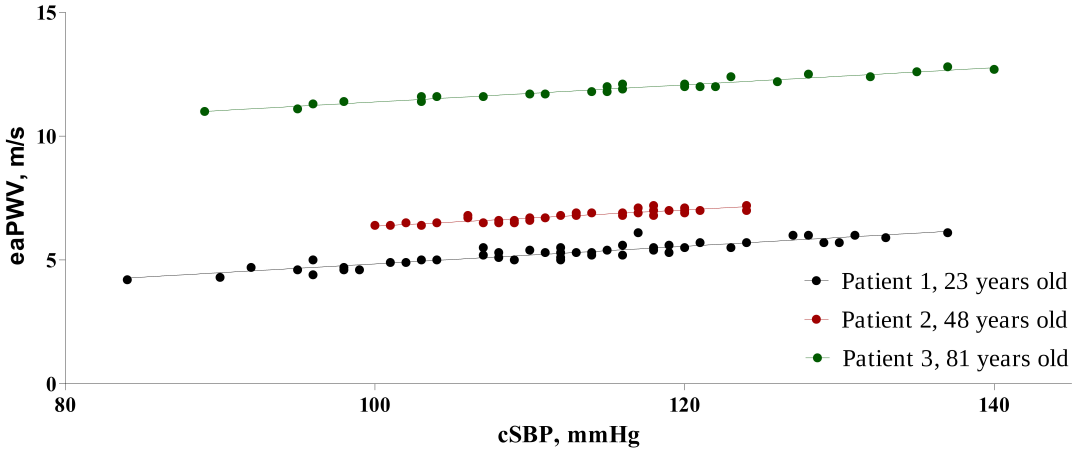

FIGURE 1 | Correlation between central blood pressure and pulse wave velocity in individual patients in three different age ranges; A < 25 years; B- 40–50 years; C > 75 years.

single regression analysis. Those with significant result in single regression analysis were included in multiple regression analysis.

Repeated Measurements

For a part of the study collective repeated measurements were recorded. One hundred and eight patients had two recordings. Twenty five patients had three recordings. Five subjects had four recordings and one patient had five recordings. Data from at least one follow up recording were compared to the initial measurement, respectively. The change of eaPWV, PWVslope, and PWVbaseline between recordings was assessed and possible factors impacting this change were evaluated.

Statistics

This study is retrospective. For each continuous variable mean and standard deviation were calculated. For each dichotomous variable number of affected subjects and the ratio related to the whole study collective in per cent were determined. Normal distribution of parameters was proofed with Kolmogorov-Smirnov-Test. In order to compare parameters from repeated measurements paired *T*-Test was used in case of proven normal distribution and Wilcoxon paired test in case of non-normal distribution. A multiple regression approach was used to determine relationship between available parameters. Two-sided *p*-values lower than 0.05 were considered as statistically significant. Statistic analysis was performed with SPSS Statistics 23.0 (IBM, New York, United States).

RESULTS

Five hundred and seven patients were included in the analysis. Approximately half of the study collective was female (48.7%). The mean age was 60.7 [18–92] years and the mean body-mass index was 27.4 kg/m^2. 92.5% of patients had established diagnosis of hypertension, 33.7% of hyperlipoproteinemia and 22.9% were smoker. Approximately a fifth had DM (20.5%) and 29.6% have had chronic kidney disease with an estimated glomerular flow rate (eGFR) below 60 ml/min/1,73 m^2 according to creatinine-based CKD-EPI equation with the mean protein/creatinine-ratio of 363 ± 1,025 mg/g and the mean albumin/creatinine-ratio of 248 ± 792 mg/g. The mean brachial SBP was 133 mmHg and DBP 80 mmHg with the mean heart rate of 69.5 beats/min. The mean cSBP was 121.6 ± 13.4 mmHg and the mean eaPWV was 9.2 ± 2.2 m/s. The mean PWVslope was 0.035 with the range from 0.026 to 0.050 m/s*mmHg and the mean PWVbaseline was 4.9 with the range from −0.21 to 11.2 m/s. Further details regarding demographic and clinical parameters as well as details about medication can be found in **Table 1**.

eaPWV and PWVbaseline increased with rising BP and age (**Figures 2**, **3**). PWVslope increased numerically with increasing age und SBP. This association was without statistical significance (**Table 2**). eaPWV and PWVbaseline were significantly higher in women compared to men (9.5 ± 2.2 vs. 8.9 ± 2.2, $p = 0.001$; and 5.2 ± 2.2 vs. 4.6 ± 2.1 m/s; $p < 0.001$). No differences in PWVslope were observed between female and male subjects.

In the single regression analysis we observed statistically significant correlation between eaPWV and age, SBP, DBP, mean BP, PP, heart rate, sex, DM, hyperlipoproteinemia, eGFR, history of hypertension, coronary artery disease, myocardial infarction, stroke, peripheral arterial disease, medication with ACE-Inhibitor/Angiotensin receptor blocker, calcium channel blocker, thiacids, beta blockers and central alpha-agonists. Multiple regression analysis revealed independent significant influence of age, SBP, DBP, eGFR and history of myocardial infarction on the eaPWV. Increased age and SBP were associated with increasing in eaPWV, while decreased DBP and eGFR were associated with the rise in eaPWV. Study patients with history of myocardial infarction had higher eaPWV than patients without previous myocardial infarction. Using the same demographic and clinical parameters inputted in single and multiple regression analyses we showed independent influence of DBP and age on PWVbaseline (**Table 3**). In contrast, we observed

TABLE 1 | Main characteristics and medication of the study collective (n = 507).

Sex	
Male, n(%)	260 (51.3)
Female, n(%)	247 (48.7)
Age, years	60.7 ± 16.3
Body mass index, kg/m^2	27.4 ± 5.3
Hypertension, n (%)	469 (92.5)
Hyperlipoproteinemia, n (%)	171 (33.7)
Smoker, n (%)*	116 (22.9)
Previous stroke, n (%)	26 (5.1)
Coronary heart disease, n (%)	123 (24.3)
Previous myocardial infarction, n (%)	36 (7.1)
Peripheral vascular disease, n (%)	22 (4.3)
Diabetes mellitus, n (%)	104 (20.5)
Chronic kidney disease (eGFR < 60 ml/min/1.73 qm CKD-EPI-Equation), n (%)	150 (29.6)
eGFR, ml/min/1.73 qm	70.4 ± 26.0
Protein/Creatinin-Ratio, mg/g$^{\#}$	363 ± 1025
Albumin/Creatinin-Ratio, mg/g$^{\$}$	248 ± 792
ABPM brachial systolic blood pressure, mmHg	133.0 ± 14.8
ABPM brachial diastolic blood pressure, mmHg	80.0 ± 10.7
ABPM mean blood pressure, mmHg	101.2 ± 11.3
ABPM pulse pressure, mmHg	52.9 ± 11.3
ABPM heart rate, beats/min	69.5 ± 10.3
ABPM central systolic blood pressure, mmHg	121.6 ± 13.4
ABPM central diastolic blood pressure, mmHg	81.7 ± 10.9
ABPM estimated aortic pulse wave velocity, m/s	9.2 ± 2.2
ABPM PWVslope, m/s*mmHg	0.035 ± 0.003
ABPM PWVbaseline, m/s	4.9 ± 2.2
Medication	
Antiplatelet therapy, n(%)	113 (22.3)
Oral anticoagulation, n(%)	30 (5.9)
Cholesterol reducing therapy, n(%)	180 (35.5)
Statins, n (%)	168 (33.1)
RAAS blocker, n(%)	355 (70)
Calcium-channel blocker, n(%)	275 (54.2)
Aldosterone antagonists, n (%)	37 (7.3)
Thiacid diuretics, n (%)	151 (29.8)
Loop diuretics, n (%)	80 (15.8)
Betareceptor-blocker, n (%)	266 (52.5)
Alphareceptor-blocker, n(%)	63 (12.4)
Central alpha-agonists, n (%)	67 (13.2)
Direct vasodilators, n(%)	15 (3)

*Available in 253 subjects; $^{\#}$available in 181 subjects; $^{\$}$available in 175 subjects.

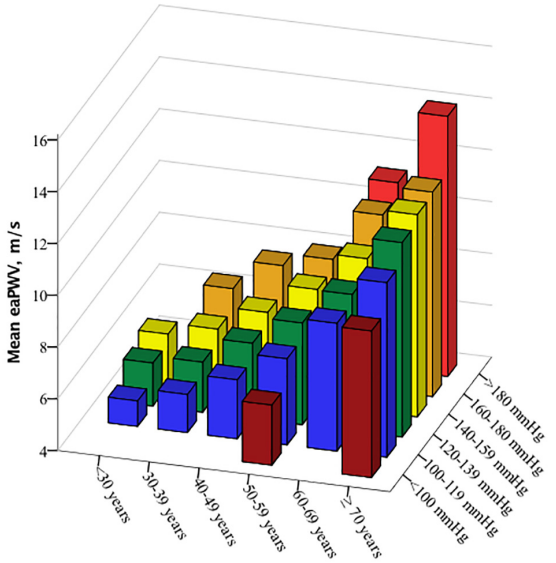

FIGURE 2 | Mean estimated aortic pulse wave velocity (eaPWV) values according to age and blood pressure categories.

no statistically significant correlation between any available demographic and clinical parameter and PWVslope, although it increased numerically with increasing age and SBP level.

One hundred and eight patients have had repeated recordings. The mean between-recording time was 4.5 ± 5.8 months. The mean age of these patients was 60 years and the BMI was 27.8 kg/m^2. 42% were female. The mean eGFR was 72.1 ml/min/1.73 m^2 according to creatinine-based CKD-EPI equation with ca. 29% of the patients having chronic kidney disease with an eGFR < 60 ml/min/1.73 m^2. The mean brachial BP was 134.9/80.1 mmHg with the mean heart rate of 67.3 beats/min. The mean eaPWV was 9.2 m/s with the mean PWVslope of 0.035 and PWVbaseline of 4.9 m/s. **Supplementary Table 1** denotes further information about the subgroup of patients with repeated recordings.

eaPWV was adjusted to the SBP level of 120 mmHg. We observed statistically significant difference in eaPWV$_{120}$, while SBP, DBP, PP and heart rate didn't change significantly between recordings (**Table 4**). We then investigated change in eaPWV$_{120}$ (delta-eaPWV$_{120}$) across the range of change in SBP, DBP, heart rate and PP as well as change in eaPWV$_{120}$ related to absolute level of initial SBP, DBP, heart rate and eaPWV$_{120}$. Increase in DBP between the measurements was statistically significant associated with decrease in eaPWV$_{120}$ (Spearman R^2 = 0.048, p < 0.01). Higher absolute value of initial PP was statistically significant associated with increase in follow-up eaPWV$_{120}$ (Spearman R^2 = 0.038, p < 0.05). We did not observe any statistically significant correlation between the change in SBP, heart rate and PP, absolute level of initial SBP, DBP, heart rate, eaPWV120 and change in eaPWV120 between the measurements (**Supplementary Figures 2, 3**).

DISCUSSION

In our study analysis of the relationship between eaPWV and cSBP based on multiple single measurements from simultaneous 24 h BP monitoring and pulse wave analysis was essential to describe individual relationship between PWV and BP.

In 2010, a landmark study was published by Arterial Stiffness' Collaboration, where reference and normal values for PWV (measured as cfPWV) were established. The authors observed a linear relationship between BP and PWV and quadratic

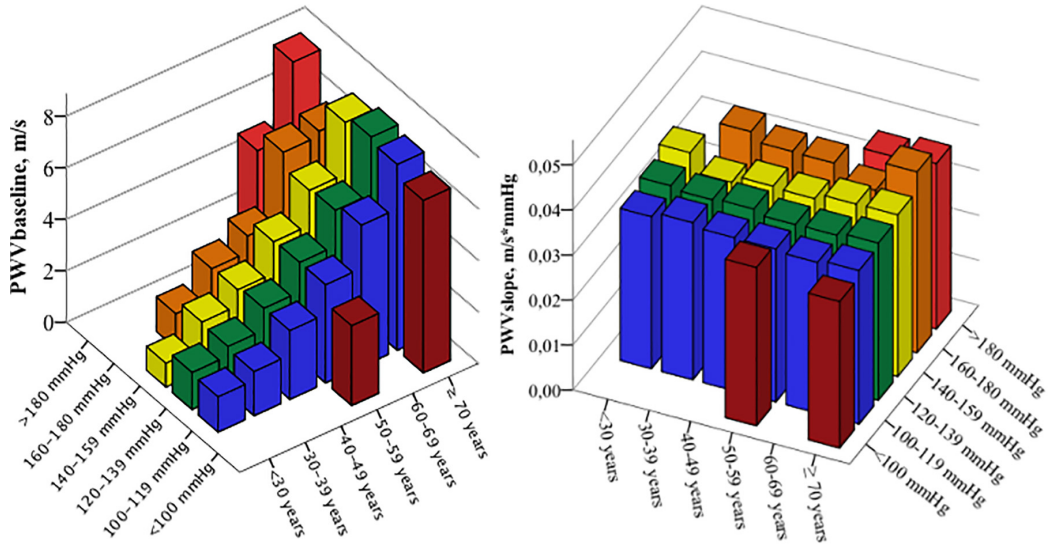

FIGURE 3 | Mean pulse wave velocity baseline (PWVbaseline) values **(right graph)** and PWVslope **(left graph)** according to the age and blood pressure categories.

TABLE 2 | Distribution of estimated aortic pulse wave velocity (eaPWV), PWVslope, and PWVbaseline in the study population according to age and blood pressure category.

Age category, years	systolic blood pressure category, mmHg					
	<100	100–119	120–139	140–159	160–180	>180
eaPWV as mean ± standard deviation, m/s						
<30		5.0 ± 0.1	5.7 ± 0.8	6.0 ± 0.2		
30–39		5.5 ± 0.2	5.9 ± 0.2	6.4 ± 0.2	7.2*	
40–49		6.3 ± 0.3	6.9 ± 0.4	7.3 ± 0.4	8.3 ± 0.2	
50–59	6.3*	7.3 ± 0.4	7.9 ± 0.4	8.4 ± 0.4	8.8 ± 0.2	
60–69		8.9 ± 0.5	9.2 ± 0.5	9.9 ± 0.6	10.8 ± 0.4	11.2*
≥70	9.7*	10.7 ± 0.9	11.5 ± 1.0	11.8 ± 0.8	11.9 ± 1.3	14.1*
PWVslope as mean ± standard deviation						
< 30		0.034 ± 0.002	0.035 ± 0.004	0.037 ± 0.005		
30–39		0.035 ± 0.003	0.035 ± 0.002	0.033 ± 0.004	0.039*	
40–49		0.034 ± 0.003	0.035 ± 0.003	0.034 ± 0.003	0.037 ± 0.002	
50–59	0.035*	0.034 ± 0.001	0.034 ± 0.002	0.035 ± 0.002	0.037 ± 0.003	
60–69		0.033 ± 0.001	0.034 ± 0.003	0.035 ± 0.003	0.034 ± 0.004	0.036*
≥70	0.033*	0.034 ± 0.002	0.035 ± 0.002	0.036 ± 0.004	0.040 ± 0.007	0.037*
PWVbaseline as mean ± standard deviation, m/s						
<30		1.4 ± 0.3	1.4 ± 0.9	0.9 ± 0.6		
30–39		1.7 ± 0.2	1.8 ± 0.3	1.9 ± 0.6	1.3*	
40–49		2.7 ± 0.4	2.7 ± 0.4	2.5 ± 0.6	2.5 ± 0.2	
50–59	3.1*	3.8 ± 0.5	3.8 ± 0.5	3.7 ± 0.5	3.1 ± 0.8	
60–69		5.5 ± 0.5	5.2 ± 0.6	5.1 ± 0.5	5.7 ± 1.0	4.9*
≥ 70	6.7*	7.2 ± 0.9	7.4 ± 1.0	7.1 ± 1.0	5.9 ± 0.8	7.7*

Standard deviation not available.

relationship between PWV and age (Reference Values for Arterial Stiffness' Collaboration, 2010). The strength of the study was that all PWV values were measured. However, only few single measurements per patient were obtained and detection of individual relationship between PWV values and corresponding BP level was not possible. Analysis of over 11,000 patients allowed to draw general conclusions about PWV course with change in age and BP in whole study collective. However, individual impact of BP-level on PWV in single patients could not be determined. This point represents a current dilemma in interpreting PWV as an additional cardiovascular risk marker.

TABLE 3 | Significant influence parameters on estimated aortic pulse wave velocity (eaPWV) and PWVbaseline in multiple regression analysis.

	Dependent parameter: eaPWV		
Independent parameter	**Regression coefficient**	**R^2-value**	***p*-value**
Age	0.13	0.86	<0.001
Systolic blood pressure	0.03	0.05	0.007
eGFR	0.002	0.0007	0.02
Myocardial infarction	0.21	0.0006	0.02
Dependent parameter: PWVbaseline			
Age	0.12	0.88	<0.001
Diastolic blood pressure	-0.018	0.007	<0.001

TABLE 4 | Comparison between initial and follow-up recording (n = 108).

	Initial recording	Follow up recording	*p*-value
Systolic blood pressure, mmHg	134.4 ± 14.3	135.6 ± 15.6	0.35#
Diastolic blood pressure, mmHg	80.0 ± 10.7	80.5 ± 11.6	0.59#
Pulse pressure, mmHg	54.4 ± 11.3	55.2 ± 11.3	0.34*
Heart rate, beats/min	67.8 ± 9.7	67.4 ± 10.5	0.57#
PWV_{120}, m/s	8.9 ± 2.1	9.0 ± 2.1	<0.001#
PWVslope	0.0347 ± 0.00297	0.03495 ± 0.00324	0.37#
PWVbaseline, m/s	4.79 ± 2.11	4.81 ± 2.08	0.56#

*$eaPWV_{120}$- estimated aortic pulse wave velocity for the systolic blood pressure of 120 mmHg according following equation: PWV_{120} = 120 mmHg*PWVslope + PWVbaseline; #paired t-test; *paired Wilcoxon-test.*

In our study, we used a device, which is able to estimate aortic PWV using oscillometric approach. Currently required parameters for the eaPWV calculation are age, measured brachial BP and data from pulse wave analysis (Wassertheurer et al., 2008). Approaching the dilemma of the BP-independent PWV we analyzed individual relationship between eaPWV and SBP based on the data coming from ABPM. Based on our findings the relationship can be described with an individual linear equation. According to determined equation PWVslope could represent individual reaction of PWV to an increase in BP, while PWVbaseline could probably reflect baseline status of the arterial vessels. Though we observed increasing PWVslope values with increasing age and BP, this association was not statistically significant. Additionally, we did not show association between PWVslope and any other clinical parameter. Thus, the clinical relevance of the PWVslope as a separate parameter is still to be proofed. A possible explanation could be a high impact of age in the determination of the eaPWV in the algorithm. Recently, the clinical relevance of the eaPWV beyond the impact of age and SBP has been questioned (Schwartz et al., 2019). Despite the known shot-cuts of the oszillometric PWV estimation this method is valid, feasible and easy to apply in the clinical practice. It is able to capture multiple PWV changes with corresponding changes in BP. Previously to the era of oszillometric PWV measurement multiple PWV recordings were sophisticated and such relationships as obtained in our study could not be established. Based on the mathematical analysis of derived data we were able to reach a "standardization" of the PWV using novel parameters PWVbaseline und PWVslope and in such a way to separate the BP-impact on it. The standardization to a particular BP level is also useful to compare PWV between the patients but also to compare PWV values in the same individual over a time course as we have done in a part of our study collective with available repeated measurements.

To our knowledge, this is the first time serial BP and corresponding PWV changes have been reported. Greve et al. (2016) assessed the performance of estimated PWV, calculated from age, mean arterial pressure, using equations published by Arterial Stiffness' Collaboration. Though estimated PWV performed well in healthy subjects, it did not add any predictive value in patients with diabetes mellitus or on antihypertensive drugs. As mentioned above, this might be due to high individual variability, which cannot be addressed by using equations coming from another study collective (Greve et al., 2017). Lim et al. (2015) observed intraindividually increasing cfPWV with increasing mean BP in healthy subjects. However, they did not describe individual relationship between cfPWV and BP in their study collective.

The relation between cSBP and eaPWV can readily be translated to the relation between obtained brachial SBP and eaPWV, as we observed well known strong correlation between SBP and cSBP in our data (Pearson correlation coefficient 0.96). We choose cSBP as an independent variable based on the original publication of the method, where authors described cSBP as one of the major determinants needed for the calculation of the eaPWV (Hametner et al., 2013).

We observed well-known association between eaPWV with age and SBP. As in the study published 2010 by Arterial Stiffness' Collaboration (Reference Values for Arterial Stiffness' Collaboration, 2010) the correlation between eaPWV and SBP was linear and the correlation between eaPWV and age was better explained by quadratic equation. Furthermore, we saw significant increase in eaPWV with a decreasing kidney function and decreasing DBP. The influence of age, SBP and chronic kidney disease on AS and PWV is well known and could be demonstrated in previous studies (Tolle et al., 2015). The impact of DM on AS (De Angelis et al., 2004) and PWV (Cardoso and Salles, 2016) as its surrogate parameter is also well known. However, we could not show significant independent influence of DM on eaPWV in our collective. One possible explanation could be a relatively low prevalence of DM in our study collective as only circa 20% of patients had DM, which was non-insulin-dependent in the majority of cases. One can speculate that changes in vascular structure might have been only moderate. Furthermore, the impact of BP, age and kidney function had statistically higher impact on eaPWV compared to DM in our analysis. Higher prevalence of isolated systolic hypertension in subjects with DM has been shown previously (Os et al., 2006). Observed increase in eaPWV with lower DBP in our study could thus been interpreted as an indirect link between DM and eaPWV. Supporting this hypothesis, diabetics showed significantly lower DBP compared to non-diabetics in our collective.

Recent data pointed out that changes in heart rate could also contribute to significant changes in PWV (Tan et al., 2016) and adjustment of PWV to a heart rate would also be necessary. We did not see any significant independent effect of heart rate on PWV in our data.

Many studies demonstrated severe differences in PWV between female and male subjects (DuPont et al., 2019). We observed higher eaPWV120 in women. However, we did not show any independent effect of sex on PWV in multiple regression analysis. Additionally, women were significantly older (63.2 ± 15.9 vs. 58 ± 16.4 years) than men in our study collective, which is probably the major reason for higher eaPWV.

Many studies demonstrated significant influence of smoking on AS (Doonan et al., 2010). We did not observe any significant independent effect of smoking on eaPWV. This result is, however, limited as data on smoking status were available in only 50% of the study subjects due to retrospective study design.

Comparison of repeated ABPM readings, which were performed on average 4.5 months apart, revealed statistically significant change in eaPWV120. However, the mean difference of 0.1 m/s is not relevant from the clinical point of view. We observed no clinically relevant impact of any hemodynamic parameter on eaPWV120, no matter whether the amount of difference between initial and follow up recording or absolute value of the initial recording were considered (**Supplementary Figures 2, 3**), although single variables (e.g., PP) indeed showed statistically significant impact on change in eaPWV120.

Assuming that remodeling of vessel wall is a very slow process, the period of 4.5 months is likely to be too short to reveal a real change in the architecture of the vessel wall explaining why the individual BP-adjusted eaPWV did not change in our study. Thus far, published studies compared initial and follow up PWV-values without individual BP-adjustment. For instance, 2011 published study by Ignace et al. compared cfPWV before and after kidney transplantation (Ignace et al., 2011). Though cfPWV was adjusted to the reduction in mean BP, individual adjustment to the particular level of BP is missing and individual degree of BP-impact on cfPWV cannot be obtained. Whether observed reduction in cfPWV of mean 0.5 m/s 3 months after transplantation in patients still on comparably high level of immunosuppression really reflects improvement in AS is debatable.

CONCLUSION

In conclusion, using simple mathematical approach by plotting eaPWV and cSBP values obtained during ABPM, it is possible to visualize unique course of individual PWV related to BP. Using PWVslope and PWVbaseline as novel parameters could be a feasible way to approach BP-independent PWV, though clinical relevance should be tested in future studies. Our data underline the importance of BP-independent expression of PWV, when we use it as a clinical surrogate parameter for the vascular damage.

We acknowledge several limitations of our study: Attributable to the oscillometric method, which we used, obtained PWV-values were not measured but estimated based on pulse wave analysis and utilization of age and central BP. BP-adjustment of eaPWV using obtained individual PWVslope could thus represent the extent of arterial damage. However, the clinical potential of the obtained novel parameters PWVbaseline and PWVslope is not yet established and the next necessary step would be to correlate these parameters to relevant clinical endpoints.

Worth mentioning is the fact that pulse wave analysis is done in the brachial artery, which is a muscular artery, used as a surrogate for PWV in the aorta, which is an elastic vessel. As the anatomy of elastic and muscular arteries is different, they could stiffer in distinct manner (Shirwany and Zou, 2010).

Retrospective design of the study precludes inferences about causal relationships. All available demographic and clinical parameters were included, however, unidentified confounders cannot be ruled out. For instance, no information about the cuff position was available, which is known to be potential influence factor on the PWV. The study population was limited to a specific group of non-severe ill subjects, with a majority having hypertension, mild kidney disease and obesity. Thus, further studies are needed in other populations to confirm and generalize our findings. Low prevalence of diabetes mellitus and advanced kidney disease might have diminished the known effect of these influence factors on PWV. Small part of the subjects with repeated measurements and short follow up period could be a reason for clinically non-relevant change in eaPWV120, obtained in the study.

DATA AVAILABILITY STATEMENT

The raw data supporting the conclusions of this article will be made available by the authors, without undue reservation.

ETHICS STATEMENT

The studies involving human participants were reviewed and approved by the Ethic Review Board Charité University Berlin. Written informed consent for participation was not required for this study in accordance with the national legislation and the institutional requirements.

AUTHOR CONTRIBUTIONS

AR and MG: conceptualization. AR: methodology, formal analysis, writing—original draft preparation. K-UE and MG: writing—review and editing. MG: project administration. All authors contributed to the article and approved the submitted version.

SUPPLEMENTARY MATERIAL

The Supplementary Material for this article can be found online at: https://www.frontiersin.org/articles/10.3389/fphys.2020.579852/full#supplementary-material

REFERENCES

Ben-Shlomo, Y., Spears, M., Boustred, C., May, M., Anderson, S. G., Benjamin, E. J., et al. (2014). Aortic pulse wave velocity improves cardiovascular event prediction: an individual participant meta-analysis of prospective observational data from 17,635 subjects. *J. Am. Coll. Cardiol.* 63, 636–646.

Cardoso, C. R., and Salles, G. F. (2016). Aortic stiffness as a surrogate endpoint to micro- and macrovascular complications in patients with type 2 diabetes. *Int. J. Mol. Sci.* 17:2044. doi: 10.3390/ijms17122044

De Angelis, L., Millasseau, S. C., Smith, A., Viberti, G., Jones, R. H., Ritter, J. M., et al. (2004). Sex differences in age-related stiffening of the aorta in subjects with type 2 diabetes. *Hypertension* 44, 67–71. doi: 10.1161/01.hyp.0000130482.81883.fd

Doonan, R. J., Hausvater, A., Scallan, C., Mikhailidis, D. P., Pilote, L., and Daskalopoulou, S. S. (2010). The effect of smoking on arterial stiffness. *Hypertens. Res.* 33, 398–410. doi: 10.1038/hr.2010.25

DuPont, J. J., Kenney, R. M., Patel, A. R., and Jaffe, I. Z. (2019). Sex differences in mechanisms of arterial stiffness. *Br. J. Pharmacol.* 176, 4208–4225. doi: 10.1111/bph.14624

Greve, S. V., Blicher, M. K., Kruger, R., Sehestedt, T., Gram-Kampmann, E., Rasmussen, S., et al. (2016). Estimated carotid-femoral pulse wave velocity has similar predictive value as measured carotid-femoral pulse wave velocity. *J. Hypertens.* 34, 1279–1289. doi: 10.1097/hjh.0000000000000935

Greve, S. V., Laurent, S., and Olsen, M. H. (2017). Estimated pulse wave velocity calculated from age and mean arterial blood pressure. *Pulse* 4, 175–179. doi: 10.1159/000453073

Hametner, B., Wassertheurer, S., Kropf, J., Mayer, C., Holzinger, A., Eber, B., et al. (2013). Wave reflection quantification based on pressure waveforms alone–methods, comparison, and clinical covariates. *Comput. Methods Programs* 109, 250–259. doi: 10.1016/j.cmpb.2012.10.005

Ignace, S., Utescu, M. S., De Serres, S. A., Marquis, K., Gaudreault-Tremblay, M. M., Lariviere, R., et al. (2011). Age-related and blood pressure-independent reduction in aortic stiffness after kidney transplantation. *J. Hypertens.* 29, 130–136. doi: 10.1097/hjh.0b013e32833f5e68

Lim, J., Pearman, M. E., Park, W., Alkatan, M., Machin, D. R., and Tanaka, H. (2015). Impact of blood pressure perturbations on arterial stiffness. *Am. J. Physiol. Regul. Integr. Comp. Physiol.* 309, R1540–R1545.

Mancia, G., Fagard, R., Narkiewicz, K., Redon, J., Zanchetti, A., Bohm, M., et al. (2013). 2013 ESH/ESC Guidelines for the management of arterial hypertension: the Task Force for the management of arterial hypertension of the european society of hypertension (ESH) and of the european society of cardiology (ESC). *J. Hypertens.* 31, 1281–1357.

Os, I., Gudmundsdottir, H., Kjeldsen, S. E., and Oparil, S. (2006). Treatment of isolated systolic hypertension in diabetes mellitus type 2. *Diabetes Obes. Metab.* 8, 381–387. doi: 10.1111/j.1463-1326.2005.00523.x

Reference Values for Arterial Stiffness' Collaboration (2010). Determinants of pulse wave velocity in healthy people and in the presence of cardiovascular risk factors: 'establishing normal and reference values'. *Eur. Heart J.* 31, 2338–2350. doi: 10.1093/eurheartj/ehq165

Reshetnik, A., Gohlisch, C., Tolle, M., Zidek, W., and Van Der Giet, M. (2017). Oscillometric assessment of arterial stiffness in everyday clinical practice. *Hypertens. Res.* 40, 140–145. doi: 10.1038/hr.2016.115

Sarafidis, P. A., Loutradis, C., Karpetas, A., Tzanis, G., Piperidou, A., Koutroumpas, G., et al. (2017). Ambulatory pulse wave velocity is a stronger predictor of cardiovascular events and all-cause mortality than office and ambulatory blood pressure in hemodialysis patients. *Hypertension* 70, 148–157. doi: 10.1161/hypertensionaha.117.09023

Schwartz, J. E., Feig, P. U., and Izzo, J. L. Jr. (2019). Pulse wave velocities derived from cuff ambulatory pulse wave analysis. *Hypertension* 74, 111–116. doi: 10.1161/hypertensionaha.119.12756

Shirwany, N. A., and Zou, M. H. (2010). Arterial stiffness: a brief review. *Acta Pharmacol. Sin.* 31, 1267–1276. doi: 10.1038/aps.2010.123

Tan, I., Spronck, B., Kiat, H., Barin, E., Reesink, K. D., Delhaas, T., et al. (2016). Heart rate dependency of large artery stiffness. *Hypertension* 68, 236–242. doi: 10.1161/hypertensionaha.116.07462

Tolle, M., Reshetnik, A., Schuchardt, M., Hohne, M., and van der Giet, M. (2015). Arteriosclerosis and vascular calcification: causes, clinical assessment and therapy. *Eur. J. Clin. Invest.* 45, 976–985. doi: 10.1111/eci.12493

Van Bortel, L. M., Laurent, S., Boutouyrie, P., Chowienczyk, P., Cruickshank, J. K., De Backer, T., et al. (2012). European society of hypertension Working Group on vascular, function, and a. european network for noninvasive investigation of large, expert consensus document on the measurement of aortic stiffness in daily practice using carotid-femoral pulse wave velocity. *J. Hypertens.* 30, 445–448. doi: 10.1097/hjh.0b013e32834fa8b0

Wassertheurer, S., Kropf, J., Weber, T., van der Giet, M., Baulmann, J., Ammer, M., et al. (2010). A new oscillometric method for pulse wave analysis: comparison with a common tonometric method. *J. Hum. Hypertens.* 24, 498–504. doi: 10.1038/jhh.2010.27

Wassertheurer, S., Mayer, C., and Breitenecker, F. (2008). Modeling arterial and left ventricular coupling for non-invasive measurements. *Simul. Model. Pract. Theory* 16, 988–997. doi: 10.1016/j.simpat.2008.04.016

Weber, T., Wassertheurer, S., Hametner, B., Parragh, S., and Eber, B. (2015). Noninvasive methods to assess pulse wave velocity: comparison with the invasive gold standard and relationship with organ damage. *J. Hypertens.* 33, 1023–1031. doi: 10.1097/hjh.0000000000000518

Conflict of Interest: The authors declare that the research was conducted in the absence of any commercial or financial relationships that could be construed as a potential conflict of interest.

frontiers in Physiology

ORIGINAL RESEARCH
published: 05 November 2020
doi: 10.3389/fphys.2020.578701

Mechanisms of Aortic Flow Deceleration and the Effect of Wave Reflection on Left Ventricular Function

*Chloe M. Park[1,2], Alun D. Hughes[2], Michael Y. Henein[1,3] and Ashraf W. Khir[1]**

[1] Brunel Institute for Bioengineering, Brunel University London, London, United Kingdom, [2] Institute of Cardiovascular Science, University College London, London, United Kingdom, [3] Umea Heart Centre, Umea University Hospital, Umea, Sweden

Increased wave reflection is an independent predictor of cardiovascular events, possibly due to effects on left ventricular (LV) function. We investigated the relationship between reflected waves in early systole, the forward decompression wave in mid-late systole and LV mechanical behavior. Invasively acquired ascending aortic velocity, pressure, and LV long and minor axes' dimensions were measured simultaneously in 11 anesthetized dogs during both control conditions and aortic occlusion to cause additional early wave reflection. Wave intensity analysis (WIA) was used to identify the arrival of the reflected wave and the onset of a forward decompression wave in mid-late systole. The arrival time of the reflected wave coincided with the time when minor axis shortening began to decline from its peak, even during aortic occlusion when this time is 12 ms earlier. The initial decline in long axis shortening corresponded to the time of the peak of the reflected wave. The forward decompression wave was consistently observed to have a slow and then rapid phase. The slow phase onset coincided with time of maximum shortening velocity of the long axis. The onset of the later larger rapid phase consistently coincided with an increased rate of deceleration of both axes during late systole. Forward decompression waves are generated by the LV when the long axis shortening velocity falls. Reflected wave arrival has a detrimental effect on LV function, particularly the minor axis. These observations lend support to suggestions that therapies directed toward reducing wave reflection may be of value in hypertension and cardiovascular disease.

Keywords: wave reflection, LV velocity of axis shortening, aortic flow deceleration, wave intensity analysis and forward decompression wave, wave intensity analysis, aortic flow

OPEN ACCESS

Edited by:
Jonathan Paul Mynard, Royal Children's Hospital, Australia

Reviewed by:
Audrey Adji, Victor Chang Cardiac Research Institute, Australia
Claire Raphael, Mayo Clinic, United States

***Correspondence:**
Ashraf W. Khir
ashraf.khir@brunel.ac.uk

Specialty section:
This article was submitted to Vascular Physiology, a section of the journal Frontiers in Physiology

Received: *03 July 2020*
Accepted: *29 September 2020*
Published: *05 November 2020*

Citation:
Park CM, Hughes AD, Henein MY and Khir AW (2020) Mechanisms of Aortic Flow Deceleration and the Effect of Wave Reflection on Left Ventricular Function. Front. Physiol. 11:578701. doi: 10.3389/fphys.2020.578701

INTRODUCTION

Increased wave reflection is an independent predictor of cardiovascular events in hypertension (London et al., 2001; Manisty et al., 2010) and has been proposed as a therapeutic target in cardiovascular disease (O'Rourke and Safar, 2005). Reflected waves arrive at the left ventricle (LV) during systole (Baksi et al., 2009) and impose an additional load on the LV, which is exaggerated in

hypertension (Merillon et al., 1983; Westerhof and O'Rourke, 1995) and heart failure (Curtis et al., 2007).

LV motion undergoes a complex pattern of change during the cardiac cycle (Codreanu et al., 2011) however, no studies have simultaneously measured the arrival of reflected waves during systole with LV long and minor axes function. Systolic LV function involves shortening of myocardial fibers oriented in circumferential, longitudinal, and oblique directions (Greenbaum et al., 1981; Henein and Gibson, 1999). This arrangement optimizes work (Torrent-Guasp et al., 2005) and has a major influence on intramural stress distribution (Arts et al., 1991). Velocity and strain patterns of various myocardial components have provided valuable information on cardiac function (Nagueh et al., 1997; Wang et al., 2005); however, the relationship between arterial wave reflection, LV mechanical function, and aortic flow remains modestly understood.

Wave intensity analysis (WIA) has proved a useful method for studying pressure-flow dynamics in conjunction with LV wall motion patterns in health and disease (Parker, 2009). Rapid shortening of the LV muscle fibers generates a large forward compression wave (FCW) in early systole, and this has been proposed as an indicator of LV systolic function (Parker et al., 1988). A backward compression wave (BCW) occurring after the initial FCW wave is attributed to reflection of the forward wave from distal sites of impedance mismatch (Zambanini et al., 2002). The origin of the late systolic (proto-diastolic) forward decompression wave (FDW) that decelerates aortic blood flow (Parker et al., 1988) is less well understood.

We hypothesized that wave reflections would influence LV minor (M) and long (L) axis function. Further, to establish mechanistic links between waves and LV function, we used aortic occlusion as means of inducing earlier and larger wave reflections and examined their effect on LV function.

MATERIALS AND METHODS

The experimental protocol was approved by the animal care committee of the University Of Calgary, Faculty of Medicine and conforms to the National Institutes of Health Guide for the Care and Use of Laboratory Animals. Eleven open chest mongrel dogs were anesthetized using 30 mg/kg of sodium pentobarbital administered intravenously, in addition to a maintenance dose of 75 mg/h for the length of the experiment. The dogs were intubated and mechanically ventilated (constant volume ventilator, model 607, Harvard Apparatus Company, Millis, MA, United States). The forelegs and left hind leg of the dogs were used for recording the ECG.

Control Conditions

An ultrasonic flow probe (model T201, Transonic Systems Inc., Ithaca, NY, United States) was snug-fitted to the ascending aorta to measure blood flow rate, from which velocity (U) was derived using the *post mortem* diameter and assuming a circular cross-sectional area. Pressure at the aortic root (P) and LV (Plv) was measured using high-fidelity pressure catheters (Millar Instruments Inc., Houston, TX, United States). The aortic root catheter was placed approximately 1 cm distal to the aortic valve and was introduced into the aorta *via* the brachial or the carotid arteries. The LV pressure catheter was also inserted into either a brachial artery or into the LV directly through the myocardium of the LV apex. A mercury manometer was used to calibrate the pressure catheters before every experiment, and all data were digitally recorded at a sampling rate of 200 Hz. LV long and minor axes' dimensions were measured throughout the cardiac cycle. Two pairs of ultrasound sonomicrometer crystals (5MH, Sonometrics, Ontario, Canada) were implanted in the mid-wall of the LV myocardium to measure the movement of the long (base–apex) and short (septum–free wall) axes throughout the cardiac cycle. The septum and free wall crystals were implanted at the mid-level, between the base and apex of the LV.

Aortic Occlusion

Total aortic occlusion was achieved by a snare positioned in the proximal descending thoracic aorta at the level of the aortic valve approximately 13 cm from the measurement site. P, U, and axial shortening velocity were measured for 30 s during control and following aortic occlusion, 3 min after the snare was applied.

The following hemodynamic parameters were determined from the basic measurements: Pulse pressure (PP) = SBP − DBP, where SBP is the systolic blood pressure and DBP is the diastolic blood pressure. Mean arterial pressure (MAP) = DBP + (PP/3) and Stroke volume (SV) = (EDV − ESV), where EDV and ESV are end diastolic and systolic volume. Cardiac output (CO) = SV × heart rate (HR), where HR is the heart rate. Total peripheral resistance (TPR) = MAP/CO, and total arterial compliance (TAC) = SV/PP. Effective arterial elastance and compliance are, respectively, (EEA) = ESBP/SV, where ESBP is end systolic blood pressure, and (C) = SV/PP.

Theoretical Analysis

Wave intensity analysis is based on the solution of the one-dimensional conservation equations of mass and momentum. Wave intensity (dI) is the rate of energy flux per unit area (W/m^2) and can be written

$$dI = dP\,dU. \tag{1}$$

The water hammer equation for forward (+) and backward (−) waves is

$$dP_{\pm} = \pm \rho c dU_{\pm} \tag{2}$$

where ρ is the density of blood 1,050 kg/m^3 and c is the wave speed, which we calculated using the PU loop, as previously described (Khir et al., 2001). Knowledge of c allows dI to be separated into its forward and backward components.

$$dI_{\pm} = \pm \frac{1}{4\rho c}(dP \pm \rho c dU)^2 \tag{3}$$

Data Analysis

Custom-written programs in MATLAB (The MathWorks Inc., MA, United States) were used to analyze the data. P and U waveforms were smoothed using a 7-point Savitzky–Golay filter, and the foot of both waveforms was aligned to take account of time lags in data processing. Shifting by no more than three

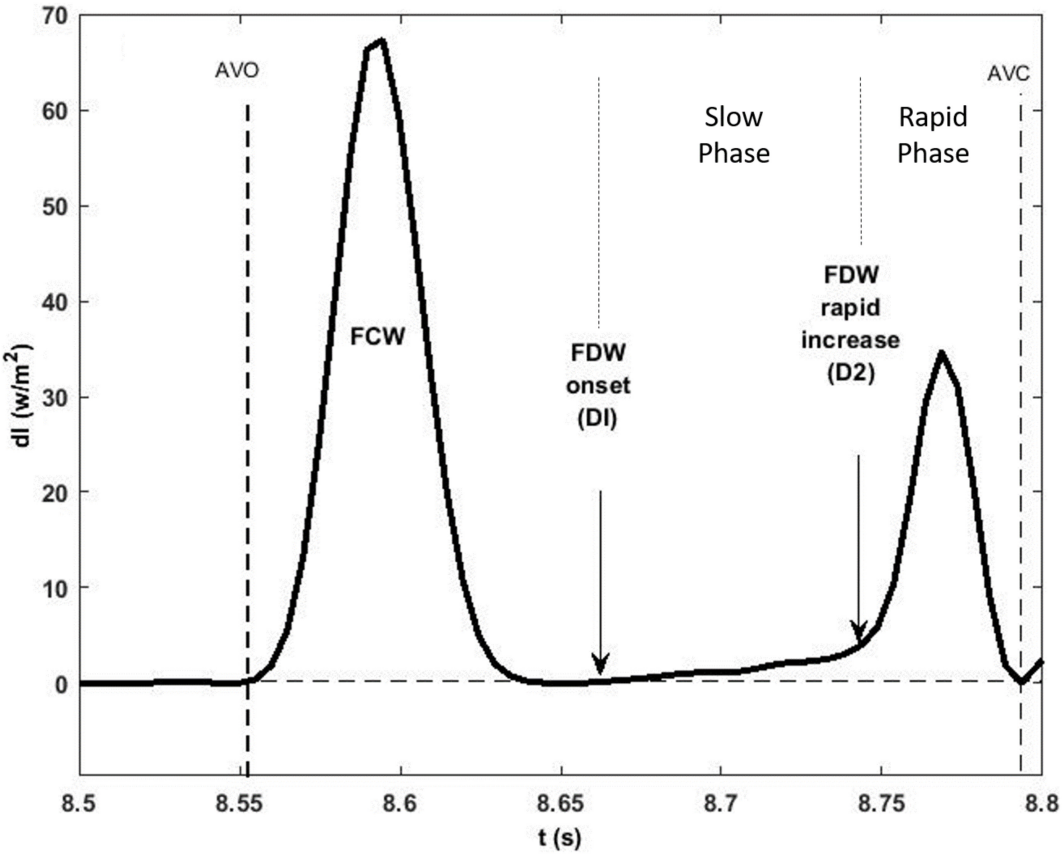

FIGURE 1 | A typical forward wave intensity analysis curve calculated from pressure and velocity measured in the ascending aorta. The rise of the forward decompression wave, FDW, comprises two phases: a slow (D1) then a rapid (D2) phase whose onset is clearly shown to occur in mid and late systole, respectively. AVO and AVC indicate opening and closing of the aortic valve. Also shown is the forward compression wave, FCW, in early systole.

sampling intervals was required to adjust for the lag caused by the filter in the ultrasonic flow meter (Hollander, 1999). Up to three representative cardiac cycles were selected from a stable sequence of beats during the 30 s recording period. Each cardiac cycle was analyzed individually and the data were averaged for each dog.

The R wave of the QRS complex was taken as time $t = 0$ and the following hemodynamic events and their timings were identified: peak aortic pressure ($P_{\max}$); peak LV pressure ($\mathrm{Plv}_{\max}$) and the derivative of Plv with respect to time ($\frac{dPlv}{dt}$); peak aortic velocity ($U_{\max}$); an inflection point on the descending limb of the aortic velocity waveform before aortic valve closure (U_i) was determined from the first derivative of U_{i} with respect to t. LV volume was calculated by considering the LV as an ellipsoid using the following equation

$$0.5\ (4/3) \times \pi \times r_1 r_2^2. \tag{4}$$

Where r_1 = LV long axis radius (base–apex) and r_2 = septum to free wall radius whose dimensions were acquired using the sonomicrometer crystals. Time to peak volume decline ($V_{\max}$) was determined by plotting the first derivative of volume with respect to time.

The onset of ejection was identified from the onset of the upstroke of the aortic flow waveform, which also indicated the onset of the FCW. The FDW wave observed in mid-to-late systole was always seen to have a "slow" (D1) then "rapid" (D2) phase as shown in **Figure 1**. The onset of each phase was determined from the first derivative of the forward wave intensity. The time of onset of the reflected waves was identified as the moment the separated backward wave intensity curve became negative. The energy carried by each wave ($\mathrm{J/m^2}$) was calculated by integrating the area under the peak of the wave with respect to time.

LV Wall Motion

Velocity of the LV long (L) and minor (M) axis shortening was determined by differentiating the axial displacement with respect to time. As reported previously (Page et al., 2010), the rate of shortening of each axis in systole could be subdivided into three phases throughout systole (I, II, III) although the onset of each phase in the long and minor axes did not occur simultaneously (**Figure 2**). Phase I represents acceleration of axis shortening during early systole; phase II is a period of slow deceleration of axial shortening beginning in mid-systole; phase III occurs near end-systole when there is a sudden increase in the rate of deceleration. The onsets of

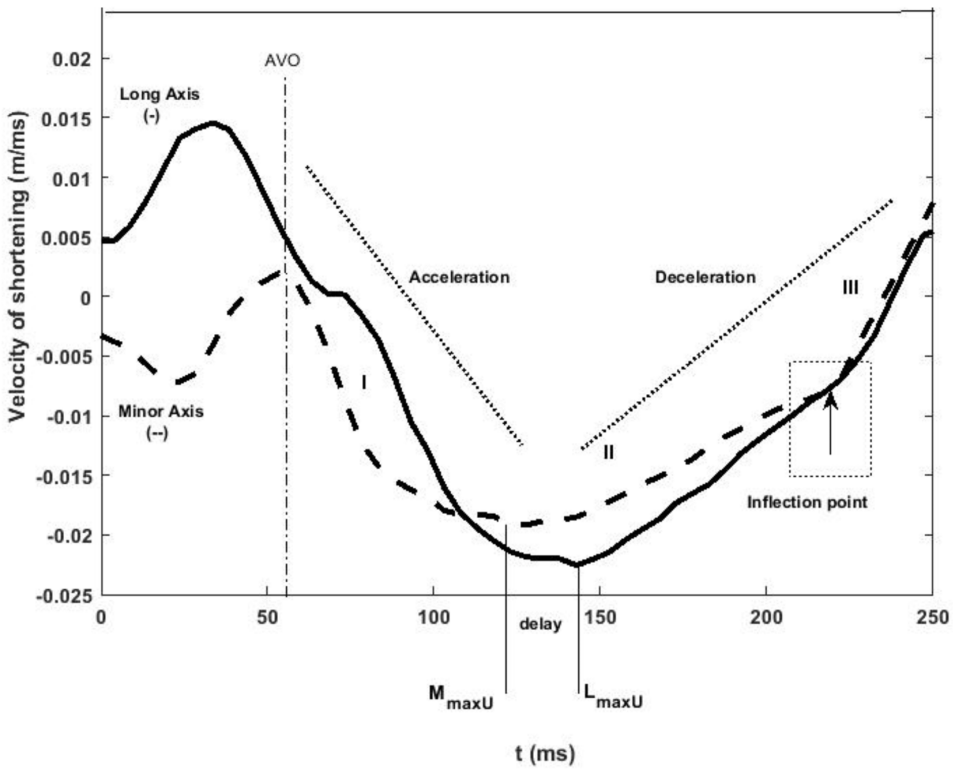

FIGURE 2 | LV minor (dashed line) and long (solid line) axes shortening speed during systole. The minor axis reaches its maximum velocity of shortening before the long axis during control conditions. The three rates of axial shortening are represented by I, II, and III sequentially. In late systole, both axes exhibit an inflection point after which their velocity of shortening decreases at an increased rate indicated as rate III. AVO and AVC indicate aortic valve opening and closing, and stages I, II, and III indicate acceleration and deceleration of the axes at early, mid, and late systole, respectively.

both phase II (M_{maxU}, L_{maxU}) and phase III (M_{III}, L_{III}) for each axis were determined from the second derivative of axial velocity of shortening. Minor and long axes rate of shortening (acceleration and deceleration) at each phase were also determined.

TABLE 1 | Baseline data during both control conditions and thoracic aortic occlusion.

Variable	Control	Occlusion	*p*-value
SBP (mmHg)	116 ± 9	173 ± 9	<0.0001
DBP (mmHg)	73 ± 7	108 ± 7	0.003
MBP (mmHg)	88 ± 7	130 ± 8	0.001
PP (mmHg)	43 ± 5	65 ± 5	0.008
HR (bpm)	86 ± 5	90 ± 5	0.5
SV (ml)	13.0 ± 1.5	11.3 ± 1.7	0.5
CO (L/min)	1.2 ± 0.6	1.5 ± 0.8	0.3
TPR (kPa/L)	12.1 ± 6.7	13.6 ± 7.2	0.7
C (ml/kPa)	2.33 ± 0.6	1.38 ± 0.3	0.001
EEA (kPa/ml)	1.19 ± 0.4	1.92 ± 0.6	0.005
SEP (ms)	194 ± 11	174 ± 12	0.2
Peak *U* (m/s)	0.7 ± 0.09	0.5 ± 0.1	0.4

SBP, systolic blood pressure; DBP, diastolic blood pressure; MBP, mean blood pressure; PP, pulse pressure; HR, heart rate; SV, stroke volume; CO, cardiac output; TPR, total peripheral resistance; C, arterial compliance; EEA, effective arterial elastance; SEP, systolic ejection period; peak U, peak velocity.

LV Wall Stress

Average fiber myocardial stress in the mid-wall (σ_m) was estimated using the equations derived by Regen (1990).

$$\sigma_{\mathrm{m}=3/2(\mathrm{V_m}/\mathrm{V_{mu}})\mathrm{P}/(\ln \mathrm{V_{ou}}-\ln \mathrm{V_{cu}})}. \quad (5)$$

Where V_m is mid-wall volume at any distension and V_{mu}, V_{ou}, and V_{cu} are mid-wall, chamber, and cavity volumes at reference distension. Based on the literature, end diastolic posterior wall thickness was assumed to be 7.1 mm in all dogs and was used to calculate LV wall volume. The average time to peak average fiber myocardial stress (σ_{max}) was recorded.

Reproducibility

Measurement of the time intervals from the peak of the R wave of the QRS complex to the peak shortening velocity of both the minor and long axes as well as to the onset of all three WIA waves was repeated on three separate occasions by a single observer. The mean difference ± SD to the time of M_{maxU} was 2 ± 2 ms (within-observer coefficient of variation (CV) = 2%). The time to L_{maxU} was 2 ± 4 ms (CV = 1%). The time to the onset of the FCW wave was 1 ± 2 ms (CV = 1.78%), the onset of the BCW was 1 ± 1 ms

TABLE 2 | All mean ± SD time intervals from the R of the QRS complex to the main hemodynamic and mechanical events during both control conditions and aortic occlusion.

	Event	Control (ms)	Occlusion (ms)
Minor axis maximum shortening velocity	M_{maxU}	110 ± 4	93 ± 36
	BCW onset	106 ± 5*CCC* = 0.96	97 ± 36*CCC* = 0.96
	V_{max}	117 ± 16*CCC* = 0.87	103 ± 34*CCC* = 0.97
Long axis maximum shortening velocity	L_{maxU}	147 ± 20	158 ± 20
	FDW (D1)	149 ± 23*CCC* = 0.97	153 ± 30*CCC* = 0.69
	BCW peak	149 ± 22*CCC* = 0.91	164 ± 15*CCC* = 0.65
Rapid phase of the forward decompression wave (D2)	FDW (D2)	191 ± 18	201 ± 22
	L_{III}	190 ± 20*CCC* = 0.86	196 ± 28*CCC* = 0.90
	M_{III}	189 ± 20*CCC* = 0.93	194 ± 25*CCC* = 0.89
	P_{max}	192 ± 27*CCC* = 0.82	204 ± 21*CCC* = 0.90
	U_i	190 ± 17*CCC* = 0.77	196 ± 27*CCC* = 0.92
Wave energies (J/m^2)	FCW	295 ± 198	232 ± 209
	BCW	−42 ± 13	−101 ± 24
	FDW	120 ± 57	78 ± 64

CCC = concordance correlations. During both control and aortic occlusion conditions, the time of maximum shortening velocity of the LV minor axis (M_{maxU}) coincides and has been compared with the time of the arrival of the BCW. The time of maximum shortening velocity of the LV Long axis (L_{maxU}) coincides and has been compared with both the slow onset of the FDW (D1) and the peak of BCW. The rapid phase of the FDW (D2) coincides and has been compared to peak aortic pressure (P), an inflection point on the descending limb of aortic velocity (U_i) and the change in rate of deceleration of the LV minor and long axis during late systole ($L_{Ø}$ and $M_{Ø}$). Plus average energies carried by the forward compression wave (S), reflected compression wave (R), and forward decompression wave (D) at control conditions and during total aortic occlusion. The forward waves are both attenuated during occlusion, while the reflected wave is significantly larger.

(CV = 1%), the onset of the FDW (D1) was 2 ± 3 ms (CV = 1%), and the onset of the FDW (D2) was 1 ± 4 ms (CV = 1%).

Statistical Analysis

All data are presented as mean ± SD. Timings were compared by calculating the mean difference between timings in each dog and the standard deviation of the difference. Statistical agreement between timings was assessed using concordance correlation coefficients (CCC; asymptotic *p*-value) (Lin, 1989). All analyses were performed using Stata 12 (StataCorp) and $p < 0.05$ was considered statistically significant.

RESULTS

Control Conditions

The baseline characteristics of the dogs during control are presented in **Table 1**.

The LV minor axis reached its maximum velocity of shortening, M_{maxU}, at 110 ± 4 ms. The time of M_{maxU} agreed very closely with the arrival time of the reflected waves ($\bar{x} \pm \mathrm{SD_{diff}} = -3 \pm 4$ ms, CCC = 0.96, $p < 0.001$) (**Table 2**) and was shortly followed by V_{max} ($\bar{x} \pm \mathrm{SD_{diff}} = 4 \pm 8$ ms, CCC = 0.87). The long axis reached its maximum velocity of shortening, L_{maxU}, approximately 40 ms after the minor axis (147 ± 20 ms) and after the time of arrival of the reflected wave. However, the time of L_{maxU} corresponded very closely with the time of the peak of the BCW (2 ± 7 ms, CCC = 0.91, $p < 0.001$) (**Table 2**). The onset of the decline in long axis velocity also corresponded with the onset time of the FDW (D1) ($\bar{x} \pm \mathrm{SD_{diff}} = 2 \pm 4$ ms, CCC = 0.97, $p < 0.001$; **Figures 3**, **4A**). Around this time, σ_{max} also occurred (143 ± 32 ms after the R wave).

A later marked decrease in the rate of LV axis shortening occurred almost simultaneously in the long and minor axes (190 ± 20 and 189 ± 20 ms, respectively). This was just prior to closure of the aortic valve (phase III) and corresponded very closely with the onset of D2 (long axis $\bar{x} \pm \mathrm{SD_{diff}} = 0 \pm 3$ ms, CCC = 0.86, $p < 0.001$; minor axis $\bar{x} \pm \mathrm{SD_{diff}} = -1 \pm 1$ ms, CCC = 0.93, $p < 0.001$) (**Figures 4B,C**). This time also coincided with the time of peak aortic pressure (P_{max}) ($\bar{x} \pm \mathrm{SD_{diff}} = 1 \pm 2$ ms, CCC = 0.82, $p < 0.001$) and the occurrence of an inflection point (U_i) on the descending limb of the aortic flow wave ($\bar{x} \pm \mathrm{SD_{diff}} = 0 \pm 1$ ms, CCC = 0.77, $p < 0.001$). As expected, D2 was also seen to coincide with a sharp decline in LV pressure ($\bar{x} \pm \mathrm{SD_{diff}} = 2 \pm 2$ ms, CCC = 0.9, $p < 0.001$) (**Figure 5**).

Aortic Occlusion

To allow mechanistic links between wave reflection and LV shortening velocity to be elucidated, aortic clamping was used to alter the magnitude and timing of the reflected wave. During occlusion, there was a significant increase in systolic, diastolic, mean, and pulse pressure (**Table 1**), and this was accompanied by a significant reduction in arterial compliance but no significant change in heart rate.

Proximal aortic occlusion had a marked effect on wave reflection (**Figure 6**) increasing the energy of the reflected wave by more than twofold and resulting in an earlier arrival of the reflected wave (93 ± 36 ms, i.e., 12 ms earlier than control) although the time of the peak reflection was slightly delayed (164 ± 15 ms, i.e., 15 ms later than control). The FCW wave and FDW wave were reduced by 21 and 35%, respectively, by aortic clamping (**Table 2**). During aortic occlusion, M_{maxU} was reduced by 20% (from 1.5 ± 0.4 to 1.2 ± 0.2 m/s) and the time of M_{maxU} also occurred earlier (97 ± 36 ms); hence, the relationship

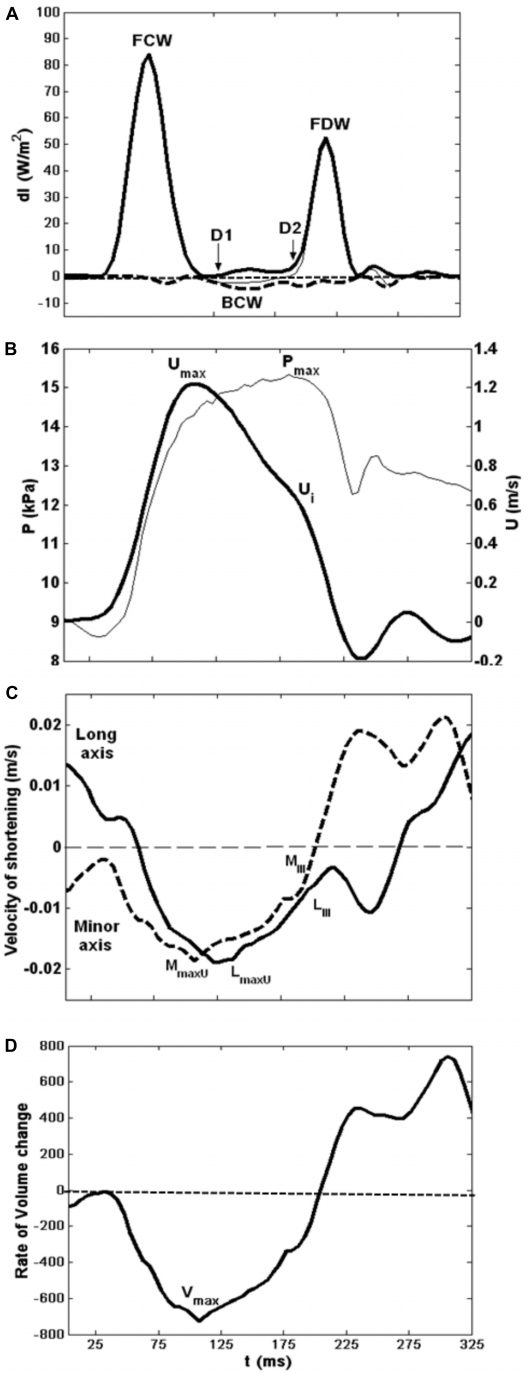

FIGURE 3 | Composite showing all major hemodynamic events in sequence with velocity of LV shortening patterns. **(A)** Wave intensity analysis curves; forward waves (thick line). **(B)** Typical flow velocity waveform (thick line) and aortic pressure trace at the aortic root. **(C)** LV minor (dashed line) and long (solid line) axes shortening speed during systole. **(D)** LV rate of volume change.

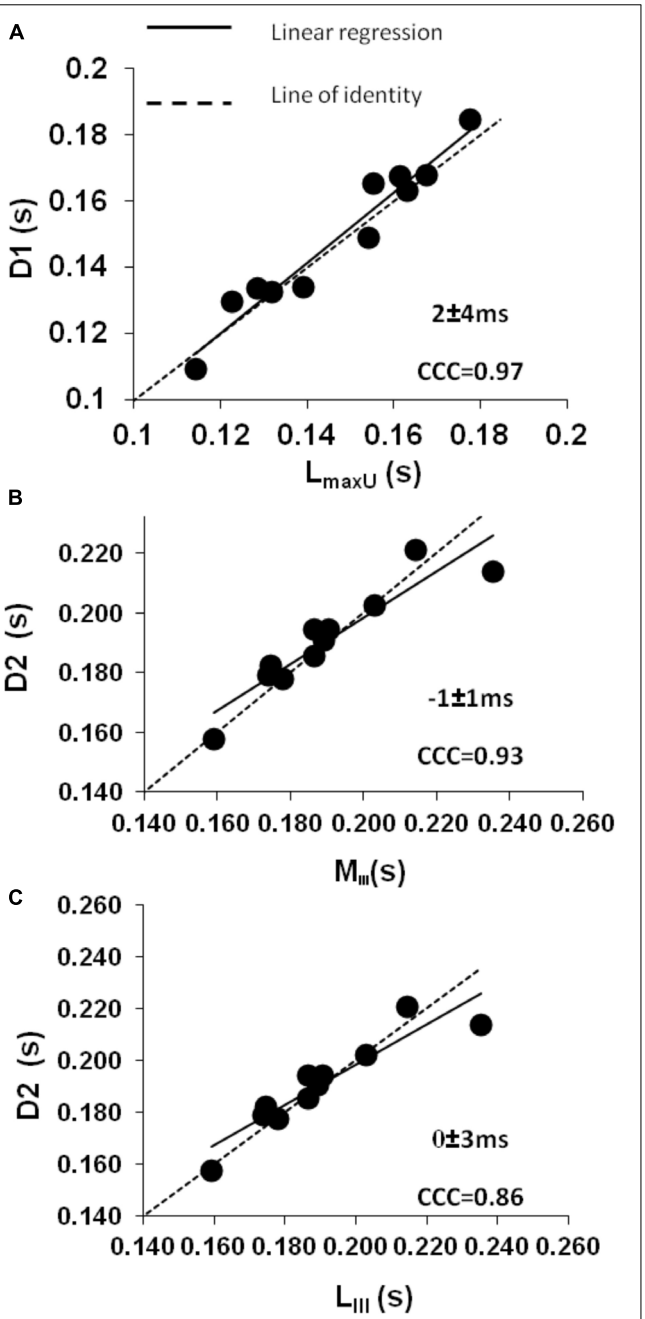

FIGURE 4 | Control conditions: **(A)** intraclass concordance correlation plot (CCC) showing the strong agreement during mid-systole between the slow onset of the forward decompression wave (D1) and the time to maximum shortening velocity of the LV long axis (L_{maxU}). **(B,C)** Intraclass concordance correlation plots (CCC) showing the strong agreement during late systole when a secondary decline in both **(B)** minor (M_{III}) and **(C)** long axis (L_{III}) shortening leads to the rapid phase of the forward decompression wave (D2) which in turn relates to a decrease in aortic pressure (P_{max}) and a further decrease in the rate of declining velocity (U_i).

between the arrival time of the reflected waves and the time of $M_{\mathrm{max}U}$ was preserved ($\bar{x} \pm \mathrm{SD_{diff}}$ = 5 ± 9 ms, CCC = 0.96, $p < 0.001$) (**Table 2** and **Figure 6**). During aortic occlusion, V_{max} still followed the time of $M_{\mathrm{max}U}$ ($\bar{x} \pm \mathrm{SD_{diff}}$ 6 ± 6 ms, CCC = 0.97, $p < 0.001$), $L_{\mathrm{max}U}$ reduced by 11% (from 0.9 ± 0.5 to 0.8 ± 0.2 m/s), and time of the peak reflected wave and $L_{\mathrm{max}U}$

was in good agreement ($\bar{x} \pm SD_{diff}$ = 4 ± 18 ms, CCC = 0.65, $p < 0.001$). This time also corresponded with the onset of FDW (D1) (**Table 2**). Aortic clamping had minimal effects on the timing of L_{III}, M_{III}, and D2 which occurred at approximately the same time (**Table 2**), and σ_{max} was significantly delayed compared to control conditions (200 ± 14 ms, $p < 0.0001$).

DISCUSSION

Waves carry important information about LV function and the interaction between LV and arterial circulation (Jones et al., 1993; Bleasdale et al., 2003). Our aims were to establish whether the arrival of reflected wave(s) affects LV long and minor axes shortening and to establish the relationship between LV shortening and the generation of the FDW in mid-late systole. The main findings are as follows: (1) arrival of reflected waves agrees very closely with the deceleration of the rate of shortening of the LV minor axis and rate of LV volume decline, even when the timing of the arrival of the reflected wave is altered by aortic clamping. This suggests that the arrival of the reflected wave initiates the deceleration of minor axis shortening; (2) the time of the peak of the reflected waves corresponds closely with the onset of deceleration of the rate of shortening of the long axis under control and aortic clamping conditions. This indicates that the reflected wave also plays a part in initiating the decline in deceleration in major axis shortening. (3) The FDW has a slow and then rapid phase, and these phases are explained by two distinct changes in the rate of shortening of the LV axes. The slow phase of the FDW (D1) is generated by deceleration of the LV long axis (i.e., its onset corresponds with the maximum velocity of shortening of the LV long axis), which in turn appears to be related to the peak of the reflected wave. The fast phase of the FDW (D2) is generated by concurrent deceleration of the rate of shortening in both long and minor axes.

Wave Reflection and LV Wall Movement

The reflected wave is believed to play a detrimental role in the pathophysiology of cardiovascular disease in renal failure (London et al., 2001), hypertension (Manisty et al., 2010), and heart failure (Curtis et al., 2007) and to contribute to LV hypertrophy (Hashimoto et al., 2008). By employing aortic clamping as an intervention to cause a defined reflection site, we provide strong evidence for a causal link between arrival of the reflected wave, slowing of minor axis shortening, and peak volume rate of decline with a lesser effect on long axis function. This may have important clinical implications. In humans, long axis shortening is responsible for only 7% of ejection fraction in normal individuals but 18% in people with hypertension (de Simone et al., 1997). We speculate that the relative reduction in the contribution of the minor axis in systemic hypertension may be related to the adverse effects of earlier arrival and larger magnitude of reflected waves although it should be noted that the increase in magnitude of the reflected wave in hypertension is somewhat smaller than that following aortic occlusion (∼70% increase in backward pressure) (Merillon et al., 1983). Differences in long and minor axes' sensitivity to reflected waves could result from differences in timing of the reflected wave in relation to the cross-bridge cycle in fibers of differing orientation. Previous studies have shown that there is a transition point in the cross-bridge cycle during systole; before this transition time, an increase in afterload prolongs contraction, whereas after this time, an increase in afterload abbreviates contraction (Brutsaert et al., 1985; Solomon et al., 1999). If the reflected wave arrives at the LV during the critical transitional time of minor axis contraction, this would promote cross-bridge detachment and early LV relaxation. Since in our study long axis contraction began after short axis contraction, it may be that this susceptible period occurs later in the cardiac cycle for the long axis. Further research on this issue is required.

Left Ventricle Wall Motion and the Forward Decompression Wave

Sugawara et al. (1997) have previously proposed that a forward decompression wave is generated in late systole by the LV due to "both the loss of tension bearing ability caused by myocardial relaxation and the deceleration of aortic blood flow caused by the reduced rate of myocardial shortening." This is analogous to the situation in isolated cardiac tissue, where contraction ceases before tension-bearing ability declines (Brutsaert and Sys, 1989). This explanation was supported by Niki et al. (1999) who showed that patients with mitral regurgitation had a much reduced FDW which increased following mitral valve surgery. Our data are consistent with this view, although they suggest a more complex pattern to the FDW in mid-late systole, with two distinct phases (D1 and D2). Jones et al. (2002) suggested that FDW may have been generated by two temporally distinct processes, such as the slowing of the myocardial shortening and complete cessation of myocardial shortening. We observed that D2 does not correspond to complete cessation of myocardial shortening but instead it coincides with a simultaneous decline in the velocity of shortening of both the minor and long axes later in systole. The mechanism responsible for the secondary change in velocity of deceleration of both LV axes is not known, but it is plausible that it corresponds to the release of torsion and radial thinning of the ventricle that is observed ∼40 ms before aortic valve closure (Rosen et al., 2004). The release of torsion would bring about a rapid decrease in LV pressure and a decrease in the rate of ejection resulting in a rapid increase in the intensity of the FDW (online **Figure 4**).

The strength of this study is the direct, invasive measurement of the reflected wave and left ventricular velocities. No assumptions about the timing and magnitude of waves were made, and measuring pressure and flow simultaneously to calculate wave intensity is superior to pressure waveform analysis alone. This work provides insight into how wave reflection influences LV function and wave generation. Wave reflection causes a deceleration in LV shortening and the function of the minor axis is particularly sensitive to the arrival of reflected waves. These observations lend support to previous suggestions that therapies directed toward reducing wave reflection may be of value in hypertension and cardiovascular disease.

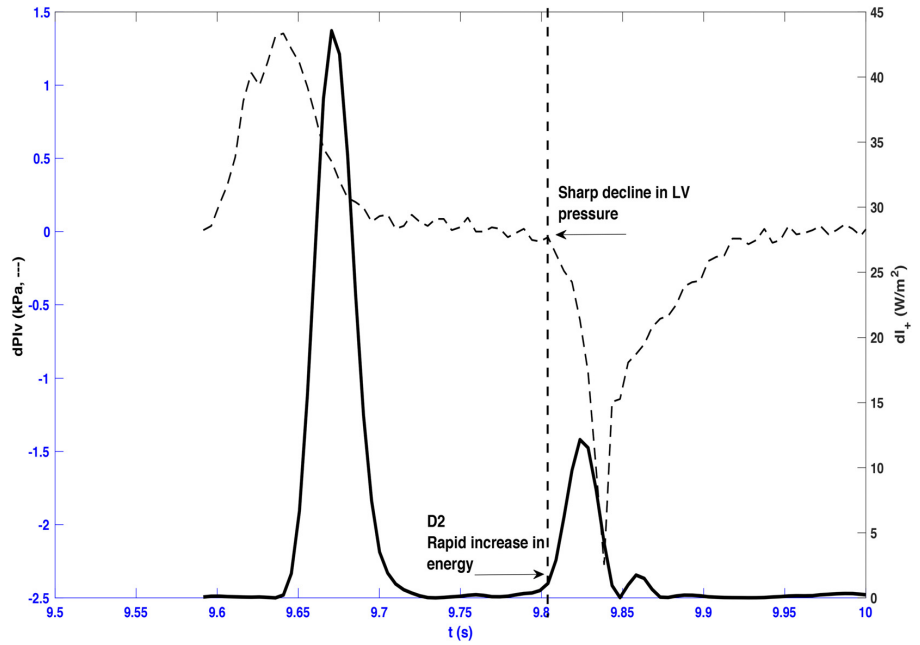

FIGURE 5 | Forward wave intensity and differentiated left ventricle pressure (dPlv) plotted from a representative beat taken from dog 3. A sharp decline in left ventricle pressure coincides with the onset of the rapid increase of the forward decompression wave (D2) as indicated by the vertical dashed line.

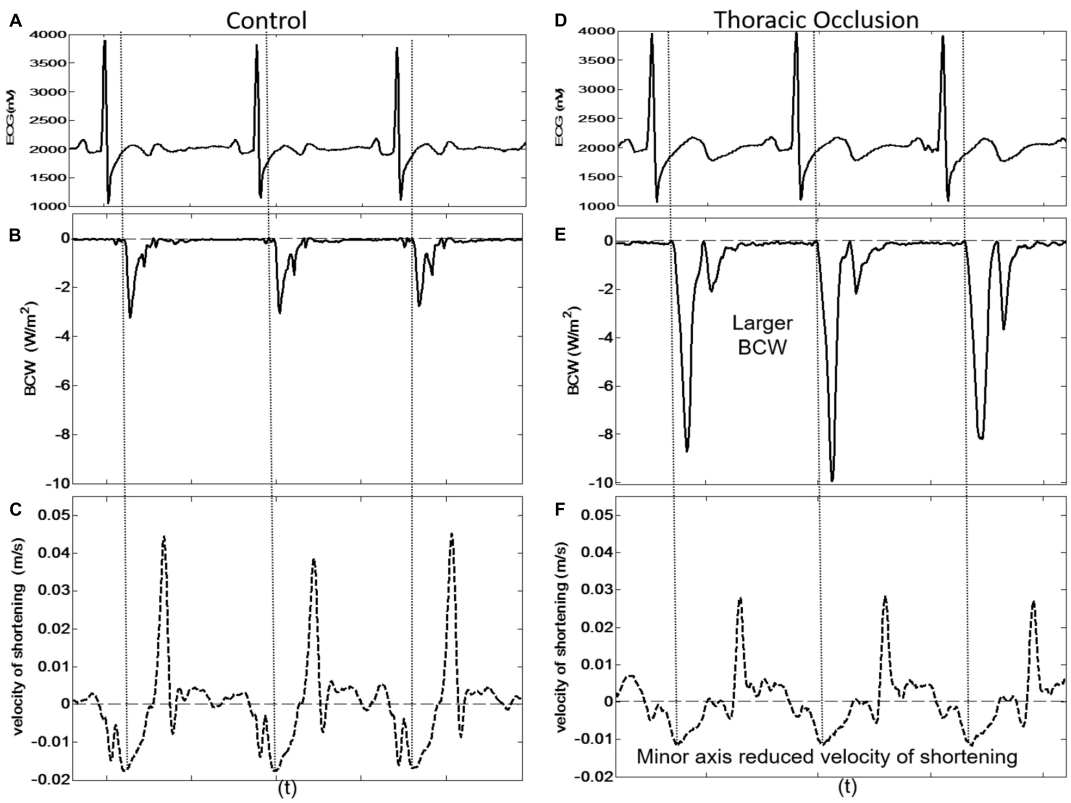

FIGURE 6 | Three consecutive beats taken from dog 9 showing the simultaneous arrival of the BCW at the LV and reduced peak velocity of shortening of the LV minor axis during control conditions [**(A)** ECG, **(B)** BCW, **(C)** minor axis velocity of shortening] and during thoracic occlusion [**(D)** ECG, **(E)** BCW, **(F)** minor axis velocity of shortening].

A limitation of the study was that only longitudinal and radial motion were studied (i.e., base–apex and septum–free wall). Changes in LV geometry over the cardiac cycle are intrinsically complex, particularly during ejection, and possible effects of rotation could not be accounted for in our study. However, the crystals used for measuring the axial movement were embedded into the myocardium at the mid-level where rotation is minimal, and thus, this should not invalidate our principal conclusions. Nevertheless, further studies resolving the full three-dimensional strain patterns in the ventricle would be valuable. A further limitation is the lack of wall thickness measurements to investigate the effect of wave reflection on myocardial stress in more detail. A final limitation is the assumption that the aortic area is uniform throughout the cardiac cycle, and we cannot rule out the possibility of aortic distortion during the cross-clamping in or variability during the cardiac cycle (de Heer et al., 2011).

CONCLUSION

In conclusion, This is the first study to simultaneously measure the arrival of reflected waves during systole with LV long and minor axes function. These measurements provided strong evidence that the arrival of the reflected wave initiates a deceleration in LV minor axis shortening. The data have also shown that the forward decompression wave generated by the LV has a slow and then rapid phase that are generated by two distinct changes in the rate of shortening of the LV axes. The results of this work are physiologically and clinically relevant as increased wave reflection causes a reduction in the contraction velocity of the LV. Reducing wave reflection may be of value in hypertension and cardiovascular disease patients.

DATA AVAILABILITY STATEMENT

The raw data supporting the conclusions of this article will be made available by the authors, without undue reservation.

ETHICS STATEMENT

The animal study was reviewed and approved by animal care committee, Calgary University.

AUTHOR CONTRIBUTIONS

CP: data analysis, manuscript drafting, figures, and table production. AH: statistical analysis, data interpretation, and manuscript editing. MH: data interpretation and clinical implication and manuscript editing. AK: manuscript concept, data collection and interpretation and manuscript editing. All authors contributed to the article and approved the submitted version.

ACKNOWLEDGMENTS

The experiments of this study were performed in the course of a doctoral fellowship in the laboratory of Prof. John V. Tyberg at the University of Calgary, whose generous cooperation the authors gratefully acknowledge. We also acknowledge the excellent technical support of Cheryl Meek and Gerry Groves.

REFERENCES

Arts, T., Bovendeerd, P. H., Prinzen, F. W., and Reneman, R. S. (1991). Relation between left ventricular cavity pressure and volume and systolic fiber stress and strain in the wall. *Biophys. J.* 59, 93–102. doi: 10.1016/s0006-3495(91)82201-9

Baksi, A. J., Treibel, T. A., Davies, J. E., Hadjiloizou, N., Foale, R. A., Parker, K. H., et al. (2009). A meta-analysis of the mechanism of blood pressure change with aging. *J. Am. Coll. Cardiol.* 54, 2087–2092. doi: 10.1016/j.jacc.2009.06.049

Bleasdale, R. A., Parker, K. H., and Jones, C. J. (2003). Chasing the wave. Unfashionable but important new concepts in arterial wave travel. *Am. J. Physiol. Heart Circ.* 284, H1879–H1885.

Brutsaert, D. L., Rademakers, F. E., Sys, S. U., Gillebert, T. C., and Housmans, P. R. (1985). Analysis of relaxation in the evaluation of ventricular function of the heart. *Prog. Cardiovasc. Dis.* 28, 143–163.

Brutsaert, D. L., and Sys, S. U. (1989). Relaxation and diastole of the heart. *Physiol. Rev.* 69, 1228–1315. doi: 10.1152/physrev.1989.69.4.1228

Codreanu, I., Robson, M. D., Rider, O. J., Pegg, T. J., Jung, B. A., Dasanu, C. A., et al. (2011). Chasing the reflected wave back into the heart: a new hypothesis while the jury is still out. *Vasc. Health Risk Manag.* 7, 365–373. doi: 10.2147/vhrm.s20845

Curtis, S. L., Zambanini, A., Mayet, J., McG Thom, S. A., Foale, R., Parker, K. H., et al. (2007). Reduced systolic wave generation and increased peripheral wave reflection in chronic heart failure. *Am. J. Physiol. Heart Circ.* 293, H557–H562.

de Heer, L. M., Budde, R. P. J., Mali, W., de Vos, A. M., van Herwerden, L. A., and Kluin, J. (2011). Aortic root dimension changes during systole and diastole: evaluation with ECG-gated multidetector row computed tomography. *Int. J. Cardiovas. Imaging* 27, 1195–1204. doi: 10.1007/s10554-011-9838-x

de Simone, G., Ganau, A., Roman, M. J., and Devereux, R. B. (1997). Relation of left ventricular longitudinal and circumferential shortening to ejection fraction in the presence or in the absence of mild hypertension. *J. Hypertens.* 15, 1011–1017. doi: 10.1097/00004872-199715090-00012

Greenbaum, R. A., Ho, S. Y., Gibson, D. G., Becker, A. E., and Anderson, R. H. (1981). Left ventricular fibre architecture in man. *Br. Heart J.* 45, 248–263. doi: 10.1136/hrt.45.3.248

Hashimoto, J., Nichols, W. W., O'Rourke, M. F., and Imai, Y. (2008). Association between wasted pressure effort and left ventricular hypertrophy in hypertension: influence of arterial wave reflection. *Am. J. Hypertens.* 21, 329–333. doi: 10.1038/ajh.2007.49

Henein, M. Y., and Gibson, D. G. (1999). Normal long axis function. *Heart* 81, 111–113. doi: 10.1136/hrt.81.2.111

Hollander, E. H. (1999). *Wave Intensity Analysis of Pulmonary Arterial Blood Flow in Anethetised Dogs*. Calgary, AB: University of Calgary.

Jones, C. J., Sugawara, M., Kondoh, Y., Uchida, K., and Parker, K. H. (2002). Compression and expansion wavefront travel in canine ascending aortic flow: wave intensity analysis. *Heart Vessels* 16, 91–98. doi: 10.1007/s003800200002

Jones, C. J. H., Sugawara, M., Davies, R. H., Kondoh, Y., Uchida, K., and Parker, K. H. (1993). "Arterial wave intensity: physical meaning and physiological significance," in *Recent Progress in Cardiovascular Mechanics*, eds H. Hosoda, T. Yaginum, M. Sugawara, M. G. Taylor, and C. G. Caro (Chur: Harwood Academic Publishers), 129–148.

Khir, A. W., O'Brien, A., Gibbs, J. S., and Parker, K. H. (2001). Determination of wave speed and wave separation in the arteries. *J. Biomech.* 34, 1145–1155. doi: 10.1016/s0021-9290(01)00076-8

Lin, L. I. (1989). A concordance correlation coefficient to evaluate reproducibility. *Biometrics* 45, 255–268. doi: 10.2307/2532051

London, G. M., Blacher, J., Pannier, B., Guerin, A. P., Marchais, S. J., and Safar, M. E. (2001). Arterial wave reflections and survival in end-stage renal failure. *Hypertension* 38, 434–438. doi: 10.1161/01.hyp.38.3.434

Manisty, C., Mayet, J., Tapp, R. J., Parker, K. H., Sever, P., Poulter, N. R., et al. (2010). Wave reflection predicts cardiovascular events in hypertensive individuals independent of blood pressure and other cardiovascular risk factors: an ASCOT (Anglo-scandinavian cardiac outcome trial) substudy. *J. Am. Coll. Cardiol.* 56, 24–30. doi: 10.1016/j.jacc.2010.03.030

Merillon, J. P., Lebras, Y., Chastre, J., Lerallut, J. F., Motte, G., Fontenier, G., et al. (1983). Forward and backward waves in the arterial system, their relationship to pressure waves form. *Eur. Heart J.* 4(Suppl. G), 13–20. doi: 10.1093/eurheartj/4.suppl_g.13

Nagueh, S. F., Middleton, K. J., Kopelen, H. A., Zoghbi, W. A., and Quinones, M. A. (1997). Doppler tissue imaging: a noninvasive technique for evaluation of left ventricular relaxation and estimation of filling pressures. *J. Am. Coll. Cardiol.* 30, 1527–1533. doi: 10.1016/s0735-1097(97)00344-6

Niki, K., Sugawara, M., Uchida, K., Tanaka, R., Tanimoto, K., Imamura, H., et al. (1999). A noninvasive method of measuring wave intensity, a new hemodynamic index: application to the carotid artery in patients with mitral regurgitation before and after surgery. *Heart Vessels* 14, 263–271. doi: 10.1007/bf03257237

O'Rourke, M. F., and Safar, M. E. (2005). Relationship between aortic stiffening and microvascular disease in brain and kidney: cause and logic of therapy. *Hypertension* 46, 200–204. doi: 10.1161/01.hyp.0000168052.00426.65

Page, C. M., Khir, A. W., Hughes, A. D., Chung, R., and Henein, M. Y. (2010). Normal asynchrony of left ventricular long and short axes: their relationship with aortic hemodynamics. *Int. J. Cardiol.* 142, 166–171. doi: 10.1016/j.ijcard.2008.12.188

Parker, K. H. (2009). An introduction to wave intensity analysis. *Med. Biol. Eng. Comput.* 47, 175–188. doi: 10.1007/s11517-009-0439-y

Parker, K. H., Jones, C. J., Dawson, J. R., and Gibson, D. G. (1988). What stops the flow of blood from the heart? *Heart Vessels* 4, 241–245. doi: 10.1007/bf02058593

Regen, D. M. (1990). Calculation of left ventricular wall stress. *Circ. Res.* 67, 245–252. doi: 10.1161/01.res.67.2.245

Rosen, B. D., Gerber, B. L., Edvardsen, T., Castillo, E., Amado, L. C., Nasir, K., et al. (2004). Late systolic onset of regional LV relaxation demonstrated in three-dimensional space by MRI tissue tagging. *Am. J. Physiol. Heart Circ. Physiol.* 287, H1740–H1746.

Solomon, S. B., Nikolic, S. D., Frater, R. W., and Yellin, E. L. (1999). Contraction-relaxation coupling: determination of the onset of diastole. *Am. J. Physiol.* 277, H23–H27.

Sugawara, M., Uchida, K., Kondoh, Y., Magosaki, N., Niki, K., Jones, C. J., et al. (1997). Aortic blood momentum–the more the better for the ejecting heart in vivo? *Cardiovasc. Res.* 33, 433–446. doi: 10.1016/s0008-6363(96)00241-6

Torrent-Guasp, F., Kocica, M. J., Corno, A. F., Komeda, M., Carreras-Costa, F., Flotats, A., et al. (2005). Towards new understanding of the heart structure and function. *Eur. J. Cardiothorac. Surg.* 27, 191–201. doi: 10.1016/j.ejcts.2004.11.026

Wang, Z., Jalali, F., Sun, Y. H., Wang, J. J., Parker, K. H., and Tyberg, J. V. (2005). Assessment of left ventricular diastolic suction in dogs using wave-intensity analysis. *Am. J. Physiol. Heart Circ.* 288, H1641–H1651.

Westerhof, N., and O'Rourke, M. F. (1995). Haemodynamic basis for the development of left ventricular failure in systolic hypertension and for its logical therapy. *J. Hypertens.* 13, 943–952. doi: 10.1097/00004872-199509000-00002

Zambanini, A., Khir, A. W., Byrd, S. M., Parker, K. H., Thom, S. A. M., and Hughes, A. D. (2002). *Wave Intensity Analysis: A Novel Non-Invasive Method for Determining Arterial Wave Transmission*. New York, NY: IEEE.

Conflict of Interest: The authors declare that the research was conducted in the absence of any commercial or financial relationships that could be construed as a potential conflict of interest.

frontiers in Physiology

ORIGINAL RESEARCH
published: 23 February 2021
doi: 10.3389/fphys.2021.608098

Estimating Central Pulse Pressure From Blood Flow by Identifying the Main Physical Determinants of Pulse Pressure Amplification

Joaquín Flores Gerónimo[1]*, *Eugenia Corvera Poiré*[2,3], *Philip Chowienczyk*[4] and *Jordi Alastruey*[1,5]

[1] Department of Biomedical Engineering, School of Biomedical Engineering and Imaging Sciences, King's College London, London, United Kingdom, [2] Departamento de Física y Química Teórica, Facultad de Química, Universidad Nacional Autónoma de México, Ciudad Universitaria, Mexico City, Mexico, [3] Universitat de Barcelona Institute of Complex Systems (UBICS), Universitat de Barcelona, Barcelona, Spain, [4] Department of Clinical Pharmacology, British Heart Foundation Centre, St Thomas' Hospital, King's College London, London, United Kingdom, [5] World-Class Research Center, Digital Biodesign and Personalized Healthcare, Sechenov University, Moscow, Russia

Several studies suggest that central (aortic) blood pressure (cBP) is a better marker of cardiovascular disease risk than peripheral blood pressure (pBP). The morphology of the pBP wave, usually assessed non-invasively in the arm, differs significantly from the cBP wave, whose direct measurement is highly invasive. In particular, pulse pressure, PP (the amplitude of the pressure wave), increases from central to peripheral arteries, leading to the so-called pulse pressure amplification (ΔPP). The main purpose of this study was to develop a methodology for estimating central PP (cPP) from non-invasive measurements of aortic flow and peripheral PP. Our novel approach is based on a comprehensive understanding of the main cardiovascular properties that determine ΔPP along the aortic-brachial arterial path, namely brachial flow wave morphology in late systole, and vessel radius and distance along this arterial path. This understanding was achieved by using a blood flow model which allows for workable analytical solutions in the frequency domain that can be decoupled and simplified for each arterial segment. Results show the ability of our methodology to (i) capture changes in cPP and ΔPP produced by variations in cardiovascular properties and (ii) estimate cPP with mean differences smaller than 3.3 ± 2.8 mmHg on *in silico* data for different age groups (25–75 years old) and 5.1 ± 6.9 mmHg on *in vivo* data for normotensive and hypertensive subjects. Our approach could improve cardiovascular function assessment in clinical cohorts for which aortic flow wave data is available.

Keywords: pulse pressure amplification, 1-D model, peripheral pressure, central pressure, analytical solutions, hemodynamics

OPEN ACCESS

Edited by:
Giovanni Biglino, University of Bristol, United Kingdom

Reviewed by:
Chloe May Park, University College London, United Kingdom
Ramakrishna Mukkamala, University of Pittsburgh, United States

***Correspondence:**
Joaquín Flores Gerónimo
joaquin.flores@kcl.ac.uk

Specialty section:
This article was submitted to Vascular Physiology, a section of the journal Frontiers in Physiology

Received: *18 September 2020*
Accepted: *18 January 2021*
Published: *23 February 2021*

Citation:
Flores Gerónimo J, Corvera Poiré E, Chowienczyk P and Alastruey J (2021) Estimating Central Pulse Pressure From Blood Flow by Identifying the Main Physical Determinants of Pulse Pressure Amplification. Front. Physiol. 12:608098. doi: 10.3389/fphys.2021.608098

1. INTRODUCTION

Peripheral systolic blood pressure is the most commonly used measure of circulatory function and cardiovascular risk. However, a significant predictive benefit has been observed when measuring central (aortic) blood pressure (cBP) (Agabiti-Rosei and Muiesan, 2015; Williams et al., 2018) and it has been suggested that cBP should be a better indicator of risk (Agabiti-Rosei et al., 2007; Avolio et al., 2009; Sharman et al., 2013; McEniery et al., 2014; Agabiti-Rosei and Muiesan, 2015; Williams et al., 2017) since it is more representative of the load exerted on major organs

(Herbert et al., 2014; Agabiti-Rosei and Muiesan, 2015; Williams et al., 2017). For instance, elevation of cBP induces coronary arteriosclerosis which in turn can lead to adverse events such as stenosis and myocardial infarction (Agabiti-Rosei et al., 2007) and causes chronic kidney disease that can advance to end-stage renal disease (Safar et al., 2002; Ohno et al., 2016). Additionally, it has been suggested that cBP assessment can improve therapeutic decisions since anti-hypertensive drugs have different effects on peripheral and central pressure values (Sharman et al., 2013; McEniery et al., 2014; Agabiti-Rosei and Muiesan, 2015).

The morphology of the peripheral blood pressure (pBP) wave, usually assessed non-invasively in the arm, differs significantly from the morphology of the cBP wave, whose direct measurement is highly invasive. In particular, pulse pressure (PP)—the difference between systolic and diastolic blood pressures—often increases from central to peripheral arteries leading to the so-called pulse pressure amplification (ΔPP) (**Figure 1**). The cBP wave can be estimated using population-based generalized transfer functions (GTFs) from a calibrated pBP wave; however the debate continues on the suitability of this approach for all patients and conditions (Avolio et al., 2009; Shih et al., 2011). Several studies have proposed an adaptive transfer function technique which personalizes some of the parameters of a single-tube transmission line model coupled to an impedance boundary condition that reflects incoming pulse waves (Swamy et al., 2009; Hahn et al., 2012; Gao et al., 2016; Natarajan et al., 2017). Such an approach can improve the accuracy of the estimated cBP waveform compared to the GTF approach. In addition, the pressure wave measured in the common carotid artery has been used as a surrogate for the cBP wave; however reproducible pressure waves are more difficult to obtain at the carotid artery than at the radial artery due to anatomical reasons (Avolio et al., 2009).

Understanding the effect of cardiovascular parameters on ΔPP could improve cBP assessment from non-invasive pBP measurements; specially central PP (cPP) assessment which has been shown to be of greater predictive value for cardiovascular outcomes than brachial PP (Safar et al., 2002; Williams et al., 2006). Large ΔPP values have been associated with male sex (Segers et al., 2009; Herbert et al., 2014), higher heart rate (Wilkinson et al., 2002), height (Asmar et al., 1997; Camacho et al., 2004), mass index (Pichler et al., 2016), pulse transit time (Gao et al., 2016; Natarajan et al., 2017), and wave reflection coefficient (Gao et al., 2016), and lower age (Wilkinson et al., 2001; Herbert et al., 2014) and pulse wave velocity (Hashimoto and Ito, 2010; Pierce et al., 2012), and is significantly influenced by cardiovascular risk factors, such as hypertension and obesity (Herbert et al., 2014). Experimental and computational models have been used to study the effect on ΔPP of cardiovascular properties (Karamanoglu et al., 1995; Figueroa and Humphrey, 2014; Mynard and Smolich, 2015; Gaddum et al., 2017) and age (Charlton et al., 2019), showing that ΔPP raises with increasing ventricular inotropy (contractile state of the ventricle), tapering, peripheral load and vessel length; and decreasing wall thickness and age. However, there are currently no methods based on the physics of blood flow in the systemic arterial tree that enable explicit analytical identification of the main cardiovascular determinants of ΔPP—and hence estimation of cPP from peripheral PP (pPP)—from data that can be acquired non-invasively for a specific subject.

The main purpose of this study was to develop a methodology for estimating cPP from non-invasive measurements of blood flow (aortic or brachial) and pPP. Our novel approach is based on a comprehensive understanding—using the physics of blood flow—of the main cardiovascular properties that determine ΔPP along the aortic-brachial arterial path. The methodology presented in this study was assessed using *in silico* data generated by blood flow modeling and *in vivo* data measured in normotensive and hypertensive subjects. These datasets included reference cPP values.

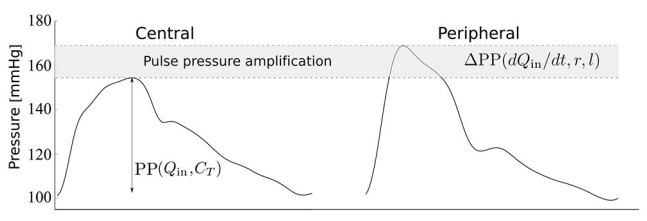

FIGURE 1 | Central and peripheral pressure waveforms. Central pulse pressure, cPP, is mainly determined by the blood flow ejected by the ventricle into the aorta, Q_{in}, and the total arterial compliance, C_T (Vennin et al., 2017). Peripheral PP amplification, ΔPP, is mainly determined by the rate of change of Q_{in} with time, t, in late systole and the radius, r, and length, l, of the brachial artery, as shown in this study.

2. MATERIALS AND METHODS

2.1. *In vivo* Data

We used previously available measurements of cBP and pBP waveforms in a group of normotensive volunteers ($n = 26$) and hypertensive subjects ($n = 57$) (Fok et al., 2014a; Li et al., 2017). Subjects were recruited from those who were evaluated for hypertension at Guy's and St Thomas' Hypertension Clinic. Although they were referred for evaluation of hypertension, blood pressure settled in some subjects and the sample included some who were normotensive (Li et al., 2017). Subjects with significant valvular disease, impaired left ventricular systolic function (ejection fraction <45%), and arrhythmia were excluded. 60% of the hypertensive subjects were on treatment with anti-hypertensive medications. Characteristics of both groups are given in **Table 1**. Radial and carotid pressure waveforms were obtained by applanation tonometry performed by an experienced operator using the SphygmoCor system (AtCor, Australia). Ensemble-averaged carotid pressure was used as surrogate for ascending aortic pressure (Chen et al., 1996). Approximately 10 cardiac cycles were obtained and ensemble averaged. Brachial blood pressure was measured in triplicate by a validated oscillometric method (Omron 705CP, Omron Health Care, Japan) and used to calibrate radial waveforms and, thus, to obtain a mean arterial pressure (MAP) through integration of the radial waveform. Carotid waveforms were calibrated from MAP and diastolic brachial blood pressures

TABLE 1 | Characteristics of the datasets: normotensive (second column) and hypertensive (third column) *in vivo* subjects and *in silico* subjects (fourth column).

Characteristic	Normotensives ($n = 26$)	Hypertensives ($n = 57$)	*In silico* ($n = 4374$)
Age (years)	44 ± 14	40 ± 13	50 ± 17
Sex (male %)	58	65	100
Height (m)	1.72 ± 0.03	1.72 ± 0.09	1.76 ± 0.00
Weight (kg)	79.2 ± 7.7	79.4 ± 13.4	-
Heart rate (bpm)	62 ± 8	62 ± 10	76 ± 9
r_{Ao} (cm)	0.96 ± 0.12	0.98 ± 0.11	1.97 ± 0.19
r_{Bra} (cm)	0.20 ± 0.03	0.20 ± 0.03	0.45 ± 0.05
SV (mL)	55.4 ± 15.8	52.4 ± 13.9	60.4 ± 12.4
$(\Delta Q_{in}/\Delta t)_{Ao}$ (mL/s^2)	1550 ± 464	1580 ± 405	1966 ± 270
$dQ_{in}/dt\|_{min,Bra}$ (mL/s^2)	96 ± 35	98 ± 31	434 ± 83
cPP (mmHg)	39.7 ± 12.3	45.6 ± 13.5	35.0 ± 15.3
pPP (mmHg)	51.0 ± 12.0	54.1 ± 14.7	50.2 ± 13.6
ΔPP (mmHg)	11.2 ± 6.4	11.5 ± 7.5	15.5 ± 5.2
R_T (mmHg s/mL)	1.96 ± 0.55	2.20 ± 0.70	1.27 ± 0.31
C_T (mL/mmHg)	1.15 ± 0.48	1.04 ± 0.40	0.85 ± 0.30

Values are percentage or mean ± SD. r_{Ao}, aortic radius; r_{Bra}, brachial radius; SV, stroke volume; $(\Delta Q_{in}/\Delta t)_{Ao}$, approximate maximum temporal rate of decrease in late-systolic flow at the ascending aorta; $dQ_{in}/dt|_{min,Bra}$, maximum temporal rate of decrease in late-systolic flow at the brachial artery; cPP, central pulse pressure; pPP, peripheral pulse pressure; ΔPP, pulse pressure amplification; R_T, total vascular resistance; C_T, total vascular compliance. r_{Bra} and $dQ_{in}/dt|_{min,Bra}$ for the in vivo datasets were estimated from the corresponding data in the aorta using Equations (16) and (17), respectively.

on the assumption of equality of these pressures at central and peripheral sites (Pauca et al., 1992). Ultrasound imaging was performed by an experienced operator using the Vivid-7 ultrasound platform (General Electric Healthcare, United Kingdom). Velocity above the aortic valve was recorded using pulsed wave Doppler obtained from an apical 5-chamber view. All ultrasound measurements were averaged over at least 3 cardiac cycles. Cross-sectional area of the aortic valve (obtained in the parasternal long-axis view) was used to estimate the aortic radius. These data were acquired in a previous study approved by the London Westminster Research Ethics Committee, for which written informed consent was obtained (Li et al., 2017).

2.2. Dataset of *in silico* Pulse Waves

We used an existing dataset containing *in silico* cBP and pBP waves measured, respectively, at the aortic root and outlet of the brachial artery, and blood flow waves measured at the aortic root, in a group of 4,374 virtual subjects. Characteristics of the *in silico* group are given in **Table 1**. Pulse waves were simulated for subjects of each age decade, from 25 to 75 years old, using a 116-artery, one-dimensional (1-D) model of blood flow in the larger systemic arteries of the thorax, limbs, and head (**Figure 2A**). The model cardiovascular properties were identified through a comprehensive literature review and simulated pulse waves were verified by comparison against clinical data [see Charlton et al. (2019) for full details].

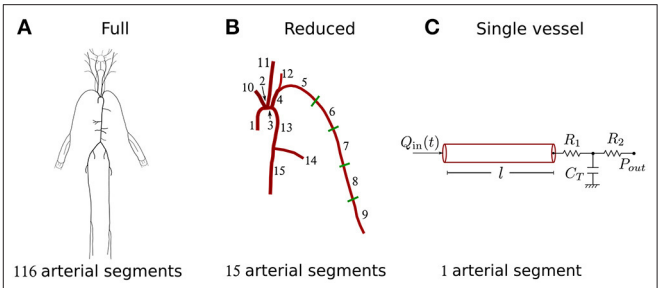

FIGURE 2 | Schematic representation of the three models used in the study. **(A)** Full 116-artery model with cardiovascular properties taken from Charlton et al. (2019). **(B)** Reduced 15-artery model containing the aortic-brachial arterial path of the full model. **(C)** Single-vessel model of the brachial artery with the nomenclature used throughout the study. Tapering in the brachial artery of the full and reduced models was represented by five straight arterial segments of different radii. The single-vessel model allowed us to identify analytically the main physical determinants of ΔPP.

2.3. Blood Flow Models

Three blood flow models with decreasing level of mathematical complexity were employed in this study (**Figure 2**). Firstly, we used the 116-artery model of the systemic circulation described above. Blood pressure and flow waves at any point in the arterial network were simulated using our in-house, linear, one-dimensional (1-D) formulation, which enables analytical solutions in the frequency domain and has previously been verified against computational 1-D and 3-D solutions (Flores Gerónimo et al., 2016). This model—hereafter referred to as the "full model"—provided reference cBP and pBP waves to assess the accuracy of the other two simpler models.

The second model simulated blood flow in the 15 arterial segments that make up the upper thoracic aorta and left brachial artery of the full model. This model hereafter referred to as the "reduced model"—has the same inflow waveform prescribed at the aortic root as the full model. Such inflow waveform was obtained by the *AorticFlowWave* script described in Charlton et al. (2019) for the desired inflow characteristics (heart rate, stroke volume and left ventricular ejection time). **Figure 3A** shows the inflow waveform for the 25 year-old baseline subject. The vascular network of the reduced model was obtained from the full model by lumping groups of arteries into optimized three-element windkessel (WK) models that preserved the total vascular compliance and resistance of the full model. Six sets of WK parameters were calculated, for the six terminal segments of the reduced model, from the flow and pressure waves produced by the full model using a gradient descent algorithm previously described in Fossan et al. (2018). **Table 2** shows the vascular parameters of the reduced model that was able to reproduce pressure and flow waves along the aortic-brachial arterial path with relative errors smaller than 3 and 10%, respectively (**Figure 3**). All relative errors in this figure were calculated using the full model as a reference, as described in **Supplementary Section 1**.

The reduced model provided accurate and workable analytical solutions for blood pressure and flow waves along the aortic-brachial arterial path. It was further simplified into a third model:

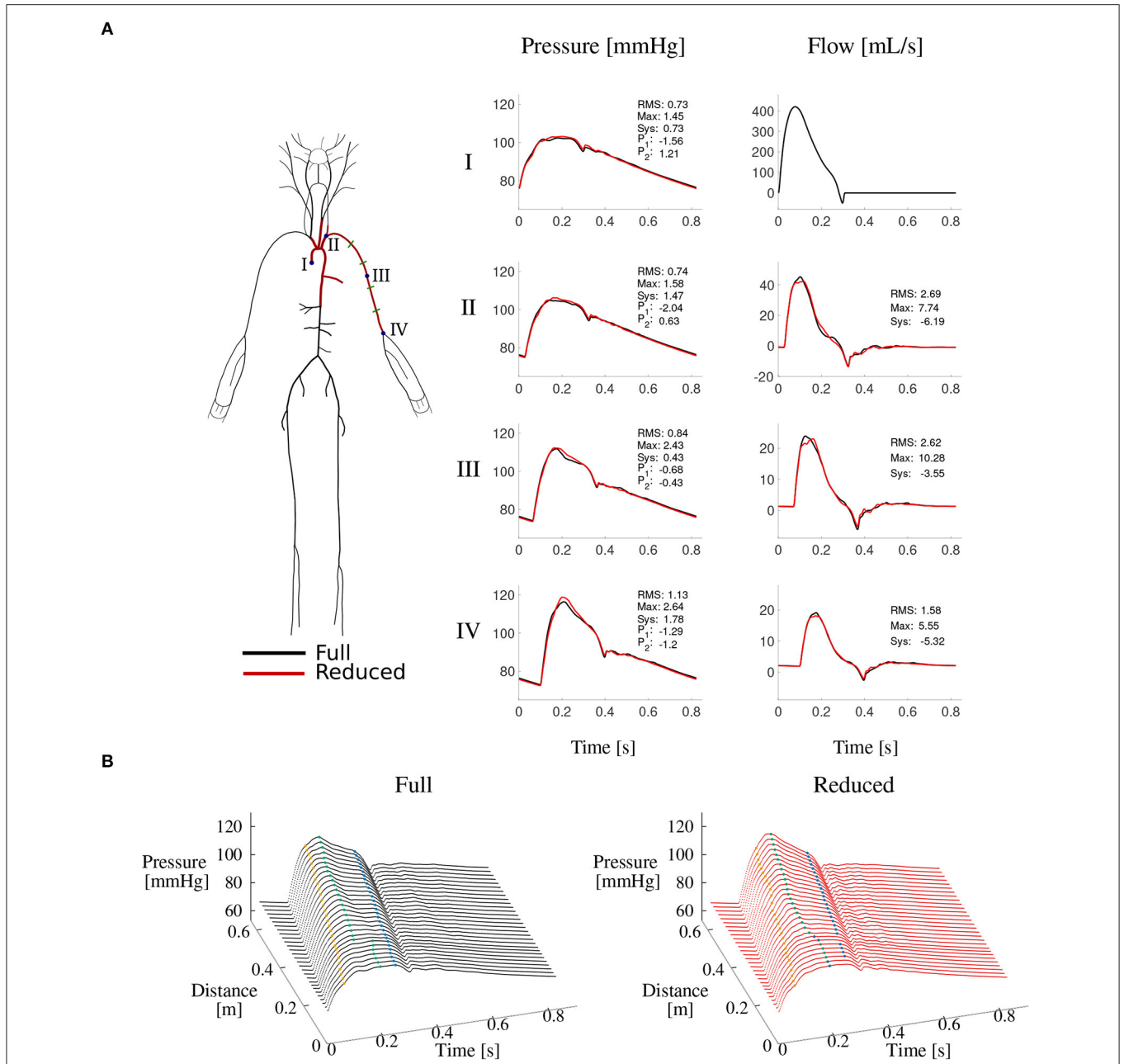

FIGURE 3 | Reduced vs. full model pressure and flow waves. **(A)** Schematic representations of both models (left) and comparison of corresponding pressure and flow waves at four locations along the aortic-brachial arterial path (right). Each plot shows relative errors (expressed as percentages) for average (RMS), maximum (Max), systolic (Sys) and characteristic pressure points P_1 and P_2 calculated as described in **Supplementary Section 1**. **(B)** Pressure wave along the same arterial path, for the full (left) and reduced (right) model. Characteristic pressure points P_1 (yellow), systolic pressure (green), and P_2 (blue) are shown in each plot.

a straight single-vessel model of the brachial artery which enabled us to identify analytically the main physical determinants of ΔPP, as described in the next sections.

2.3.1. Single-Vessel Model

Blood pressure in the frequency domain, $\hat{p}(x,\omega)$, along the single-vessel model (**Figure 2C**) can be described by the summation of an attenuation, $\hat{T}_1(x,\omega)$, and an amplification, $\hat{T}_2(x,\omega)$, term based on the formulation described by Flores Gerónimo et al. (2016) (see **Supplementary Section 2**); i.e.,

$$\hat{p} = \hat{T}_1 + \hat{T}_2, \tag{1}$$

where

$$\hat{T}_1 = \left[\frac{\cos(k_c l)\hat{Z}M + \sin(k_c l)}{\cos(k_c l) - \hat{Z}M\sin(k_c l)}\right]\cos(k_c x)\frac{\hat{Q}_{\text{in}}}{M}, \tag{2}$$

TABLE 2 | Vascular parameters of the reduced model.

Arterial segment	Length (cm)	r_d (mm)	Eh (Pa m)	R_1 (mmHg s mL^{-1})	R_2 (mmHg s mL^{-1})	C_{Wk} (mL mmHg^{-1})
1. Asc. aorta	6.00	18.1	975.7	-	-	-
2. Aortic arch I	2.00	15.8	851.0	-	-	-
3. Aortic arch II	3.90	15.2	817.8	-	-	-
4. L. subclavian	3.40	6.4	346.4	-	-	-
5. Brachial I	8.44	5.4	292.3	-	-	-
6. Brachial II	8.44	4.8	262.9	-	-	-
7. Brachial III	8.44	4.3	234.4	-	-	-
8. Brachial IV	8.44	3.7	207.5	-	-	-
9. Brachial V	8.44	3.1	173.2	1.548	10.982	0.046
10. Brachiocephalic	3.40	8.6	461.1	0.123	4.523	0.252
11. L. Com. carotid	6.95	4.4	239.6	0.406	10.333	0.047
12. L. vertebral	3.70	2.2	152.2	1.582	57.410	0.008
13. Desc. Thor. aorta I	5.20	12.8	691.7	-	-	-
14. Intercostal	8.00	1.5	139.7	9.115	3.081	0.051
15. Desc. Thor. aorta II	10.40	9.7	520.3	0.125	0.964	0.683

They were taken from the 25-year-old baseline subject in Charlton et al. (2019). Segment numbers are displayed in ***Figure 2B****. The remaining parameters are: blood density* $\rho = 1,060$ *Kg m*$^{-3}$*, blood viscosity* $\eta = 2.5 \times 10^{-3}$ *Pa s and outflow pressure* $P_{out} = 33$ *mmHg.* r_d *is the diastolic luminal radius, E is the Young modulus, h is the wall thickness,* R_1*,* R_2*, and* C_{Wk} *are the two resistances and compliance, respectively, of the outflow windkessel models. L, left; Com, common; Desc, descending; Thor, thoracic.*

$$\hat{T}_2 = -\sin(k_c x)\frac{\hat{Q}_{\text{in}}}{M}, \tag{3}$$

with x the axial direction, ω the angular frequency, l the vessel length, $\hat{Q}_{\text{in}}$ the Fourier transform of $Q_{\text{in}}(t)$ the flow wave at the inlet, and

$$k_c^2(\omega) = \frac{i\omega C\eta}{A_0 K(\omega)}, \qquad M^2(\omega) = \frac{i\omega C A_0 K(\omega)}{\eta},$$
$$\hat{Z}(\omega) = \frac{R_1 + R_2 - i\omega R_1 R_2 C_{\text{Wk}}}{1 - i\omega R_2 C_{\text{Wk}}}. \tag{4}$$

η is the blood viscosity, A_0 is the average luminal cross-sectional area, $C = \frac{3\pi r_0 r_d^2}{2Eh}$ is the vessel compliance – with E the Young modulus, h the wall thickness, and r_0 and r_d the average and diastolic luminal radii, respectively—C_{Wk} is the WK-model compliance, and R_1 and R_2 are the WK-model resistances. $K(\omega) = -\frac{\eta}{i\omega\rho}\left[1 - \frac{2J_1(kr_0)}{kr_0 J_0(kr_0)}\right]$ is the dynamic permeability where J_0 and J_1 are the Bessel functions of order zero and one, respectively, $k^2 = \frac{i\omega\rho}{\eta}$ and ρ is the blood density. Inverse Fourier transforms can be applied to obtain time-domain blood pressure, $p(x,t)$, and its attenuation and amplification components $T_1(x,t)$ and $T_2(x,t)$, respectively.

Figure 4 compares the pressure waves simulated by the reduced and single-vessel models along the brachial artery. It includes the terms T_1 and T_2 calculated using the single-vessel model (Equations 2 and 3), with $Q_{\text{in}}(t)$ the flow wave measured at the inlet of the brachial artery of the reduced model, $l = 42.2$ cm the total length of the brachial artery, $r_0 \approx r_d = 4.3$ mm, the average radii at diastolic pressure of the 5 arterial segments that make up the brachial artery in the reduced model, and $Eh = 234$ Pa m the average Eh value along the brachial artery, and $C = 0.205$ mm^2/mmHg. The approximation for $r_0 \approx r_d$ was used given that the difference between r_0 and r_d was smaller than 2.5%, which allowed us to reduce the number of parameters in the model. The WK parameters C_{Wk}, R_1, R_2 and P_{out} are equal to those of the WK model coupled to the outlet of the segment 'Brachial V' in the reduced model (see **Table 2**). We note that PP along the vessel is indeed slightly attenuated by T_1 and considerably amplified by T_2. Next, we derive an approximate expression for the amplification term T_2.

2.3.2. Approximate Amplification Term

A Taylor series expansion of the amplification term $\hat{T}_2(x,\omega)$ about $\omega = 0$ yields

$$\hat{T}_2 \approx -\frac{x\eta}{A_0 K^0}\left[1 - i\omega\left(\frac{\rho r_0^2}{6\eta} + \frac{C\eta x^2}{6A_0 K^0}\right)\right]\hat{Q}_{\text{in}}, \tag{5}$$

where $K^0 = r_0^2/8$ is the steady state permeability. The time-domain solution of Equation (5) is given by

$$T_2(x,t) = -\frac{8x\eta}{\pi r_0^4}Q_{\text{in}}(t) - \frac{4x\eta}{3\pi r_0^4}\left(\frac{\rho r_0^2}{\eta} + \frac{8C\eta x^2}{\pi r_0^4}\right)\frac{dQ_{\text{in}}(t)}{dt}. \tag{6}$$

For all segments of the aortic-brachial arterial path, the term containing dQ_{in}/dt dominates. Moreover, the viscous time $\frac{\rho r_0^2}{\eta}$ is at least three orders of magnitude larger than $\frac{8C\eta x^2}{\pi r_0^4}$ (see **Supplementary Section 2.1**). As a result, Equation (6) can be further approximated as

$$T_2(x,t) = -\frac{4x\rho}{3\pi r_0^2}\frac{dQ_{\text{in}}(t)}{dt}. \tag{7}$$

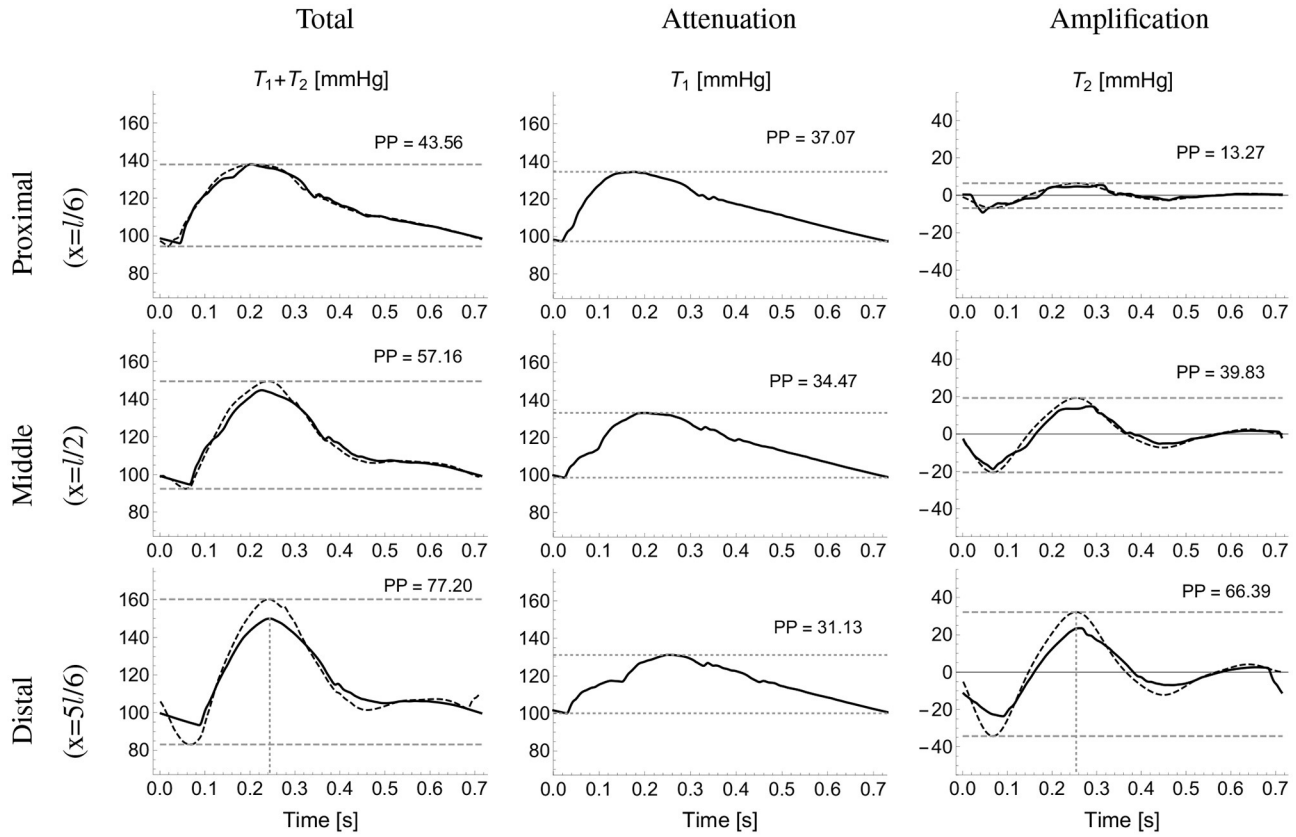

FIGURE 4 | Analytical pressure wave decomposition. The total pressure wave calculated using the reduced model (first column) at proximal **(top)**, midpoint **(middle)**, and distal **(bottom)** sites along the brachial artery was decomposed into the attenuation, T_1 (second column) and amplification, T_2 (third column) terms calculated using the single-vessel model (Equations 2 and 3). The approximated total (sum of Equations 2 and 7) and T_2 pressures (computed using Equation 7) are shown in dotted lines (first and third columns, respectively). Horizontal dashed lines highlight pulse pressure (PP) values. Vertical dashed lines (bottom plots) indicate the time of minimum dQ_{in}/dt.

According to this equation the main determinants of T_2 along an arterial segment are its radius, length, and the rate of change of Q_{in} with time. Moreover, the amplification term T_2 is maximum when dQ_{in}/dt is minimum and, hence, systolic blood pressure, $P_{Sys}(x)$, along an arterial segment can be estimated as

$$P_{Sys}(x) = P_{Sys}^{In} - \frac{4x\rho}{3\pi r_0^2}\left.\frac{dQ_{in}}{dt}\right|_{min}, \quad (8)$$

where P_{Sys}^{In} is the systolic pressure at the inlet and $dQ_{in}/dt|_{min}$ denotes the maximum temporal rate of decrease in late-systolic flow at the inlet. Assuming equal diastolic pressure at any point along the arterial segment, PP and ΔPP can be expressed as a function of the distance x from the inlet as

$$PP(x) = PP^{In} - \frac{4x\rho}{3\pi r_0^2}\left.\frac{dQ_{in}}{dt}\right|_{min}, \quad (9)$$

$$\Delta PP(x) = -\frac{4x\rho}{3\pi r_0^2}\left.\frac{dQ_{in}}{dt}\right|_{min}, \quad (10)$$

with PP^{In} the pulse pressure at the inlet. **Figure 4** (third column) compares the exact T_2 term along the brachial artery given by Equation (3) with the corresponding approximated term calculated using Equation (7). To avoid high-frequency noise, the time derivative of Q_{in} was filtered by computing the Fourier series of dQ_{in}/dt and keeping terms up to 15 Hz to reproduce the filtered signal. The vertical dotted lines in the first and third columns indicate the time of the maximum temporal rate of decrease in late-systolic flow, $dQ_{in}/dt|_{min}$, which approximately corresponds to the time of peak pressure for the reduced model and the exact T_2 term. The approximated pressure given by the sum of Equations (2) and (7), and shown on **Figure 4** (first column) with dotted lines, overestimates systolic pressures calculated by the reduced model, shown on **Figure 4** (first column) with continuous lines, by less than 6%.

2.4. Methodology for Estimating cPP

Based on the previous analytical expressions for the amplification term T_2, two methods can be developed for estimating cPP at the aortic root from the flow at the aortic root or the brachial artery

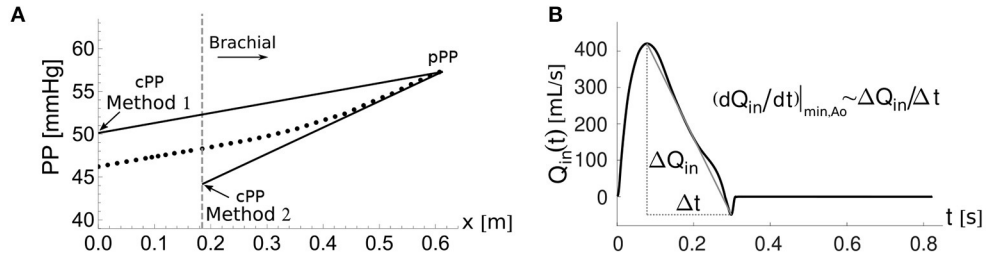

FIGURE 5 | The two cPP estimation methods. **(A)** Pulse pressure, PP(x), along the aortic-brachial arterial path with distance, x, from the aortic root. The start of the brachial artery is indicated by the dashed vertical line. PP values calculated along the path using the reduced model (dots). Methods 1 and 2 estimate cPP (solid lines) based on the approximate expression for PP(x) given by Equation (11), starting from the PP value at the outlet of the brachial artery, pPP. **(B)** Approximate calculation of the maximum temporal rate of decrease in late-systolic flow, $\left(dQ_{\text{in}}/dt\right)\big|_{\text{min,Ao}}$, from the aortic flow waveform, $Q_{\text{in}}(t)$.

and pPP at the outlet of the brachial artery. Both are illustrated in **Figure 5**.

2.4.1. Method 1

This method assumes that Equation (9) can be applied to the entire aortic-brachial arterial path as

$$\text{PP}(x) = \text{cPP} - \frac{4x\rho}{3\pi\,(\bar{r})^2}\left.\frac{dQ_{\text{in}}}{dt}\right|_{\text{min,Ao}}, \tag{11}$$

with x the distance from the aortic root, cPP the PP at the aortic root, $\left(dQ_{\text{in}}/dt\right)\big|_{\text{min,Ao}}$ the maximum temporal rate of decrease in late-systolic flow at the aortic root and $\bar{r}$ the mean radius of the aortic-subclavian arterial segments. Note that the suffix Ao stands for aortic. Equation (11) can be used to compute cPP from the PP at the brachial artery, pPP, as

$$\text{cPP} = \text{pPP} + \frac{4\,\rho\,l_{\text{Ao-Bra}}}{3\pi\,(\bar{r})^2}\left.\frac{dQ_{\text{in}}}{dt}\right|_{\text{min,Ao}}, \tag{12}$$

where $l_{\text{Ao-Bra}}$ is the length of the aortic-brachial arterial path.

Equation (12) was used to estimate cPP for the *in silico* dataset. The following assumptions were used for the *in vivo* dataset. When using *in vivo* aortic flow data with low temporal resolution, such as the Doppler ultrasound data used in this study, $\left(dQ_{\text{in}}/dt\right)\big|_{\text{min,Ao}}$ can be approximated by (**Figure 5B**)

$$\left.\left(\frac{dQ_{\text{in}}}{dt}\right)\right|_{\text{min,Ao}} \approx \left(\frac{\Delta Q_{\text{in}}}{\Delta t}\right)_{\text{Ao}}, \tag{13}$$

with ΔQ_{in} the end-systolic flow minus the peak flow and Δt the time of end of systole minus the time of peak flow. $l_{\text{Ao-Bra}}$ was estimated using the empirical expression (Sugawara et al., 2018)

$$\begin{aligned} l_{\text{Ao-Bra}}(\text{mm}) &= 37.9 \times \text{sex(male} = 1, \text{female} = 0) \\ &+1.4 \times \text{age(years)} + 2.5 \times \text{height(cm)} - 14.8. \end{aligned} \tag{14}$$

The radius of the aorta was used as a surrogate of the mean radius of the aortic-subclavian arterial segments, that is, $\bar{r} \approx r_{\text{Ao}}$.

2.4.2. Method 2

This method assumes that all the change in PP along the aortic-brachial arterial path occurs in the brachial artery. As a result, Equation (12) becomes

$$\text{cPP} = \text{pPP} + \frac{4\,\rho\,l_{\text{Bra}}}{3\pi\,(r_{\text{Bra}})^2}\left.\frac{dQ_{\text{in}}}{dt}\right|_{\text{min,Bra}}, \tag{15}$$

where l_{Bra} and r_{Bra} are the length and mean radius of the brachial artery, and $dQ_{\text{in}}/dt\big|_{\text{min,Bra}}$ is the maximum rate of decrease of late systolic blood flow at the inlet of the brachial artery.

Equation (15) was used to estimate cPP for the *in silico* dataset. The following correlations and assumptions were used for the *in vivo* dataset. According to the *in silico* dataset, r_{Bra} is strongly correlated with the radius of the aortic root, r_{Ao} (both in cm) through

$$r_{\text{Bra}} = 0.246\,r_{\text{Ao}} - 0.04, \tag{16}$$

with a correlation coefficient $R = 0.98$. Moreover, $dQ_{\text{in}}/dt\big|_{\text{min,Bra}}$ is correlated with the corresponding value at the aortic root (both in mL/s^2), through

$$\left.\frac{dQ_{\text{in}}}{dt}\right|_{\text{min,Bra}} = 0.0763\left.\frac{dQ_{\text{in}}}{dt}\right|_{\text{min,Ao}} + 22, \tag{17}$$

with $R = 0.80$. We therefore estimated the brachial radius and maximum temporal rate of decrease of brachial flow from the corresponding *in vivo* data at the aortic root.

The length of the brachial artery was estimated by multiplying the aortic-brachial length computed using Equation (14) by a factor of 0.73. This corresponds to the ratio of the brachial artery length to the total aortic-brachial length measured in the *in silico* dataset.

3. RESULTS

3.1. Approximate Pressure Calculations Using the Single-Vessel Model

Figures 6A,B shows the ability of the single-vessel model to describe—through Equations (8) and (9), respectively—systolic pressure, P_{Sys}, and PP for each segment along the aortic-brachial

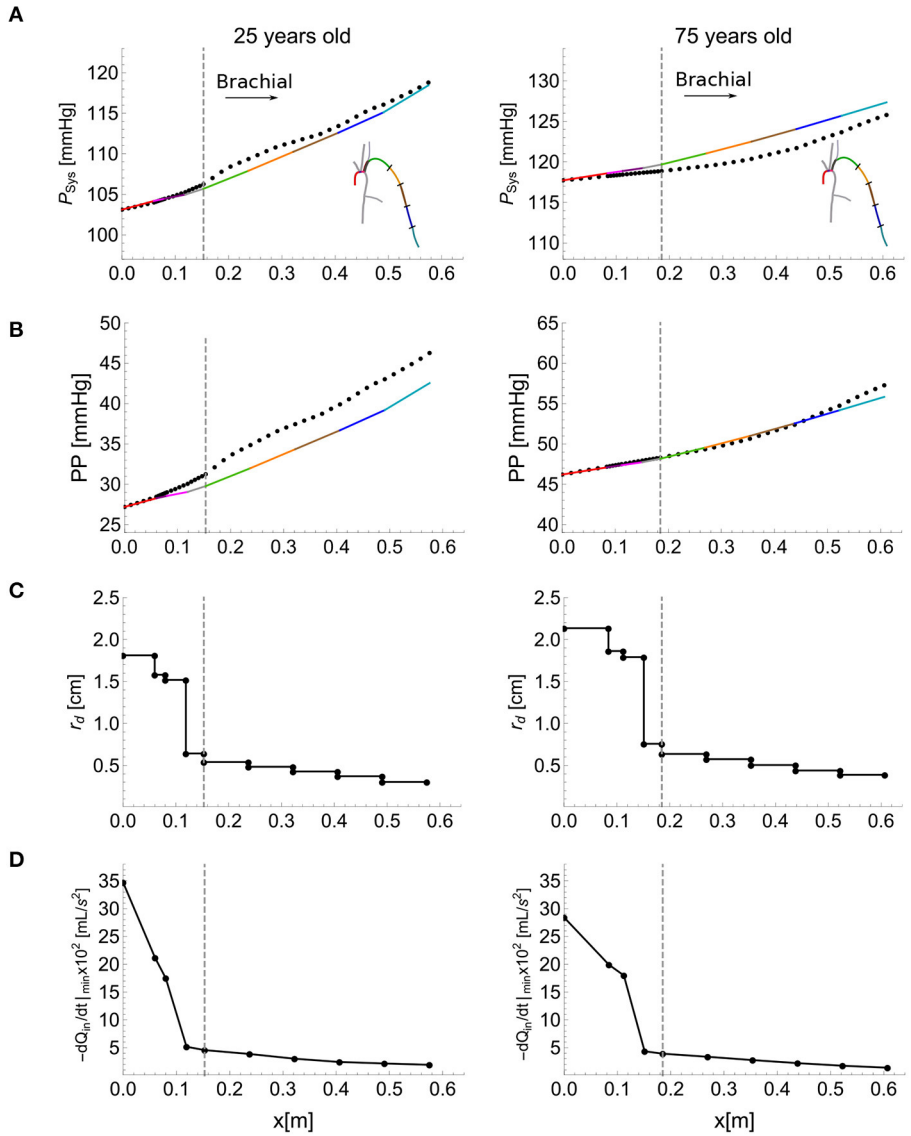

FIGURE 6 | Calculation of systolic blood pressure, P_{Sys}, and pulse pressure, PP, using the single-vessel model. P_{Sys} **(A)**, and PP **(B)** (solid lines) calculated using Equations (8) and (9), respectively. The dots show the corresponding values obtained by the reduced model. Luminal diastolic radius, r_d **(C)**, and maximum temporal rate of decrease in late-systolic flow, $-dQ_{in}/dt|_{min}$ from the reduced model **(D)** at the inlet and outlet of each segment of the aortic-brachial arterial path, for the baseline 25 (left) and 75 (right) year-old subject from the *in silico* dataset. Dashed vertical lines indicate the start of the brachial artery.

arterial path, for the 25 (left) and 75 (right) year-old baseline subjects of the *in silico* dataset. Results are compared with corresponding P_{Sys} and PP values obtained from reduced models of each subject. The inlet systolic pressure, P_{Sys}^{In}, in Equation (8) and inlet pulse pressure, PP^{In}, in Equation (9) for the first arterial segment (ascending aorta) were taken from the values provided by the corresponding reduced model. For the remaining segments, P_{Sys}^{In} and PP^{In} were assumed to be equal to the values calculated at the outlet of the adjacent upflow segment using Equations (8) and (9), with the luminal diastolic radius and maximum temporal rate of decrease in late-systolic blood flow shown in **Figures 6C,D** computed from the reduced model. Relative errors were smaller than 1.3% for P_{Sys} and 13.7% for PP for the 25 year-old *in silico* subject and 1.8% for P_{Sys} and 2.5% for PP for the 75 year-old *in silico* subject, along the aortic-brachial arterial path. The larger luminal radii and smaller rate of blood flow decrease in late systole in the 75-year-old subject led to a smaller pulse pressure amplification from aortic root to brachial artery, compared to the 25-year-old subject.

Starting from the PP values at the outlet of the brachial artery of the reduced model and assuming that the PP at the inlet of an arterial segment is equal to the PP at the outlet of the adjacent one, Equations (9) and (10) applied to each arterial segment from the brachial artery to the aortic root enabled

us to calculate cPP and ΔPP with variations in cardiovascular properties. Cardiovascular properties variations for the 25-year-old *in silico* subjects led to relative errors smaller than 18% for cPP and 24% for ΔPP when the morphology of the aortic flow wave was modified to account for changes in stroke volume, heart rate and left ventricular ejection time (results are shown in the **Supplementary Figure 3A**). On the other hand, variations in total vascular resistance, total vascular compliance, total path length and average network radius (for the same aortic root waveform) led to relative errors smaller than 20% for cPP and 29% for ΔPP (**Supplementary Figure 3B**).

According to Equation (10), ΔPP along an arterial segment is proportional to the segment length and the maximum temporal rate of decrease in late systolic-flow; and inversely proportional to the square of the vessel radius. These proportionalities were verified in all the arterial segments of the aortic-brachial arterial path for the 25- and 75-years-old *in silico* subjects. Proportionalities for length and temporal rate of decrease in late systolic-flow exhibited linear correlations with the smallest correlation coefficient (R^2) of 0.91. Proportionality in radius exhibited a power-decay with exponents of −1.73 and −2.18 for the 25- and 75-year-old *in silico* subjects, respectively, both exponents are close to the expected value of −2. Results are shown in the **Supplementary Figure 2**.

3.2. *In silico* Verification of cPP Estimation Methods

Figure 7 shows the ability of the cPP estimation methods to describe—through Equation (12) for Method 1 and Equation (15) for Method 2—changes in cPP and ΔPP, respectively, with variations in cardiovascular properties. Mean and standard deviation (SD) for stroke volume, heart rate, left ventricular ejection time, total vascular resistance and total vascular compliance correspond to the 25-year-old *in silico* subjects. The length and the radius of each vessel of the 25-year-old baseline subject were changed by 14% and 11%, respectively. These percentages were calculated from the covariance (SD/Mean) of the aortic arch length (Bensalah et al., 2014) and brachial artery radius (van der Heijden-Spek et al., 2000), respectively. Both methods were able to capture changes in cPP and ΔPP produced by the variations in cardiovascular properties. Excluding radii variations, Method 1 led to relative errors smaller than 20% for cPP and 28% for ΔPP. Excluding radii variations, Method 2 led to smaller relative errors: 18% for cPP and 24% for ΔPP. Except for radii variation where a competing effect arises, approximate PP and ΔPP values followed the trends provided by the reduced model. For all the cardiac variations ΔPP increases with the maximum temporal rate of decrease in late-systolic flow and length; and is almost not affected by the total vascular resistance and total compliance as described by Equation (10) and consequently by Equations (12) and (15).

We tested the accuracy of the two new cPP estimation methods on the dataset of *in silico* pulse waves (**Figure 8**, left). For the whole dataset, estimated cPP was strongly correlated with measured cPP, with R-squared (R^2) values of 0.97 for both methods (**Figures 8A,B**, top). Overall, Method 1 (Equation 12) overestimated cPP (**Figure 8A**, bottom) and Method 2 underestimated cPP (**Figure 8B**, bottom). The mean ± SD error was 3.3 ± 2.8 mmHg for Method 1 and -1.2 ± 2.7 mmHg for Method 2. Estimated cPP values were closer to measured cPP values for Method 2. When only the 75-year-old subjects were considered (blue dots), the agreement between cPP obtained from Method 1 and measured values was much closer, with R^2 values and mean ± SD errors of 0.99 and 0.1 ± 2.7 mmHg for Method 1, respectively, and 0.99 and −3.4 ± 2.7 mmHg for Method 2, respectively.

3.3. *In vivo* Verification of cPP Estimation Methods

We also tested the accuracy of the two new cPP estimation methods on the *in vivo* data (**Figure 8**, right). For the whole dataset, estimated cPP was strongly correlated with measured cPP, though with R^2 values smaller than those obtained for the *in silico* dataset: 0.74 for Method 1 and 0.75 for Method 2. Method 1 led to a smaller mean error than the one obtained for the *in silico* dataset (−2.0 vs. 3.3 mmHg). However, the SD was greater in the *in vivo* dataset (7.0 vs. 2.8 mmHg). For Method 2, both the mean error and SD were larger in the *in vivo* dataset (5.1 ± 6.9 vs. −1.2 ± 2.7 mmHg). For both methods, no considerable differences in mean, SD or R^2 values were observed between normotensive (Method 1: −2.4 ± 6.7 mmHg, R^2 = 0.72; Method 2: 4.9 ± 6.4 mmHg, R^2 = 0.75) and hypertensive (Method 1: −1.9 ± 7.4 mmHg, R^2 = 0.74; Method 2: 5.3 ± 7.4 mmHg, R^2 = 0.74) subjects.

4. DISCUSSION

We have developed and tested two methods for estimating cPP from aortic or brachial blood flow and peripheral blood pressure. Both methods originated from a model of blood flow in the larger arteries of the systemic circulation based on physical principles (conservation of mass and linear momentum). The mathematical complexity of this full model was simplified based on the physics of blood flow, resulting in a reduced model of blood flow in the upper thoracic aorta and left brachial artery that allows for workable analytical solutions in the frequency domain. This reduced model enabled us to obtain an approximation for blood pressure, in time domain, along each segment of the aortic-brachial arterial path from which the main cardiovascular determinants of ΔPP could be identified, leading to the two new cPP estimation methods. Both methods were able to (i) capture changes in cPP and ΔPP produced by variations in cardiovascular properties and (ii) estimate cPP with mean differences smaller than 3.3 ± 2.8 mmHg on *in silico* data for different age groups (25–75 years old) and 5.1 ± 6.9 mmHg on *in vivo* data for normotensive and hypertensive subjects.

4.1. Main Cardiovascular Determinants of Pulse Pressure Amplification

We have obtained a simple expression highlighting the main cardiovascular determinants of ΔPP along an arterial segment. According to Equation (10), ΔPP is directly proportional to the

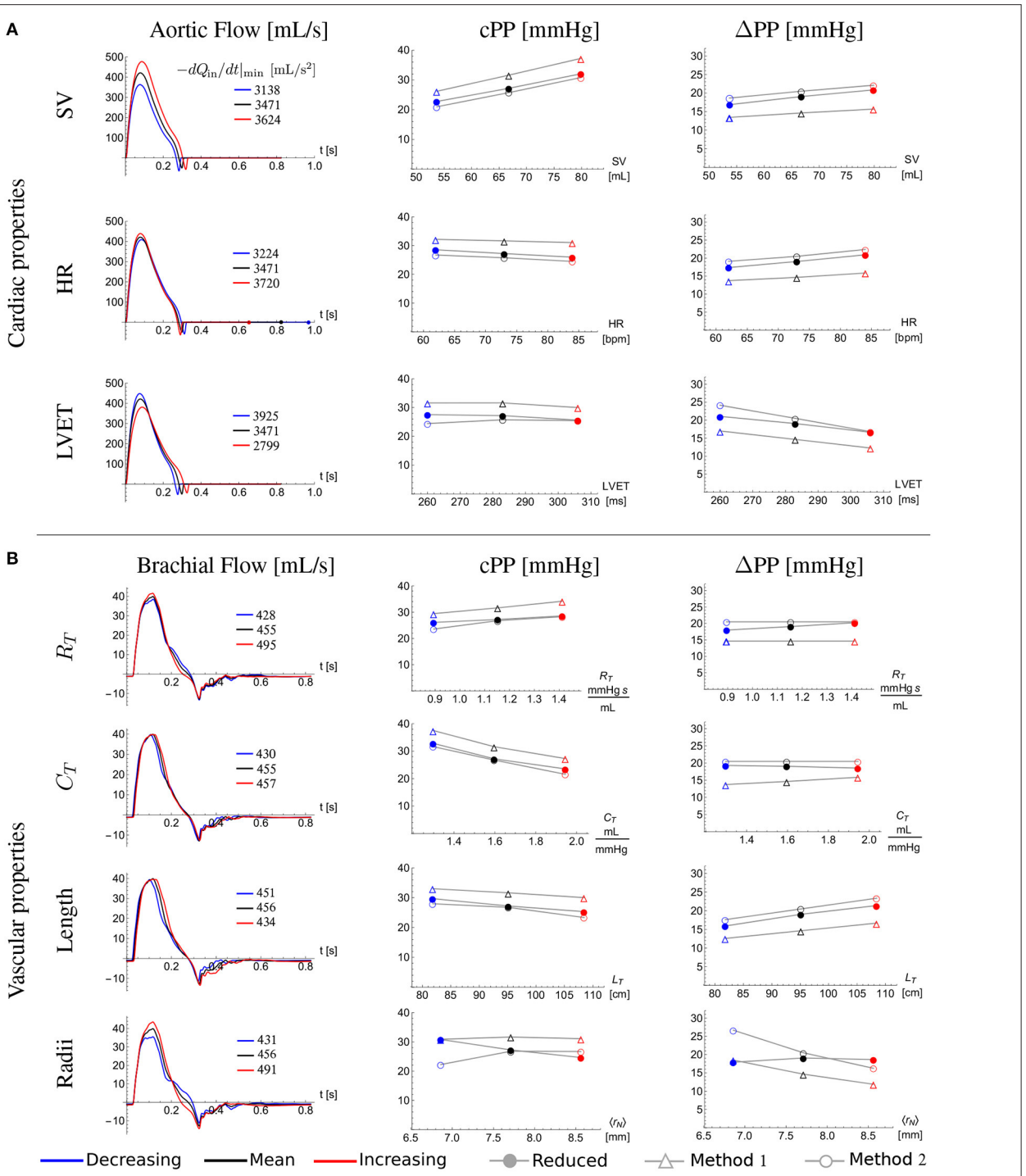

FIGURE 7 | Effect of cardiovascular properties on central pulse pressure, cPP, and its amplification from the aortic root to the outlet of the brachial artery, ΔPP. Aortic root **(A)** and brachial artery **(B)** flow wave (first column), cPP (second column), and ΔPP (third column) for the 25-year-old baseline subject (black) and with a standard deviation (SD) decrease (blue) and a SD increase (red) in **(A)** stroke volume (SV), heart rate (HR) and left ventricular ejection time (LVET), and **(B)** total vascular resistance (R_T) and total vascular compliance (C_T); and with a 14% decrease (blue) and 14% increase (red) in the total network length (L_T) and with a 11% decrease (blue) and 11% increase (red) in the average radius of the network ($\langle r_N \rangle$). The closed dots were calculated using the reduced model, the open triangles were calculated using Equation (12) of Method 1 and the open dots were calculated using Equation (15) of Method 2. Legends in the first column indicate the maximum temporal rate of decrease in late systolic-flow in mL/s^2 for all flow waves.

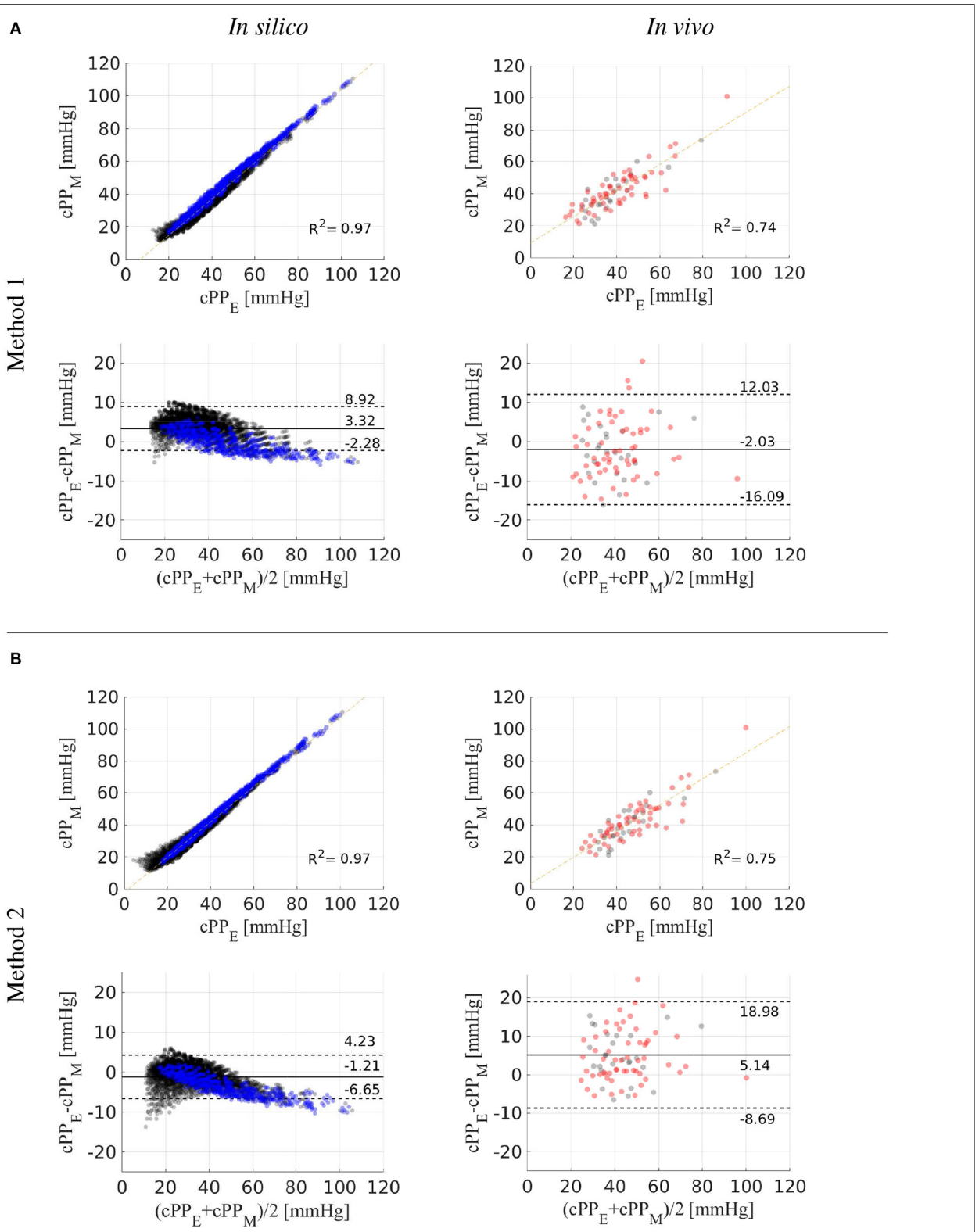

FIGURE 8 | Estimated (cPP_E) vs. measured (cPP_M) central pulse pressure. Correlation and Bland-Altman plots comparing cPP_E values calculated using Methods 1 **(A)** and 2 **(B)** with (cPP_M) values for the *in silico* (left) and *in vivo* (right) datasets. *In vitro* 75-year-old subjects are shown in blue dots. *In vivo* hypertensive subjects are shown in red dots. Dotted horizontal lines show the limits of agreement (±1.96*SD*) between estimated and reference cPP values.

distance along the arterial segment and the maximum temporal rate of decrease in late-systolic flow, and inversely proportional to the square of the vessel radius. Vascular geometry, therefore, plays a very important role in changing PP from central to peripheral arterial sites. This result is in agreement with previous studies in which ΔPP was associated with higher height and, hence, greater vessel length (Asmar et al., 1997; Camacho et al., 2004) and greater tapering and, hence, greater decrease in vessel radius (Belardinelli and Cavalcanti, 1992; Mynard and Smolich, 2015). Mynard and Smolich (2015) found, using computational modeling, that brachial artery tapering is a major factor leading to wave intensity amplification in the arm. They suggested that this may explain why amplification of wave intensity, which is directly related to the rate of change of pressure with time (and hence PP), was not found in other regions where the degree of tapering was lower. Our analytical results further support this finding. We have shown that changes in PP mainly occur in the brachial artery rather than in the aorta (**Figure 6B**), despite the rate of decrease in systolic flow being greater in the aorta than in the brachial artery (**Figure 6D**). This is because (i) the brachial artery is longer than the upper thoracic aorta and (ii) the vessel radius, which has an inversely quadratic contribution to ΔPP in Equation (10), is much smaller in the brachial artery (**Figure 6C**).

Equation (10) highlights the predominant role that flow wave morphology in late systole plays in ΔPP. Cardiac properties such as stroke volume (SV), heart rate (HR) and left ventricular ejection time (LVET) introduce variations in late-systolic aortic flow resulting in changes in ΔPP (**Figure 7**). In particular, increasing SV or HR and decreasing LVET augments the rate of decrease in late-systolic aortic flow and causes a greater ΔPP, as predicted by Equation (10) and consequently by Equations (12) and (15). This result is in agreement with previous studies underlining the potential importance of ventricular dynamics in determining ΔPP (O'Rourke, 1970; Asmar et al., 1997; Gaddum et al., 2017); e.g., O'Rourke (1970) found that, in human subjects, ΔPP increases with decreasing LVET. Equation (10) provides a mechanistic explanation of this result since a smaller LVET would lead to a greater temporal rate of decrease in late-systolic flow and, hence, greater ΔPP.

Interestingly, ΔPP is independent of the total compliance of the network (**Figure 7B**), again in agreement with Equation (10) and despite cPP decreasing with the increasing compliance. Indeed, cPP is mainly determined by total arterial compliance and left ventricular ejection dynamics affecting SV (Vennin et al., 2017). Except for radii variation, where the effects of the radius and the maximum temporal rate of decrease in late systolic-flow (induced by radii variation) are competing, approximate PP and ΔPP values followed the trends provided by the reduced model (**Figure 7**).

Our analytical results are in concordance with the experimental observation of a linear increase in ΔPP with the distance along an arterial segment (Gaddum et al., 2017) and further analysis of cardiac variables could be performed in experimental setups to corroborate our analytical results. Observed tendencies of *in vivo* measurements, like the difference in ΔPP with gender (Segers et al., 2009), can be analyzed in terms of our results, namely, the brachial artery length correlates with the height which in turn is significantly different with gender (Max Roser and Ritchie, 2019), however, *in vivo* measurements of radius and proximal flow at the brachial artery would be needed to corroborate the correlations between ΔPP and its determinants.

4.2. Aging and Pulse Pressure Amplification

Aging is associated with increased PP (Pinto, 2007) and decreased ΔPP (Herbert et al., 2014). It has been shown to increase PP more rapidly in central rather than distal arteries and, consequently, it has been suggested that ΔPP attenuation is predominantly caused by an increase in central systolic BP (cSBP) which, in turn, is induced by a rise in arterial stiffness (Safar et al., 2002). Other studies have highlighted the importance of ventricular dynamics—in addition to arterial stiffness—in determining PP (Fok et al., 2014b; Vennin et al., 2017; Li et al., 2019). Our study shows that the decrease in ΔPP with age is mainly caused by the increase in arterial radius and decrease in the rate of change of aortic flow with time in late systole (see Equation 10) strongly correlated with left ventricular ejection dynamics. The mechanisms behind the age-related increase in diameter are still unclear, though they may be the result of a compensatory adaptation to plaque formation and/or increases in wall thickness (Thijssen et al., 2015).

4.3. Central Pulse Pressure Estimation Methods

We have developed two methods that estimate cPP from measurements of the aortic flow wave and pPP that can be obtained by non-invasive means; e.g., Doppler ultrasound or magnetic resonance imaging for aortic flow and an oscillometric device for pPP. We have tested both methods on a dataset of *in silico* pulse waves and on a cohort of normotensive and hypertensive subjects, which covered a wide range of pressure wave morphologies and cPP values including those seen in hypertensive subjects (**Table 1**). Stronger linear correlations between estimated and reference cPP values were observed for the in *in silico* data compared to the *in vivo* data, the same was true for the smaller values for the mean and SD of the errors for cPP estimates (**Figure 8**). This is due to the larger experimental errors of the *in vivo* measurements, compared to the uncertainties of the *in silico* data due to model assumptions.

Recent (2017) clinical guidelines for the validation of non-invasive central blood pressure devices propose a mean absolute difference $\leq$ 5 mmHg with a SD $\leq$ 8 mmHg compared with the reference cSBP (Sharman et al., 2017). Method 1 led to mean absolute differences within recommended values (2.0 ± 7.0 mmHg), though Method 2 did not (5.1 ± 6.9 mmHg). Direct implementation of Method 2 requires measurements of the flow wave, vessel length and vessel radius in the brachial artery, which were not available for our *in vivo* cohorts and could lead to smaller mean absolute differences within recommended values. Indeed, Method 2 led to smaller differences than Method 1 when tested using *in silico* measurements in the brachial artery.

By using transfer functions, the influence of the large arteries and peripheral load on pulse pressure amplification has been studied (Karamanoglu et al., 1995). Using a single-tube transmission line model enables personalization of some of the transfer function parameters, improving the accuracy of the estimated cBP waveform (Swamy et al., 2009; Hahn et al., 2012; Gao et al., 2016; Natarajan et al., 2017). Further improvement in cBP assessment could be achieved by including additional patient-specific information to transfer functions based on the results of our study; i.e., the geometry of the brachial artery and the flow morphology. It is worth mentioning that our model approach differs from the lossless transmission line model approach used by Swamy et al. (2009), Hahn et al. (2012), Gao et al. (2016), Natarajan et al. (2017). First, starting from continuum mechanics (fluid dynamics, and a model for vessel elasticity), our approach accounts for the spatial and temporal variations of blood pressure and flow in the brachial artery. Second, it accounts for viscous losses along the vessel. Third, it decomposes pressure along the vessel into space-varying attenuation and amplification terms, whereas the transmission line model does a decomposition into forward and backward waves that are independent of position (the distance between the peripheral and central positions is introduced by adding a time delay). The main determinants of ΔPP are also different in both models: the pulse transit time and reflection coefficient in the transmission line model, and the inflow wave morphology and arterial geometry in our model. Notably, the main determinants of ΔPP in our model are independent of peripheral vascular properties.

Machine learning approaches could also be used to estimate cPP from aortic or brachial flow and pPP. However, like transfer function methods, they should be trained on datasets covering the large range of physiological and pathophysiological conditions encountered in healthy and diseased subjects, to make them widely applicable. The ability to numerically generate datasets containing hemodynamic data for thousands of virtual subjects (Charlton et al., 2019) could facilitate this process.

4.4. Limitations

This study is subject to several important limitations. Our non-invasive measurements of pressure and the flow were not simultaneous and subject to experimental error. Carotid pressure is also an imperfect surrogate of aortic pressure and subject to calibration errors. Both Methods 1 and 2 require a flow wave measurement in addition to the peripheral pulse pressure. Calculation of the maximum temporal rate of flow decrease in late systole requires differentiation of the flow wave, which can be challenging when working with noisy flow waves; e.g., those acquired by Doppler ultrasound. To facilitate this calculation, we have approximated this maximum temporal rate by the slope given from peak flow to end of systolic flow (see **Figure 5B**). Further validation of both methods using more accurate techniques for measuring flow, such as magnetic resonance, would be valuable, as well as further validation of Method 2 using measurements of blood flow and vascular geometry in the brachial artery. We tested both methods only in normotensive subjects and in otherwise hypertensive subjects. Although comparison with the dataset of *in silico* pulse waves has provided a wider range of pressure and flow wave morphologies and hemodynamic conditions, indicating that both methods would be equally valid in pathological conditions, such as systolic hypertension in older subjects and in heart failure, this needs testing prospectively.

4.5. Perspectives

Assessment of cPP has been shown to be of greater predictive value for cardiovascular outcomes than brachial PP. It is, therefore, essential to understand the hemodynamic determinants of PP amplification. The results that we have presented here show that blood flow is a key determinant of PP amplification, confirming the importance of measuring flow and the key role played by ventricular ejection. Therefore, conditions and drugs that influence cardiac function may influence pulse wave morphology independent of arterial function. Moreover, the two methods proposed here allow for a more regular assessment of a patient's cPP, due to their non-invasive nature which removes the risk of complications due to cardiac catheterization.

5. CONCLUSION

We have identified the main determinants of pulse pressure amplification—highlighting the important role of flow morphology—and presented two methods based on the physics of blood flow for estimating central pulse pressure from non-invasive measurements of aortic flow and peripheral blood pressure. We have tested both methods on *in silico* data for different age groups (25–75 years old) and *in vivo* data for normotensive and hypertensive subjects. Our approach could improve cardiovascular function assessment in clinical cohorts for which aortic ultrasound or magnetic resonance imaging data are available.

DATA AVAILABILITY STATEMENT

The raw data supporting the conclusions of this article will be made available by the authors, without undue reservation.

AUTHOR CONTRIBUTIONS

All authors contributed to the article and approved the submitted version.

FUNDING

JFG acknowledges support of a postdoctoral fellowship from CONACyT [CVU:288182]. ECP and JA acknowledge the UK-Mexico Visiting Chair for a mobility grant. ECP acknowledges funding from the Centre for Mexican Studies UNAM-UK, for financing a short stay; CONACyT (Mexico), through project no. 219584 and agreement no. 2018-000007- 01EXTV-00183; the Faculty of Chemistry UNAM, through PAIP 5000-9011; and DGAPA, UNAM, through a PASPA programme,

during a sabbatical leave. PC and JA were partially funded by the British Heart Foundation (BHF) [PG/15/104/31913 and PG/17/50/32903]. The authors also acknowledge financial support from the Wellcome EPSRC Centre for Medical Engineering at King's College London [WT 203148/Z/16/Z], Department of Health through the National Institute for Health Research (NIHR) Cardiovascular MedTech Co-operative at Guy's and St Thomas' NHS Foundation Trust (GSTT) and the Ministry of Science and Higher Education of the Russian Federation within the framework of state support for the creation and development of World-Class Research Centers Digital biodesign and personalized healthcare [075-15-2020-926]. The views expressed are those of the authors and not necessarily those of the UNAM, CONACyT, AMEXCID, EPSRC, BHF, Wellcome Trust, NIHR, GSTT or Ministry of Science.

ACKNOWLEDGMENTS

The authors thank Drs. Ye Li (King's College London), Jorge Aramburu (Navarra University), and Peter Charlton (King's College London) for data and programming support.

SUPPLEMENTARY MATERIAL

The Supplementary Material for this article can be found online at: https://www.frontiersin.org/articles/10.3389/fphys.2021.608098/full#supplementary-material

REFERENCES

Agabiti-Rosei, E., Mancia, G., O'Rourke, M. F., Roman, M. J., Safar, M. E., Smulyan, H., et al. (2007). Central blood pressure measurements and antihypertensive therapy. *Hypertension* 50, 154–160. doi: 10.1161/HYPERTENSIONAHA.107.090068

Agabiti-Rosei, E., and Muiesan, M. L. (2015). Understanding and treating central blood pressure. *Dialog. Cardiovasc. Med*. 20, 169–184. Available online at: https://www.dialogues-cvm.org/

Asmar, R., Brisac, A., Courivaud, J., Lecor, B., London, G., and Safar, M. (1997). Influence of gender on the level of pulse pressure: the role of large conduit arteries. *Clin. Exp. Hypertens*. 19, 793–811. doi: 10.3109/10641969709083187

Avolio, A. P., Bortel, L. M. V., Boutouyrie, P., Cockcroft, J. R., McEniery, C. M., Protogerou, A. D., et al. (2009). Role of pulse pressure amplification in arterial hypertension. *Hypertension* 54, 375–383. doi: 10.1161/HYPERTENSIONAHA.109.134379

Belardinelli, E., and Cavalcanti, S. (1992). Theoretical analysis of pressure pulse propagation in arterial vessels. *J. Biomech*. 25, 1337–1349. doi: 10.1016/0021-9290(92)90289-D

Bensalah, M. Z., Bollache, E., Kachenoura, N., Giron, A., De Cesare, A., Macron, L., et al. (2014). Geometry is a major determinant of flow reversal in proximal aorta. *Am. J. Physiol. Heart Circ. Physiol*. 306, H1408–H1416. doi: 10.1152/ajpheart.00647.2013

Camacho, F., Avolio, A., and Lovell, N. H. (2004). Estimation of pressure pulse amplification between aorta and brachial artery using stepwise multiple regression models. *Physiol. Meas*. 25, 879–889. doi: 10.1088/0967-3334/25/4/008

Charlton, P., Mariscal Harana, J., Vennin, S., Li, Y., Chowienczyk, P., and Alastruey, J. (2019). Modelling arterial pulse waves in healthy ageing: a database for *in silico* evaluation of haemodynamics and pulse wave indices. *Am. J. Physiol. Heart Circ. Physiol*. 317, H1062–H1085. doi: 10.1152/ajpheart.00218.2019

Chen, C.-H., Ting, C.-T., Nussbacher, A., Nevo, E., Kass, D. A., Pak, P., et al. (1996). Validation of carotid artery tonometry as a means of estimating augmentation index of ascending aortic pressure. *Hypertension* 27, 168–175. doi: 10.1161/01.HYP.27.2.168

Figueroa, C. A., and Humphrey, J. D. (2014). Pressure wave propagation in full-body arterial models: a gateway to exploring aging and hypertension. *Proc. IUTAM* 10, 382–395. doi: 10.1016/j.piutam.2014.01.033

Flores Gerónimo, J., Alastruey, J., and Corvera Poiré, E. (2016). A novel analytical approach to pulsatile blood flow in the arterial network. *Ann. Biomed. Eng*. 44, 3047–3047. doi: 10.1007/s10439-016-1625-3

Fok, H., Guilcher, A., Brett, S., Jiang, B., Li, Y., Epstein, S., et al. (2014a). Dominance of the forward compression wave in determining pulsatile components of blood pressure. *Hypertension* 64, 1116–1123. doi: 10.1161/HYPERTENSIONAHA.114.04050

Fok, H., Guilcher, A., Li, Y., Brett, S., Shah, A., Clapp, B., et al. (2014b). Augmentation pressure is influenced by ventricular contractility/relaxation dynamics. *Hypertension* 63, 1050–1055. doi: 10.1161/HYPERTENSIONAHA.113.02955

Fossan, F. E., Mariscal-Harana, J., Alastruey, J., and Hellevik, L. R. (2018). Optimization of topological complexity for one-dimensional arterial blood flow models. *J. R. Soc. Interface* 15:20180546. doi: 10.1098/rsif.2018.0546

Gaddum, N., Alastruey, J., Chowienczyk, P., Rutten, M. C. M., Segers, P., and Schaeffter, T. (2017). Relative contributions from the ventricle and arterial tree to arterial pressure and its amplification: an experimental study. *Am. J. Physiol. Heart Circ. Physiol*. 313, H558–H567. doi: 10.1152/ajpheart.00844.2016

Gao, M., Rose, W. C., Fetics, B., Kass, D. A., Chen, C.-H., and Mukkamala, R. (2016). A simple adaptive transfer function for deriving the central blood pressure waveform from a radial blood pressure waveform. *Sci. Rep*. 6:33230. doi: 10.1038/srep33230

Hahn, J., Reisner, A. T., Jaffer, F. A., and Asada, H. H. (2012). Subject-specific estimation of central aortic blood pressure using an individualized transfer function: a preliminary feasibility study. *IEEE Trans. Inf. Technol. Biomed*. 16, 212–220. doi: 10.1109/TITB.2011.2177668

Hashimoto, J., and Ito, S. (2010). Pulse pressure amplification, arterial stiffness, and peripheral wave reflection determine pulsatile flow waveform of the femoral artery. *Hypertension* 56, 926–933. doi: 10.1161/HYPERTENSIONAHA.110.159368

Herbert, A., Cruickshank, J. K., Laurent, S., and Boutouyrie, P. (2014). Establishing reference values for central blood pressure and its amplification in a general healthy population and according to cardiovascular risk factors. *Eur. Heart J*. 35, 3122–3133. doi: 10.1093/eurheartj/ehu293

Karamanoglu, M., Gallagher, D. E., Avolio, A. P., and O'Rourke, M. F. (1995). Pressure wave propagation in a multibranched model of the human upper limb. *Am. J. Physiol. Heart Circ. Physiol*. 269, H1363–H1369. doi: 10.1152/ajpheart.1995.269.4.H1363

Li, Y., Gu, H., Fok, H., Alastruey, J., and Chowienczyk, P. (2017). Forward and backward pressure waveform morphology in hypertension. *Hypertension* 69, 375–381. doi: 10.1161/HYPERTENSIONAHA.116.08089

Li, Y., Jiang, B., Keehn, L., Gu, H., Boguslavskyi, A., Cecelja, M., et al. (2019). Hemodynamic mechanism of the age-related increase in pulse pressure in women. *Hypertension* 73, 1018–1024. doi: 10.1161/HYPERTENSIONAHA.118.12402

Max Roser, C. A., and Ritchie, H. (2019). *Human Height. Our World in Data*. Available online at: https://ourworldindata.org/human-height

McEniery, C. M., Cockcroft, J. R., Roman, M. J., Franklin, S. S., and Wilkinson, I. B. (2014). Central blood pressure: current evidence and clinical importance. *Eur. Heart J*. 35, 1719–1725. doi: 10.1093/eurheartj/eht565

Mynard, J. P., and Smolich, J. J. (2015). One-dimensional haemodynamic modeling and wave dynamics in the entire adult circulation. *Ann. Biomed. Eng*. 43, 1443–1460. doi: 10.1007/s10439-015-1313-8

Natarajan, K., Cheng, H.-M., Liu, J., Gao, M., Sung, S.-H., Chen, C.-H., et al. (2017). Central blood pressure monitoring via a standard automatic arm cuff. *Sci. Rep*. 7:14441. doi: 10.1038/s41598-017-14844-5

Ohno, Y., Kanno, Y., and Takenaka, T. (2016). Central blood pressure and chronic kidney disease. *World J. Nephrol.* 5, 90–100. doi: 10.5527/wjn.v5.i1.90

O'Rourke, M. F. (1970). Influence of ventricular ejection on the relationship between central aortic and brachial pressure pulse in man. *Cardiovasc. Res.* 4, 291–300. doi: 10.1093/cvr/4.3.291

Pauca, A. L., Wallenhaupt, S. L., Kon, N. D., and Tucker, W. Y. (1992). Does radial artery pressure accurately reflect aortic pressure? *Chest* 102, 1193–1198. doi: 10.1378/chest.102.4.1193

Pichler, G., Martinez, F., Vicente, A., Solaz, E., Calaforra, O., and Redon, J. (2016). Pulse pressure amplification and its determinants. *Blood Press* 25, 21–27. doi: 10.3109/08037051.2015.1090713

Pierce, G. L., Zhu, H., Darracott, K., Edet, I., Bhagatwala, J., Huang, Y., et al. (2012). Arterial stiffness and pulse-pressure amplification in overweight/obese African-American adolescents: relation with higher systolic and pulse pressure. *Am. J. Hypertens.* 26, 20–26. doi: 10.1093/ajh/hps014

Pinto, E. (2007). Blood pressure and ageing. *Postgrad. Med. J.* 83, 109–114. doi: 10.1136/pgmj.2006.048371

Safar, M. E., Blacher, J., Pannier, B., Guerin, A. P., Marchais, S. J., Guyonvarc'h, P.-M., et al. (2002). Central pulse pressure and mortality in end-stage renal disease. *Hypertension* 39, 735–738. doi: 10.1161/hy0202.098325

Segers, P., Mahieu, D., Kips, J., Rietzschel, E., Buyzere, M. D., Bacquer, D. D., et al. (2009). Amplification of the pressure pulse in the upper limb in healthy, middle-aged men and women. *Hypertension* 54, 414–420. doi: 10.1161/HYPERTENSIONAHA.109.133009

Sharman, J. E., Avolio, A. P., Baulmann, J., Benetos, A., Blacher, J., Blizzard, C. L., et al. (2017). Validation of non-invasive central blood pressure devices: ARTERY Society task force consensus statement on protocol standardization. *Eur. Heart J.* 38, 2805–2812. doi: 10.1093/eurheartj/ehw632

Sharman, J. E., Marwick, T. H., Gilroy, D., Otahal, P., Abhayaratna, W. P., and Stowasser, M. (2013). Randomized trial of guiding hypertension management using central aortic blood pressure compared with best-practice care. *Hypertension* 62, 1138–1145. doi: 10.1161/HYPERTENSIONAHA.113.02001

Shih, Y.-T., Cheng, H.-M., Sung, S.-H., Hu, W.-C., and Chen, C.-H. (2011). Quantification of the calibration error in the transfer function-derived central aortic blood pressures. *Am. J. Hypertens.* 24, 1312–1317. doi: 10.1038/ajh.2011.146

Sugawara, J., Tomoto, T., and Tanaka, H. (2018). Arterial path length estimation for heart-to-brachium pulse wave velocity. *Hypertens. Res.* 41, 444–450. doi: 10.1038/s41440-018-0019-3

Swamy, G., Xu, D., Olivier, N. B., and Mukkamala, R. (2009). An adaptive transfer function for deriving the aortic pressure waveform from a peripheral artery pressure waveform. *Am. J. Physiol. Heart Circ. Physiol.* 297, H1956–H1963. doi: 10.1152/ajpheart.00155.2009

Thijssen, D. H. J., Carter, S. E., and Green, D. J. (2015). Arterial structure and function in vascular ageing: are you as old as your arteries? *J. Physiol.* 594, 2275–2284. doi: 10.1113/JP270597

van der Heijden-Spek, J. J., Staessen, J. A., Fagard, R. H., Hoeks, A. P., Boudier, H. A. S., and Bortel, L. M. V. (2000). Effect of age on brachial artery wall properties differs from the aorta and is gender dependent. *Hypertension* 35, 637–642. doi: 10.1161/01.HYP.35.2.637

Vennin, S., Li, Y., Willemet, M., Fok, H., Gu, H., Charlton, P., et al. (2017). Identifying hemodynamic determinants of pulse pressure. *Hypertension* 70, 1176–1182. doi: 10.1161/HYPERTENSIONAHA.117.09706

Wilkinson, I. B., Franklin, S. S., Hall, I. R., Tyrrell, S., and Cockcroft, J. R. (2001). Pressure amplification explains why pulse pressure is unrelated to risk in young subjects. *Hypertension* 38, 1461–1466. doi: 10.1161/hy1201.097723

Wilkinson, I. B., Mohammad, N. H., Tyrrell, S., Hall, I. R., Webb, D. J., Paul, V. E., et al. (2002). Heart rate dependency of pulse pressure amplification and arterial stiffness. *Am. J. Hypertens.* 15, 24–30. doi: 10.1016/S0895-7061(01)02252-X

Williams, B., Brunel, P., Lacy, P. S., Baschiera, F., Zappe, D. H., Kario, K., et al. (2017). Application of non-invasive central aortic pressure assessment in clinical trials: clinical experience and value. *Artery Res.* 17, 1–15. doi: 10.1016/j.artres.2016.10.154

Williams, B., Lacy, P. S., Thom, S. M., Cruickshank, K., Stanton, A., Collier, D., et al. (2006). Differential impact of blood pressure; lowering drugs on central aortic pressure and clinical outcomes. Principal results of the conduit artery function evaluation (CAFE) study. *Circulation* 113, 1213–1225. doi: 10.1161/CIRCULATIONAHA.105.595496

Williams, B., Mancia, G., Spiering, W., Agabiti Rosei, E., Azizi, M., Burnier, M., et al. (2018). ESC/ESH guidelines for the management of arterial hypertension: the task force for the management of arterial hypertension of the European Society of Cardiology and the European Society of Hypertension. *J. Hypertens.* 36, 1956–2041. doi: 10.1097/HJH.0000000000001940

Conflict of Interest: The authors declare that the research was conducted in the absence of any commercial or financial relationships that could be construed as a potential conflict of interest.

frontiers in Pediatrics

ORIGINAL RESEARCH
published: 04 March 2021
doi: 10.3389/fped.2020.557407

Feasibility of Wave Intensity Analysis in Patients With Conotruncal Anomalies Before and After Pregnancy: New Physiological Insights?

Maria Victoria Ordonez[1,2*], *Sandra Neumann*[2], *Massimo Caputo*[1,2], *Stephanie Curtis*[1] and *Giovanni Biglino*[1,2,3]

[1] Bristol Heart Institute, University Hospitals Bristol, Bristol, United Kingdom, [2] Bristol Medical School, University of Bristol, Bristol, United Kingdom, [3] National Heart and Lung Institute, Imperial College London, London, United Kingdom

Background: Conotruncal anomalies (CTA) are associated with ongoing dilation of the aortic root, as well as increased aortic stiffness, which may relate to intrinsic properties of the aorta. Pregnancy hormones lead to hemodynamic changes and remodeling of the *tunica media*, resulting in the opposite effect, i.e., increasing distensibility. These changes normalize post-pregnancy in healthy women but have not been fully investigated in CTA patients.

Methods: We examined aortic distensibility and ventriculo-arterial coupling before and after pregnancy using cardiovascular magnetic resonance (CMR)-derived wave intensity analysis (WIA). Pre- and post-pregnancy CMR data were retrospectively analyzed. Aortic diameters were measured before, during, and after pregnancy by cardiac ultrasound and before and after pregnancy by CMR. Phase contrast MR flow sequences were used for calculating wave speed (c) and intensity (WI). A matched analysis was performed comparing results before and after pregnancy.

Results: Thirteen women ($n = 5$, transposition of the great arteries; $n = 6$, tetralogy of Fallot; $n = 1$, double outlet right ventricle, $n = 1$, *truncus arteriosus*) had 19 pregnancies. Median time between delivery and second CMR was 2.3 years (range: 1–6 years). The aortic diameter increased significantly after pregnancy in nine ($n = 9$) patients by a median of 4 ± 2.3 mm (range: 2–7.0 mm, $p = 0.01$). There was no difference in c pre-/post-pregnancy ($p = 0.73$), suggesting that increased compliance, typically observed during pregnancy, does not persist long term. A significant inverse relationship was observed between *c* and heart rate (HR) after pregnancy ($p = 0.01$, $r = 0.73$). There was no significant difference in cardiac output, aortic/pulmonary regurgitation, or WI peaks pre-/post-pregnancy.

Conclusions: WIA is feasible in this population and could provide physiological insights in larger cohorts. Aortic distensibility and wave intensity did not change before and after pregnancy in CTA patients, despite an increase in diameter, suggesting that pregnancy did not adversely affect coupling in the long-term.

Keywords: conotruncal anomalies, pregnancy, aorta distensibility, aorta diameter, wave intensity analysis

OPEN ACCESS

Edited by:
Oswin Grollmuss, Université Paris-Sud, France

Reviewed by:
Michal Schäfer, University of Colorado, United States
Aurelio Secinaro, Bambino Gesù Children Hospital (IRCCS), Italy

***Correspondence:**
Maria Victoria Ordonez
victoria.ordonez@uhbw.nhs.uk

Specialty section:
This article was submitted to Pediatric Cardiology, a section of the journal Frontiers in Pediatrics

Received: *30 April 2020*
Accepted: *16 December 2020*
Published: *04 March 2021*

Citation:
Ordonez MV, Neumann S, Caputo M, Curtis S and Biglino G (2021) Feasibility of Wave Intensity Analysis in Patients With Conotruncal Anomalies Before and After Pregnancy: New Physiological Insights? Front. Pediatr. 8:557407. doi: 10.3389/fped.2020.557407

INTRODUCTION

Conotruncal cardiac anomalies (CTA) include a variety of congenital heart defects, such as tetralogy of Fallot (ToF), *truncus arteriosus* (TA), double outlet right ventricle (DORV), and transposition of the great arteries (TGA). These defects represent 5–10% of congenital heart disease (1) and generally lead to severe cyanosis, necessitating repair in the newborn period or early in infancy. A common observation in CTA is thoracic aortic dilation. Landmark work by Niwa demonstrates that the incidence of aorta dilation (AD) in adults with repaired ToF approaches 15% despite early ToF repair (1). Progressive dilation of the neo-aortic root is out of proportion to somatic growth in TGA after repair with arterial switch surgery (2), and AD is also found in the majority of patients with TA who survive initial repair (3).

Some independent variables can have an impact on the structure and size of the aorta, such as age, hypertension, smoking, diabetes, and pregnancy. However, there are a few hypotheses for why AD in CTA occurs principally. The first is that AD occurs due to hemodynamic stress on the aorta from an early right-left shunt. Evidence to support this hypothesis includes data showing that AD is worse with worsened degrees of right ventricular outflow tract stenosis and in patients with pulmonary atresia more than in patients with pulmonary stenosis (4). A second hypothesis is that volume loading of the aorta, *via* a surgical systemic-to-pulmonary shunt, will increase flow through the aortic valve, thus leading to dilation of the proximal aorta *via* increased wall stress (5). A longer duration between shunting and complete repair has been found to correlate with AD in repaired ToF (3–5). Other observations that have been associated with larger aortic dimensions in ToF include having a right rather than left aortic arch and male sex (5, 6). Recent evidence demonstrates that early ToF repair does not normalize aortic compliance and that abnormal ascending aortic flow patterns based on 4D flow cardiac magnetic resonance (CMR) are prevalent and might affect long-term cardiac performance (7).

Pivotal questions are whether these abnormalities are inherent or acquired, whether congenital heart disease plays a causal or facilitating role and whether genetic determinants are important. Recent data suggest that CTA may be associated with a primary problem with aortic histology and should be considered a true aortopathy (6). Patients with CTA present with impaired distensibility of the aorta (6). Interestingly, patients with ToF present with a higher degree of aortic dilation and aorta distensibility than d-TGA patients (8). In addition, in patients with d-TGA, impaired distensibility has only been found at the level of the ascending aorta, whereas in ToF patients both the ascending and descending aorta have been shown to be affected (9).

In this context, it is known that pregnancy represents an independent risk factor as it impacts the elastic properties of the aorta (9). This is due to a combination of the hemodynamic stress of pregnancy in producing changes in arterial structure and integrity and increasing the risk of arterial dissection and rupture, as well as changes to the independent role of female hormones. These structural changes are believed to regress to pre-pregnancy levels after delivery; however, whether or not these changes persist is unknown (9, 10).

Aortic distensibility, as well as ventriculo-arterial coupling, can be assessed by an established mathematical technique called wave intensity analysis (WIA) (11). This is traditionally derived from pressure and velocity data, but it can also be formulated using velocity and area, thus rendering the analysis applicable to phase contrast cardiac magnetic resonance (PC-CMR) (12).

This study aims to evaluate possible changes in aortic distensibility and ventriculo-arterial coupling in a CTA cohort before and after pregnancy non-invasively, based on the hypothesis that stiffness of the aorta and mechanical ventricular properties would be adversely affected by the hemodynamic stress and hormonal changes imposed by pregnancy.

METHODS AND MATERIALS

This was a retrospective feasibility study performed at a single NHS site. Therefore, no approval from the NHS UK research and ethics committee was sought in line with the Health Regulatory Authority guidelines.

Participants

The inclusion criteria were (i) conotruncal anomaly and (ii) phase contrast scan in the aorta available before and after pregnancy. Twenty-eight women with surgically repaired congenital conotruncal anomalies who had undergone pregnancy and had cardiac magnetic resonance scans at the University Hospitals Bristol NHS Foundation Trust were retrospectively assessed. Of these, 15 in total were removed from the analysis: 13 women had the appropriate scans available only at one time point (i.e., before or after pregnancy) and a further two patients who had insufficient scan quality (velocity encoding artifacts).

Thirteen patients ($n = 13$) were therefore entered into the analysis. Of these, five had transposition of the great arteries, six had tetralogy of Fallot, one had a double outlet right ventricle, and one had *truncus arteriosus*. Baseline characteristics are reported in **Table 1**.

Image Acquisition

Clinical ECG-gated phase contrast MR angiography in the ascending aorta was acquired on a 1.5T Siemens Avanto Magnetom (Siemens Healthineers, Erlangen, Germany). Flow data were acquired in the axial plane above the valves during free breathing. The acquisition parameters of the phase contrast MR angiography (PC-MRA) were as follows: field of view = 250 mm, slice thickness = 5 mm, matrix = 256 × 100, voxel = 1.0 × 1.0 × 5 mm, TR = 10.95 ms, TE = 2.61 ms, phase reconstructions = 20–30, velocity encoding (VENC) = 150–500 cm/s. See **Table 2**.

Segmentation

The ascending aortas were manually segmented using the magnitude image (CVI42, Circle Cardiovascular Imaging Inc, Calgary, Canada). This allowed for the quantification of the

TABLE 1 | Baseline characteristics.

CHD	*n*	Age at pregnancy (years)	*N* pregnancies	Weight (kgs)	Height (cm)	Body mass index (BMI)*	HTA	Blood pressure Pre vs. Post (mmHg)	Smoking
ToF	7	29.5	10	58.3	159.5		1	112/70	1
TA	1	19	1	53.0	156.0		0	108/70	0
d-TGA	5	26	8	55.0	161.0		0	119/65	3
Total	13	34	19	58.3	159.5	24.6	1	116/64 vs. 120/67	4

**Weight, height, and BMI (body mass index) values correspond to 2.3 years post pregnancy. Data are expressed as means ± s.d.*
HT, arterial hypertension; ToF, tetralogy of Fallot; TA, truncus arteriosus; d-TGA, transposition of the great arteries; CHD, congenital heart defect.

TABLE 2 | Imaging parameters, presented as median (range).

	Before	After	*P*-value
VENC (cm/s)	200 (150–400)	200 (150–500)	0.84
TR (ms)	31 (29.9–47.15)	47.15 (29.9–47.15)	0.23
TE (ms)	3.8 (2.0–3.8)	2.0 (2.0–2.18)	0.025
Reconstructed phases	30 (20–30)	30 (20–30)	0.43

average blood flow velocity (U) in each frame over the cross-sectional area (A).

Aortic Dimensions

Echocardiographic data were reviewed in repaired CTA at baseline (1 year before pregnancy), during pregnancy in the third trimester, and >3 years after pregnancy. Two-dimensional echo measurements of the diameter of the sinus of Valsalva and sinotubular junction were made in the parasternal long-axis view at end-diastole using the inner edge-inner edge technique.

Aortic measurements from cross-sectional cardiac CMR images were taken before and after pregnancy, considering only changes >1.5 mm (pixel size).

Physiological Parameters

Within the segmented area, cardiac output (L/min), mean flow velocity (cm/s), regurgitation fraction (%), and net negative volume of the flow (ml) were quantified. A 3-lead ECG measured the mean heart rate during the scan. Volumetric data were also calculated (end-diastolic volume EDV, end systolic volume ESV, and stroke volume SV). A ratio SV/ESV was derived from these as an accepted indicator of ventricular-vascular coupling (13).

Wave Intensity Analysis

The A and U data were smoothed by the application of a Savitsky-Golay filter with a window size of 11 and a second-degree polynomial. Following the wave intensity analysis method outlined by Biglino et al. (12), the U-ln$A$ loop was plotted and the linear portion of the slope selected during early systole to calculate wave speed (c) where $c = dU/d\ln A$. The net wave intensity, $dI = dUd\ln A$, as well as the forward and backward wave components were fitted in MATLAB (The MathWorks Inc., Natick, MA, USA). Wave energy was quantified by the area under the curve of the forward compression wave (FCW), forward expansion wave (FEW), and backward compression wave (BCW).

Wave intensity defined as $dI_{(A)} = dUd\ln A$ differs from the definition of wave intensity $dI_{(P)} = dPdU$ by a difference in dimensions [wave intensity $dI_{(P)}$ has the units W/m^2 and $dI_{(A)}$ has the units m/s] (14, 15). However, it can be shown that they differ only by a scaling factor, ρc^2, where ρ = blood density (16). We report $dI_{(A)}$ as wave energy in m/s.

Statistical Analysis

Normality of the data was assessed by D'Agostino-Pearson test of normality.

The FEW and BCW, as well as the regurgitation fraction and net negative volume, did not pass normality and was analyzed using non-parametric tests, namely Wilcoxon matched-pairs signed rank test. All other comparisons were run as Student paired *t*-tests, comparing the measure before and after pregnancy. Correlations were assessed by Pearson's correlation coefficient. All analyses were performed in GraphPad Prism version 7.0d (GraphPad, La Jolla, CA, USA). Data are reported as mean ± standard deviation. Alpha was set at 0.05. In the figures, the asterisk signifies the following: $^{*}p < 0.05$, $^{**}p < 0.01$, $^{***}p < 0.001$.

RESULTS

Demographics

Thirteen pregnant women were analyzed, with a mean age at pregnancy of 28.5 ± 4.6 years. The total number of pregnancies was 19. Baseline data, including blood pressure, smoking status, body mass index, and age at pregnancy are reported in **Table 3**.

Structural Changes

Four patients (31%) did not present a change in aortic dimensions. The other patients showed median aortic growth of 4 mm (2–7 mm), representing a significant growth compared to pre pregnancy values ($p = 0.01$) based on cross-sectional images (**Table 4**). Overall, ultrasound measurements confirmed a significant change in aortic dimensions during pregnancy (**Table 5**).

TABLE 3 | Baseline data.

CHD pathologies (*n*):	
Arterial Switch	2
Atrial Switch	3
TA	1
TOF	7
Corrective procedures (*n*)	
TAP	1
TAP/PVR	1
DORV/PVR	1
TOF/PVR	3
TOF	1
Senning	3
AVR/PVR	1
Age at last pregnancy (years)	27.5 ± 4.7
Number of pregnancies	1.5 ± 0.9
Time from last pregnancy to MRI (years)	3.2 ± 1.7
Pre-pregnancy blood pressure (mmHg)	124 (±26)/64 (±10) ($n = 9$)
Post-pregnancy blood pressure (mmHg)	123 (±13)/68 (±9) ($n = 9$)
Body Mass Index (kg/m^2)	24.7 ± 5.0
Diabetes	1
Smoking	4

Table shows demographics of the patients as mean ± standard deviation unless otherwise stated.
TA, Truncus Arteriosus; TAP, transannular patch; PVR, pulmonary valve replacement; DORV, double-outlet right ventricle; TOF, Tetralogy of Fallot; AVR, aortic valve replacement.

TABLE 4 | Aorta diameters before and after pregnancy.

CHD	Pre_SV (mm)	Pre_STJ (mm)	Pre_mid (mm)	Post_SV (mm)	Post_STJ (mm)	Post_mid (mm)
ToF	29	23	27	27	23	29
TA	28	19	25	35	26	30
d-TGA	24	23	21	27	24	26.5
P-value (pre_post)				$p = 0.1$	$p < 0.01$	$p = 0.2$

CHD, congenital heart defect; SV, sinus of Valsalva; STJ, sinotubular junction; TA, truncus arteriosus; d-TGA, transposition of the great arteries.

Physiological Parameters

There was no difference in the cardiac output before or after pregnancy (5 ± 1 vs. 4.8 ± 1.5 L/min; $p = 0.71$). There was also no difference in SV/ESV before or after pregnancy (1.7 ± 0.5 vs. 1.9 ± 0.7; $p = 0.53$). Mean velocity across the cardiac cycle ($p = 0.13$), regurgitation fraction ($p = 0.64$), and net negative volume ($p = 0.38$) also did not change after pregnancy. None of the patients presented clinical signs of aortic stenosis. Results are shown in **Figure 1**.

Wave Speed

There was no difference in wave speed before and after pregnancy ($p = 0.7$) (**Figure 2**). A significant negative correlation was seen between wave speed and heart rate ($p = 0.01$, $r = -0.73$), suggesting that increased stiffness was associated with lower heart rate (**Figure 3**). This was not observed before pregnancy ($p = 0.8$, $r = -0.08$). Wave speed results are shown in **Figure 2**.

TABLE 5 | Ultrasound aorta diameters before, during, and after pregnancy.

CHD	Pre_SV(mm)	During_SV (mm)	Post_SV (mm)
Arterial switch	28.5	34.5	31
TOF	30	35	33
Atrial switch	26.5	31.5	27
TA	33	38	35
Total (mean)	29.25	34.75	32
P-value*		0.01	

CHD, congenital heart defect; SV, sinus of Valsalva; TA, truncus arteriosus; d-TGA, transposition of the great arteries.
**P-value represents the difference of the aorta dimeter between before and during pregnancy.*

There was no correlation between cardiac output and wave speed before ($p = 0.16$, $r = 0.43$) or after pregnancy ($p = 0.057$, $r = -0.56$). Similarly, there was no correlation between wave speed and number of pregnancies (pre: $r = 0.0083$, $p = 0.98$; post: $r = -0.17$, $p = 0.60$), pre-pregnancy systolic blood pressure (pre: $r = -0.11$, $p = 0.79$, $n = 8$), or diastolic blood pressure (pre: $r = -0.42$, $p = 0.30$; post $r = -0.02$, $p = 0.94$, $n = 8$). However, a significant correlation was observed between wave speed and systolic pressure post-pregnancy (post $r = 0.73$, $p = 0.006$).

Wave Intensity

There was no difference in either the FCW ($p = 0.45$), or the FEW ($p = 0.62$) before and after pregnancy. Nor was there a difference in the BCW ($p = 0.24$, $n = 11$) or net WI ($p = 0.79$, $n = 13$) before and after pregnancy.

There was no correlation between FCW, BCW, net *dI* and age, number of pregnancies, SV/ESV, or blood pressure before or after pregnancy. Nor was there a correlation between FEW and age, number of pregnancies or blood pressure before pregnancy. FEW showed a positive correlation between the number of pregnancies ($r = 0.68$, $p = 0.01$).

DISCUSSION

Patients with congenital heart disease including CTA may present with dilatation of the thoracic aorta during their lifetime. Histological abnormalities of the aortic wall have been identified in patients with ToF and d-TGA as responsible for the early presentation of aorta dilation despite early surgical repair (10, 12, 14, 15).

Tobias et al. have shown that a CTA diagnosis and the presence of aortic regurgitation were independent predictors of an increased aortic sinus diameter (8). Moreover, they add that the diagnosis of a conotruncal defect and age are independent predictors of ascending aorta distensibility. Some independent variables are also known to influence this outcome, such as age, hypertension, smoking, diabetes, and additive pregnancies. These variables are thought to lead to changes in the structure of the

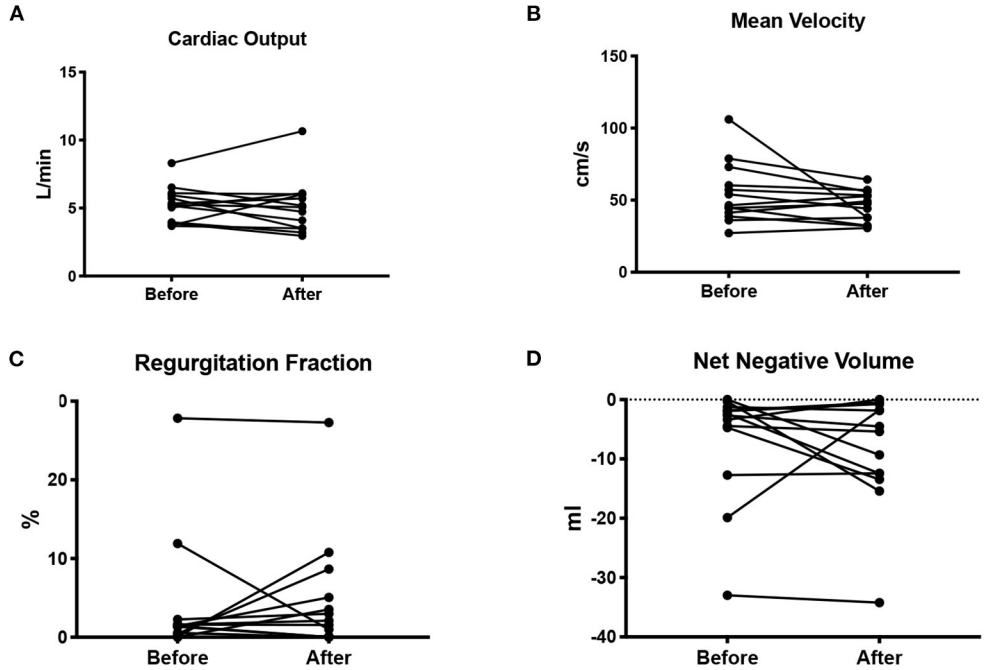

FIGURE 1 | Cardiac output in L/min **(A)**, mean blood flow velocity in cm/s **(B)**, regurgitation fraction as a percentage of the cardiac output **(C)**, and net negative blood volume **(D)** measured before and after pregnancy.

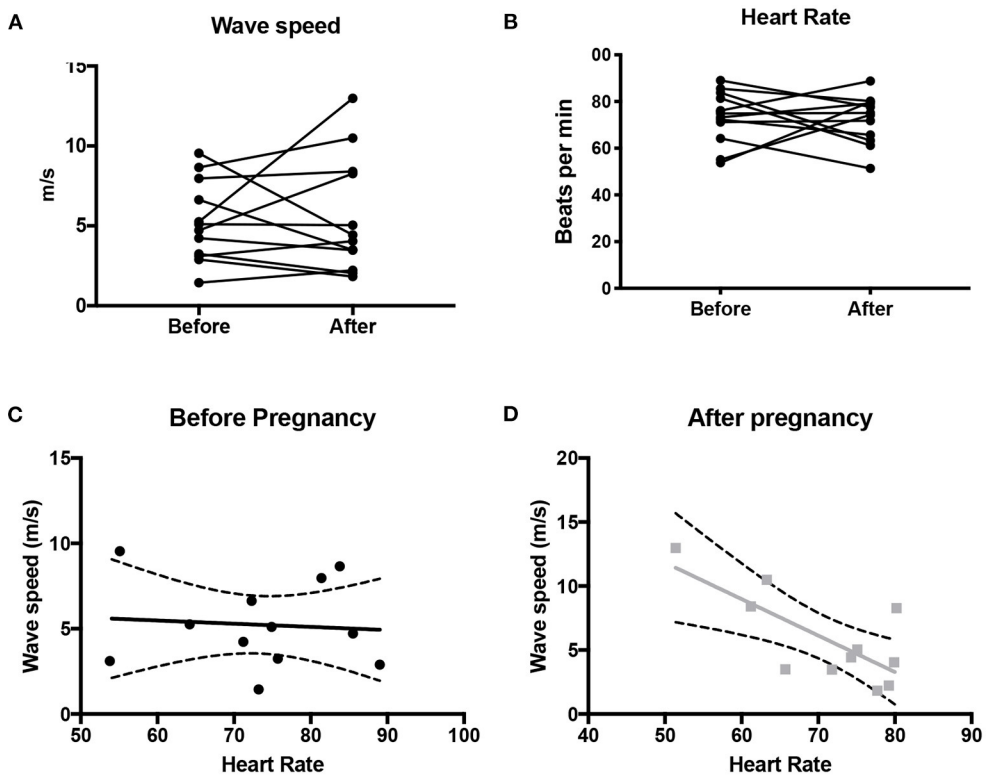

FIGURE 2 | Wave speed **(A)** and heart rate **(B)** in the ascending aorta before and after pregnancy. Also shown is the correlation (+/- 95% CI) between wave speed and heart rate before pregnancy **(C)** and after pregnancy **(D)**.

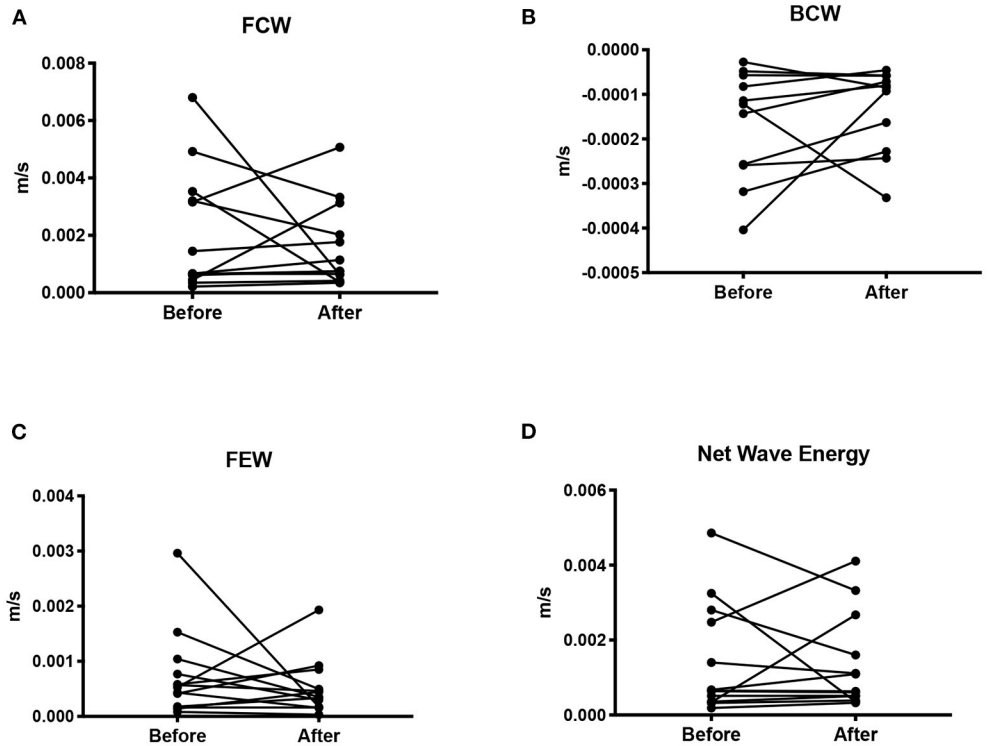

FIGURE 3 | Wave intensity shown as the mean wave energy (AUC) for the forward compression wave **(A)**, backward compression wave **(B)**, forward expansion wave **(C)**, and net wave energy **(D)**.

aortic media, leaving the aortic wall more vulnerable to dilation and eventually rupture and dissection (10).

There is an association between pregnancy and arterial aneurysm and dissections (9) in females without underlying aortopathy. This risk is secondary to a combination of the hemodynamic stress and hormonal changes imposed during pregnancy on the aortic wall. Nolte et al. reported histological changes in the aortic wall in two women without underlying aortopathy, strongly suggesting that these findings were associated with pregnancy stress plus hormonal changes. It is possible that, after repeated pregnancies, arterial walls might become abnormal because of a combination of hemodynamic stresses and hormonal changes, potentially enhancing the development of pathological changes in the arterial wall. Pregnancy is accompanied by fragmentation of elastic fibers, a decrease in mucopolysaccharides, and an increase in smooth muscle cells in the aortic wall (10). To what extent these changes normalize after delivery is unknown. Since more women with CTAs are reaching childbearing age, it is sensible to investigate if these changes persist temporarily or permanently after pregnancy or even if additive pregnancies enhance the progression of further histological changes.

Persistence of histological changes after pregnancy in CTA patients will lead to increased stiffness and reduced aortic distensibility (10). Stiffness of the aorta will have a negative impact on the ventricular function due to increased afterload, resulting in unfavorable ventriculo-arterial coupling. Recent evidence has suggested that patients with D-TGA and hypoplastic left heart syndrome (HLHS) have unfavorable ventricular-vascular coupling in light of reduced aortic distensibility (11, 12). Moreover, another study, which compared aorta distensibility between arterial and atrial switches, has shown that both groups had reduced distensibility, but the arterial switch cohort presented stiffer aortas. In addition, both had compromised ventricular-arterial coupling based on WIA, likely a result of increased impedance caused by the stiffer ascending aorta (17).

Our study has analyzed aortic distensibility and ventriculo-arterial efficiency in patients with CTA before and after pregnancy, aiming to evaluate whether pregnancy physiology modifies aortic elastic properties and, consequently, mechanical function of the ventricle. No significant changes of aortic distensibility or ventricular-vascular coupling were found. Nonetheless, a significant increase in aortic diameter was seen during pregnancy, based on ultrasound measurements, which persisted 2.3 years post-partum. This is similar to recent evidence that showed that pregnant women with CTA presented with a significant increase in aorta diameter during pregnancy, based on echocardiographic measurements, without reversion to a baseline diameter after 6 months of follow-up (18).

Wave speed has shown a positive correlation with HR, suggesting that higher wave speed presents with lower heart

rate in this population. We can suggest that, in CTA patients, heart rate tends to decrease over time in the context of sinus node dysfunction, mainly in patients with congenitally corrected (CCTGA) and D-TGA who have undergone a Mustard or Senning operation. Four out of 13 patients decreased more than 10 beats per minute after pregnancy, of which three were D-TGA patients, in whom increased aortic stiffness over time has also been reported (18). Nonetheless, it is known that heart rate can be a confounding variable that varies depending on systolic blood pressure measurements (19, 20). Further investigation is needed in order to fully explore this observation in a larger sample.

Furthermore, wave speed was found to be associated with systolic blood pressure after pregnancy in this cohort. An increment in systolic blood pressure could be associated with the aging process, albeit over a small number of years and other risk factors associated such as diabetes, smoking, or BMI >25 kg/m^2. We observed that patients with increased systolic blood pressure post-pregnancy were overweight (four out of 13 had a BMI $\geq$ 25 kg/m^2 post-pregnancy), two were smokers, and another was diabetic.

Another interesting finding was the significant positive correlation between FEW and number of pregnancies. While again limited by the small sample size, this could be clinically interesting given that FEW has been previously associated with the diastolic time constant tau (16). This would suggest that repetitive pregnancies may improve ventricular compliance, thus reflecting diastolic function. There is a possible explanation to address this finding: preload increases during pregnancy that lead to an increment in the stretching mechanism of the myocardium that regresses after 6–8 weeks post-delivery (18). After repetitive pregnancies, we can assume that ventricular compliance reaches the maximum point of stretching based on the Frank Starling mechanism, leading to more compliant ventricles. This remains speculative at this stage, as observed in a small number of cases, and should be explored in a larger sample allowing for sufficient power for subgroup analysis.

Indeed, the major limitation of this study is the small available sample, due in part to the number of patients with CTA undergoing pregnancy as well as the availability of the required imaging data. If a larger sample were available, it would be interesting to explore some of the associations mentioned here, particularly the possible association between wave energy (both FCW and FEW) and SV/ESV as a different CMR-derived indicator of ventriculo-vascular coupling.

Larger samples would likely require multicenter collaborations, thus allowing the exploration of the effect of multiple pregnancy or subtle differences between different diagnoses within CTA. Nevertheless, the study demonstrates the feasibility of performing the analysis in this patient population and the kind of physiological insight that could be gathered with regards to functional changes post pregnancy and the overall impact on ventriculo-arterial coupling.

From a methodological standpoint, it is worth remembering that several methods can be employed for the calculation of wave propagation, and even with a non-invasive approach, different techniques could be employed, with respective advantages and pitfalls (21). While an in-depth comparison and discussion of different techniques are beyond the scope of this article, it is worth considering that research is addressing the consistency and robustness of regional and local CMR-derived indices according to the theoretical model (Bramwell-Hill), demonstrating their relevance (22). Interestingly, WIA has been recently performed by combining standard CMR flow-velocity and non-invasive central blood pressure waveforms (23), but our study was purposely based solely on clinically available CMR data. Furthermore, measures of net wave intensity do not require knowledge of wave speed and thus are not influenced by the wave speed measurements.

CONCLUSION

Aortic distensibility did not change after pregnancy in CTA patients, but an increase in aortic diameter was observed. Serial measurement of the aortic root during and after pregnancy is clearly important. Wave intensity analysis is feasible in this population and could provide physiological insights in larger cohorts.

DATA AVAILABILITY STATEMENT

The original contributions presented in the study are included in the article/supplementary materials, further inquiries can be directed to the corresponding author/s.

ETHICS STATEMENT

This was a retrospective feasibility study performed at a single NHS site. Therefore, no approval from NHS UK research and ethics committee was sought in line with the Health Regulatory Authority guidelines.

AUTHOR CONTRIBUTIONS

MO: contributed with the idea, writing, analysis of the wave intensity analysis results, and the clinical significance. SN: did the analysis of the data and the wave intensity analysis. MC: supervised the study and writing. SC: lead the pregnancy input and helped in the writing process. GB: coordinated the study and writing and analysis of the data. All authors contributed to the article and approved the submitted version.

ACKNOWLEDGMENTS

The authors also acknowledge the generous support of the Grand Appeal (Bristol Royal Hospital for Children Charity) and the British Heart Foundation.

REFERENCES

1. Niwa K. Aortic root dilatation in tetralogy of Fallot long-term after repair—histology of the aorta in tetralogy of Fallot: evidence of intrinsic aortopathy. *Int J Cardiol.* (2005) 103:117–9. doi: 10.1016/j.ijcard.2004.07.002
2. Schwartz ML, Gauvreau K, del Nido P, Mayer JE, Colan SD. Long-term predictors of aortic root dilation and aortic regurgitation after arterial switch operation. *Circulation.* (2004) 110(11suppl.1):II−128. doi: 10.1161/01.CIR.0000138392.68841.d3
3. Carlo WF, Dean McKenzie E, Slesnick TC. Root dilation in patients with truncus arteriosus. *Congenital Heart Dis.* (2011) 6.3:228–33. doi: 10.1111/j.1747-0803.2011.00520.x
4. Niwa K, Siu SC, Webb GD, Gatzoulis MA. Progressive aortic root dilatation in adults late after repair of tetralogy of Fallot. *Circulation.* (2002) 106.11:1374–8. doi: 10.1161/01.CIR.0000028462.88597.AD
5. Capelli H, Ross D, Somerville J. Aortic regurgitation in tetrad of Fallot and pulmonary atresia. *Am J Cardiol.* (1982) 49.8:1979–83. doi: 10.1016/0002-9149(82)90218-1
6. Kay WA. Molecular and genetic insights into thoracic aortic dilation in conotruncal heart defects. *Front Cardiovasc Med.* (2016) 3:18. doi: 10.3389/fcvm.2016.00018
7. Schäfer M, Barker AJ, Jaggers J, Morgan GJ, Stone ML, Truong U, et al. Abnormal aortic flow conduction is associated with increased viscous energy loss in patients with repaired tetralogy of Fallot. *Eur J Cardio-Thoracic Surg.* (2020) 57.3:588–95. doi: 10.1093/ejcts/ezz246
8. Rutz T, Max F, Wahl A, Wustmann K, Khattab K, Pfammatter J-P, et al. Distensibility and diameter of ascending aorta assessed by cardiac magnetic resonance imaging in adults with tetralogy of fallot or complete transposition. *Am J Cardiol.* (2012) 110.1:103–8. doi: 10.1016/j.amjcard.2012.02.055
9. Nolte JE, Rutherford RB, Nawaz S, Rosenberger A, Speers WC, Kruspski WC et al. Arterial dissections associated with pregnancy. *J Vasc Surg.* (1995) 21:515–20. doi: 10.1016/S0741-5214(95)70296-2
10. Niwa K, Perloff JK, Bhuta SM, Laks H, Drinkwater DC, Child JS, et al. Structural abnormalities of great arterial walls in congenital heart disease: light and electron microscopic analyses. *Circulation.* (2001) 103.3:393–400. doi: 10.1161/01.CIR.103.3.393
11. Neumann S, Sophocleous F, Kobetic MD, Hart EC, Nightingale AK, Parker KH, et al. Wave intensity analysis in the internal carotid artery of hypertensive subjects using phase-contrast MR angiography and preliminary assessment of the effect of vessel morphology on wave dynamics. *Physiol Measure.* (2018) 39.10:104003. doi: 10.1088/1361-6579/aadfc5
12. Biglino G, Steeden JA, Baker C, Schievano S, Taylor AM, Parker KH, et al. A non-invasive clinical application of wave intensity analysis based on ultrahigh temporal resolution phase-contrast cardiovascular magnetic resonance. *J Cardiovasc Magnet Resonance.* (2012) 14.1:57. doi: 10.1186/1532-429X-14-57
13. Truong U, Patel S, Kheyfets V, Dunning J, Fonseca B, Barker AJ, et al. Non-invasive determination by cardiovascular magnetic resonance of right ventricular-vascular coupling in children and adolescents with pulmonary hypertension. *J Cardiovasc Magnet Resonance.* (2015) 17:81. doi: 10.1186/s12968-015-0186-1
14. Tan JL, Davlouros PA, McCarthy KP, Gatzoulis MA, Ho SY. Intrinsic histological abnormalities of aortic root and ascending aorta in tetralogy of Fallot: evidence of causative mechanism for aortic dilatation and aortopathy. *Circulation.* (2005) 112.7:961–8. doi: 10.1161/CIRCULATIONAHA.105.537928
15. Schäfer M, Browne LP, Morgan GJ, Barker AJ, Fonseca B, Dunbar Ivy D, et al. Reduced proximal aortic compliance and elevated wall shear stress after early repair of tetralogy of Fallot. *J Thoracic Cardiovasc Surg.* (2018) 156.6:2239–49. doi: 10.1016/j.jtcvs.2018.08.081
16. Biglino G, Ntsinjana H, Plymen C, Tann O, Giardini A, Derrick G, et al. Ventriculovascular interactions late after atrial and arterial repair of transposition of the great arteries. *J Thoracic Cardiovasc Surg.* (2014) 148.6:2627–33. doi: 10.1016/j.jtcvs.2014.07.072
17. Biglino G, Schievano S, Steeden JA, Ntsinjana H, Baker C, Khambadkone S, et al. Reduced ascending aorta distensibility relates to adverse ventricular mechanics in patients with hypoplastic left heart syndrome: non-invasive study using wave intensity analysis. *J Thoracic Cardiovasc Surg.* (2012) 144.6:1307–14. doi: 10.1016/j.jtcvs.2012.08.028
18. Horiuchi C, Kamiya CA, Ohuchi H, Nakanishi A, Tsuritani M, Iwanaga N, et al. Impact of pregnancy on aortic root in women with repaired conotruncal anomalies. *Pediatr Cardiol.* (2019) 40:1134–43. doi: 10.1007/s00246-019-02112-4
19. Lantelme P, Mestre C, Lievre M, Gressard A, Milon H. Heart rate: an important confounder of pulse wave velocity assessment. *Hypertension.* (2002) 39.6:1083–7. doi: 10.1161/01.HYP.0000019132.41066.95
20. Tan I, Butlin M, Liu YY, Ng K, Avolio AP, et al. Heart rate dependence of aortic pulse wave velocity at different arterial pressures in rats. *Hypertension.* (2012) 60.2:528–33. doi: 10.1161/HYPERTENSIONAHA.112.194225
21. Elmenhorst J, Weberruss H, Mayr M, Pfister K, Oberhoffer R. Comparison of two measurement devices for pulse wave velocity in children: which tool is useful to detect vascular alterations caused by overweight? *Front Pediatr.* (2019) 7:334. doi: 10.3389/fped.2019.00334
22. Dogui A, Kachenoura N, Frouin F, Lefort M, De Cesare A, Mousseaux E, et al. Consistency of aortic distensibility and pulse wave velocity estimates with respect to the Bramwell-Hill theoretical model: a cardiovascular magnetic resonance study. *J Cardiovasc Magnetic Resonance.* (2011) 13:11. doi: 10.1186/1532-429X-13-11
23. Bhuva AN, D'Silva A, Torlasco C, Nadarajan N, Jones S. Non-invasive assessment of ventriculo-arterial coupling using aortic wave intensity analysis combining central blood pressure and phase-contrast cardiovascular magnetic resonance. *Eur Heart J Cardiovasc Imag.* (2020) 21:805–13. doi: 10.1093/ehjci/jez227

Conflict of Interest: The authors declare that the research was conducted in the absence of any commercial or financial relationships that could be construed as a potential conflict of interest.

frontiers in Cardiovascular Medicine

ORIGINAL RESEARCH
published: 27 August 2021
doi: 10.3389/fcvm.2021.701267

The Use of Maximum Entropy to Enhance Wave Intensity Analysis: An Application to Coronary Arteries in Hypertrophic Obstructive Cardiomyopathy

Nadine Francis[1,2*], *Peter P. Selwanos*[3], *Magdi H. Yacoub*[1,3,4,5,6] *and Kim H. Parker*[2]

[1] *Biomedical Engineering and Innovation Laboratory, Department of Research, Aswan Heart Centre, Magdi Yacoub Heart Foundation, Aswan, Egypt,* [2] *Department of Bioengineering, Imperial College, London, United Kingdom,* [3] *Department of Cardiology, Aswan Heart Centre, Magdi Yacoub Heart Foundation, Aswan, Egypt,* [4] *Harefield Heart Science Centre, Harefield, United Kingdom,* [5] *Department of Surgery, Aswan Heart Centre, Magdi Yacoub Heart Foundation, Aswan, Egypt,* [6] *National Heart and Lung Institute, Imperial College, London, United Kingdom*

OPEN ACCESS

Edited by:
Giovanni Biglino, University of Bristol, United Kingdom

Reviewed by:
Erhan Tenekecioglu, University of Health Sciences, Turkey
Ernst Wellnhofer, Charité-Universitätsmedizin Berlin, Germany

****Correspondence:***
Nadine Francis
nadine.samy.francis@hotmail.com

Specialty section:
This article was submitted to Cardiovascular Imaging, a section of the journal Frontiers in Cardiovascular Medicine

Received: *27 April 2021*
Accepted: *05 August 2021*
Published: *27 August 2021*

Citation:
Francis N, Selwanos PP, Yacoub MH and Parker KH (2021) The Use of Maximum Entropy to Enhance Wave Intensity Analysis: An Application to Coronary Arteries in Hypertrophic Obstructive Cardiomyopathy. Front. Cardiovasc. Med. 8:701267. doi: 10.3389/fcvm.2021.701267

Background: Wave intensity analysis is useful for analyzing coronary hemodynamics. Much of its clinical application involves the identification of waves indicated by peaks in the wave intensity and relating their presence or absence to different cardiovascular events. However, the analysis of wave intensity peaks can be problematic because of the associated noise in the measurements. This study shows how wave intensity analysis can be enhanced by using a Maximum Entropy Method (MEM).

Methods: We introduce a MEM to differentiate between "peaks" and "background" in wave intensity waveforms. We apply the method to the wave intensity waveforms measured in the left anterior descending coronary artery from 10 Hypertrophic Obstructive Cardiomyopathy (HOCM) and 11 Controls with normal cardiac function. We propose a naming convention for the significant waves and compare them across the cohorts.

Results: Using a MEM enhances wave intensity analysis by identifying twice as many significant waves as previous studies. The results are robust when MEM is applied to the log transformed wave intensity data and when all of the measured data are used. Comparing waves across cohorts, we suggest that the absence of a forward expansion wave in HOCM can be taken as an indication of HOCM. Our results also indicate that the backward compression waves in HOCM are significantly larger than in Controls; unlike the forward compression waves where the wave energy in Controls is significantly higher than in HOCM. Comparing the smaller secondary waves revealed by MEM, we find some waves that are present in the majority of Controls and absent in almost all HOCM, and other waves that are present in some HOCM patients but entirely absent in Controls. This suggests some diagnostic utility in the clinical measurement of these waves, which can be a positive sign of HOCM or a subgroup with a particular pathology.

Conclusion: The MEM enhances wave intensity analysis by identifying many more significant waves. The method is novel and can be applied to wave intensity analysis in all arteries. As an example, we show how it can be useful in the clinical study of hemodynamics in the coronary arteries in HOCM.

Keywords: maximum entropy method, wave intensity analysis, Hypertrophic Obstructive Cardiomyopathy, coronary artery, wave identification

1. INTRODUCTION

Wave Intensity Analysis (WIA) is useful for analyzing arterial hemodynamics, particularly in the coronary arteries. Many different types of waves can exist in the elastic arteries (1), but the dominant wave that we are considering is the elastic axial wave; which exchanges energy between the kinetic energy of the blood flow and the potential energy in the elastic arterial wall (2, 3). Wave intensity is defined as the product of the pressure and velocity differences across a wave front, $dI = dPdU$, and represents the energy flux per unit area carried by the wave (4, 5).

Waves propagate in both the forward and backward direction in the arteries; wave intensity is positive for forward waves and negative for backward waves. Wave intensity calculated from the measured pressure and velocity at a given site in an artery is the sum of the forward and backward wave intensities; so that the wave intensities of simultaneous forward and backward waves tend to cancel each other. If the wave speed is known, it is possible to separate the forward and backward wave intensities.

Separated wave intensity analysis measures both the magnitude and the direction of waves in the artery. **Figure 1** is an example of the separated wave intensity calculated from pressure and flow measurements in a human circumflex artery (6). The ability of wave intensity to separate the effects of forward and backward waves is one of its main advantages, particularly in coronary arteries where the contraction of the myocardium directly causes both forward and backward waves.

Much of the clinical application of wave intensity analysis has involved identifying waves from the peaks in the wave intensity and relating these waves (or their absence) to events in the ventricle or alterations in the downstream sites of reflection (2, 7). In **Figure 1**, the authors have identified 6 peaks and identified them by their timing, their direction of travel and their affect on the blood velocity (acceleration or deceleration). Comparing wave intensity measurements from diseased and normal patients has been useful in determining the affect of different pathologies on arterial hemodynamics (7).

In other retrospective clinical studies, the relative magnitude of wave intensity peaks has been shown to be a significant predictor of cardiovascular risk (3). In all of these studies, peaks in the wave intensity have been identified "by eye," which is straightforward for the larger peaks but becomes problematic for smaller peaks. As seen in **Figure 1**, there are many local maxima in all wave intensity measurements. In this paper, we explore the use of information theory, in particular the Shannon entropy of the wave intensity signal, to distinguish "peaks" from "background" thereby enhancing wave intensity analysis.

The analysis of wave intensity peaks can be problematic because of the associated physiological noise in the measurements (e.g., heart rate variations) as well as the inevitable noise in the measurement of pressure and velocity. We introduce a method for differentiating between "peaks" and "background" in the wave intensity waveform based on the Maximum Entropy Method (MEM). The idea is very simple in concept and we believe its application to wave intensity analysis is novel.

We conclude the paper by comparing wave intensity waveforms measured in the left anterior descending coronary artery in a small cohort of patients with Hypertrophic Obstructive Cardiomyopathy (HOCM) and a small cohort of patients with normal cardiac function. This study demonstrates how MEM can enhance the identification of waves from the wave intensity analysis of pressure and flow in coronary arteries.

2. MATERIALS AND METHODS

2.1. Maximum Entropy Method

Information theory was introduced in the study of communications (8) but can be extended to any subject that involves probability and statistics. Central to information theory is the concept of *entropy* (usually called Shannon entropy to distinguish it from thermodynamic entropy). The probability of any event p is a measure of our expectation that it will occur in any trial; when p is small the event will occur infrequently, and when it is large it will occur frequently. Obversely, the reciprocal $\frac{1}{p}$ can be thought of as a measure of our uncertainty about the occurrence of an event. For subtle axiomatic reasons, Shannon defined uncertainty as $\log\frac{1}{p}$, and entropy as the expected outcome over all possible events $n = 1...N$.

$$H = \sum_{n=1}^{N} p_n \log\left(\frac{1}{p_n}\right) = -\sum_{n=1}^{N} p_n \log p_n \tag{1}$$

Thus, the entropy H is the average uncertainty about the outcome of a trial. p is non-dimensional and so H is non-dimensional, however its magnitude depends upon the base of the logarithm used; when logarithm to the base 2 is used, as in this study, entropy is given in "bits."

The link between entropy and information is the realization that when a trial is performed and the outcome is known uncertainty is removed, and so the information that we have received from the trial is equal to the entropy before the trial was performed. Despite its name, information in this sense is

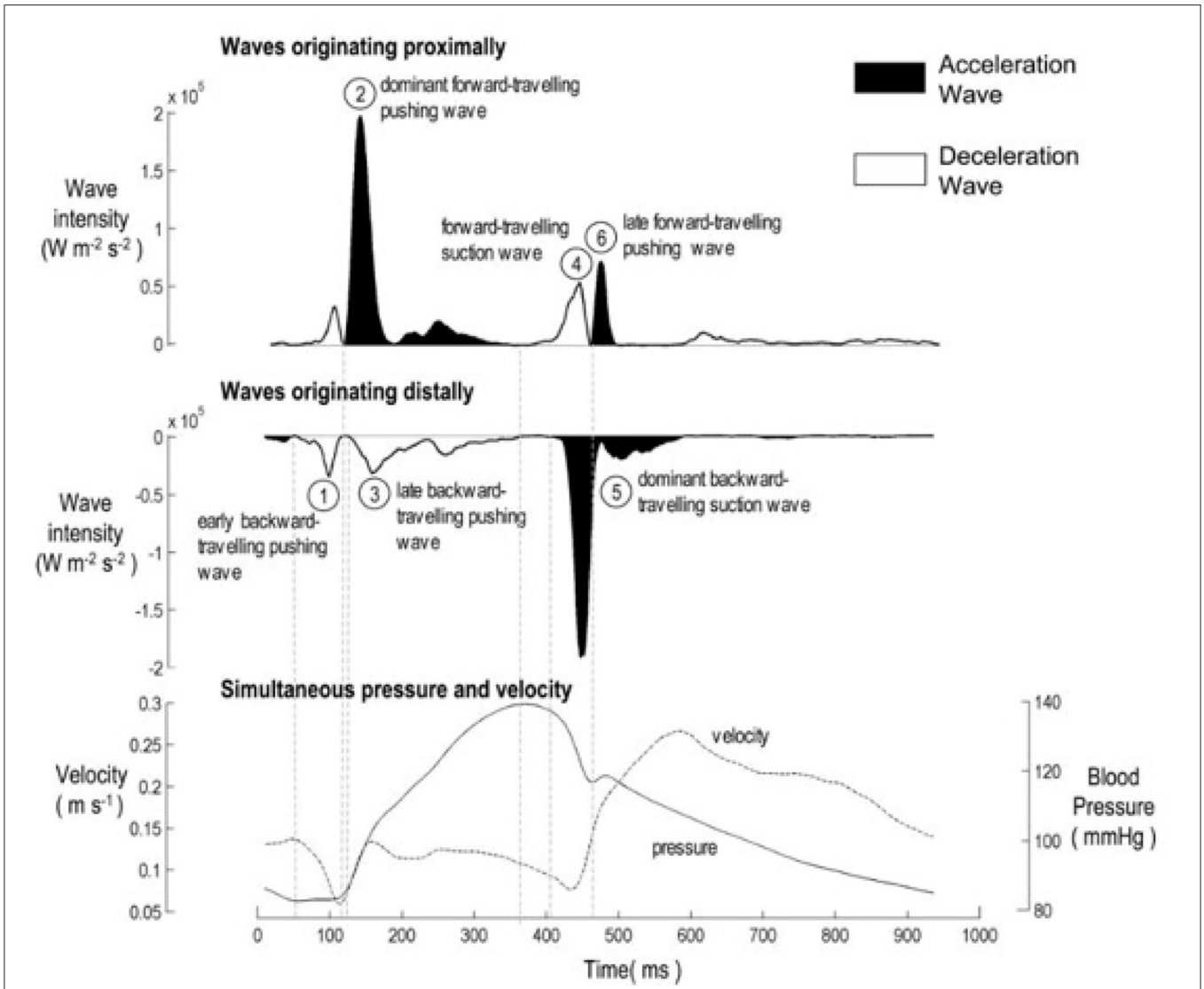

FIGURE 1 | The six characteristic waves in healthy unobstructed coronary arteries, adapted from Davies et al. (6). **(Top)** Forward wave intensity originating near the aorta. **(Middle)** Backward wave intensity originating near the microcirculation. **(Bottom)** Total pressure and velocity waveforms used in the calculation of wave intensity analysis. The peaks are identified as 1: Early Backward Compression Wave (BCW_0); 2: Forward Compression Wave (FCW_1); 3: Backward Compression Wave (BCW_1); 4: Forward Expansion Wave (FEW_2); 5: Backward Expansion Wave (BEW_2); 6: Late Forward Compression Wave (FCW_2).

not a measure of the value of the outcome; the entropy of a Shakespearean sonnet is exactly equal to the entropy of the same letters jumbled up in any random order.

The Maximum Entropy Method (MEM) involves partitioning data in a way that maximizes the entropy of the data (9). Its utility has been demonstrated in many areas such as the treatment of missing data in clinical trials, artificial intelligence, computer vision, and the optimal categorization of data.

In this study, we investigate the use of MEM to separate a measured wave intensity waveform into "peaks" and "background" using the Bayesian statistical principle; the probability distribution function that best represents the categorized data is the one with the largest entropy. This reduces the problem to finding the optimal threshold between peaks and background. This separation is particularly important in wave intensity analysis because of the inherent noisiness of wave intensity, which is defined as the product of two noise-enhancing derivatives.

The main problem in applying MEM is that we do not have prior knowledge of the probability distribution of the data; the probability must be estimated from the observed data. In our study, the data X is a time series of wave intensities x_n measured at discrete time intervals t_n. The probability of each x_n is estimated from the histogram of data h, which lies within bins b. h_j is the number of data points that fall within each bin b_j, and the sum of h_j is equal to N. Thus, $p_j = \frac{h_j}{N}$ is an estimate of the probability,

which enables us to calculate the entropy of the signal using:

$$H = -\sum_{j=1}^{J} p_j \log p_j \quad (2)$$

where J is the number of bins in the histogram; determined in our case by rounding the square root of the length of data. When the data X are categorized into two categories by a threshold x_T: peaks Π ($x_n \geq x_T$) and background Φ ($x_n < x_T$), the total entropy H_T is calculated using entropy H_Π and H_Φ:

$$H_T = H_\Pi + H_\Phi = -\sum_{j\in\Pi} p_j \log p_j - \sum_{j\in\Phi} p_j \log p_j \quad (3)$$

Since the entropy is a measure of the information in the signal, MEM asserts that the optimal threshold is the one that maximizes the total entropy of the partitioned data. Finding the maximum can be done iteratively or, more simply, by calculating the maximum net entropy over an equi-spaced array of thresholds and determining the maximum by interpolation.

2.2. Application of Maximum Entropy Method to Wave Intensity Analysis

Wave intensity is an inherently noisy signal. It is the product of differences which tends to emphasize the inevitable measurement noise in the pressure and velocity, and it is sensitive to physiological "noise" such as breathing and heart rate variations. Also, the use of an estimated local wave speed in the separation of wave intensity into its forward and backward components introduces systematic error which is very difficult to model. Given the level of noise and the difficulty in analyzing wave intensity peaks, MEM provides a convenient way to separate significant peaks from the noisy background.

Assuming that the noise is the same for the forward wave intensity (dI_+) and the backward wave intensity (dI_-), then the signal $X = dI_+ \cup |dI_-|$ is categorized using the same threshold (dI_T), where "peaks" are $\geq dI_T$, and "background" is $< dI_T$. The optimal threshold is defined as the threshold that maximizes the total entropy $H_T(dI_T)$, see **Figure 2**.

From our experience in applying MEM to wave intensity waveforms, there are two techniques that greatly increase the robustness and reproducibility of the method. The first technique arises from the highly skewed nature of the distribution of clinical wave intensity measurements, see **Figure 3**. The exponential shape of the histogram introduces a number of difficulties in estimating the probabilities. By introducing the log transform $X = log(dI)$, the resulting histogram is much more normally distributed, and the results of the entropy calculations are much more robust. All of our results are obtained by performing the entropy calculations on the log transformed data and then transforming the optimal threshold back to the original units by taking its exponential.

Second, it is best to perform the analysis using all of the data rather than the ensemble averaged wave intensity. Estimating the underlying probability density function used in calculating the entropy from the data itself is a fundamental problem in statistics. We tried a number of methods, including kernel smoothing methods, but found that estimating the probability from the more highly populated histograms using the total log transformed data is superior for our data, see **Figure 4**.

2.3. Data Acquisition

WIA was performed using the simultaneously measured pressure and flow via a 0.014 inch diameter velocity and pressure sensor wire (Combowire, Volcano Corporation, San Diego, California) positioned appropriately in the proximal left anterior descending coronary artery in 10 patients (age 30 ± 8 years old) with

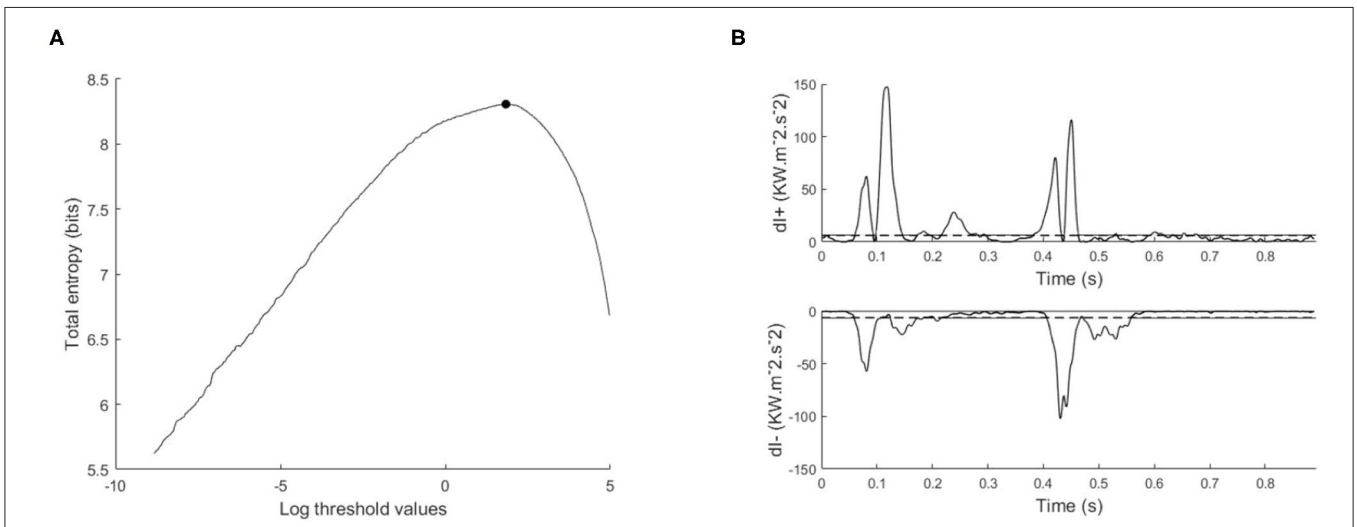

FIGURE 2 | Illustration of maximum entropy method and its application to the wave intensity signal, **(A)** total entropy as a function of the thresholds calculated on the log transformed data, with the optimal threshold indicated with a black circle, **(B)** separated wave intensity waveforms; forward (dI_+) and backward (dI_-). The horizontal dashed line is the exponential of the optimal threshold.

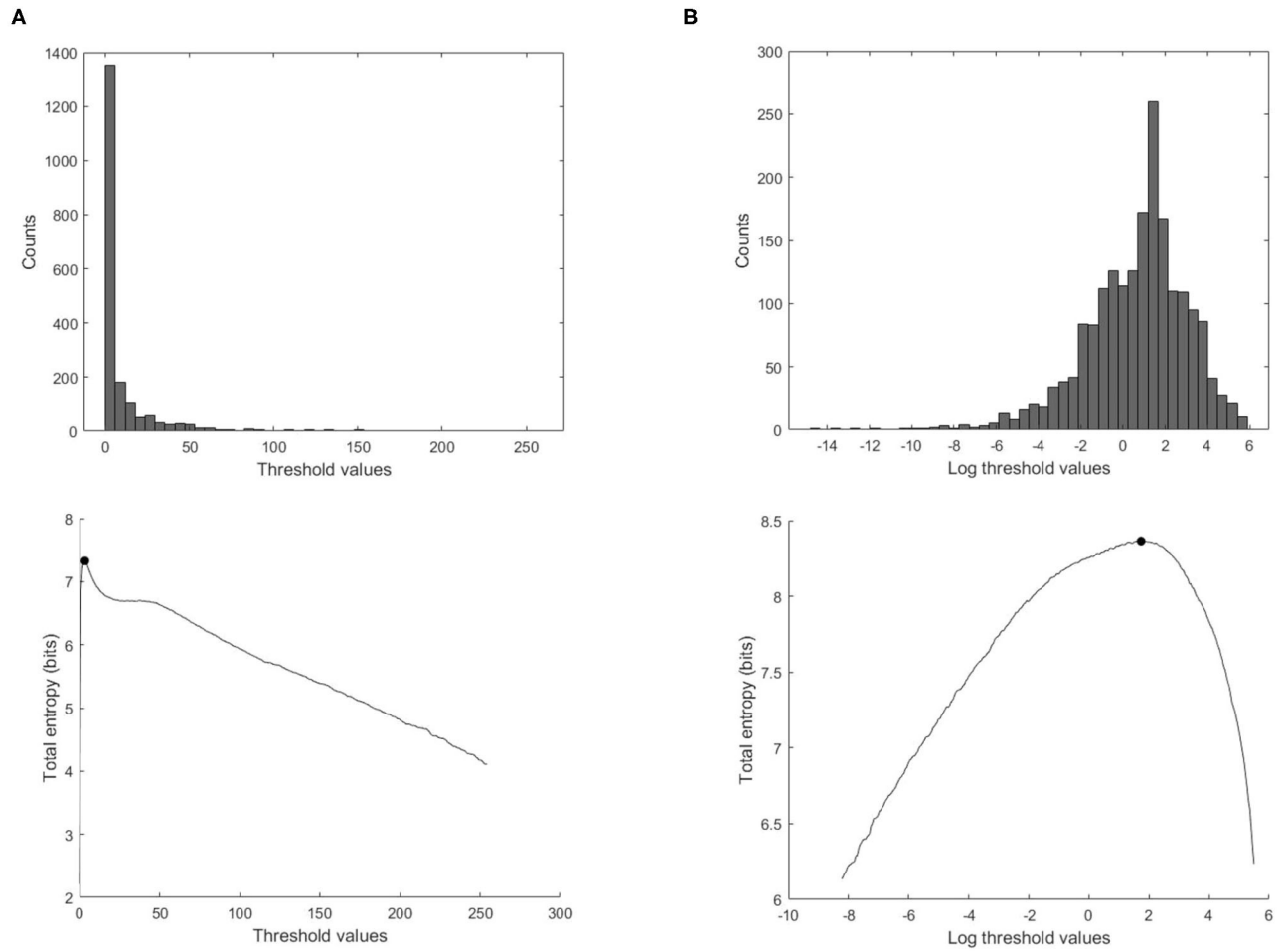

FIGURE 3 | Effect of using the log transform data on the calculation of the total entropy. **(Top)** Histogram of the ensemble wave intensity data of a control subject. **(Bottom)** Total entropy as a function of the threshold calculated on the wave intensity data, with the optimal threshold indicated with the black solid circle, **(A)** threshold values in the original units, **(B)** threshold values transformed to the logarithmic values.

symptomatic HOCM (10–13) prior to undergoing myectomy at Aswan Heart Center-Magdi Yacoub Heart Foundation; and in 11 normal Controls were patients who presented at St. Mary's Hospital for coronary angiography and were found to have structurally normal hearts with absence of valvular pathology or coronary artery obstruction (6). All patients and controls signed consent forms following ethical approval from the ethical committees at Aswan Heart Center-Magdi Yacoub Heart Foundation or St. Mary's Hospital, as appropriate.

The output from the Combowire console of the recordings of pressure, velocity, and ECG were digitized, processed offline and imported into MATLAB (The MathWorks, Inc., Natick, Massachusetts) for the post-processing using a custom-made MATLAB program (6, 7).

For details about the signal processing and the physics behind the analysis, see (5). Briefly, the measured pressure and velocity data P and U were converted into pressure and velocity differences dP and dU using a Savitsky-Goalay filter (2nd order, sliding frame of 11 samples), where 'd' is defined as 'd/dt', and dt is the sampling time, to accommodate different data sampling rates. The net wave intensity $dI = dPdU$ can be useful but does not differentiate between forward and backward traveling waves. This separation requires knowledge of the local wave speed c which can be estimated by the sum of squares method (calculated over an integral number of cardiac cycles)

$$c = \frac{1}{\rho}\sqrt{\frac{\sum(dP^2)}{\sum(dU^2)}} \tag{4}$$

where the density of blood ρ is assumed to be 1,050 kgm^{-3} (3, 6). From the water hammer equation

$$dP_{\pm} = \pm\rho c(dU_{\pm}) \tag{5}$$

and the assumption that the forward (+) and backward (–) waves are additive, $dP = dP_+ + dP_-$ and $dU = dU_+ + dU_-$, the forward and backward pressure and velocity changes are (2, 5)

$$dP_{\pm} = \tfrac{1}{2}(dP \pm \rho c dU) \tag{6}$$

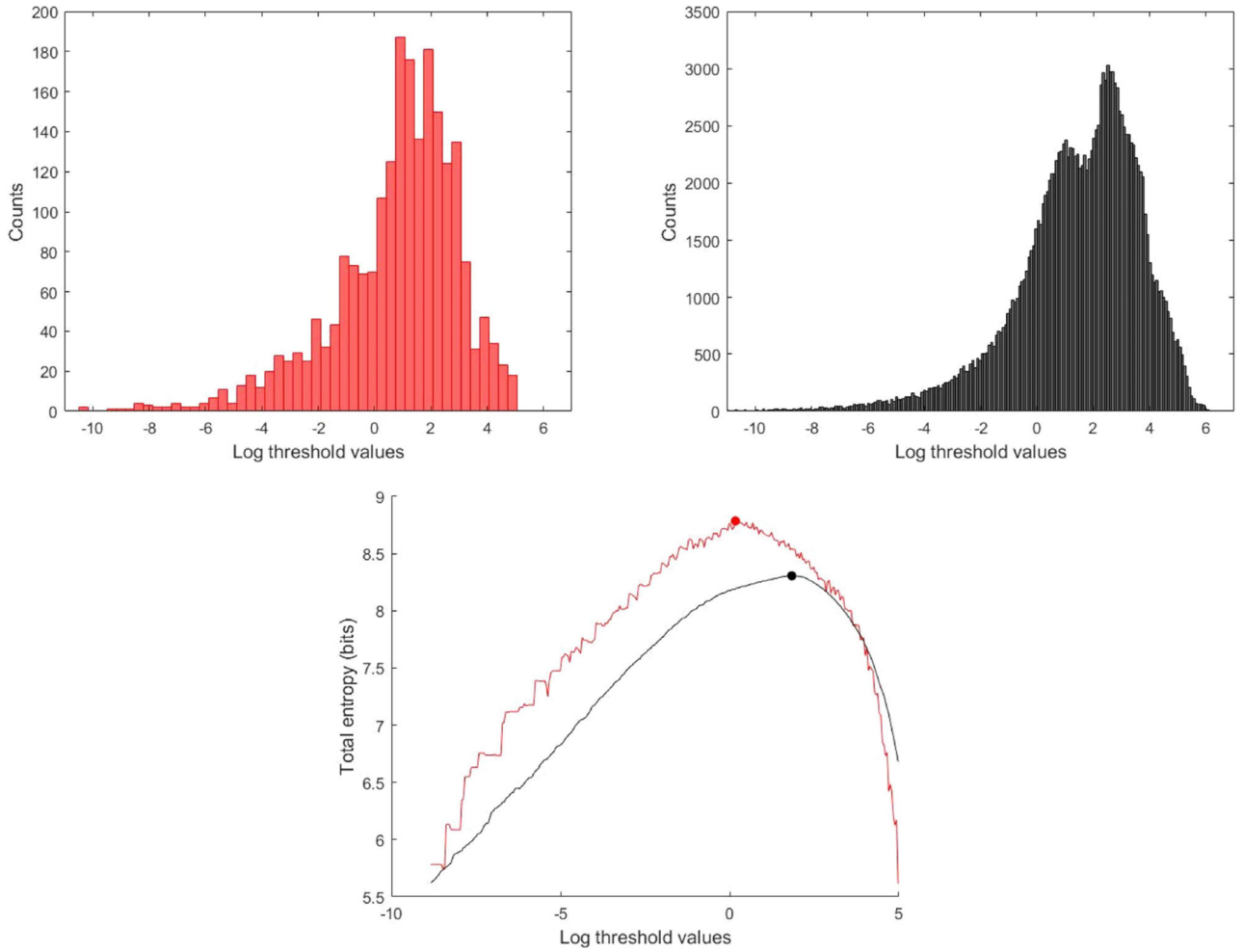

FIGURE 4 | Histogram and total entropy as a function of the thresholds for the log transformed data, **(Red)** Histogram and total entropy calculated using the ensemble averaged wave intensity signal, **(Black)** calculated using the total wave intensity data.

$$dU_{\pm} = \pm \frac{1}{2\rho c}(dP_{\pm}\ \rho c dU) \tag{7}$$

Finally, the forward and backward wave intensities are calculated as

$$dI_{\pm} = dP_{\pm} dU_{\pm}. \tag{8}$$

2.4. Identification of Significant Wave Intensity Peaks

The separated wave intensities can be thought of as the magnitude of the forward and backward wave fronts that are passing the measurement site at any particular time. Peaks in the separated wave intensities are usually referred to, rather confusingly, as "waves." The direction of these waves is determined by the sign of the wave intensity; positive for forward waves and negative for backward waves. The nature of the waves is determined by the sign of dP; waves with positive dP are compressive waves and those with negative dP are expansion waves. There are therefor four types of waves in the arteries: Forward Compression Waves (FCW), Forward Expansion Waves (FEW), Backward Compression Waves (BCW) and Backward Expansion Waves (BEW). The effect of the waves on the velocity are determined by the sign of dU; waves with positive dU are acceleration waves and those with negative dU are deceleration waves. Both FCW and BEW are acceleration waves and both FEW and BCW are deceleration waves.

The timing of the waves is indicated by subscripts 0, 1 and 2 depending upon the phase of the cardiac cycle when they appear. The three phases are marked by the R-wave of the ECG (the iso-volumic contraction phase), the start of the rapid rise in pressure (early systole) and the start of the rapid rise in velocity (late systole/early diastole). We note that these phases are unique to the coronary arteries; in other arteries the start of the rapid rise in velocity is simultaneous with the start of the rapid rise in pressure. Occasionally other waves of the same nature occur in the same phase and the subsequent waves are denoted by appending the subscripts "a" and "b."

The ability to relate the magnitude, the direction and the timing of the waves to events, both upstream and downstream, in the coronary arteries is the main value of wave intensity analysis. For each significant wave, as determined by the MEM analysis, we measure the peak value, time of the peak, wave duration, wave energy (time integral of power) and the percentage of the wave energy (wave energy fraction) calculated from dividing each wave energy by the cumulative wave energy of all the waves in that subject. In this study, we report results for measurements in 21 subjects (11 Controls, 10 HOCM).

2.5. Statistical Analysis

Data are expressed as mean ± standard deviation for different parameters. The wave intensity data were calculated from a single, simultaneous measurement of pressure, velocity and ECG for each subject. For data comparison between HOCM and Controls, we used the Mann-Whitney U test. A $p \leq 0.05$ is considered statistically significant, which indicates that the observations from HOCM patients differ from those from Controls.

3. RESULTS

The primary purpose of this paper is to introduce the application of MEM for the identification of significant waves in an artery by the detection of significant peaks in the wave intensity waveform. This is relevant to all wave intensity analysis. The secondary purpose is to present some preliminary results from a small study of HOCM patients. These patients are scheduled for myectomy and will eventually be part of a larger study measuring the clinical and mechanical effects of myectomy. The methodological results will use representative data from HOCM and Control subjects. The more clinical results will compare the MEM results in a cohort of 21 subject, 10 HOCM and 11 Controls.

3.1. Methodological Results

3.1.1. Estimation of the Probability Density Function of Wave Intensity

Calculation of the entropy of a digitized signal depends on the probability of each measurement. In clinical measurements, this probability is not known and must be inferred from the data itself. Due to the highly skewed distribution of wave intensity data (dI) observed in most cases, we have explored transforming the distribution of the data from a skewed distributed data to a more Gaussian distribution using the log transform of the data "log (dI)" (see **Figure 3**).

3.1.2. Ensemble Averaged vs. Total Wave Intensity Data

Because of the quasi-periodic nature of the cardiac cycle, most dynamic measurements of cardiovascular parameters are presented as a single "representative" beat or, preferably, as an ensemble average of the measurements over an ensemble of beats. Most wave intensity results, for example those shown in **Figure 1**, are calculated from the ensemble averaged P and U. In our study, we determined that the ensemble average of the instantaneous wave intensity is very close to the wave intensity calculated from the ensemble average P and U. Therefore, all of our preliminary studies of MEM were done using the ensemble average dI. The results were encouraging but not very robust, being very sensitive to various parameters in the calculations and producing an unacceptable number of outliers. We then tried MEM using the instantaneous dI calculated from all of the measured P and U, and found the results to be much more satisfactory. **Figure 4** shows the histograms and the maximum total entropy for the categorized data using the two methods: wave intensity calculated from the ensemble averaged P and U or from the total P and U data.

3.2. Clinical Results

Wave intensity analysis provides a quantitative description of the timing, magnitude and direction of the waves that determine the pressure and velocity in an artery. This is particularly useful in the coronary arteries because the contraction of the ventricle causes disturbances to the distal intra-myocardial blood vessels which profoundly affect coronary artery hemodynamics. Previous studies have concentrated on the main waves, manifested as large peaks in the wave intensity waveforms, comparing the differences between normal and pathological conditions such as HOCM (7). We seek to extend this work by identifying smaller but still significant waves using a MEM to differentiate between peaks and background in the clinically measured wave intensity waveforms.

The benefits of MEM can be seen by comparing **Figure 1**, a previously published wave intensity analysis in a normal subject, with **Figure 5**, a normal subject in our study. The previous study identified 6 waves while using MEM we have identified 6 additional significant waves, most of which are present in **Figure 1** but presumably considered to be noise.

In this study, we introduce a systematic nomenclature for waves in coronary arteries which may be useful in future studies. Our cohort of subjects is too small to reach any clinical results but we do present preliminary results for guidance and the statistical information necessary to properly power future clinical studies. Our approach is to divide the waves into dominant and secondary waves. We further divide the secondary waves into categories depending on the frequency that we observe them in our subjects, discussing their probable origin and their possible value in diagnosis.

The waves are named using the following convention:

F/B for Forward/Backward where forward is defined by the mean direction of blood flow.

C/E for Compression/Expansion depending on whether the pressure Increases/Decreases across the wave.

0/1/2 depending on the phase of the cardiac cycle in which they appear.

a/b/... refers to the successive individual waves with the same nature, that are occasionally observed.

For instance, FCW_{1a} is a Forward Compression Wave that follows FCW_1, which appears in the period between the rapid rise of pressure in early systole and the rapid rise of velocity in late systole.

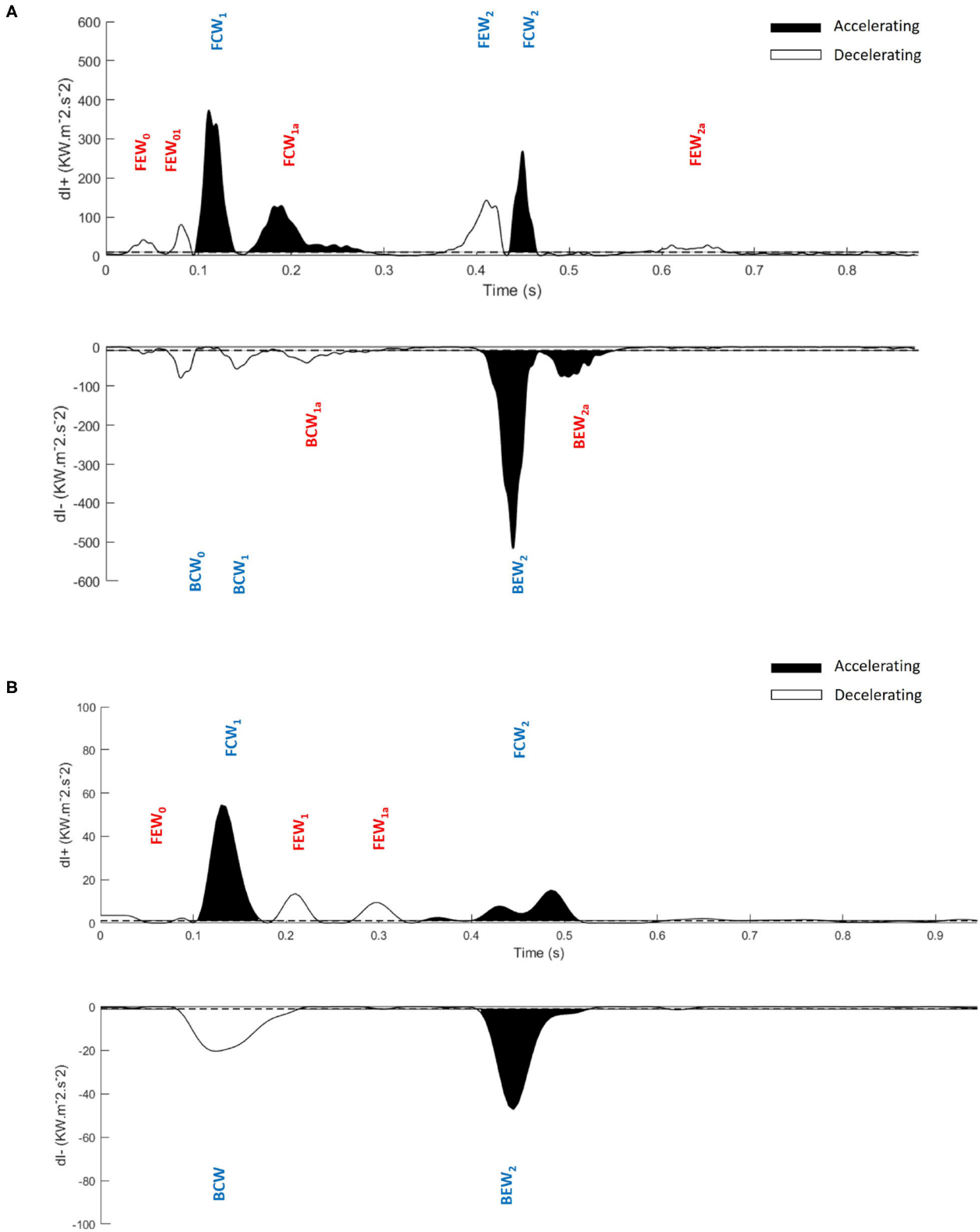

FIGURE 5 | Application of the maximum entropy method to wave intensity waveforms and identification of significant peaks. Significant peaks in the separated ensemble average wave intensity waveforms; forward (dI_+) and backward (dI_-), **(A)** Control subject, **(B)** Hypertrophic Obstructive Cardiomyopathy patient. FEW, Forward Expansion Wave; FCW, Forward Compression Wave; BCW, Backward Compression Wave; BEW, Backward Expansion Wave. The blue colored waves are the dominant waves, and red colored waves are the secondary waves. Note the difference in scales between **(A,B)**.

3.2.1. Dominant Waves

As expected, the total wave energy was much larger in Controls than in HOCM patients; the average over Controls was 27 ± 9 $kWm^{-2}s^{-1}$ compared to 15 ± 8 $kWm^{-2}s^{-1}$ in HOCM. Statistically, this difference is significant with $p < 0.01$. To enable comparisons of individual waves between the two groups, we define the relative wave energy as the wave energy in a single wave, the time integral of the wave energy over the duration of the peak, divided by the total wave energy in that subject.

Waves are classified as "dominant" if they are present in all the subjects and their relative wave energy is >3%. The properties of the individual dominant waves are given in **Table 1**. The classification is essentially independent of the MEM analysis and comparison of **Figure 1** and **Table 1** shows that the dominant waves correspond to the numbered waves identified in previous studies (2, 6, 7, 14).

3.2.2. Secondary Waves

The secondary waves are described in **Table 2** where they are classified into four categories depending on their frequency of observation in our subjects:

A waves that are observed in more than 40% of both Controls and HOCM subjects.
B waves that are observed in more than 40% of Controls but not in HOCM.
C waves that are observed in more than 40% of HOCM patients but not in Controls.
D waves that are observed in <40% of both groups.

The secondary waves observed in both Controls and HOCM are listed in **Table 2** together with their frequency of observation, their average wave energy and wave energy fraction.

4. DISCUSSION

4.1. Methodological Discussion

Our original efforts to apply MEM to wave intensity measurements were disappointing, probably because of the highly skewed distribution of dI, see **Figure 3**. Observing that the log transformed data, $[\log(dI)]$, exhibited a much more normal distribution, we applied the analysis to the log transformed data which gave reasonable and robust results. Thus, the probability density is estimated from the log transform of the observed data using a histogram function for regularly spaced thresholds over the range $[T_{min}, max(dI)]$. T_{min} is determined from the histogram of all of the data as the smallest bin containing more than 1 count. Tests indicated that the total entropy results are not sensitive to slight changes in the value of T_{min}.

TABLE 2 | The secondary waves.

Secondary waves:

	Wave	# with wave		Wave energy		Wave energy fraction	
		Control ($n = 11$)	HOCM ($n = 10$)	Control ($n = 11$)	HOCM ($n = 10$)	Control ($n = 11$)	HOCM ($n = 10$)
A	FEW_0	11	9	0.8 ± 1.1	0.6 ± 0.7	3 ± 4	3 ± 3
A	FEW_{2a}	11	9	0.4 ± 0.5	0.2 ± 0.2	2 ± 2	2 ± 2
A	FEW_{2b}	7	5	0.2 ± 0.3	0.1 ± 0	1 ± 1	0 ± 0
B	FCW_{1a}	8	2	1.9 ± 1.9	0.1 ± 0.1	6 ± 5	1 ± 0
B	BEW_{2a}	5	1	0.8 ± 0.6	0.3	4 ± 3	3
B	FEW_{01}	6	-	0.7 ± 0.7	-	2 ± 2	-
B	BCW_{1a}	6	2	0.6 ± 0.8	0.1 ± 0	2 ± 2	1 ± 0
B	FCW_{1b}	8	-	0.4 ± 0.3	-	3 ± 2	-
C	FEW_1	-	9	-	0.3 ± 0.2	-	3 ± 3
C	BEW_1	-	4	-	0.2 ± 0.2	-	2 ± 2
D	FCW_{2a}	1	1	0.5	0.2	8	2
D	FEW_{1a}	-	1	-	0.3	-	7
D	BCW_2	4	3	0.1 ± 0.1	0.2 ± 0.3	0 ± 0	3 ± 4

The waves are divided into 4 subcategories based on their frequency of observation and their wave energy, as discussed in the text. Wave energy ($kWm^{-2}s^{-1}$) and the wave energy fraction (%) for each wave are given as (mean ± standard deviation). HOCM, Hypertrophic Obstructive Cardiomyopathy.

TABLE 1 | The dominant waves.

Dominant waves:

Wave	# with wave		Wave energy			Wave energy fraction		
	Control ($n = 11$)	HOCM ($n = 10$)	Control ($n = 11$)	HOCM ($n = 10$)	*P*-value	Control ($n = 11$)	HOCM ($n = 10$)	*P*-value
FCW_1	11	10	6.7 ± 2.4	2.2 ± 1.3	< 0.001	27 ± 10	15 ± 6	< 0.001
FEW_2	11	-	2.3 ± 1.3	-	-	8 ± 3	-	-
FCW_2	11	10	3.4 ± 1.5	0.9 ± 0.5	< 0.001	14 ± 5	6 ± 3	< 0.001
BCW_0	11	10	1.0 ± 1.0	5.5 ± 4.0	< 0.001	4 ± 3	32 ± 10	< 0.001
BCW_1	11		1.4 ± 0.6			6 ± 3		
BEW_2	11	10	8.1 ± 4.4	5.5 ± 2.9	0.1	29 ± 10	35 ± 9	0.1

Wave energy ($kWm^{-2}s^{-1}$) and the wave energy fraction (%) for each wave are given as (mean ± standard deviation). HOCM: Hypertrophic Obstructive Cardiomyopathy.

Similarly, we found that MEM applied to wave intensity calculated for an ensemble averaged beat gave less reliable results than MEM applied to the wave intensity calculated from all of the instantaneous measurements of P and U. This is shown for a typical subject in **Figure 4**. The total entropy H_T calculated for the total wave intensity data (black) is much smoother than H_T calculated for the ensemble averaged data (red). More importantly, the maximum which is used to find the optimal threshold is shifted to a smaller value when the ensemble averaged data are used. The explanation for this shift is not obvious to us but it was observed consistently in our subjects. We therefore recommend that MEM should be used with the total rather than the ensemble averaged wave intensity data.

4.2. Clinical Discussion

We have used MEM to categorize the data and separate the significant peaks from the non-peaks. We refer to the noisy non-informative peaks as "background" because they include physiological noise, instrumental noise and any other unknown noise. We have applied MEM to WIA in one clinical application, HOCM, where wave intensity is thought to have predictive value of risk (3) but it is frequently difficult to identify the significant peaks from the background. Because of the small size of our cohort (21 subjects), all of the clinical observations should be considered to be preliminary; providing pointers to future clinical studies.

For convenience, we have divided the measured waves into dominant and secondary waves. The dominant wave coincide almost exactly with the waves measured in previous studies (2, 6, 7, 14) and their data are in **Table 1**.

Our results confirm the observation that the wave FEW_2 (i.e., the Forward Expansion Wave occurring in late systole/early diastole) that is observed in all Controls is not observed in any of the HOCM patients. This suggests that the absence of this wave could be taken as a clinical indication of HOCM. In this case, the MEM analysis could be useful because it gives a quantitative measure for the "absence" of the wave. Because of the small number of patients in our cohort, these results are preliminary and not clinically definitive. They do, however, suggest future clinical studies exploring the link between the absence of FEW_2 and changes in the myocardium in HOCM.

Our results also indicate that the two backward compression waves, BCW_0, occurring during the iso-volumic contraction period, and BCW_1, occurring during early systole, which are distinct in Controls present as a summation wave in all of our HOCM patients. The wave energy of this summation wave in HOCM is significantly larger than the combined energy of the two separate waves in Controls. This is not the case for other dominant waves FCW_1 or FCW_2 where the wave energy in Controls is significantly higher than the wave energy in HOCM. This large BCW, a deceleration wave, is responsible for the majority of differences between the pressure and velocity waveforms in HOCM and Controls. Also, the reduced FCW in HOCM suggest that HOCM pathology could significantly derange the forward waves originating near the aorta, which suggests that the aorta may play a role in perturbing the coronary flow dynamics.

The relatively small secondary waves that are revealed using MEM are listed in **Table 2** together with their properties, wave energy and fractional wave energy. For convenience we have divided these secondary waves into four categories depending on their frequency of observation in our subjects.

Category A waves are relatively small waves that are observed in both Controls and HOCM. Their wave energy in HOCM is approximately half that in Controls, which is comparable to the difference in total wave energy between HOCM and Controls. This suggests that their etiology is similar in both groups and their study may increase our understanding of the detailed interaction between the heart and the coronary arteries.

Category B waves are present in the majority of Controls and absent in almost all HOCM. This suggests that a study involving a larger number of subjects could find some diagnostic utility in the clinical measurement of these waves. Any future studies should be guided by the function of these waves. For example, the largest wave in Category B is FCW_{1a}, which is a second forward compression wave that accelerates the blood during mid-systole and is generally missing in HOCM. Similarly, the second largest wave BEW_{2a} is a second backward expansion wave that accelerates blood during early diastole and is also present in most Controls but absent in most HOCM.

Category C waves are present in some of our HOCM patients but entirely absent in Controls. The largest of these waves is FEW_1 which decelerates blood in early systole in some HOCM patients but is not present in any of our control subjects. Again, further study of this wave could provide supplementary evidence to the standard clinical tests for HOCM that may be useful in difficult cases or in differential diagnosis.

Category D waves are included only for completeness. They are not discussed because the observations are purely anecdotal.

5. CONCLUSION

The application of MEM to WIA for the identification of the significant peaks is novel and may enhance WIA in future study of coronary arteries. We demonstrate robust and reasonable results when we applied MEM to the log transformed wave intensity data, and smoother and more reliable results with the total rather than the ensemble averaged wave intensity data. Comparing the significant peaks in the wave intensity waveforms of Controls and HOCM patients, we have found an increase of backward compression waves and perturbed forward waves which altogether could perturb the coronary and aortic flow dynamics. We have also shown that some of the secondary waves identified using MEM are lost in HOCM patients, presumably due to the disease pathology, and that the appearance of FEW_1 and BEW_1 in HOCM patients could be predictor markers of HOCM. Thus, our provided data could help in elucidating the mechanisms involved in the complex interaction between coronary flow regulation and pathobiology of HOCM. However, the small number of subjects in our cohort is a serious limitation of our study and all our clinical results should be taken as preliminary.

DATA AVAILABILITY STATEMENT

The raw data supporting the conclusions of this article will be made available by the authors, without undue reservation.

ETHICS STATEMENT

The studies involving human participants were reviewed and approved by St. Mary's Hospital Research Ethics Committee, Imperial College Healthcare National Health Service Trust, St. Mary's Hospital and Aswan Heart Centre Research Ethics Committee, Aswan Heart Centre, Magdi Yacoub Heart Foundation. The patients/participants provided their written informed consent to participate in this study.

AUTHOR CONTRIBUTIONS

NF, MY, and KP were involved in the conception of the research and the writing of the manuscript. NF and KP were involved in the computing, data analysis and other technical matters. NF, PS, and MY were involved in the data collection and other clinical matters. All authors approved the final version of the manuscript.

REFERENCES

1. Maxwell JA, Anliker M. The dissipation and dispersion of small waves in arteries and veins with viscoelastic wall properties. *Biophys J*. (1968) 8:920–50. doi: 10.1016/S0006-3495(68)86529-4
2. Parker K, Davies JE, Escaned JE, Broyd CJ, Hughes A. Wave intensity analysis and its application to the coronary circulation. *Glob Cardiol Sci Pract*. (2016) 2015:64. doi: 10.5339/gcsp.2015.64
3. Broyd CJ, Rigo F, Davies J. Non-invasive coronary wave intensity analysis. *Int J Cardiovasc Imaging*. (2017) 33:1061–8. doi: 10.1007/s10554-017-1185-0
4. Sun YH, Anderson TJ, Parker KH, Tyberg JV. Wave-intensity analysis: a new approach to coronary hemodynamics. *J Appl Physiol*. (2000) 89:1636–44. doi: 10.1152/jappl.2000.89.4.1636
5. Parker KH. An introduction to wave intensity analysis. *Med Biol Eng Comput*. (2009) 47:175–88. doi: 10.1007/s11517-009-0439-y
6. Davies JE, Whinnett ZI, Francis DP, Manisty CH, Aguado-Sierra J, Willson K, et al. Evidence of a dominant backward-propagating "suction" wave responsible for diastolic coronary filling in humans, attenuated in left ventricular hypertrophy. *Circulation*. (2006) 113:1768–78. doi: 10.1161/CIRCULATIONAHA.105.603050
7. Raphael CE, Cooper R, Parker KH, Collinson J, Vassiliou V, Pennell DJ, et al. Mechanisms of myocardial ischemia in hypertrophic cardiomyopathy: insights from wave intensity analysis and magnetic resonance. *J Am Coll Cardiol*. (2016) 68:1651–60. doi: 10.1016/j.jacc.2016.07.751
8. Shannon CE. A mathematical theory of communication. *Bell Syst Techn J*. (1948) 27:379–423. doi: 10.1002/j.1538-7305.1948.tb01338.x
9. Papoulis A. *Probability, Random Variables, and Stochastic Processes, 2 Edn*. Singapore: McGraw-Hill International (1984).
10. Maron BJ, Maron MS. Hypertrophic cardiomyopathy. *Lancet*. (2013) 381:242–55. doi: 10.1016/S0140-6736(12)60397-3
11. Maron BJ. Hypertrophic cardiomyopathy: a systematic review. *JAMA*. (2002) 287:1308–20. doi: 10.1001/jama.287.10.1308
12. Elliott PM. 2014 ESC guidelines on diagnosis and management of hypertrophic cardiomyopathy. *Russ J Cardiol*. (2015). 121:7–57. doi: 10.1093/eurheartj/ehu284
13. Yacoub MH, Afifi A, Saad H, Aguib H, ElGuindy A. Current state of the art and future of myectomy. *Ann Cardiothorac Surg*. (2017) 6:307. doi: 10.21037/acs.2017.06.04
14. Hadjiloizou N, Davies JE, Malik IS, Aguado-Sierra J, Willson K, Foale RA, et al. Differences in cardiac microcirculatory wave patterns between the proximal left mainstem and proximal right coronary artery. *Am J Physiol Heart Circ Physiol*. (2008) 295:H1198–205. doi: 10.1152/ajpheart.00510.2008

Conflict of Interest: The authors declare that the research was conducted in the absence of any commercial or financial relationships that could be construed as a potential conflict of interest.

Publisher's Note: All claims expressed in this article are solely those of the authors and do not necessarily represent those of their affiliated organizations, or those of the publisher, the editors and the reviewers. Any product that may be evaluated in this article, or claim that may be made by its manufacturer, is not guaranteed or endorsed by the publisher.

frontiers in Pediatrics

ORIGINAL RESEARCH
published: 28 January 2022
doi: 10.3389/fped.2021.770754

Wave Reflection and Ventriculo-Arterial Coupling in Bicuspid Aortic Valve Patients With Repaired Aortic Coarctation

Elena Giulia Milano[1,2], *Sandra Neumann*[3], *Froso Sophocleous*[3], *Giulia Pontecorboli*[4], *Stephanie L. Curtis*[1], *Radwa Bedair*[1], *Massimo Caputo*[1,3], *Giovanni Battista Luciani*[2], *Chiara Bucciarelli-Ducci*[5] *and Giovanni Biglino*[3,6]*

[1] Bristol Heart Institute, University Hospitals Bristol & Weston, NHS Foundation Trust, Bristol, United Kingdom, [2] Department of Surgery, Dentistry, Pediatrics and Gynecology, University of Verona, Verona, Italy, [3] Bristol Medical School, University of Bristol, Bristol, United Kingdom, [4] Cardiovascular and Thoracic Department, Careggi University Hospital, Florence, Italy, [5] Royal Brompton and Harefield Clinical Group, Guy's and St Thomas' NHS Foundation Trust, London, United Kingdom, [6] National Heart and Lung Institute, Imperial College London, London, United Kingdom

OPEN ACCESS

Edited by:
Christian Apitz,
Ulm University Medical Center, Germany

Reviewed by:
Inga Voges,
University Medical Center Schleswig-Holstein, Germany
Ludger Sieverding,
University of Tuebingen, Germany

***Correspondence:**
Giovanni Biglino
g.biglino@bristol.ac.uk

Specialty section:
This article was submitted to Pediatric Cardiology, a section of the journal Frontiers in Pediatrics

Received: 04 September 2021
Accepted: 01 December 2021
Published: 28 January 2022

Citation:
Milano EG, Neumann S, Sophocleous F, Pontecorboli G, Curtis SL, Bedair R, Caputo M, Luciani GB, Bucciarelli-Ducci C and Biglino G (2022) Wave Reflection and Ventriculo-Arterial Coupling in Bicuspid Aortic Valve Patients With Repaired Aortic Coarctation. Front. Pediatr. 9:770754. doi: 10.3389/fped.2021.770754

Background: Ventriculo-arterial (VA) coupling in bicuspid aortic valve (BAV) patients can be affected by the global aortopathy characterizing BAV disease and the presence of concomitant congenital lesions such as aortic coarctation (COA). This study aimed to isolate the COA variable and use cardiovascular magnetic resonance (CMR) imaging to perform wave intensity analysis non-invasively to shed light on VA coupling changes in BAV. The primary hypothesis was that BAV patients with COA exhibit unfavorable VA coupling, and the secondary hypothesis was that BAV patients with COA exhibit increased wave speed as a marker of reduced aortic distensibility despite successful surgical correction.

Methods: Patients were retrospectively identified from a CMR database and divided into two groups: isolated BAV and BAV associated with repaired COA. Aortic and ventricular dimensions, global longitudinal strain (GLS), and ascending aortic flow data and area were collected and used to derive wave intensity from CMR data. The main variables for the analysis included all wave magnitudes (forward compression/expansion waves, FCW and FEW, respectively, and reflected backward compression wave, BCW) and wave speed.

Results: In the comparison of patients with isolated BAV and those with BAV associated with repaired COA ($n = 25$ in each group), no differences were observed in left ventricular ejection fraction, GLS, or ventricular volumes, whilst significant increases in FCW and FEW magnitude were noted in the BAV and repaired COA group. The FCW inversely correlated with age and aortic size. Whilst the BCW was not significantly different compared with that in patients with/without COA, its magnitude tends to increase with a

lower COA index. Patients with repaired COA exhibited higher wave speed velocity. Aortic wave speed (inversely related to distensibility) was not significantly different between the two groups.

Conclusion: In the absence of a significant restenosis, VA coupling in patients with BAV and COA is not negatively affected compared to patients with isolated BAV. A reduction in the magnitude of the early systolic FCW was observed in patients who were older and with larger aortic diameters.

Keywords: aortic coarctation, bicuspid aortic valve, congenital heart disease, wave intensity analysis, cardiac magnetic resonance, ventriculo-arterial coupling, ventricular strain

INTRODUCTION

Changes in ventriculo-arterial (VA) coupling are a key determinant of ventricular energetics (1). Considering the arterial side of the VA equation, both global and local changes can result in alterations of coupling efficiency. These changes can include overall alterations in arterial stiffness of the vessel as well as local changes in the vessel anatomy such as focal stenoses or sites of bifurcations. In this light, patients with bicuspid aortic valve (BAV) represent an interesting population in which to assess VA coupling, considering the presence of both global vascular abnormalities (BAV aortopathy) and the presence of concomitantly associated congenital lesions such as aortic coarctation (COA).

Wave intensity analysis (2) is an established method to measure the interaction between the ventricle and the remainder of the vasculature, and it has been used in other congenital heart diseases such as hypoplastic left-heart syndrome as well as aortic COA. In particular, previous studies exploring the hemodynamics of COA using wave intensity analysis observed that its presence results in a substantial backward reflection wave, in turn associated with left ventricular (LV) hypertrophy (3) and unfavorable LV energetics.

This demonstrates how the analysis of VA coupling can highlight the relationship between changes on the arterial side and the function of the LV and their possible repercussions on ventricular remodeling.

Importantly, wave intensity analysis lends itself to both invasive and non-invasive formulations, the latter making the analysis compatible with routinely acquired medical imaging data.

In this study, wave intensity analysis was performed non-invasively from cardiovascular magnetic resonance (CMR) data. This study focuses specifically on the assessment of the presence of a repaired COA in a population of patients with BAV, trying to isolate the COA variable from the BAV-associated aortopathy. The hypothesis underpinning the study is that BAV patients with COA exhibit unfavorable VA coupling. A secondary hypothesis is that BAV patients with COA also exhibit increased wave speed as a marker of reduced arterial distensibility.

The aim is to explore the difference in VA coupling between patients with isolated BAV and patients with BAV and repaired COA.

METHODS

Patient Population

Patients for this study were retrospectively identified from a database of 525 clinical CMR scans in patients with BAV acquired at the Bristol Heart Institute between 2011 and 2016 (4).

Ethical approval was not required by the local Research and Innovation Department in light of the retrospective nature of the study.

Patients were excluded based on the following criteria: (i) previous surgery on the aortic valve and/or surgery of the aortic root or ascending aorta, (ii) associated congenital heart defects apart from repaired aortic COA, (iii) undefined aortic valve morphology, (iv) presence of aortic valve stenosis (any degree), (v) presence of moderate to severe aortic regurgitation, (vi) presence of severe reCOA (COA index >0.5), and (vii) suboptimal image quality.

Twenty-five patients with BAV and repaired COA and 25 patients with isolated BAV were ultimately included from the above-mentioned sample.

CMR Imaging

All scans were acquired at 1.5 T (Avanto, Siemens Healthineers, Erlangen, Germany). Demographic and clinical information were gathered from CMR reports, together with aortic dimensions, valvular anatomy, presence of COA, presence and severity of valve dysfunction, LV volumes, LV mass, and LV ejection fraction (LVEF).

Aortic regurgitation was graded, according to regurgitant fraction quantification, as mild (<30%), moderate (31–49%), and severe (>50%). Aortic stenosis was classified, according to valve planimetry, as mild (>1.5 cm^2), moderate (1.0–1.5 cm^2), and severe (<1 cm^2) (5).

Severity of the reCOA was defined based on a COA index (6), i.e., a ratio of the aortic diameter at the level of the isthmus over the diameter of the descending aorta at the level of the diaphragm. Severity of reCOA was thus graded as absent (COA index >0.85), mild–moderate (COA index = 0.5–0.85), or severe (COA index <0.5).

Global longitudinal strain (GLS) was measured with the dedicated tool in the CVI42 software (Circle Cardiovascular Imaging, Calgary, Canada) by manually contouring the endocardial and epicardial borders of three long axis projections (four-chamber, three-chamber, and two-chamber views of the

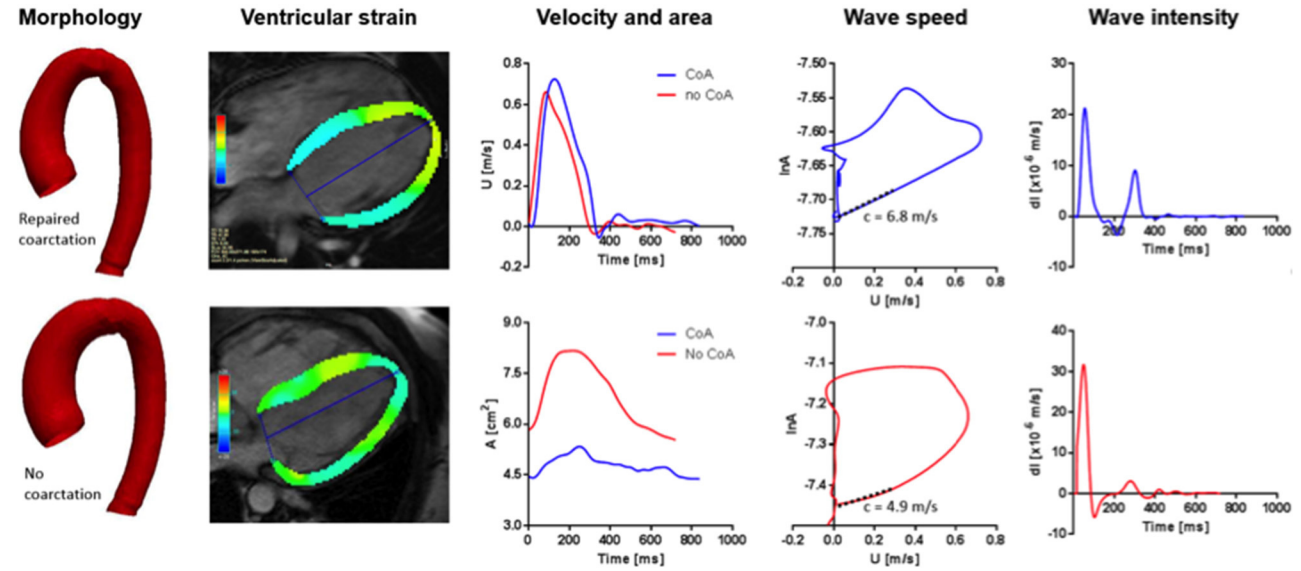

FIGURE 1 | From left to right: Aortic arch template of patients with BAV and repaired aortic COA (upper) and isolated BAV (lower); four-chamber view for GLS analysis in the diastole (upper) and systole (lower); velocity (upper) and area (lower) curves derived from phase-contrast analysis at the level of the ascending aorta; wave speed in patients with repaired COA (upper) and isolated BAV (lower); examples of wave intensity analysis patterns in a patient with repaired COA (upper) and isolated BAV (lower).

LV) in end-systole and end-diastole and propagating the regions of interest (ROIs) semiautomatically throughout the cardiac cycle, followed by manual correction.

The phase-contrast (PCMR) flow sequences acquired in the proximal ascending aorta at the level of the left pulmonary artery were selected for wave intensity analysis (7). Image segmentation was performed using the Flow package of CVI42 (Circle Cardiovascular Imaging), contouring the area of the aorta and propagating the ROI semiautomatically throughout the cardiac cycle, obtaining the corresponding flow velocity and area curves (**Figure 1**). The latter were used to derive fractional changes in area (dlnA) and velocity differentials (dU) to calculate wave speed and perform wave intensity analysis.

Aortic Distensibility

Processing of the aortic velocity (U) and area (A) signals and subsequent calculations were all performed in Matlab (MathWorks, Natick, MA, USA) using an in-house script, including steps of interpolation and resampling of the signals to 1 ms. Changes in U and A are related through the water hammer equation:

$$dU_{\pm} = \pm c\, dlnA_{\pm} \quad (1)$$

where the + and – subscripts indicate the forward-traveling and the backward-traveling components of the wavefront, respectively.

Similar to the pressure–velocity loop method (8), the U and lnA signals were plotted against each other, and the slope of the early systolic linear portion of the loop yields an estimate of wave speed (c). This approach, mathematically based on the Riemann method of characteristics, is based on the observation that in early systole the relationship between pressure and velocity is generally linear, with the slope of the first portion of the loop being proportional to c (9). Knowledge of c, in turn, allows direct estimation of aortic distensibility (D) based on the Bramwell–Hill equation (10):

$$D = 1/\rho c^2 \quad (2)$$

where ρ is the density of blood.

Wave Intensity Analysis

Wave intensity is a haemodynamic index that describes the working condition of the heart in relation to the remainder of the vasculature (3, 9), defined as the product of simultaneous pressure and velocity differentials at a given point in the circulation:

$$(dP/dt) \times (dU/dt) \quad (3)$$

where dP/dt and dU/dt represent changes in pressure and velocity measured simultaneously at a given location. As an analytical tool, wave intensity offers insights into haemodynamic changes and wave propagation, as it quantifies the intensity and energy carried by waves traveling in the blood (both forward, i.e., away from the heart, and backward, i.e., toward the heart) in the time domain (11). The clinical meaning of changes in wave intensity has been discussed extensively in the relevant literature, particularly indicating that the magnitude of the first positive peak of the aortic wave intensity pattern positively correlates with ventricular dP/dt and the second positive peak in late systole

negatively correlates with the diastolic time constant τ (12). The first peak (a forward-traveling compression wave, FCW) can thus be considered an indicator of contractile performance of the ventricle, whilst the second peak (a forward-traveling expansion wave, FEW) can be considered an indicator of isovolumic relaxation. Wave intensity thus carries information on both contractility and protodiastolic relaxation of the left ventricle (12, 13), and it has been shown to hold prognostic value, predicting cardiovascular events independently of other cardiovascular risk factors or being independently associated with cognitive decline (14, 15).

Data Analysis

Statistical analysis was carried out in Stata (v 13.1, StataCorp, College Station, TX, USA). Continuous variables are reported as mean ± SD, when normally distributed, and median (IQR) when not normally distributed, based on visual assessment of the data. Differences between continuous variables were assessed with either a Student's *t*-test or Mann–Whitney test, as appropriate. Categorical variables are reported as proportions or percentages, and differences between categorical variables were assessed with chi-square test. Associations between clinical, anatomical, and functional variables were investigated using univariate linear regression analysis. If multiple predictors were found to be significantly associated with an outcome of interest, these were further tested in a multivariable regression model. A $p < 0.05$ was taken to indicate statistical significance.

RESULTS

Demographic characteristics of the study population, together with anatomical and functional data, are summarized in **Table 1**. There were no statistically significant differences in age (at the time of the CMR scan), sex, or BSA amongst the two groups.

Patients with BAV and repaired COA presented overall with smaller diameters at the sinus of Valsalva compared to patients with isolated BAV (17.3 vs. 20.3 mm/m^2, $p = 0.001$), ascending aorta (14.6 vs. 20.8 mm/m^2, $p < 0.001$), and the transverse aortic arch (16 vs. 22 mm, $p < 0.001$).

The majority of patients with BAV and repaired COA underwent a surgical repair (92%), whereas only 8% of the patients underwent and interventional repair with stenting. Surgical procedures included end-to-end anastomosis ($n = 11$), subclavian flap aortoplasty ($n = 2$), and unknown ($n = 10$). None of the patients had a significant reCOA (median COA index = 0.73).

Patients with isolated BAV had a higher degree of aortic regurgitation compared to those with repaired COA (regurgitant fraction 2 vs. 6%, $p = 0.01$).

No differences were observed in LVEF and GLS between the two groups, as reported in **Table 2**. Indexed end-diastolic and end-systolic volumes also did not differ significantly between the two groups.

An example of the results is illustrated in **Figure 1**. Significant increases in FCW and FEW magnitudes were noted in the repaired COA subgroup, as reported in **Table 3**. Furthermore, wave intensity revealed the presence of a backward compression wave (BCW), although it was not significantly different when comparing the BAV-with-repaired-COA group with the isolated-BAV group.

Linear regression analysis, in BAV patients with repaired COA, revealed that FCW was inversely associated with age (rho = −0.49, $p = 0.037$) and with increasing diameters at the level of the ascending aortic (rho = −0.625, $p = 0.001$), aortic root (rho = −0.55, $p = 0.005$), and descending aorta (rho = −0.44, $p = 0.034$). It was also noted that the FEW magnitude decreased as aortic diameters increased at the ascending aortic and aortic root (rho = −0.55, $p = 0.008$ and rho = −0.0441, $p = 0.04$, respectively). The BCW in patients with BAV and repaired COA increased in magnitude with worsening of the COA index (rho = −0.435, $p = 0.043$).

Aortic wave speed was higher in the group of BAV with repaired COA (suggesting a degree of reduction of aortic distensibility in these patients), but this difference did not reach statistical significance (c = 5.9 vs. 4.2 m/s, $p = 0.08$).

TABLE 1 | Demographic characteristic, anatomical, and functional data.

	BAV + repaired COA	Isolated BAV	*p*-value
Age (years)	30.7 (21.7–34.9)	33.5 (26.9–50.0)	0.09
Male sex (%)	68	48	0.25
BSA	1.8 (1.7–2.0)	1.9 (1.7–2.2)	0.10
BAV–RL fusion pattern (%)	88	76	0.47
Presence of AR (%)	36	52	0.39
Peak AoV velocity (m/s)	1.2 (1.1–1.7)	1.4 (1.2–1.6)	0.95
Forward flow (ml)	82 (71.5–92.5)	85 (74–99)	0.50
Net forward flow (ml)	75 (69.0–90.5)	75 (66.5–92.5)	0.98
Cardiac output (l/min)	5.2 (4.3–6.4)	5.6 (4.8–6.4)	0.38
AoV regurgitant fraction (%)	2 (1.0–6.5)	6 (3.5–11.5)	0.01*
SOV (mm/m^2)	17.3 (15.6–18.9)	20.3 (17.5–21.9)	0.001*
AA (mm/m^2)	14.6 (12.1–18.9)	20.8 (17.7–22.4)	<0.001*
COA index	0.73 (0.6–0.8)	–	
Transverse arch (mm)	16 (14.0–18.0)	22 (19.5–24.0)	<0.001*
Descending aorta—mid (mm)	19 (16.0–22.0)	21 (19.5–22.5)	0.19
Descending aorta—diaphragm (mm)	16.5 ± 2.7	18.1 ± 2.2	0.024*
Arch hypoplasia index	1.0 ± 0.2	1.2 ± 0.2	0.006*

AA, ascending aorta; AoV, aortic valve; AR, aortic regurgitation; BSA, body surface area; SOV, sinus of Valsalva.
** $p < 0.05$.*

TABLE 2 | Results from CMR analysis.

	BAV + repaired COA	BAV	*p*-value
LVEDVi (ml/m^2)	74 (66–95)	81 (76–97)	0.23
LVESVi (ml/m^2)	33 (28–37)	30 (23.0–38.5)	0.36
LVEF (%)	61 (57–66)	62 (57.5–69.5)	0.28
GLS (%)	−19 (−20.8 to −16.7)	−18.7 (−21.2 to 16.7)	0.75

LVEDVi, left ventricular end diastolic volume indexed; LVESVi, left ventricular end systolic volume indexed; LVEF, left ventricular ejection fraction; GLS, global longitudinal strain.

TABLE 3 | Wave intensity analysis results for the BAV patients with and without COA (BAV + COA vs. isolated BAV).

	BAV + repaired COA	Isolated BAV	*p*-value
c (wave speed) m/s	5.9 (3.3–7.8)	4.2 (2.5–6.3)	0.08
D (distensibility) 1/mmHg × 10^{-3}	0.0035 (0.002–0.111)	0.0068 (0.003–0.019)	0.08
FCW (m/s) × 10^{-5}	2.8 ± 2.0	1.7 ± 1.6	0.04*
FEW (m/s) × 10^{-5}	0.42 ± 0.30	0.2 ± 0.2	0.02*
BCW (m/s) × 10^{-5}	−0.3 ± 0.5	−0.2 ± 0.1	0.10
FCW/FEW	8.5 ± 5.7	10.4 ± 9.0	0.50
FCW/BCW	15.4 ± 15.6	23.6 ± 38.4	0.60

FCW, forward compression wave; FEW, forward expansion wave; BCW, backward compression wave.

A ratio of "VA efficiency," measured as the FCW/FEW ratio, was not different between the two groups (8.5 ± 5.7 vs. 10.4 ± 9.0, $p = 0.5$), as well as the ratio FCW/BCW, both reported in **Table 3**.

DISCUSSION

This study examined properties of the aortic arch in a population of BAV patients, assessing the effect of repaired COA on aortic hemodynamics. The main observations from this study were that patients with BAV and repaired COA without any significant reCOA exhibit VA efficiency comparable to those with isolated BAV, as shown by the wave intensity analysis results, and that the presence of residual narrowing, albeit not clinically significant based on the COA index, appeared to be associated with an increment in the magnitude of backward reflected waves. This study also complements and adds to the overall wave intensity literature, particularly because it provides information on patients with BAV only, whereas the literature has generally focused on the presence of the COA, its haemodynamic effect, and different types of COA repair (16, 17).

The study analyzed VA coupling based on the hypothesis that patients with repaired COA would exhibit a reduction in the wave intensity values, reflecting an unfavorable VA coupling scenario, possibly due to anatomical and functional abnormalities.

As far as the aortic arch morphology is concerned, in our population, patients with COA had smaller aortic diameters compared to isolated-BAV patients, with lower diameters at the level of the root and in the ascending aorta, with a degree of transverse arch hypoplasia (4, 18).

With regard to LV functional parameters, there were no differences in global LV systolic function, assessed with LVEF and GLS. Likewise, a difference in VA efficiency was not observed between the two groups. Compared with other studies, ours did not show a correlation between LV deformation parameters and vascular indices (19). However, patients with BAV and repaired COA presented higher values of wave speed (and thus reduced aortic distensibility), compared to isolated-BAV patients, suggesting an increase in aortic stiffness in the first group, albeit results did not reach statistical significance.

A prior larger study employing wave intensity analysis in a population of COA patients reported a significant increase in ascending aortic stiffness compared to healthy controls (2). These results are not confirmed in our population, and this is possibly due to the fact that both our groups, being affected by BAV and related aortopathy, are carriers of structural abnormalities of the aortic wall.

Insight into post-operative COA physiology, especially through exercise studies, highlighted different features, at times conflicting (20), and different factors beyond the aortic anatomy itself have been suggested to be at play, including increased systemic arterial resistance and a hyperdynamic state which can lead to increased systolic blood pressure (20, 21).

The presence of an important BCW has already been described in repaired COA patients (3). Our results confirm the presence of a backward wave in patients with BAV and repaired COA, which was not significantly different in magnitude from that measured in patients with isolated BAV. The presence of the BCW derives from the anatomical restriction representing a reflection site or from an increase in aortic stiffness at the site of COA, or a combination of both factors. It should also be considered that, above and beyond local changes at the COA site, the overall aortopathy may play a role in such a population with isolated BAV, explaining the absence of significant differences amongst the two groups. The presence and magnitude of the BCW have also been associated with increasing LV mass in patients with atherosclerosis (22, 23). Furthermore, hypertensive therapy has been suggested to reduce the magnitude of the BCW in the aorta (22).

This analysis indicated a trend toward an increase of the magnitude of the BCW increases as the COA index decreases, even when the reCOA is not clinically significant (median COA index 0.73). Hashimoto et al. demonstrated that in the absence of an anatomical narrowing or in the presence of a mild reCOA, daily systolic blood pressure is independently associated with the COA index (24). The mechanism through which this phenomenon occurs is not entirely understood and may be in part explained by the increased aortic stiffness in these patients, also presenting histological changes and a reduction in smooth muscle cells vs. collagen (25, 26). The magnitude of the BCW may represent an additional tool to stratify these patients and potentially contribute to inform their treatment. However, additional studies are required to verify the relationship between increasing BCW and significant alterations in blood pressure and/or clinical endpoints.

Despite not observing significant alterations in VA coupling, we found that older patients and those with increased aortic diameters (at the level of the aortic root and in the descending aorta) present a reduction of the FCW, as a surrogate for dP/dt. This finding suggests the possible presence of subgroups with unfavorable anatomical and functional characteristics. Also, whilst this study focused on comparing BAV patients with and without repaired COA, comparison with values reported in the literature for healthy controls in a similar age range suggests a substantial difference, which should be explored further in a single prospective study.

The uptake of parameters derived from imaging-based methodologies, such as statistical shape modeling (27) and wave intensity analysis, could potentially represent a contribution of diagnostic value allowing identification of patient subgroups at

risk of developing aortic dilatation, LV systolic and diastolic dysfunction, or systemic hypertension and thus requiring more frequent follow-up (28). In particular, future prospective studies should explore the relationship between morphological characteristics of the aortic arch and changes in aortic distensibility with VA coupling and the development of hypertension (at rest and during exercise).

Limitations

The main limitations of this study are due to its retrospective nature. Data on arterial blood pressure (cuff measurements) at the time of CMR were not available for most patients as well as LV mass. Whilst the main aim of the study was to explore changes in wave intensity parameters comparing BAV patients with and without COA and as such lacked a group of healthy controls, the small sample size of the study limited subgroup comparisons of interest, such as comparing patients with different COA repairs (different surgical approaches and/or stenting). It would also be interesting to explore any relationship between age of COA repair and wave intensity variables. Whilst the study was based on routinely acquired CMR data, high-temporal-resolution PCMR would be desirable in future prospective studies to confirm observations on changes in wave speed.

CONCLUSION

In conclusion, this study explored the effect of the presence of repaired aortic COA on VA coupling in a population of patients with BAV. Patients with BAV and repaired COA, in the absence of a significant reCOA, are not negatively affected with regard to VA coupling compared to patients with isolated BAV. On the other hand, the study suggests that further studies assessing the effect of BAV aortopathy on ventricular energetics are warranted, expanding the current BAV literature.

DATA AVAILABILITY STATEMENT

The raw data supporting the conclusions of this article will be made available by the authors, without undue reservation.

AUTHOR CONTRIBUTIONS

GB and CB-D designed the study. EM, FS, and GP collected the data and performed the analysis on CMR images. SN and GB performed the WIA. GB performed the statistical analysis. SC, RB, MC, GL, and CB-D contributed to the critical interpretation of the data and revision of the manuscript. All authors reviewed the manuscript.

FUNDING

The authors acknowledge the generous support from the British Heart Foundation and the Cardiovascular Theme of the NIHR Bristol Biomedical Research Centre. The funders played no role in the design of the study, in the collection, analysis, and interpretation of data, or in the decision to submit the manuscript for publication.

REFERENCES

1. Chantler PD, Lakatta EG, Najjar SS. Arterial-ventricular coupling: mechanistic insights into cardiovascular performance at rest and during exercise. *J Appl Physiol.* (2008). 105:1342–51. doi: 10.1152/japplphysiol.90600.2008
2. Parker KH, Jones CJ. Forward and backward running waves in the arteries: analysis using the method of characteristics. *J Biomech Eng.* (1990) 112:322–6. doi: 10.1115/1.2891191
3. Quail MA, Short R, Pandya B, Steeden JA, Khushnood A, Taylor AM, et al. Abnormal wave reflections and left ventricular hypertrophy late after coarctation of the aorta repair. *Hypertension.* (2017) 69:501–9. doi: 10.1161/HYPERTENSIONAHA.116.08763
4. Sophocleous F, Biffi B, Milano EG, Bruse J, Caputo M, Rajakaruna C, et al. Aortic morphological variability in patients with bicuspid aortic valve and aortic coarctation. *Eur J Cardiothorac Surg.* (2019) 55:704–13. doi: 10.1093/ejcts/ezy339
5. Otto CM, Nishimura RA, Bonow RO, Carabello BA, Erwin JP, Gentile F, et al. 2020 ACC/AHA guideline for the management of patients with valvular heart disease: a report of the American College of Cardiology/American Heart Association Joint Committee on Clinical Practice Guidelines. *Circulation.* (2021). 143:e72–227. doi: 10.1161/CIR.0000000000000923
6. Egbe A, Miranda W, Connoly H. Predictors of left ventricular reverse remodeling after coarctation of aorta intervention. *Eur Heart J Cardiovasc Imaging.* (2021) 22:1168–73. doi: 10.1093/ehjci/jeaa199
7. Biglino G, Steeden JA, Baker C, Schievano S, Taylor AM, Parker KH, et al. A non-invasive clinical application of wave intensity analysis based on ultrahigh temporal resolution phase-contrast cardiovascular magnetic resonance. *J Cardiovasc Magn Reson.* (2012) 14:57. doi: 10.1186/1532-429X-14-57
8. Khir AW, O'Brien A, Gibbs JS, Parker KH. Determination of wave speed and wave separation in the arteries. *J Biomech.* (2001) 34:1145–5. doi: 10.1016/S0021-9290(01)00076-8
9. Li Y, Borlotti A, Parker KH, Khir AW. Variation of wave speed determined by the PU-loop with proximity to a reflection site. *Annu Int Conf IEEE Eng Med Biol Soc.* (2011) 2011:199–202. doi: 10.1109/IEMBS.2011.6090032
10. Bramwell JC, Hill AV. The velocity of the pulse wave in man. *Proc R Soc Lond B.* (1922) 93:298–306. doi: 10.1098/rspb.1922.0022
11. Hughes AD, Park C, Ramakrishnan A, Mayet J, Chaturvedi N, Parker KH. Feasibility of estimation of aortic wave intensity using non-invasive pressure recordings in the absence of flow velocity in man. *Front Physiol.* (2020) 11:550. doi: 10.3389/fphys.2020.00550
12. Parker KH. An introduction to wave intensity analysis. *Med Biol Eng Comput.* (2009) 47:175–88. doi: 10.1007/s11517-009-0439-y
13. Ohte N, Narita H, Sugawara M, Niki K, Okada T, Harada A, et al. Clinical usefulness of carotid arterial wave intensity in assessing left ventricular systolic and early diastolic performance. *Heart Vessels.* (2003) 18:107–11. doi: 10.1007/s00380-003-0700-5
14. Manisty C, Mayet J, Tapp RJ, Parker KH, Sever P, Poulter NR et al. Wave reflection predicts cardiovascular events in hypertensive individuals independent of blood pressure and other cardiovascular risk factors: an ASCOT (Anglo-Scandinavian Cardiac Outcome Trial) substudy. *J Am Coll Cardiol.* (2010) 56:24–30. doi: 10.1016/j.jacc.2010.03.030
15. Chiesa ST, Masi S, Shipley MJ, Ellins EA, Fraser AG, Hughes AD, et al. Carotid artery wave intensity in mid- to late-life predicts

cognitive decline: the Whitehall II study. *Eur Heart J.* (2019) 40:2300–9. doi: 10.1093/eurheartj/ehz189
16. van den Wijngaard JPHM, Siebes M, Westerhof BE. Comparison of arterial waves derived by classical wave separation and wave intensity analysis in a model of aortic coarctation. *Med Biol Eng Comput.* (2009) 47:211–20. doi: 10.1007/s11517-008-0387-y
17. Schäfer M, Morgan GJ, Mitchell MB, Ross M, Barker AJ, Hunter KS et al. Impact of different coarctation therapies on aortic stiffness: phase-contrast MRI study. *Int J Cardiovasc Imaging.* (2018) 34:1459–69. doi: 10.1007/s10554-018-1357-6
18. Bruse JL, Khushnood A, McLeod K, Biglino G, Sermesant M, Pennec X, et al. How successful is successful? Aortic arch shape after successful aortic coarctation repair correlates with left ventricular function. *J Thorac Cardiovasc Surg.* (2017) 153:418–27. doi: 10.1016/j.jtcvs.2016.09.018
19. Lee MG, Kowalski R, Galati JC, Cheung MM, Jones B, Koleff J, et al. Twenty-four-hour ambulatory blood pressure monitoring detects a high prevalence of hypertension late after coarctation repair in patients with hypoplastic arches. *J Thorac Cardiovasc Surg.* (2012) 144:1110–6. doi: 10.1016/j.jtcvs.2012.08.013
20. Hauser M. Exercise blood pressure in congenital heart disease and in patients after coarctation repair. *Heart.* (2003) 89:125–6. doi: 10.1136/heart.89.2.125
21. Ong CM, Canter CE, Gutierrez FR, Sekarski DR, Goldring DR. Increased stiffness and persistent narrowing of the aorta after successful repair of coarctation of the aorta: relationship to left ventricular mass and blood pressure at rest and with exercise. *Am Heart J.* (1992) 123:1594–600. doi: 10.1016/0002-8703(92)90815-D
22. Chirinos JA, Kips JG, Jacobs DR, Brumback L, Duprez DA, Kronmal R, et al. Arterial wave reflections and incident cardiovascular events and heart failure: MESA (Multiethnic Study of Atherosclerosis). *J Am Coll Cardiol.* (2012) 60:2170–7. doi: 10.1016/j.jacc.2012.07.054
23. Zamani P, Bluemke DA, Jacobs DR, Duprez DA, Kronmal R, Lilly SM, et al. Resistive and pulsatile arterial load as predictors of left ventricular mass and geometry: the multi-ethnic study of atherosclerosis. *Hypertension.* (2015) 65:85–92. doi: 10.1161/HYPERTENSIONAHA.114.04333
24. Hashimoto J, Westerhof BE, Westerhof N, Imai Y, O'Rourke MF. Different role of wave reflection magnitude and timing on left ventricular mass reduction during antihypertensive treatment. *J Hypertens.* (2008) 26:1017–24. doi: 10.1097/HJH.0b013e3282f62a9b
25. Vriend JW, Zwinderman AH, de Groot E, Kastelein JJ, Bouma BJ, Mulder BJ. Predictive value of mild, residual descending aortic narrowing for blood pressure and vascular damage in patients after repair of aortic coarctation. *Eur Heart J.* (2005) 26:84–90. doi: 10.1093/eurheartj/ehi004
26. de Divitiis M, Pilla C, Kattenhorn M, Zadinello M, Donald A, Leeson P, et al. Vascular dysfunction after repair of coarctation of the aorta: impact of early surgery. *Circulation.* (2001) 104(12 Suppl. 1):I165–70. doi: 10.1161/hc37t1.094900
27. Bruse JL, McLeod K, Biglino G, Ntsinjana HN, Capelli C, Hsia TY, et al. A statistical shape modelling framework to extract 3D shape biomarkers from medical imaging data: assessing arch morphology of repaired coarctation of the aorta. *BMC Med Imaging.* (2016) 16:40. doi: 10.1186/s12880-016-0142-z
28. Brown ML, Burkhart HM, Connolly HM, Dearani JA, Cetta F, Li Z, et al. Coarctation of the aorta: lifelong surveillance is mandatory following surgical repair. *J Am Coll Cardiol.* (2013) 62:1020–5. doi: 10.1016/j.jacc.2013.06.016

Conflict of Interest: CB-D is the CEO (part-time) of the Society for Cardiovascular Magnetic Resonance, and she received speaker's fees from Circle Cardiovascular Imaging and Siemens.

The remaining authors declare that the research was conducted in the absence of any commercial or financial relationships that could be construed as a potential conflict of interest.

Publisher's Note: All claims expressed in this article are solely those of the authors and do not necessarily represent those of their affiliated organizations, or those of the publisher, the editors and the reviewers. Any product that may be evaluated in this article, or claim that may be made by its manufacturer, is not guaranteed or endorsed by the publisher.

Advantages of publishing in Frontiers

OPEN ACCESS
Articles are free to read for greatest visibility and readership

FAST PUBLICATION
Around 90 days from submission to decision

HIGH QUALITY PEER-REVIEW
Rigorous, collaborative, and constructive peer-review

TRANSPARENT PEER-REVIEW
Editors and reviewers acknowledged by name on published articles

Frontiers
Avenue du Tribunal-Fédéral 34
1005 Lausanne | Switzerland

Visit us: www.frontiersin.org
Contact us: frontiersin.org/about/contact

REPRODUCIBILITY OF RESEARCH
Support open data and methods to enhance research reproducibility

DIGITAL PUBLISHING
Articles designed for optimal readership across devices

FOLLOW US
@frontiersin

IMPACT METRICS
Advanced article metrics track visibility across digital media

EXTENSIVE PROMOTION
Marketing and promotion of impactful research

LOOP RESEARCH NETWORK
Our network increases your article's readership